SANDIA REPORT

SAND2017-8032X
Unlimited Release
Printed August 2017

Probability of Detection Study to Assess the Performance of Nondestructive Inspection Methods for Wind Turbine Blades

Dennis Roach
Tom Rice
Josh Paquette
Sandia National Laboratories

Prepared by
Sandia National Laboratories
Albuquerque, New Mexico 87185 and Livermore, California 94550

Issued by Sandia National Laboratories, operated for the United States Department of Energy by Sandia Corporation.

Available to DOE and DOE contractors from

U.S. Department of Energy
Office of Scientific and Technical Information
P.O. Box 62
Oak Ridge, TN 37831

Telephone: (865) 576-8401
Facsimile: (865) 576-5728
E-Mail: reports@adonis.osti.gov
Online ordering: http://www.osti.gov/bridge

Available to the public from

U.S. Department of Commerce
National Technical Information Service
5285 Port Royal Rd.
Springfield, VA 22161

Telephone: (800) 553-6847
Facsimile: (703) 605-6900
E-Mail: orders@ntis.fedworld.gov
Online order: http://www.ntis.gov/help/ordermethods.asp?loc=7-4-0#online

SAND2017-8032X
Unlimited Release
Printed August 2017

Probability of Detection Study to Assess the Performance of Nondestructive Inspection Methods for Wind Turbine Blades

Dennis Roach
Tom Rice
Transportation Safeguards and Surety Organization

Josh Paquette
Wind Energy Technologies

Sandia National Laboratories
P.O. Box 5800
Albuquerque, NM 87185

ABSTRACT

Wind turbine blades pose a unique set of inspection challenges that span from very thick and attentive spar cap structures to porous bond lines, varying core material and a multitude of manufacturing defects of interest. The need for viable, accurate nondestructive inspection (NDI) technology becomes more important as the cost per blade, and lost revenue from downtime, grows. NDI methods must not only be able to contend with the challenges associated with inspecting extremely thick composite laminates and subsurface bond lines, but must also address new inspection requirements stemming from the growing understanding of blade structural aging phenomena. Under its Blade Reliability Collaborative program, Sandia Labs quantitatively assessed the performance of a wide range of NDI methods that are candidates for wind blade inspections. Custom wind turbine blade test specimens, containing engineered defects, were used to determine critical aspects of NDI performance including sensitivity, accuracy, repeatability, speed of inspection coverage, and ease of equipment deployment. The detection of fabrication defects helps enhance plant reliability and increase blade life while improved inspection of operating blades can result in efficient blade maintenance, facilitate repairs before critical damage levels are reached and minimize turbine downtime. The Sandia Wind Blade Flaw Detection Experiment was completed to evaluate different NDI methods that have demonstrated promise for interrogating wind blades for manufacturing flaws or in-service damage. These tests provided the Probability of Detection information needed to generate industry-wide performance curves that quantify: 1) how well current inspection techniques are able to reliably find flaws in wind turbine blades (industry baseline) and 2) the degree of improvements possible through integrating more advanced NDI techniques and procedures.

Sandia National Laboratories is a multimission laboratory managed and operated by National Technology and Engineering Solutions of Sandia, LLC, a wholly owned subsidiary of Honeywell International, Inc., for the U.S. Department of Energy's National Nuclear Security Administration under contract DE-NA0003525.

Acknowledgments

This program is sponsored by the U.S. Department of Energy (DOE) - Energy Efficiency & Renewable Energy department under the sponsorship and direction of Jose Zayas, Mike Derby, Jim Ahlgrimm Cash Fitzpatrick and program managers Megan McCluer and Nick Johnson.

The NDI development work and the Wind Blade Flaw Detection Experiment (WBFDE) were formulated with the Sandia National Laboratories Wind Energy Technologies department and conducted in concert with the Sandia-organized Blade Reliability Collaborative (BRC) team. Many of these BRC members provided information and served as reviewers and advisors for the activities described in this report. The contributions of the following team members are gratefully acknowledged: Derek Berry (NREL),Scott Hughes (NREL), Steve Nolet (TPI Composites), Kyle Wetzel (Wetzel Engineering), Gary Kanaby (Molded Fiber Glass Companies), Chris Bley (InspecTools), Doug Cairns (Montana State University), Ganzalo Palacio (Gamesa), Marty Crotty (Upwind), Joshua Crayton (Rope Partner Inc.), Maya Nissim (EDP Renewables), Carsten Westergaard (Vestas/Sandia), Yong Huang (Siemens), Ole Kils (Clipper Windpower), Christophe Mattei (Exova), Chris Yetter (GE Wind Energy), Daniel Nies (Nordex), Theis Hecker (Senvion), Steffen Szmaglinski (Enercon), Aaron Wahlstrom (Broadwind), Richard Roberts (Hexcel). Test specimen fabrication was supported by TPI Composites. The authors would like to thank Nick Altoff and his TPI team (Ethan Brown, Tim Fallon, Herminio DeOliveira and Alicia Poole). The authors would also like to thank Stephen Neidigk (Sandia Labs) and Randy Duvall (formerly Sandia Labs) for their assistance in setting up the experiment protocols.

Special thanks goes to the following companies who participated in the experiment and the employees who assisted with factory floor deployment of the WBFDE: Nick Althoff (TPI Composites), Martin Leong (Siemens), Johnny Jakobsen (Aalborg University), James Martin (Blade Dynamics), Alon Goldis (LM Windpower), Ryan Brashier (GE Windpower), Joan Reffs (Force Technology), Anurag Gupta (Vestas), Josu Badiola (Gamesa), Jason Habermehl (Olympus), Francis Boudreault-LeClerc (Nucleom), Juan Hodelin (Physical Optics Corp.), Steve Shepard (Thermal Wave Imaging), and Ciji Nelson (Sandia National Labs).

Probability of Detection Study to Assess the Performance of Nondestructive Inspection Methods for Wind Turbine Blades

TABLE OF CONTENTS

Section	Title	Page
ABSTRACT		3
1.0	INTODUCTION TO BLADE RELIABILITY COLLABORATIVE NONDESTRUCTIVE INSPECTION INITIATIVES	7
1.1	Objectives	10
1.2	Blade Reliability Collaborative Task Descriptions	12
1.3	Introduction to Wind Blade Flaw Detection Experiment	14
2.0	WIND BLADE FLAW DETECTION NEEDS	17
2.1	Post-Production Inspection of New Blades	17
2.2	In-Service Inspection of Operating Blades	21
3.0	WIND BLADE FLAW DETECTION EXPERIMENT DESIGN	33
3.1	Developing a Blade Probability of Flaw Detection Study	33
3.2	Design of Wind Blade POD Specimens with Engineered Flaws	39
3.3	Use of NDI Feedback Specimens	44
3.4	Manufacture of Flawed Wind Blade POD Specimens	53
3.5	NDI Characterization of Wind Blade POD Specimens	60
4.0	WIND BLADE FLAW DETECTION EXPERIMENT IMPLEMENTATION	71
5.0	DESCRIPTION OF CONVENTIONAL AND ADVANCED INSPECTION METHODS FOR WIND BLADES	77
5.1	Pulse-Echo and Phased/Linear Array Ultrasonics	77
5.1.1	Optimization of Single Element Contact and Phased Array UT Using Deployment Aids	100
5.1.2	Optimization of Single Element Contact and Phased Array UT Using Specialized Data Acquisition	115
5.1.2.1	Advantages and Deployment of Proper Transducer Frequency and Transducer Type	115
5.1.2.1	Advantages and Use of Proper Gate Settings	117
5.2	Pulsed Thermography	119
5.3	Microwave	125
6.0	RESULTS FROM WIND BLADE FLAW DETECTION EXPERIMENT	131

6.1 Conventional Pulse-Echo Ultrasonics ……... 131
6.1.1 WBFDE – Overall POD Results for All Specimens (Spar Cap with Shear Web and Box Spar Construction)…..…….. 131
6.1.2 WBFDE – Overall Probability of Detection Results for Spar Cap with Shear Web Construction……...….. 143
6.1.3 WBFDE – Overall Probability of Detection Results for Box Spar Construction……...……... 150
6.1.4 WBFDE – Overall POD Results Representing the Expected Inspection Performance within the Wind Industry…… 154
6.1.5 Improving Conventional POD - Value of NDI Training and Exposure to Wind Blade Inspections…..……... 162
6.2 Phased/Linear Array and Pulse Echo Scanning Ultrasonics ……..…. 173
6.2.1 WBFDE –POD Results Omniscan, P-Scan and Focused Single Element C-Scan Systems…..……... 174
6.2.2 Improvements Stemming from Additional Analysis and Proper Equipment Deployment - Value of NDI Training and Exposure to Wind Blade Inspections …..…….... 206
6.2.3 WBFDE – Preliminary Assessment of GE RotoArray Device …..….. 214
6.3 Pulsed Thermography ……... 218
6.4 Microwave ……..……..……. 228
6.5 Preliminary Efforts to Explore Wind Blade Inspection Training……. 247

7.0 CONCLUSIONS AND RECOMMENDATIONS…….……... 229
7.1 Overview Thoughts on NDI for Wind Blade Structures……... 259
7.2 WBFDE - Steps to Improve Probability of Flaw Detection and Exposure to Wind Blade Inspections …..……..……... 261
7.3 Inspection Improvement Via Technology Transfer and Focused Wind Inspector NDI Training …..……..…… 268
7.4 Summary of Key Points and Best NDI Practices ……..……..... 276

APPENDICES

A — Experimenter Briefing for Wind Blade Flaw Detection Experiment…….. 279

DISTRIBUTION LIST ……..……. 305

Probability of Detection Study to Assess the Performance of Nondestructive Inspection Methods for Wind Turbine Blades

CHAPTER 1

1.0 Introduction to Blade Reliability Collaborative NDI Initiatives

As the application of wind turbines continues to expand, there is an increased emphasis on ensuring the quality, and thus the reliability, of wind turbine blades. Blade reliability is rapidly becoming one of the most costly elements of plant operations because blade failure can cause extensive down time and lead to expensive repairs. In addition, blades are being delivered to the site in a condition that occasionally requires additional treatment of quality issues before they can be installed. Blade repair contractors for US wind plant developers and operators report that a significant percentage of the blades they repair have never been operated. Blade reliability issues need early attention because of the lost production and cost of significant failures. A reliability effort, centered around nondestructive inspection (NDI), was initiated at Sandia Labs to address these important reliability issues as they impact development and operations costs. This effort recognizes and is addressing the need to improve the quality of blades as they are delivered to the field through enhanced inspection capabilities and associated quality metrics.

Nondestructive inspection requirements, methods and practices vary widely within the wind industry and different blade manufacturers utilize different levels of rigor and different inspection methods on their product before it leaves the factory. As the length of blades increase and more advanced materials are being used to manufacture blades, it has become increasingly important to detect fabrication defects during blade production. In addition, small defects can propagate to levels of concern during blade use while fatigue loading, impact, lightning strike and other in-service conditions can lead to new damage in the blades. Operational environments produce high stress levels in the blades, it has become increasingly important to detect the onset of damage or the propagation of fabrication defects during blade operation. The need for in-service NDI of blades at wind farms is growing. One aspect of this program is to determine how advanced NDI methods can be gracefully integrated into wind farm operations. These include both up-tower NDI deployment and equipment for inspecting blades that have been removed from the wind turbine. The first task is to determine the inspection requirements as they exist now, as well as those that are expected to exist in the near-future.

The goals of this study are to determine what Nondestructive Inspection (NDI) is being performed on blades during and after the manufacturing process, determine the level of inspection requirements and standardization within the industry, develop new and customized NDI methods to meet the inspection needs of the industry and work with blade inspectors to test and apply state of the art inspection techniques in manufacturing environments. This includes the possible introduction of automated inspections, a comprehensive assessment of various conventional and advanced NDI techniques in manufacturing environments, close interface with blade original equipment manufacturers (OEMs) to determine inspection requirements, and the completion of NDI technology transfer activities with the wind turbine blade industry.

The purpose of the "Non-Destructive Inspection for Wind Turbine Blades" effort within the *Blade Reliability Collaborative* (BRC) is to develop, evaluate and validate the potential nondestructive inspection methods that could be deployed to effectively detect flaws in composite wind turbine blades. This effort has also allowed Sandia Labs to establish a national capability – including a physical presence and methodology - to comprehensively evaluate blade inspection techniques. The primary benefit to the wind industry is the optimum deployment of automated or semi-automated NDI to detect undesirable flaws in blades before the blades enter service while minimizing the time and cost required to complete the inspections.

Figure 1-1 shows various operating wind turbines along with a blade in production. Figure 1-2 shows the main components of a wind turbine blade and Figure 1-3 shows several different cross sections of blades highlighting some variations in blade design. Such variations give rise to unique inspection needs and challenges. Typical flaws encountered during production include: disbonds, interply delaminations, dry or resin-starved regions, porosity, voids, wrinkles, ply waviness, and snowflaking. In addition to these flaws, wind turbine blades operating in the field may also sustain damage stemming from transportation, installation, stress, erosion, impact, lightning strike, and fluid ingress.

A completed SAND report has already presented the details of the BRC NDI program and the infrastructure that was established to conduct the development and evaluation of advanced NDI methods for wind turbine blades reference [1-1]. It also describes the development of a highly-sensitive NDI method that is capable of inspecting through the thick composite sections and attenuative bond lines in blades to meet the inspection requirements of blade manufacturers. Preliminary testing was completed in this first phase of the BRC program to assess some NDI methods on actual wind blade test specimens. This first SAND report was intended to describe the promising NDI methods but not to assign any quantitative performance metric with respect to the inspection of wind turbine blades.

The report contained in this SAND document takes the next step of providing quantitative NDI validation through the implementation of a Probability of Flaw Detection (POD) experiment. This report describes the design and implementation of the Wind Blade Flaw Detection Experiment (WBFDE). WBFDE was deployed to quantitatively assess the performance of the best and most viable NDI methods as determined in the preliminary testing described in reference [1-1]. This report describes the top nondestructive inspection (NDI) techniques that might possibly be applied to address the fabrication quality assurance and in-service inspection of wind turbine blades. It provides an overview description of the various methods while introducing specific instruments that are available to implement each method. A series of Probability of Detection (POD) curves are presented to clearly show the ability of both conventional inspection methods – as deployed by current wind blade inspectors – and advanced inspections methods. Such comparisons are used to provide insights into the advantages, limitations, optimized deployment and training needs associated with each technology along with results from the application of these NDI methods to the set of WBFDE POD test specimens. Insights gained during the WBFDE testing are being used to develop both NDI reference

standards, formal inspection procedures and an inspector training regimen to further improve the inspection performance on wind blades.

Figure 1-1: Sample Wind Turbine Blades in Production and Operation

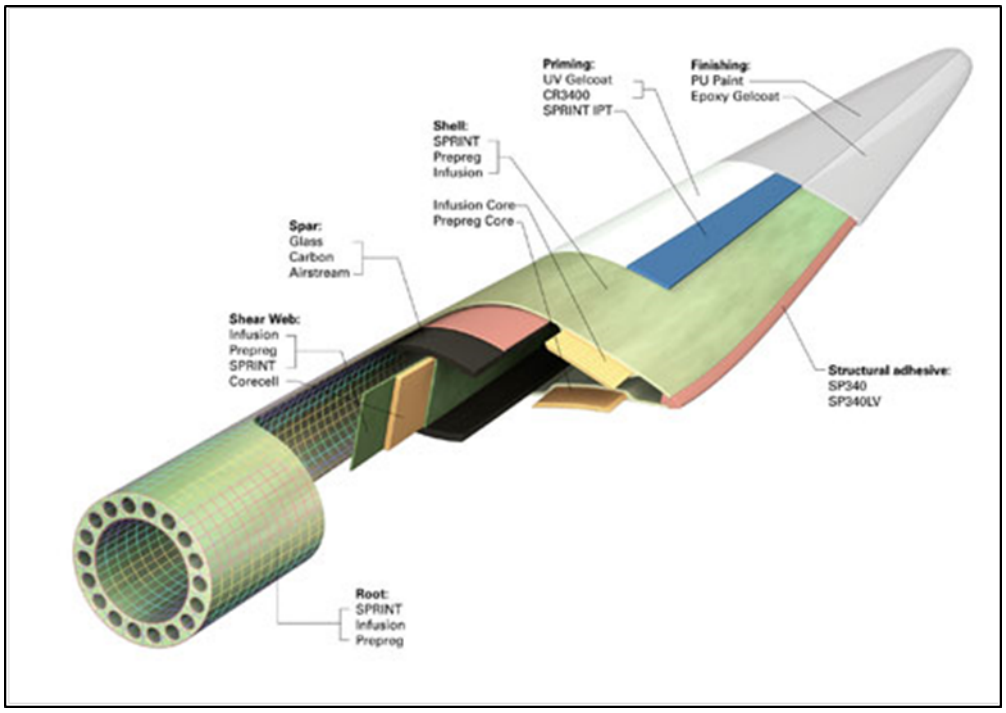

Figure 1-2: Components of a Wind Turbine Blade Construction

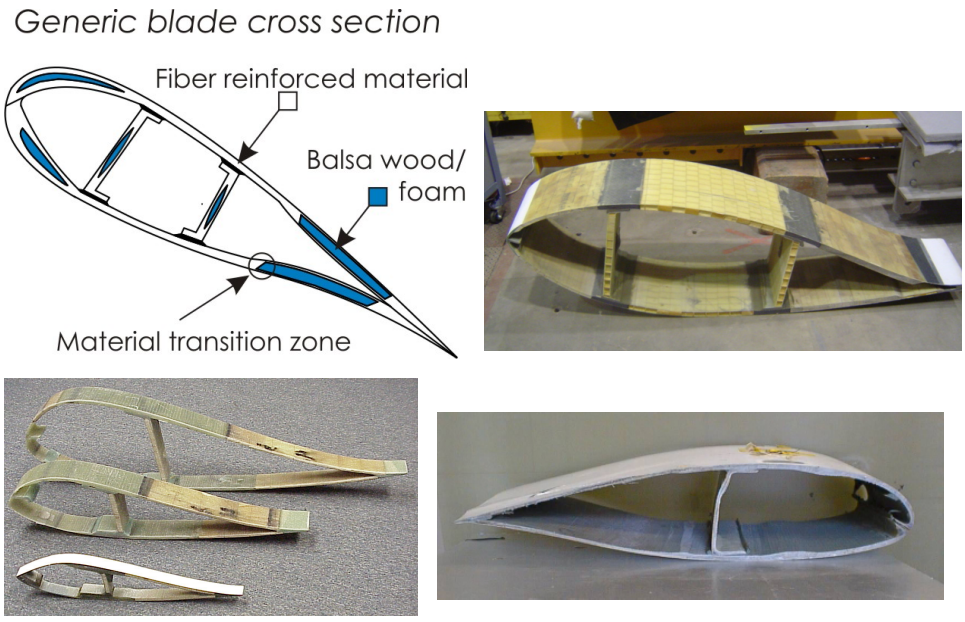

Figure 1-3: Sample Wind Turbine Blade Cross Sections Showing Different Design and Construction Scenarios

1.1. Objectives

The overall objectives of this NDI activity are:

- Plan and implement a national capability – including a physical presence and methodology - to comprehensively evaluate blade inspection techniques.
- Develop, evaluate and validate the array of potential nondestructive inspection methods for the detection of flaws in composite wind turbine blades. Transfer this NDI technology to wind blade production facilities.
- Produce optimum deployment of automated or semi-automated NDI to reliably detect undesirable flaws in blades (major criteria are time, cost and sensitivity).
- Create the ability for manufacturers to determine the quality of their product before it leaves the factory. Develop an array of inspection tools to comprehensively assess blade integrity (determine needs, challenges, and NDI limitations).
- Possibly use successful NDI to extend blade operational life.

Inspections must address all field deployment issues:

- Vertical and horizontal inspection surfaces
- Hand scan vs. attachable scanner
- Signal coupling into part
- Wide range of thicknesses
- Quantitative information

- Ease and rate of inspection

Inspections must overcome all inspection impediments

- Some methods may need access to both sides of blade
- Wide area inspection method needed (scanners)
- Porosity/attenuation levels of blades are high
- Depth of penetration and sensitivity at depth is needed
- Inspections must accommodate surface curvature and complex geometries

The BRC NDI initiative is addressing multiple methods to improve performance:

- Evolve existing NDI
- Introduce advanced NDI
- Assess NDI performance – conventional baseline and advanced NDI improvements
- Improve and/or add training
- Develop NDI standards
- Training – including feedback on experiment
- Process optimization
- Inspector certification

Figure 1-4 depicts the approach used to arrive at the desired NDI performance levels. Structural analysis and testing, which include a damage tolerance assessment, are used to determine the level of damage that can be sustained by the blade such that it can still achieve its desired function and lifetime. Inspection methods must then be developed and validated to ensure that all flaws can be detected prior to reaching a critical size. Damage tolerance assessments (DTA) are difficult to complete in composite materials, especially those produced with the VARTM process, and are exceptionally challenging in structures as large as wind turbine blades. Wide variations in operational environments and sources of damage onset also exacerbate a damage tolerance assessment. As a result, this NDI effort uses a conservative approach and includes flaw sizes that are expected to be below the DTA levels. This ensures that the results from the NDI evolution work will produce NDI methods that perform at or above the desired performance levels. DTA analysis and testing conducted to date has confirmed that the flaw sizes used in the NDI test specimens are conservative.

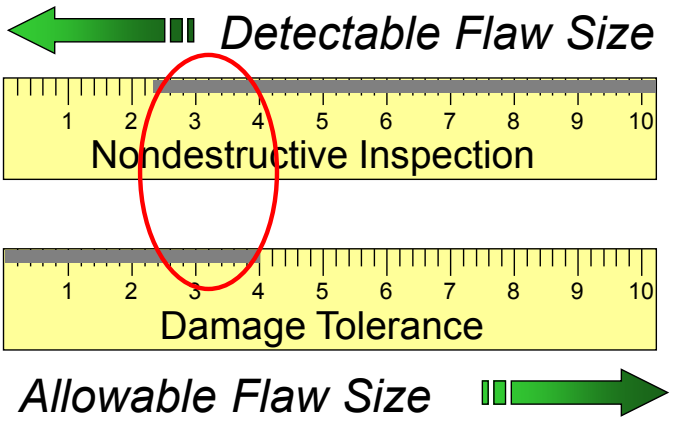

Figure 1-4: Required Relationship Between Structural Integrity and Inspection Sensitivity

Figure 1-5 shows the five key pieces of an NDI system that include the method, the equipment, inspection procedures and training needed to produce the optimum results in a repeatable manner. They include:

- Use of NDI reference standards to form a sound basis of comparison and ensure proper equipment set-up.
- Use of material property and calibration curves (e.g. attenuation, velocity) to guide NDI deployment and signal interpretation and to set proper accept-reject thresholds.
- Human factors – use of extensive NDI deployment testing to adjust procedures and minimize human factors concerns.
- Improved flaw detection via:
  - Advanced NDI
  - Hybrid inspection approach - stack multiple methods which address array of flaw types (data fusion)

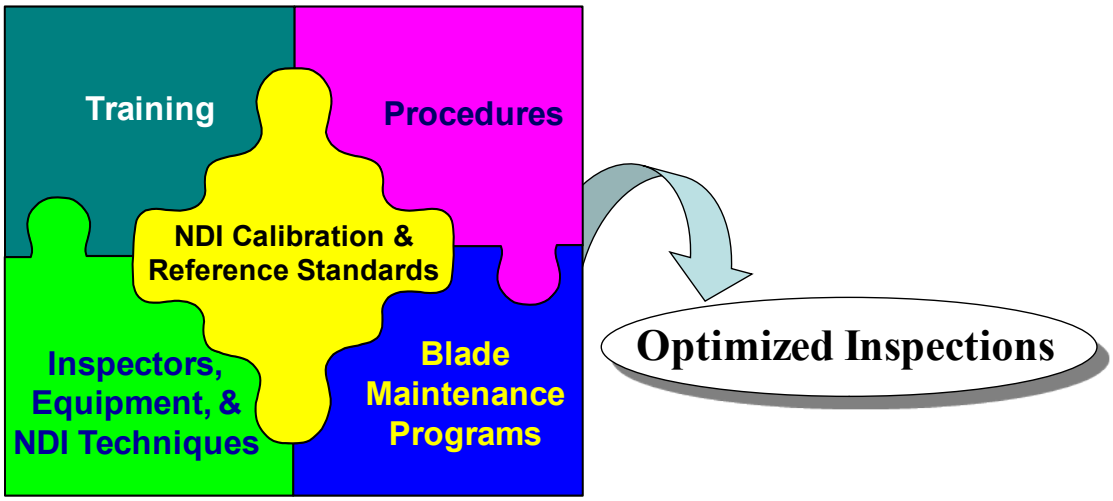

Figure 1-5: Depiction of the Critical Elements Contained in an

1.2. BRC Task Descriptions

One of the primary, early, activities conducted by Sandia Labs was the development and evaluation of ultrasonic (UT) inspection methods to improve the current state of blade inspection capabilities. These methods, categorized into single-element pulse-echo UT and phased array UT, were then used to accurately characterize the wind blade test specimens that were fabricated with engineered flaws and to propose an advanced NDI method for improving wind turbine blade inspections. The flaws include an array of interply delmainations, spar-to-shear web disbonds, contamination/FOD, laminate waves, porosity and dry regions. The Sandia-evolved ultrasonic NDI methods were demonstrated to produce some of the best sensitivity (highest contrast C-scan images) on wind turbine blades to date. A series of tasks developed deployment devices to: 1) allow the UT techniques to be conducted on rough surfaces at any orientation, and 2) produce reliable and optimized signal coupling to produce the strongest and most sensitive signal possible. The use of multiple gates, along with customized time-corrected gain, was explored in order to detect the full set of flaws through the assembly thickness. The combined use of A-scan (raw UT signal), B-scan (section view), C-scan (2-D planform view) data was also evaluated to enhance flaw detection and characterization. In order to better explain the subsequent NDI performance evaluations that were completed as part of the WBFDE, some of the NDI developments – primarily hardware and data acquisition improvements – are also briefly described in this report.

Activities from the completed portion of the BRC NDI initiative produced an initial screening of NDI methods; to identify the methods that show the greatest promise for flaw detection and potential deployment on wind turbine blade geometry reference [1-1]. A series of NDI Reference Standards and NDI Feedback Specimens were designed and fabricated to facilitate initial assessments of candidate NDI methods. Blade design and fabrication information from multiple manufacturers was digested into general construction scenarios so that this NDI effort could address the wind industry as a whole. The specimen designs, and associated fabrication processes, were reviewed by several wind energy experts to insure specimen realism. The NDI specimens were applied in a "feedback" mode where the inspector was aware of the flaw profile in each specimen (i.e. not blind mode inspections). Inspection systems at NDI vendors, research labs including Sandia Labs, and universities were evaluated using the representative test standards. The results were compiled in a structured manner to arrive at preliminary rankings of performance. The candidate array of flaws that were studied include: snowflaking, porosity, resin-starved regions, adhesive voids, interply delaminations, spar and shear web disbonds, and wrinkles. Discussions with blade manufacturers coupled with operational history were used to identify the most representative flaw types to be used in this study. The flaw sizes deemed necessary to be detected were determined by a complimentary BRC "Effects of Defects" study. Custom test panels with engineered flaws were supplemented by full-scale blades and blade sections that contain natural flaws found in the field along with engineered flaws. Candidate NDI methods are presented in Chapter 6.

Major tasks included:

- Acquire retired blade sections and add engineered flaws

- Understand blade designs and define blade NDI issues (design, inspection requirements, NDI impediments, desired deployment)
- Inspect retired blades using various NDI methods to understand challenges and characterize flaws
- Choose flaw types to include and the optimum methods to produce these flaws
- Perform trials to consistently reproduce realistic flaws
- Complete final design of NDI Reference Standards and NDI Feedback Specimens
- Complete fabrication of NDI Feedback Specimen set
- Identify NDI methods to be included in the WINDIE screening effort
- Develop WINDIE experiment protocols and invite participants
- Complete flaw characterization of NDI Feedback specimens
- Implement WINDIE - conduct round-robin testing on NDI Feedback specimens with "advanced" NDI methods
- Complete analysis of inspection results with NDI comparisons (sensitivity, repeatability, coverage, adaptability, deployment, cost, etc.)
- Assess NDI in the field - deploy NDI methods to allow for routine use of validated NDI method(s) in blade production environments (technology transfer)
    1) Develop, then evaluate technology in full-scale factory testing environment and obtain inspector feedback
    2) Conduct training and develop inspection procedures aimed at manufacturer needs using advanced NDI
    3) Carry out technology transfer to industry

1.3. Introduction to Wind Blade Flaw Detection Experiment

The development and deployment of advanced nondestructive inspection (NDI) methods must keep pace with the rapidly-increasing size and complexity of modern wind turbine blades. Nondestructive inspection requirements, methods and practices vary widely within the wind industry. Different blade manufacturers utilize different levels of rigor and different inspection methods on their product before it leaves the factory. As the length of blades increase and more advanced materials are being used to manufacture blades, it has become increasingly important to detect fabrication defects during blade production, thus enhancing plant reliability. Additional information on the Sandia Labs Wind Inspection Program can be obtained from references [1-1 to 1-3]. Formal discussions on industry-wide flaw detection studies conducted for aviation composite structures can be found in references [1-4] and [1-5].

Nondestructive inspection (NDI) requirements, methods and practices vary widely within the wind industry and different blade manufacturers utilize different levels of rigor and different inspection techniques on their product before it leaves the factory. However, small defects can propagate to levels of concern during blade use while fatigue loading, impact, lightning strike and other in-service conditions can lead to new damage in the blades. As the length of blades increase and operational environments produce high stress levels in the blades, it has become increasingly important to detect the onset of damage or the propagation of fabrication defects during blade operation. The need for in-service NDI of blades at wind farms is growing.

Additional NDI fidelity beyond what can be provided by visual methods is required to identify and repair defects before they reach a critical size.

The purpose of the Wind Blade Flaw Detection Experiment (WBFDE) was to determine the capability of conventional and advanced Nondestructive Inspection (NDI) methods to identify flaws in wind turbine blades. The WBFDE effort was used to study the capabilities and limitations of applicable NDI methods in identifying the different flaw types in wind blade construction. The general goal was to determine which NDI method(s) have high sensitivity, accuracy and reliability in order to facilitate improvements in both quality assurance measures during blade production and critical damage detection during service. This effort also identified the factors influencing composite wind blade inspections on this type of structure so that improved methods and procedures can be developed.

The topic of this report is a formal, statistical, quantitative assessment of wind blade inspection methods including current limitations and the use of NDI devices to improve inspection coverage of blades in the field while also improving damage detection sensitivity and reliability. The Sandia Wind Blade Flaw Detection Experiment was completed to evaluate different NDI methods that have demonstrated promise for interrogating wind blades for manufacturing flaws or in-service damage. NDI performance attributes were evaluated with the expected results of:

1. Assessing NDI accuracy & sensitivity (hits, misses, false calls, sizing)
2. Assessing NDI versatility, portability, complexity, inspection time (human factors)
3. Producing guideline documents to improve inspections
4. Using tech transfer initiatives to introduce advanced NDI where warranted

The Wind Blade Flaw Detection Experiment (WBFDE) was conducted to quantify the flaw detection performance of NDI in composite wind turbine blades. This experiment determined Probability of Detection (POD) curves for the wind turbine blade industry. In general, inspectors were asked to locate and size hidden flaws in the test specimens which mimic the construction and include damage types found in today's wind turbine blades. These POD experiments were conducted to assess the performance of both conventional and advanced NDI techniques. Once a sufficient number of inspectors completed the experiment, industry-wide performance curves were established that determine: 1) how well current inspection techniques are able to reliably find flaws/damage in wind turbine blades (industry baseline), and 2) the degree of improvements possible through the integration of more advanced NDI techniques and procedures. Ultimately, the proper combination of several inspections methods may be required to produce the best inspection sensitivity and reliability for both near-surface and deep, subsurface damage.

The experiment tasks associated with the WBFDE were: 1) fabrication of representative test specimens to be used with all inspection methods, 2) comprehensive, in-house characterization of the NDI test specimens to ensure flaw realism, 3) production of experiment protocols, NDI candidate list, and invitation to possible participants, 4) completion of blind POD testing on NDI test specimens with a wide range of qualified inspectors, and 5) completion of analysis of inspection results with NDI comparisons (sensitivity, repeatability, coverage, adaptability deployment, cost, etc.). Other information gathered during the inspections included: a) duration of inspection, b) fieldability, c) deployment issues, d) inspection method difficulties, e) cost of

new system, f) accessories needed to make the inspection device fieldable, g) ease of data interpretation.

Current results from the BFDE will be presented in this report along with procedures that have been identified to improve critical NDI methods. The end product of this project includes NDI technology transfer activities with both wind service companies and wind farm operators. Improved detection of fabrication defects helps enhance plant reliability and increase blade life while improved inspection of operating blades can result in efficient blade maintenance, facilitate repairs before critical damage levels are reached and minimize turbine downtime. The optimum deployment of automated or semi-automated NDI to detect undesirable damage in blades will help the blades reach their design lifetime or beyond.

References

1-1. Roach, D., Neidigk, S., Rice, T., Duvall, R., Paquette, J., "Blade Reliability Collaborative: Development and Evaluation of Nondestructive Inspection Methods for Wind Turbine Blades," Sandia DOE Report, SAND2014-16965, September 2014.

1-2. Neidigk, S., Duvall, R., Roach, D., Rice, T., "Preliminary Assessment of In-Service NDI Needs and Field-Deployable NDI," Dept of Energy Report, Oct. 2015.

1-3. Roach, D., Rice, T., "Use of Probability of Detection Studies to Establish the Reliability of Quality Assurance Measures in the Wind Industry," Int'l Wind Turbine Blade Manufacturing Conference, Dusseldorf, Germany, December 2015.

1-4. Roach, D., Rice, T., "A Quantitative Assessment of Advanced NDI Techniques for Detecting Flaws in Composite Laminate Aircraft Structures," US Dept. of Transportation Report DOT/FAA/AR-15/23, July 2015.

1-5. Roach, D., "A Quantitative Assessment of Conventional and Advanced NDI Techniques for Detecting Flaws in Composite Honeycomb Aircraft Structures," Dept. of Transportation Report DOT/FAA/AR-15/15, May 2014.

1-6. Neidigk, S., Duvall, R., Roach, D., Rice, T., "Preliminary Assessment of In-Service NDI Needs and Field-Deployable NDI," Sandia report to DOE, Oct. 2015.

CHAPTER 2

2.0 Wind Blade Flaw Detection Needs

2.1. Post-Production Inspection of New Blades

While there are a wide array of blade designs and customized production processes, there are common flaws that can be produced in composite wind blade structures. Typical flaws encountered during production include: disbonds, interply delaminations, dry or resin-starved regions, porosity, adhesive voids, wrinkles, ply waviness, and snowflaking. In addition to these flaws, wind turbine blades operating in the field may also sustain damage stemming from stress, erosion, impact, lightning strike, fluid ingress and other stress risers that may occur during shipping and installation. Figure 2-1 shows a cross section of a blade highlighting some primary inspection regions. Blade design variations give rise to unique inspection needs and challenges. Sample flaws found in the thick, fiberglass and carbon blades are shown in Figure 2-2 through Figure 2-5.

The most general list of flaws, damage and non-standard production items that the industry would like to detect are:

- Thickness variations
- Disbonds, including kissing (intimate contact) disbonds
- Presence of adhesive (ensuring proper bond line width)
- Missing adhesive (voids)
- Width and placement of adhesive
- Interply delaminations
- Dry regions (incomplete resin transfer)
- Gelcoat disbonds

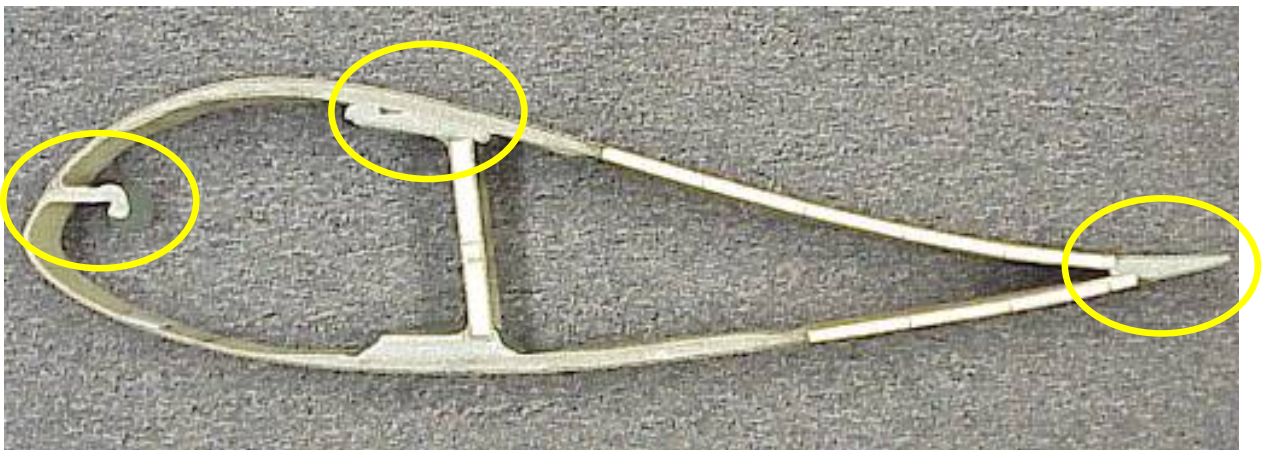

Figure 2-1: Inspection Areas of Interest – 1) Leading Edge Bond, 2) Spar Cap, 3) Spar Cap-to-Shear Web Flange Bond Line and 4) Trailing Edge

- Snowflaking
- Porosity
- In-plane and out-of-plane waves
- Composite fiber fracture (cracks)
- In-service damage such as erosion, overstress, impact, lightning strike and fluid ingress.

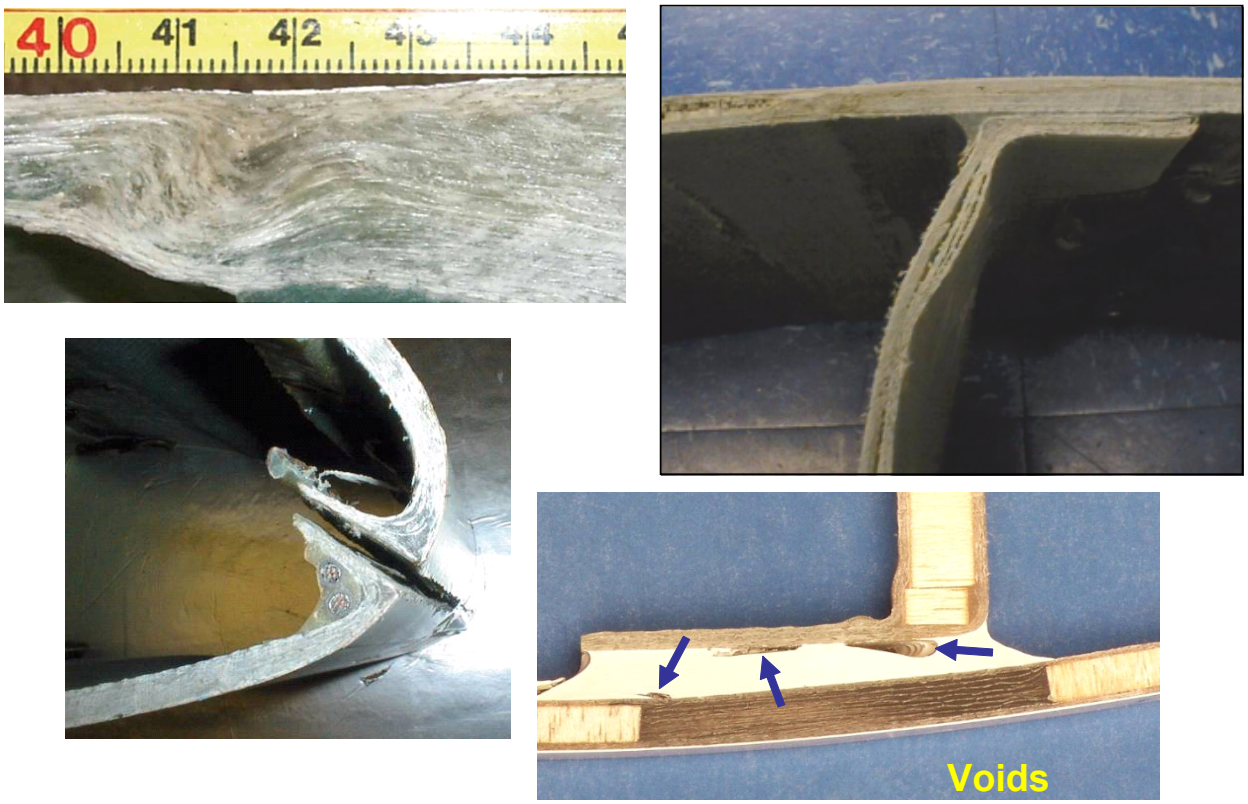

Figure 2-2: Flaw Types That Are Desirable to Detect with NDI Including Ply Wrinkles and Delaminations, Adhesive Voids and Joint Disbonds

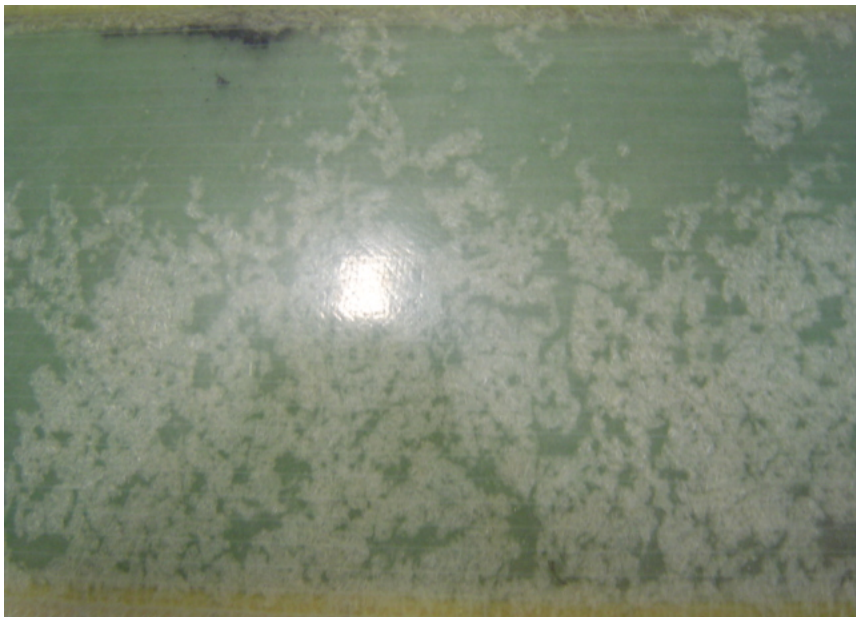

Figure 2-3: "Snowflaking" Flaws in Spar Cap Created by Entrapped Air During Cure

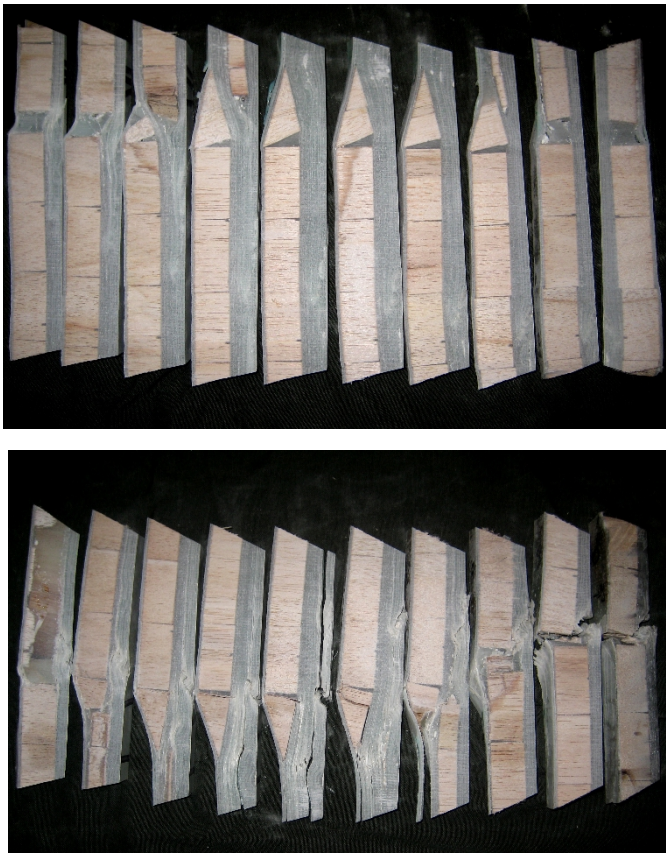

Figure 2-4: Figure Comparing Pristine Blades with Cracks, Delaminations and Other Laminate Fractures that Can Occur in Wind Blades

The inspections must address all deployment issues including: a) vertical and horizontal inspection surfaces, b) hand scan vs. attachable scanner, c) signal coupling via water flow or other signal couplant, d) wide range of thicknesses which may require equipment adjustments such as transducer selection and gate adjustments in ultrasonic inspections, e) need for quantitative information, f) ease of equipment use to minimize human factors concerns and performance variations, and g) rate of inspection to produce necessary coverage.

Some inspection considerations and impediments that must be overcome in order to produce the desired NDI performance include: a) some methods may need access to both sides of blade, b) wide area inspection methods may be needed (scanners), c) porosity/attenuation levels of blades are high, d) depth of penetration and sensitivity at depth is needed, and e) inspections must accommodate surface curvature and complex geometries.

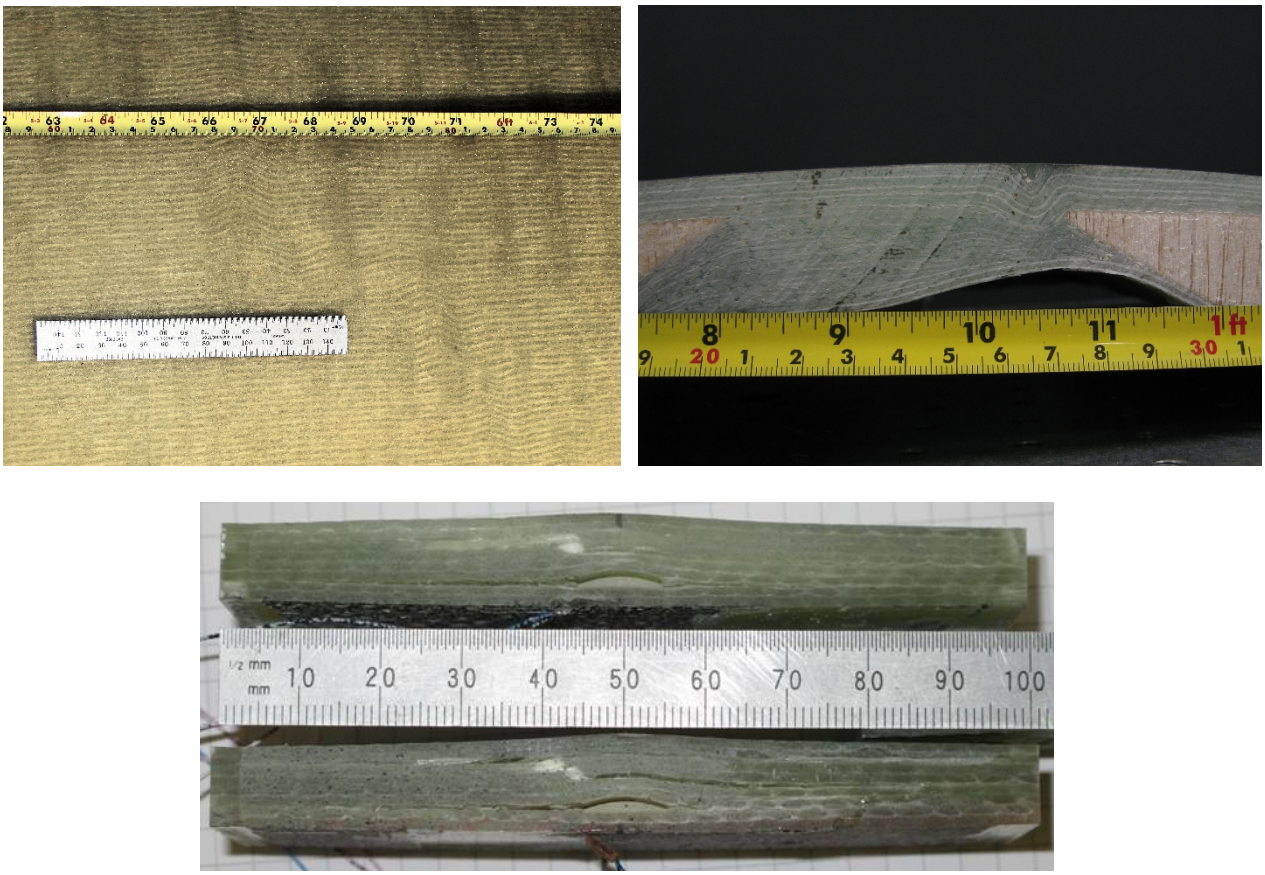

Figure 2-5: In-Plane (left) and Out-of-Plane (right) Wave Flaws in Wind Blade Composite Laminate

2.2. In-Service Inspection of Operating Blades

Background on In-Service NDI Needs - Small defects can propagate to levels of concern during blade use while fatigue loading, impact, lightning strike and other in-service conditions can lead to new damage in the blades. As the length of blades increase and operational environments produce high stress levels in the blades, it has become increasingly important to detect the onset of damage or the propagation of fabrication defects during blade operation. The need for in-service NDI of blades at wind farms is growing. Additional NDI fidelity beyond what can be provided by visual methods is required to identify and repair defects before they reach a critical size. In addition, the use of larger and more expensive blades means that it will be necessary to install more invasive repairs and repairs to primary blade structure in order to avoid the cost of blade removal and replacement. These more extensive repairs will require close scrutiny from NDI methods to ensure the long-term viability of the repair.

One aspect of this program is to determine how advanced NDI methods can be gracefully integrated into wind farm operations. These include both up-tower NDI deployment and equipment for inspecting blades that have been removed from the wind turbine. The first task is to determine the inspection requirements as they exist now, as well as those that are expected to exist in the near-future. This includes the identification of current inspection practices at wind farms, the level of standardization across the industry and the ability of operators to deploy NDI methods in the field. This information will allow us to focus our activities on developing new and customized NDI methods to meet these inspection needs while ensuring the ability of wind farm operators to avail themselves of such inspections. The latter item could involve the use of wind service companies to provide skilled inspectors with proven equipment and procedures.

Thus, this project includes close interactions with wind farm operators to test and apply state of the art inspection techniques in in-service environments. This project also includes NDI technology transfer activities with both wind service companies and wind farm operators. The benefit will be optimum deployment of automated or semi-automated NDI to detect undesirable flaws and damage in blades in order to help the blades reach their design lifetime or beyond.

Application of NDI technology in the field, and specifically up-tower has the same challenges associated with deployment as factory inspections, with the addition of many more. Wind farms are typically located in rural, rugged areas of the country with high winds, elevated work areas, and dangerous conditions. Nondestructive inspection technology being proposed for field use needs to be portable, battery powered and durable so that inspectors can bring the equipment to different locations on the blade including areas that may only accommodate rope access. The most common use of NDI applied up-tower has been to inspect specific, critical regions of a blade that have been identified as having a high probability of containing a serial manufacturing defect that was not detected at the plant on a large number of blades. These have been very specialized and confined to a particular set of blades. The operator typically identifies the issue over time because the defect manifests itself as early damage onset and eventually failure in more than one blade. Often when an issue like this is identified the first question is: “How many of the blades are affected and can the blades be repaired before the defect grows?” In-service NDI is critical to assess and detect defects, even those that were not seeded by manufacturing problems.

In-Service Blade Damage - The most common operational damage is from surface impact and rain/dust erosion. Other damage stems from bird strikes, lightning strikes, other object strikes, the propagation of manufacturing anomalies and the origination of new damage stemming from normal fatigue stress loads, off-design overloads or other environmental conditions. Figure 2-6 to Figure 2-8 show various types of wind blade damage. Note that all photos feature damage that is extreme or that has propagated to the point of blade failure. The goal of this effort to conduct nondestructive inspections before minor damage can grow to levels of concern. Figure 2-9 shows several images of subsurface damage that can be detected via NDI methods.

Lightning Strike Damage

Impact Damage

Figure 2-6: Types of Damage to Wind Blades Experienced During Operation (1)

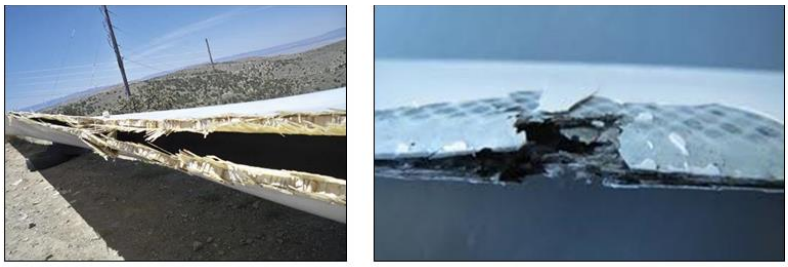

Trailing Edge Disbond and Fracture Damage

Erosion and Impact Damage

Damage from Shipping and Installation Handling

Figure 2-7: Types of Damage to Wind Blades Experienced During Operation (2)

Severe Growth of Fiber Fracture

Delamination and Subsequent Laminate Fracture

Erosion Damage

Figure 2-8: Types of Damage to Wind Blades Experienced During Operation (3)

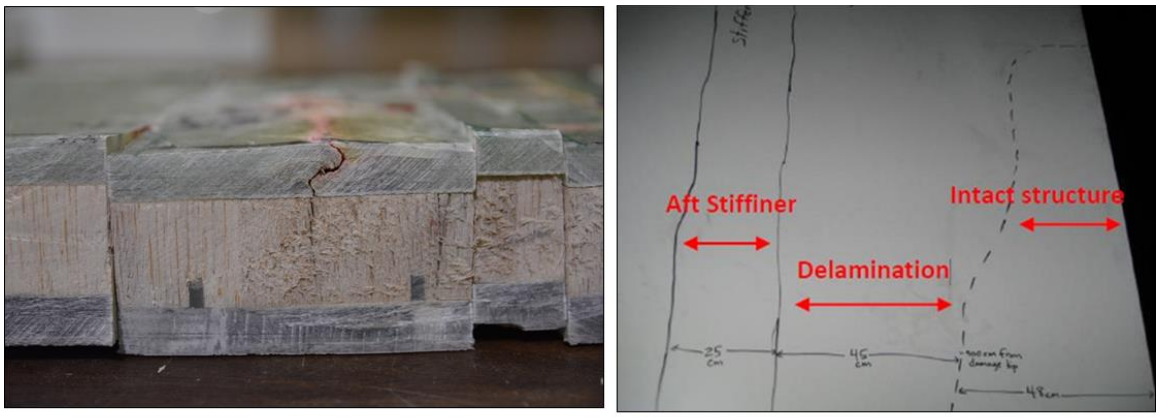

Skin Laminate Fracture

Interply Delamination in Skin and Spar Cap

Figure 2-9: Subsurface Wind Blade Damage Detectable Using NDI Methods in the Field

In-Service Blade Repairs - The same techniques used to detect damage may also be used to determine the integrity of a structural repair to a blade. Enhanced NDI techniques could open up new opportunities for more invasive and complete spar cap and root repairs. The integrity of the structural repair could be verified through inspection, giving repair designers and engineers added confidence that the blade can be recertified for use, which would lead to significant cost savings. In order to assess these challenges, collaborative relationships with blade maintenance and inspection companies has been pursued by Sandia Labs. Increased damage detection sensitivity in the field will improve blade reliability and minimize blade downtime.

Most turbine blade damage from erosion or impact is repaired with primary near-surface type of repairs using epoxy or polyurethane filler material or with the addition of a ply or two of material using an ambient bond adhesive. Repairs to core structure are common and can extend to double-sided repairs of through-thickness damage. While core structure is not considered primary structure, extensive damage to the core region can affect the overall stability and structural integrity of the blade. As the wind blades have become larger and more expensive, there is a corresponding desire to install more extensive repairs that reach many layers in depth and are placed on and around primary structure such as spar caps and root sections. The criticality of these repairs will then require the use of through-thickness depth inspection methods to ensure the quality of the repair. Periodic up-tower inspections may also be required, depending on the repair analysis conducted by the wind farm operator in concert with the original blade manufacturer. The repair, the post-repair inspection and subsequent in-service inspection could be carried out in a centralized fashion by a third-party wind service company. This allows for a centralized location of expertise, repeatable inspection methods and reliable results. Blade repairs require consideration of both aerodynamic and aeroelastic loads to the structure. The repair design is adjusted to meet the zone requirements as shown in Figure 2-10. Repairs conducted in Zones (1) and (4) involve primary structure (blade root or spar cap) and must be designed and installed for structural purposes.

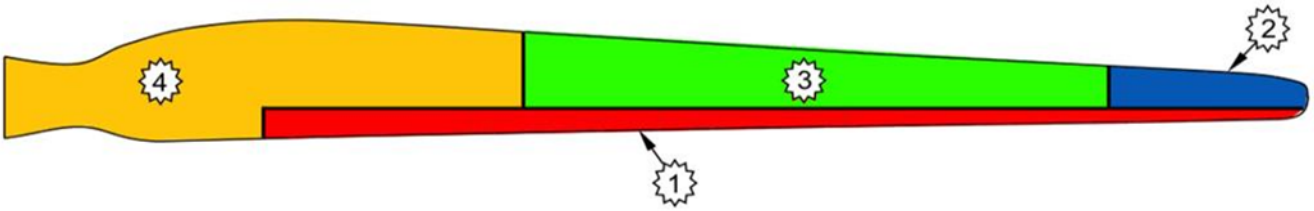

Figure 2-10: Repair Zones on Wind Blades that Identify Criticality and Limits on Level of Repair Allowed

A typical repair process is shown in Figure 2-11 where a tapered sanding process is used to remove the damaged region. Then, replacement plies of similar material and orientation are placed into the repair region and cured using in-situ vacuum and heating equipment (if elevated cure temperatures are needed). An example of a blade tip repair is shown in Figure 2-12. The success of a repair can be affected by numerous factors including: surface preparation, the ambient temperature and humidity conditions during curing, proper mixing and uniform application of the resin, improper curing profiles and improper placement/orientation of the plies. Most of the problems associated with improper repairs will result in damage within the repair that can be detected by NDI methods. Normally, the damage could be detectable during a post-installation inspection or within 6-12 months of operation.

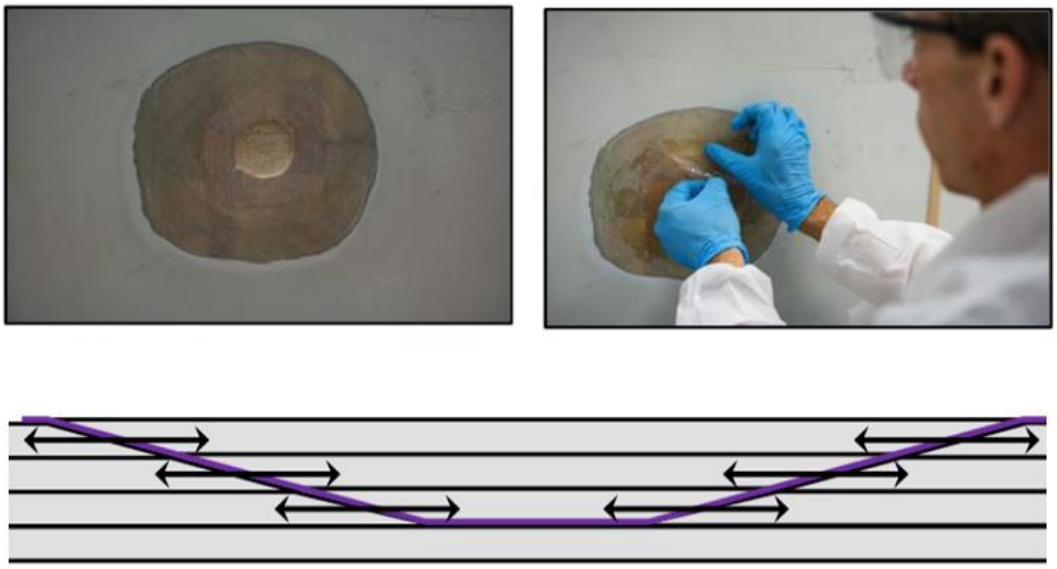

Figure 2-11: Tapered Scarf Angle, Replacement of Plies and Resulting Shear Stress Distribution in the Scarfed Repair Joint

Manual tap testing is the most common method of NDI used to evaluate damaged areas of a blade in the field. This method involves the use of a coin or other small, hard item such as hammer/tool to tap on the structure while the inspector or repairman listens to audible changes in

the sound of the tapping. This is a fairly effective method to size damage in core materials (moisture ingress and skin delamination), but not effective in the critical, thicker structures such as solid laminate spar caps and thick bond lines in the trailing edge.

Figure 2-12: Picture of a Lightning Strike Tip Repair

Repairmen also use a method of visual inspection and evaluation of wind blade structure during the repair process. Once a repairable damage is identified and the mechanic begins to remove damaged material, they visually determine how much material needs to be removed and replaced. In this case, in-field NDI to assess damage in sandwich structure, leading and trailing edges, and other aero shell components may be needed to identify the initial damage and subsequently ensure the success of the repair.

In-Service Repair Inspections - Manufacturers perform repairs on blades quite often in the manufacturing plant. Repairs can range from the simple addition of adhesive to a joint that was insufficiently wide, to multi-ply depth scarfed repairs on spar caps and root laminates. The type of repairs a company will perform depends on the original construction process (e.g. shear web to spar or box beam configurations) and their tolerance for invasive repairs on primary structure. Repairs in the manufacturing plant are not typically inspected with NDI after they are performed, but they are visually inspected by quality personnel.

Repairs performed in the manufacturing plant can be much larger than repairs made up-tower. This is because manufacturers have much better access to resources - such as engineering support, materials, and larger work spaces – and can maintain the proper control over the repair

process. Wind blades that have been significantly damaged in the field are typically taken down and replaced with a new blade. Typical service repair companies will not repair spar cap-to-shear web adhesive bond lines due to warranty issues, structural criticality of the area, and the extensive amount of work it requires up-tower. Although this scenario is rare, if the damage is extensive and non-repairable up-tower, then the blade can be taken down, repaired in the field, and put back on the tower.

Enhanced NDI techniques could open up new opportunities for spar cap and root repairs in the field. The integrity of the structural repair could be verified through inspection, giving repair designers and engineers added confidence that the blade can be recertified for use. This would lead to significant cost savings.

Up-Tower Blade Access - With a growing number of blades now in service - many well outside their warranty periods - rotor blade maintenance is becoming a major issue. One of the most challenging aspects of wind farm operations is the means to conduct periodic maintenance of the blades while they are still installed on the rotor hub (i.e. up-tower maintenance). Access to the blades and deployment of equipment severely hinders both the ability of workers to conduct their tasks but also limits the amount and type of work that can be carried out up-tower. Up until recently, the excellent reputation of composite materials for high durability has induced wind farm operators to defer general blade maintenance and oversight tasks. The increasing knowledge of wind blade aging issues has produced an increase in demand for blade inspection, maintenance and repair. In response, several wind service companies have been formed to supply a new breed of worker called skyworkers. These workers combine skills in the inspection and repair of wind blades with climbing skills. The technicians themselves are normally suspended from the rotor hub, working on the subject blade – which is stopped in the down position as shown in Figure 2-13. Anchor lines may be deployed to the tower or around the blade.

Almost all of the inspections are confined to visual assessments. Erosion, surface fracture and, to a lesser extent, impact damage can be identified with visual inspections. However, many of the more aggressive and destructive types of damage that can severely reduce blade life do not manifest themselves as surface demarcations. Such subsurface damage must be detected via high-penetration, inspections methods such as ultrasonics.

Currently most repairs are of the ‘cut out and fill’ type or, in the case of laminate repairs, wet lay-up. However, a smaller number of technicians can also handle infusion and prepreg repairs, along with restitution of gel-coats and surface finishes. Vacuum bagging and heat curing up-tower is a challenge and workers must execute everything from small surface repairs to medium structural repairs, dealing with a wide range of materials including polyester, vinyl ester and epoxy resins, along with glass, carbon, aramid and biocomposite fibers. A technician's visit can encompass anything from a close visual inspection with report, through blade cleaning, to a modest structural repair – a damaged tip or edge for example. Because a skyworker has either to take everything required for a job with him (or her), or have it hoisted up or lowered down to the working position, repair procedures have to be carefully pre-planned and managed, with adequate back-up from other team members.

Figure 2-13: Use of Skyworkers to Access Blades Via Climbing Ropes

A variation on this theme involves the use of adaptive platforms to provide an enhanced work area with the ability to provide more controlled use of extensive equipment in an up-tower environment. Figure 2-14 shows several different types of work platforms that can accommodate more extensive blade maintenance activities.

Deployment of NDI Methods - The platforms highlighted in Figure 2-14 allow for the direct application of proven NDI methods (see Sandia report: Roach, D., Neidigk, S., Rice, T., Duvall, R., Paquette, J., "Blade Reliability Collaborative: Development and Evaluation of Nondestructive Inspection Methods for Wind Turbine Blades," Sandia DOT Report, SAND2014-16965, September 2014). These could be deployed manually or in a scan mode. However, the use of these platforms is very rare at this time and quite expensive. Thus, there is a need for more frequent, rapid inspections means that other NDI deployment options should be pursued for use in the absence of such expensive work platform deployments.

Remote Visual Inspections - The use of Unmanned Aerial Systems (UAS) or ground-based telescopic devices to inspect wind blades has received a lot of attention in the last 2-3 years. Such devices, such as the ones shown in Figure 2-15, utilize high resolution optics to produce excellent visual inspections of the surface of the blade. While these are quite useful for identifying surface-based damage such as erosion, these inspections are not useful for detecting the more extensive subsurface damage that can be present in wind blades. This damage, such as delaminations, disbonds and fracture in the composite fibers, represent damage that can reduce blade life and even result in catastrophic failure in-service. This critical damage must be

detected using NDI methods that can interrogate the entire thickness of the blade (e.g. spar cap and shear web bond line, thick laminate root and transition sections).

Figure 2-14: Use of Adaptive Platforms to Provide Larger Work Space for Blade Maintenance Activities

Remote and Semi-Automated Access to Blades - In order to obtain a more accurate picture of the overall health of wind turbine blades in operation, it is important to consider independent deployment of up-tower inspection devices without the aid of work platforms or other personnel present along the blade. Several different scanning systems have been developed to accommodate automated inspections and even more are in the concept stage. The scanners shown in Figure 2-16 can produce C-scan images which Sandia has shown to be very beneficial in improving flaw detection accuracy. Such scanning systems, that utilize X-Y motion carriages to move a transducer across a wide area of the blade, do require some level of access to the area of interest. Sandia's scanning system (Figure 2-16, right side) was successfully deployed in a factory setting and could be adapted for up-tower inspections. A true, remotely controlled inspection could be performed using a robotic crawler device that can scale a wind tower (see Figure 2-17 for concept crawlers and those used in other industries). These are concept devices that could be adapted to allow for ground-based, easy access to remote portions of the blade. This would allow wind farm operators to quickly inspect their blades if they need to respond to unanticipated overload conditions. Such inspections are necessary to make GO – NO GO

decisions and to determine the need for any immediate repairs. This will minimize the risk of failure or forced down-time of the turbine. Power and data connection requirements may require a tether to be added to the concept crawler. Another option for remote inspections might be accomplished by adapting NDI methods onto UAS vehicles. Experienced gained from expanding visual assessments via UAS vehicles could be leveraged to provide more detailed inspection data. Integration of minimal NDI hardware (i.e. weight) would be stressed as would on-board power and data logging capabilities. Problem spots, such as high stress regions or areas thought to contain systemic manufacturing flaws, could be routinely and quickly inspected with such and NDI vehicle.

Figure 2-15: Unmanned Aerial Systems and Ground-Based Devices Used to Conduct Visual Inspection of Wind Blades

Figure 2-16: X-Y Scanning Systems Can Temporarily Adhere to the Surface of Interest to Produce High-Quality, Through-Thickness Flaw Detection Images Over Wide Areas

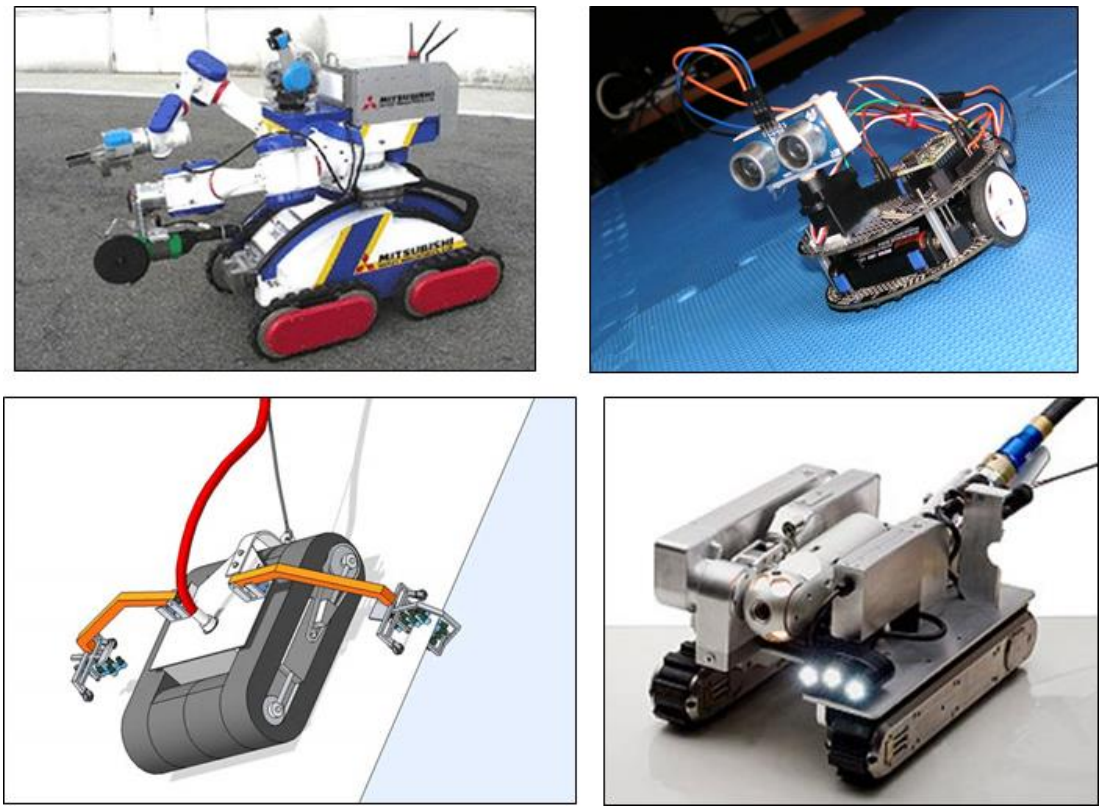

Figure 2-17: Remotely Controlled Auto Crawler Devices for Possible Deployment of NDI Equipment

THIS PAGE INTENTIONALLY LEFT BLANK

CHAPTER 3

3.0 Wind Blade Flaw Detection Experiment Design

3.1 Developing a Blade Probability of Flaw Detection Study

For the larger blades being employed on current designs, weight and aeroelastic limitations have put added pressure on blade design and manufacturing. This has placed greater emphasis on the development of improved nondestructive inspection (NDI) methods that are more reliable and sensitive than conventional NDI. Blade flaws include ply transitions and waves, fiber misalignment, porosity, interply delaminations and disbonds in the structural assemblies. NDI practices have increased on the manufacturing floor to assess the quality of blade structures, especially critical sections like spar caps and spar cap-to-shear web bond lines. However, reliable data on the accuracy of these systems is difficult to ascertain and is the subject of ongoing research. Under its Blade Reliability Collaborative program, Sandia National Labs has quantitatively assessing the performance of a wide range of NDI methods that are currently deployed, as well as new NDI candidates for wind blade inspections. As part of previous Blade Reliability Collaborative efforts, Sandia conducted a brief Wind Inspection NDI Experiment (WINDIE) completed a preliminary screening of the advanced NDI methods that may be candidates for inspecting blades [3-1]. The top performing methods then became candidates for the more structured WBFDE Probability of Detection study discussed in this report. Custom wind turbine blade test specimens, containing engineered defects, were used to determine critical aspects of NDI performance including sensitivity, accuracy, repeatability, speed of inspection coverage, and ease of equipment deployment.

Following is a description of the experiment that was developed to quantify the ability of both conventional and advanced NDI techniques to detect the array of flaws and damage that may occur in wind blades. A series of solid laminate, bonded composite specimens with statistically relevant flaw profiles were inspected using conventional, hand-held pulse echo UT, as well as, advanced NDI methods that Sandia Labs has evaluated and deemed suitable to improve sensitivity and repeatability of blade inspections. The majority of the testing was in the form of blind Probability of Detection (POD) studies while other portions of the testing measured signal-to-noise ratios from which flaw detection can be inferred. The primary factors affecting flaw detection in laminates and laminate bond lines are included in this study: material type, flaw profiles, presence of complex geometries involving thick, bonded joints, and environmental conditions. One phase of this effort utilized wind blade production personnel to study POD at factories and to formulate improvements to existing inspection techniques. In addition, advanced NDI methods for laminate inspections – such as thermography, shearography, scanning pulse-echo UT, ultrasonic spectroscopy, microwave, and phased array UT – were applied to quantify the improvements achievable through the use of more sophisticated NDI.

The WBFDE Probability of Detection study was conducted to quantify the flaw detection performance of NDI in composite wind turbine blades. The general goal was to determine which NDI method(s) have high sensitivity, accuracy and reliability in order to identify those with promise for continued development and application. This effort also identified the factors

influencing composite wind blade inspections on this type of structure so that improved methods and procedures can be developed.

The experiment was conducted in a blind mode where the type, location and size of flaws were not known by inspector. The statistically relevant flaw distribution allowed for the calculation of POD curves using the resulting flaw hit-miss data. The overall performance of each inspector and each NDI method was analyzed using hits, misses, false-calls, flaw sizing, human factors observations, and deployment procedures. The basic experimental design parameters included: 1) representative blade design and manufacturing (all panels painted with wind turbine blade paint), 2) various parts of blade such as spar cap, bonded joints, leading and trailing edge (spar cap thickness ranges from 0.45" to 1.80"), 3) statistically valid POD (number, size of flaws and inspection area), 4) random flaw location, and 5) exercising deployment obstacles. In order to obtain data from multiple inspectors at each factory site while minimizing disruption to normal plant operations, the WBFDE was designed to require a maximum of 2 1/2 days to perform the experiment. Design and fabrication considerations included: 1) realistic, random flaw locations, 2) portable sample set, 3) range of thickness, and 4) range of material types (fiberglass and adhesives).

WBFDE Experiment Design Process – The following activities were completed and design parameters considered in order to produce the WBFDE:

1. Investigate current NDI practices being used by industry.
2. Work with OEMs to identify the various flaw types that need to be found during inspections.
3. Identify the critical flaw size for each flaw type (define inspection requirements).
4. Identify the most common thicknesses of blade sections to determine minimum, average, and maximum specimen thicknesses to be fabricated in the test specimens.
5. Identify any special geometry or structural elements on wind turbine blades that should be included in the test specimen designs.
6. Investigate the inspection environment requirements (e.g. single side access, access limitations, degree of coverage, geometry to accommodate).
7. Identify the most common materials used in fabrication including the method used to infuse the resin.
8. Include all flaw types identified by industry. Size the flaws based on current inspection requirements and locate the flaws at three different depths (25, 50, and 75% of full thickness).
9. Design the specimens around two basic, structural configurations: one that represents the skin and spar construction configurations and the second that represents the bondline between the spar cap and shear web (adhesive layer).
10. Statistically distribute the following array of flaws: delaminations, gross disbonds, "kissing" disbonds, spar cap skin-to-core disbonds, dry fabric, adhesive voids, resin voids, out-of-plane waves, porosity, snowflaking, thin adhesive (below specifications), thick adhesive (above specifications), chemical contamination, and non-uniform resin flow.
11. Utilize flaw sizes of 0.5", 1.0", 1.5" and 2.0" diameter.

12. Provide adequate spacing between all flaws such that there is sufficient "unflawed" area to allow for assessment of "false calls" in the inspection images.
13. Utilize specimen thicknesses with a spar cap thickness range of 0.25" to 2.14" and a spar cap plus adhesive layer thickness range of 0.85" to 2.65".
14. Produce fiberglass specimens.
15. Produce a set of test specimens with the identified flaw types and sizes that are smaller than and greater than the determined critical flaw size.
16. Determine the most prevalent manufacturing process used in the industry and use this process for test specimen fabrication. This includes the ply lay-up process, resin transfer via VARTM and the mixing and application of adhesive in the spar-to-shear web joint.
17. Characterize all test specimens to confirm the final flaw sizes and locations.
18. Evaluate inspection results from all methods on the suite of NDI specimens to determine Probability of Detection values.

The experiment development tasks involved in this POD testing were: 1) fabrication of representative test specimens to be used with all inspection methods, 2) comprehensive, in-house characterization of the NDI test specimens to ensure flaw realism, 3) production of experiment protocols, NDI candidate list, and invitation to possible participants, 4) completion of round-robin testing on NDI test specimens with "advanced" NDI methods, and 5) completion of analysis of inspection results with NDI comparisons (sensitivity, repeatability, coverage, adaptability deployment, cost, etc.). The tests allowed for the quantification of capabilities and identification of limitations of all the selected NDI methods as they attempted to detect the different flaw types in the various construction scenarios.

Other information gathered during the WBFDE included:

- Duration of inspection
- Fieldability (portable)
- Deployment issues
- Inspection method difficulties
- Cost of new system
- Accessories needed to make the inspection device fieldable
- Ease of data interpretation

<u>Testing Approach for Application of NDI:</u>

1. Apply NDI devices with knowledge of flaw types and locations to determine quantitative signal-to-noise (S/N) ratios; flaw detection can be inferred by studying S/N levels.
2. Apply NDI devices with knowledge of flaw depths to determine quantitative signal-to-noise (S/N) ratios at the various depths of flaws. Determine if there are any limits to depth of penetration for specific inspection methods.

Figure 3-1 shows the primary target for the POD assessment: ultrasonic NDI methods. The figure depicts the evolution of ultrasonics from single-element to phased array and from manually deployed to automated scanning with sophisticated, real time data analysis capabilities. The single-element UT method deployed by hand over the surface is still the most widely-used NDI technique found in wind blade production facilities. This will be the baseline POD evaluation to which the advanced UT methods, and other NDI methods, will be compared.

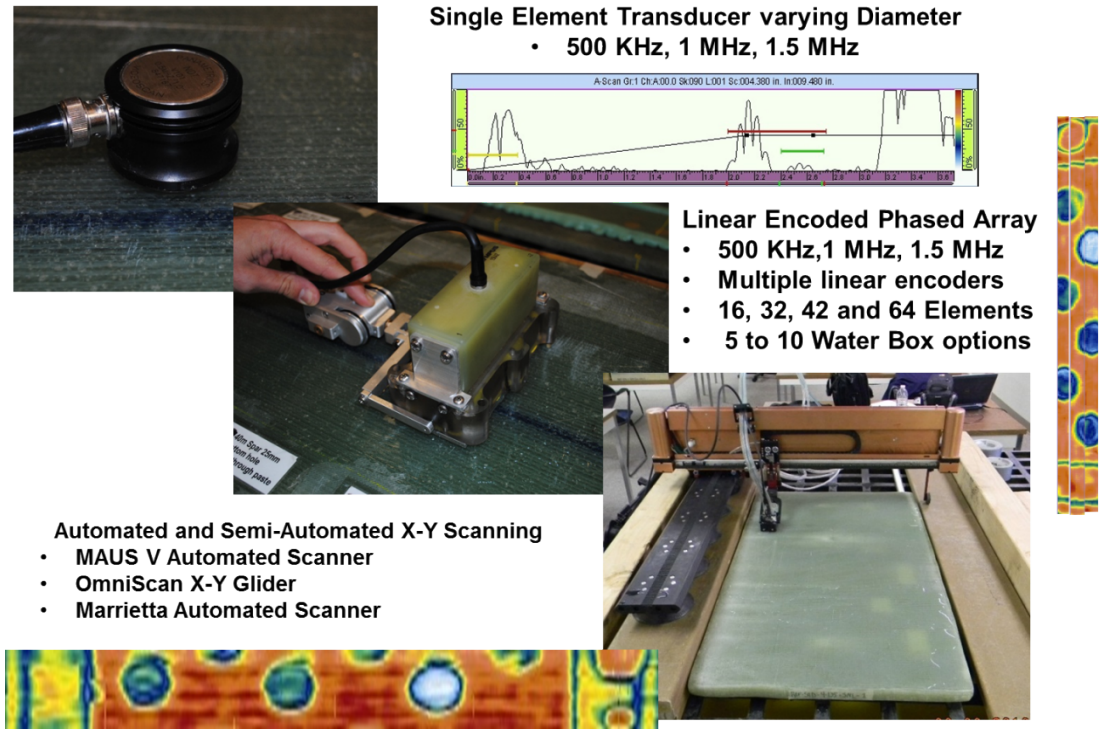

Figure 3-1: Progression of Ultrasonic Deployment Showing Primary Target for POD (Single Element UT, Manually Deployed) and Advanced Technology (Phased Array UT on Scanner System) Being Evaluated

Figure 3-2 shows one of the curves used in the specimen design phase to ensure the proper distribution of flaws within the specimen set. Within the spar cap laminate structures, there was an even distribution of near surface, mid-depth and back wall flaws. Within the bond line between the spar cap and the shear web, the flaws were positioned at both interfaces of the bond line (top and bottom) and some bond porosity (simulated with drilled holes) was located at the mid-depth of the bond line.

All of the WBFDE design and production activities described above were conducted in concert with an industry review team. This team reviewed preliminary and final specimen designs, assisted with specimen production and reviewed the experiment implementation plans. Figure 3-3 shows the industry participants that provided consultation or assistance on the WBFDE review team to ensure the relevance of all aspects of the POD testing and specimen design. Finally, Figure 3-4 and Figure 3-5 provide a summary of the flaw types and location distribution within the Spar Cap & Shear Web and Box Type specimen designs. A total of 11 test specimens were included in the WBFDE. Nine of them were the Spar Cap & Shear Web construction and two of them were the Box Type construction. These specimens included 48.9 $ft.^2$ of total inspection area. The total flaw areas within these specimens was 2.6 $ft.^2$ so the ratio of unflawed-to-flawed area in the POD specimen set is 19:1. This provided sufficient unflawed

area to assess the human vigilance factor and also provide inspection regions to assess the Probability of False Alarms (POFA).

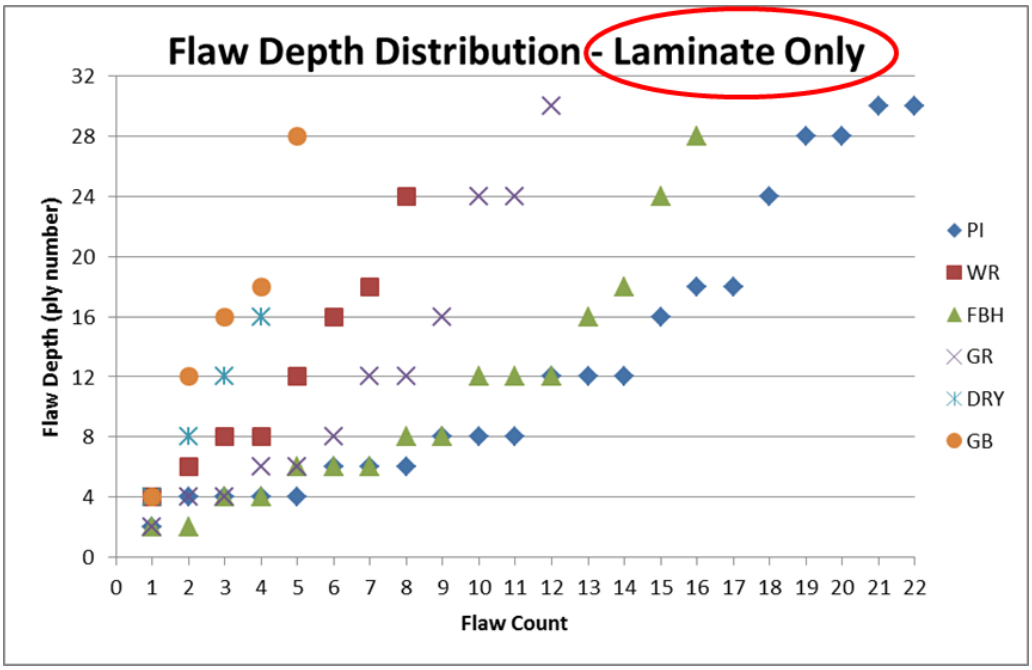

Figure 3-2: Design Plot Used to Guide Distribution of Different Flaws in the WBFDE POD Experiment

Figure 3-3: Wind Blade Flaw Detection POD – Experiment Review Team Used to Ensure Representative Blade Construction and Materials

Spar Cap & Shear Web Construction

Flaw Types Used:
PI - Pillow Insert (delamination in the laminate, void or bubble in the adhesive)
GB - Glass Beads (porosity)
GR - Grease (kissing bond)
FBH - Flat Bottomed Hole (gross delamination in laminate, not enough adhesive in the bond line)
WR - Wrinkle (Out of plain)
DRY - Dry Area (resin starved)
PT - Pull Tab (disbond, between adhesive and laminate or shear web)
VD - Void through the adhesive thickness

Flaw Locations Used:
INT-A - Flaw is located between the spar cap and the adhesive interface (box type, skin and adhesive)
INT-B - Flaw is located between the adhesive and the shear web flange interface (box type, adhesive and spar cap)
THRU - Refers to a void going through the thickness of the adhesive

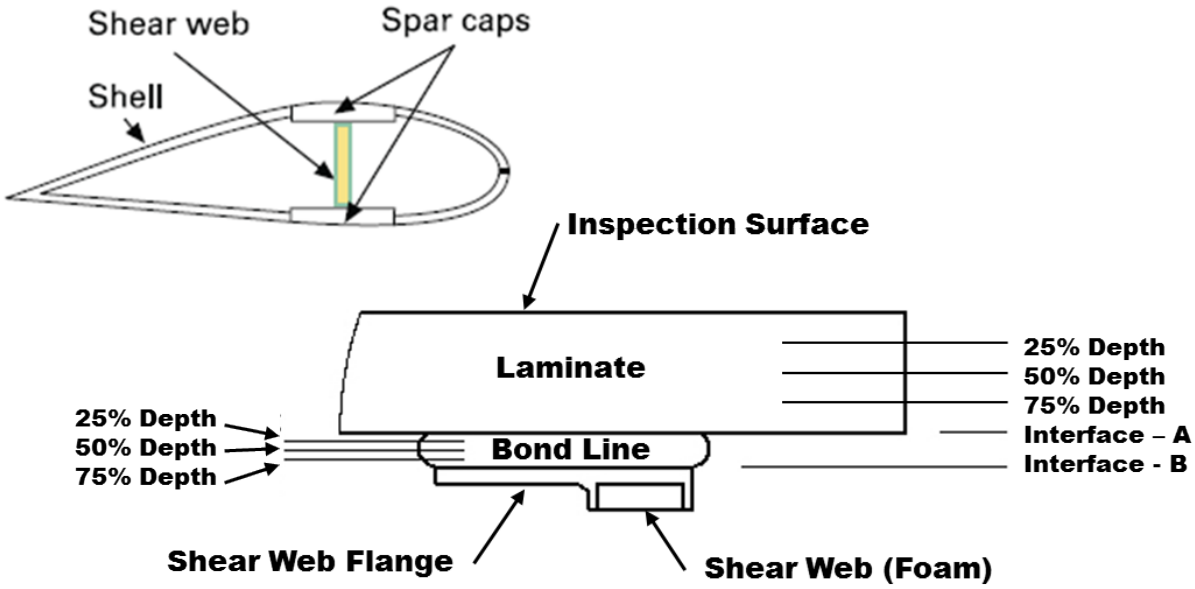

Figure 3-4: Spar Cap and Shear Web Specimens – Description of Configuration, Flaw Types and Locations Within the Laminate and Bond Line

Box Spar Construction

Flaw Types Used:
PI - Pillow Insert (delamination in the laminate, void or bubble in the adhesive)
GB - Glass Beads (porosity)
GR - Grease (kissing bond)
FBH - Flat Bottomed Hole (gross delamination in laminate, not enough adhesive in the bond line)
WR - Wrinkle (Out of plain)
DRY - Dry Area (resin starved)
VD - Void through the adhesive thickness
Note: No Pull Tabs used in Box Construction

Flaw Locations Used:
INT-A - Flaw is located between the spar cap and the adhesive interface (box type, skin and adhesive)
INT-B - Flaw is located between the adhesive and the shear web flange interface (box type, adhesive and spar cap)
THRU - Refers to a void going through the thickness of the adhesive

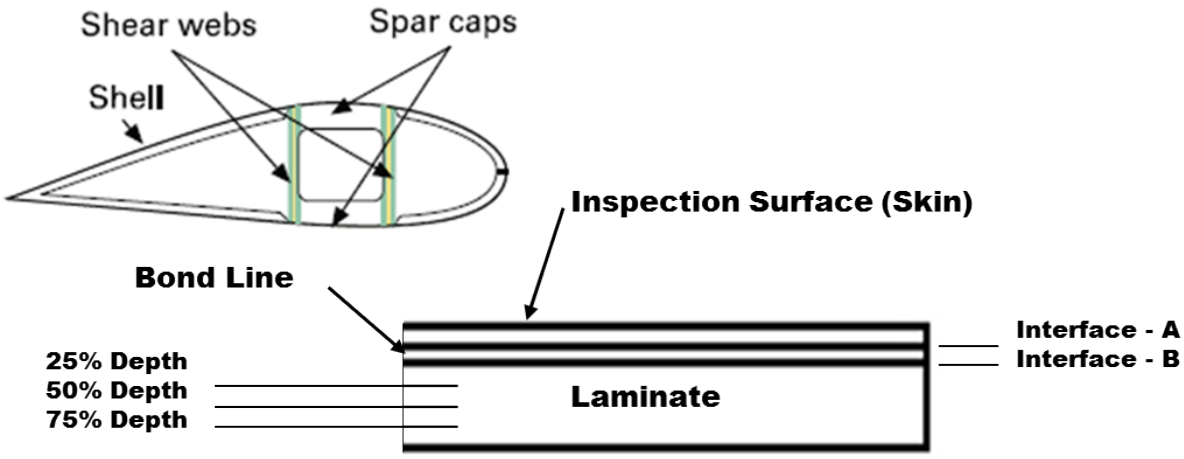

Figure 3-5: Box Spar Specimens – Description of Configuration, Flaw Types and Locations Within the Laminate and Bond Line

3.2 Design of Wind Blade POD Specimens with Engineered Flaws

The test specimens used to evaluate the maturity and viability of a wide range of NDI methods contained an array of different, representative flaw types and wind turbine blade construction types. Discussions with blade manufacturers coupled with operational history were used to identify the most representative flaw types to be used in this study. Engineered test specimens were used to establish the ability of advanced NDI methods to detect manufacturing flaws and in-service damage including: snowflaking, voids, interply delaminations, resin-starved regions, spar and shear web disbonds, ply waviness, adhesive voids, fiber fracture, erosion, impact, lightning strike, and fluid ingress. Figure 3-6 shows the two major categories of blade types included in the WBFDE specimen designs: 1) spar cap with shear web and 2) box spar construction.

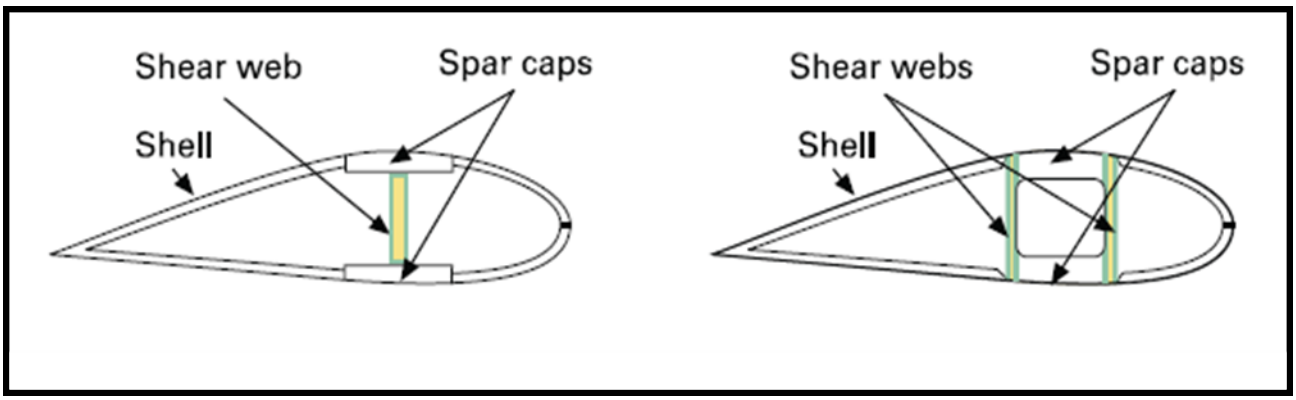

Figure 3-6: Two Major Specimen Design Types Used to Represent the Most Common Blade Construction

Figure 3-7 shows a sample test specimen design. Note that this is not one of the "blind" POD test specimens but is a "Feedback Specimen" which is used to allow inspectors to set-up their equipment and gain experience on the blind specimens before moving into the actual POD testing. The most common flaws found in wind turbine blade bonded joints are lack of adhesive, adhesive voids (air pockets), presence of foreign material or contamination in the laminate and bond line and disbonds between the laminate and the adhesive. In order to create realistic NDI test specimens, various methods were developed for producing engineered flaws that are representative of actual flaws found in wind turbine blades. The methods used to create real but controlled, engineered damage in wind blade specimens are described in detail in Section 3.2.

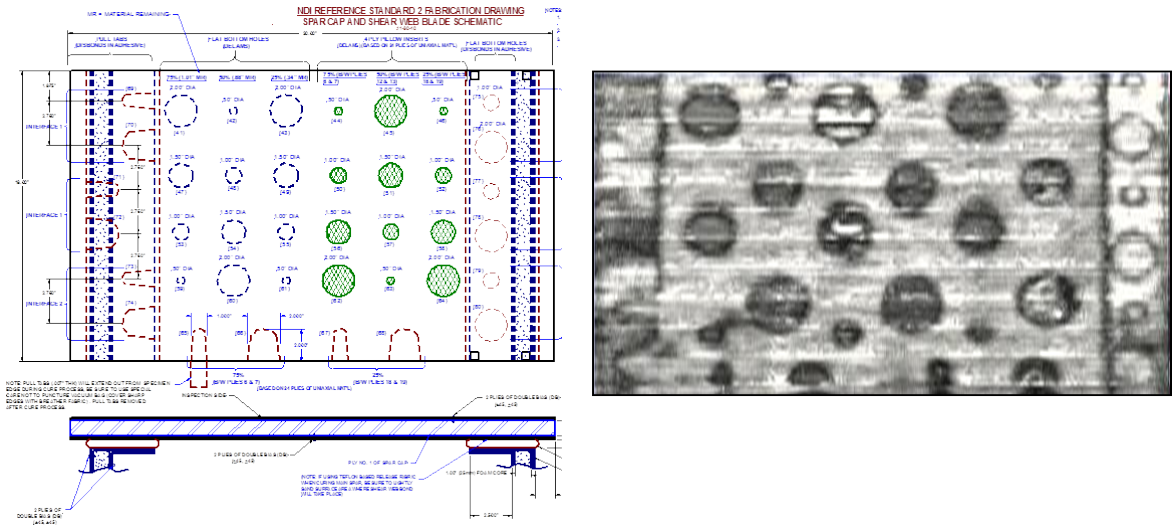

Figure 3-7: Sample Design Drawing of NDI Feedback Test Specimen and NDI Characterization Scan - Representative of Blind POD Specimens but Flaw Profiles are Provided for Educational Purposes

Design Guidelines for NDI POD Test Specimens:

- Include all flaw types identified by industry; the flaws will be sized around current inspection requirements and located at three different depths (25, 50, and 75% of full thickness).
- Produce three different thicknesses for each flaw scenario to cover the full range of design variables.
- There will be two basic standard types, one which will represent the skin and spar construction configurations, and the second will represent the bond line between the spar cap and shear web (adhesive layer).
- It should be noted that in order to induce some of the flaw types that occur during the production of these standards it may not be completely possible to control the final flaw size and location as shown on drawings. In this case all standards were characterized to determine final flaw size and location.
- Figure 3-8 to Figure 3-11 show the flaw types and some sample test specimen drawings.

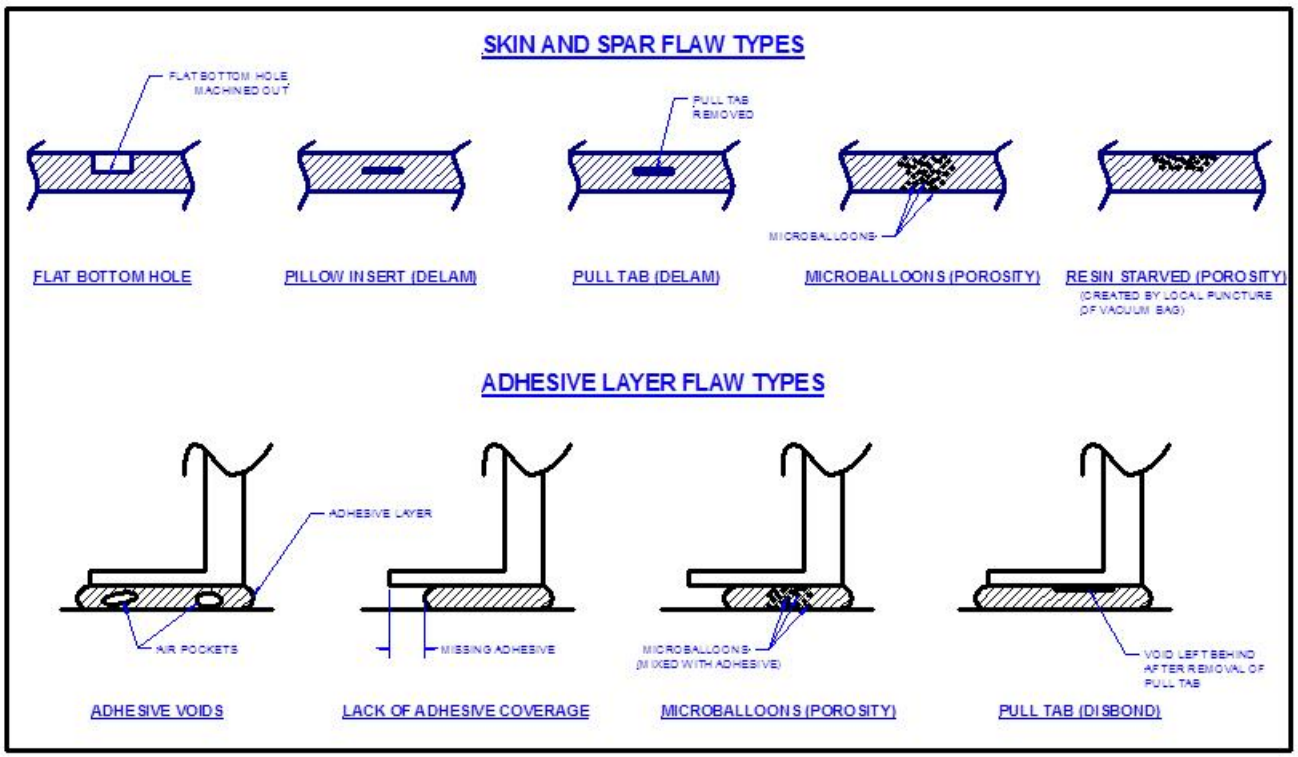

Figure 3-8: Skin, Spar, and Adhesive Layer Flaw Schematics

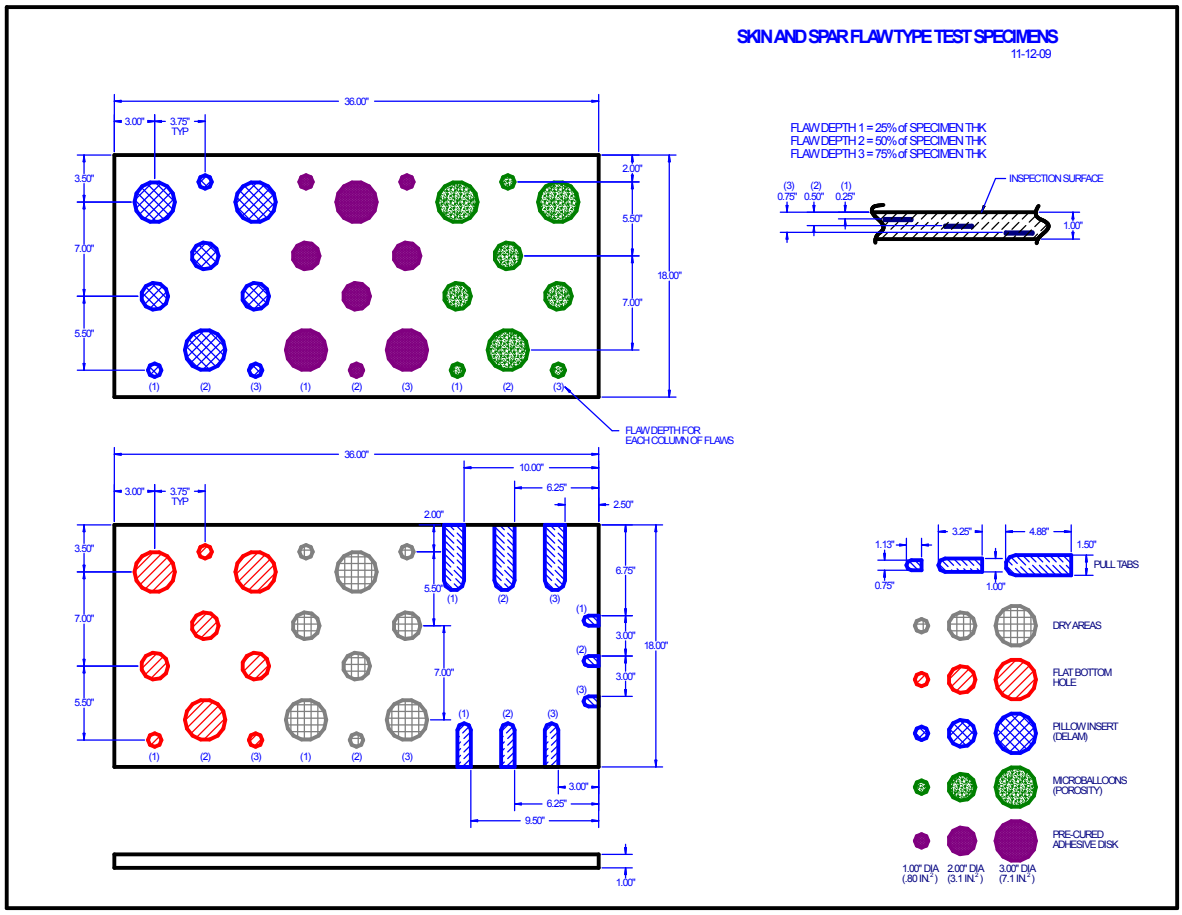

Figure 3-9: Skin and Spar Reference Standard Drawing 1

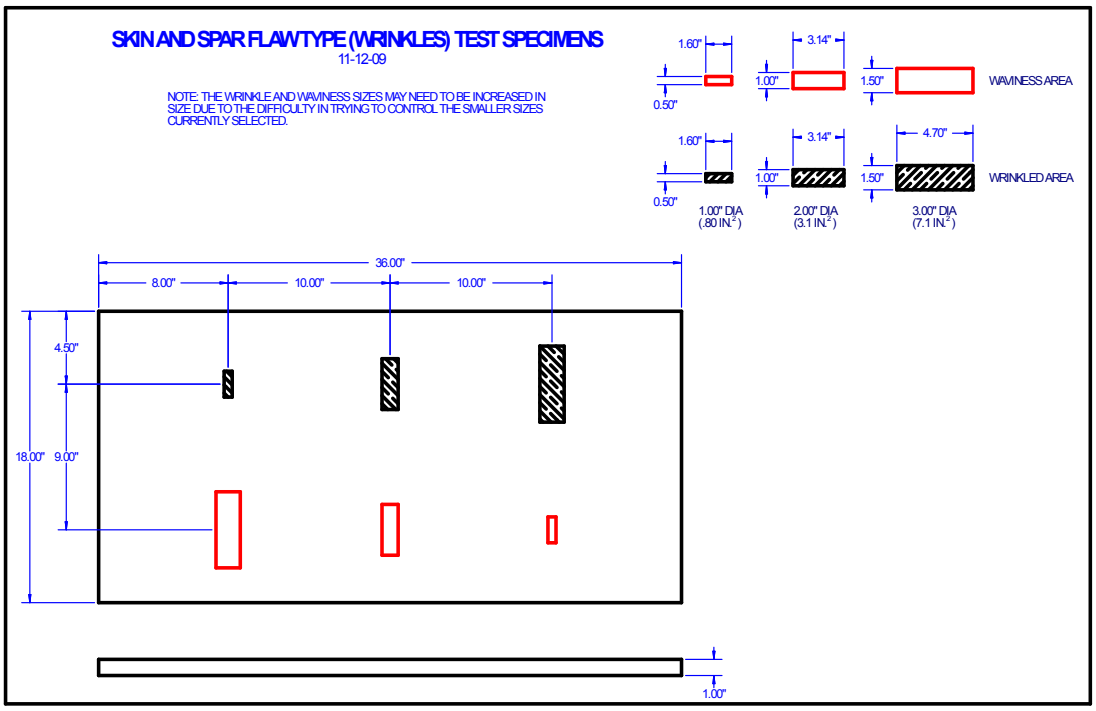

Figure 3-10: Skin and Spar Reference Standard Drawing 2

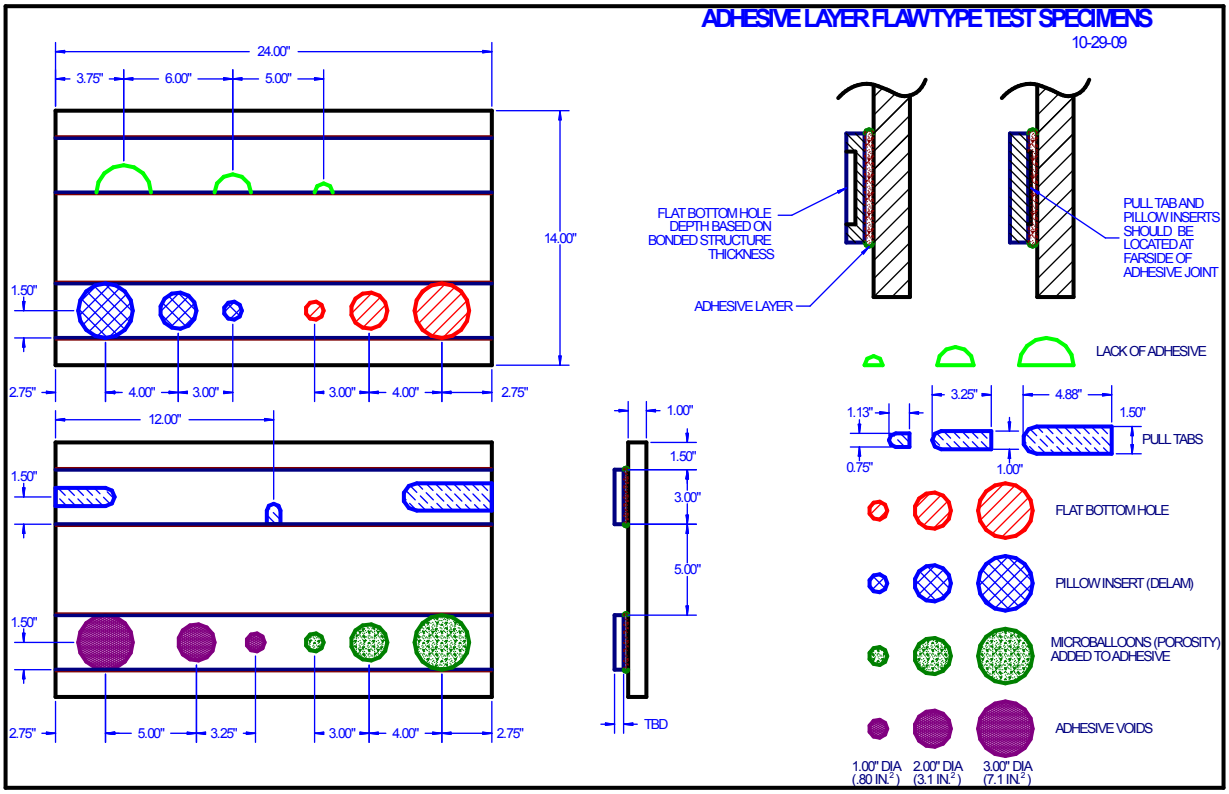

Figure 3-11: Adhesive Layer Reference Standard Drawing

3.3 Use of NDI Feedback Specimens

A series of NDI Feedback Specimens were designed and fabricated to allow inspectors to familiarize themselves with the type of specimens and flaws included in the WBFDE. The feedback specimens are representative of the POD test specimens that were inspected by each experiment participant in a blind mode. So, to provide adequate preparation for the blind inspections, the NDI Feedback Specimens – which mimicked the POD specimens - were utilized first in a "feedback" mode where the inspector is told the exact flaw profile in each specimen. Inspectors are provided with the drawings of these specimens and knows both the flaw locations type. Inspectors could spend a much time as desired on the NDI Feedback Specimens and could revisit them multiple times during the course of their blind POD inspections.

The NDI Feedback Specimens were fabricated using the same materials and manufacturing processes as the actual blade POD specimens. They contain representative, seeded defects, that model those found in the field, and are produced using real manufacturing environments. Thus, optimum equipment settings could be produced and any signal changes associated each flaw type and specimen configuration could be established before the POD testing is initiated. The NDI Feedback Specimens could also be used by inspectors to setup and calibrate their inspection equipment to verify that their hardware is functioning properly before an inspection takes place.

Among their many uses, NDI Feedback Specimens help inspectors gain a preliminary assessment of depth of penetration of their NDI technique and the various reflections stemming from items at different depths in the part. One part of the NDI Feedback Specimens consisted of a series of fiberglass spar cap reference calibration blocks. The calibration depths range from 0.40" to full thickness of 1.80", with depth increments of 0.05". These NDI Feedback Specimens were fabricated from a section of a 40 meter fiberglass spar cap by cutting four, 9"x 6.5" blocks and milling 1.5" diameter flat bottom holes in them. The spar cap that the specimens were cut from was considered very good by the manufacturer and preliminary NDI results supported this assessment. Figure 3-12 shows the fiberglass laminate thickness NDI Feedback Specimens that allow for an accurate calibration of depth of NDI penetration. Examples of other flaws embedded in feedback specimens include disbonds, porosity, contaminates and interply delaminations. The NDI Feedback Specimens are intended to be used for flaw detection in the following inspections:

- Spar cap
- Spar cap assembly (integrated into blade with fiberglass skins)
- Shear web to spar cap bond line
- Shear web bond line thickness with fiberglass spar cap
- Shear web bond line thickness with carbon spar cap
- Trailing edge bond line.

NDI Feedback specimen design considerations include:

- Designs were generalized and cover a range of thicknesses and blade designs
- Flaw sizes deemed necessary to be detected were determined by a complimentary BRC "Effects of Defects" study and manufacturer requirements

- Flaw depth, location and type were determined through discussions with manufacturers (flaw types considered include: snowflaking, porosity, resin-starved regions, adhesive voids, interply delaminations, spar and shear web disbonds, ply waviness, erosion, impact, lightning strike, and fluid ingress)
- Design parameters were varied and flaws engineered in a uniform array to better assess sensitivity
- Flaw locations focused on identified critical areas – blade root, spar, shear web bond lines, leading and trailing edges
- Custom test panels with engineered flaws were supplemented by full-scale blades and blade sections that contain natural flaws.

Figure 3-12: Laminate Thickness NDI Feedback Specimens Made From a Retired Blade – Flat Bottom Holes Placed in Representative Laminate Section to Simulate Delaminations and Backside Disbonds

The full set of five NDI Feedback Specimens are contained in Figure 3-12 through Figure 3-25.

These drawings and photos show key features of the test specimen designs along with the approach to engineering and placing of flaws within the specimens. These specimen designs depict the use of pull tabs, microballoons and pillow inserts to create disbonds at the laminate-to-adhesive interface and porosity in the adhesive layer. A detailed description of how the NDI

Feedback Specimens and WBFDE POD Specimens were made and the methods used to engineer the flaws in these specimens is provided in Section 3.4. Figure 3-13 shows one of the basic blade construction scenarios focusing on the blade spar cap and the adhesive joint connecting the spar cap to the foam core shear web. Another of the NDI Feedback Specimens that was designed to assess NDI performance in this region of the blade is shown in Figure 3-19. Notice that two shear webs and associated bond lines are included in this test specimen to increase the amount of inspection bond line area and the number of flaws in this critical inspection region. NDI Feedback Specimen No. 7, shown in Figure 3-19 through Figure 3-21, has a spar cap laminate thickness of 2.14" and a total thickness of 2.65" at the shear web adhesive bond line. The basic set of materials used in the fabrication of the fiberglass test specimen is: 1) foam core – Airex C70.5, 2) fiberglass uniaxial plies –Vector ply ELT 5500 or Saertex 1250 gsm UD, 3) fiberglass biaxial (0/90) plies – Vectorply ELT 2400-7P or Saertex VU-90079-00830, 4) fiberglass double bias (±45/±45) Vectorply EBX2400-5, 5) resin – Hexion epoxy MGS Rim R 135 with M GS RIMH 136 or 137 hardener, and 6) adhesive – Hexion EP 135G3 with EKH 137G hardener.

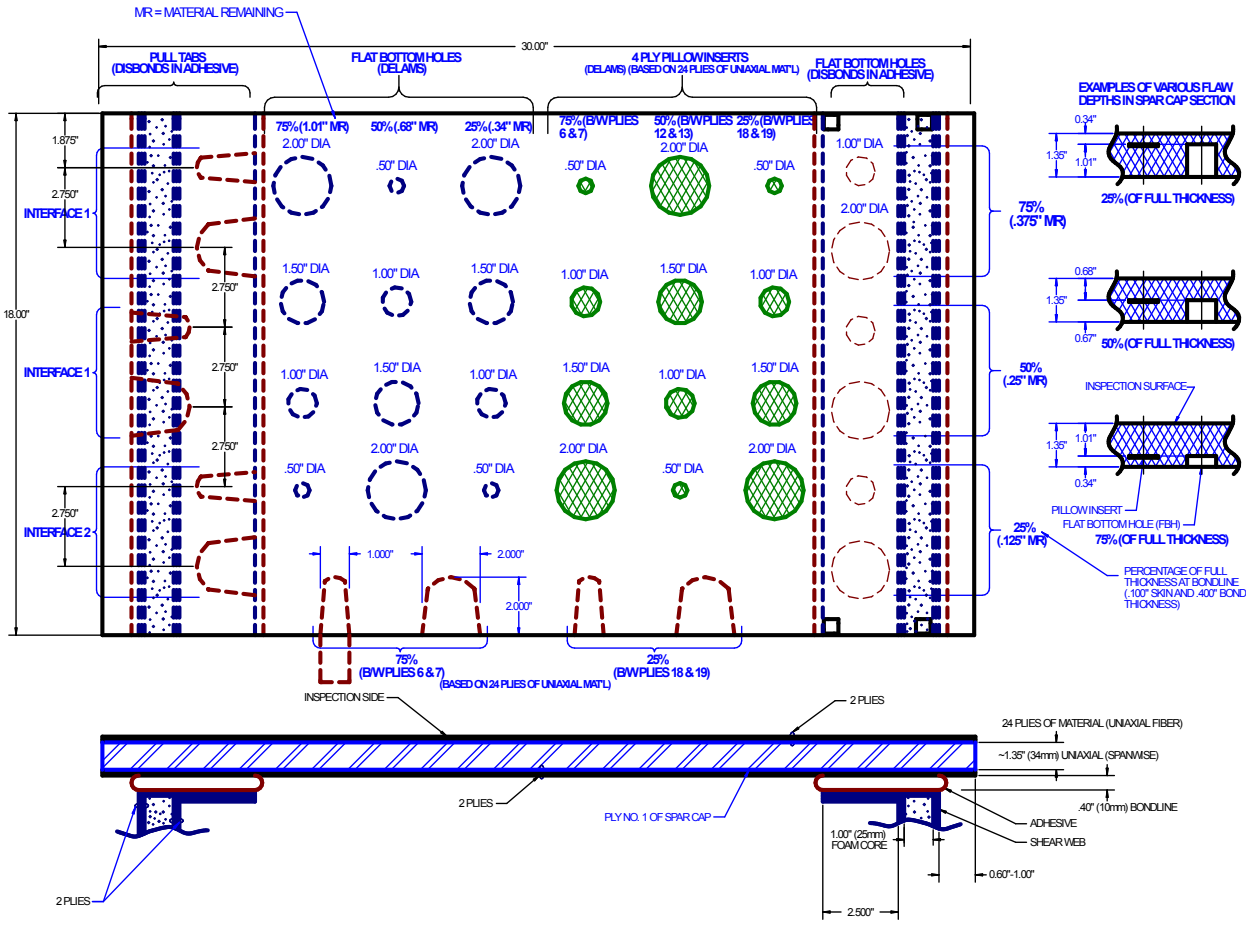

Figure 3-13: Spar Cap and Shear Web NDI Feedback

Specimen No. 2 (REF-STD-2-127-173-SXX-1)

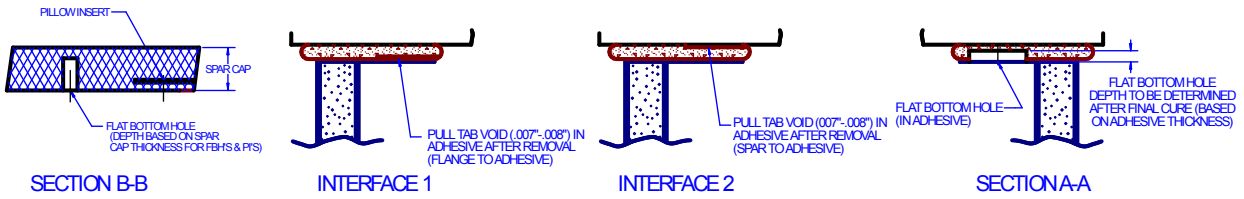

Figure 3-14: Additional Information on How Flaws Were Engineered into REF-STD-2-127-173-SXX-1

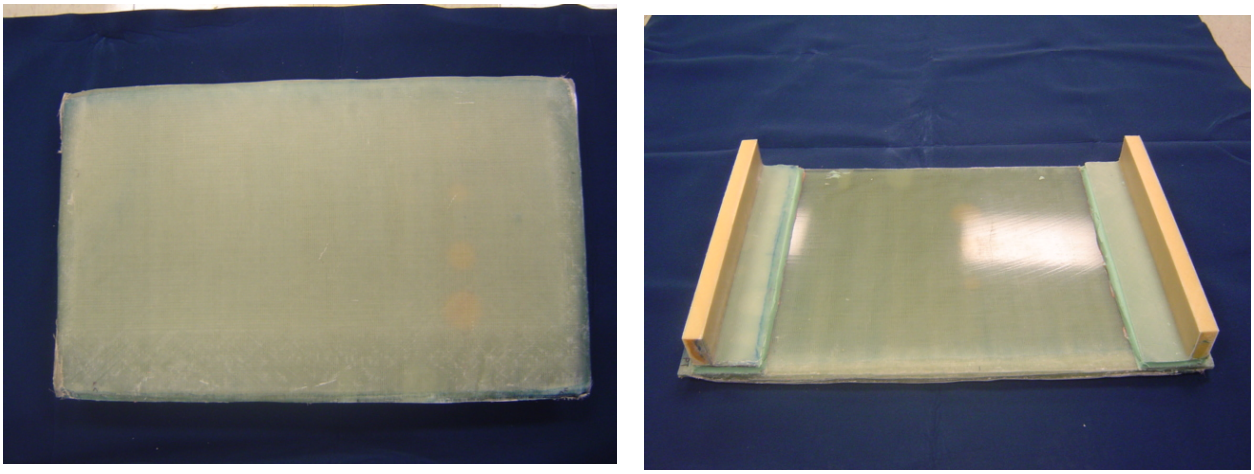

Figure 3-15: Photos of NDI Feedback Specimen REF-STD-2-127-173-SXX-1

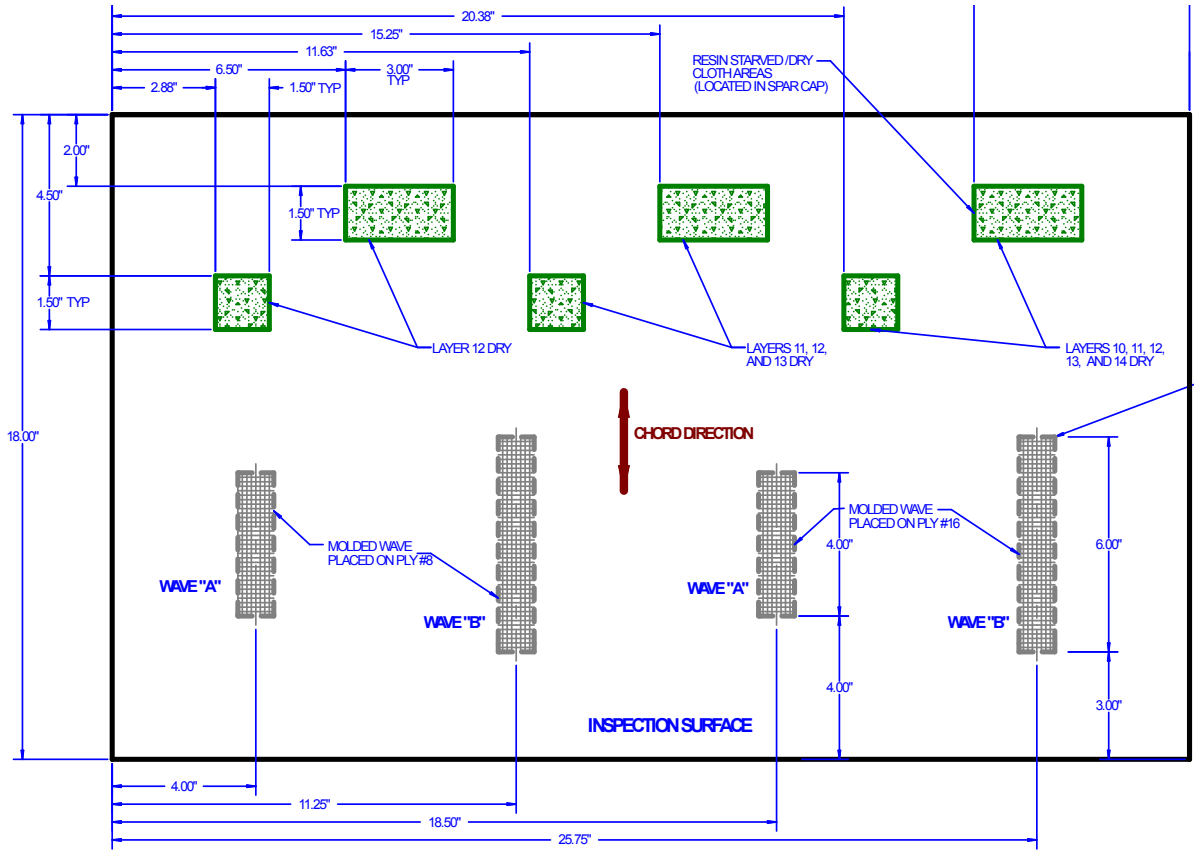

Figure 3-16: Laminate Dry Resin Wrinkle (Out-of--Plane Wave) NDI Feedback Specimen No. 4 (REF-STD-4-135-SXX-1)

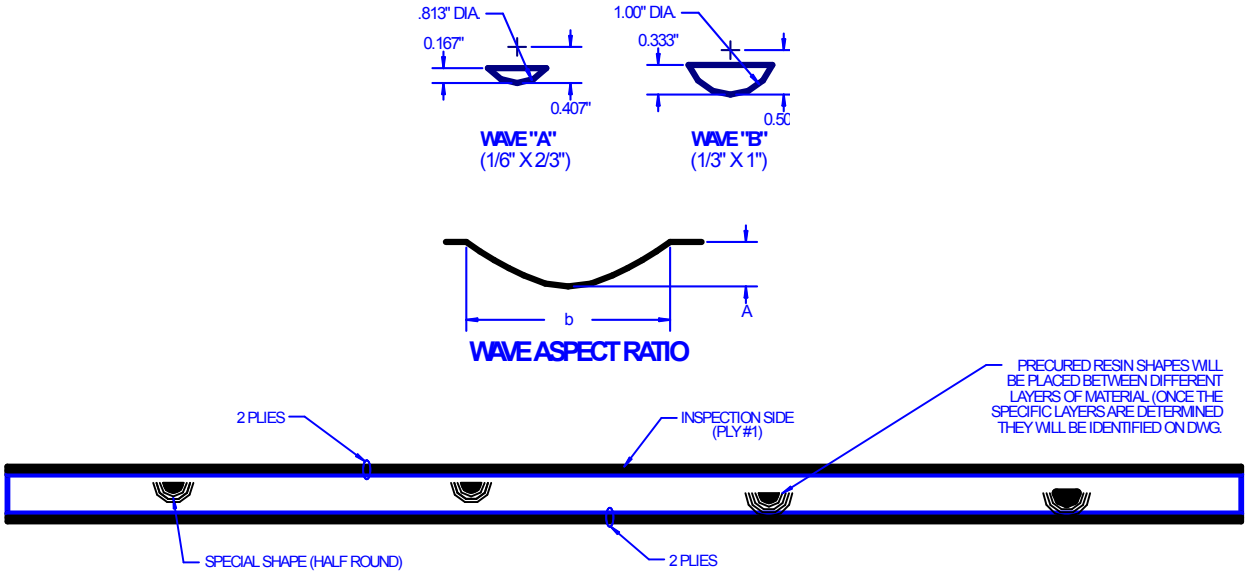

Figure 3-17: Additional Information on How Flaws Were Engineered into REF-STD-4-135-SXX-1

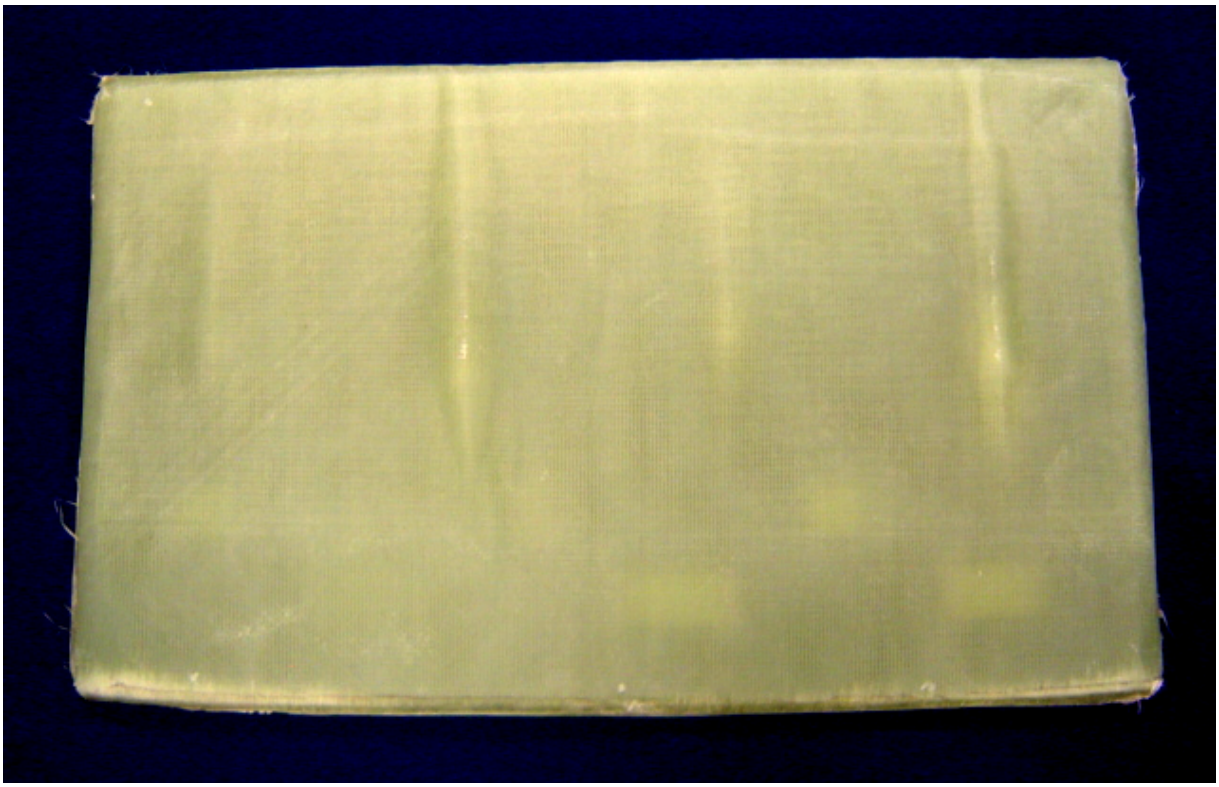

Figure 3-18: Photos of NDI Feedback Specimen REF-STD-4-135-SXX-1

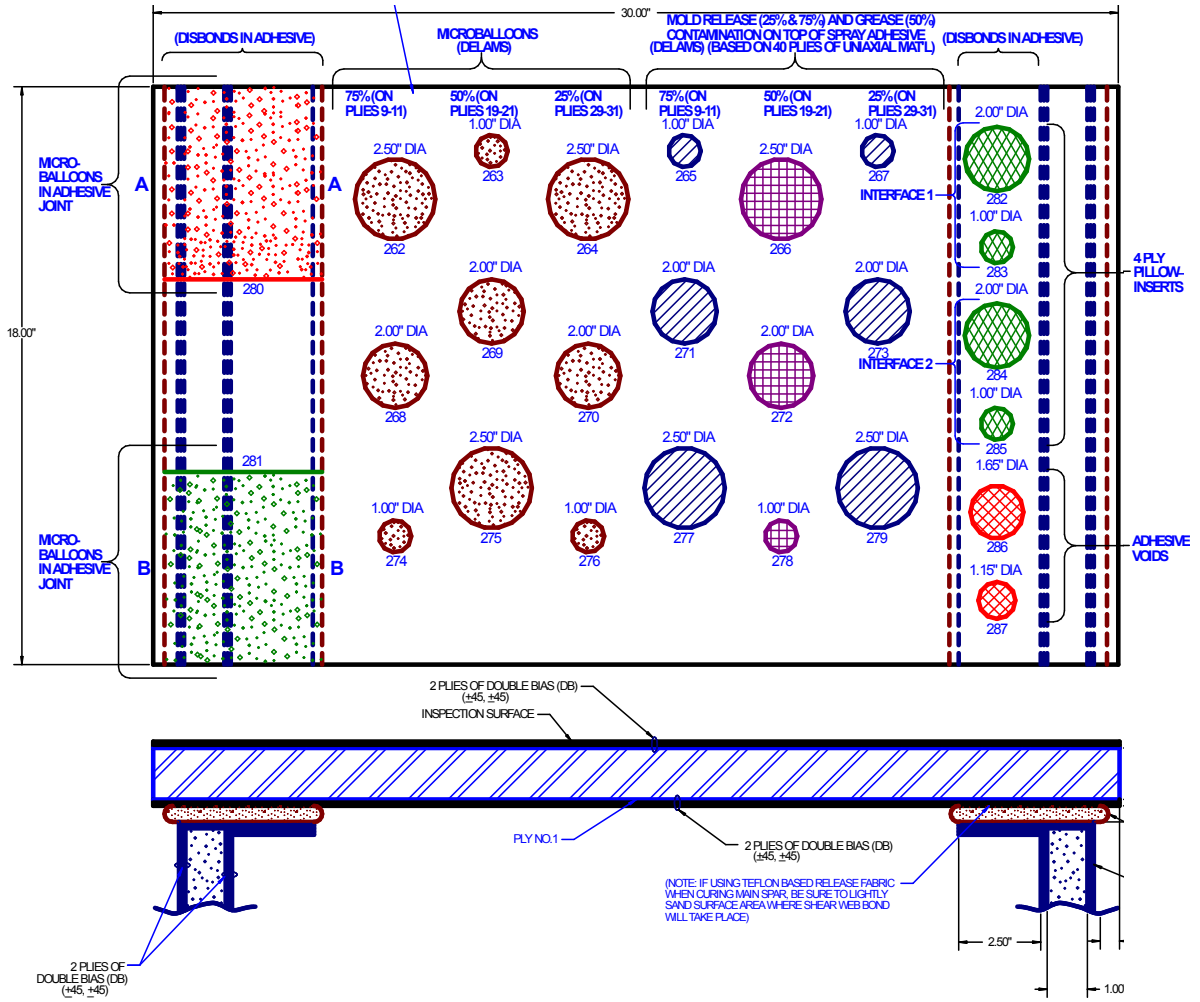

Figure 3-19: Thick Spar Cap and Shear Web NDI Feedback Specimen No. 7 (REF-STD-7-214-265-SNL-1)

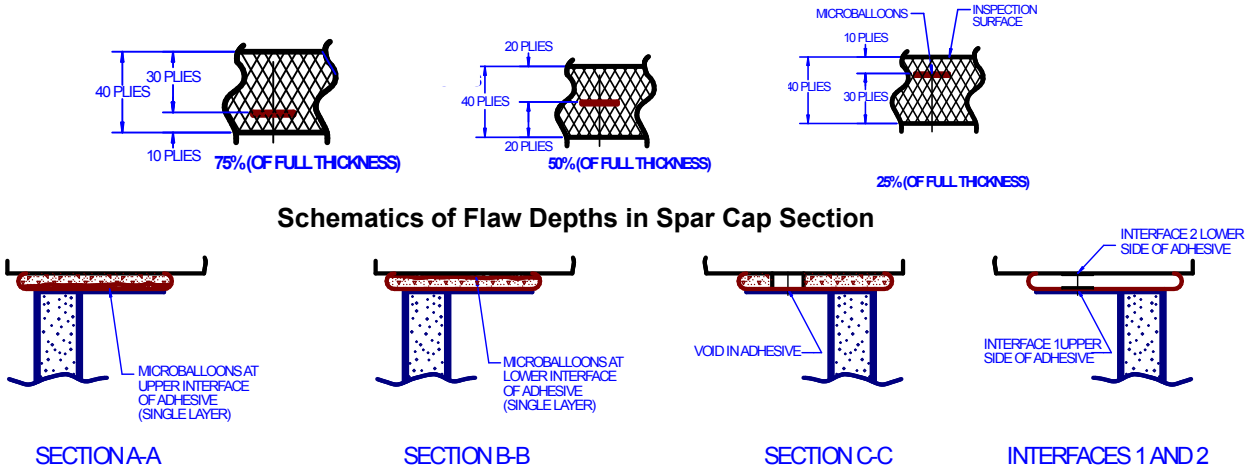

Figure 3-20: Additional Information on How Flaws Were Engineered into REF-STD-7-214-265-SNL-1

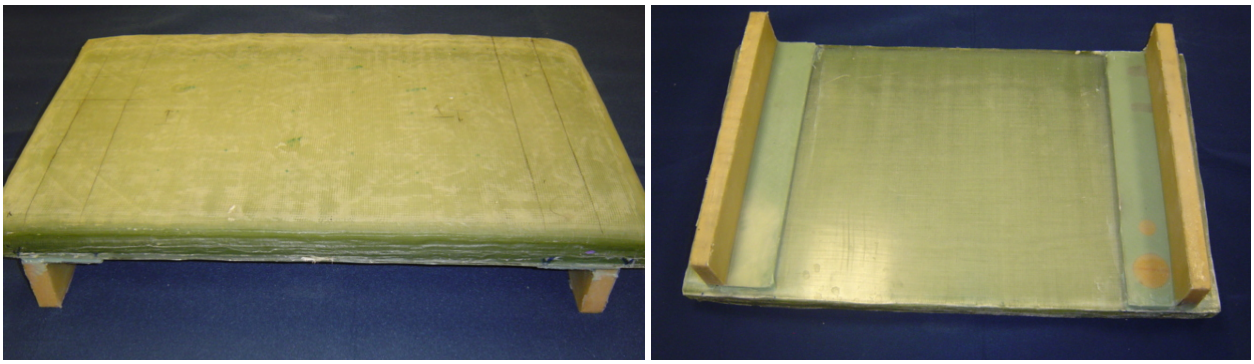

Figure 3-21: Photos of NDI Feedback Specimen REF-STD-7-214-265-SXX-1

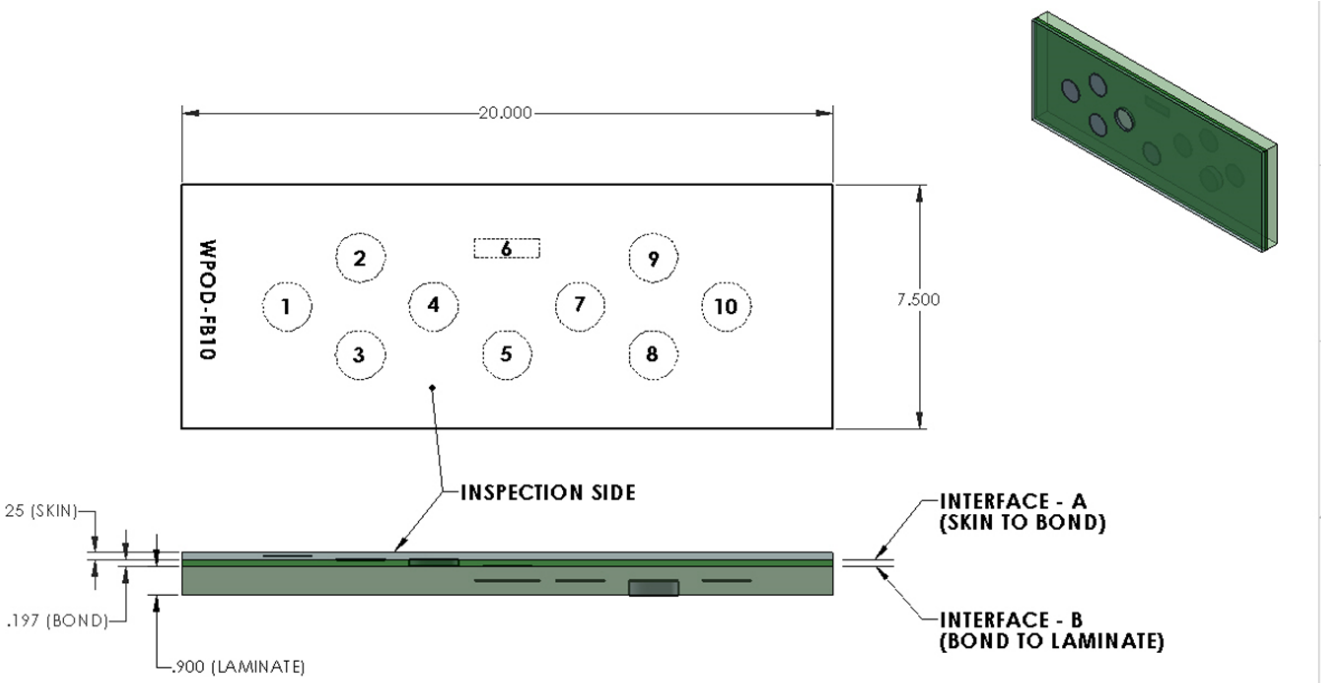

FLAW #	FLAW TYPE	LOCATION	FLAW SIZE	FLAW DEPTH
1	PILLOW INSERT	SKIN	DIA. 1.50"	50% OF SKIN
2	GLASS BEADS	BOND	DIA. 1.50"	INTERFACE -A
3	PILLOW INSERT	BOND	DIA. 1.50"	INTERFACE -A
4	VOID	BOND	DIA. 1.50"	THRU BOND
5	PILLOW INSERT	BOND	DIA. 1.50"	INTERFACE -B
6	WRINKLE	LAMINATE	2.00" X 0.60"	50% OF LAMINATE
7	GREASE	LAMINATE	DIA. 1.50"	50% OF LAMINATE
8	FLAT BOTTOMED HOLE	LAMINATE	DIA. 1.50"	50% OF LAMINATE
9	GLASS BEADS	LAMINATE	DIA. 1.50"	50% OF LAMINATE
10	PILLOW INSERT	LAMINATE	DIA. 1.50"	50% OF LAMINATE

Figure 3-22: Spar Cap and Shear Web Bond Line NDI Feedback Specimen No. 10 (WPOD FB-10) with Flaw Type and Depth Description

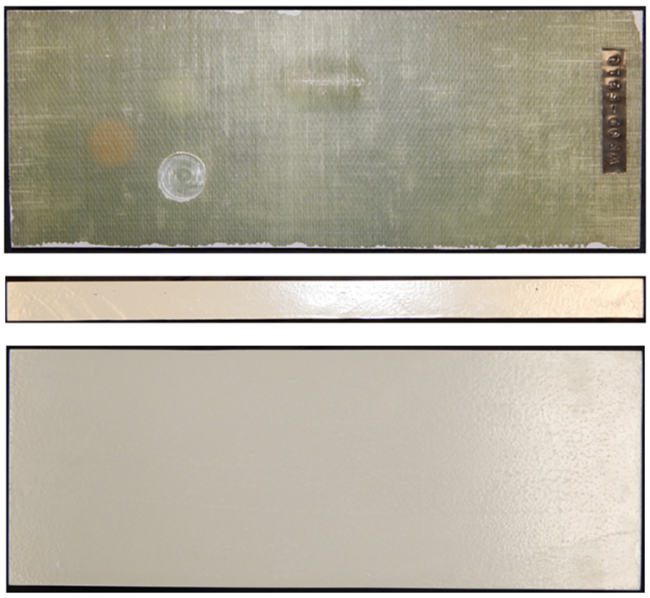

Figure 3-23: Photos of NDI Feedback Specimen No. 10 (WPOD FB-10)

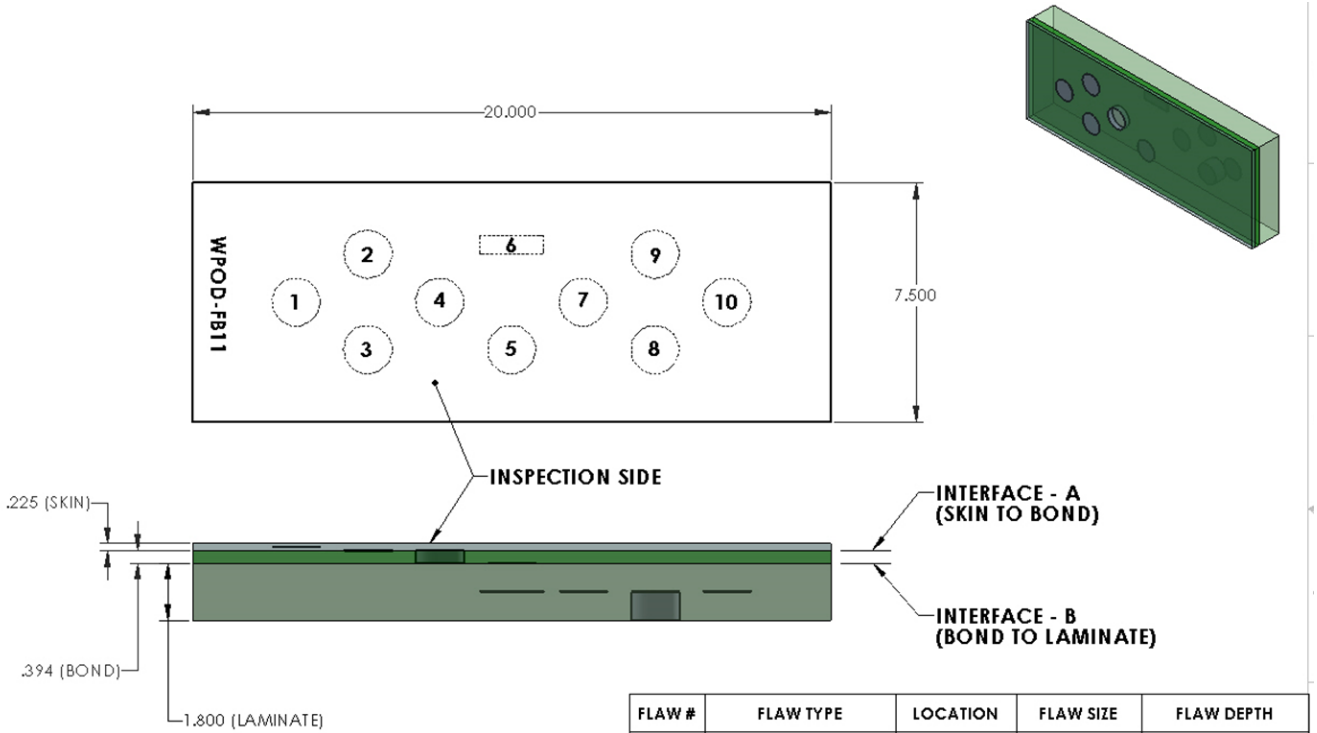

FLAW #	FLAW TYPE	LOCATION	FLAW SIZE	FLAW DEPTH
1	PILLOW INSERT	SKIN	DIA. 1.50"	50% OF SKIN
2	GLASS BEADS	BOND	DIA. 1.50"	INTERFACE -A
3	PILLOW INSERT	BOND	DIA. 1.50"	INTERFACE -A
4	VOID	BOND	DIA. 1.50"	THRU BOND
5	PILLOW INSERT	BOND	DIA. 1.50"	INTERFACE -B
6	WRINKLE	LAMINATE	2.00" X 0.60"	50% OF LAMINATE
7	GREASE	LAMINATE	DIA. 1.50"	50% OF LAMINATE
8	FLAT BOTTOMED HOLE	LAMINATE	DIA. 1.50"	50% OF LAMINATE
9	GLASS BEADS	LAMINATE	DIA. 1.50"	50% OF LAMINATE
10	PILLOW INSERT	LAMINATE	DIA. 1.50"	50% OF LAMINATE

Figure 3-24: Spar Cap and Shear Web Bond Line NDI Feedback Specimen No. 11 (WPOD FB-11) with Flaw Type and Depth Description

Figure 3-25: Photos of NDI Feedback Specimen No. 11 (WPOD FB-11)

3.4 Manufacture of Flawed Wind Blade Specimens

Through joint efforts with wind turbine blade manufacturers, a set of VARTM fiberglass NDI Feedback Specimens and Probability of Detection Specimens were designed and fabricated in order to conduct the WBFDE on thin and thick wind blade structures. A total of 11 POD Specimens were designed and fabricated. The specimen designs, and associated fabrication processes, were reviewed by a team of wind energy experts to insure specimen realism. This work included new design drawings, flaw fabrication, and templates for proper flaw location.

The most common flaws found in wind turbine blade bonded joints are lack of adhesive, adhesive voids (air pockets), presence of foreign material or contamination in the laminate and bond line and disbonds between the laminate and the adhesive. In order to create realistic NDI test specimens, various methods were developed for producing engineered flaws that are representative of actual flaws found in wind turbine blades. Figure 3-26 shows the several methods used to produce flaws in the wind blade NDI test specimens. Glass beads (microballoons) are used to represent concentrated pockets of porosity in the adhesive or within a single ply layer of a specimen. The hollow nature of the glass beads (trapped air) creates higher attenuation levels for ultrasonic inspection similar to actual small voids. Grease and mold release are used to represent foreign object damage (FOD) which can create kissing disbonds when stressed. Such tight disbonds are often difficult to detect as they possess intimate contact between the adjacent layers but no adhesive strength. Pillow inserts are made with layers of

tissue paper between Kapton tape to represent a disbond or tight delamination either between plies of the laminate or at bond line interfaces.

Figure 3-27 shows another set of methods used to engineer flaws. Engineered voids are created by using cylinders during the application of the adhesive, then removing the cylinders prior to bonding leaving a circular area without adhesive. To create tight disbonds, pull tabs are made from thin, tapered steel shim stock and placed between the laminate and the adhesive. Once the adhesive is cured, the pull tabs are removed, creating a disbond (air gap) between the adhesive and the laminate. Wrinkles, or out-of-plane waves, are created using resin rods or pyramid stacks of dry fiber before being placed between plies during the layup process. Dry areas are represented by using plies of dry fabric sandwiched between pre-cured fiberglass disks, limiting the amount of resin that can wet the fiber during infusion. Figure 3-28 and Figure 3-29 depict how the pre-cured disks are used to isolate one or more dry plies during the resin transfer process so that regions of dry fabric (extreme porosity) are produced. Several cross sections of dry fabric are shown in the photos of Figure 3-29.

Test specimen fabrication included the following steps:

- Design – material specifications, panel size, number of plies, ply types, flaw types, flaw sizing and flaw locations
- Flaw fabrication – producing flaws prior to visit with manufacturer
- Template creation – a Mylar/plastic template that is dimensionally identical to the drawing with cut-outs for flaw placement including labels for flaw type, size and ply insertion layer
- Ply cutting – cutting dry fiberglass and pre-preg carbon material to the proper size
- Ply layup – starting with the tool side down laying up each ply
- Flaw insertion – using the flaw templates to place each flaw in the proper location and ply layer
- Vacuum bagging and curing – panels are vacuum bagged, resin is infused and panels are cured on a heat table.

Additional fabrication steps for spar caps with bonded shear webs:

- Double bias fiberglass – two plies of double bias fiberglass added to the top and bottom of the spar cap. This represents what is performed on an actual blade when the spar cap is placed in the blade layup
- Resin infusion – VARTM method used to infuse the double bias plies to the carbon spar cap
- Adhesive and shear web installation – adhesive is applied and shear webs installed. Proper bond thickness is established by using pre-cured adhesive shims that are cut to the desired thickness
- Adhesive and laminate post curing – the entire spar cap specimen with bonded shear webs is placed into an oven for post curing.

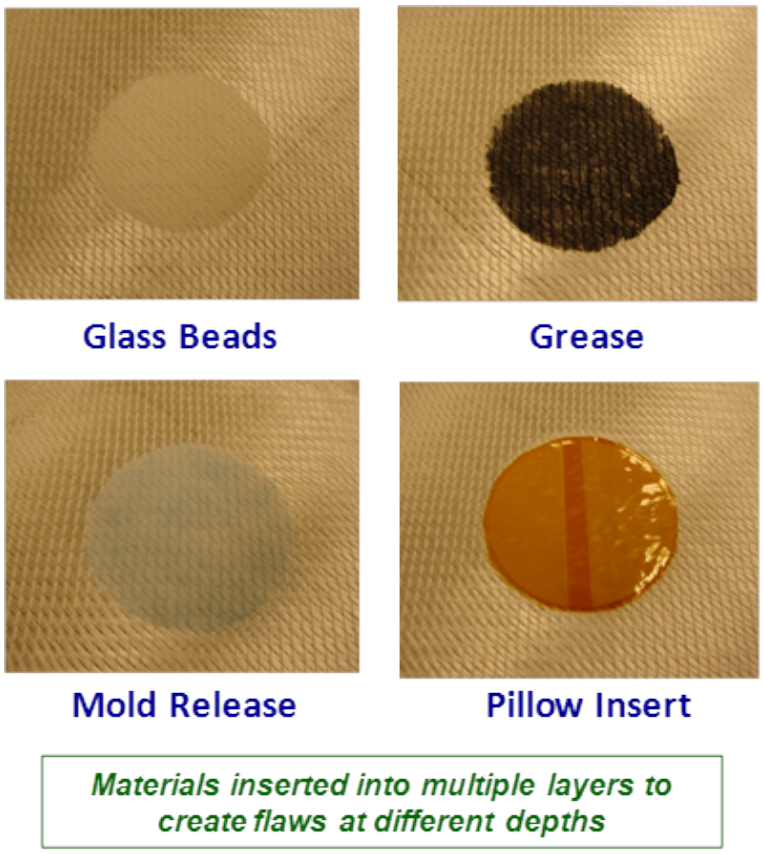

Figure 3-26: Inserts and Foreign Materials Placed at Various Layers to Produce Representative Flaws in Wind Blade Test Specimens

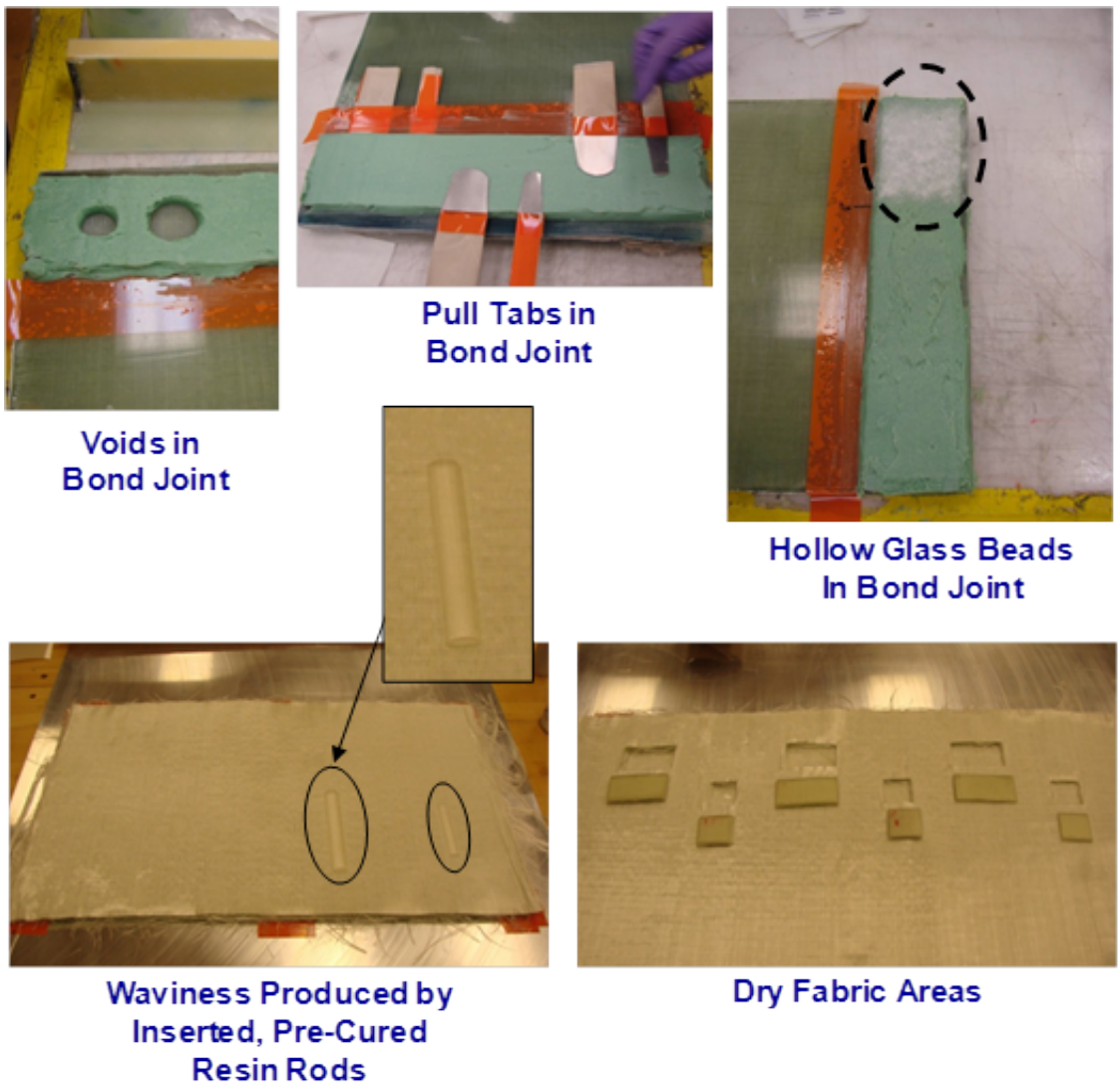

Figure 3-27: Methods Used to Produce Representative Flaws in Wind Blade Test Specimens

To create a representative sample set, it was essential to work with a manufacturer to guarantee the use of proper construction materials, bonding methods, resin transfer process and curing. Photos showing the fiberglass specimens during fabrication, including the ply lay-ups, VARTM resin transfer, flaw engineering methods and secondary bonding processes can be seen in Figure 3-30 and Figure 3-31. To create a representative sample set, it was essential to work with a manufacturer to guarantee the use of proper construction materials, bonding methods, resin transfer process and curing. Figure 3-32 and Figure 3-33 contain a series of schematics that explain the methods used to embed engineered flaws into the test specimens the placement of the flaws at various depths within each test specimen.. They also highlight the difference between near-side (flaw between spar cap and adhesive layer) and far-side (flaw between adhesive layer and shear web flange) adhesive flaws. These flaw types were used often in the NDI test specimens and will appear in a number of the NDI characterization images that follow.

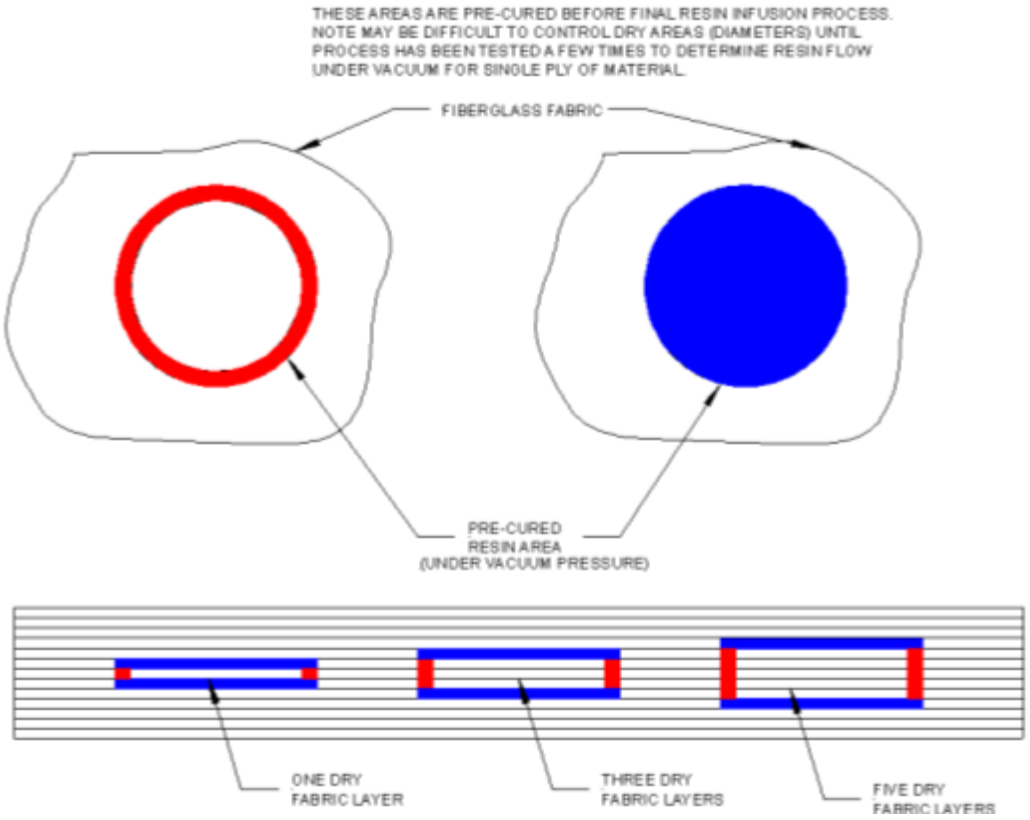

Figure 3-28: Schematic of Method Used to Engineer Dry Fabric Flaws into Wind Blade NDI Specimens

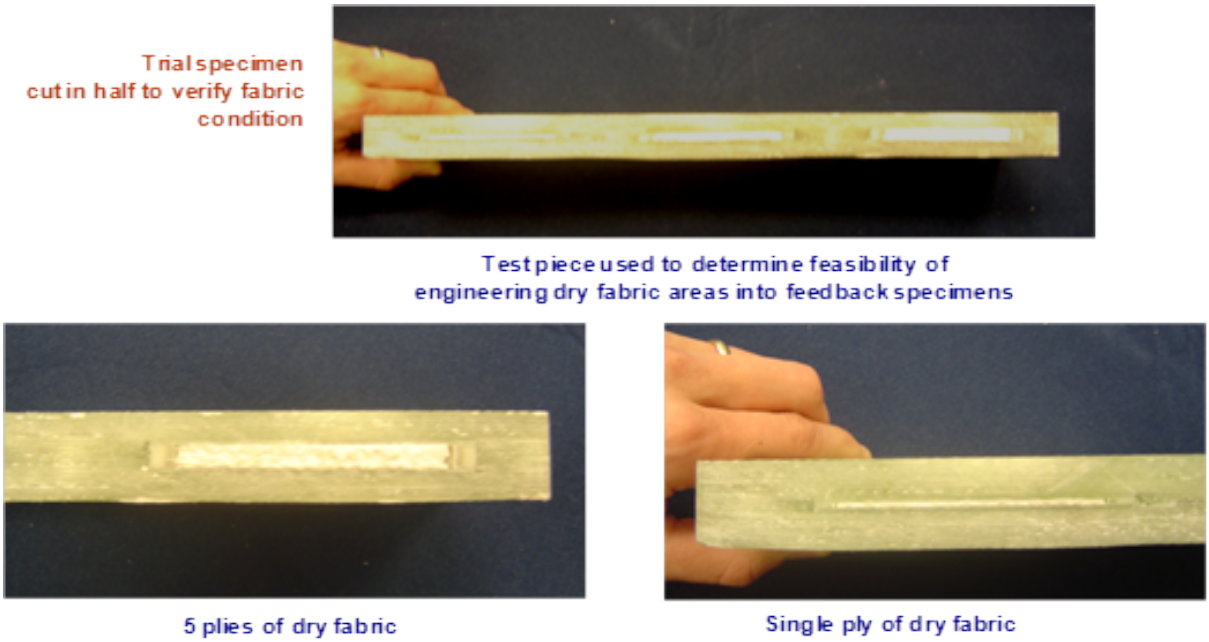

Figure 3-29: Cross Section Views of Trail Samples Showing Successful Engineering of Dry Fabric Flaws in Wind Blade NDI Specimens

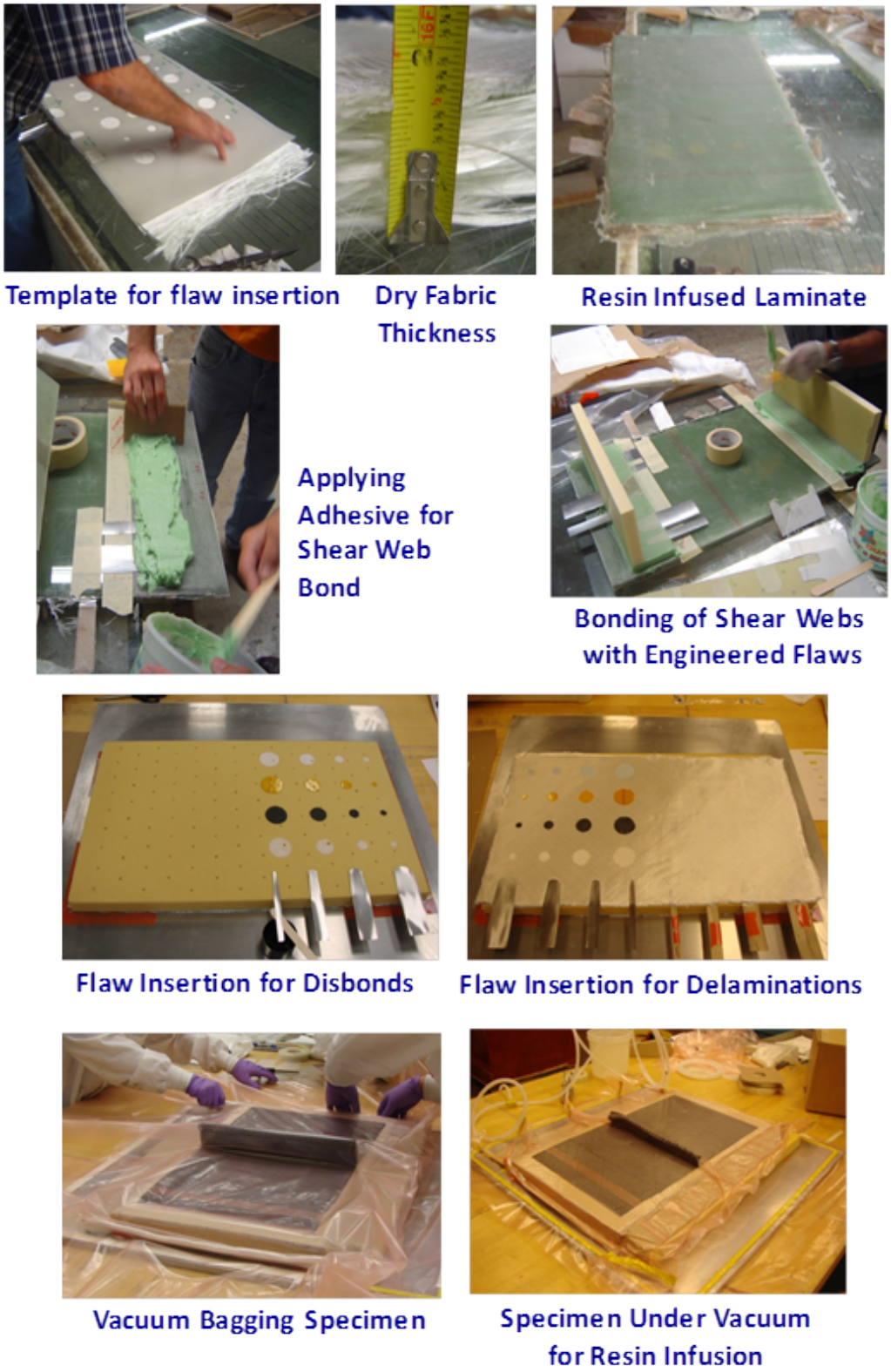

Figure 3-30: Fabrication Steps Used to Produce Representative Fiberglas Wind Blade Test Specimens with Engineered Flaws

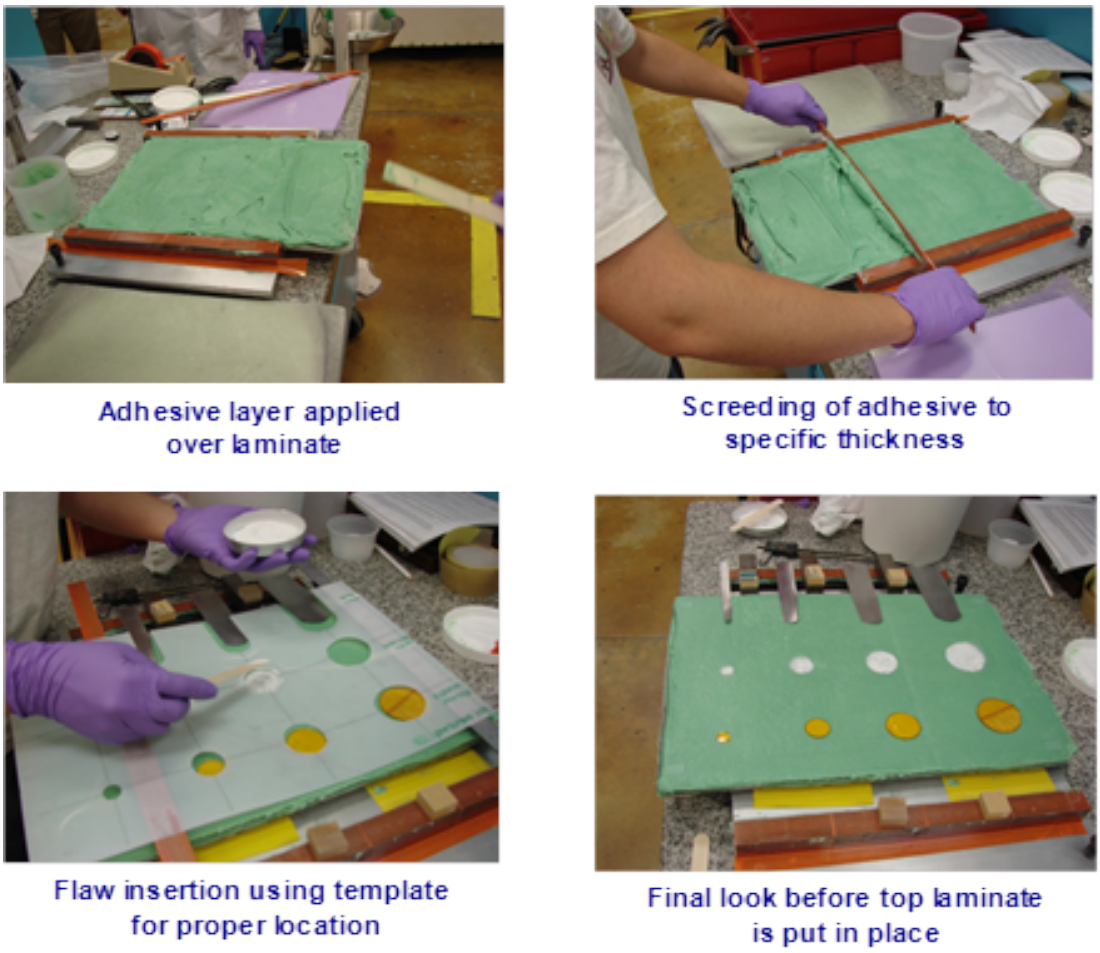

Figure 3-31: Fabrication of Trailing Edge Specimen - NDI Feedback Specimen No. 5

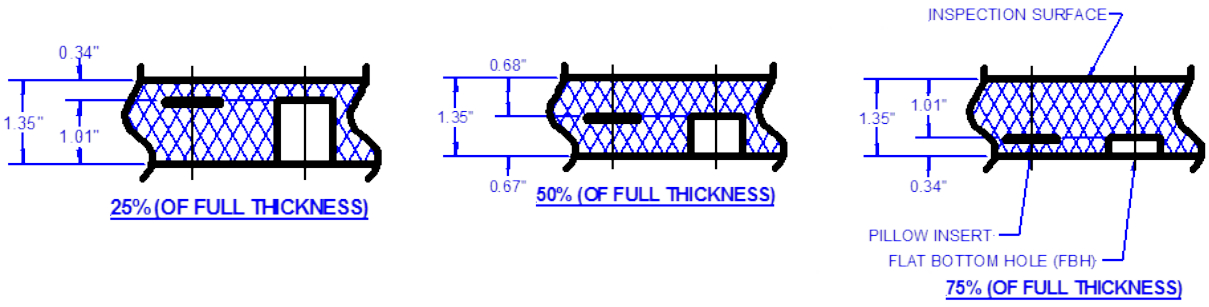

Figure 3-32: Cross Section View Showing Flaws Engineered at Different Depths in the Laminate

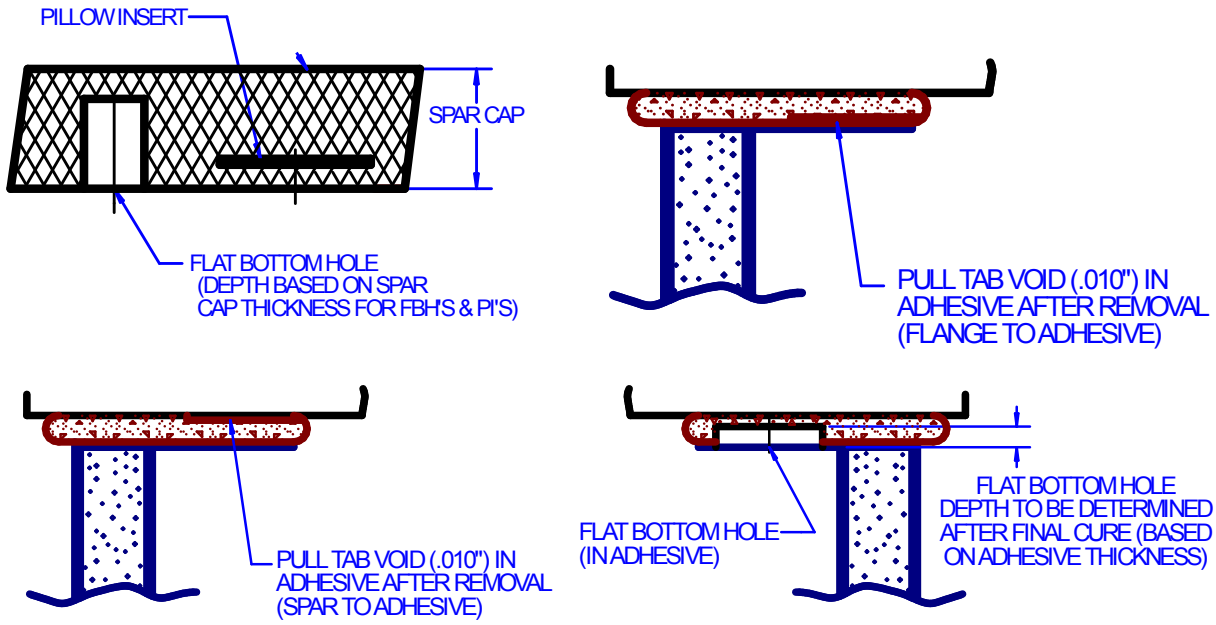

Figure 3-33: Schematics Depicting the Methods Used to Engineer Flaws in Blade Specimens and Their Various Locations within the Blade Construction

3.5 NDI Characterization of Wind Blade POD Specimens

In addition to detailed visual inspection of blade components after fabrication, there are typically two types of inspections performed by blade manufacturers in the spar cap region of the blade. The first inspection is conducted on the spar cap after fabrication but before it is inserted into the blade layup assembly. This is usually a visual inspection for fiberglass spars and a UT inspection for carbon spars. The second inspection is performed after the spar cap is inserted into the blade layup and bonded to the shear webs. Due to manufacturer's need for various types of spar cap inspections, some of the NDI test specimens were manufactured to represent pre blade assembly spar caps (cured spar caps before being inserted into the blade assembly) and some were manufactured to simulate post manufacturing spar caps (blade fully assembled with bond line).

Once the test specimens were fabricated, a series of conventional and advanced UT inspection methods were used to conduct the characterization of the NDI test specimens described above. The primary purpose was to ensure that the test specimens and their flaws were representative of those that will be encountered in the field. In addition to flaw detection based on C-scan imaging or amplitude and time-of-flight deviations, Signal-to-Noise (S/N) calculations were also produced to establish that each flaw provided sufficient deviation from the norm to elicit a "flaw call." Thus, it was determined that all flaws included in the WBFDE POD Experiment were ones that a manufacturer or operator would like to detect.

One of the chief activities conducted by Sandia Labs was the development and evaluation of ultrasonic (UT) inspection methods to improve the current state of blade inspection capabilities. These methods, categorized into single-element pulse-echo UT and phased array UT, were then used to accurately characterize the wind blade test specimens that were fabricated with engineered flaws. The flaws include an array of interply delmainations, spar-to-shear web disbonds, contamination/FOD, laminate waves, porosity and dry regions. The Sandia-evolved ultrasonic NDI methods were demonstrated to produce some of the best sensitivity (highest contrast C-scan images) on wind turbine blades to date. The combined use of A-scan (raw UT signal), B-scan (section view), C-scan (2-D planform view) data was also evaluated to enhance flaw detection and characterization. In addition, custom probe housings (shoes) were developed to facilitate phased array inspections through a wide range of material thicknesses, adjust for slight contours, maximize UT signal strength and make deploying a phased array probe on blades more effective than conventional housings. Figure 3-34 shows the inspection of an NDI Feedback Specimen using phased array UT, a specialized water box shoe (transducer housing) and a mechanical X-Y scanning unit. Figure 3-35 shows one of the inspection test set-ups used to characterize the NDI Feedback and blind, POD Specimens. In this case, the MAUS scanning system was deployed in pulse-echo UT mode with a single-element 500 KHz contact transducer. Multiple NDI methods were used to comprehensively characterize all of the specimens used in the WBDE study.

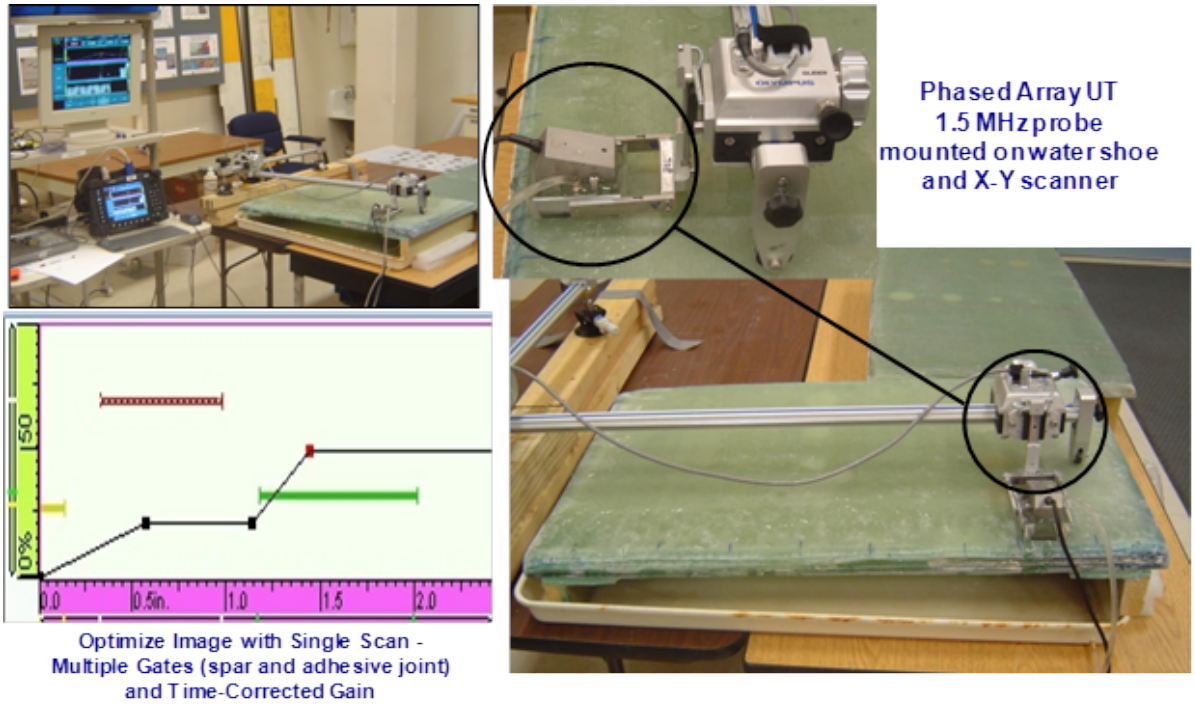

Figure 3-34: OminScan Phased Array UT Scanning System Inspecting an NDI Feedback Specimen

Figure 3-35: Characterization of Wind Blade Flaw Detection Experiment Specimens Using MAUS C-Scan System in Pulse-Echo UT Mode and 0.5 MHz Single Element Probe

Some sample results from the NDI specimen characterization will now be presented to demonstrate the types of signals and images that correspond to typical wind blade damage. Specific information on the UT inspection methods, the transducers, specialized hardware and custom data acquisition approaches will all be presented in Chapter 5. Figure 3-36 shows several images produced from a single element UT inspection of an actual blade section that contains resin starved (high porosity) regions while Figure 3-37 contains images produced from both single element and phased array UT inspections of out-of-plane waves (wrinkles) in the laminate. Figure 3-38 shows how resin pools placed between plies were used to create out-of-plane waviness. It also shows the B-scan and C-scan images to detect these flaws. All flaws in these specimens are clearly imaged and are candidates for detection by an inspector.

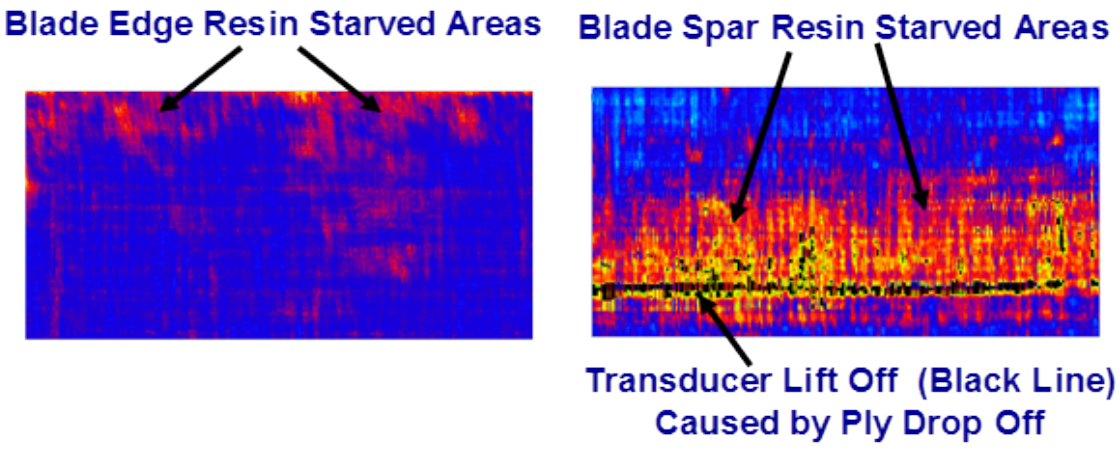

Figure 3-36: Inspection Results from Boeing MAUS System using a 1 MHz, 2" Focused Probe on Thick Blade Section with Resin Starved Areas

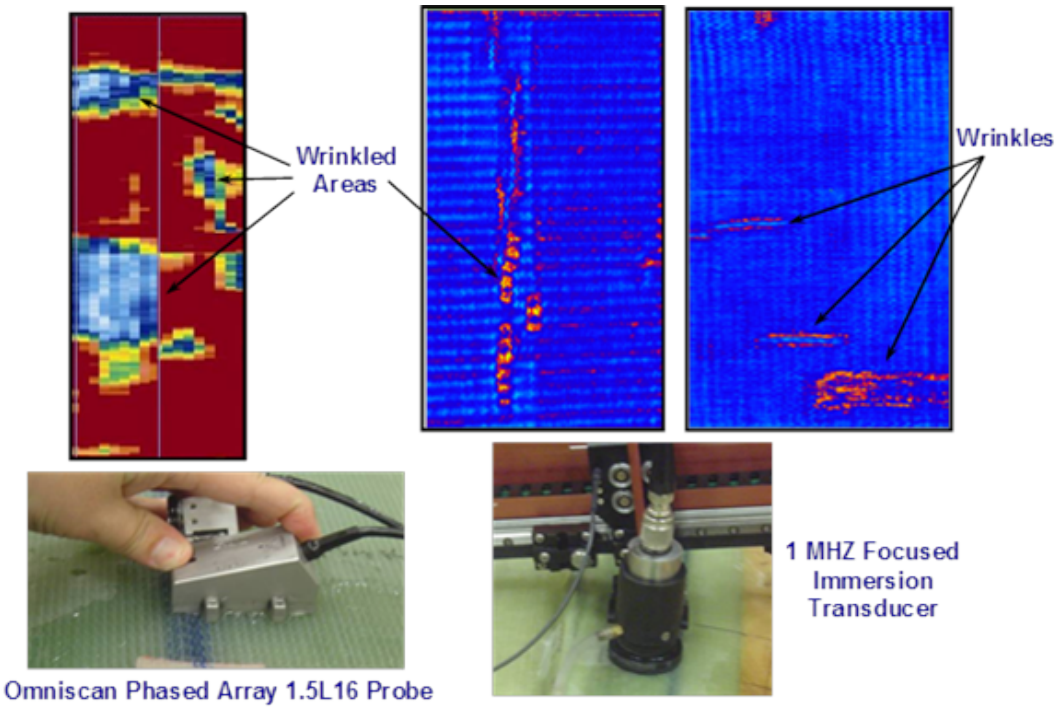

Figure 3-37: Inspection Results from Phased Array UT (OmniScan Device) and UT Focused Immersion Transducer (MAUS Device) on Test Specimens with Wrinkles

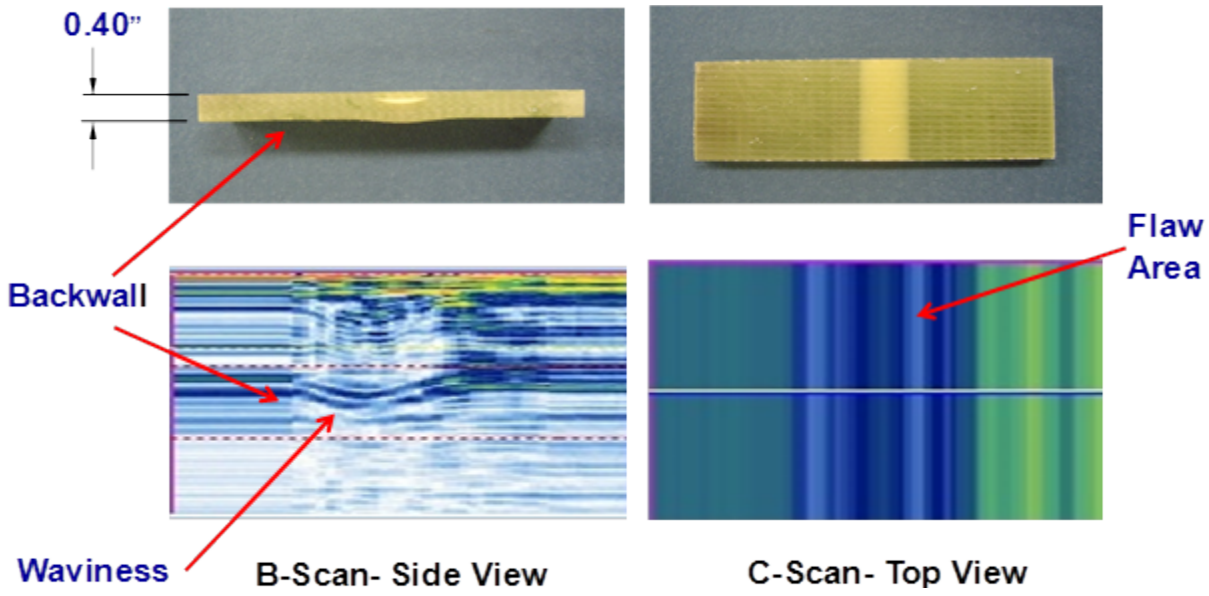

Figure 3-38: Phased Array UT C-scan Image of Out-of-Plane Waviness Coupons

Figure 3-39 and Figure 3-40 show several of the test specimen designs along with the inspection results of WBFDE specimens using phased array UT with a specialized water box shoe

(transducer housing) and a mechanical X-Y scanning unit. These results show that all engineered flaws can be detected.

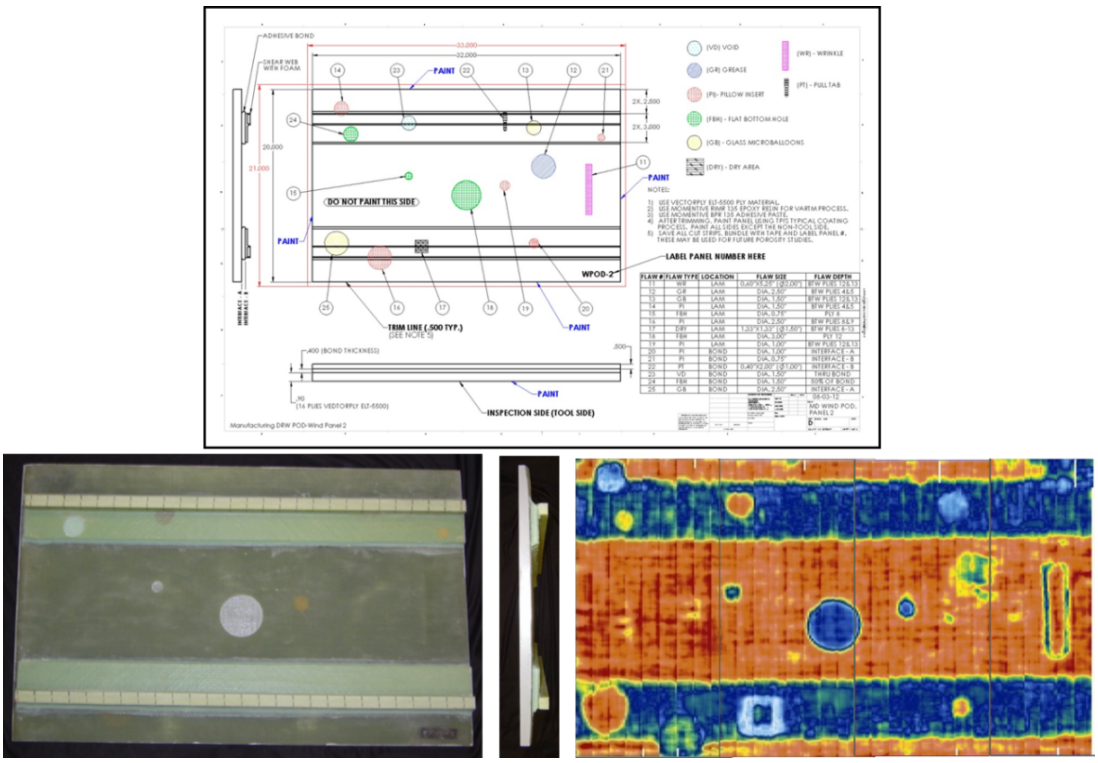

Figure 3-39: Wind POD Test Specimen Design Drawing with Flaw Layout Along with Photo of Specimen and C-Scan Image Produced by Phased Array UT

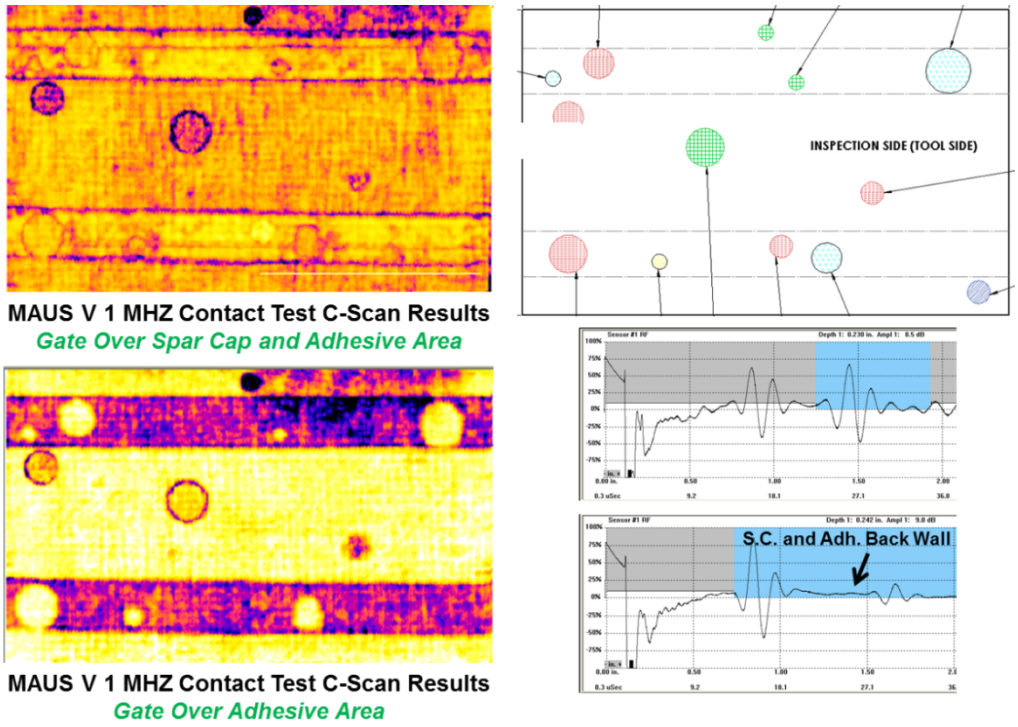

Figure 3-40: Inspection Images Depicting the Process Used to Characterize the Flaw Profiles of Each Specimen and Ensure Each Flaw was Viable for Detection

Figure 3-41 to Figure 3-46 contain NDI test specimen schematics and inspection results from both single-element and phased array UT inspections of the NDI Feedback Specimens used in this POD study. It is not prudent to list provide the characterization results for all of the blind POD Specimens as this would provide the "answers" to the WBFDE and compromise the ability to utilize this experiment for future NDI evaluation testing. NDI Feedback Specimen 2 (REF-STD-2-127-173-SXX-1) contains both a spar cap laminate and two spar cap-to-shear web adhesive joints. The engineered flaws were imaged in the scans. Some of the more subtle and challenging flaws to detect included the mold release (tight delamination with small adhesive strength remaining) and microballoon (porosity) flaws. In addition, the backside (far-side) adhesive bond line flaws (see MB and PI at interface 1 in Figure 3-14) are difficult to image. This is due to the thinness of the shear web flange and the resulting close proximity of these backside flaws to the overall back surface of the part. Figure 3-42 addresses the wrinkles and dry regions in thick laminates (REF-STD-4-135-SXX-1). It can be seen that all of the flaws in these specimens were detected and imaged with the phased array UT inspection method except for some of the smallest 0.5" diameter flaws. Single element and phased array UT inspection results for NDI Feedback Specimen No. 7 (REF-STD-7-214-265-SXX-1)are shown in Figure 3-43 and Figure 3-44. Shifts in the UT signals associated with different regions on the blade are highlighted in Figure 3-43. These signal shifts, along with unique signal shifts associated with damage in the part, are exploited to produce the C-scan images shown in Figure 3-44. All of the flaws, including the challenging ones at the backside of the adhesive layer, are clearly imaged. The details of the single element, focused UT transducer approach and the custom deployment of the phased array transducer will be described in detail in Chapter 5.

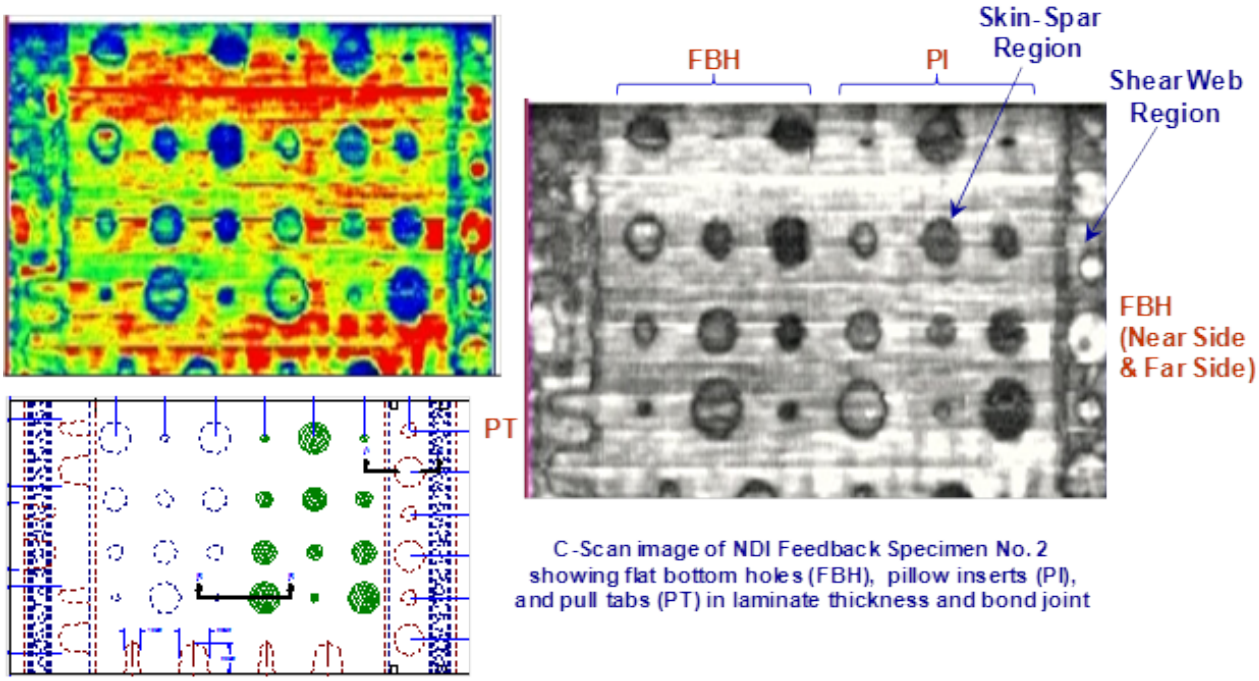

Figure 3-41: Phased Array UT C-Scan of NDI Feedback Specimen No. 2 (REF-STD-2-127-173-SXX-1)

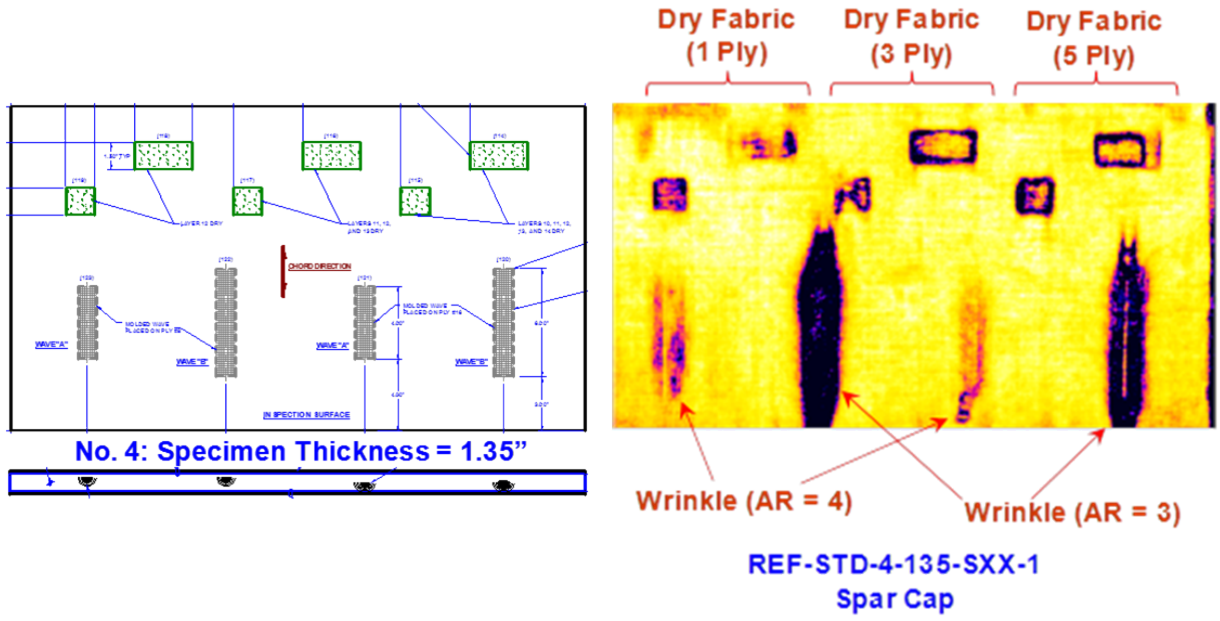

Figure 3-42: Spar Cap with Waviness & Dry Regions NDI Feedback Specimen No. 4 (REF-STD-4-135-SXX-1) and Characterization Image Produced by Phased Array UT C-Scan

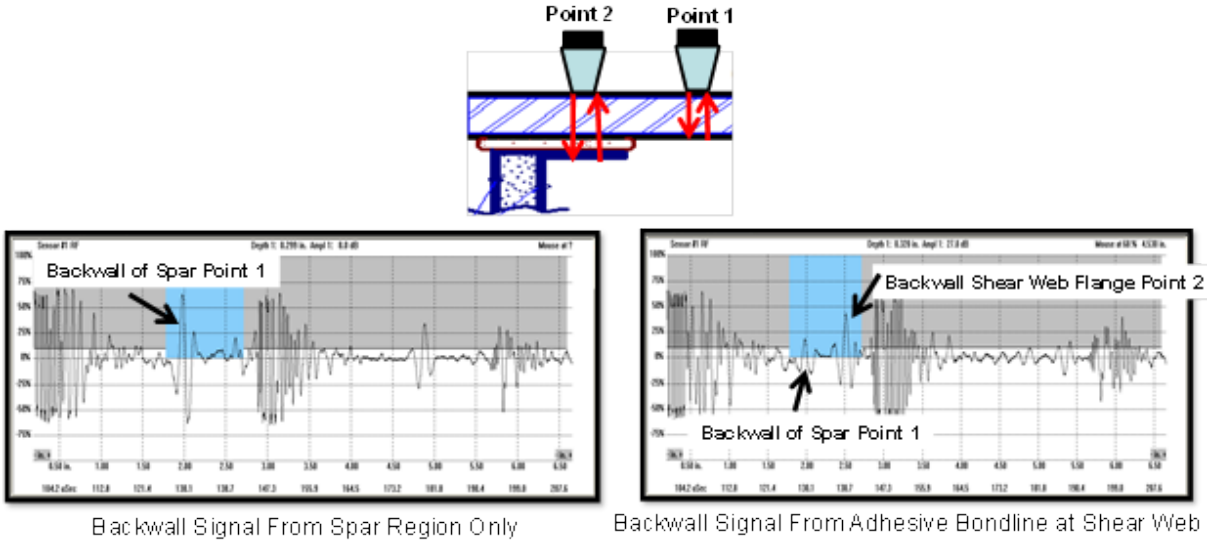

Figure 3-43: UT A-Scans of NDI Feedback Specimen No. 7 (REF-STD-7-214-265-SXX-1) – Generated by 1 MHz, 2" Focused "Immersion" Probe

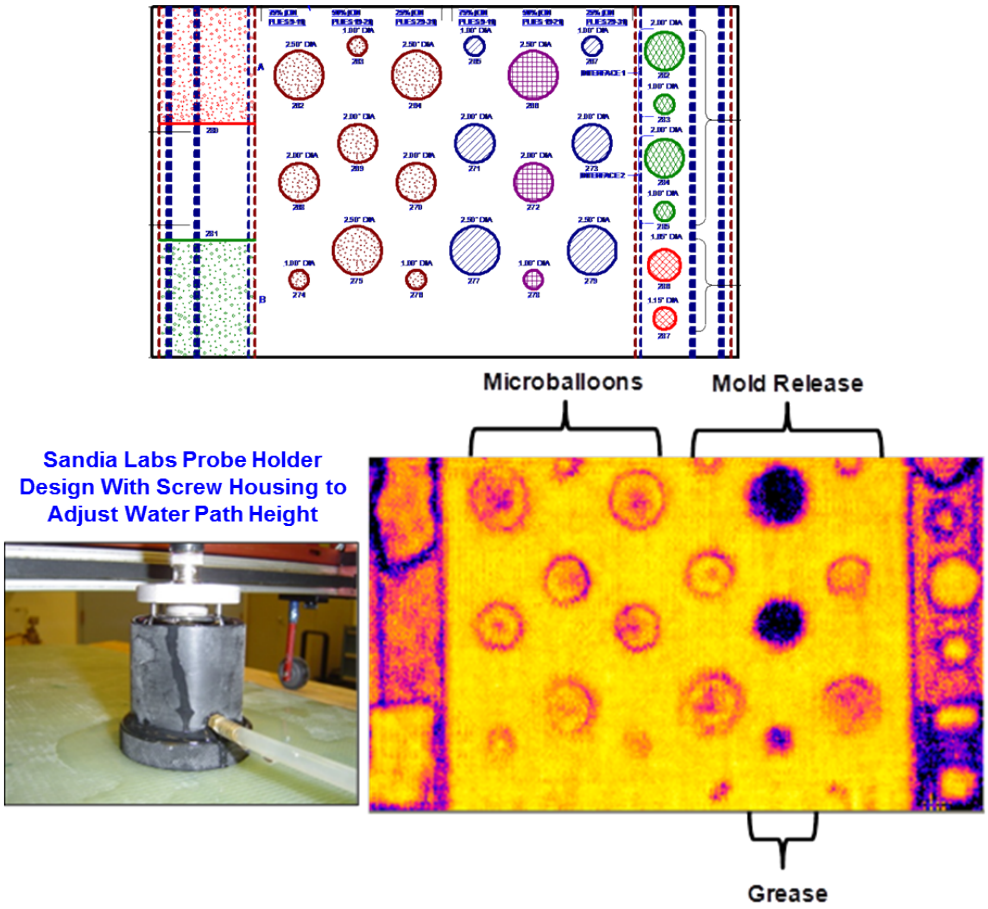

Figure 3-44: UT C-Scans of NDI Feedback Specimen No. 7 (REF-STD-7-214-265-SXX-1) - Generated by 1 MHz, 2" Focused "Immersion" Probe

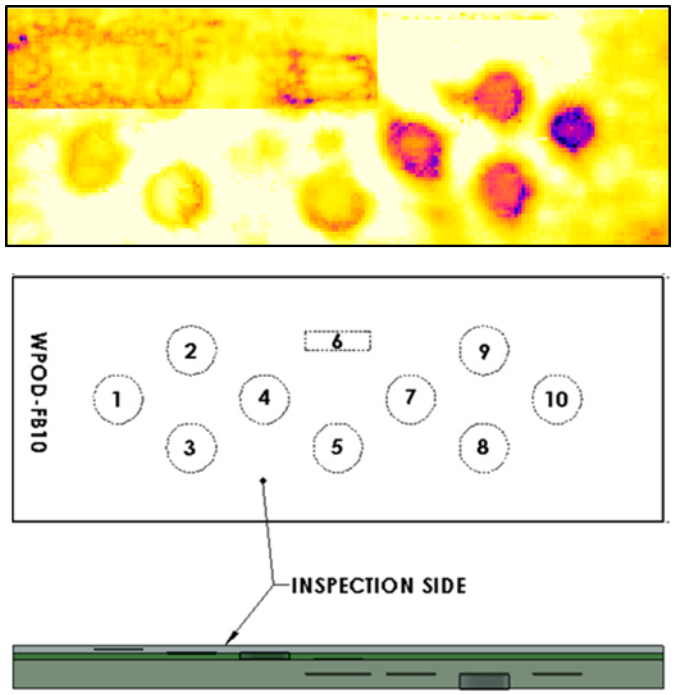

Figure 3-45: Phased Array UT C-Scans of NDI Feedback Specimen No. 10 (WFB-10) - Generated by MAUS Scan with a 0.5 MHz, 1" Dia. Single-Element UT Transducer

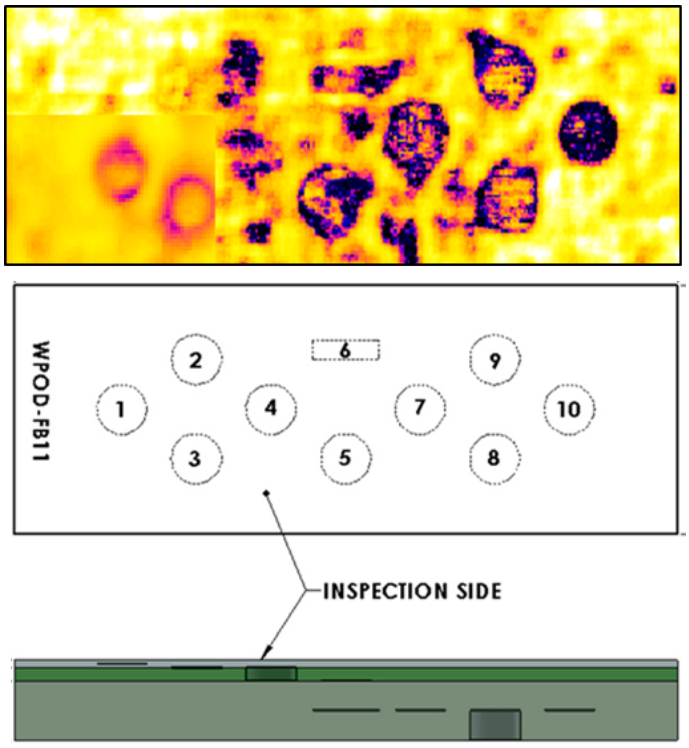

Figure 3-46: Phased Array UT C-Scans of NDI Feedback Specimen No. 11 (WFB-11) - Generated by MAUS Scan with a 0.5 MHz, 1" Dia. Single-Element UT Transducer

References

3-1. Roach, D., Neidigk, S., Rice, T., Duvall, R., Paquette, J., “Blade Reliability Collaborative: Development and Evaluation of Nondestructive Inspection Methods for Wind Turbine Blades,” Sandia DOT Report, SAND2014-16965, September 2014.

THIS PAGE INTENTIONALLY LEFT BLANK

CHAPTER 4

4.0 Wind Blade Flaw Detection Experiment Implementation

This Wind Blade Flaw Detection Probability of Detection Experiment involved traveling to different wind blade production facilities to capture data from current blade inspectors, as well as hosting different advanced NDI vendors/developers in the Sandia Labs WIND Reliability Center facility and having them inspect the POD blade test. Experimenters provided their inspection results so that it was possible to intercompare them and determine the capabilities and limitations of the various methods.

A set of experiment protocols were written to guide every aspect of the WBFDE implementation. The experiment protocols ensured that the information provided to all experiment participants was consistent and comprehensive such that all participants received similar guidance and inspection aids. The experiment protocols also provided step-by-step guidance to the experiment monitors so that all data and observations associated with the WBFDE were acquired in a consistent manner. A thorough "Experiment Briefing Package" (See Appendix A) was read by each inspector prior to any testing. The set of NDI Feedback Specimens, with flaw locations clearly marked, were also sent out in advance so that experiment participants could conduct inspections to familiarize themselves with the wind blade structures and flaw detection requirements.

The first day of each experiment started with the presentation of the Experimenter Briefing. Figure 4-1 shows one of the briefings being provided to inspectors while Figure 4-2 and Figure 4-3 show inspectors and their equipment while conducting the WBFDE inspections. The briefing explained the purpose of the experiment and the process the inspectors will use to indicate their flaw findings. The briefing was used at each facility to ensure a consistent presentation on the experiment goals and a thorough explanation of how the experiment will proceed. It also allowed the inspectors to ask questions. During the course of the NDI tests, the experiment monitors logged various observations along with the exact flaw calls provided by the inspectors.

Once the briefing was completed, each blind inspection process was preceded by inspections on appropriate NDI Feedback Specimens supplied by the experiment monitors. The inspector was provided with information on the manufactured flaws present in the NDI Feedback Specimens and was allowed to use the specimens for check-out and set-up of their inspection equipment. The NDI Feedback Specimens have similar construction as the blind test specimens and include similar flaws. Thus, they were also used to allow inspectors to become familiar with an inspection device and to learn about a specific equipment's response to various composite structures and about the flaws within those structures. Information gathered during the WBFDE inspections included: 1) flaw detection performance (type, sensitivity), 2) duration of inspection, 3) deployment issues; range of thicknesses limitations, 4) inspection difficulties, 5) accessories needed to make device fieldable, and 6) ease of data interpretation.

Figure 4-1: Wind POD Experiment Briefing

Figure 4-2: Deployment of Wind Blade Flaw Detection Experiment

Figure 4-3: Inspectors and Typical Equipment and Signals During the Wind Blade Flaw Detection Experiment

Once the inspectors were comfortable with their set-up on the NDI Feedback Specimens, experiment monitors distributed the blind specimens to them for inspection. Each experimenter was provided with drawings of each specimen type. They were asked to inspect each specimen/blade section and provide any information about the presence of flaws. If they determined that the flaws are detectable, they marked the location and size of the flaw directly on the test specimen. Inspectors were asked only to locate and properly size the flaws they find by marking directly on the specimens using standard grease pencils. This data was then recorded and graded to determine their Probability of Detection level, number of false calls, and inspectors' accuracy in sizing the flaws. Other secondary data was collected such as timing (inspection time on each panel), inspector experience, NDI training level, inspection frequency,

probe type, and equipment used for inspection. The typical set-up for the experiment deployment is shown in Figure 4-2 where each inspector has a workstation to set-up their equipment and test specimens.

Table 4-1 lists the WBFDE participants that completed the testing, as well as the full set of blade inspection candidates for the POD experiment. It can be seen that ultrasonic-based inspections are emphasized and that a good cross-section of industry participation has been achieved. A wide array of wind blade manufacturing companies and applicable wind blade NDI equipment companies were contacted. The goal was to obtain inspection data from at least 10 inspectors deploying the conventional UT inspection method.

Company	NDI Method	Number of Inspectors
TPI	Conventional Pulse Echo Ultrasonics	5
Force Technology	Conventional Pulse Echo Ultrasonics	1
Vestas	Conventional Pulse Echo Ultrasonics	*
Siemens	Conventional Pulse Echo Ultrasonics	2
Blade Dynamics	Conventional Pulse Echo Ultrasonics	1 *
Sandia Labs	Conventional Pulse Echo Ultrasonics	2
LM-Wind Power	Phased Array Ultrasonics (Omniscan, Hand Scanned)	3
Force Technology	Phased Array Ultrasonics (P-Scan Device)	3
Siemens	Phased Array Ultrasonics (P-Scan Device)	4
Olympus	Phased Array Ultrasonics (Omniscan with Scanner)	*
Sonatest	Phased Array Ultrasonics (RapidScan Rolling Wheel)	*
Sandia Labs	Phased Array Ultrasonics (MAUS Scanner)	*
Sandia Labs	Single Element UT with Custom Focus Probe Scanner	*
GE	Phased Array Ultrasonics (RotoArray Rolling Wheel)	*
Iowa State Univ	Terahertz	*
LTI	Shearography	1
Thermal Wave Imaging	Thermography	1
Siemens	Thermography (FLIR XX6540 SC IR Camera)	1

* Initial experiment, or additional testing, in planning stage

Table 4-1: List of Participants in the Wind Blade Flaw Detection Experiment

There were some excellent benefits provided to the wind blade manufacturing plant participants. First, all inspectors were provided with feedback on their individual performance. This includes their POD levels overall and broken down by various design features and by different areas of the blades. Inspectors are provided with information on the number of flaws detected, the number of flaws missed, the number of false calls, flaw sizing capability and the location and type of flaws missed. Each participant also gained valuable experience regarding the implementation of their inspection method/device on representative wind turbine blades. Additional interactions were used to assist inspectors with improving any deficiencies noted or in improving issues such as deployment of equipment set-up. In addition, when several inspectors from the same company participate in the experiment, we provide the company with an overall assessment of its Quality Assurance process and NDI practices.

The WBFDE was applied to 12 wind blade inspectors deploying conventional inspection methods (pulse-echo UT with single-element transducers and A-scan data only) five advanced NDI methods including: three phased array ultrasonic systems, the MAUS scanner system with a focused transducer and thermography. Chapter 5 describes the basic physics of each inspection method while Chapter 7 presents the associated inspection results from the WBFDE along with some final assessments of the inspection methods. Figure 4-4 shows some of the organizations that participated in the WBFDE experiment. All results obtained from this experiment are presented in this report.

Figure 4-4: Participants in Sandia Labs Wind Blade Flaw Detection POD Experiment

THIS PAGE INTENTIONALLY LEFT BLANK

CHAPTER 5

5.0 Description of NDI Methods Applied to WINDIE Experiment

5.1 Pulse-Echo Single-Element and Phased/Linear Array Ultrasonics

Conventional ultrasonic transducers for NDI commonly consists of either a single active element that both generates and receives high frequency sound waves, or two paired elements, one for transmitting and one for receiving. Phased array probes, on the other hand, typically consist of a transducer assembly with 16 to as many as 256 small individual elements that can each be pulsed separately. A phased array system will also include a sophisticated computer-based instrument that is capable of driving the multi-element probe, receiving and digitizing the returning echoes, and plotting that echo information in various standard formats. Unlike conventional flaw detectors, phased array systems can sweep a sound beam through a range of refracted angles or along a linear path, or dynamically focus at a number of different depths, thus increasing both flexibility and capability in inspection setups.

In Pulse-Echo Ultrasonic (PE UT) inspections, short bursts of high frequency sound waves are introduced into materials for the detection of surface and subsurface flaws in the material. Ultrasonic test equipment usually operates in the range of 200KHz to 25 MHz. The speed with which the sound waves travel through a material is dependent on the composition and density of the material. The sound waves travel through the material with some attendant loss of energy (attenuation) and are reflected at interfaces. The reflected beam is displayed and then analyzed to define the presence and location of flaws. Ultrasonic inspection methods currently provide the best option for inspecting wind blades due to its exceptional depth of penetration, signal resolution and wide variation in deployment options. This chapter describes the customized UT inspection methods and hardware that were developed and deployed by Sandia Labs to optimize wind blade NDI.

A-Scan Mode - Ultrasonic testing involves one or more of the following measurements: time of wave transit (or delay), path length, frequency, phase angle, amplitude, impedance, and angle of wave deflection (reflection and refraction). In conventional Pulse-Echo Ultrasonics (PE UT), pulses of high frequency sound waves are introduced into a structure being inspected. A-Scan signals represent the response of the stress waves, in amplitude and time, as they travel through the material. As the waves interact with defects or flaw interfaces within the solid and portions of the pulse's energy are reflected back to the transducer, the flaws are detected, amplified and displayed. The interaction of the ultrasonic waves with defects and the resulting time vs. amplitude signal produced depends on the wave mode, its frequency and the material properties of the structure. Flaw size can be estimated by comparing the amplitude of a discontinuity signal with that of a signal from a discontinuity of known size and shape. Flaw location (depth) is determined from the position of the flaw echo along a calibrated time base. In the pitch-catch UT method, one transducer introduces a pressure wave into the specimen and a second transducer detects the transmitted wave. A complex wave front is generated internally in the material as a result of velocity characteristics, acoustical impedance, and thickness. The time and amount of energy is affected by the changes in material properties, such as thickness,

disbonds, and discontinuities. The mechanical vibration (ultrasound) is introduced into the specimen through a couplant and travels by wave motion through the specimen at the velocity of sound. If the pulses encounter a reflecting surface, some or all of the energy is reflected and monitored by the transducer. The reflected beam, or echo, can be created by any normal or abnormal (flaw) interface. Complete reflection, partial reflection, scattering, or other detectable effects on the ultrasonic waves can be used as the basis of flaw detection.

In most pulse-echo systems, a single transducer acts alternately as the sending and receiving transducer. If the pulses encounter a reflecting surface, some or all of the energy is reflected and monitored by the transducer. Figure 5-1 shows a schematic of the pulse-echo technique. It shows the interaction of UT waves with various interfaces within a structure and the corresponding A-scan waveforms that are displayed on an ultrasonic inspection instrument. Complete reflection, partial reflection, scattering, or other detectable effect on the ultrasonic waves can be used as the basis of flaw detection. In addition to wave reflection, other variations in the wave that can be monitored include: time of transit through the test piece, attenuation, and features of the spectral response [5.1, 5.2]. The degree of reflection depends largely on the physical state of the materials forming the interface. Cracks, delaminations, shrinkage cavities, pores, disbonds, and other discontinuities that produce reflective interfaces can be detected.

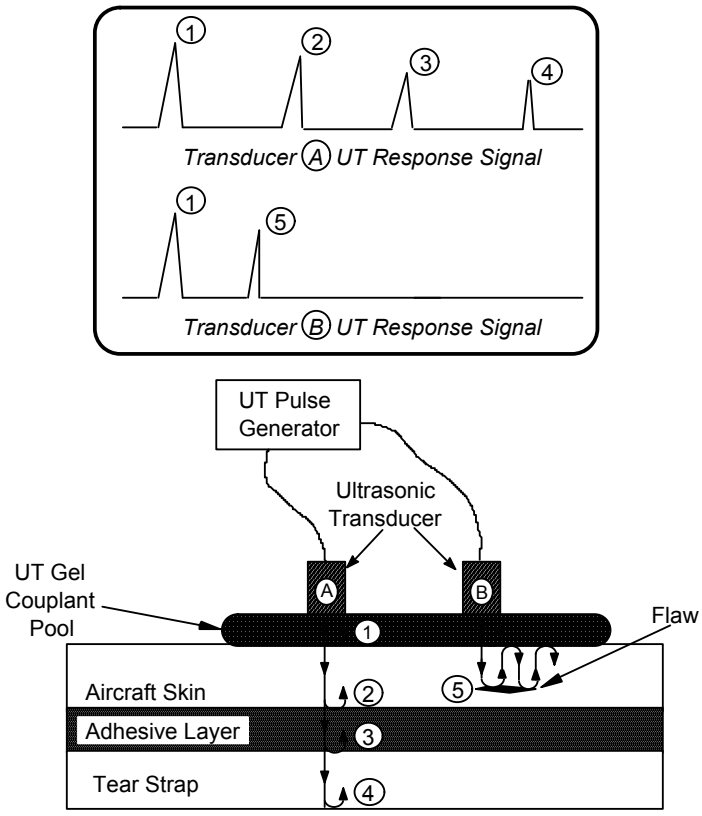

Figure 5-1: Schematic of Pulse-Echo Ultrasonic Inspection and A-Scan Signal Showing Reflection of UT Waves at Assorted Interfaces

C-Scan Mode: Use of UT Scanning Technology - It is sometimes difficult to clearly identify flaws using ultrasonic A-Scan signals alone. Small porosity pockets commonly found in composites, coupled with signal fluctuations caused by material nonuniformities can create signal interpretation difficulties. Significant improvements in disbond and delamination detection can be achieved by taking the A-scan signals and transforming them into a single C-scan image of the part being inspected. C-scans are two-dimensional images (area maps) produced by digitizing the point-by-point signal variations of an interrogating sensor while it is scanned over a surface. A computer converts the point-by-point data into a color representation and displays it at the appropriate point in an image. Specific "gates" can be set within the data acquisition software to focus on response signals from particular regions within the structure. C-scan area views provide the inspector with easier-to-use and more reliable data with which to recognize flaw patterns. This format provides a quantitative display of signal amplitudes or time-of-flight data obtained over an area. The X-Y position of flaws can be mapped and time-of-flight data can be converted and displayed by image processing-equipment to provide an indication of flaw depth. A variety of PC-based manual and automated scanning devices can provide position information with digitized ultrasonic signals [5.3].

In the basic C-scan system, shown schematically in Figure 5-2, the scanning unit containing the transducer is moved over the surface of the test piece using a search pattern of closely spaced parallel lines. A mechanical linkage connects the scanning unit to X-axis and Y-axis position indicators which feed position data to the computer. The echo signal is recorded, versus its X-Y position on the test piece, and a color coded image is produced from the relative characteristics of the sum total of signals received. A photograph of an automated (motorized) scanner, the Boeing MAUS system, inspecting an aircraft fuselage section is shown in Figure 5-3. The entire ultrasonic C-Scan device is attached to the structure using suction cups connected to a vacuum pump. The unit is tethered to a remotely located computer for control and data acquisition. Figure 5-4 shows a comparison of A-scan signals, from damaged and undamaged portions of a composite structure that were produced by the pulse-echo ultrasonic inspection method. Note the clear reflection peak produced by uninterrupted signal travel to the back wall in the "undamaged" A-scan signal. Compare this to the A-scan signal from the "damaged" region where the amplitude of the back wall signal is decreased and a new intermediate peak (reflection) is observed. Both of these A-scan changes indicate the presence of damage or other anomaly.

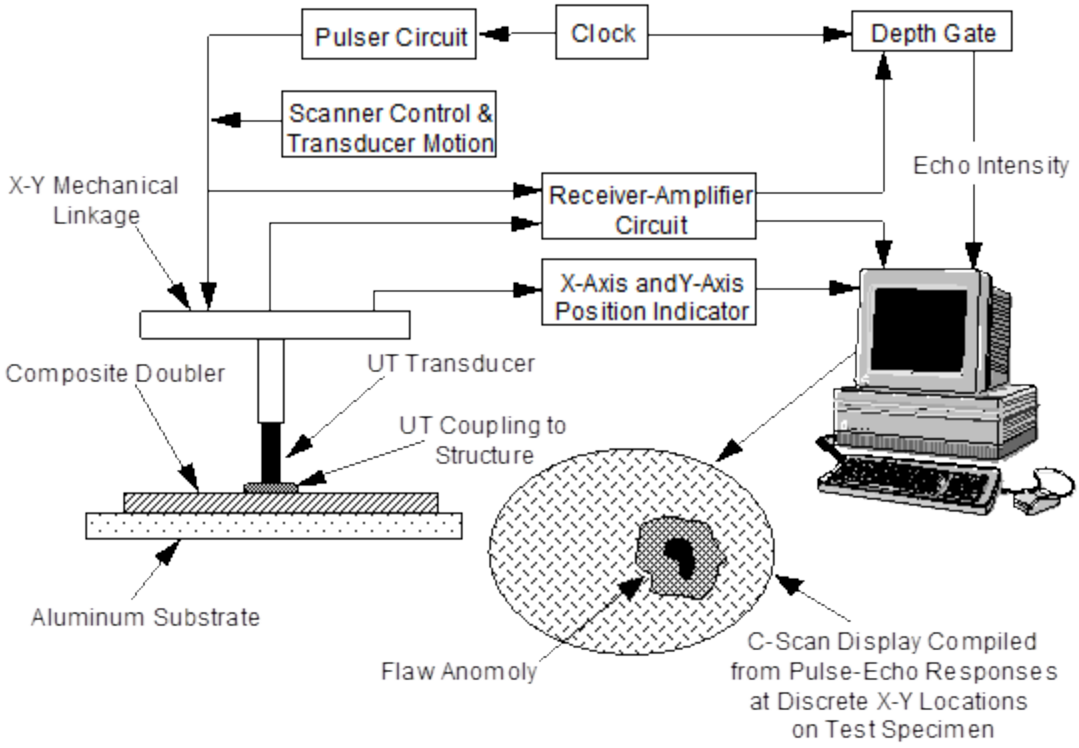

Figure 5-2: Schematic of C-Scan Setup for Pulse-Echo Ultrasonic Inspection

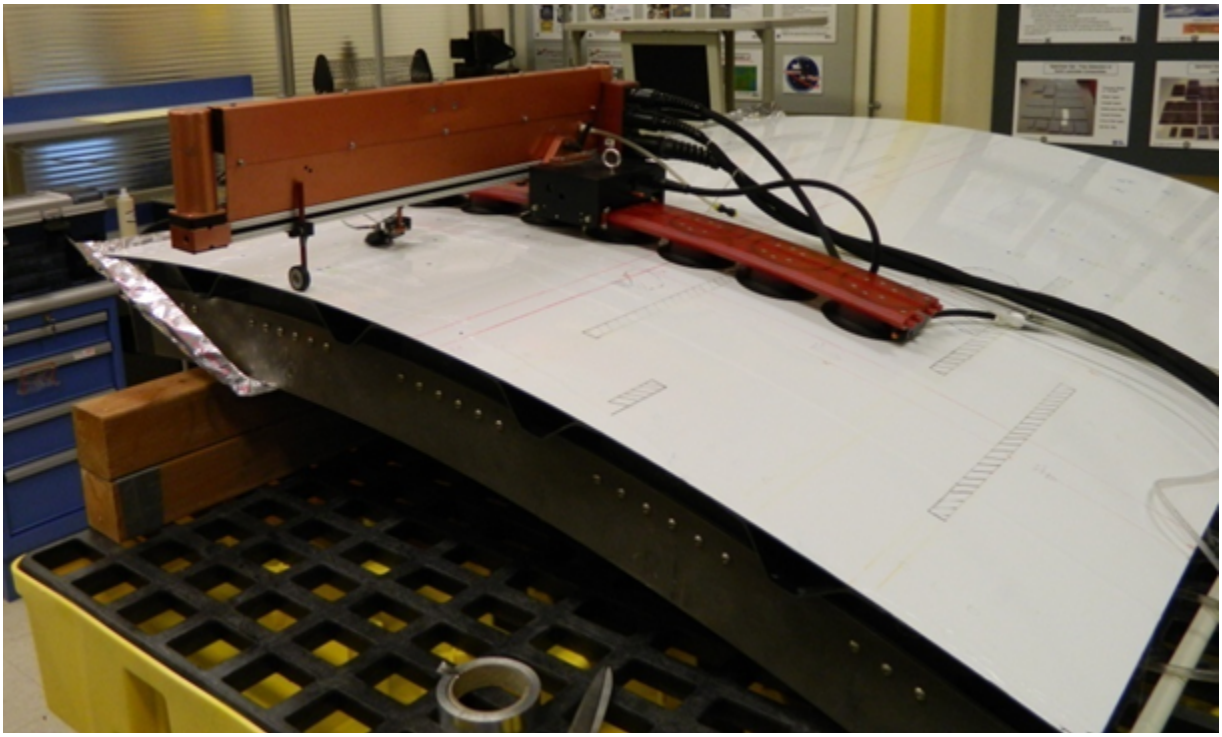

Figure 5-3: MAUS Automated Ultrasonic Scanning System

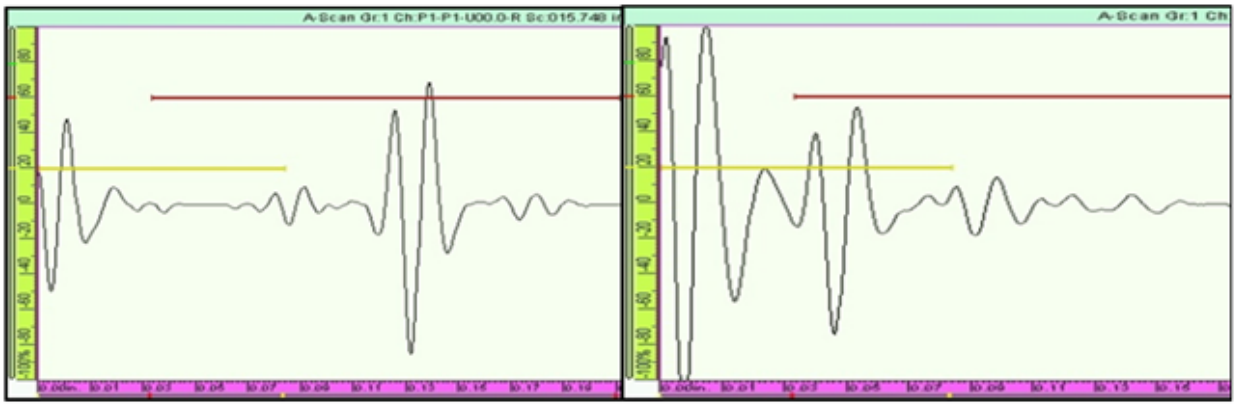

Figure 5-4: Sample Ultrasonic Signals Generated from: a) Structure Without Damage and b) Structure With Damage

Figure 5-5 shows a sample C-scan image (based on amplitude) from a pulse-echo UT inspection of a composite fuselage structure containing stringers and frame shear ties. Dark spots and irregularly-shaped regions of nonuniform color indicate the presence of impact damage in this panel. The value of using two-dimensional color coding, stemming from the sum total of the A-scan signals, to identify and size composite flaws is evident in this C-scan image. The discussion below describes the use of both A-scan and C-scan data to inspect wind turbine blades.

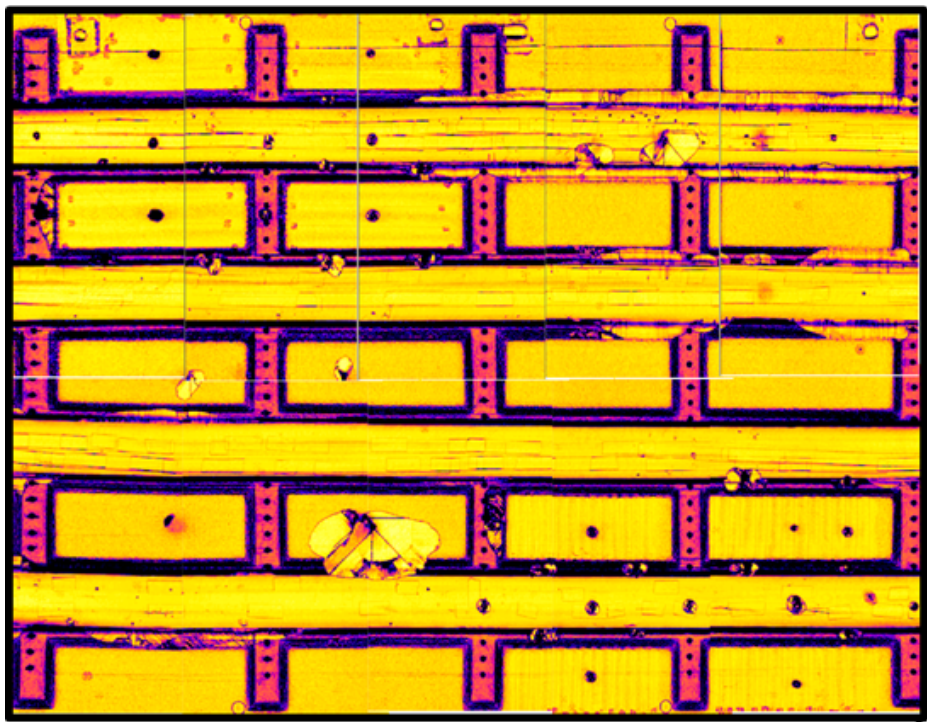

Figure 5-5: Sample C-Scan produced by an Automated Ultrasonic Scanning Device

Phased Array Ultrasonics (PA-UT) involves the use of multiple signals from a contained series of transducers (phased arrays) to produce diagnostic images in the form of ultrasonic C-scans. Conventional ultrasonic transducers for NDI commonly consist of either a single active element that both generates and receives high frequency sound waves, or two paired elements, one for transmitting and one for receiving. Phased array probes, on the other hand, typically consist of a transducer assembly with 16 to as many as 256 small individual elements that can each be pulsed separately. A phased array system will also include a sophisticated computer-based instrument that is capable of driving the multi-element probe, receiving and digitizing the returning echoes, and plotting that echo information in various formats. Unlike conventional flaw detectors, phased array systems can sweep a sound beam through a range of refracted angles or along a linear path, or dynamically focus at a number of different depths, thus increasing both flexibility and capability in inspection setups.

PA-UT operation is similar to single-element UT transducers, however, the simultaneous use of multiple sensors allows for rapid coverage and two-dimensional images from which to assess structural integrity. A linear array of ultrasonic sensors is placed within a single, scanning probe. The width of the linear probe array determines the swath of the inspection "scan" as the probe is moved along the surface. A compression wave beam is electronically scanned along the array at pulse repetition frequencies in excess of 10 KHz. The response of each individual sensor is monitored and assessed using the ultrasonic wave analysis approaches described above. High speed pulsing combined with rapid data capture permits the array to be quickly moved over the structure. The individual responses from each UT sensor are integrated to produce a real-time, C-scan image of the covered area. An example of a linear array UT inspection device deployed

by Sonatest in a rolling wheel arrangement is shown in Figure 5-6. The physics of how the ultrasonic array works is depicted in Figure 5-7. By carefully controlling the generation of UT signals and data acquisition from select elements in a phased array, it is possible to produce customized focusing of the array to improve the sensitivity of the inspection. Electronic focusing permits optimizing the beam shape and size at the expected defect location, thus further optimizing probability of flaw detection. The ability to focus at multiple depths also improves flaw sizing of critical defects in volumetric inspections. Focusing can significantly improve signal-to-noise ratio in challenging applications, and electronic scanning across many groups of elements allows for C-Scan images to be produced very rapidly. The main difference between a phased array and a linear array is that linear arrays aren't capable of steering the sound beam at different angles or focusing the beam. Thus, the sound waves stay parallel to each other regardless of the depth.

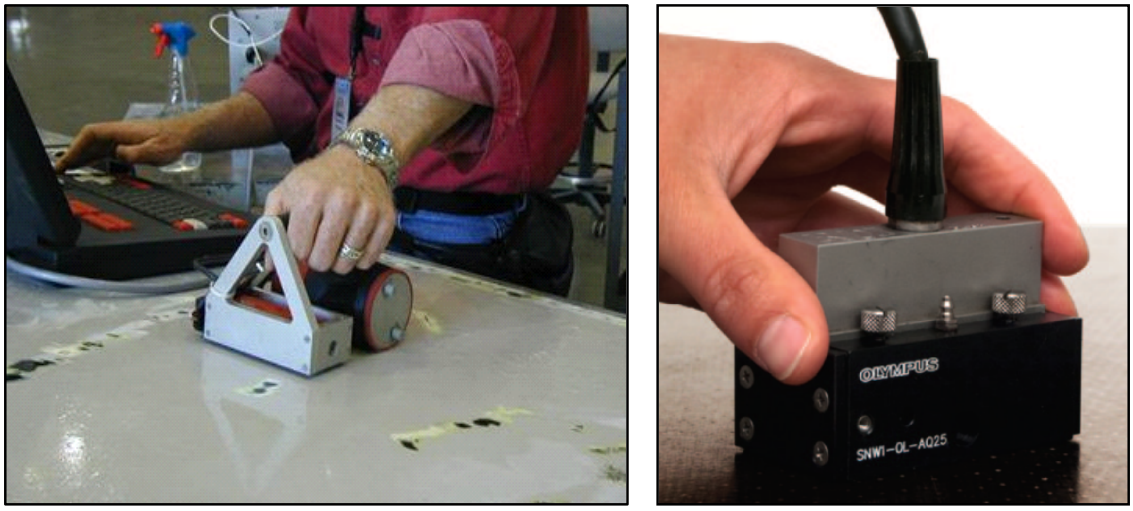

Figure 5-6: Phased Array UT Deployed in Rolling Wheel Mechanism (left) and Contained in a Single Probe Housing (right)

Associated with this effort, a series of new and unique phased array probe housings were designed and fabricated to improve field deployment. The custom probe housing facilitates phased array inspections through a wide range of material thicknesses, adjusts for slight contours, maximizes UT signal strength and makes deploying a phased array probe on blades more effective than conventional housings. Various probe offset designs (water column heights) were studied in order to eliminate the confounding effects of signal harmonics which are prevalent in thick composite structures.

To provide a baseline understanding of the current ultrasonic inspection method used in wind blades, Figure 5-8 and Figure 5-9 present some of the basic, building-block UT signals that are used to conduct the wind blade inspections. Figure 5-8 is a schematic of a bonded joint between a spar cap and a shear web flange. This particular bonded joint has some adhesive squeeze-out. Figure 5-8 also shows an ultrasonic transducer moving over four different construction regions in a typical blade which includes: 1) the spar cap laminate alone, 2) the adhesive squeeze out

adjacent to the near side of the bonded shear web joint, 3) the adhesive thickness at the spar cap-to-shear web joint, and 4) the adhesive squeeze out adjacent to the far side of the bonded shear web joint.

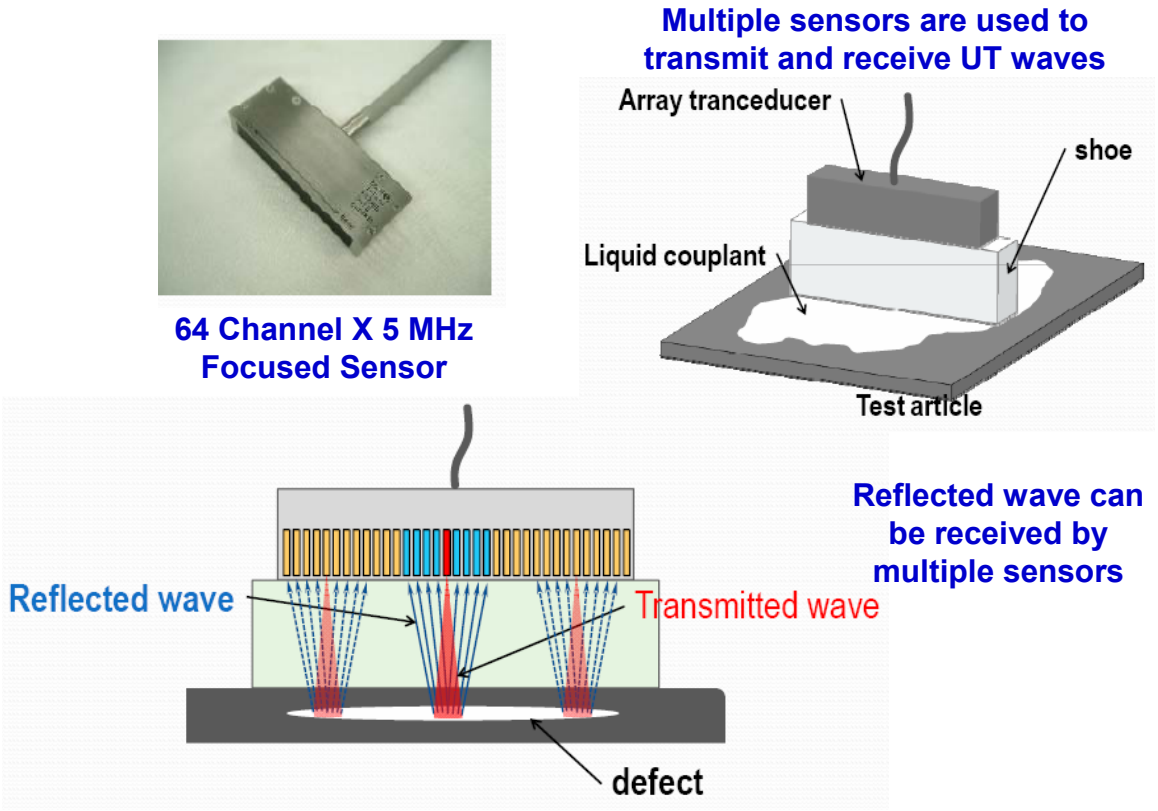

Figure 5-7: Schematic Showing the Operation of an Ultrasonic Array – Contains Multiple UT Elements in a Single Transducer Which Allows for the Generation and Acquisition of Multiple UT Signals

Figure 5-8 also depicts a scenario where the adhesive paste bulges out and can be detected using ultrasonics. It also shows the UT A-scan signals that are produced when a transducer is placed over various regions of the bond line. These distinct signals can be used to detect the presence of the desired adhesive bond width. The resulting, expected A-scan signals that are generated at each of these points are also shown to demonstrate critical signal interpretation needs. In addition, gate settings can be selected based on these desired signals such that deviations from the norm can be detected and imaged in UT C-scans. Many of the existing, routine inspections tend to focus on the upper and lower portions of the bond line and use the presence of adhesive squeeze-out to infer a successful bonded joint. Figure 5-9 provides another example of UT signals generated from different depths of penetration in the blade structure. Several different phased array UT devices will now be described in order to introduce some different deployment approaches which may lend themselves quite well to wind blade inspections.

Olympus OmniScan Phased Array UT System - The OmniScan device, shown in Figure 5-10, is manufactured by Olympus. The one-line scan capability of the OmniScan allows inspectors to collect data in one axis and visualize it using the top view. This feature is easy to set up and allows the data to be played back after the acquisition for offline analysis and reporting. Data can be encoder- or time-based and phased array images can be displayed in real time. Transducers are available with up to 128 elements. The OmniScan device can be operated in manual mode or can be connected to an X-Y scanner to automate the inspection of large areas. The hardware and equipment set-up used for the OmniScan phased array UT inspections were:

- 1.5 MHz, 42 and 64 element phased array probes
- Custom ABWX1935 water fed housing (multiple housing used for full experiment)
- OmniScan MX2 unit (module 16/128)
- Software MXU 3.0R2
- Mini-wheel encoder and X-Y glider (manual X-Y scanner)
- CFU-05 water pump
- Probes/Wedges: Three probe and wedge combinations were used with the majority of the tests performed with the two large aperture combinations. The 25 mm water column (WC) shoe used a contained water column to provide the UT coupling between the probe and the part. The contact wedge used a solid block of an impedance-matching plastic material with a thin film of base water to provide the offset and coupling to the part. The Aqualene wedge used a delay line block made from Aqualene along with a wetted surface to provide the offset and coupling to the part. The details of these shoe designs are discussed in Chapter 4.

Figure 5-11 and Figure 5-12 show the OmniScan equipment set-up and deployment for phased array UT inspections of wind blade specimens while Figure 5-12 and Figure 5-13 highlight the various features of the UT transducers and the shoes or wedges used to optimize the NDI signals. Ultrasonic phased array technology, along with the widely adaptable range of probe housings and deployment options were shown to have strong flaw detection capabilities in multiple wind turbine blade structures. These include both thin and thick fiberglass spar cap laminates and bond line interfaces. Figure 5-14 and Figure 5-15 show sample results produced by the OmniScan from the inspection of carbon laminate test specimens that contain engineered flaws. Damage in the parts are shown in the photos and schematics while the accompanying C-scan images show the ability of the inspection method and equipment to detect the flaws.

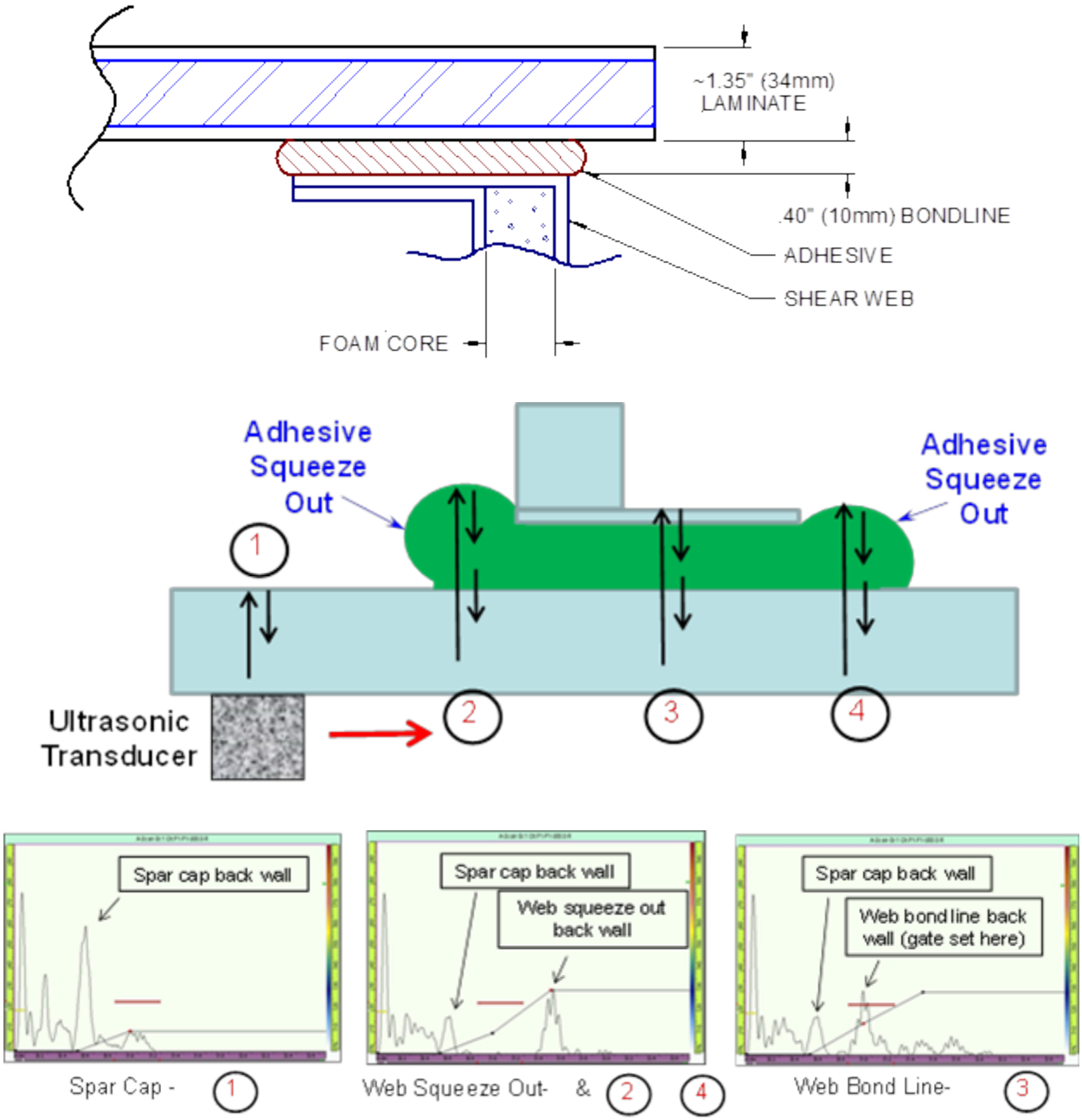

Figure 5-8: Typical Bond Joint Configuration Used in NDI Feedback and NDI Reference Standard Specimens

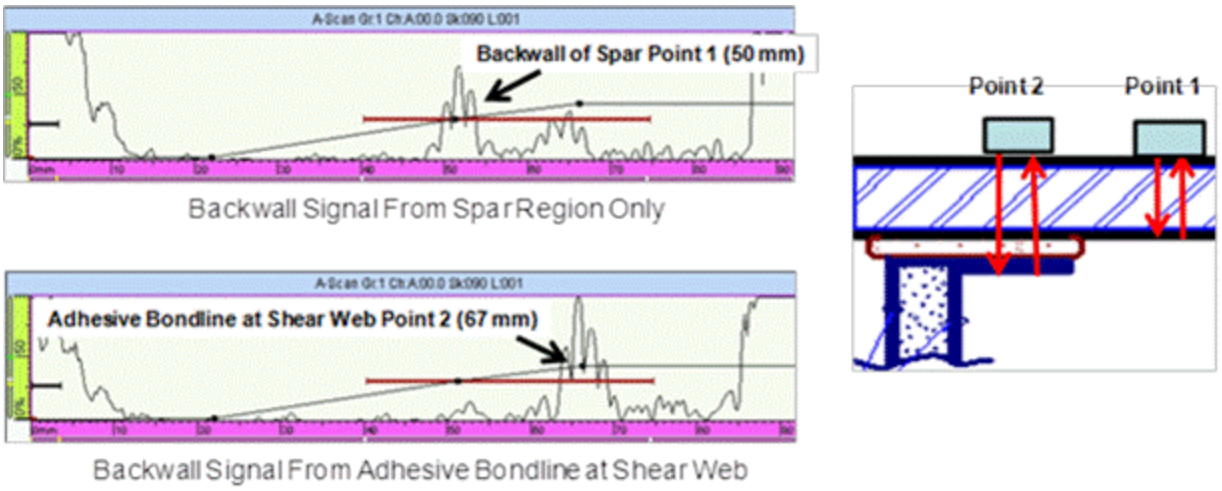

Figure 5-9: Schematic of Two Different Depth of Penetration Regions in a Blade and the Resulting A-scan Signals Generated for Each Thickness

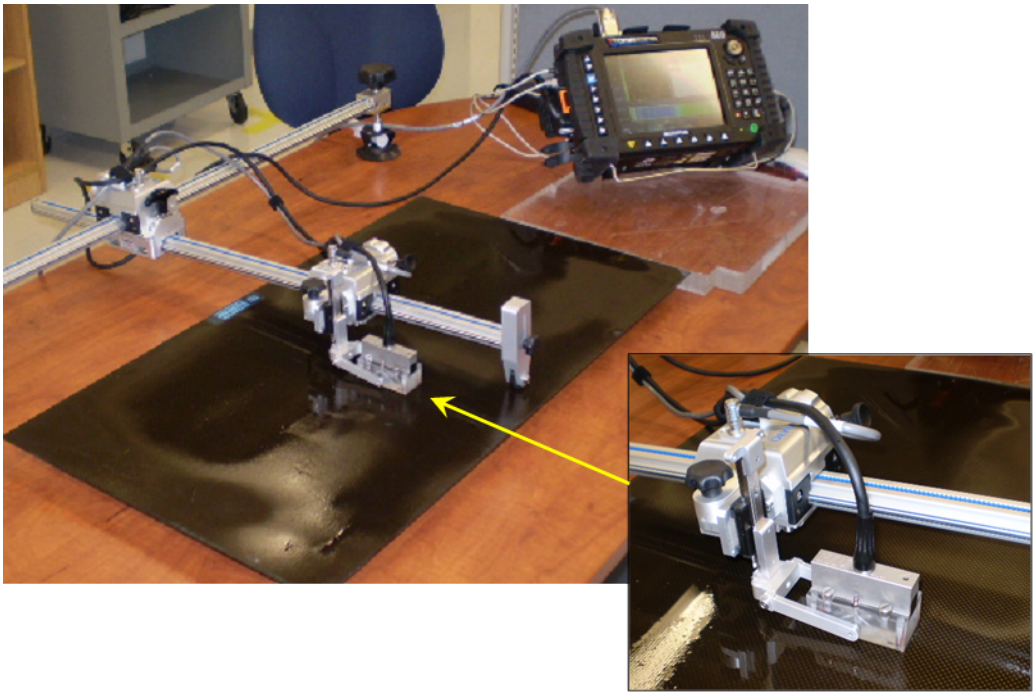

Figure 5-10: Olympus OmniScan Device with a 16:128 Phased Array Module

Figure 5-11: Phased Array Ultrasonics Inspection with OmniScan System

Figure 5-12: Phased Array Probes and OmniScan Deployment on Wind Blade NDI Specimens

	Configuration 1 Large aperture	Configuration 2 Large Aperture	Configuration 3 Small Aperture
Probe	1.5L42 (XAAB-10011)	1.5L42 (XAAB-10118)	1.5L64-I4
Wedge	25mm water column (ABWX1875)	Contact wedge (ABWX1935)	Aqualene wedge (SNW1-0L-AQ25)

	Configuration 1	Configuration 2	Configuration 3
Probe Name	1.5L42	1.5L42	1.5L64-I4
Part #	XAAB-10118	XAAB-10011	1.5L64-I4
Housing	Custom	Custom	I4
Frequency	1.5MHz	1.5MHz	1.5MHz
Number of elements	42	42	64
Pitch	2.8mm	2.8mm	1mm
Elevation	26mm	26mm	7mm
		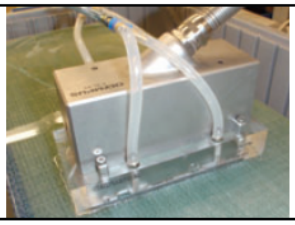	

Figure 5-13: Summary of Prototype Phased Array Probes and Wedges Used with the OmniScan Device to Conduct the Phased Array UT Inspections

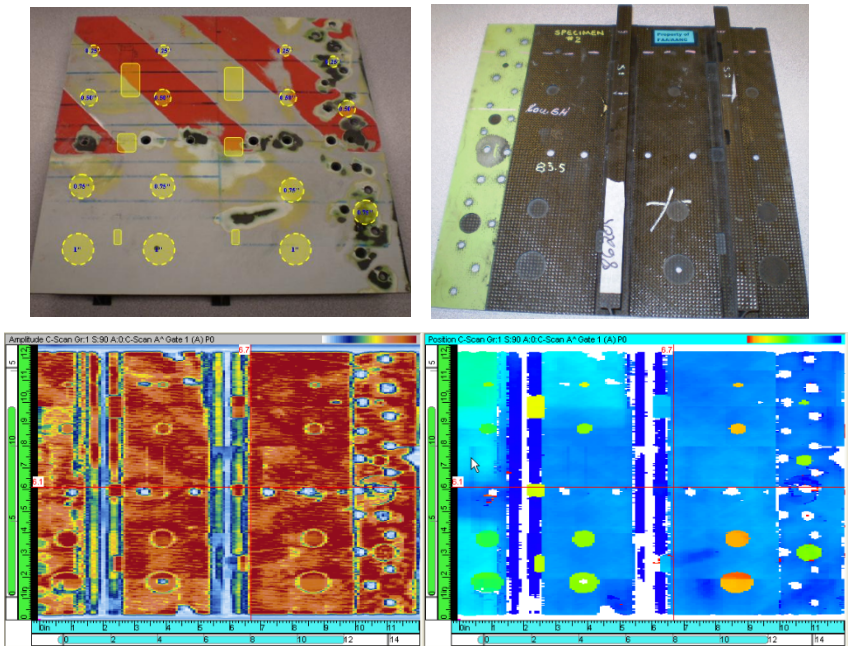

Figure 5-14: Amplitude (right) and Time of Flight (left) Data Produced by OmniScan Inspection of Composite Laminate Aircraft Panel with Flaw Profile as Shown

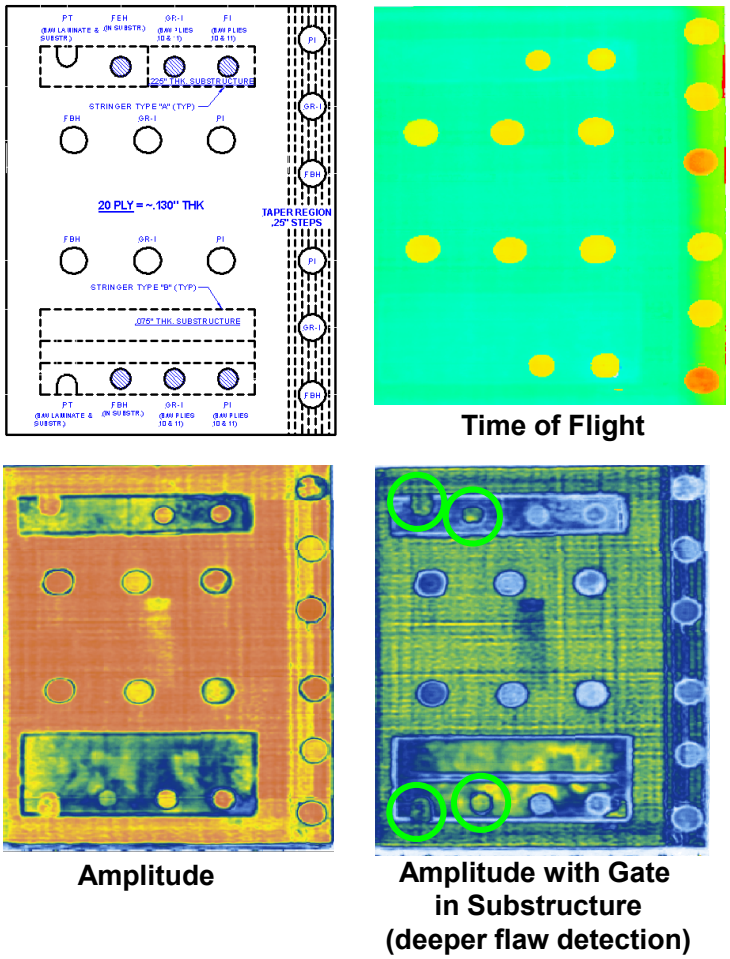

Figure 5-15: C-Scan Images Produced by OmniScan Phased Array UT Inspection of 20 Ply Composite Laminate Feedback Panel with the Flaw Profile as Shown

Sample Inspection Results Demonstrating Capabilities of Phased Array UT – This section presents results from OmniScan PA-UT inspections conducted on several Sandia specimens from the Wind Blade Test Specimen Library. Figure 5-16 and Figure 5-17 show the details of an adhesive step wedge that includes a section with adhesive of different thicknesses and a section where the stepped adhesive is bonded to a composite laminate (spar cap). This is an example of a specimen produced to study specific capabilities of NDI methods. Inspections of this specimen allow for the assessment of the ability of NDI to quantify adhesive thickness which would allow it to determine if an adhesive layer is outside of a required thickness range (i.e. too thick or too thin). Figure 5-18 shows two different characterizations of this NDI test specimen. The upper graph plots the UT velocity of the material. It is fairly consistent across the various thicknesses which ensures that the adhesive properties are consistent. The lower graph plots the signal attenuation through the various thicknesses. As expected, the relationship between the bond line thickness and the associated attenuation level is linear.

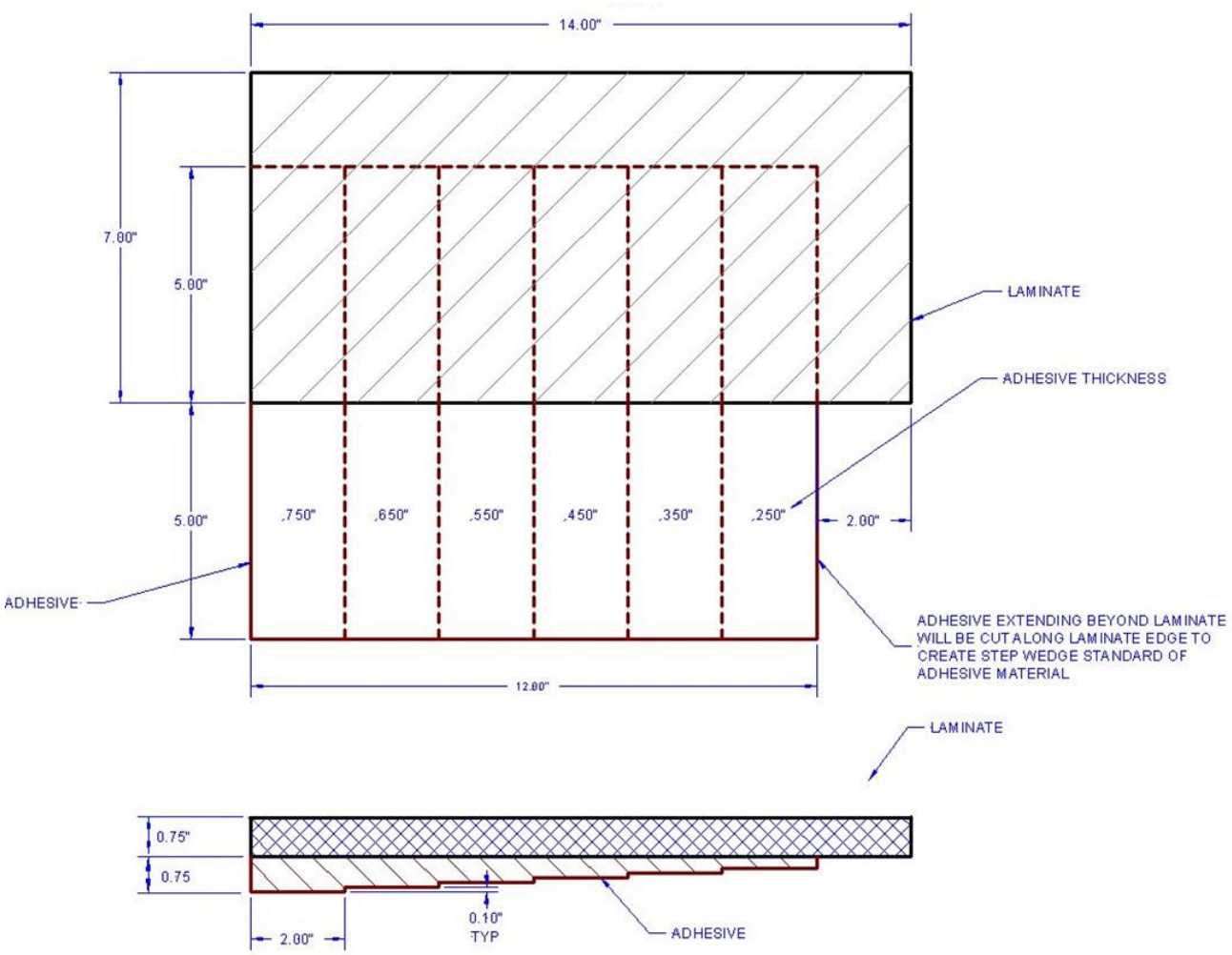

Figure 5-16: Adhesive Step Wedge NDI Reference Standard - Schematic

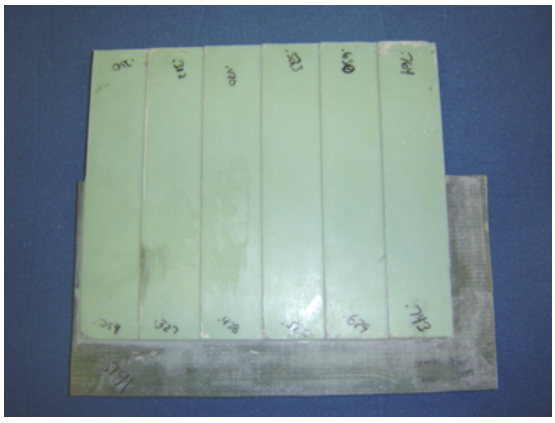

Bottom View

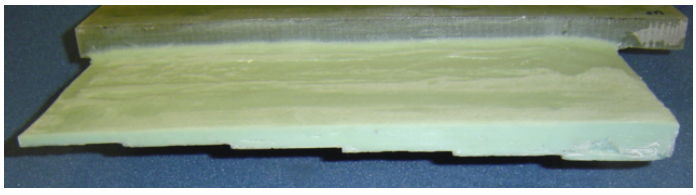

Side-Adhesive Area

Figure 5-17: Adhesive Step Wedge NDI Reference Standard

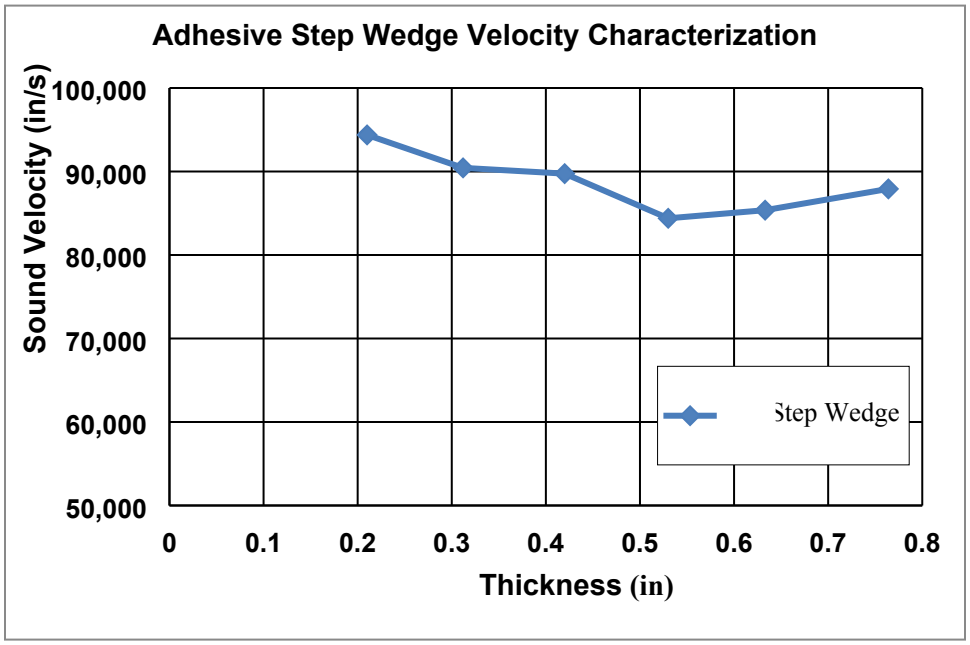

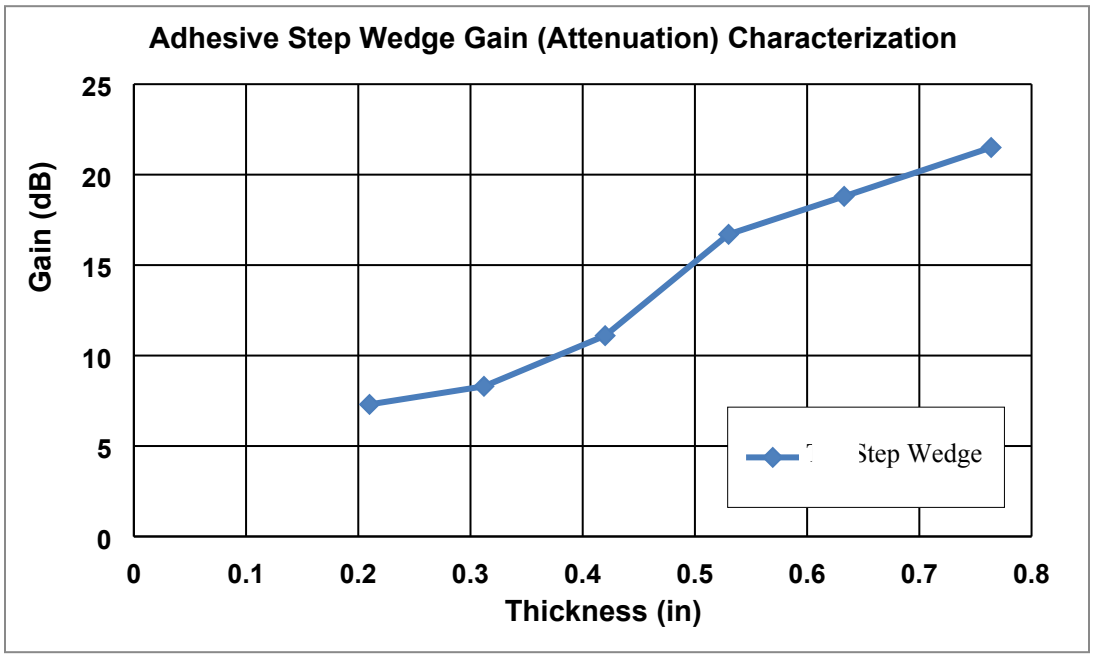

Figure 5-18: Pulse-Echo Ultrasonic Wave Velocity and Attenuation Results Showing Consistency of Adhesive Step Wedge and Linear Relationship Between Bond Line Thickness and Attenuation

Figure 5-19 and Figure 5-20 show a phased array UT inspection deployment and the resulting C-scan image of the various specimen thicknesses. The results show that this inspection method

is able to differentiate the various adhesive thicknesses even when inspecting through a thick spar cap laminate. Each bond line thickness is assigned a color code that can then be calibrated to a specific thickness or tight thickness range. Figure 5-21 shows the results from a single element UT inspection of this same specimen. Again, it was possible to differentiate the various adhesive thicknesses and each bond line thickness is assigned a color code in the C-scan that is related to an adhesive tight thickness range. Figure 5-22 shows the set of A-scan signals generated at each thickness step and the associated shift in the back wall peaks which allow the thickness to be determined.

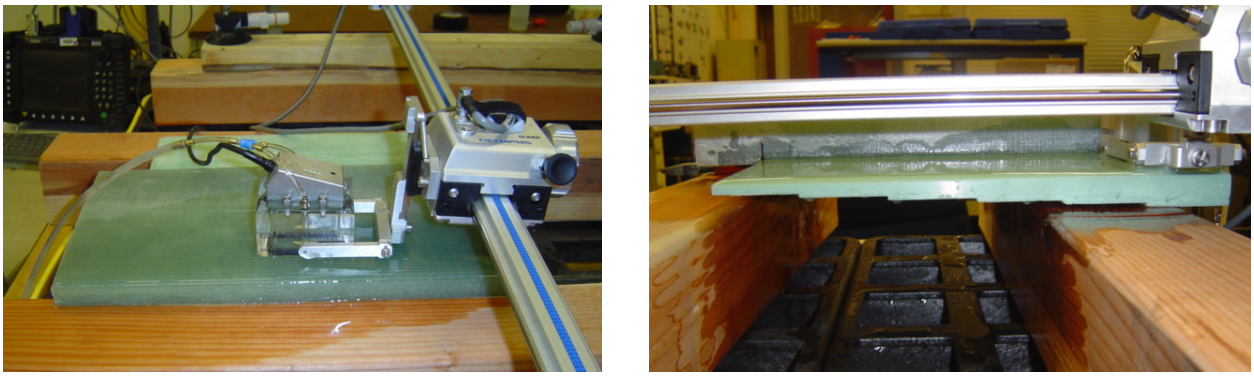

Figure 5-19: Phased Array PE-UT Inspection of Fiberglass Step Wedge Bond Line Specimen Using 1.5 MHz, 16 Element Array and a 40 mm Thick Open Water Box Shoe

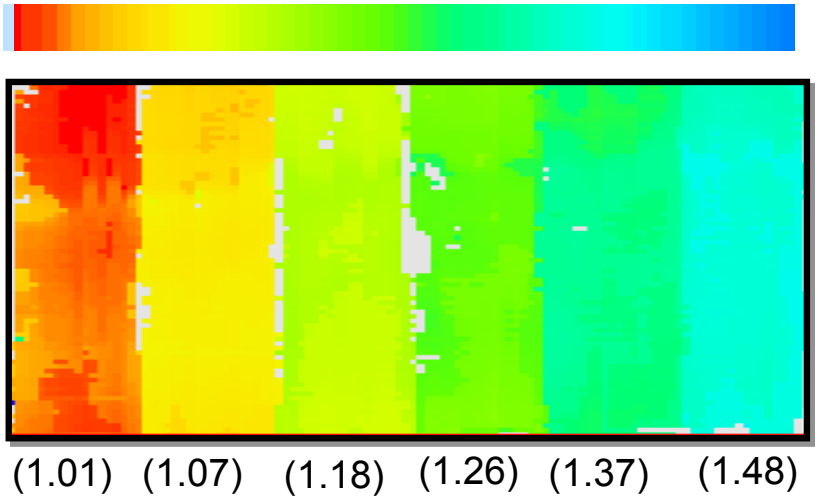

Figure 5-20: Color Coded Time-of Flight C-scan Generated by Phased Array PE-UT Inspection of Fiberglass Step Wedge Bond (OmniScan system with 1.5 MHz phased array probe and 40 mm thick shoe) – Shows Ability of UT to Differentiate the Various Bond Line Thicknesses Beneath the Laminate (labeled below each color segment)

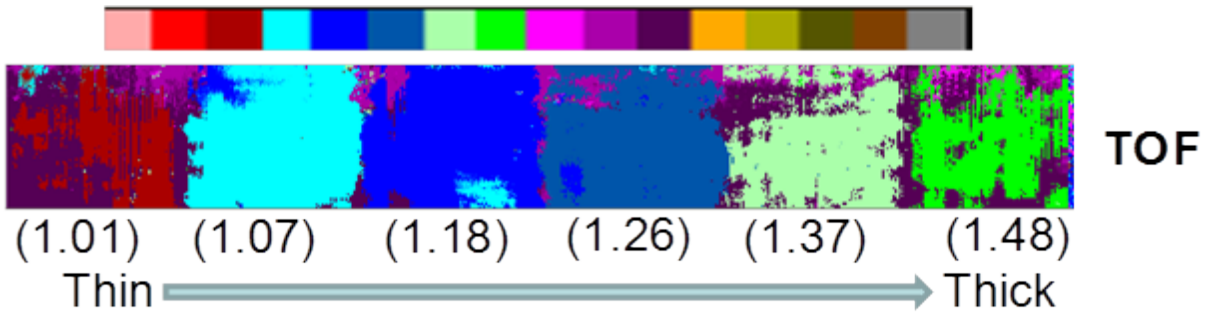

Figure 5-21: Color Coded Time-of Flight C-scan Generated by Pulse Echo UT (MAUS V system with 1 MHz contact probe) – Shows Ability of UT to Differentiate the Various Bond Line Thicknesses Beneath the Laminate (labeled below each color segment)

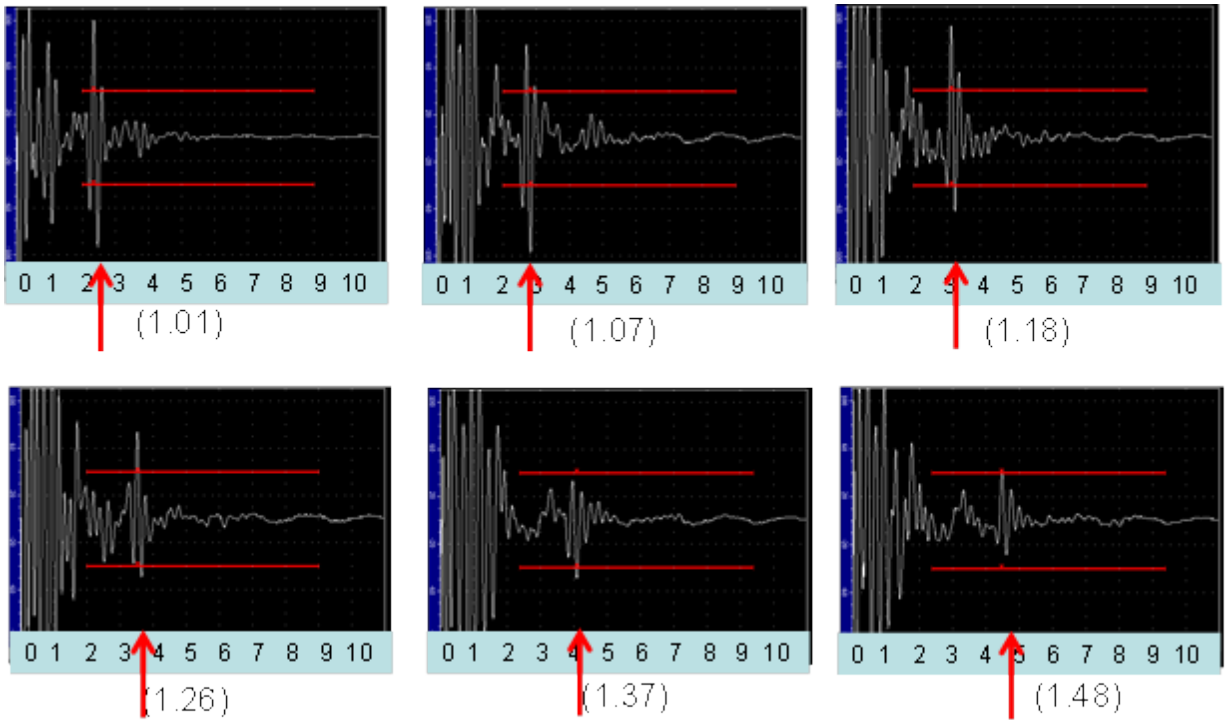

Figure 5-22: A-scan Amplitude Plots Generated by Pulse-Echo UT (MAUS V system with 1 MHz contact probe) – Shows Amplitude Decrease and Time to Back Wall Increase (indicated by red arrow) as Bond Line Thickness Increases

As part of the WBFDE, the OmniScan completed inspections on the NDI Feedback Specimens. Figure 5-23 through Figure 5-25 show the PA-UT results for wind specimen REF-STD-2-127-173-SNL-1 (see Figure 3-41 for design drawing). The 25 mm water column on the OmniScan PA-UT device (1.5L42 probe) provided good coupling to the specimen and the needed offset (delay line) to avoid the interference of the harmonic signals. Thus, the 25 mm water column

allows for inspecting the adhesive joint on this specimen (between the spar and adhesive and between adhesive and shear web). Flat bottom holes in spar cap laminate were detected at the various depths and the flat bottom holes in the bonded shear web joint were also detected. It appears that all sizes of the flat bottom holes were detected (difficult to see 75% FBH – 1.0" diameter in bonded shear web joint). Pull tab flaws in laminate at 25% depth and at 75% depth were detected. The pull tabs in the shear web bonded joint, both at the upper and lower adhesive interface, were detected. Figure 5-23 shows the amplitude and B-scan (flaw depth) images produced by a back wall gate ranging from 0.4" to 1.6" in depth. Figure 5-25 shows how the various gate settings can focus the inspections to detect flaws at various depths. The back wall gating worked well for inspecting the laminate for delamination flaws. Alternative gating can be used to specifically look at the adhesive joint. Most indications within the laminate showed up relatively well including the 0.50" diameter FBHs and pillow inserts, especially when gating the off of the back wall of the laminate.

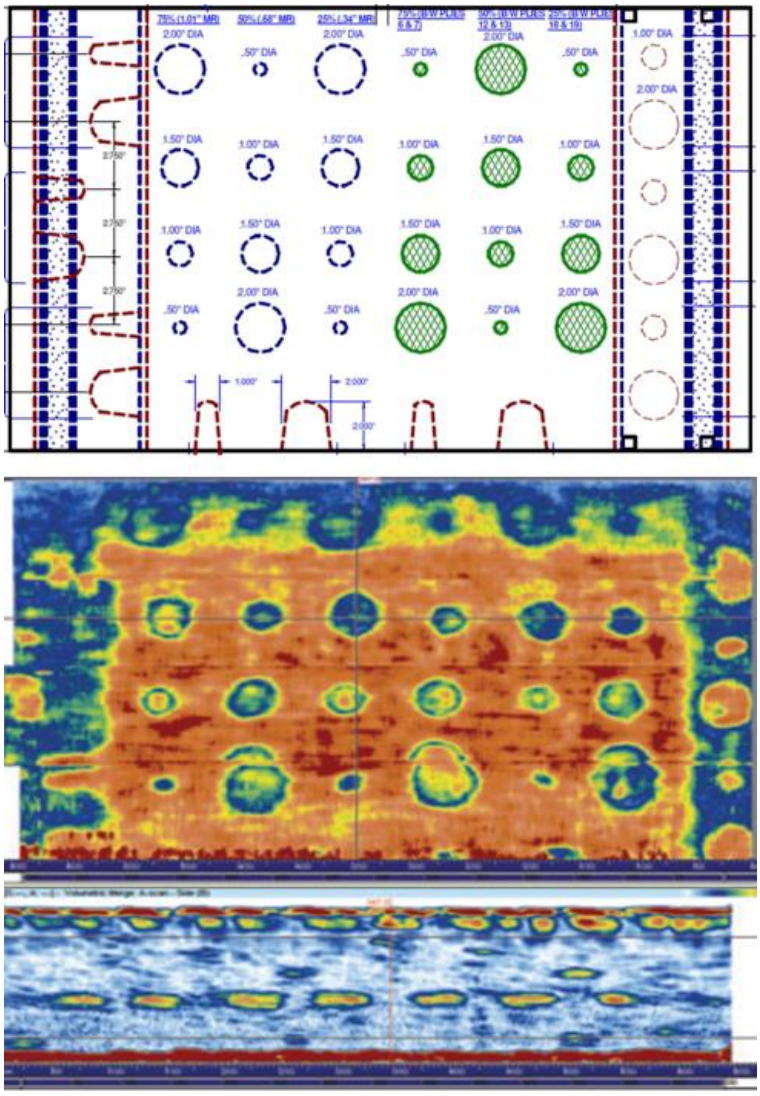

Figure 5-23: OmniScan PA-UT C-Scan of REF-STD-2-127-173-SNL-1 Produced by the 25 mm Water Column Shoe

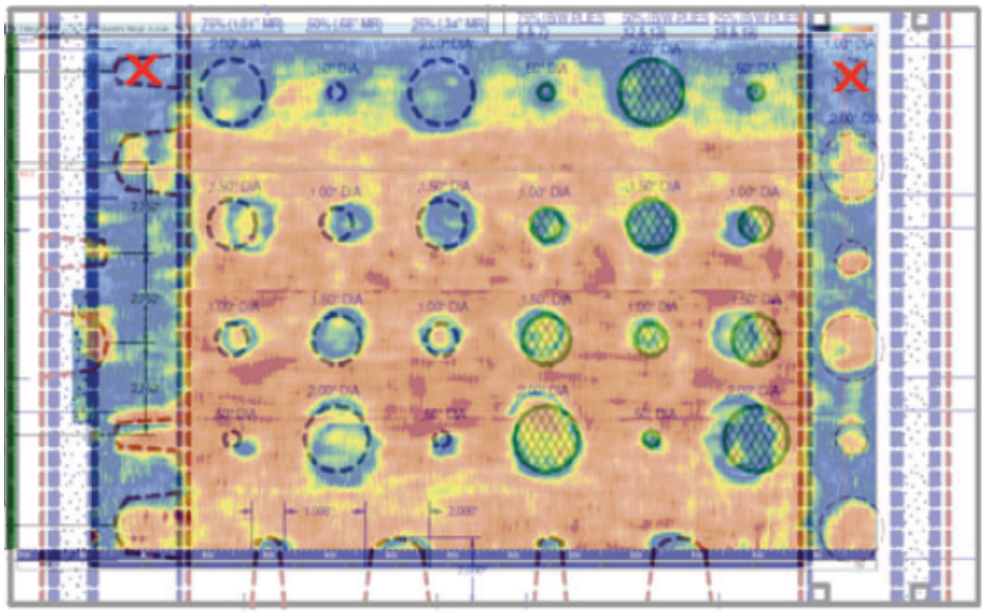

Figure 5-24: Overlay of Flaw profile with PA-UT Image Showing the Two Small Flaws Not Detected by the OmniScan Inspection (Water Column Shoe)

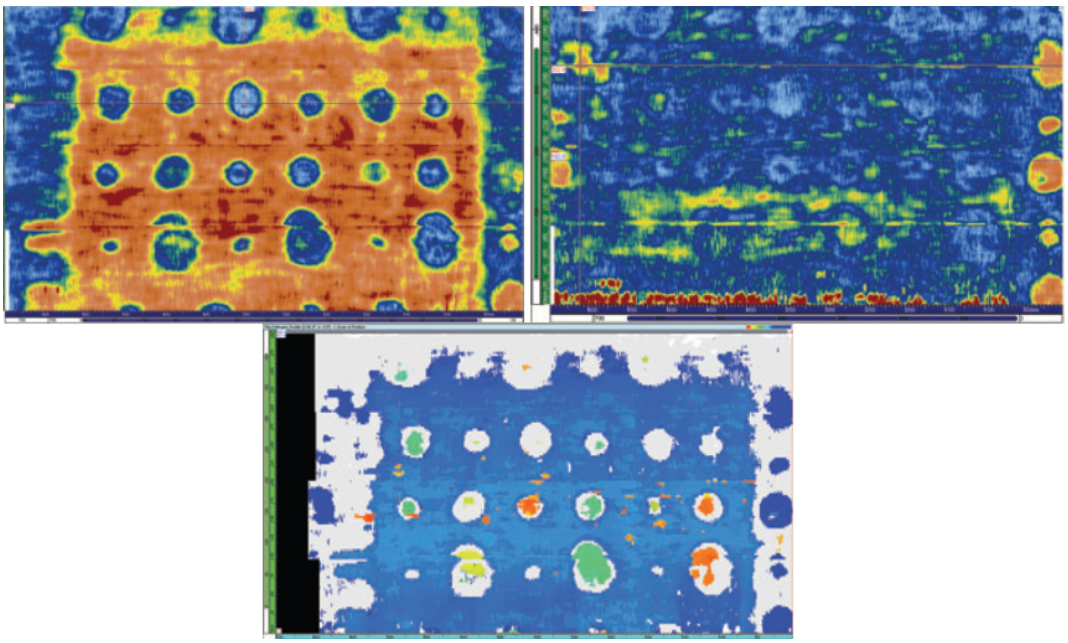

Figure 5-25: OmniScan PA-UT C-Scans of REF-STD-2-127-173-SNL-1 – Gate Set on Back Wall Only (top left), Gate Set Between Back Wall (1.3”) and Wedge Reflection Echo (1.7” depth) (top right) and Time-of-Flight Image (bottom)

The OmniScan PA-UT system was also applied to wind specimen REF-STD-5-154-SNL-1. Specimen REF-STD-5-154-SNL-1 is a sample dedicated to inspecting the adhesive joint between the spar cap and the adhesive. All of the flaws are located at this junction. Figure 7-58 shows the PA-UT inspection results. All flaw types – Pillow Inserts, microballoons and Pull Tabs – were detected. Only the smallest flaws of each type (0.5" or smaller) along the left hand side were not adequately detected. It is assumed that this is due to the very large probe elevation that is not optimal for these flaws.

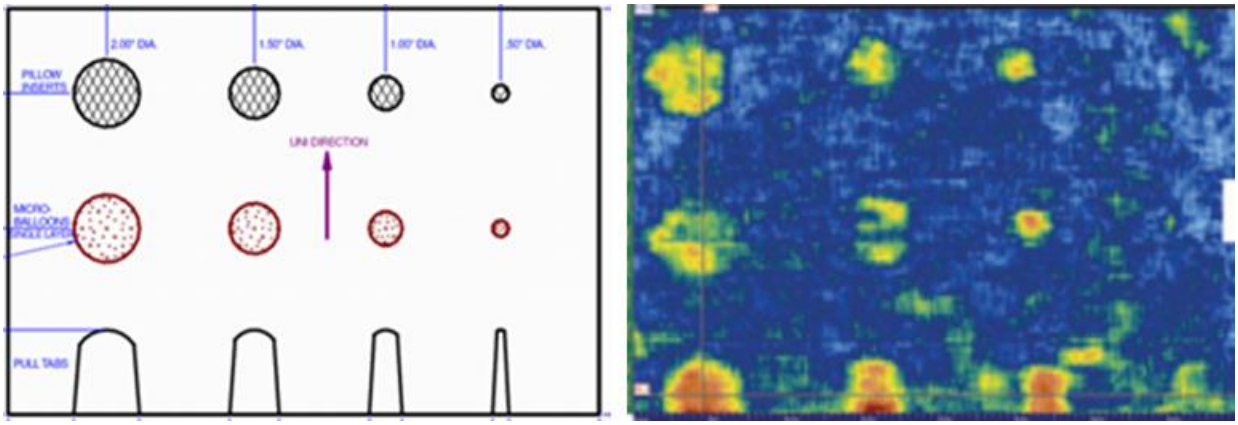

Figure 5-26: OmniScan PA-UT C-Scan of REF-STD-5-154-SNL-1 Produced by the 25 mm Water Column Shoe

Sonatest RapidScan 2 - The RapidScan rolling array WheelProbe was developed by Sonatest and provides a capability for A, B and C-scan inspections. It uses a novel, rubber-coupled sensor array that provides rapid, wide area C-scan data in the field. Powerful gating and evaluation tools are used to ensure proper analysis of the ultrasonic signals. RapidScan 2, shown in Figure 5-27, operates in a pulse-echo mode suitable for inspecting medium to large areas. A water film coupling that can be sprayed onto the inspection surface is used to transmit the UT pulse and return signals from the rolling wheel and back to the linear array transducer housed within the wheel. Multiple scan strips can be assembled to produce images of entire structures such as the horizontal stabilizer image shown in Figure 5-28. The high resolution C-scans, such as those in the examples of Figure 5-29 through Figure 5-31, show time of flight and amplitude data. Both A and B-scans can be simultaneously displayed. The system includes a 128-channel multiplexing pulser/receiver module; data capture electronics and a standard PC laptop, housed in a low-profile plastic enclosure for easy portability. Array WheelProbes incorporate a 64 element linear array (50mm) or 128 element linear array (100mm) with 0.8mm resolution, and a high resolution position encoder. The array WheelProbe provides high quality, high resolution data. Current array probes are available in 1, 2, 5, and 10 MHz to provide a range of resolutions and depth of penetration in thick and highly-attenuative structures.

Figure 5-27: RapidScan UT Rolling Wheel Array Device

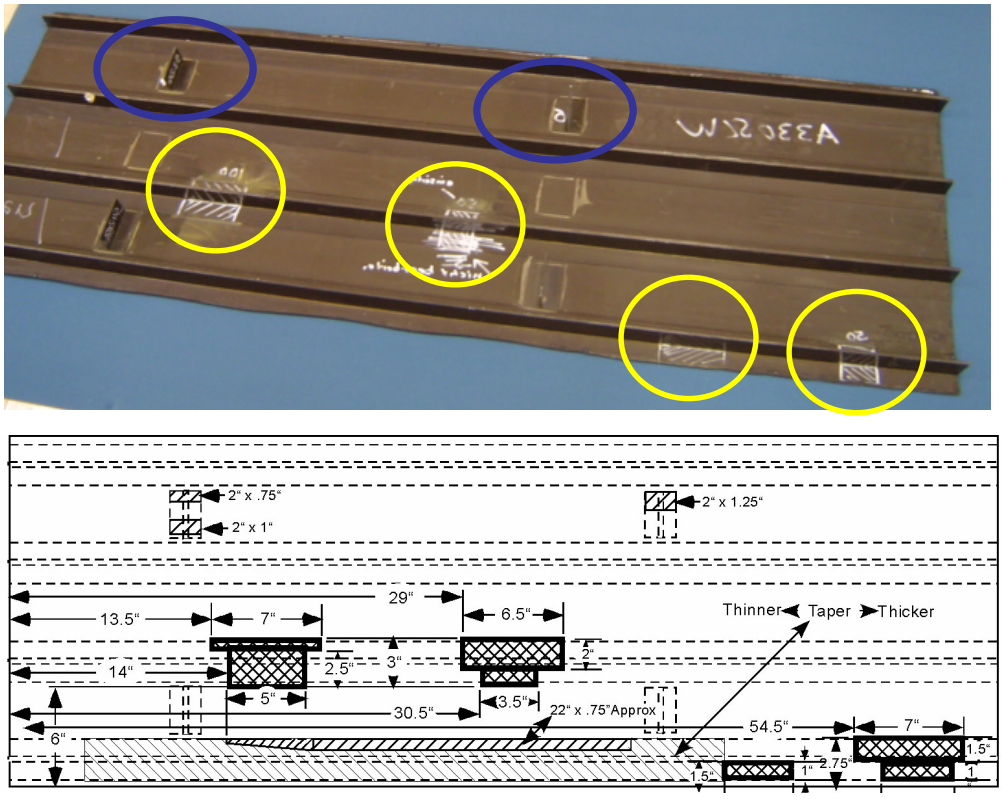

Figure 5-28: Carbon Composite Panel with Stringers, Ribs and Engineered Flaws Three stringer-to-skin disbonds (yellow) Two rib to-skin-partial disbonds (blue)

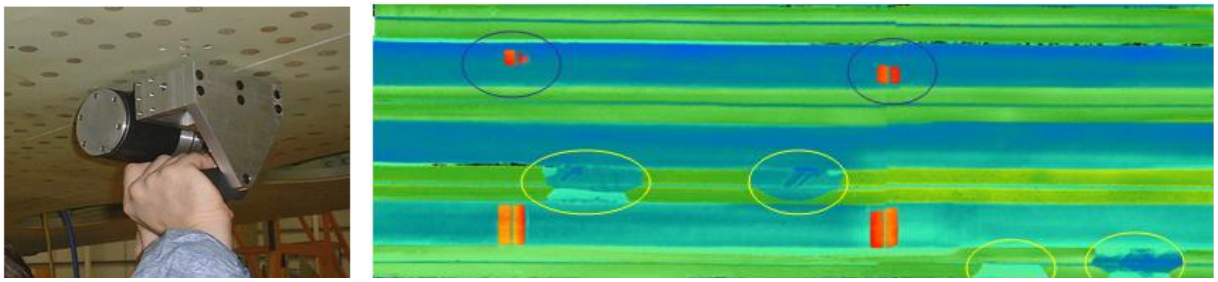

Figure 5-29: Inspection Scans of Composite Panel Produced by the RapidScan UT Array Device

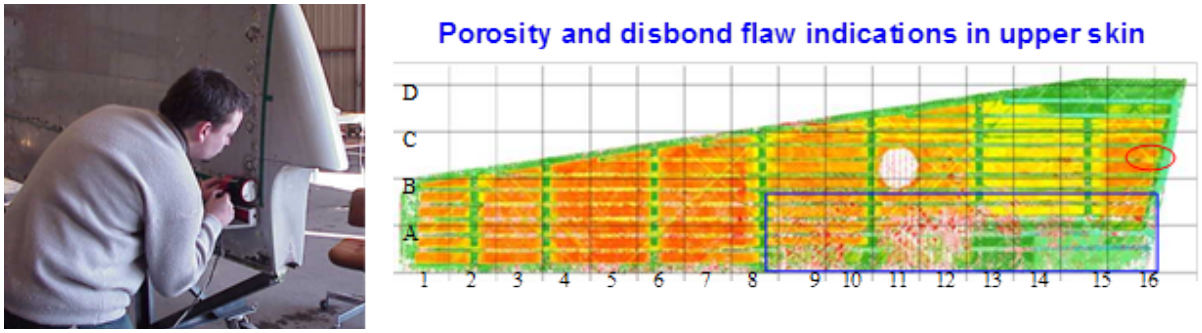

Figure 5-30: Scan of Composite Horizontal Stabilizer with Ultrasonic Rapidscan Array Probe

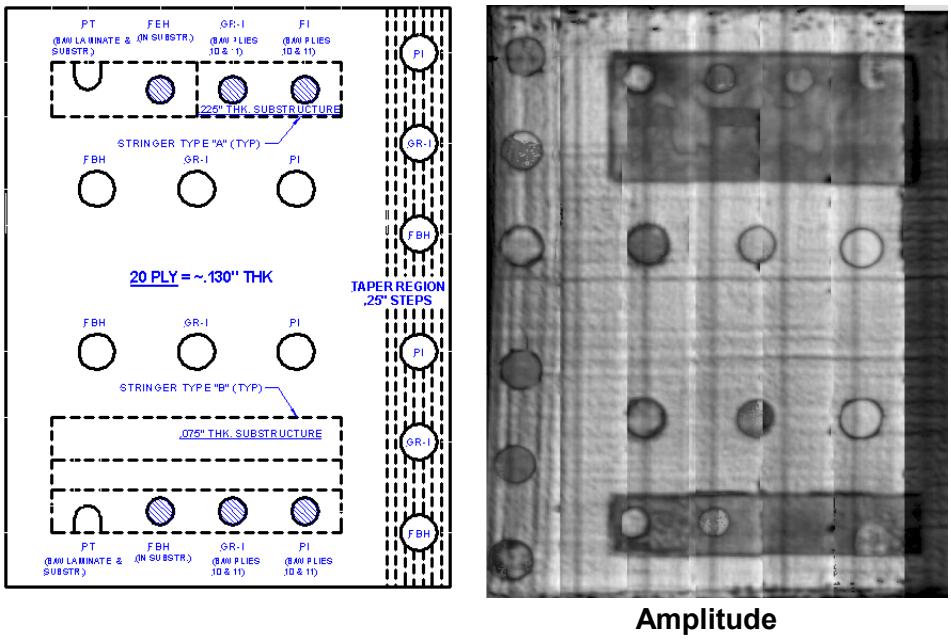

Figure 5-31: C-Scan Images Produced by Rapidscan Array WheelProbe on a20 Ply Composite Laminate Feedback Panel with the Flaw Profile as Shown

5.1.1 Optimization of Single Element Contact and Phased Array UT Using Deployment Aids

Sections 5.1.1 and 5.1.2 describe the array of custom hardware that can be added to the ultrasonic equipment and the unique data acquisition methods that were developed to optimize the ultrasonic inspection results. This hardware includes custom transducer shoes used to properly deploy the probe while producing the best UT coupling to the inspection surface and overcoming the inspection impediments. Inspection impediments include rough surfaces, curved surfaces and structure orientation. On the data acquisition side, a wide range of UT gate settings were studied to determine which ones were needed to identify the various flaw types and to determine which ones would produce the clearest C-scan images. All of the customized hardware is described here because it is important to understand the various hardware and data acquisition aspects of UT deployment and how they can affect the overall inspection performance. This will allow the reader to understand some of the differences in POD levels that were observed in the WBFDE study.

Enhanced hardware and data acquisition methods for both single-element and multi-element (Phased Array UT) transducers were developed in this NDI activity. Similar A-scan signals can be obtained from either transducer type, however, the single element transducer will acquire data from a narrow-width of the structure (like covering a surface with an artist's paint brush) while a phased array transducer will acquire data from a wider width of the structure that is determined by the number of elements in the array (like covering a surface using a house painter's brush). A schematic showing the make-up of the multiple UT elements in a phased array UT transducer is shown in Figure 5-7. Figure 5-32 and Figure 5-33 contain close-up photos of a phased array UT transducer, or probe.

The proper transmission of the UT signal into and out of the inspection part is critical to the performance of the inspection system. This section discusses the use of custom shoes mounted to the bottom of the UT transducers to optimize the signal strength and to control the signal travel such that key signals of interest are emphasized. The overall goal is to develop a sealed water path that produces a clear signal through a wide range of thicknesses (up to 2.5 inches) and curvatures. Figure 5-32 shows one of the shoes, or water boxes, that was tested in this program. In one version of this shoe, the water column is in an "open" water box configuration where it was not supported or contained. The open water box (i.e. no base – unsupported water column) experienced problems during deployment on representative blade structures. Loss of seal with the inspection surface was common and the coupling water column was lost during inspection. Oftentimes, a curved surface required a custom shoe contour. The use of a seal ring at the base of the box can help for thin seals (i.e. very gradual curve); however, the box cannot tolerate a thick foam seal at the base. Thick seals lead to uneven deployment of the transducer such that the transducer is not perpendicular to the surface and the resulting transmitted signals are dispersed rather than returned to the transducer. Finally, it is difficult to maintain a seal when deploying this set-up vertically. As a result, a second configuration was developed that used a gasket seal at the base of the shoe as shown in Figure 5-32. This set-up allowed for constant retention of the water column and better coupling of the UT signal with the part. So, the focus of this effort shifted to the use of a clear membrane at the base of the water box which seals against

the gasket labeled in the schematic. The end result is a fully-enclosed water column to optimize signal transmission.

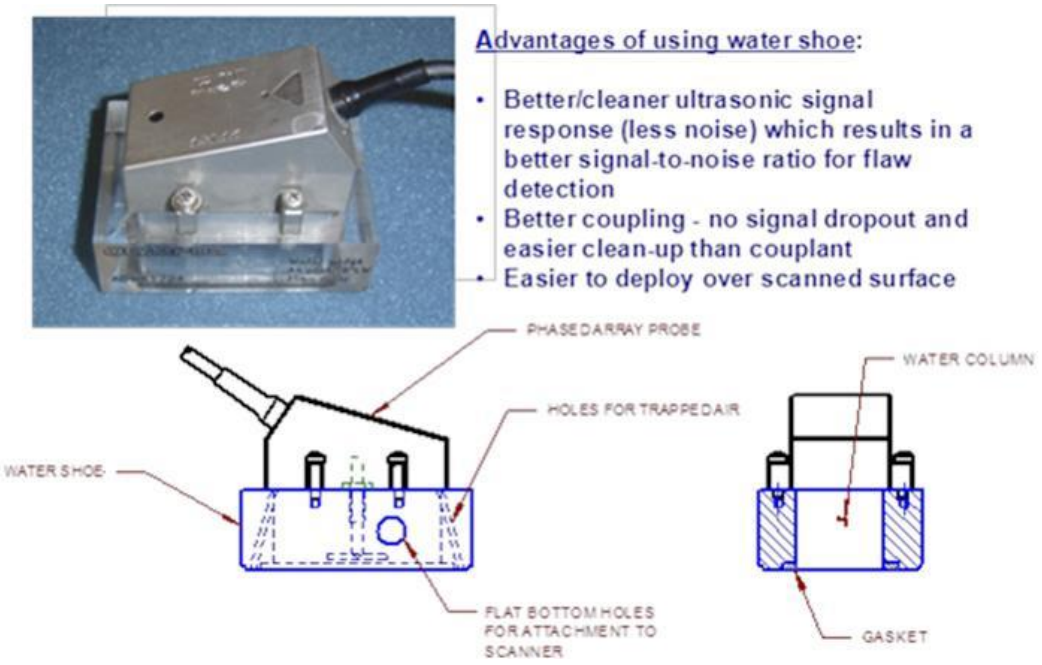

Figure 5-32: Use of Custom Water Shoe to Eliminate Inspection Impediments

Next, the height of the water box was adjusted. Figure 5-33 shows a phased array UT transducer with several different probe shoe configurations. These different configurations allowed the height of the water column to be adjusted. Further study revealed that the water column height is critical to accurate inspections in thick parts. Figure 5-33 also shows the use of an encoder to create a hand-held device that can produce a linear C-scan of the region covered by the rolling PA-UT transducer. Figure 5-34 shows the PA-UT transducer mounted in two different shoe thicknesses, a 25 mm and a 40 mm shoe. The schematic in Figure 5-32 shows the water column that is set up within the shoe in order to couple (transmit) the UT signal from the transducer to the inspection surface. The height of the water column is determined by the height of the shoe. Data acquisition from each of the different water shoes is shown in Figure 5-34. Note the use of time corrected gains to emphasize the specific signals of interest, in this case, the peak return from the back wall of the spar cap.

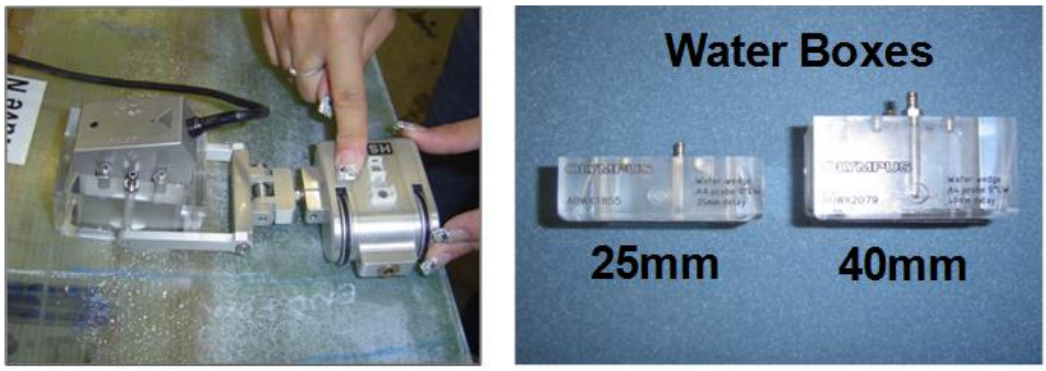

Figure 5-33: Integration of Linear Encoder with Phased Array UT Probe to Produce C-scans and Variation in Water Box Shoes Used to Overcome Signal Interference Issues

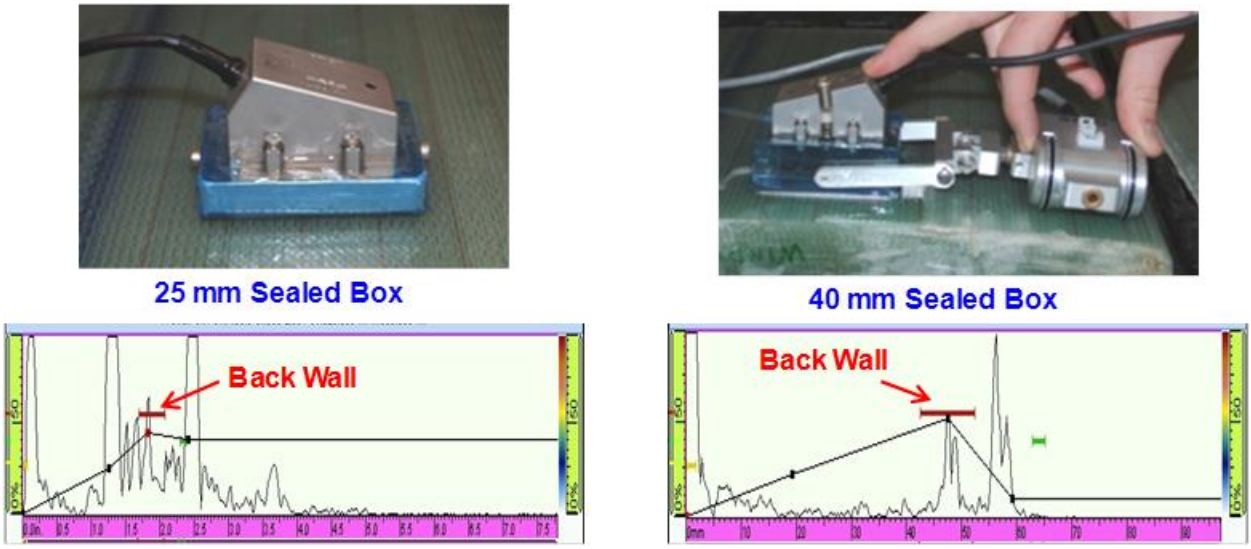

Figure 5-34: Design of Probe Housing to Acquire Optimized Signal and Use of Time Corrected Gain to Emphasize Signals in the Region of Interest

Multiple inspections using the "membrane" version of the shoe shown in Figure 5-32 were used to confirm the proper operation of the device. During these inspections, it was noticed that certain, expected signatures within the UT A-scan signal were absent. When analog signals are digitized and displayed there are harmonics that occur in the data acquisition process. These harmonics - the time position of which are determined by the thickness of the material being inspected – can sometimes appear within the area of interest for UT signal analysis. It was determined that when inspecting thick blades (on the order of 2" or greater), these harmonics appear at approximately the same time as the reflection of interest from the back wall of the spar cap. Figure 5-35 summarizes this issue along with the solution that Sandia Labs developed. The UT signal on the left was produced using the thinner, 25 mm thick water box. In this signal trace, the harmonic from the front surface UT wave interaction happens to appear at the same time as the back wall signal of interest. The back wall signal has a smaller amplitude and thus,

cannot be seen. The UT signal on the right was produced using the thicker, 40 mm thick water box. In this signal trace, the harmonic from the front surface UT wave interaction is moved further down the timeline and away from the back wall signal of interest. The back wall signal with its smaller amplitude can now be clearly seen and interrogated using the gate setting shown. This is a critical finding as it allowed the deeper flaws that were masked by this probe deployment impediment to be detected and accurately imaged. The use of a 40mm thick water box solves this inspection problem by moving the harmonic return signal further out in time, thus revealing the signal of interest.

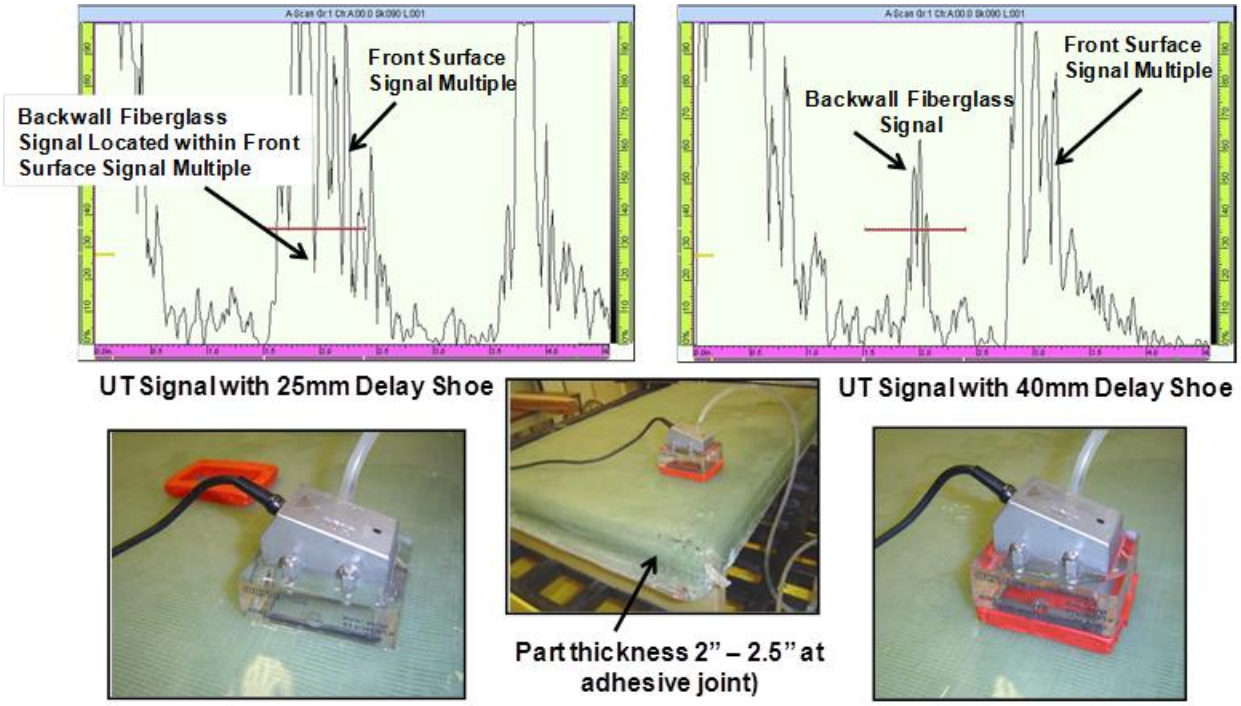

Figure 5-35: Signals Showing the Signal of Interest That is Hidden when Using the Thinner Water Box Shoe and the Ability of the Thicker Water Box Shoe to Properly Display the Signal of Interest in Thicker Composite Structures (1.5 MHz Phased Array UT Probe)

The water box signal analysis displayed in Figure 5-35 shows how the 25mm thick water box causes the back wall signal of interest to occur at the same time (be hidden by) the harmonic signals generated by the front wall reflections. It also shows how the 40mm thick water box allows the important signal of interest to be acquired. Figure 5-36 through Figure 5-38 show the successful results that were obtained using the thicker water box with the PA-UT inspection method. First, Figure 5-36 shows the use one of the NDI Reference Standards with flat bottom holes simulating damage at various depths. The C-scan image on the left shows how the flaws nearer to the surface were clearly imaged but the deeper flaws were somewhat masked by the presence of the harmonics as shown in Figure 5-35. However, the C-scan image on the right demonstrates how the deeper flaws can be imaged using the thicker water box shoe. Also note

that the background signals are more uniform so that the overall signal-to-noise levels are improved.

C-scan results from the 40 mm water box and PA-UT for the thicker NDI Feedback Specimen No. 6 (2" spar cap with a 2.5" total thickness at the adhesive joint) are presented in Figure **5-37**. Finally, a PA-UT inspection result from one of the thickest and most challenging test specimens in shown in Figure 5-38. The schematic shows the 2.65" thick joint (shear web adhesive and spar cap) and the engineered flaws that were placed at various depths in the test specimen. Note that the adhesive disbonds were placed in the near-side, between the spar cap and the adhesive layer, and the far-side, between the adhesive layer and the flange of the shear web. The latter location (upper left flaw), due to its very close proximity to the back wall of the entire assembly, is especially hard to detect and image. However, using the custom, enclosed water box, it was possible to obtain a clear C-scan image of all flaws throughout the test specimen. Even the subtle kissing disbonds, represented by the insertion of thin grease and mold release contaminants, were clearly imaged.

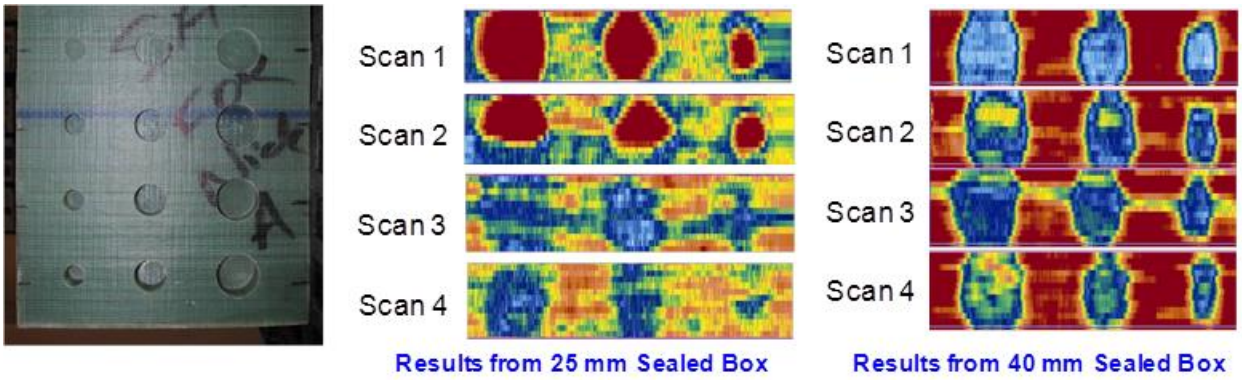

Figure 5-36: Photo of NDI Test Specimen and UT C-Scan Inspection Images Showing Greater Clarity Achieved Using a 40 mm Transducer Shoe (Delay Line)

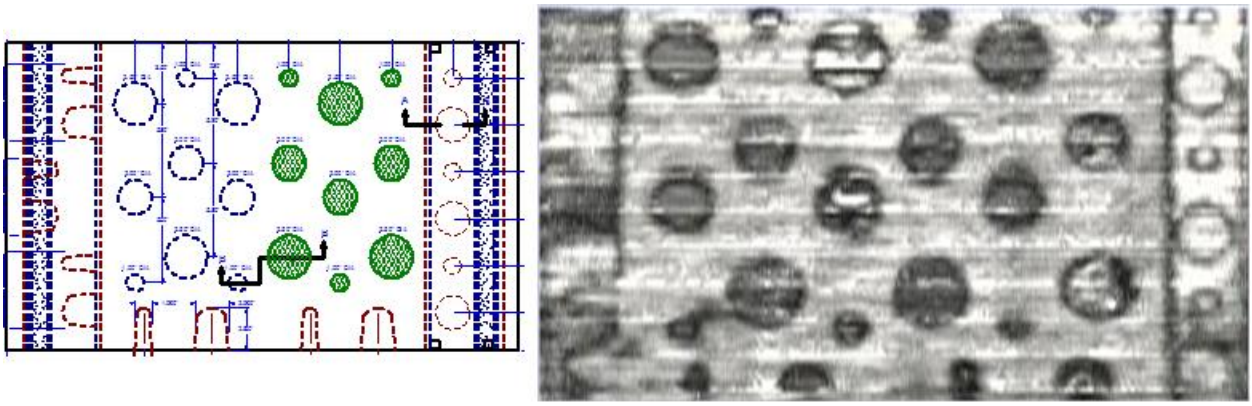

Figure 5-37: Phased Array UT C-Scan of NDI Feedback Specimen No. 6 (REF-STD-6-202-250-SNL-1) Generated by OmniScan with 1.5 MHz PA-UT Probe & 40 mm Water Box

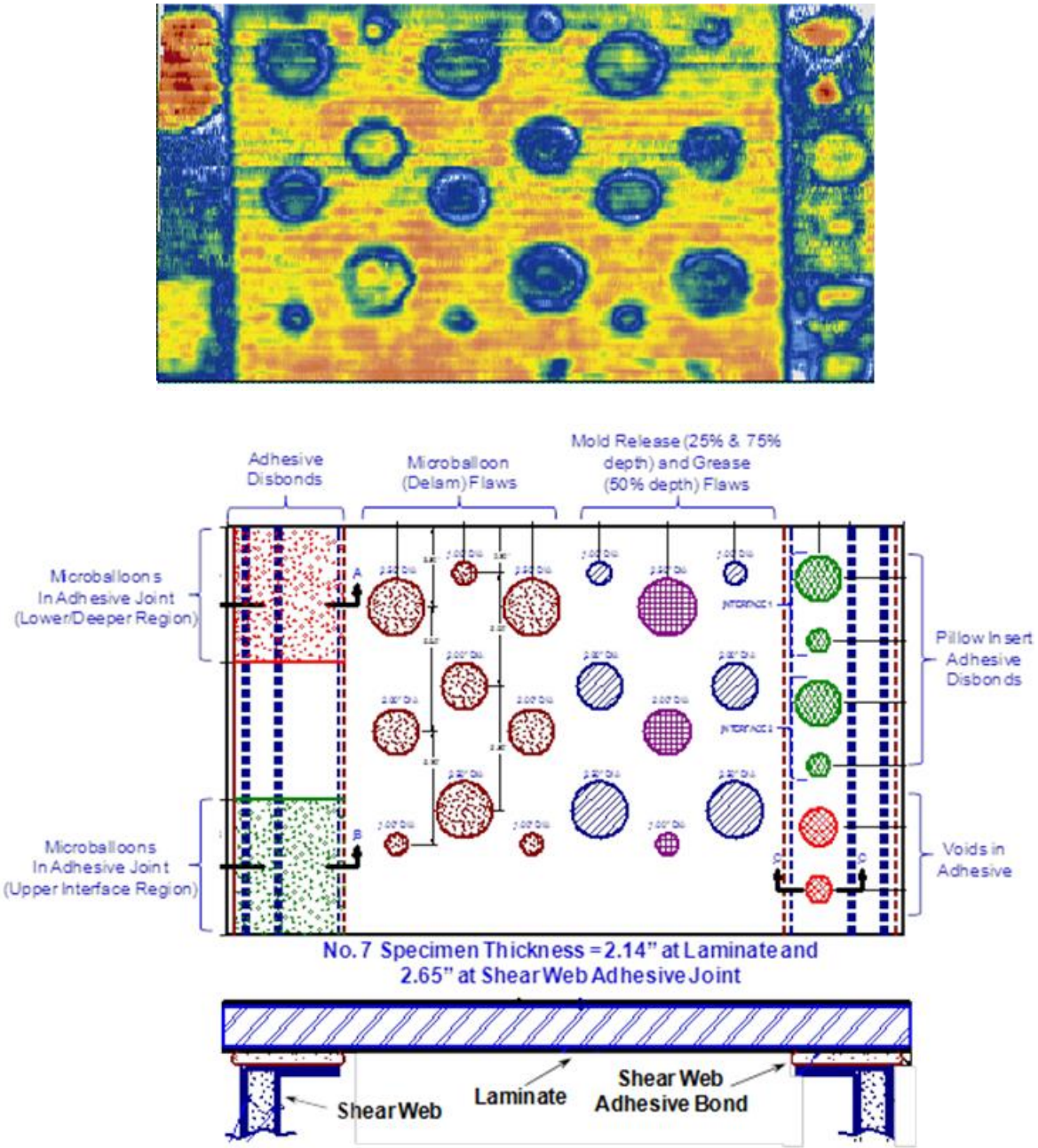

Figure 5-38: Phased Array UT C-Scan of NDI Feedback Specimen No. 7 (REF-STD-7-214-265-SNL-1) Generated by OmniScan with 1.5 MHz PA-UT Probe & 40 mm Water Box

This study also looked at the benefits stemming from the use of single-element transducers. It was determined that the normal, flat, single-element UT transducers can produce clear C-scan images in thick blade sections; however, experiments with focused transducers demonstrated their value as well. Figure 5-39 shows a focused transducer which uses a hemispherical-shaped end to focus its UT energy. Such a focus allowed for increased energy at the points of interest

and enhanced signal strength at greater depths. The focused probe is normally used for immersion UT testing in a water tank. Thus, it had to be deployed in the "captured water column" shown in the Figure 5-39 schematic. It can be seen that the focused transducer is placed at some offset distance from the inspection surface. This is the height of the captured water column. In order to overcome the harmonics inspection impediment that is described above, a threaded housing was developed to allow the offset distance to be adjusted. The focused UT transducer can be moved within the housing to create the optimum offset distance that avoids placing signal harmonics on top of the true signals of interest. Figure 5-40 and Figure 5-41 show the threaded housing arrangement which allows for the operator to adjust the water column between the transducer and the inspection surface. Figure 5-40 also shows some sample A-scan signals from various depths within a test specimen. Peak return signals from the 1.4" and 1.52: depth flaws can be detected but the peak signal from the 1.65" depth flaw is hidden inside the signal harmonics (i.e. not detected).

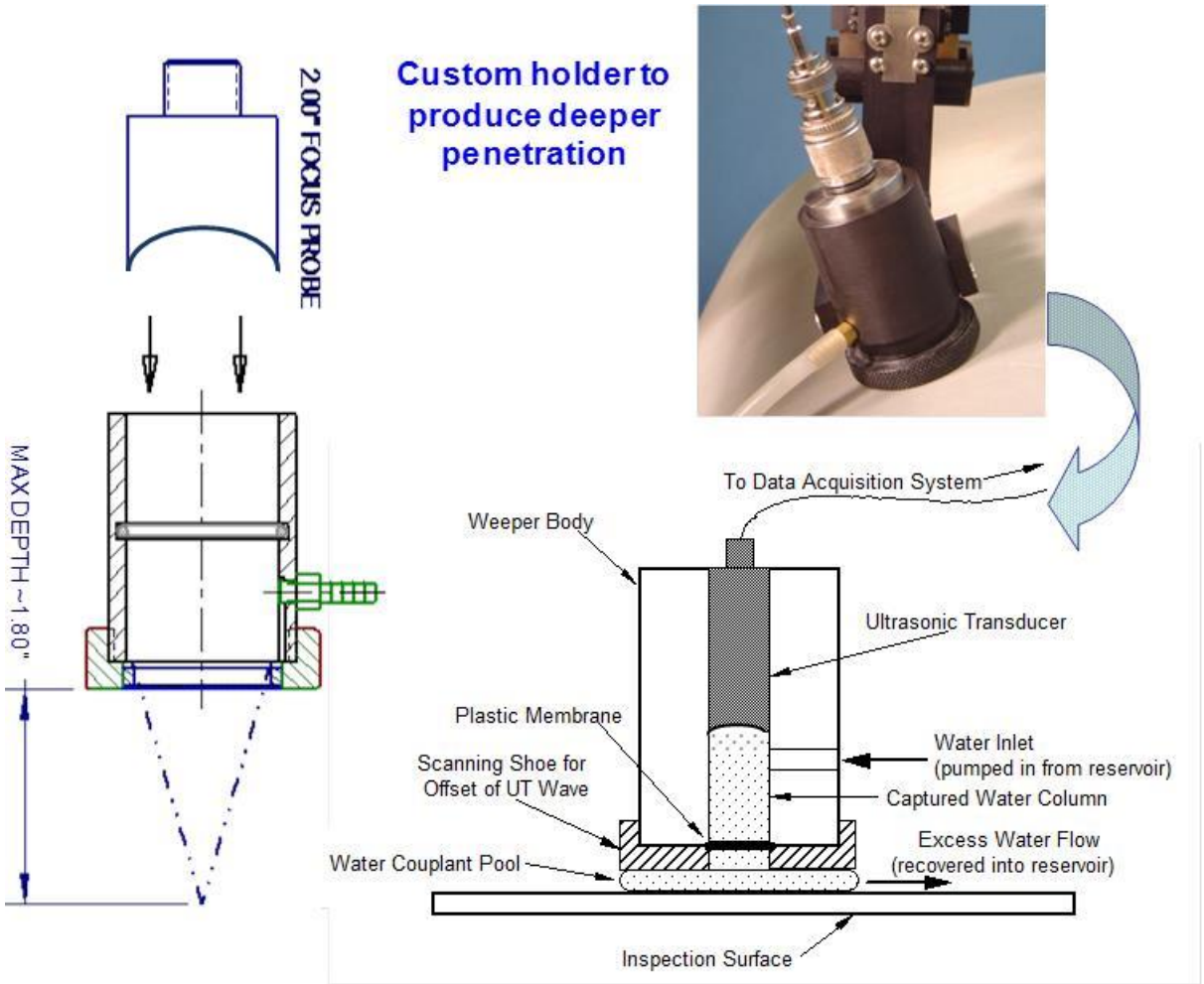

Figure 5-39: Design of Custom Water-Column Shoe to Allow for Field Use of Focused "Immersion" Probe and Allow for Deeper UT Wave Penetration

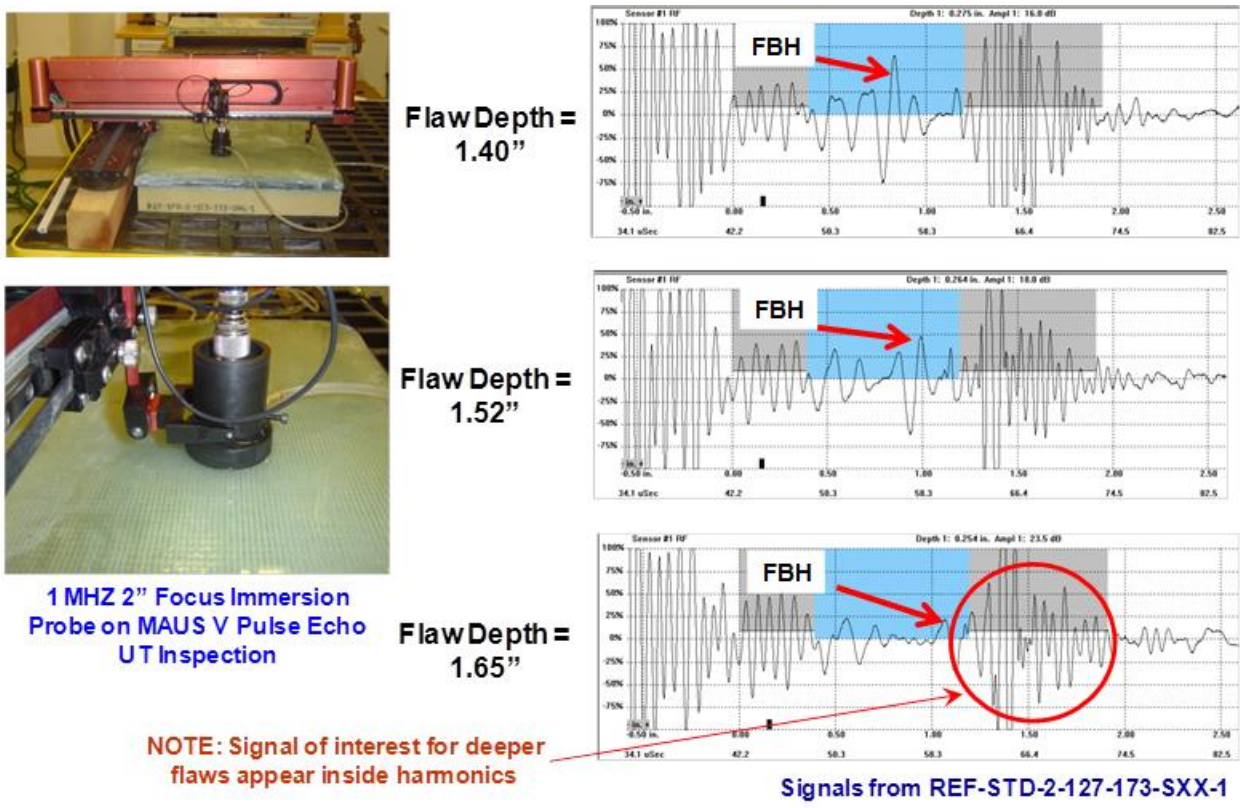

Figure 5-40: Ultrasonic A-Scan Signals Highlighting Inspection Impediment Where Deeper Signals of Interest are Hidden Within Harmonics from Earlier Arriving Signals

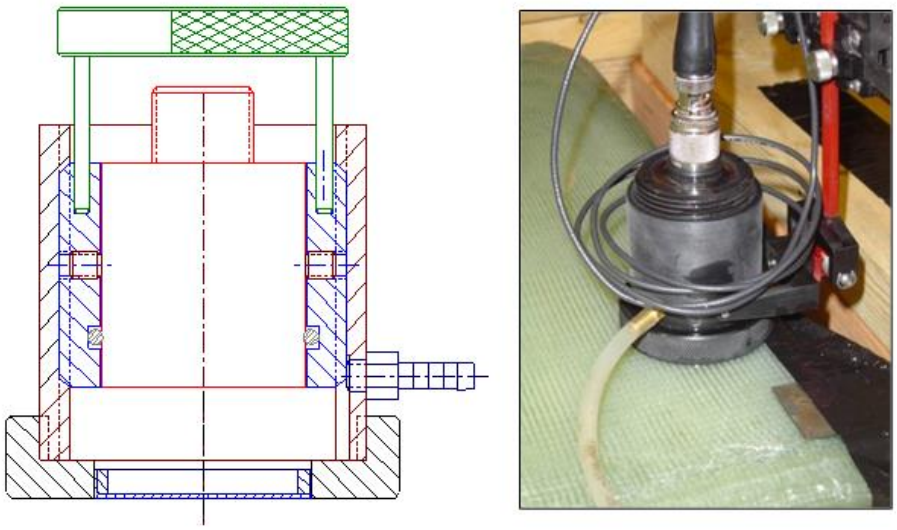

Figure 5-41: Variation on Water Column Shoe that Includes a Threaded Housing to Allow for Adjusting the Length of the Water Path or Column Height (Patent Pending)

Figure 5-42 shows ultrasonic A-scan signals that highlight: 1) the inspection impediment where deeper signals of interest are hidden within harmonics from earlier arriving signals, and 2) the clear back wall signal that is now separated from the front surface multiple (harmonics) when the focused UT probe is moved out to create a longer water column (increased offset distance). The adjustable water column shoe allows for real-time changes in the height of the water column (offset). This allows the transducer deployment to be adjusted such that the signal harmonics are moved outside the signal region of interest as depicted and discussed above. This custom water shoe was added to a UT scanning system to produce a C-scan image of the wind blade test specimen shown in Figure 5-43 (NDI Feedback Specimen No. 6 with a 2" spar cap with a 2.5" total thickness at the adhesive joint). All of the flaws in this specimen are imaged when the water column optimization is deployed. Once again, it is important to note that the flaws on the back side of the adhesive layer are detected with this NDI deployment. The schematic for NDI Feedback Specimen No. 7 (2.14" spar cap with a 2.65" total thickness at the adhesive joint) is shown in Figure 5-44. The presence of the more challenging deeper flaws (back side of adhesive) and contamination flaws (mold release and grease) are shown. Figure 5-45 shows the resulting C-scan image where, once again, all of the various flaws are clearly imaged. Thus, it can be seen that both the phased array and single-element UT methods, modified with the custom hardware described here, can detect deep flaws in thick wind blades and can detect a wide range of defect types.

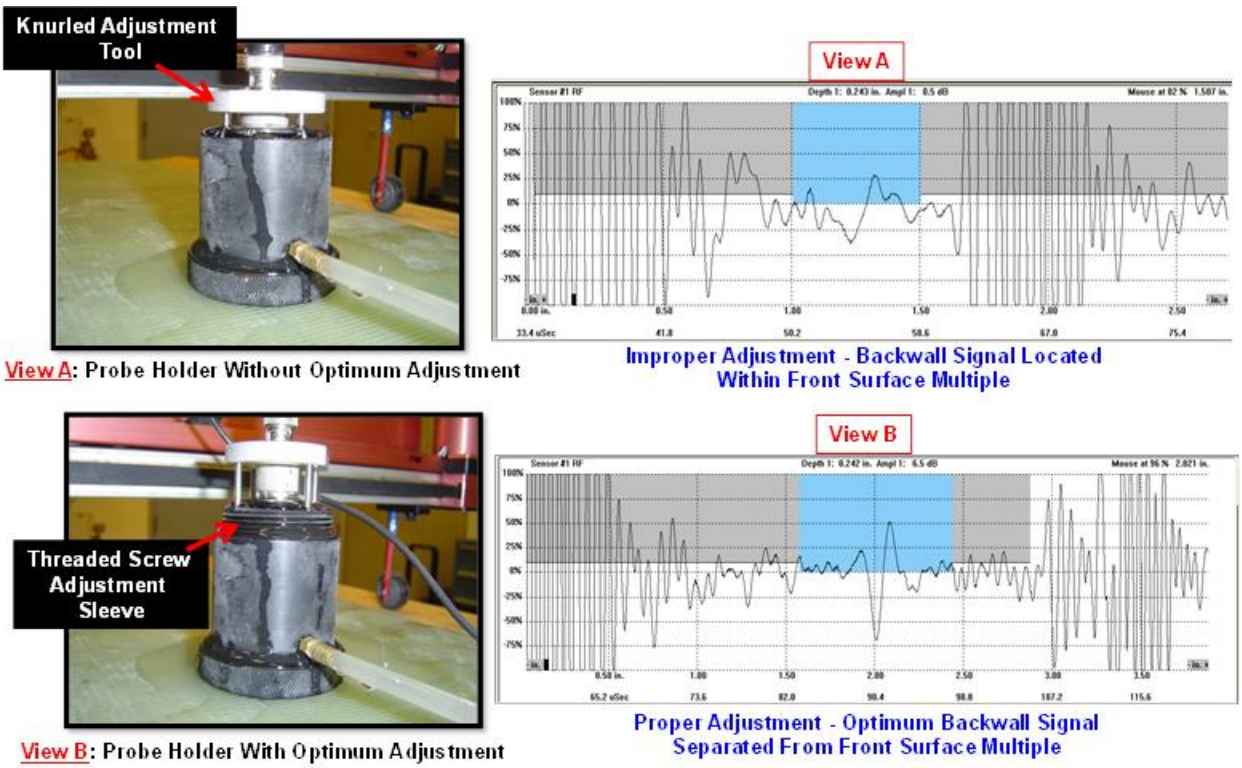

Figure 5-42: Use of 1 MHZ/2" Focus UT "Immersion" Probe with Adjustable Water Path Shoe to Optimize Performance

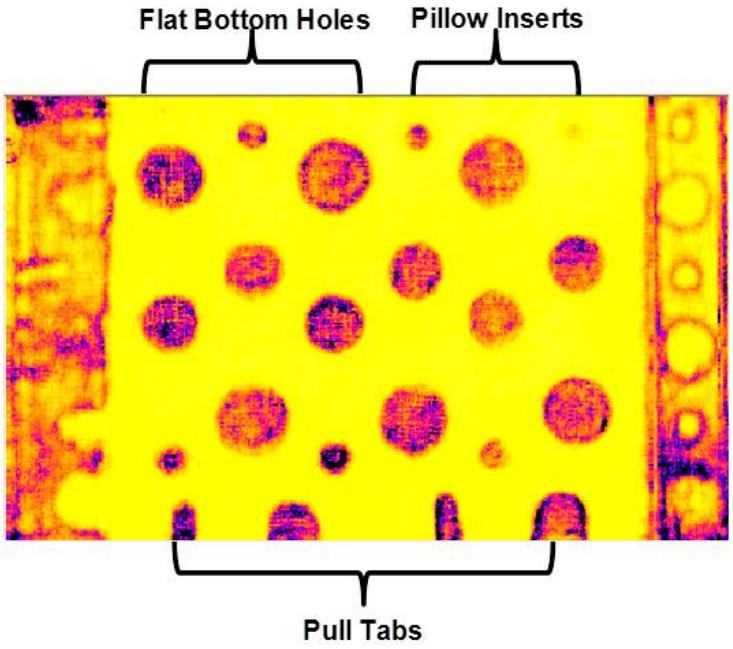

Figure 5-43: C-Scan Image Produced by MAUS PE-UT on NDI Feedback Specimen No. 6 with the Focused Probe (1 MHz, 2" Focus) and Optimized Adjustable Water Path Shoe

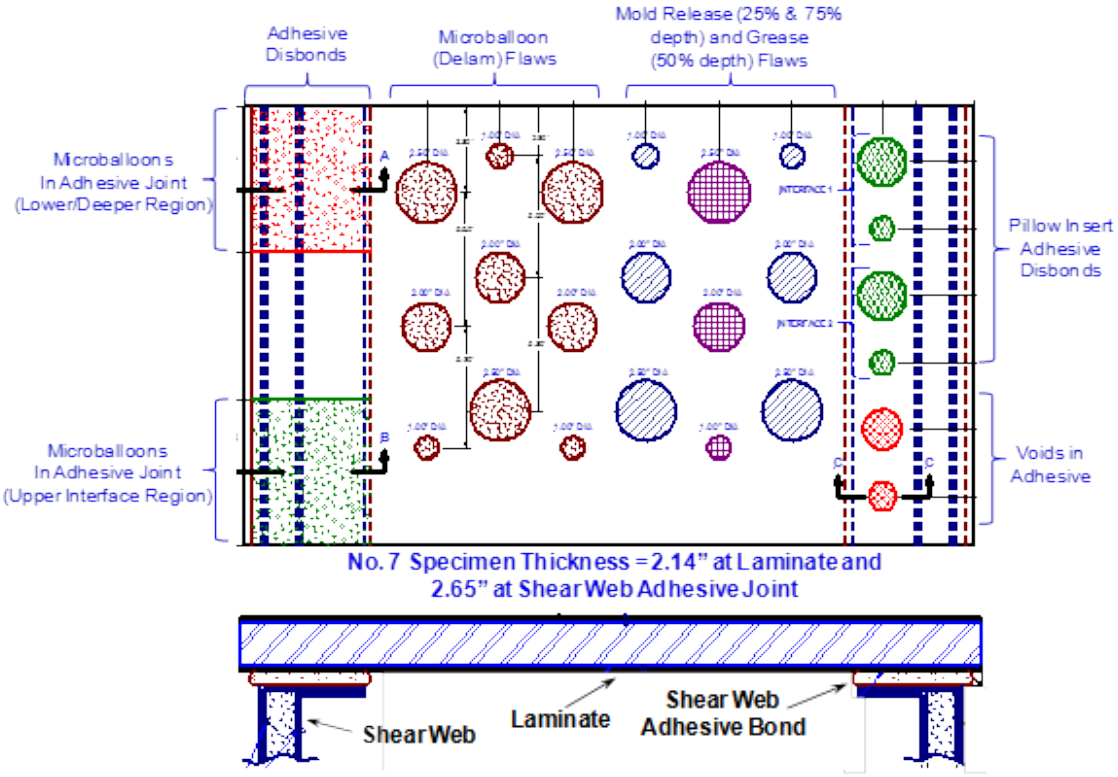

Figure 5-44: Spar Cap and Shear Web and Adhesive Joint NDI Feedback Specimen No. 7 (REF-STD-7-214-265-SNL-1)

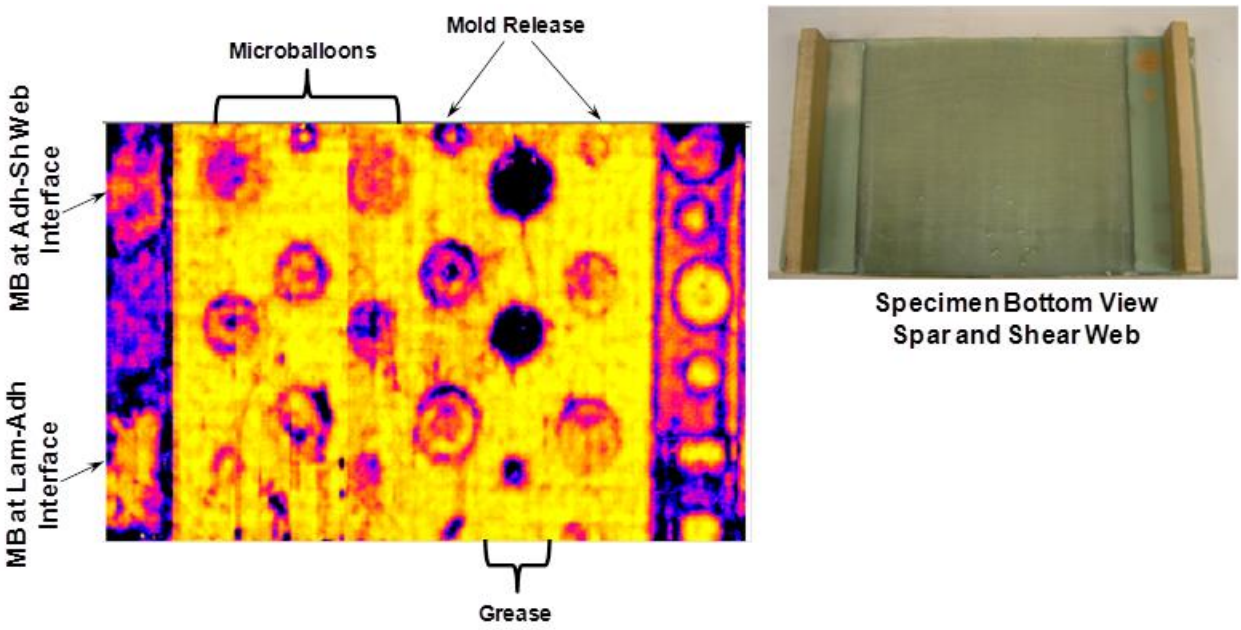

Figure 5-45: C-Scan Image Produced by MAUS PE-UT on NDI Feedback Specimen No. 7 with the Focused Probe (1 MHz, 2" Focus) and Water Column Shoe

In summary, the adjustable water column shoe allows for real-time changes in the height of the water column (offset). This allows the transducer deployment to be adjusted such that the signal harmonics are moved outside the signal region of interest as depicted and discussed above. The overall assessment of the pulse-echo UT method using the focused probe with signal optimization is:

- Overall noise levels and harmonics are a concern as they mask signals of interest.
- Use of immersion probe with custom probe holder (water column coupling) improves signals beyond normal contact transducers.
- 1 MHz, 2" focus probe (1.25" dia.) produced the strongest signals at an offset of 1.15" from the inspection surface.
- New probe holder was designed with larger membrane diameter to allow transducer positioning close to inspection surface (optimize focus to specimen thickness).
- UT signals contain what appears to be transducer ringing (adjacent peaks) and flat (non-focus) UT probe is especially susceptible.
- Adjustable water path probe holder is able to eliminate the presence of the confounding signals in the time-base region of interest.
- Adhesive studies and UT signal modeling may reveal additional methods to optimize penetration into the adhesive layer and improve flaw recognition in laminate-to-shear web joints.

Sandia has focused on the development of sealed water column shoes with customized heights to optimize UT inspections. Overall, the advantages of using water shoes to optimally deploy

single-element or phased array UT include: a) better/cleaner scanning signal response (less noise) which results in a better signal-to-noise ratio for flaw detection, b) better coupling - no signal dropout and easier clean-up than gel couplant, and c) easier to deploy over a scanned surface, and d) the enclosed water column which uses a bladder system allows the inspector to maintain a seal when deploying vertically. Several different water shoes were designed and evaluated as part of this program. Figure 5-46 provides a schematic of one of the NDI test specimens that were used to evaluate each shoe while Figure 5-47 through Figure 5-50 provide a photo of the shoe design along with a sample C-scan produced by PA-UT when deployed using each shoe. The advantages and disadvantages associated with each water shoe design were compiled and used to produce a final, optimized design that was used for all UT inspection tasks thereafter.

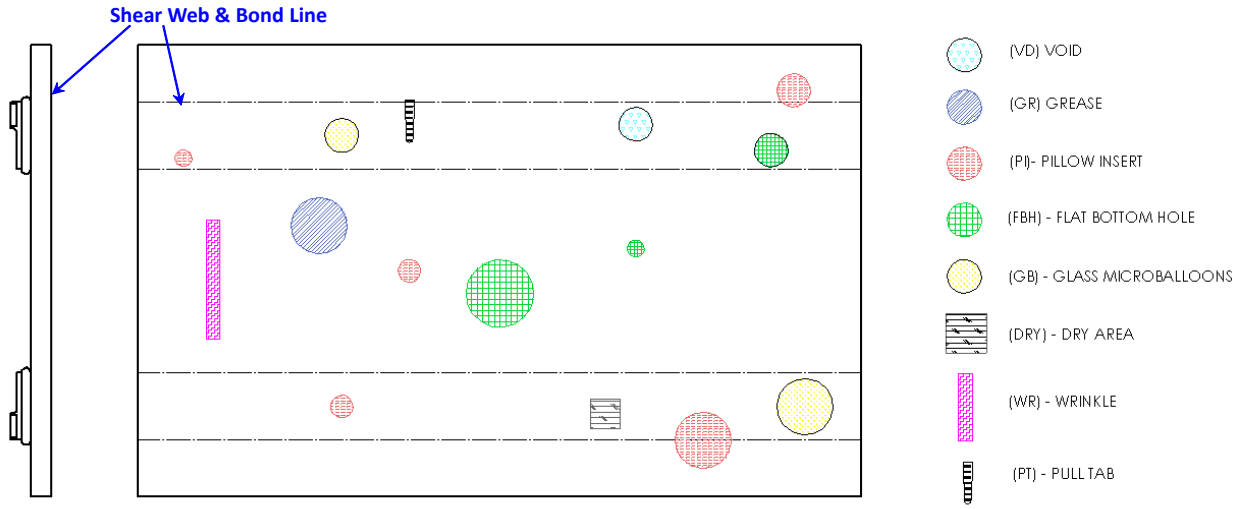

Figure 5-46: Schematic of NDI Test Specimen Used to Compare Results from Different Water Shoe Designs

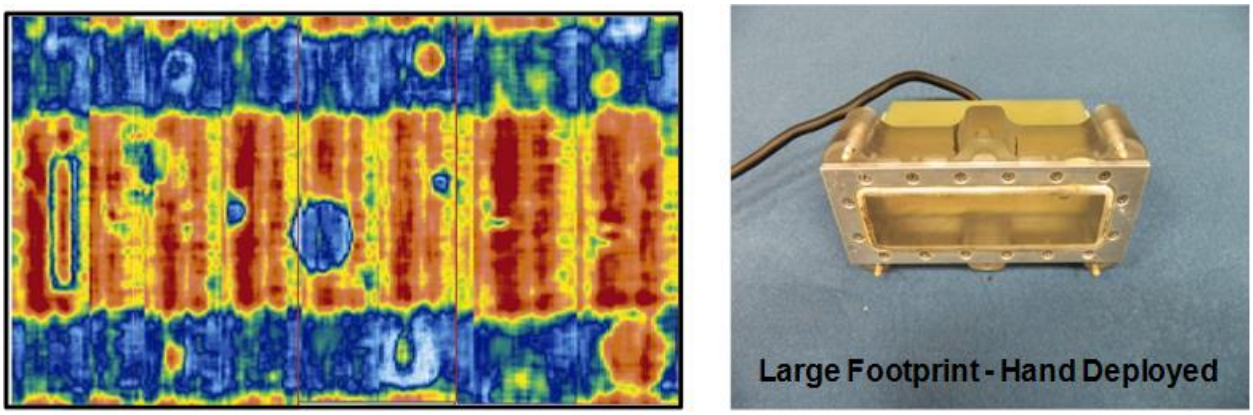

Figure 5-47: PA-UT C-Scans of Fiberglass NDI Specimen Generated by Sandia "Crab" 40mm Sealed Water Box 1.5L42 Probe with Uniaxial Encoder

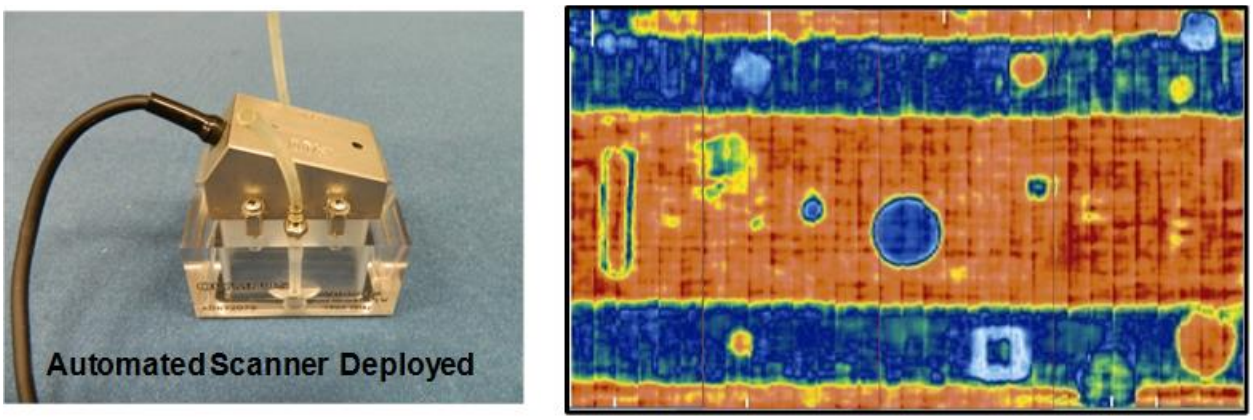

Figure 5-48: PA-UT C-Scans of Fiberglass NDI Specimen Generated by Olympus 40mm Open Water Box 1.5L16 Probe on Automated Scanner

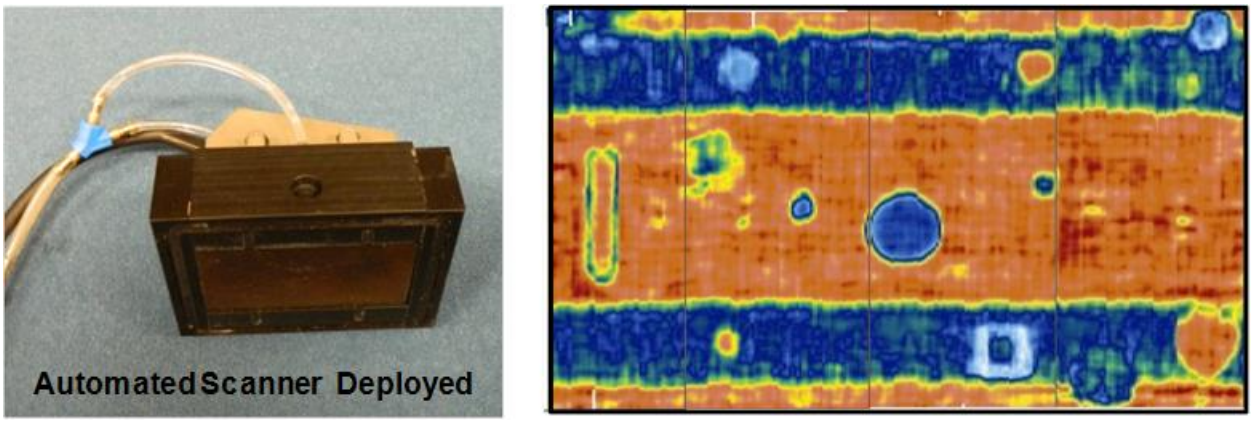

Figure 5-49: PA-UT C-Scans of Fiberglass NDI Specimen Generated by Sandia 25mm Aqualene Box with Water Pool and 1.5L16 Probe on Automated Scanner

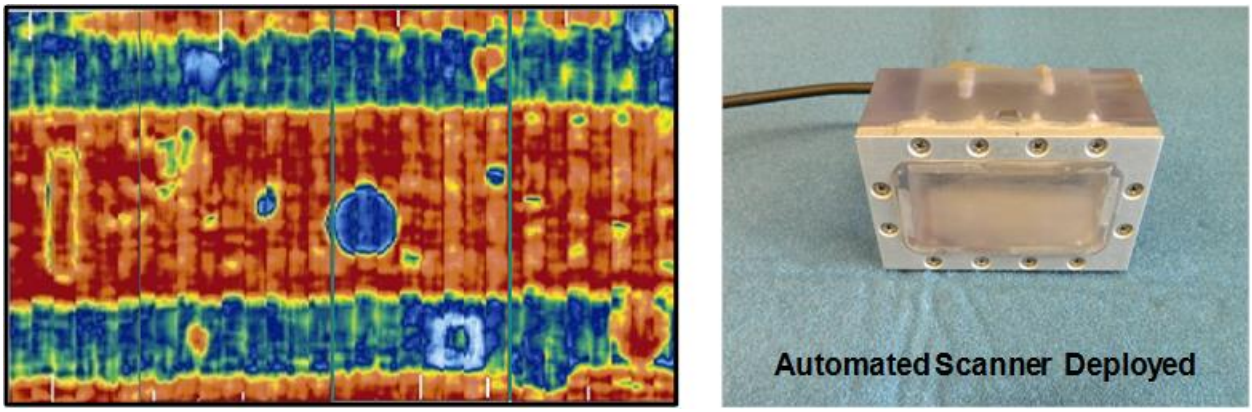

Figure 5-50: PA-UT C-Scans of Fiberglass NDI Specimen Generated by Sandia Sealed 40mm Sealed Water Box 1.5L16 Probe on Automated Scanner

Next, a larger phased array UT transducer was studied. The 1.5L42 (42 element) PA-UT transducer shown in Figure 5-51 produces approximately a 3.8" wide inspection stripe. If sensitivity and deployment flexibility similar to that observed with the 1.5L16 (~1.0" stripe) phased array UT transducer shown in Figure 5-32 could be achieved, then the larger transducer would allow for faster inspections. The bladder water box was deployed with the 1.5L42, 42 element phased array probe as shown in the Figure 5-37 photo. The UT transducer assembly was attached to a linear encoder to track position. Figure 5-52 shows another thick blade specimen that contains two spar cap bond lines and an array of different, engineered flaws. It also contains the resulting C-scan image which is composed of a series of linear stripes that are connected to give an overall view of the entire specimen. It can be seen that all of the flaws are imaged although the deepest flaws in the bond joint region are not as clear and evident as the flaws located in the spar cap (nearer to the inspection surface).

The challenge with wide, flat PA deployment is that it requires a custom contour of the shoes in high radius of curvature areas and/or a change in the scan direction to avoid rapid changes in contour. Figure 5-53 shows the issue associated with deploying UT transducers that have large footprints. In this photo, the transducer and water box shoe are scanning along the line of the spar cap in a region of relatively high curvature. This produces transducer lift-off on either side of the probe and results in loss of signal. The solution is to either fabricate a custom shoe that matches the contour of the inspection region or to turn the probe assembly 90^{o} and scan in a direction that moves across the spar cap. Both options were studied in this program and both provide good inspection results.

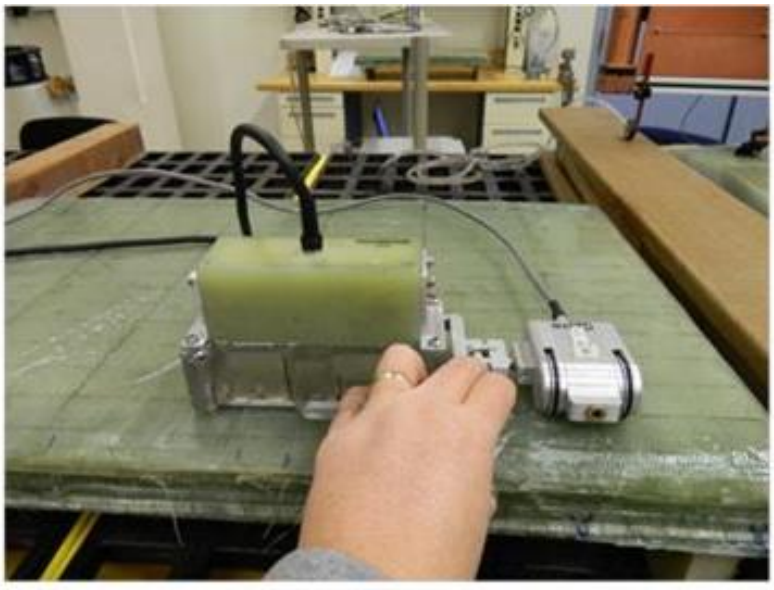

Figure 5-51: 1.5L42 Phased Array Ultrasonic Transducer with 42 Elements and a 3.8" Inspection Width Connected to a Linear Position Encoder

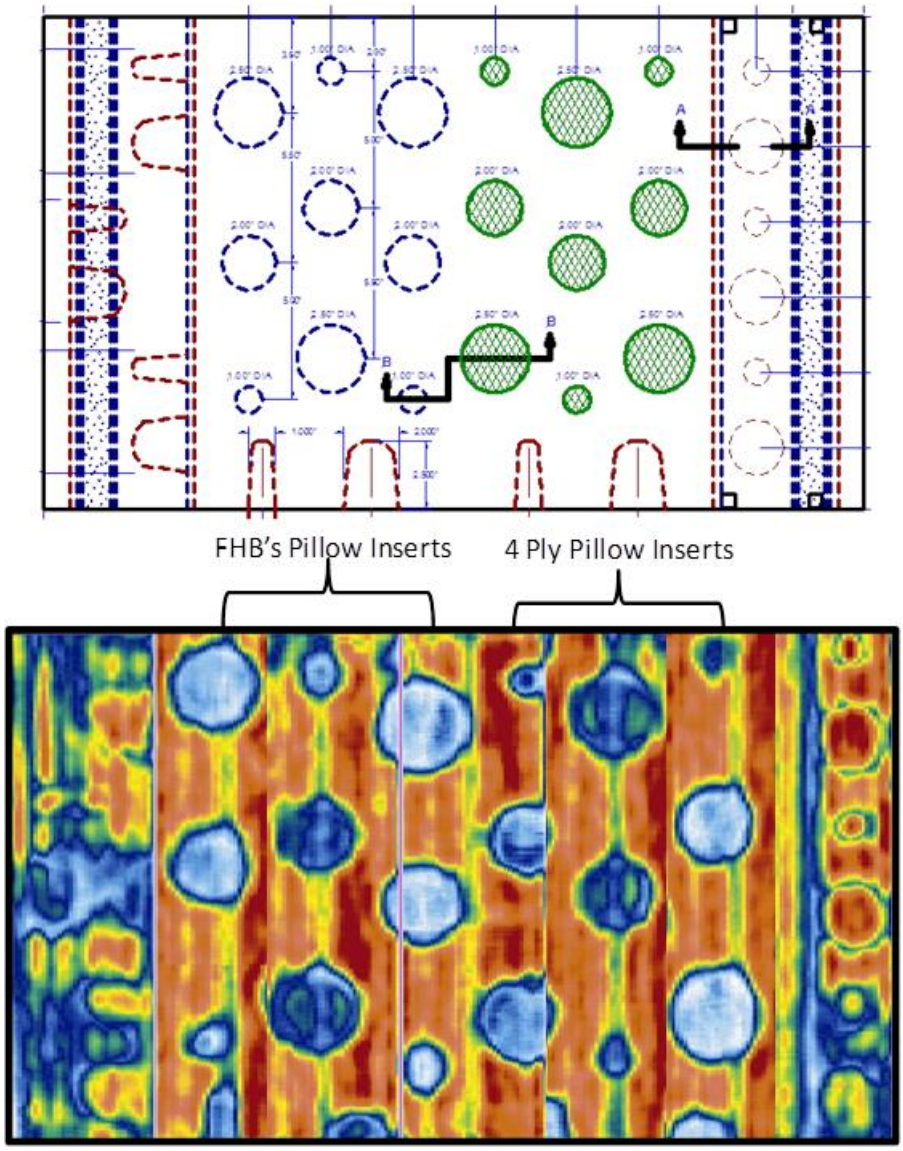

Figure 5-52: Specimen Flaw Layout and C-scan Produced by PA-UT Using the 1.5L42 Probe in the Sandia "Crab" 40mm Sealed Water Box and a Uniaxial Encode

Figure 5-53: Curvature of Blade Presents a Limitation on the Width of the Phased Array UT Probe if Inspection is Performed Along the Line of the Spar Cap

5.1.2 Optimization of Single Element Contact and Phased Array UT Using Specialized Data Acquisition

5.1.2.1 Advantages and Deployment of Proper Transducer Frequency and Type

In ultrasonic inspections, increased depth of penetration can be achieved through the use of lower frequency UT transducers. However, the longer waves associated with lower frequencies mean that the resolution of these transducers are relatively lower than similar high frequency probes. When dealing with thick and highly attenuative materials, lower frequencies are often necessary to produce sufficient wave penetration. So, selection of the inspection frequency becomes a matter of balancing signal strength and clarity with achieving proper depth of penetration. In this study, it was determined that the optimum frequency range for spar cap inspection was 500 KHz to 1.5 MHz, depending on the thickness of the blade spar cap and adhesive joint at the shear web. Figure 5-54 and Figure 5-55 compare inspection results from similar specimens when inspected by a 1 MHz and a 500 KHz transducer, respectively. The test specimen is the wind blade test specimen shown in Figure 5-38 (NDI Feedback Specimen No. 7, REF-STD-7-214-265-SNL-1). This specimen was chosen because it has a 2.14" thick spar cap and a 2.65" thick adhesive joint (shear web adhesive and spar cap) both of which provide excellent depth-of-penetration challenges. Note the presence of engineered porosity in the bond line at the spar cap interface (upper region – front side of adhesive) and the shear web flange (lower/deeper region – back side of adhesive) which makes signal penetration exceptionally difficult. In this example, the lower, 500 KHz frequency produces a cleaner crisper C-scan image (stronger UT signals and improved signal-to-noise ratio) with better contrast than the 1 MHz inspection frequency. This demonstrates the importance of signal optimization and inspection frequency selection in obtaining the best flaw inspection results. In actual deployment, the inspection procedures can specify the use of particular frequencies along designated portions of the blade.

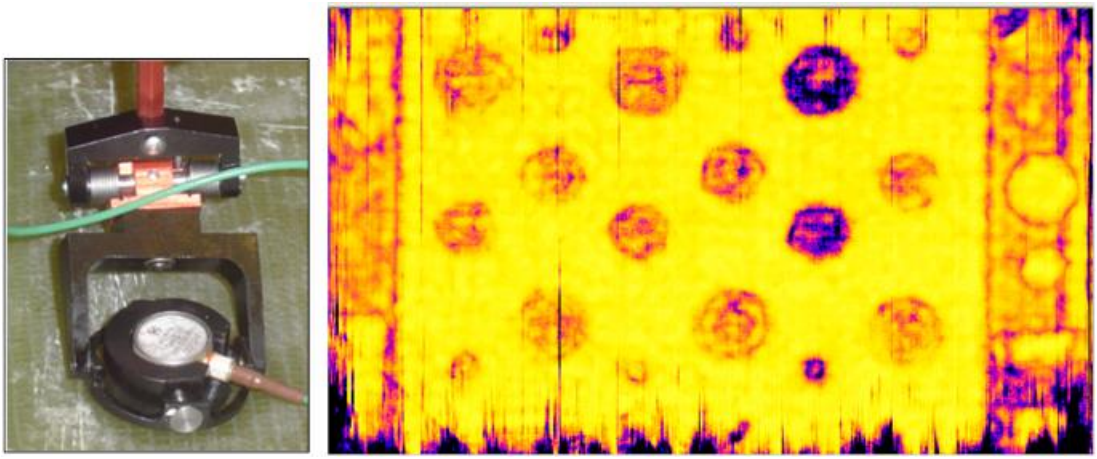

Figure 5-54: PE-UT C-Scan Produced by the 1 MHz, Single-Element Contact Transducer on the MAUS Scanner System

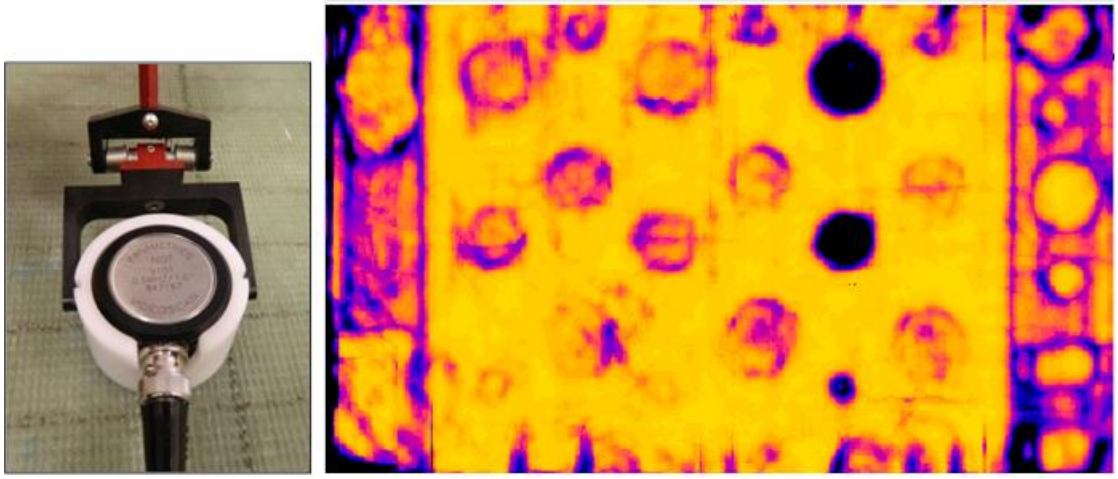

Figure 5-55: PE-UT C-Scan Produced by the 0.5 MHz, Single-Element Contact Transducer on the MAUS Scanner System

In order to further evaluate the capabilities if the single-element focused probe discussed in Section 5.1.1 above (ref. Figure 5-39 to Figure 5-42), the 1 MHz focused probe in its custom water column housing was applied to the challenging NDI Feedback Specimen No. 7. Figure 5-56 shows the optimized results for this transducer deployed with an automated scanning unit. It shows that slightly cleaner C-scan images can be produced with this shorter wave length, higher frequency transducer and that the focusing aspect of the probe allows for more concentrated energy and better depth of penetration than the simple, 1 MHz single-element probe shown in Figure 5-54.

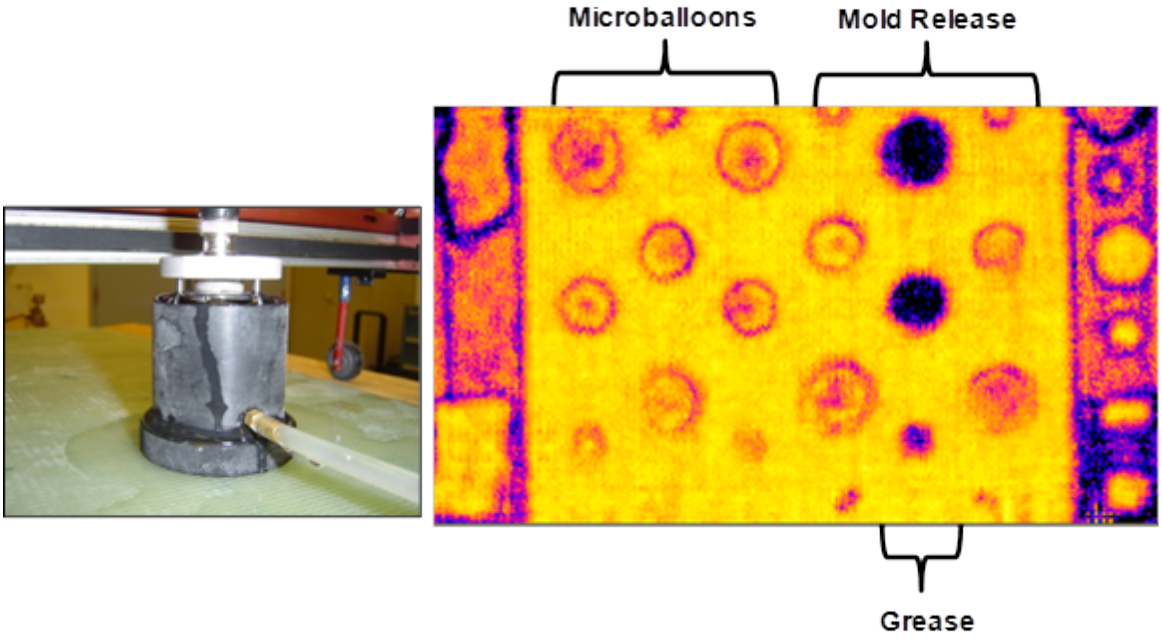

Figure 5-56: Optimized PE-UT C-Scan Produced by the 1 MHz, Single-Element Focused Transducer Displaying Good Flaw Contrast at All Depths

5.1.2.1 Advantages and Use of Proper Gate Settings

During the acquisition of ultrasonic inspection data, it is possible to use one or more gates to emphasize the signals associated with certain arrival times (depths of penetration). Optimum gate settings are critical to detecting all flaws and clearly imaging them. For example, defects at the shear web flange and adhesive layer may, or may not, be detected depending on gate settings and part thickness. To detect all flaws in the spar cap laminate and the adhesive layer, an operator could place one long gate along this entire region of the resulting UT signal. This is shown in Figure 5-57. However, the large, peak response associated with return from the spar cap back wall dominates the activity in this gate setting such that some of the more subtle flaws are not detected and imaged in the C-scan (see highlighted misses in the Figure 5-57 C-scan). Figure 5-58 shows the use of a second gate that focuses only on the signals that return from the adhesive layer region. In this case, the C-scan shows that it is possible to detect and image the deeper, more subtle flaws. This study determined that optimum results are obtained from the use of two gates, one that is narrow and focuses on the back wall of the spar cap laminate and one that focuses on the back wall of the shear web beneath the adhesive layer.

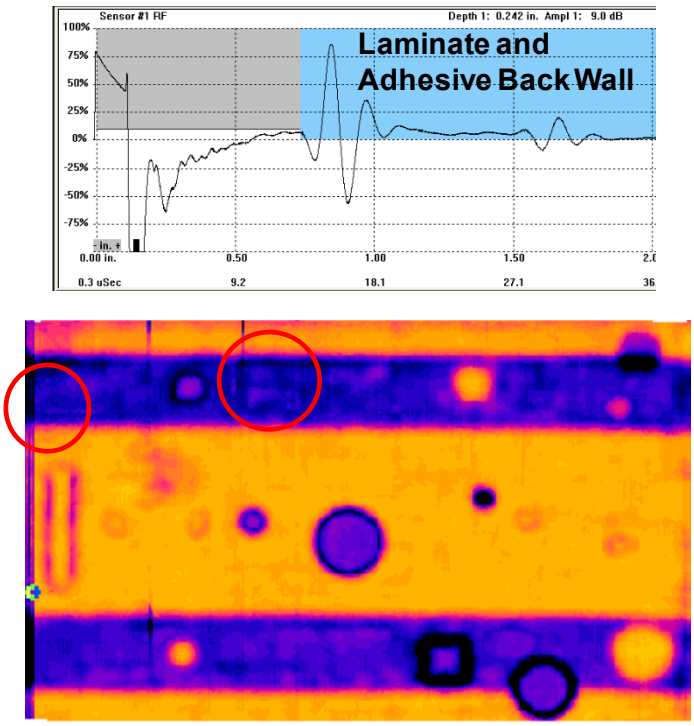

Figure 5-57: UT Gate Set to Cover Both the Spar Cap Back Wall and the Back Wall of the Adhesive Layer - PE-UT C-Scan Produced by the 0.5 MHz, Single-Element Transducer

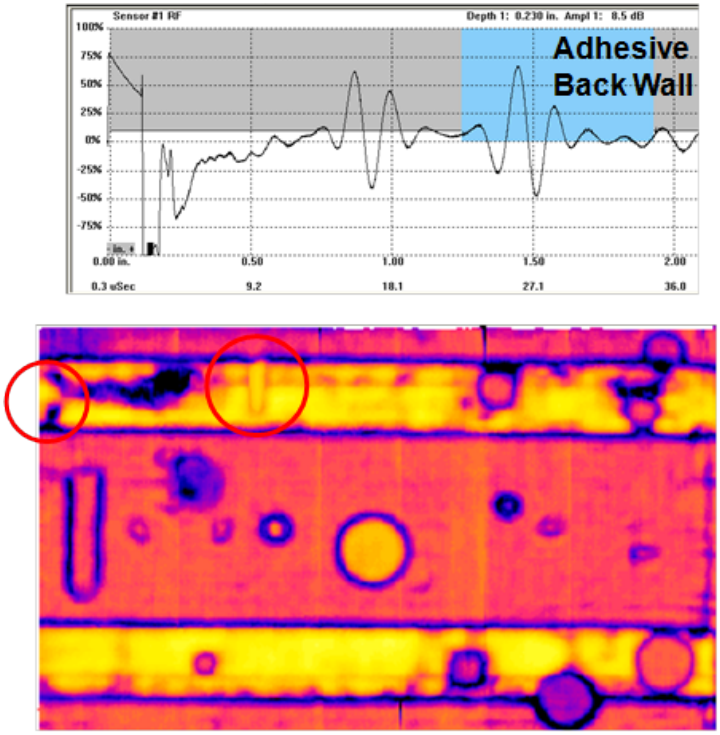

Figure 5-58: UT Gate Set to Cover Only the Back Wall of the Adhesive Layer – PE-UT C-Scan Produced by the 0.5 MHz, Single-Element Transducer

5.2 Pulsed Thermography

Thermography is a nondestructive inspection method that uses thermal gradients to analyze the physical characteristics of a structure such as internal defects. This is done by converting a thermal gradient into a visible image by using a thermally sensitive detector such as an infrared (IR) camera [5.4 to 5.6]. Flash thermography relies on the heat absorption characteristics of the structure to indicate the presence of defects. In thermographic NDI, part of the IR band of the electromagnetic spectrum is used to map the surface temperature of an inspected item. The temperature distribution on a structure can be measured optically by the radiation that it produces at infrared wavelengths. Many defects affect the thermal properties of materials. Examples are corrosion, disbonds, cracks, impact damage, panel thinning, and fluid ingress into composite or honeycomb materials. In general, a source of energy is used to create a temperature difference between the specimen and the surrounding environment. Variations in the structure or material properties result in variations in heat flow and surface temperature which are recorded by the IR camera. Figure 5-59 shows a schematic of a thermographic inspection system and highlights the physics of flaw detection.

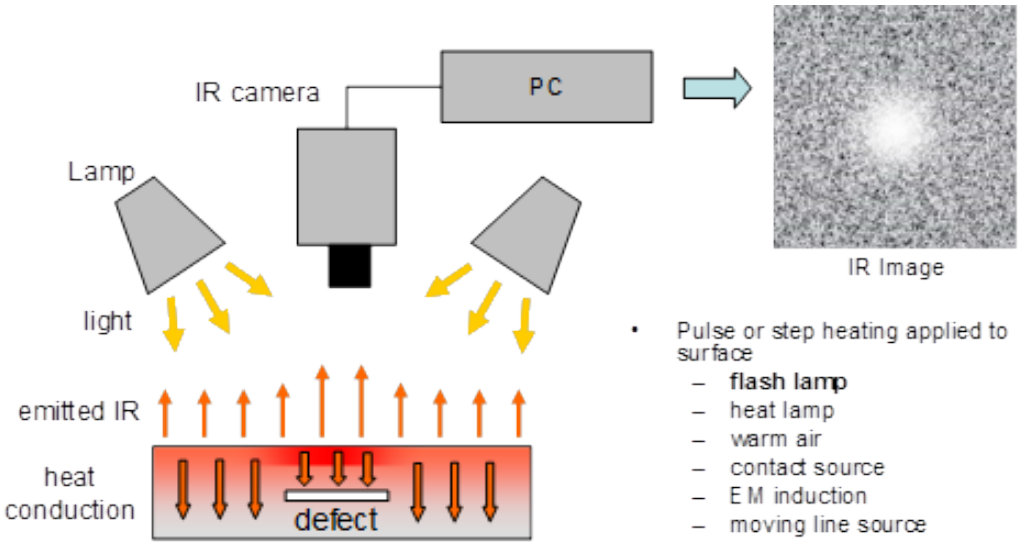

Figure 5-59: Principle of Active Pulsed Thermography

Thermographic inspection is accomplished using high-power flash lamps or other heat source, an infrared video camera, and image processing hardware and software, all of which are controlled by a personal computer. By the judicious application of external heat sources, common composite defects can be detected by an appropriate infrared survey. The heat source, such as flash lamps, is used to raise the surface temperature of the structure. The subsequent heat transfer into the material is affected by any defects that may be present. The resulting temperature distribution is then recorded by the IR camera and displayed on the computer monitor. As the heat diffuses through the structure the surface temperature is monitored for a period of time by an infrared camera. In practice, the computer actually obtains several images

at progressively later times after each flash. Areas that appear hotter than normal may indicate the presence of a delamination or disbond beneath the surface that is preventing heat diffusion into deeper layers. By using a computer to analyze and manipulate the infrared data captured over time, subtle variations can be enhanced in the image. Typical computer enhancements include analysis of the first and second derivatives of the heat versus time signatures at each point in the time sequence to produce images showing rates of change. Through the use of temperature versus time images produced by the thermography system, it is possible to determine the depths of disbonds, delaminations and other flaws in a structure. Typical gantry-based and hand-held thermographic inspection systems are shown in Figure 5-60.

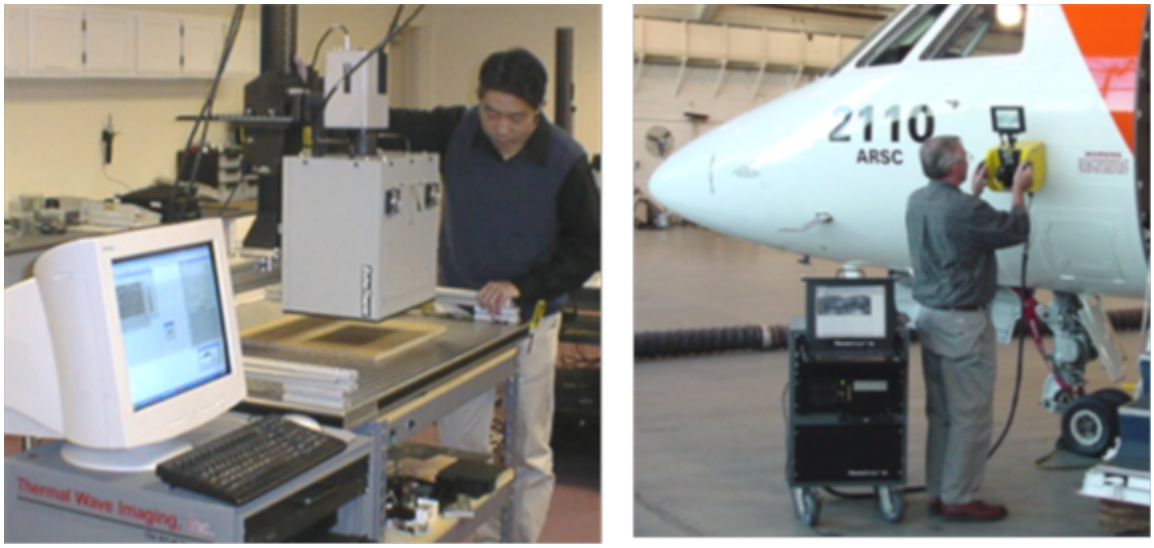

Figure 5-60: Laboratory Thermal Wave Imaging System Inspecting Composite Flaw Detection Panels and Portable Field System Inspecting an Aircraft Fuselage

Thermographic inspection procedures on composite parts can be used to detect certain local changes in materials that occur in homogenous parts. These may typically be considered (but not exclusively) as voids, inclusions, disbonds, fluid ingress or contamination, foreign objects and damaged or broken structural assemblies. The means of excitation, the detection method and the inspection parameters can be varied depending on the material to be inspected and the flaws to be detected.

The advantages of the thermography inspection method include: 1) thermography can be performed without physical contact with the surface, 2) single images can include relatively large areas (1-2 ft^2) allowing for rapid inspections of large surface areas, and 3) two-dimensional image of the inspected surface helps the operator visualize the location and extent of any defect. The primary disadvantages of thermography are: 1) it is often necessary to apply a high-emissivity coating during inspections to obtain an acceptable image; steps have been taken to minimize the labor time associated with this task, 2) damage to layers deep within a structure is more difficult to detect than damage in surface layers because the larger mass of material tends to dissipate the applied heat energy.

After presenting the thermography principles and equipment, it is worthwhile to discuss some specifics on the critical component: the infrared camera. An infrared camera is a non-contact device that detects infrared energy (heat) and converts it into an electronic signal, which is then processed to produce a thermal image on a video monitor and perform temperature calculations. Heat sensed by an infrared camera can be very precisely quantified, or measured to monitor thermal performance, as well as to identify and evaluate the relative severity of heat-related problems. Recent innovations, in particular detector technology, the incorporation of built-in visual imaging, automatic functionality, and infrared software development, deliver more cost-effective thermal analysis solutions. A brief comparison of some infrared cameras used for thermographic inspection systems is provided in Figure 5-61.

	A40	Merlin Mid	Phoenix
Detector Material:	Vanadium Oxide (VOx)	Indium Antimonide (InSb)	Indium Antimonide (InSb)
Detector Cooling:	Uncooled Microbolometer	Integral Stirling or LN2	Integral Stirling or LN2
Spectral Range:	7.5-13 micron	3-5 micron	3-5 micron
Thermal Sensitivity:	0.08° C	0.025 °C	0.025 °C
Focal Plane Array:	320 x 240	320 x 256	640 x 512
Frame Rate:	60 Hz	60 Hz	30 Hz
Weight:	3.1 lbs	9 lbs	Camera: 7 lbs & RTIE: 6 lbs
Size:	8.2" x 4.3" x 3.6"	9.8" x 5.5" x 5.0"	Camera: 7.5" x 4.4" x 5.2"

Figure 5-61: Comparison of Infrared Cameras for Thermography Inspection

Figure 5-62 and Figure 5-63 show sample results from thermographic inspections on bonded tear straps and composite honeycomb structure, respectively. Figure 6-51 shows how a disbond between an aircraft skin and the substructure tear strap affects the thermographic image by changing the heat transfer in that local region. Similarly, the IR image in Figure 5-63 indicates the various flaws that were engineered into the honeycomb panel. Figure 5-64 and Figure 5-65 contain additional IR images of various flaws in composite honeycomb and composite laminate structures. One of the limitations of thermography is the depth of penetration of the inspection. For composite laminates, the inspection depth limit is in the range of 0.6" to 0.7" depending on a number of factors within the part. Only flaws that manifest themselves as variations in the surface temperature of the structure can be readily imaged by the infrared camera. Novel heating methods are currently being used to infuse higher levels of heat energy into the structure and improve the detection of deeper flaws.

The Thermal Wave Imaging (TWI) system was applied to a bonded, composite doubler repair which was installed on a DC-9 fuselage section in the Sandia Labs' FAA Airworthiness Assurance hangar. Figure 5-66 shows a schematic of the 10 ply doubler highlighting the size,

shape, and location of the embedded flaws. The resultant sequence of images produced by a TWI inspection is also contained in Figure 5-66. The features seen at early times are defects closest to the outside surface of the patch (note appearance of flaws #1 and #2 in the first few frames). The disbonds, located at the base of the doubler, and the deeper delaminations appear in the later frames corresponding to their delayed effect on the thermal field. All six embedded flaws were identified in the TWI images and flaws smaller than 0.5" in diameter could be detected.

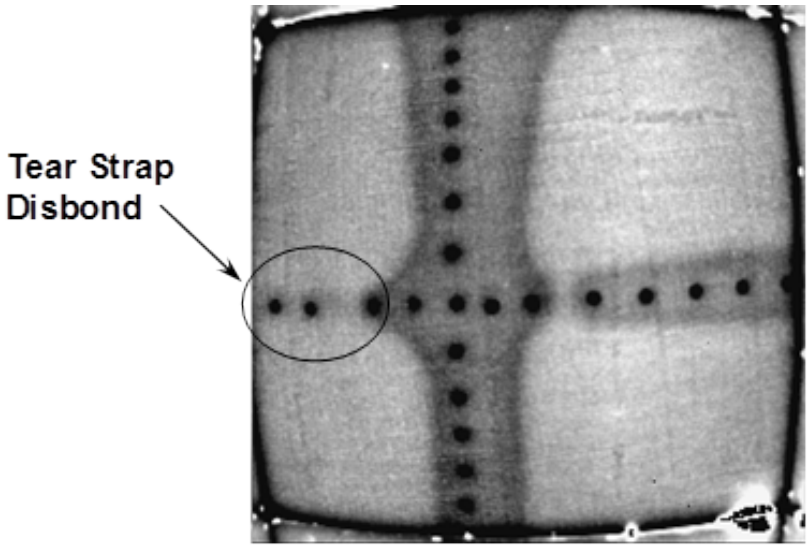

Figure 5-62: Sample Thermography Image Showing a Disbond in an Aluminum Fuselage-Tear Strap Structure

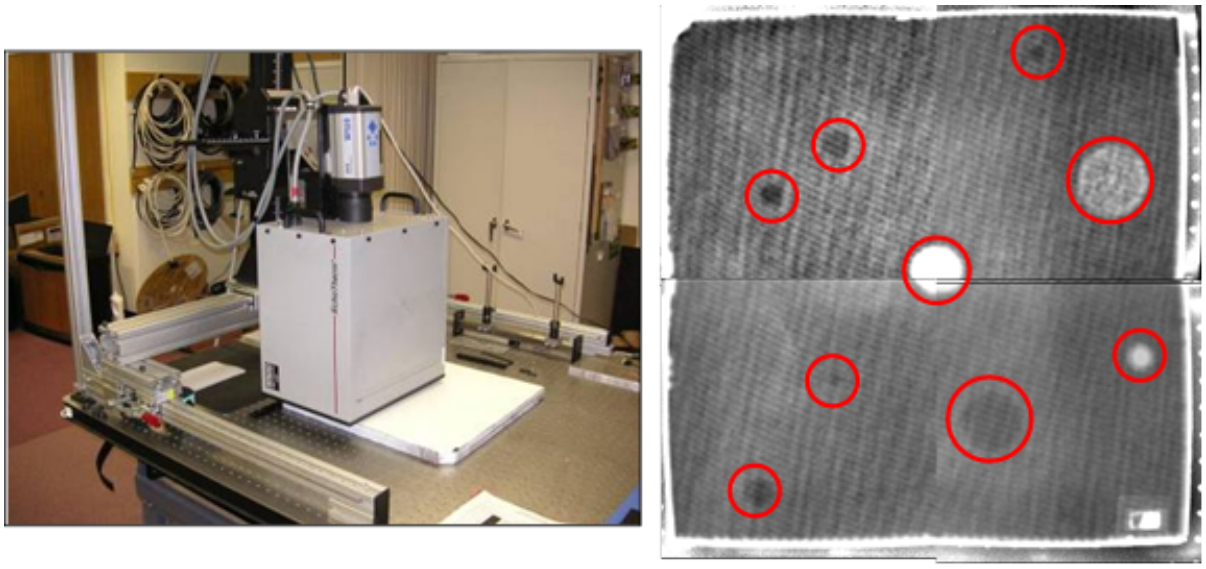

Figure 5-63: FLIR A40 Uncooled Camera Inspecting the Honeycomb Test Panels and a Sample IR Image from a Fiberglass Panel

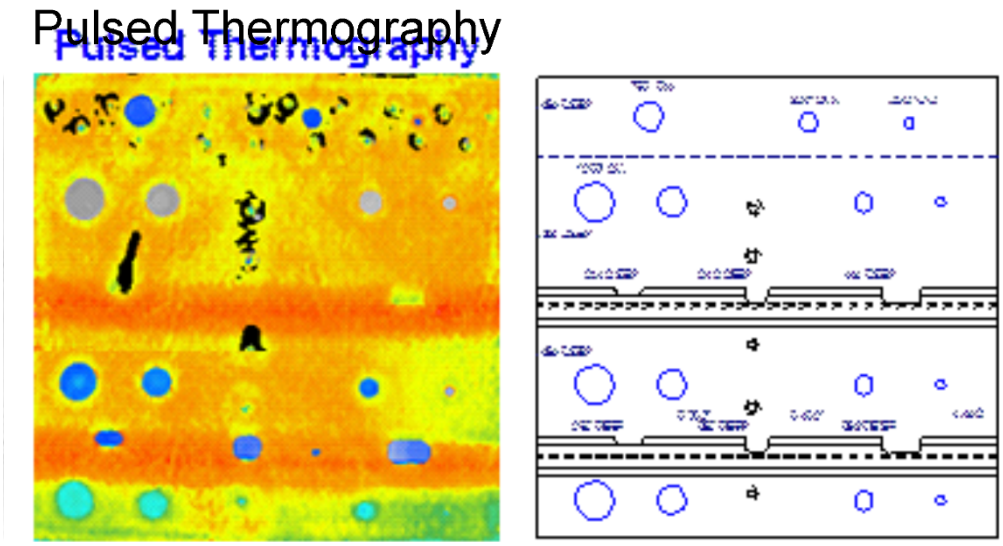

Figure 5-64: Thermography Image Produced from Inspection of Composite Laminate Panel with Flaw Profile as Shown in Drawing on the Right

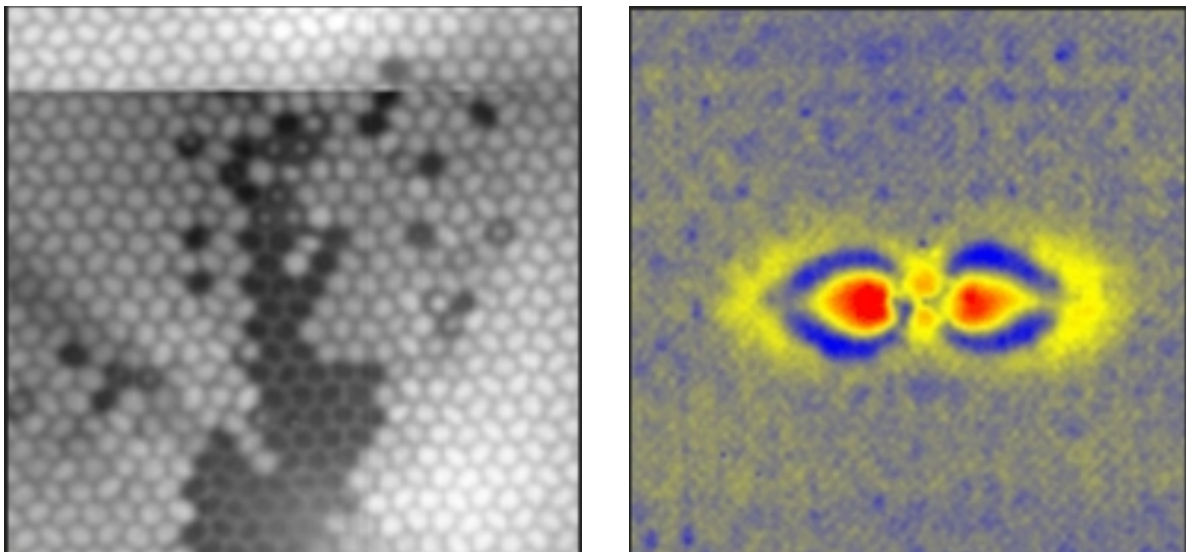

Figure 5-65: Sample Thermography Images Showing a Damage in Composite Structures

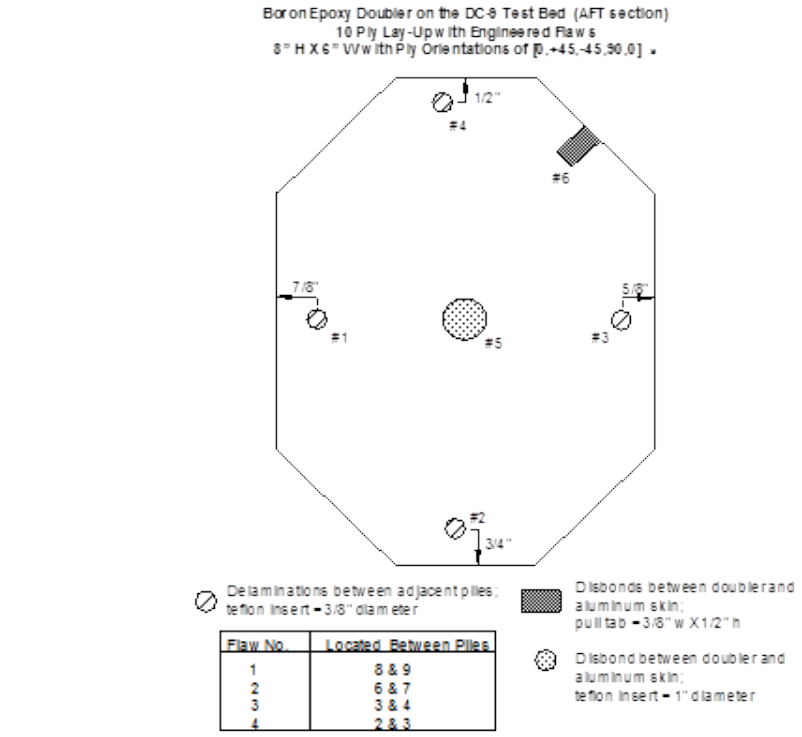

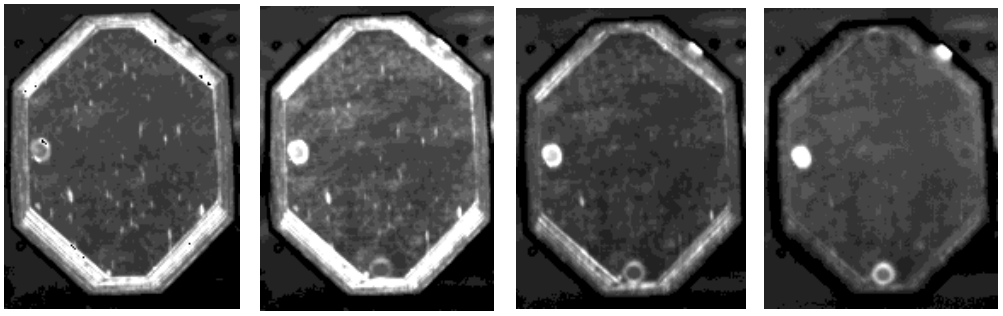

gate 1: 5 f gate 2: 20 f gate 3: 43 f gate 5: 115 f

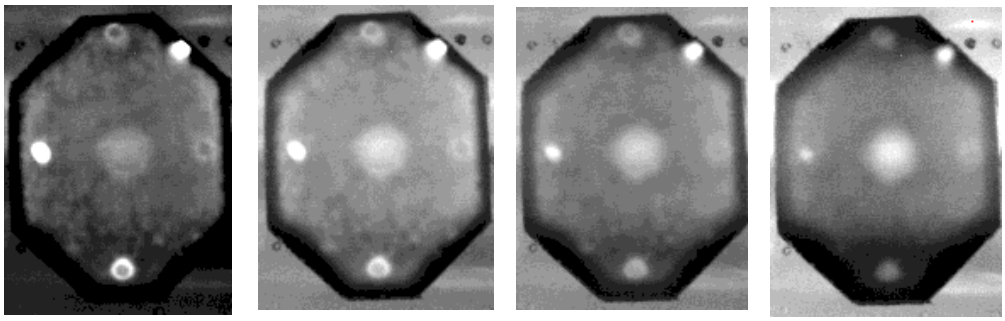

gate 7: 205 f gate 9: 305 f gate 11: 413 f gate 14: 660 f

frame time ("f") = 1/60 of a second

Figure 5-66: Sequence of Thermal Wave Images from a

5.3 Microwave

Microwave inspection works by using a specialized transducer to bathe the material of interest in microwave energy of an essentially constant frequency. Several different system set-ups for Microwave inspection are shown in Figure 5-67 and Figure 5-68. The energy is reflected from each interface between materials possessing differing dielectric constants within the specimen. The reflected energy is superimposed, creating a signal that is acquired as an analog voltage which is digitized. This signal is sampled at numerous discrete locations across the sample to create a two-dimensional image of the surface as shown in Figure 5-69 and Figure 5-70.

The ability of microwaves to penetrate inside dielectric materials makes microwave inspections an NDT technique very suitable for interrogating structures made of non-conductive composites. Additionally, the sensitivity of microwaves to the presence of dissimilar layers in such materials allows for accurate thickness measurement and variation detection. The quality of the experimental images captured with these systems has demonstrated the potential of the technique for material NDT purposes. Basically, these systems utilize an antenna (a horn antenna used in the first experiments or open-ended rectangular waveguide used in recent years) to illuminate the composite with electromagnetic waves (for this particular applications the EM wavelength go from 1 up to 100 mm) and monitor the reflected waves. The EM waves penetrate deep into the dielectric material where they interact with its interior and reflect back to the antenna. The properties of the reflected wave will convey the needed information about the composite at hand. The Imaging mechanism is based on the idea that microwaves are very sensitive to discontinuities in the material space and the presence of water (the water reflects specularly with the wavelength of microwaves).

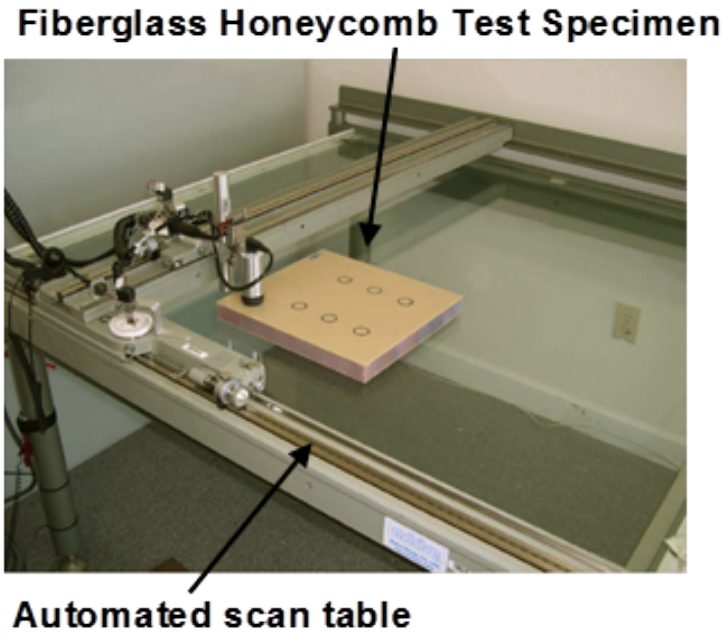

Figure 5-67: Configuration of Microwave Inspection System on a Laboratory Scan Table

Figure 5-68: Basic Equipment Set-up for Microwave Inspection

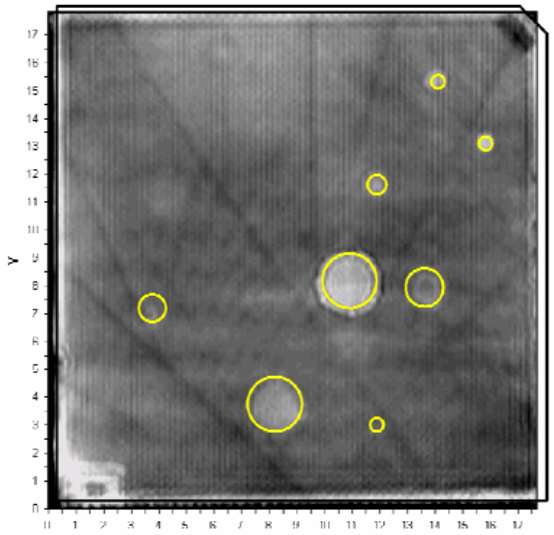

Figure 5-69: Sample Microwave Inspection Results for 3 Ply Fiberglass Panel with Engineered Flaws in the Laminate and Bond Line (Fiberglass Skin Bonded to Nomex Honeycomb)

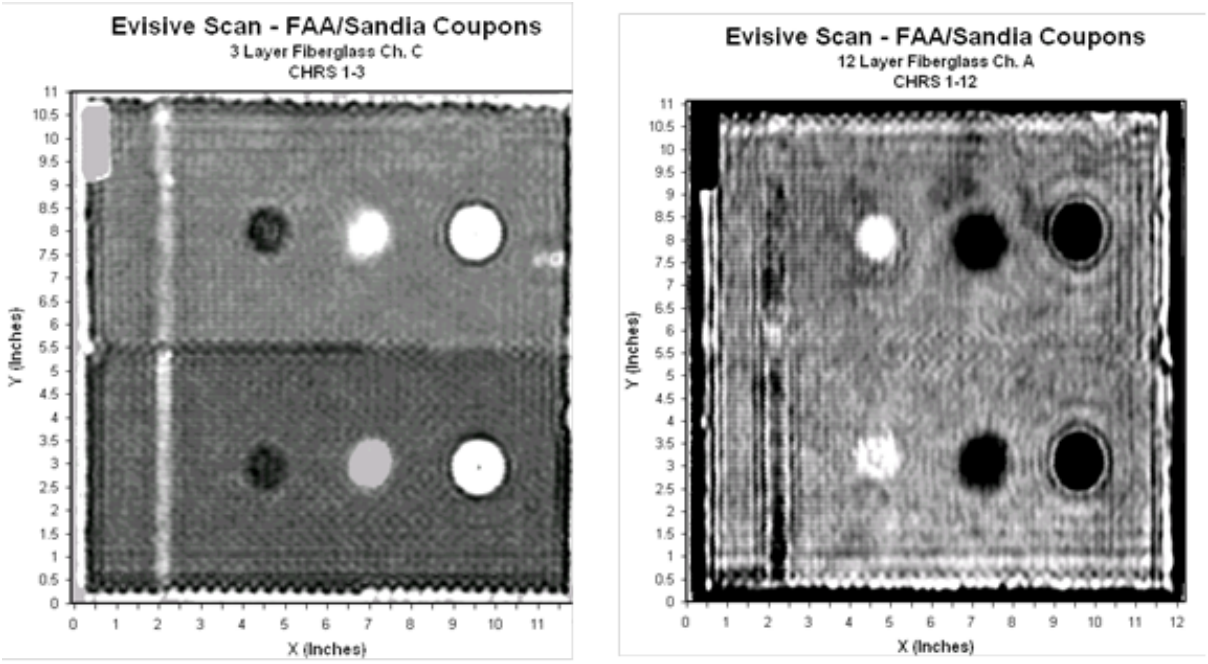

Figure 5-70: Sample Microwave Inspection Results for 3 Ply and 12 Ply Fiberglass Panels with Delamination, Disbonds, Potted Core and Core Splice

Microwave NDT techniques may be conducted on a contact or non-contact basis. In addition, these techniques are conducted from only one side of the sample (reflection techniques).

Furthermore, when compared with ultrasonic techniques, microwave NDT approaches require no coupling material and do not suffer from signal attenuation. Microwave techniques are able to detect voids, delaminations, porosity variation in a variety of materials as well as impact damage and water infiltration. These are all problems that affect composite materials and also provide the possibility of process control during the manufacturing. Finally, microwave NDT techniques do not require a high level of expertise from an operator and can be conducted in real time with simple, portable hardware. The main limitation of the Microwave method is that it is limited to non-conductive materials. Thus, it has been successfully applied to fiberglass composite structures but cannot be used to inspect carbon graphite composites.

Physical Optics Corporation, a small business located in Torrance, CA, has developed a Microwave Inspection Tool (MIT) for the nondestructive inspection of composite multi-layer components and structures. The MIT is based on the use of a near-field microwave probe along with novel property reconstruction and data visualization algorithms to inspect nonconductive, multi-layer composites. In particular, MIT is designed to detect and identify structural defects (e.g., delaminations, inclusions, voids, and disbonds), as well as variations in material layer thickness. MIT can be used for nondestructive inspection and manufacturing verification of non-conducting parts providing defect data and layer-by-layer material property data in a portable system compatible with use in the field, as well as manufacturing and storage environments. POC's MIT provides an alternative in-situ technique to ultrasonic testing (UT) capable of penetrating thick parts and a safer and lower cost alternative to X-ray inspection.

The MIT probe is designed to operate in the X band around 12 GHz frequency. The probe can be guided by hand, and only requires access to a single-side of the part, similar to ultrasonic phased array widely fielded for UT. The low energy microwaves penetrate through the thickness of the part and the probe collects the back-scattered energy. Discontinuities in the material dielectric properties caused by defects enable the detection of defects throughout the thickness of composite parts. By manually scanning the handheld probe over the part and tracking its position in real-time using an onboard six degree-of-freedom position sensor, a C-scan image of the data can be generated. The probe need not be guided in a controlled path—the user simply needs to uniformly cover the majority of the region under test in order for the software to produce a representative C-scan data product. The probe contacts the part with four Teflon feet that maintain a fixed stand-off distance of a few millimeters between the microwave aperture and the part surface. This approach allows the probe to follow the curves and contours of the sample under test and enables the C-scan data to be rendered conformally (i.e. as a 3D shell with a shape corresponding to the curvature of the part). The data is collected by a vector network analyzer (VNA) and processed and visualized by POC's software which runs on a Windows laptop. The handheld probe and VNA along with a Sandia wind blade sample are shown in Figure 5-71 Figure 1. The handheld transducer (blue) includes the microwave near-field probe and an integrated position tracking sensor. The VNA and laptop (not shown) are used for data acquisition, processing, and data visualization for analysis.

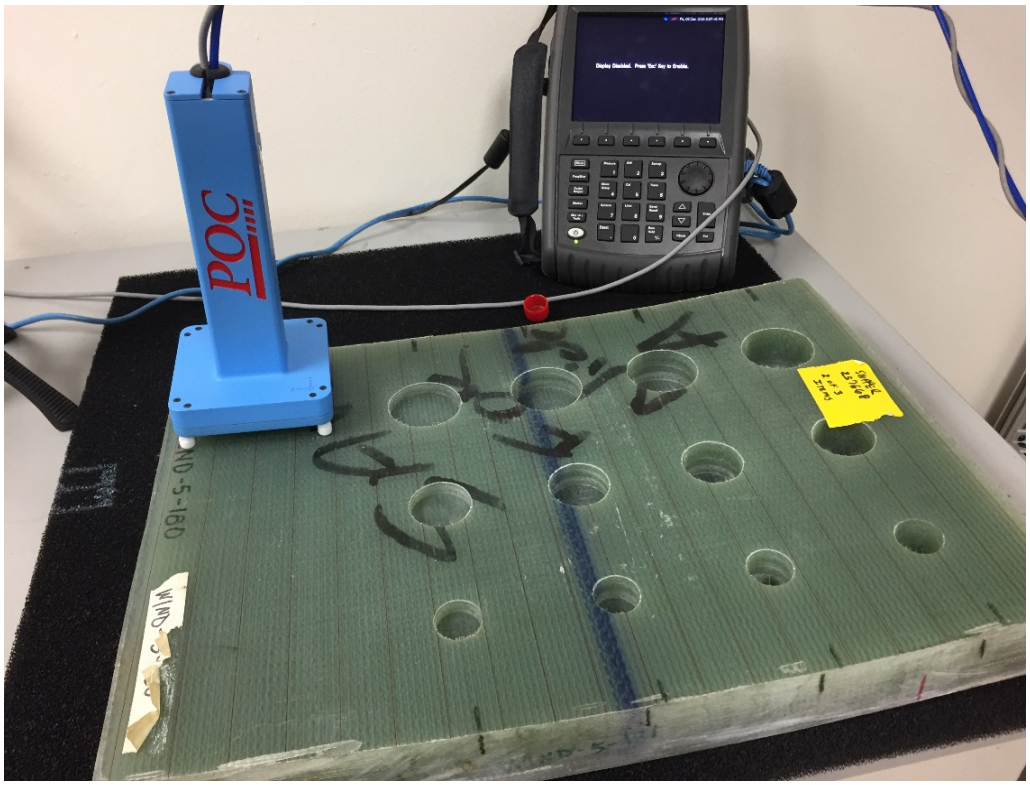

Figure 5-71: Microwave Inspection Tool (MIT) on a Sandia Wind Blade Test Specimen – Hand-Deployed Probe Includes Near Field Microwave and Position Tracker

References

5.1 Roach, D.P., Moore, D., and Walkington, P., "Nondestructive Inspection of Bonded Composite Doublers for Aircraft", Proceedings of SPIE Conference on Nondestructive Evaluation of Aging Aircraft, December 1996.

5.2 Roach, D., Beattie, A., Dahlke, L., Gieske, J., Hansche, B., Phipps, G., Shagam, R., and Thompson, K., "Emerging Nondestructive Inspection Methods for Aging Aircraft"; Dept. of Energy SAND Report 92-2732, March 1994; Dept. of Transportation Report No. DOT/FAA/CT-94/11, October 1994.

5.3 Palmer, D.D., Wood, N.O., "Development of MAUS Enhancements for Large Area Wing Inspections," Air Force Structural Integrity Conf., Dec. 1999.

5.4 Thomas, R., Favro, L., Han, X. and Zhong, O. "Thermal Methods Used in Composite Inspection," *Comprehensive Composite Materials*, vol. 5 Pergamon/Elsevier Science, Oxford, 2000.

5.5 Favro, L., Han, X. and Thomas, R.,"Quantitative Thermal-wave measurement of defects in composite aircraft structures", 44th International SAMPE Symposium and Exhibition, 1999.

5.6 Shepard, S., Roach, D., "Signal Enhancement and Noise Reduction Strategies for Thermographic Inspections," FAA/DOD/NASA Aging Aircraft Conference, May 2009.

THIS PAGE INTENTIONALLY LEFT BLANK

Chapter 6

6.0 Results from Wind Blade Flaw Detection Experiment

Each inspection technique that was applied in this blind flaw detection experiment was evaluated using the following performance attributes: 1) accuracy and sensitivity, 2) data analysis capabilities, 3) versatility, 4) portability, 5) complexity, 6) human factors and 7) inspection time. The most important of these parameters was the quantitative metrics since they are objective standards that can be numerically counted or quantified. Accuracy is the ability to detect flaws reliably and correctly in composite structures and repairs without false calls. Sensitivity is the extent to which the inspection system responds to flaws as a function of size, type, and location in the structure (e.g., proximity to edges, taper regions, underlying or adjacent structural elements). The total inspection area for the set of 11 panels in the WBFDE was 49 ft ^{2}.

The set of graphs in this report present all of the detailed results for all aspects of the WBFDE. These include the Probability of Detection (POD) curves for each inspector, as well as the resulting cumulative POD curve for overall wind blade inspections (industry baseline). The curves show the variation within the group of inspectors that completed each experiment. The results are also broken down into those obtained for specific wind blade designs (Spar Cap and Shear Web Construction and Box Spar Construction), as well for specific features/regions within each of these blade designs. The primary quantitative assessments involve Probability of Detection curves based on a statistical hit-miss analysis, along with assessments of false calls, flaw sizing capabilities and detection levels and challenges associated with different, typical flaws found in wind blades.

6.1 Conventional Pulse-Echo Ultrasonics

6.1.1. WBFDE – Overall Probability of Detection Results for All Specimens (Spar Cap with Shear Web and Box type Construction)

Table 6-1 summarizes the various pulse-echo ultrasonic devices that were utilizes in the WBFDE. The equipment array does allow this POD study to capture any potential variations that may be associated with equipment response. However, the goal of the POD testing was to establish an overall performance baseline for the wind industry as a whole. Thus, the array of UT devices, used in combination with the standard 0.5 MHz transducer, provides a good overall view of flaw detection capabilities for today's wind blade inspections. Figure 6-1 compares the maximum likelihood estimate ($POD_{[90]}$) to the POD curve that is calculated when a 90% flaw detection is combined with a 95% confidence bound ($POD_{[90/95]}$). This solid line in Figure 6-1 provides the performance curve that the industry normally uses to measure the performance of NDI methods as deployed by representative inspectors. Thus, this curve provides the overall POD for all inspectors representing the baseline for the entire wind industry. For these experiments, POD values were calculated using a pass/fail analysis with a log normal model. It

can be seen in Figure 6-1 that the overall cumulative $POD_{[90/95]}$ for all flaws in the WBFDE was $POD_{[90/95]}$ = 1.33" diameter flaw.

Wind Blade Flaw Detection Experiment Inspector Equipment Used - Conventional Pulse-Echo UT		
Inspector	**Probe Frequency Used**	**Equipment Used**
A	0.5 MHz	Olympus Epoch XT
B	0.5 MHz	Sonatest VEO
C	0.5 MHz	Olympus Epoch XT
D	0.5 MHz	Olympus Epoch XT
E	0.5 MHz	Olympus Epoch XT
F	0.5 MHz	Olympus Epoch XT
G	0.5 MHz	Sonatest VEO
H	0.5 MHz	Sonotron NDT ISONIC utPod
I	0.5 MHz	Olympus Epoch 1000I
J	0.5 MHz	Sonotron NDT ISONIC utPod
K	0.5 MHz	Olympus Epoch XT
L	0.5 MHz	GE USN 60

Table 6-1: List of Pulse-Echo A-Scan Equipment Used in the Conventional NDI Portion of the Wind Blade Flaw Detection Experiment

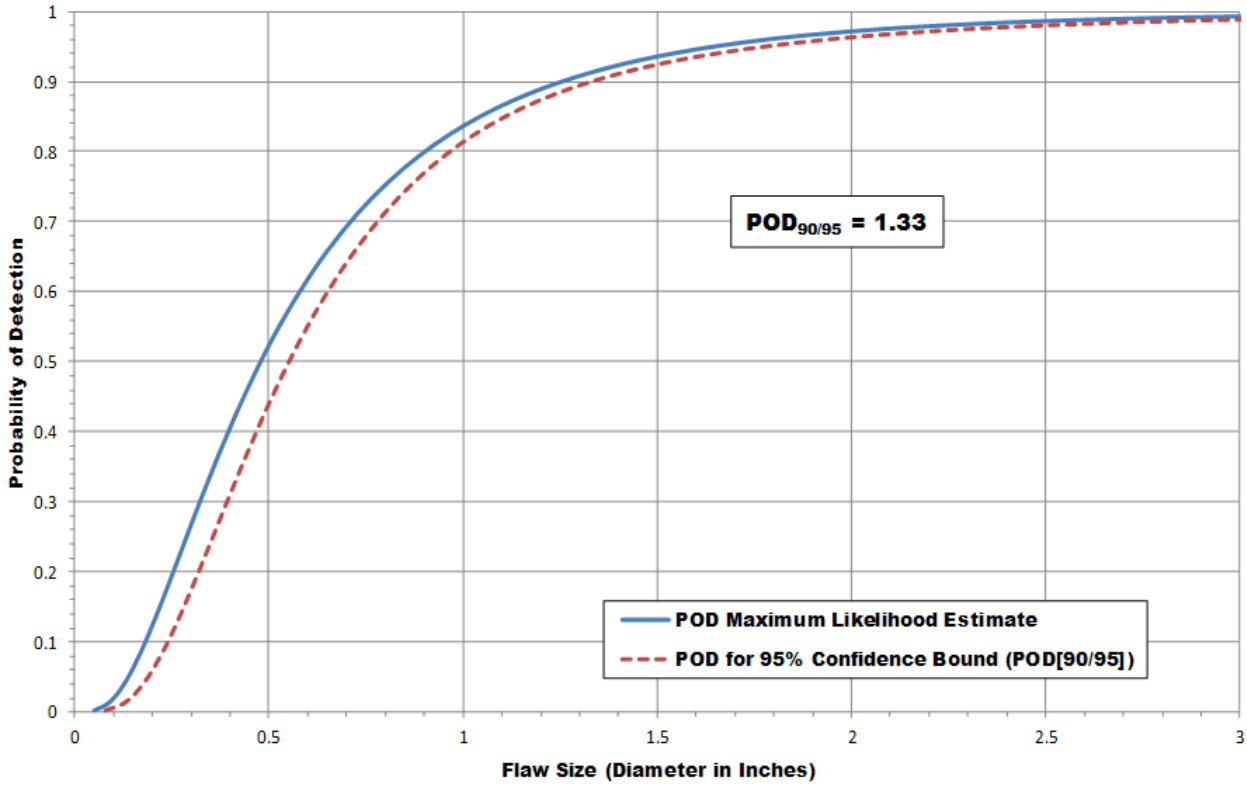

Figure 6-1: Cumulative POD Curve Representing Conventional PE-UT from All 12 Inspectors Inspecting All WBFDE Test Specimens (Spar Cap & Shear Web and Box Spar Construction)

Table 6-2 summarizes the cumulative $POD_{[90/95]}$ for the entire set of WBFDE specimens and for specific regions within those test specimens. First it shows that the overall $POD_{[90/95]}$ value was 1.33". Next, a check was conducted on the entire data set obtained in the conventional NDI testing. If the high (worst performing) and low (best performing) inspectors are removed from the overall calculation, the POD result remains essentially unchanged. This demonstrates the robustness of the data obtained and indicates that the performance statistics are viable. Finally, three subset categories of regions within the test specimens are also listed. For the constant thickness regions, representing the spar cap laminates and skins above the bond line, the $POD_{[90/95]}$ value dropped to 1.24" indicating a relatively easier inspection. For the complex geometry regions, representing all flaws in the bond lines and all flaws in spar cap laminates located beneath the bond line, the $POD_{[90/95]}$ value jumps to 1.49" indicating a relatively more difficult inspection. The third category focuses on the inspection for flaws within the bond lines. In this case, the $POD_{[90/95]}$ values is 1.23" indicating that the bond lines inspections provide the highest inspection performance.

Cumulative POD Results Table - Wind Blade Flaw Detection Experiment Conventional Pulse-Echo UT - All Spar Cap & Shear Web and Box Type Construction	
Condition	**$POD_{90/95}$ (Dia. In Inches)**
All Flaws - 12 Inspectors - Panels (1-11)	1.33
All Flaws - 10 Inspectors (High and Low Removed) - Panels (1-11)	1.30
Only Constant Thickness Flaws * - 12 Inspectors - Panels (1-11)	1.24
Only Complex Geometry Flaws ** - 12 Inspectors - Panels (2, 4, 6, 8, 10 &11)	1.49
Only Bond Line Flaws - 12 Inspectors - Panels (2, 4, 6, 8, 10 &11)	1.23

* Constant Thickness – All laminate and skin flaws above the bond line.

** Complex Geometry – Pertains to all flaws in the bond lines and all flaws in the laminates below the bond lines in box type construction.

Table 6-2: Cumulative Results Representing the Overall Performance (POD90/95 Values) of the Wind Blade Manufacturing Industry

Figure 6-2 shows the summary of the Probability of Detection results for the entire set of blind POD Specimens and all inspectors using conventional pulse-echo ultrasonics with a single-element transducer deployed in A-scan mode only. It plots the spread of all the individual inspector $POD_{[90]}$ curves (dashed lines) compared to the cumulative $POD_{[90]}$ curve (solid line) for all 12 inspectors. In the WBFDE, the best performing inspector produced a $POD_{[90/95]}$ = 0.98" diameter flaw, the worst inspector produced a $POD_{[90/95]}$ = 2.67" diameter, and the overall cumulative result was a $POD_{[90/95]}$ = 1.33" diameter. The individual inspection results had a

172% spread from best to worst performance. Data spread, or variation in performance from one inspector to another, is an expected occurrence and is the reason that multiple inspectors are used to arrive at an overall, cumulative POD value that properly represents the wind industry. However, Section 6.1.5 will address methods and procedures that can be deployed to reduce this spread and achieve more uniform NDI performance across the industry. Overall, this data indicates that a wind blade production company deploying conventional UT equipment can expect to detect a 1.33" diameter flaw anywhere in the critical structural region of the blade (spar cap region) with a 90% probability of detection and a 95% confidence factor. The Box Spar construction was more difficult to inspect than the spar cap with shear web construction. When the data from these two specimen sets are analyzed separately, the results in Section 6.1.2 show that the POD level for the Spar Cap and Shear Web construction drops to 1.25" (~ 9% improvement).

Figure 6-3 to Figure 6-6 contain the actual plots of the data summarized in Table 6-2. First, Figure 6-3 shows that there is no shift in the overall POD level when the high (worst performing) and low (best performing) inspectors are removed from the overall calculation. Figure 6-4 to Figure 6-6 highlight that the constant thickness region of the test specimens produce a better/lower POD and are designated as relatively easier regions to inspect, the complex geometry regions produce a poorer/higher POD and are designated as relatively harder regions to inspect, and that, in the bond line regions, the flaw detection was the best for what is probably the primary area of interest. In addition, the inspections in the bond lines region were much more repeatable as the range/spray in results was reduced from 172% for all specimens to 156% in bond lines only.

Performance brackets were used to place inspectors into groups and then calculate the resulting $POD_{[90/95]}$ for each performance bracket. Table 6-3 divides the participants into categories of outstanding (top 4), good (middle 4) and average (bottom 4) inspectors to assess their performance as a group. These performance brackets utilized the inspectors that fell into the 30, 70 and 90 percentile categories. The inspectors that fell into the "outstanding" group (4 inspectors, each having a $POD_{[90]}$ less than 1.2") produced a 30% improvement to $POD_{[90/95]}$ = 0.1.03" diameter flaw value compared to the overall cumulative, industry baseline $POD_{[90/95]}$ = 1.33" diameter flaw. The "good" inspector group (4 inspectors, each having a $POD_{[90]}$ less than 1.6") produced approximately the same results as the whole group. The "average" inspector group (4 inspectors, each having a $POD_{[90]}$ less than 2.0") showed an 35% poorer performance with an overall $POD_{[90/95]}$ = 1.79" diameter flaw. These performance brackets might be useful to wind blade companies who can judge where their inspectors fall within the brackets and the resulting performance they will obtain from their inspectors. These results reveal the degree of inspection improvements that are possible if inspectors can shift their performance from the average (worse) performance brackets to the outstanding (better) performance brackets. This shift in performance can be brought about by improved or more extensive composite inspection training and through optimized inspection procedures including the use of NDI Reference Standards. This topic will be discussed and analyzed further in Section 6.1.4.

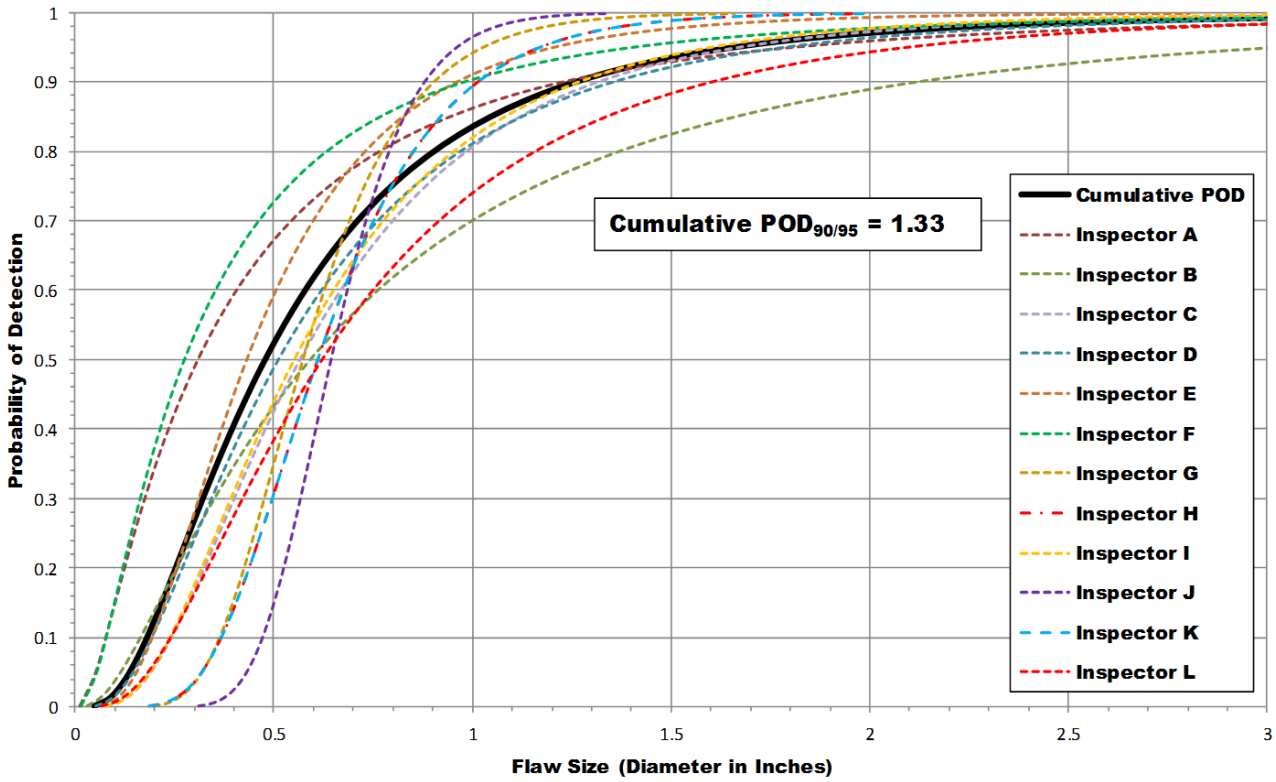

Individual Inspector POD Results Table All Spar Cap & Shear Web and Box Type Construction Conventional PE-UT - All Flaws - All Panels (1-11)	
Inspector	**$POD_{90/95}$ (Dia. In Inches)**
Inspector A	1.51
Inspector B	2.67
Inspector C	1.58
Inspector D	1.65
Inspector E	1.19
Inspector F	1.36
Inspector G	1.78
Inspector H	1.04
Inspector I	1.52
Inspector J	0.98
Inspector K	1.17
Inspector L	1.96
Overall Cumulative $POD_{90/95}$	**1.33**
Range Spread	**172.45%**

Figure 6-2: Individual Inspectors & Cumulative POD_{90} Curve Comparisons for All Panels Plus $POD_{90/95}$ Values for Each Inspector and the Cumulative Result Representing the Overall Performance of the Wind Blade Manufacturing Industry (Spar Cap with Shear Web and Box Spar Construction Types)

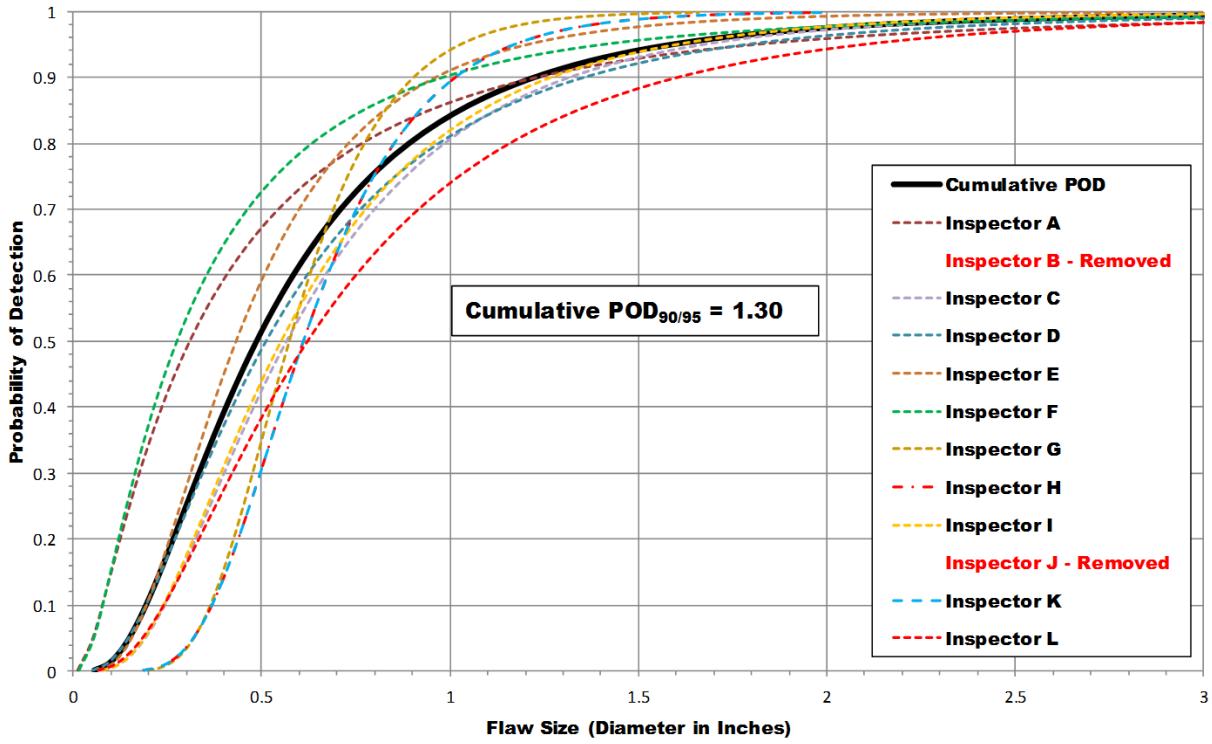

Figure 6-3: Individual Inspectors & Cumulative POD Curve Comparisons for All Panels Showing the Overall Performance When the Best and Worst Performers are Removed

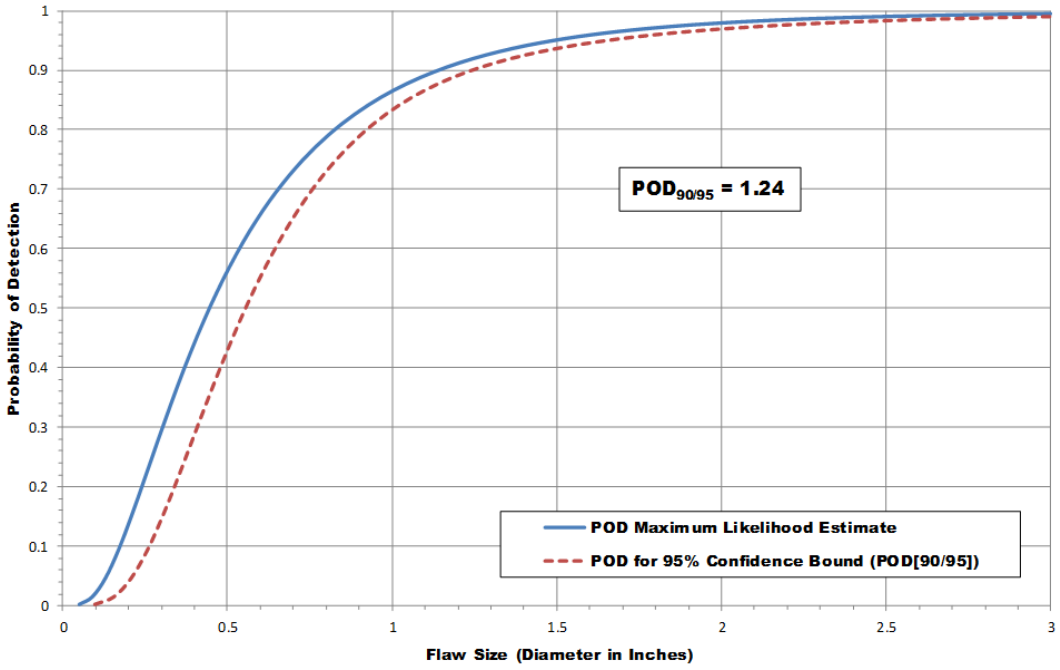

Figure 6-4: Cumulative POD Curve Representing Conventional PE-UT from All 12 Inspectors Inspecting Only the Constant Thickness Regions of the WBFDE Test Specimens (Laminate and Skin Flaws)

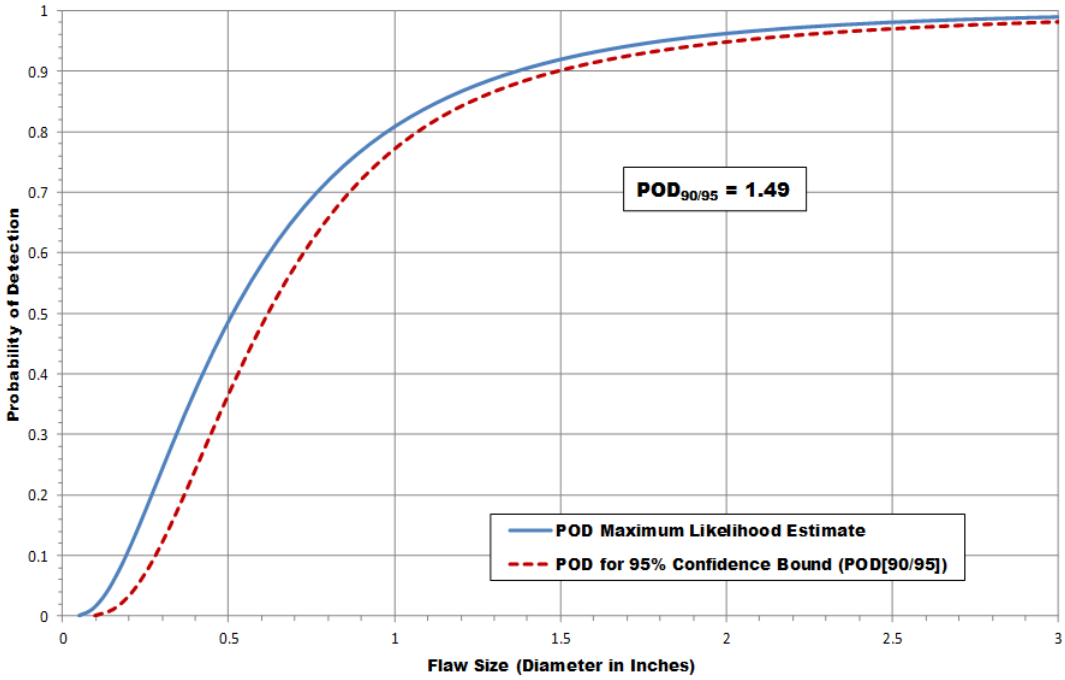

Figure 6-5: Cumulative POD Curve Representing Conventional PE-UT from All 12 Inspectors Inspecting Only the Complex Geometry Regions of the WBFDE Test Specimens (Bond Line & Laminate Under Bond)

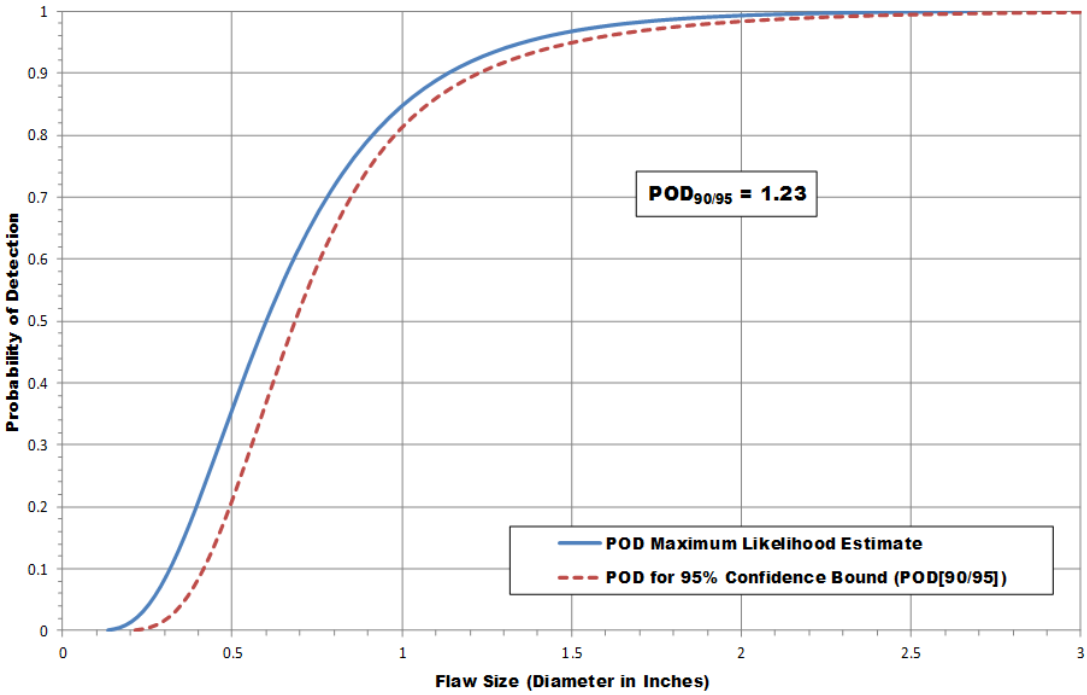

Figure 6-6: Cumulative POD Curve Representing Conventional PE-UT from All 12 Inspectors Inspecting Only the Bond Line Regions of the WBFDE Test Specimens (Bond Line Flaws Only)

Cumulative POD Results Table - Wind Blade Flaw Detection Experiment Conventional Pulse-Echo UT - All Spar Cap & Shear Web and Box Type Construction Inspector Performance Levels	
Condition	**$POD_{90/95}$ (Dia. In Inches)**
All Flaws - 12 Inspectors - Panels (1-11)	1.33
All Flaws - Top 4 Inspectors - Panels (1-11)	1.03
All Flaws - Middle 4 Inspectors - Panels (1-11)	1.34
All Flaws - Bottom 4 Inspectors - Panels (1-11)	1.79

Table 6-3: Overall POD Results When Top, Middle and Bottom Performing Inspectors Are Grouped and Considered Separately

Table 6-4 summarizes the total time and inspection rates for each inspector during the WBFDE testing. This data can be further analyzed to determine an optimum inspection coverage rate. This, of course, will depend on the deployment mechanism. For example, a hand-deployed UT inspection will proceed much slower than an automated scanner-deployed UT inspection, for similar area coverage. Overall, the average inspection time for all 11 panels was just over 10 hours for a coverage rate of 11.8 min/ft.^{2} (5.1 ft.^{2}/hour). If the individual specimen types are considered, the spar cap and shear web construction specimens required an average of 50 minutes per panel for a coverage rate of 5.3 ft.^{2}/hour. The Box Spar construction required slightly more time with an average inspection time of 75 minutes per panel for a coverage rate of 7.1 ft.^{2}/hour. Figure 6-7 plots the array of inspector inspection rates vs. their resulting overall POD; this shows the effect of inspection rate on POD; for the inspection rates encountered in this experiment, it was determined that the rates observed had no effect on the resulting POD values; this indicates that inspection rates from 8 to 18 min/ft.^{2} can produce similar performance values although the deviation in POD results was reduced significantly for inspections using a rate in excess of 12 min/ft. ^{2}.

Experiment Timing Summary Wind BFDE - All Inspectors - All Panels (1 - 11) - Conventional Pulse Echo UT													
	Spar Cap & Spar Cap with Shear Web Construction									Box Construction		Total Insp. Time (hr:min)	100% Inspection Area Coverage Rate (hr:min:sec)/ft^2
	Specimen WPOD-1	Specimen WPOD-2	Specimen WPOD-3	Specimen WPOD-4	Specimen WPOD-5	Specimen WPOD-6	Specimen WPOD-7	Specimen WPOD-8	Specimen WPOD-9	Specimen WPOD-10	Specimen WPOD-11		
Inspector A	1:03	2:22	0:55	1:15	0:35	0:55	1:13	0:32	0:33	2:00	1:25	**12:48**	0:15:43
Inspector B	0:45	0:43	0:34	0:49	0:38	0:46	0:38	0:37	0:28	0:36	0:33	**7:07**	0:08:44
Inspector C	0:58	1:18	0:56	2:28	0:50	1:21	1:40	1:09	0:46	2:05	1:16	**14:47**	0:18:09
Inspector D	1:28	2:05	0:29	0:56	1:13	0:45	0:48	0:49	0:59	1:12	2:08	**12:52**	0:15:47
Inspector E	0:32	1:12	0:17	0:51	0:39	0:54	0:37	1:07	0:21	1:14	1:34	**9:18**	0:11:25
Inspector F	0:19	0:37	0:37	0:35	1:08	0:37	0:22	0:36	0:18	0:44	0:25	**6:18**	0:07:44
Inspector G	0:40	0:47	0:37	1:08	0:51	0:52	0:52	0:36	0:40	0:47	0:45	**8:35**	0:10:32
Inspector H	0:41	1:10	0:21	0:51	0:29	0:44	0:22	0:35	0:25	0:59	1:11	**7:48**	0:09:34
Inspector I	0:20	1:02	0:24	0:58	0:37	1:26	0:37	1:14	0:25	0:38	1:04	**8:45**	0:10:44
Inspector J	1:01	1:44	0:39	0:49	0:30	1:10	0:31	0:35	0:30	0:47	0:40	**8:56**	0:10:58
Inspector K	0:35	0:59	0:35	0:40	0:42	0:47	0:50	0:51	0:40	1:24	1:34	**9:37**	0:11:48
Inspector L	0:44	0:37	0:30	0:56	0:52	0:46	0:29	0:31	0:32	1:42	0:58	**8:37**	0:10:34
Ave. Insp. Time (hr:min)	**0:45**	**1:13**	**0:34**	**1:01**	**0:45**	**0:55**	**0:44**	**0:46**	**0:33**	**1:10**	**1:07**	9:37	**11:48 min/ft^2**
Total Inspection Area (11 Panels) = 48.89 ft^2													

Table 6-4: Inspection Timing and Inspection Coverage Rate for All WBFDE Participants

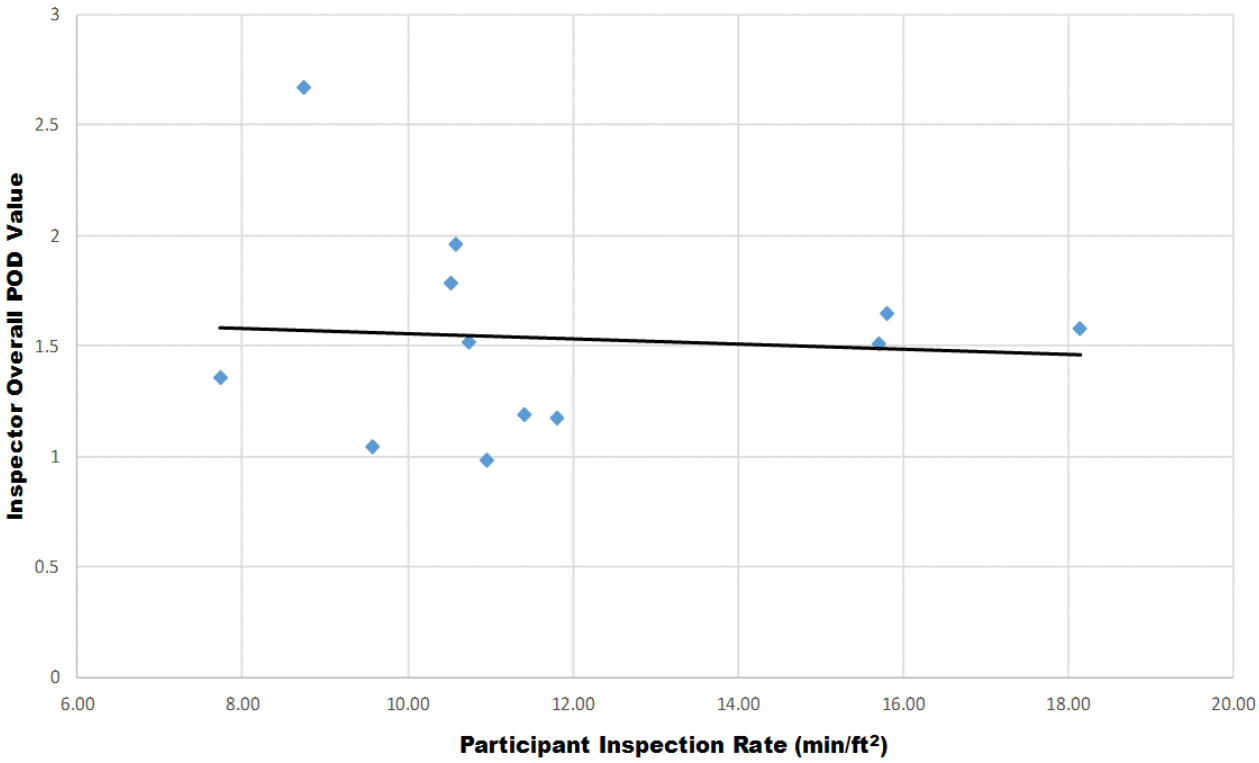

Figure 6-7: Participant Inspection Rate vs. Resulting Inspector POD Value for Conventional UT Inspections on All Panels

Tabulated results are also provided to summarize various aspects of the experiment. Table 6-5 through Table 6-8 present the percentage of flaws detected for each flaw size along with the ability of each inspector to accurately size the flaw once it is detected. In this latter category, it can be seen that 60-70% of the flaws were sized in the 75% to 100% of actual size. Thus, flaw sizing after detection is not a significant issue. Note that Table 6-5 presents the results for all data from all test specimens while Table 6-6 presents the data for only flaws in the Constant Thickness regions, Table 6-7 presents the data for only flaws contained in the Complex Geometry regions and Table 6-8 presents the data for only flaws contained in the Bond Line regions. Constant Thickness Geometry is defined as the inspection regions where the number of plies remain constant. These are the flaws in the outer laminate spar cap in the spar cap-to-shear web construction and the flaws in the outer skin of the Box Spar construction. The Complex Geometry regions are defined as those areas beneath the outer laminate in the spar cap-to-shear web construction or the outer skin in the Box Spar construction (i.e. flaws at the bond line and below. While we might expect the flaw detection in the more challenging, deeper Complex Geometry regions to be worse than in the upper, Constant Thickness regions, this was not the case. Table 6-5 through Table 6-8 **Error! Reference source not found.**show that the flaw detection was almost the same for all flaws distributed throughout the wind blade assemblies. Thus, the inspectors displayed almost equal performance for both the laminate and bond line flaws. Figure 6-8 displays the similarities in the percent flaw detection in all four categories: 1) all flaws in the WBFDE, 2) only flaws in the Constant Thickness region, and 3) only flaws in the Complex Geometry regions, and 4) only flaws in the Bond Line regions.

Overall Flaw Detection Percentage & Accuracy in Determining Flaw Size All Panels (1-11) - 12 Inspectors - All Flaws Conventional Pulse Echo UT							
Accuracy in Sizing the Flaws That Were Detected (1546 Total Flaws Detected)						Flaw Detection Percentage (1704 Total Flaws)	
Flaw Size	5 (100%)	4 (76%-99%)	3 (51%-75%)	2 (25%-50%)	1 (< 25%)	Flaw Size	Percent Detected
0.75	42%	18%	16%	10%	15%	0.75	74%
1.00	35%	32%	19%	9%	6%	1.00	83%
1.50	24%	40%	19%	10%	7%	1.50	93%
2.00	22%	47%	16%	10%	4%	2.00	97%
2.50	20%	46%	22%	9%	4%	2.50	99%
3.00	16%	52%	13%	8%	12%	3.00	99%
Overall Sizing Performance	26%	40%	18%	10%	7%	Overall Flaw Detection	91%

Table 6-5: Summary of Inspector Flaw Detection and Flaw Sizing Accuracy – All Flaws

Overall Flaw Detection Percentage & Accuracy in Determining Flaw Size All Panels (1-11) - 12 Inspectors - All Constant Thickness Flaws Conventional Pulse Echo UT							
Accuracy in Sizing the Flaws That Were Detected (801 Total Flaws Detected)						Flaw Detection Percentage (864 Total Flaws)	
Flaw Size	5 (100%)	4 (76%-99%)	3 (51%-75%)	2 (25%-50%)	1 (< 25%)	Flaw Size	Percent Detected
0.75	38%	23%	20%	10%	10%	0.75	77%
1.00	28%	36%	21%	11%	4%	1.00	87%
1.50	27%	41%	22%	6%	4%	1.50	94%
2.00	29%	49%	10%	7%	4%	2.00	99%
2.50	22%	45%	23%	6%	4%	2.50	99%
3.00	22%	55%	12%	8%	3%	3.00	100%
Overall Sizing Performance	27%	42%	18%	8%	5%	Overall Flaw Detection	93%

Table 6-6: Summary of Inspector Flaw Detection and Flaw Sizing Accuracy – Constant Thickness Flaws Only

Overall Flaw Detection Percentage & Accuracy in Determining Flaw Size Panels (2, 4, 6, 8, 10 & 11) - 12 Inspectors - All Complex Geometry Flaws Conventional Pulse Echo UT							
Accuracy in Sizing the Flaws That Were Detected (745 Total Flaws Detected)						Flaw Detection Percentage (840 Total Flaws)	
Flaw Size	5 (100%)	4 (76%-99%)	3 (51%-75%)	2 (25%-50%)	1 (< 25%)	Flaw Size	Percent Detected
0.75	46%	12%	12%	9%	21%	0.75	70%
1.00	40%	28%	17%	8%	7%	1.00	80%
1.50	21%	38%	15%	15%	11%	1.50	92%
2.00	16%	45%	21%	13%	4%	2.00	95%
2.50	16%	46%	19%	15%	4%	2.50	99%
3.00	12%	49%	13%	7%	18%	3.00	99%
Overall Sizing Performance	24%	38%	17%	12%	9%	Overall Flaw Detection	89%

Table 6-7: Summary of Inspector Flaw Detection and Flaw Sizing Accuracy – Complex Geometry Flaws Only

Overall Flaw Detection Percentage & Accuracy in Determining Flaw Size Panels (2, 4, 6, 8, 10 & 11) - 12 Inspectors - All Bond Line Flaws Only Conventional Pulse Echo UT							
Accuracy in Sizing the Flaws That Were Detected (516 Total Flaws Detected)						Flaw Detection Percentage (576 Total Flaws)	
Flaw Size	5 (100%)	4 (76%-99%)	3 (51%-75%)	2 (25%-50%)	1 (< 25%)	Flaw Size	Percent Detected
0.75	52%	11%	8%	8%	23%	0.75	69%
1.00	39%	32%	17%	7%	6%	1.00	84%
1.50	31%	41%	15%	8%	5%	1.50	95%
2.00	25%	47%	19%	4%	3%	2.00	98%
2.50	18%	56%	18%	7%	1%	2.50	100%
3.00	21%	67%	10%	0%	2%	3.00	100%
Overall Sizing Performance	31%	41%	16%	6%	6%	Overall Flaw Detection	90%

Table 6-8: Summary of Inspector Flaw Detection and Flaw Sizing Accuracy – Bond Line FlawsOnly

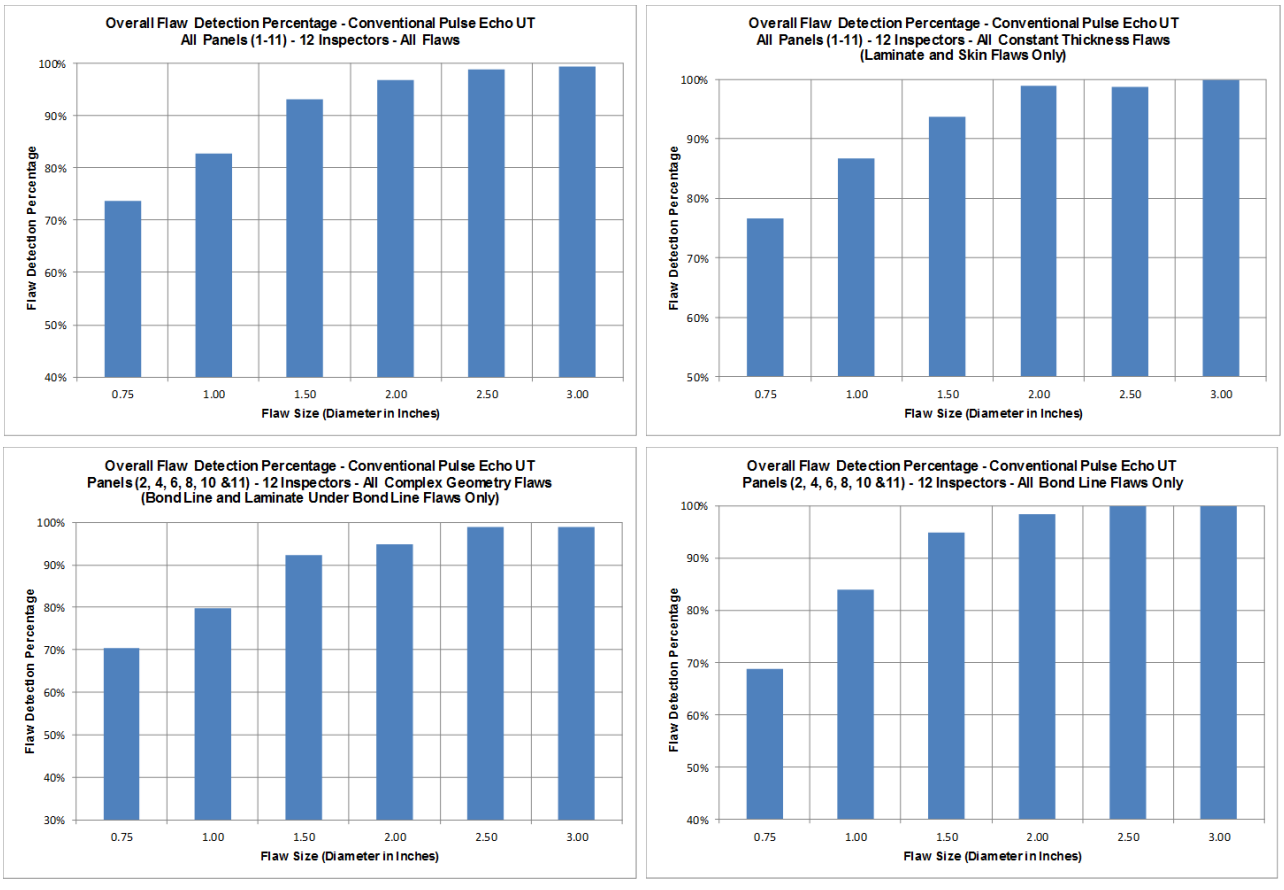

Figure 6-8: Comparison of Flaw Detection Levels for Flaws in Each of the Four Major WBFDE Categories

Table 6-9 summarizes the number of false calls made by each inspector. This table shows the number of false calls made by each inspector for the entire WBFDE specimen set and lists the sizing category that incorporates each false call. The average number of false calls made was determined to be 0.25 false calls per inspector (49 ft.^{2} inspection area) with an average of one false call per 16.3 ft^2 of inspection area. This table shows that false calls do not appear to be an issue as the overall false call rate was determined to be very low. In addition, when follow up inspections are included with final determinations, it is believed that false calls will be close to zero.

Inspection False Calls for All Panels (1-11) - All Inspectors - Pulse Echo UT														
Configuration/Sizing (in.²)	Insp. A	Insp. B	Insp. C	Insp. D	Insp. E	Insp. F	Insp. G	Insp. H	Insp. I	Insp. J	Insp. K	Insp. L	Total	Avg.
Constant Thickness (CT)														
0 - .75in.²	0	0	0	1	0	0	0	0	0	0	0	0	1	0.08
.76in.² - 1.50in.²	0	0	0	0	0	1	0	0	0	0	0	0	1	0.08
1.51in.² - 2.00in.²	0	0	0	0	0	0	0	0	0	0	0	0	0	0.00
2.01in.² - 3.00in.²	0	0	0	0	0	0	0	0	0	0	0	0	0	0.00
> 3.00in.²	0	0	0	0	0	0	0	0	0	0	0	0	0	0.00
CT Total	0	0	0	1	0	1	0	0	0	0	0	0	2	0.17
Complex Geometry (CG)														
0 - .75in.²	0	0	0	0	0	0	0	0	0	0	0	0	0	0.00
.76in.² - 1.50in.²	0	0	0	0	0	0	0	0	0	0	0	0	0	0.00
1.51in.² - 2.00in.²	0	0	0	0	0	0	0	0	0	0	0	0	0	0.00
2.01in.² - 3.00in.²	0	0	0	0	0	0	0	0	0	0	0	0	0	0.00
> 3.00in.²	0	0	1	0	0	0	0	0	0	0	0	0	1	0.08
CG Total	0	0	1	0	0	0	0	0	0	0	0	0	1	0.08
Total (All Flaws)	0	0	1	1	0	1	0	0	0	0	0	0	3	0.25
1 False Call on Average Per 16.3 ft^2 of Inspection Area														

Table 6-9: False Call Rate for All Inspectors and All WBFDE Specimens

6.1.2. WBFDE – Overall Probability of Detection Results for Spar Cap with Shear Web Construction

Table 6-10 shows the summary of the Probability of Detection results when only considering only the Spar Cap with Shear Web type specimens in the WBFDE and all inspectors using conventional pulse-echo ultrasonics with a single-element transducer deployed in A-scan mode. First it shows that the overall $POD_{[90/95]}$ value for the Spar Cap with Shear Web type specimens was reduced to 1.25". Next, a check was conducted on the entire data set obtained in the conventional NDI testing. If the high (worst performing) and low (best performing) inspectors are removed from the overall calculation, the POD result remains essentially unchanged. This demonstrates the robustness of the data obtained and indicates that the performance statistics are viable. Finally, two subset categories of regions within the test specimens are also listed. For

the spar cap laminate regions, the $POD_{[90/95]}$ value was 1.23". For the bond line regions, the $POD_{[90/95]}$ value increases to 1.34" indicating a relatively more difficult inspection for this blade construction type.

Figure 6-9 compares the maximum likelihood estimate ($POD_{[90]}$) to the POD curve that is calculated when a 90% flaw detection is combined with a 95% confidence bound ($POD_{[90/95]}$). This solid line in Figure 6-9 provides the performance curve that the industry normally uses to measure the performance of NDI methods as deployed by representative inspectors. Thus, this curve provides the wind industry baseline when inspecting Spar Cap with Shear Web type blade designs. It can be seen in Figure 6-9 that the overall cumulative $POD_{[90/95]}$ for all flaws in the Spar Cap with Shear Web specimens was $POD_{[90/95]}$ = 1.25" diameter flaw.

Figure 6-10 shows the summary of the Probability of Detection results for the Spar Cap with Shear Web specimens only and all inspectors using conventional pulse-echo ultrasonics with a single-element transducer deployed in A-scan mode only. For the Spar Cap with Shear Web specimens, the best performing inspector produced a $POD_{[90/95]}$ = 1.04" diameter flaw, the worst inspector produced a $POD_{[90/95]}$ = 1.98" diameter, and the overall cumulative result was a $POD_{[90/95]}$ = 1.25" diameter. The individual inspection results had a 90% spread from best to worst performance. This is much lower than the 172% spread observed for all specimens indicating that the inspections in Spar Cap with Shear Web construction is more repeatable. Overall, this data indicates that a wind blade production company deploying conventional UT equipment can expect to detect a 1.25" diameter flaw anywhere in a Spar Cap with Shear Web blade with a 90% probability of detection and a 95% confidence factor. The Box Spar construction was more difficult to inspect than the Spar cap with Shear Web construction and this will be discussed in detail in Section 6.1.3.

Cumulative POD Results Table - Wind Blade Flaw Detection Experiment Conventional Pulse-Echo UT - Spar Cap & Shear Web Type Construction Only	
Condition	**$POD_{90/95}$ (Dia. In Inches)**
All Flaws - 12 Inspectors - Panels (1-9)	1.25
All Flaws - 10 Inspectors (High and Low Removed) - Panels (1-9)	1.25
Only Laminate Flaws - 12 Inspectors - Panels (1-9)	1.23
Only Bond Line Flaws - 12 Inspectors - Panels (2, 4, 6, & 8)	1.34

Table 6-10: Results Representing the Performance ($POD_{90/95}$ Values) of the Wind Blade Manufacturing Industry for the Spar Cap with Shear Web Construction Only, Along with Flaw Detection Performance for Specific Specimen Regions

Figure 6-11 and Figure 6-12 contain the actual plots of the data summarized in Table 6-10. They indicate that the spar cap laminate regions of the test specimens produce approximately the same POD as the overall set and the bond line regions produce a poorer/higher POD and are designated as relatively harder regions to inspect for this type of design configuration.

Tabulated results are also provided to summarize various aspects of the experiment when only the Spar cap with Shear Web construction is considered. Table 6-11 through Table 6-13 present the percentage of flaws detected for each flaw size along with the ability of each inspector to accurately size the flaw once it is detected. In this latter category, it can be seen that 60-70% of the flaws were sized in the 75% to 100% of actual size. Thus, flaw sizing after detection is not a significant issue. Note that Table 6-11 presents the results for all data from all Spar Cap with Shear Web test specimens while Table 6-12 presents the data for only Spar Cap Laminate flaws in the Spar Cap with Shear Web test specimens, and Table 6-13 presents the data for only Bond Line flaws contained in the Spar Cap with Shear Web test specimens. Table 6-11 through Table 6-13 show that the flaw detection was almost the same for all flaws distributed throughout the Spar Cap with Shear Web test specimens. Thus, the inspectors displayed almost equal performance for both the laminate and bond line flaws. Figure 6-8:Figure 6-13: displays the similarities in the percent flaw detection in all three categories: 1) all flaws in the Spar Cap with Shear Web test specimens, 2) only flaws in the Spar Cap Laminate region of the Spar Cap with Shear Web test specimens, and 3) only flaws in the Bond Line regions of the Spar Cap with Shear Web test specimens.

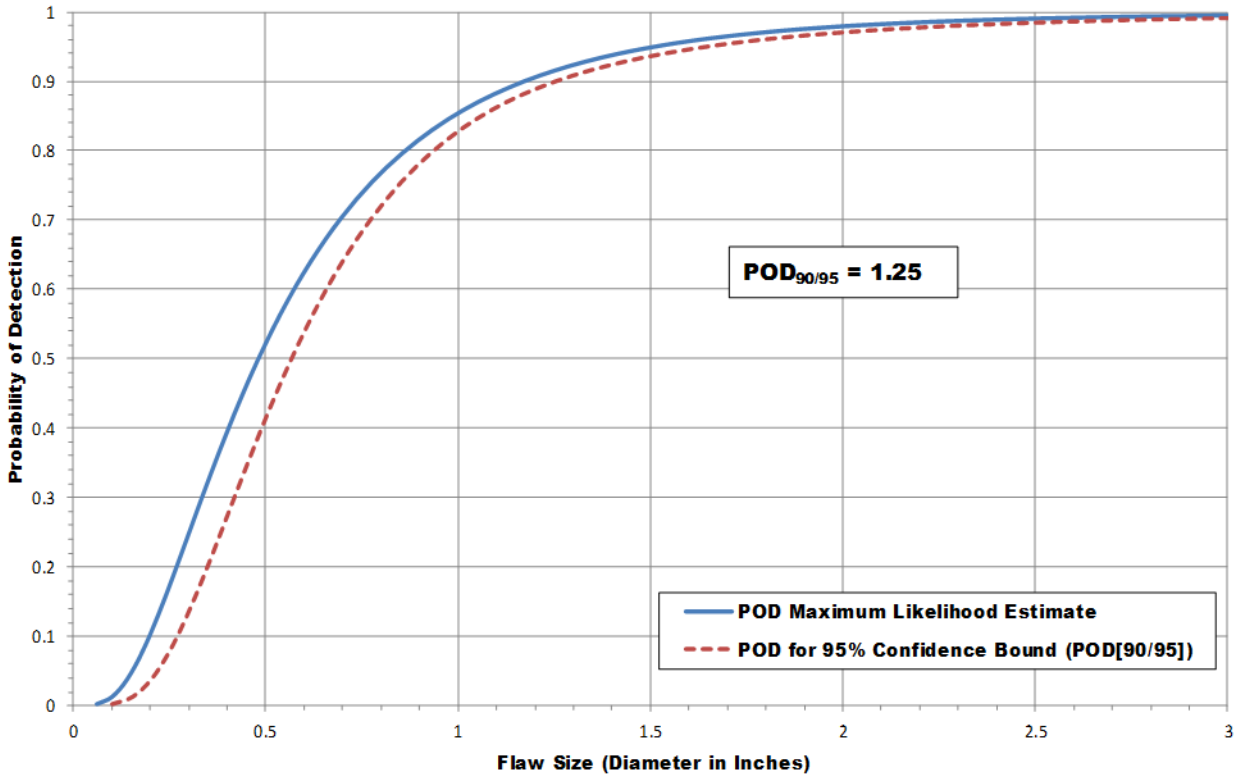

Figure 6-9: Cumulative POD Curve Representing Conventional PE-UT from All 12 Inspectors Inspecting Spar Cap with Shear Web Test Specimens Only

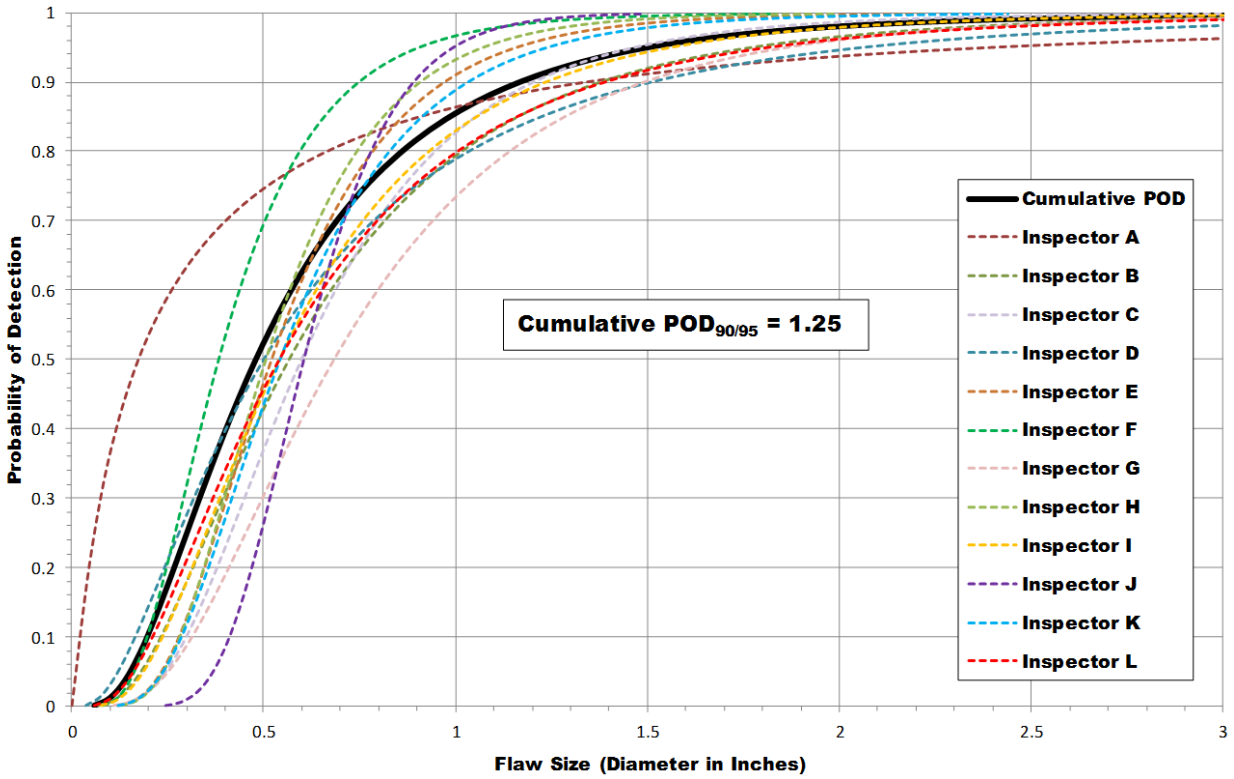

Individual Inspector POD Results Table All Spar Cap & Shear Web Type Construction Conventional PE-UT - All Flaws - Panels (1-9) Only	
Inspector	**$POD_{90/95}$ (Dia. In Inches)**
Inspector A	1.83
Inspector B	1.56
Inspector C	1.46
Inspector D	1.98
Inspector E	1.19
Inspector F	1.09
Inspector G	1.84
Inspector H	1.12
Inspector I	1.54
Inspector J	1.04
Inspector K	1.26
Inspector L	1.76
Overall Cumulative $POD_{90/95}$	**1.25**
Range Spread	**90.38%**

Figure 6-10: Individual Inspectors & Cumulative POD_{90} Curve Comparisons for Spar Cap with Shear Web Panels Only, Plus $POD_{90/95}$ Values for Each Inspector and the Cumulative Result Representing the Overall Performance of the Wind Blade Manufacturing Industry

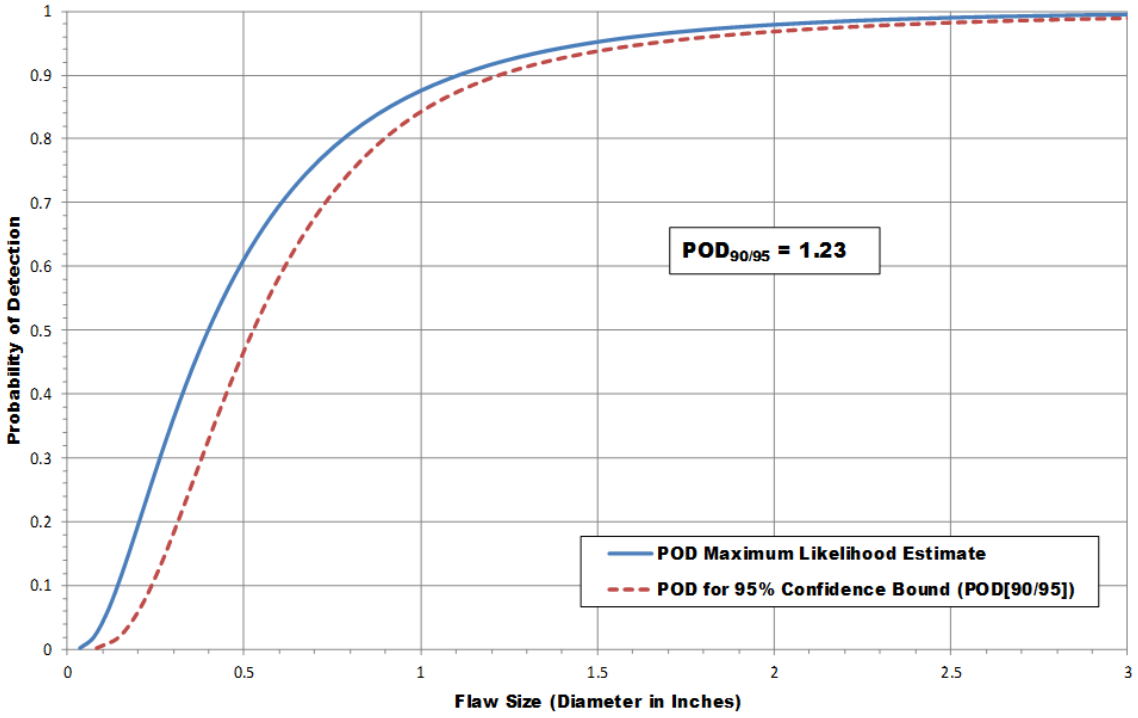

Figure 6-11: POD Curve Representing Conventional PE-UT from All 12 Inspectors Considering Only the Laminate Flaws in the Spar Cap with Shear Web Specimens of the WBFDE

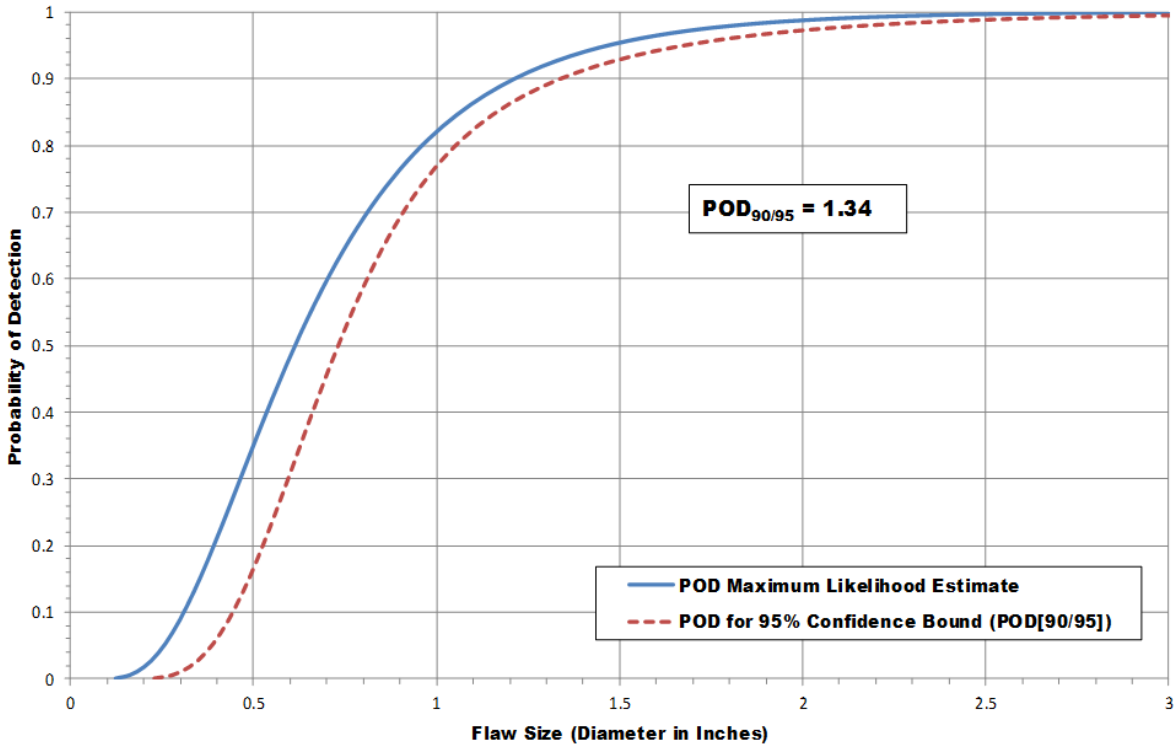

Figure 6-12: POD Curve Representing Conventional PE-UT from All 12 Inspectors Considering Only the Bond Line Flaws in the Spar Cap with Shear Web Specimens of the WBFDE

Overall Flaw Detection Percentage & Accuracy in Determining Flaw Size Spar Cap & Shear Web Panels (1-9) Only - 12 Inspectors - All Flaws Conventional Pulse Echo UT							
Accuracy in Sizing the Flaws That Were Detected (1069 Total Flaws Detected)						Flaw Detection Percentage (1164 Total Flaws)	
Flaw Size	5 (100%)	4 (76%-99%)	3 (51%-75%)	2 (25%-50%)	1 (< 25%)	Flaw Size	Percent Detected
0.75	36%	21%	17%	12%	15%	0.75	77%
1.00	31%	35%	20%	10%	4%	1.00	84%
1.50	29%	40%	19%	7%	6%	1.50	93%
2.00	25%	51%	13%	6%	4%	2.00	98%
2.50	21%	47%	21%	7%	3%	2.50	99%
3.00	20%	60%	11%	6%	4%	3.00	100%
Overall Sizing Performance	27%	42%	17%	8%	6%	Overall Flaw Detection	92%

Table 6-11: Summary of Inspector Flaw Detection and Flaw Sizing Accuracy in All the Spar Cap with Shear Web Specimens

Overall Flaw Detection Percentage & Accuracy in Determining Flaw Size Spar Cap & Shear Web Panels (1-9) Only - 12 Inspectors All Laminate Flaws Only - Conventional Pulse Echo UT							
Accuracy in Sizing the Flaws That Were Detected (750 Total Flaws Detected)						Flaw Detection Percentage (804 Total Flaws)	
Flaw Size	5 (100%)	4 (76%-99%)	3 (51%-75%)	2 (25%-50%)	1 (< 25%)	Flaw Size	Percent Detected
0.75	36%	24%	20%	10%	10%	0.75	81%
1.00	28%	36%	21%	11%	4%	1.00	86%
1.50	28%	39%	20%	7%	5%	1.50	93%
2.00	29%	49%	10%	7%	4%	2.00	99%
2.50	22%	45%	23%	6%	4%	2.50	99%
3.00	22%	55%	12%	8%	3%	3.00	100%
Overall Sizing Performance	27%	42%	18%	8%	5%	Overall Flaw Detection	93%

Table 6-12: Summary of Inspector Flaw Detection and Flaw Sizing Accuracy in All the Spar Cap with Shear Web Specimens – Laminate Flaws Only

Overall Flaw Detection Percentage & Accuracy in Determining Flaw Size Spar Cap & Shear Web Panels (2, 4, 6 & 8) Only - 12 Inspectors All Bond Line Flaws Only - Conventional Pulse Echo UT							
Accuracy in Sizing the Flaws That Were Detected (319 Total Flaws Detected)						Flaw Detection Percentage (360 Total Flaws)	
Flaw Size	5 (100%)	4 (76%-99%)	3 (51%-75%)	2 (25%-50%)	1 (< 25%)	Flaw Size	Percent Detected
0.75	36%	12%	9%	15%	27%	0.75	69%
1.00	35%	32%	18%	9%	5%	1.00	80%
1.50	31%	40%	15%	6%	7%	1.50	93%
2.00	14%	54%	21%	4%	6%	2.00	97%
2.50	19%	54%	17%	8%	2%	2.50	100%
3.00	17%	71%	8%	0%	4%	3.00	100%
Overall Sizing Performance	26%	43%	16%	7%	8%	Overall Flaw Detection	89%

Table 6-13: Summary of Inspector Flaw Detection and Flaw Sizing Accuracy in All the Spar Cap with Shear Web Specimens – Bond Line Flaws Only

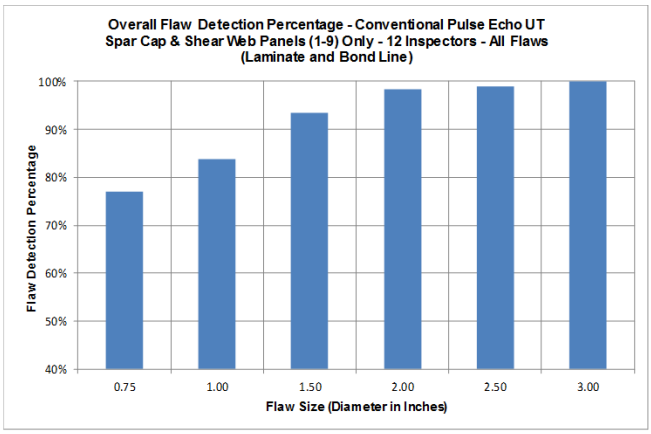

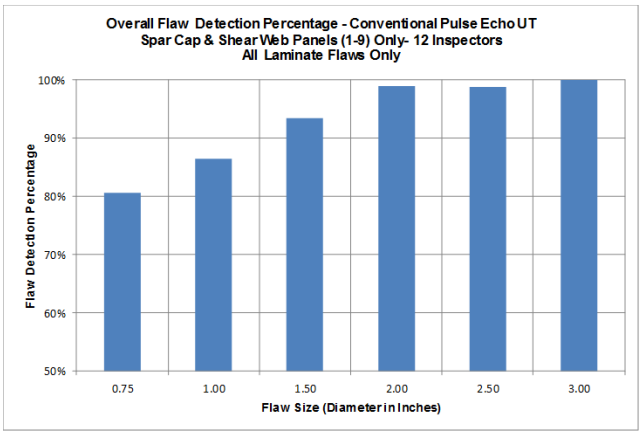

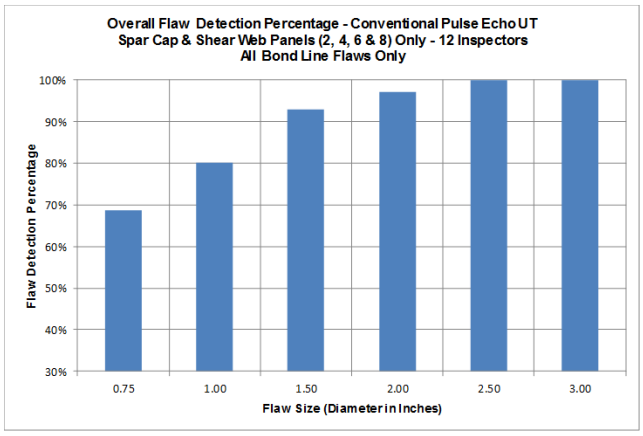

Figure 6-13: Comparison of Flaw Detection Levels for Flaws in Each of the Three Major Categories in the Spar Cap with Shear Web Specimens

6.1.3. WBFDE – Overall Probability of Detection Results for Box Spar Construction

Table 6-14 shows the summary of the Probability of Detection results when only considering only the Box Spar type specimens in the WBFDE and all inspectors using conventional pulse-echo ultrasonics with a single-element transducer deployed in A-scan mode. First it shows that the overall $POD_{[90/95]}$ value for the Box Spar type specimens is higher than the other categories at 1.62". Three subset categories of regions within the test specimens are also listed. For the Skin laws, located above the bond line, the $POD_{[90/95]}$ value was 1.40", for the Spar Cap Laminate flaws, located beneath the bond line, the $POD_{[90/95]}$ value was 2.22", and for the Bond Line flaws, located between the outer skin and the lower spar cap, the $POD_{[90/95]}$ value was 1.06". The shows that, within the Box Spar specimen set, the Bond Line flaws are easier to detect and the Spar Cap Laminate flaws are more difficult to detect

Figure 6-14 compares the maximum likelihood estimate ($POD_{[90]}$) to the POD curve that is calculated when a 90% flaw detection is combined with a 95% confidence bound ($POD_{[90/95]}$). This solid line in Figure 6-14 provides the performance curve that the industry normally uses to measure the performance of NDI methods as deployed by representative inspectors. Thus, this curve provides the wind industry baseline when inspecting Box Spar type blade designs. It can be seen in Figure 6-14 that the overall cumulative $POD_{[90/95]}$ for all flaws in the Box Spar specimens was $POD_{[90/95]}$ = 1.62" diameter flaw.

Figure 6-15 shows the summary of the Probability of Detection results for the Box Spar panels only and all inspectors using conventional pulse-echo ultrasonics with a single-element transducer deployed in A-scan mode only. For the Box Spar specimens, the best performing inspector produced a $POD_{[90/95]}$ < 0.75" diameter flaw, the worst inspector produced a $POD_{[90/95]}$ > 3.00" diameter, and the overall cumulative result was a $POD_{[90/95]}$ = 1.62" diameter. The individual inspection results had a 300% spread from best to worst performance which is quite extreme. It is highly desirable to reduce such data spread so that there is greater uniformity of inspection results across the wind industry. Section 6.1.4 will address methods and procedures that can be deployed to reduce this spread and achieve more uniform NDI performance across the industry. Overall, this data indicates that a wind blade production company deploying conventional UT equipment can expect to detect a 1.62" diameter flaw anywhere in a Box Spar blade with a 90% probability of detection and a 95% confidence factor. The Box Spar construction was more difficult to inspect than the Spar Cap with Shear Web construction and produced a POD level that was 34% higher. In addition the repeatability is less in the Box Spar construction as the spread in results was 300% versus only 90% in the Spar Cap with Shear Web specimens.

Figure 6-16 and Figure 6-17 contain plots of the data summarized in Table 6-14. Figure 6-16 shows that within the Spar Cap Laminate region, which is located beneath the bond line in the Box Spar type specimens, POD is worse at this added depth. The Spar Cap Laminate POD = 2.22" vs POD = 1.23" for the Spar Cap with Shear Web (80% higher/worse). Figure 6-17 shows that within the Bond Line region, probably the primary area of interest in the Box Spar type construction, the POD is better since the Bond Line is now nearer to the surface with a thick

backwall provided by the Spar Cap Laminate. Thus, these inspections are easier and the POD for the Bond Line in the Box Spar configuration is POD = 1.06" vs POD = 1.34" in the Bond Line of the Spar Cap with Shear Web (26% lower/better).

Cumulative POD Results Table - Wind Blade Flaw Detection Experiment Conventional Pulse-Echo UT - Box Spar Type Construction Only	
Condition	**$POD_{90/95}$ (Dia. In Inches)**
All Flaws - 12 Inspectors - Panels (10-11)	1.62
Only Skin Flaws - 12 Inspectors - Panels (10-11)	1.40
Only Spar Cap Laminate Flaws Under Bond Line - 12 Inspectors - Panels (10-11)*	2.22
Only Bond Line Flaws - 12 Inspectors - Panels (10-11)	1.06

Table 6-14: Results Representing the Performance ($POD_{90/95}$ Values) of the Wind Blade Manufacturing Industry for the Box Spar Construction Only, Along with Flaw Detection Performance for Specific Specimen Regions

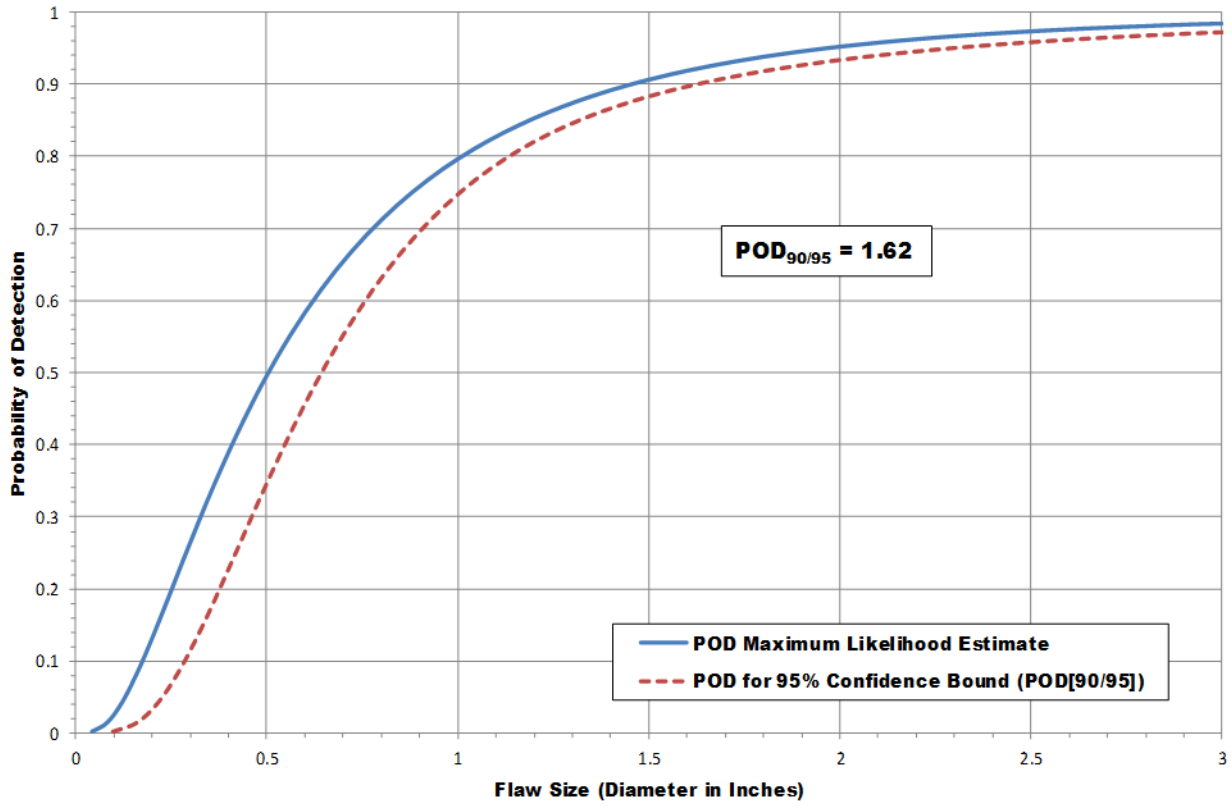

Figure 6-14: Cumulative POD Curve Representing Conventional PE-UT from All 12 Inspectors Inspecting the Box Spar Specimens Only

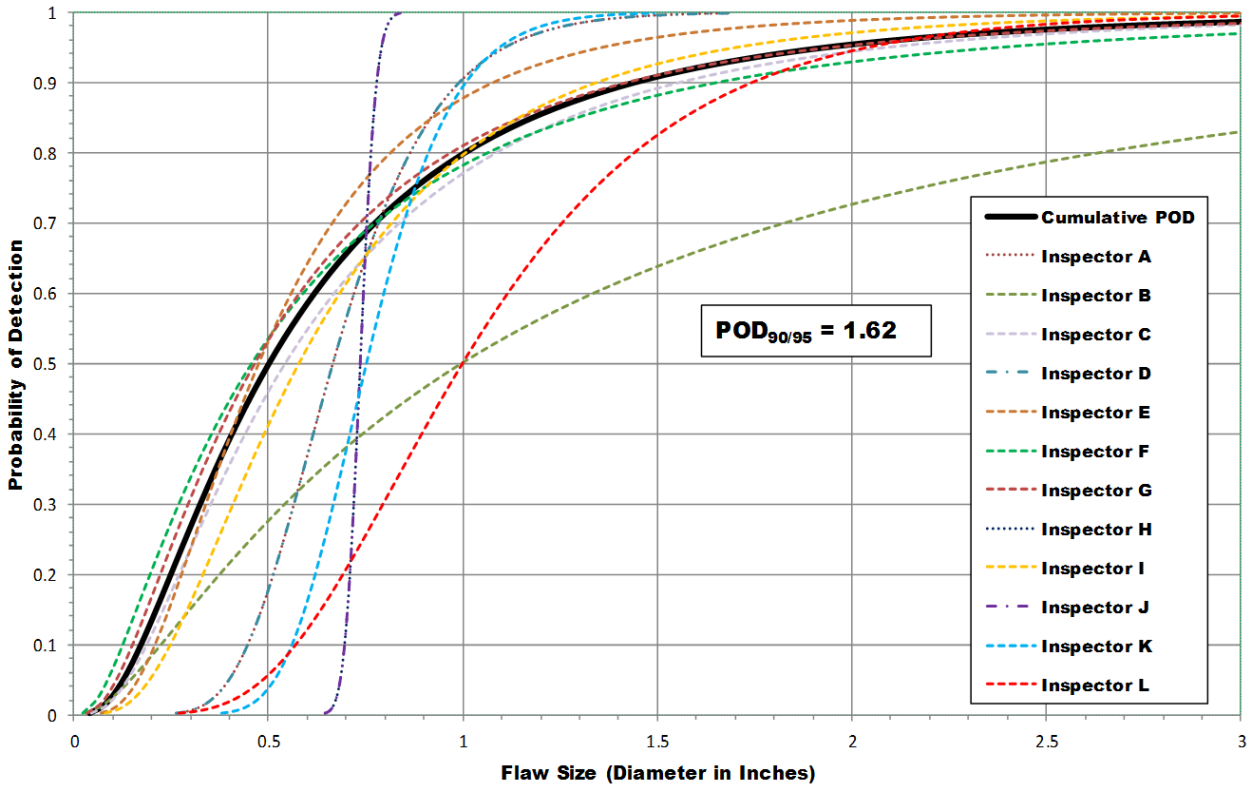

Individual Inspector POD Results Table All Box Spar Type Construction Conventional PE-UT - All Flaws - Panels (10-11) Only	
Inspector	**$POD_{90/95}$ (Dia. In Inches)**
Inspector A	1.24
Inspector B	>3.00
Inspector C	2.31
Inspector D	1.25
Inspector E	1.53
Inspector F	2.64
Inspector G	2.13
Inspector H	<0.75
Inspector I	1.87
Inspector J	<0.75
Inspector K	1.22
Inspector L	2.16
Overall Cumulative $POD_{90/95}$	**1.62**
Range Spread	**300.00%**

Figure 6-15: Individual Inspectors & Cumulative POD_{90} Curve Comparisons for Box Spar Specimens Only, Plus $POD_{90/95}$ Values for Each Inspector and the Cumulative Result Representing the Overall Performance of the Wind Blade Manufacturing Industry

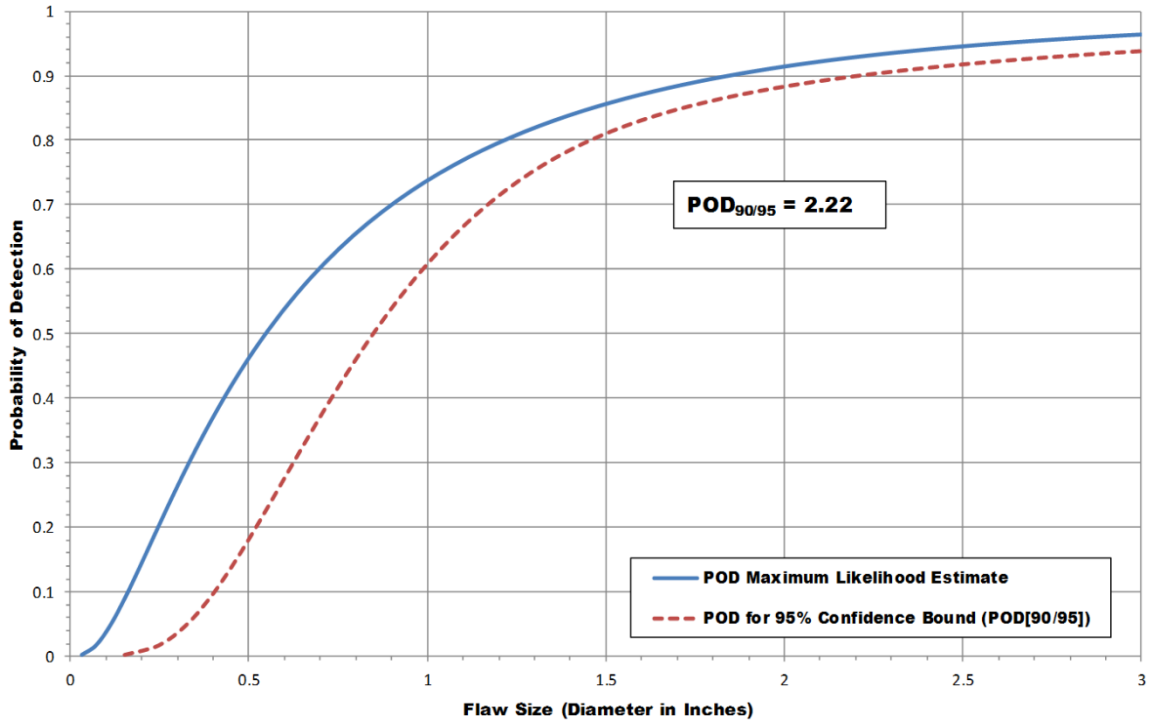

Figure 6-16: POD Curve Representing Conventional PE-UT Considering Only the Spar Cap Laminate Flaws Under the Bond Line in the Box Spar Specimens

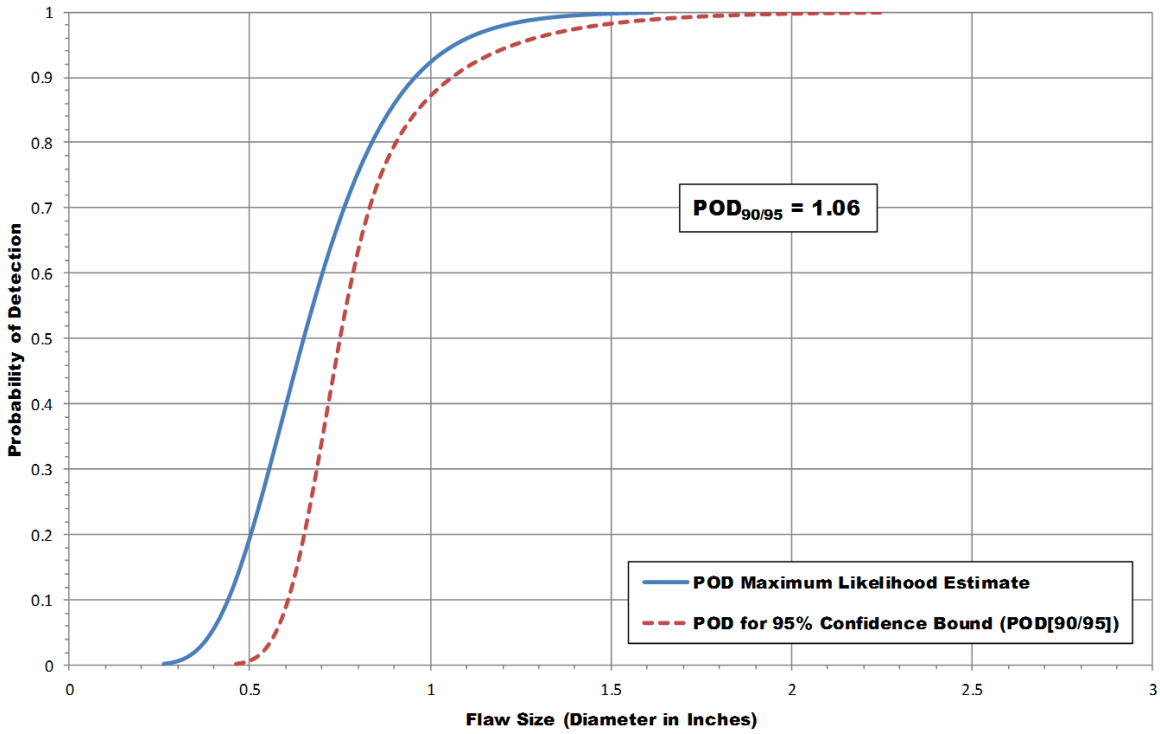

Figure 6-17: POD Curve Representing Conventional PE-UT Considering Only the

Bond Line Flaws in the Box Spar Specimens

6.1.4. WBFDE – Overall POD Results Representing the Expected Inspection Performance within the Wind Industry

Table 6-15 and Table 6-16 provide an overall summary of the flaw detection level (or missed flaw level) associated with each flaw type and location within each specimen. Chapter 3 describes the exact make-up of each flaw type so that it is possible to understand which flaw might be more subtle, tighter versus creation of air gaps, and voids versus more drastic internal changes in material. It can be seen that contamination flaws such as the presence of grease and porosity created by the insertion of micro-balloons, are the most difficult to detect. In addition, flaws located along the backside of the bond region (Interface-B) are more challenging to identify due to their closeness to the overall backwall of the assembly. This produces a very slight shift in the UT signal which may not be appreciated by the inspector. It is also possible to determine that the bond lines flaws in the Box Spar construction are easier to detect than those in the Spar Cap and Shear Web construction because of their location nearer to the inspection service. Similarly, the laminate flaws in the Spar Cap and Shear Web construction are easier to detect that those in the Box Spar construction for the same reason.

Table 6-17 provides an overall summary of the cumulative POD results (all inspectors combined) for the full set of specimens and then broken down for the different blade designs (Spar Cap & Shear Web construction or Box Spar construction) and the different regions within those designs. This table represents the measured and expected performance of wind industry inspections for each of the categories listed. This table provides a good overall evaluation of the likelihood of finding damage/flaws in new or in-service blades. For the most part, damage in the 1.25 to 1.5" diameter should be detected by inspectors deploying hand-held, single-element pulse-echo ultrasonic inspections regardless of the blade construction type. This number will go up depending on the addition of other degrees of difficulty including deployment access limitations or other challenging conditions. Poor or faulty NDI equipment set-up, calibration or other preliminary processes can also detract from these results. Conversely, additional training, formalized procedures and the use of industry-wide NDI standards can produce improvements in these results such that: 1) it offsets other inspection difficulties to produce similar end results, or 2) compounds with current successful practices to improve the repeatability and sensitivity of inspection. This latter results will be especially useful when considering repair needs and producing the ability to install more invasive and effective repairs.

These results assume that full coverage of the spar cap and bond line region is achieved. If the inspector is conducting a "spot check" type of inspection which only samples portions of the spar cap and bond line region using some type of regular pattern, then the possibility of missing some larger flaws exists. This experiment was not conducted to assess the POD for such a spot check inspection but could be adapted to determine a POD for different NDI search patterns such as those described below.

All Flaws (All Construction Types)					
Type	#	Insp	Total Flaws	Miss	% Missed
VD	14	12	168	24	14.29%
PI	56	12	672	55	8.18%
GR	14	12	168	38	22.62%
GB	13	12	156	6	3.85%
FBH	26	12	312	26	8.33%
WR	10	12	120	2	1.67%
DRY	6	12	72	2	2.78%
PT	3	12	36	5	13.89%
Total Flaws	142		1704	158	9.27%

Bond Line Flaws by Location (All Construction Types)					
Type	#	Insp	Total Flaws	Miss	% Missed
Location INT-A	16	12	192	6	3.13%
Location INT-B	13	12	156	23	14.74%

Bond Line Flaws (All Construction Types)					
Type	#	Insp	Total Flaws	Miss	% Missed
VD	14	12	168	24	14.29%
PT	3	12	36	5	13.89%
GB	6	12	72	2	2.78%
FBH	5	12	60	8	13.33%
PI	20	12	240	23	9.58%
Total Flaws	48		576	62	10.76%

Bond Line Flaws (Spar Cap & Shear Web Type Construction)					
Type	#	Insp	Total Flaws	Miss	% Missed
VD	8	12	96	13	13.54%
PT	3	12	36	5	13.89%
GB	4	12	48	2	4.17%
FBH	5	12	60	8	13.33%
PI	10	12	120	15	12.50%
Total Flaws	30		360	43	11.94%

Bond Line Flaws (Box Type Construction)					
Type	#	Insp	Total Flaws	Miss	% Missed
VD	6	12	72	11	15.28%
GB	2	12	24	0	0.00%
PI	10	12	120	8	6.67%
Total Flaws	18		216	19	8.80%

Table 6-15: Detection Levels Associated with Each Flaw Type and Location Within the WBFDE Specimens – Part 1

Skin Flaws (Box Type Construction Only)					
Type	#	Insp	Total Flaws	Miss	% Missed
PI	5	12	60	9	15.00%
Total Flaws	5		60	9	15.00%

Laminate Flaws (All Construction Types)					
Type	#	Insp	Total Flaws	Miss	% Missed
PI	31	12	372	23	6.18%
GR	14	12	168	38	22.62%
GB	7	12	84	4	4.76%
FBH	21	12	252	18	7.14%
WR	10	12	120	2	1.67%
DRY	6	12	72	2	2.78%
Total Flaws	89		1068	87	8.15%

Laminate Flaws (Spar Cap & Shear Web Type Construction)					
Type	#	Insp	Total Flaws	Miss	% Missed
PI	22	12	264	11	4.17%
GR	11	12	132	28	21.21%
GB	5	12	60	3	5.00%
FBH	17	12	204	8	3.92%
WR	8	12	96	1	1.04%
DRY	4	12	48	1	2.08%
Total Flaws	67		804	52	6.47%

Laminate Flaws (Box Type Construction)					
Type	#	Insp	Total Flaws	Miss	% Missed
PI	9	12	108	12	11.11%
GR	3	12	36	10	27.78%
GB	2	12	24	1	4.17%
FBH	4	12	48	10	20.83%
WR	2	12	24	1	4.17%
DRY	2	12	24	1	4.17%
Total Flaws	22		264	35	13.26%

Table 6-16: Detection Levels Associated with Each Flaw Type and Location Within the WBFDE Specimens – Part 2

Cumulative POD Results Table - Wind Blade Flaw Detection Experiment Conventional Pulse-Echo UT	
All Spar Cap & Shear Web and Box Type Construction	**$POD_{90/95}$ (Dia. In Inches)**
All Flaws - 12 Inspectors - Panels (1-11)	1.33
All Flaws - 10 Inspectors (High and Low Removed) - Panels (1-11)	1.30
Only Constant Thickness Flaws - 12 Inspectors - Panels (1-11)	1.24
Only Complex Geometry Flaws - 12 Inspectors - Panels (2, 4, 6, 8, 10 &11)	1.49
Only Bond Line Flaws - 12 Inspectors - Panels (2, 4, 6, 8, 10 &11)	1.23
Spar Cap & Shear Web Type Construction Only	**$POD_{90/95}$ (Dia. In Inches)**
All Flaws - 12 Inspectors - Panels (1-9)	1.25
All Flaws - 10 Inspectors (High and Low Removed) - Panels (1-9)	1.25
Only Laminate Flaws - 12 Inspectors - Panels (1-9)	1.23
Only Bond Line Flaws - 12 Inspectors - Panels (2, 4, 6, & 8)	1.34
Box Spar Type Construction Only	**$POD_{90/95}$ (Dia. In Inches)**
All Flaws - 12 Inspectors - Panels (10-11)	1.62
Only Skin Flaws - 12 Inspectors - Panels (10-11)	1.40
Only Spar Cap Laminate Flaws Under Bond Line - 12 Inspectors - Panels (10-11)*	2.22
Only Bond Line Flaws - 12 Inspectors - Panels (10-11)	1.06

Table 6-17: Overall Summary of Cumulative POD Results Representing the Expected Wind Industry Flaw Detection Performance for Different Blade Designs and Specific Regions Within those Designs

Possible Largest Flaw Missed - Instead of only addressing the smallest flaw that can be found, it is also important to study the largest flaw that can possibly be missed during an inspection. In this WBFDE, inspectors were asked to provide full coverage of each specimen in order to detect flaws in any location across the footprint of the specimen. This may have changed the inspection pattern from what is normally used in wind blade production facilities.

Oftentimes, the primary ultrasonic inspection performed on an assembled blade before it leaves the factory is an inspection of the spar cap-to-shear web bonded joint inspection. The purpose of the inspection is to ensure that there is sufficient adhesive bond width between the spar cap and the shear web and to determine if there are any voids larger than 25 mm in the bond line. The inspection is performed by hand normally using a 1/2" diameter 500 KHz probe. The blade is positioned with the trailing edge towards the ceiling and the inspector moves the probe vertically over the bond line, checking for adhesive "squeeze-out" to determine if the bond line is sufficiently wide. This is done along the entire length of the bond line. Figure 6-18 shows a schematic of the bond line cross section over a shear web flange**Error! Reference source not found.**. With the current inspection procedures, there is no image/scan that is saved from the inspection to review after the inspection has been performed. Such data could be very helpful if

there is a questionable area. Only pictures of markings on the blade placed by the inspector during the inspection are saved. The current inspection coverage pattern is shown in Figure 6-18**Error! Reference source not found.**.

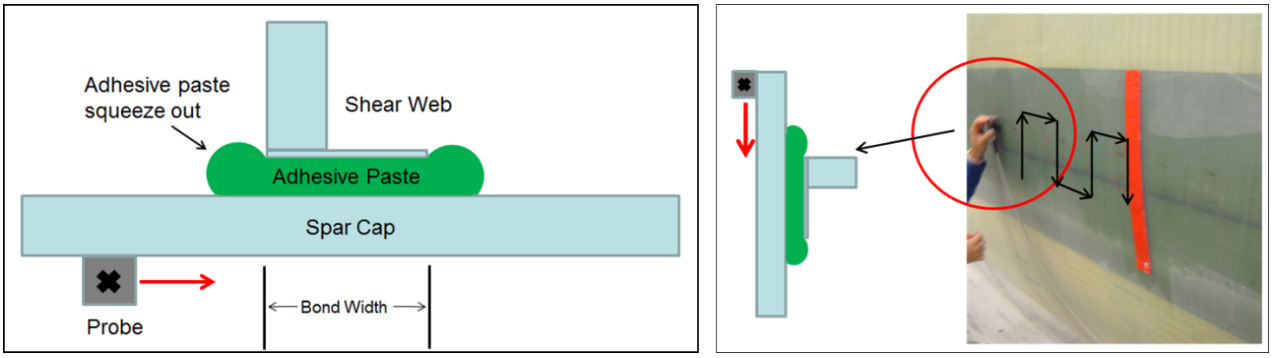

Figure 6-18: Schematic of Adhesive Bond Line and Inspector Coverage Pattern with a Single Element Transducer to Measure Bond Line Width

Figure 6-19 below shows a square wave UT coverage pattern that Sandia has observed in some wind blade factories. The green path represents the expected swath of coverage associated from a 1" diameter UT transducer. The pink area represents the region that is not inspected as a result of the hand-held inspection scan pattern. The yellow region represents ½ of the transducer width because normally one would expect a flaw to be detected if it engages at least ½ of the transducer. Finally, a series of sample flaws are superimposed on this inspection region to show: 1) flaws that should be detected, 2) flaws that may be detected and, 3) flaws that will not be detected, based on the square wave coverage pattern shown. Figure 6-19 also summarizes the maximum flaw size that could potentially be missed by square wave coverage patterns of different widths. They range from 0" for a tight transducer step width (probe spacing) of 1" to a 10 $in.^2$ flaw that might be missed in the case of a transducer step width of 3". In fact, some guidance has been observed to direct inspectors to use a 25mm (1") probe spacing during inspections. Thus, this inspection would be expected to detect all flaws. This example simply shows showing potential flaws that could be missed when 100% coverage isn't obtained by an inspector during conventional pulse-echo inspections. By using a square wave inspection pattern, there is potential for 2.5 $in.^2$ of missed bond line for every 0.5" of probe spacing that an inspector is off from the desired spacing while hand scanning.

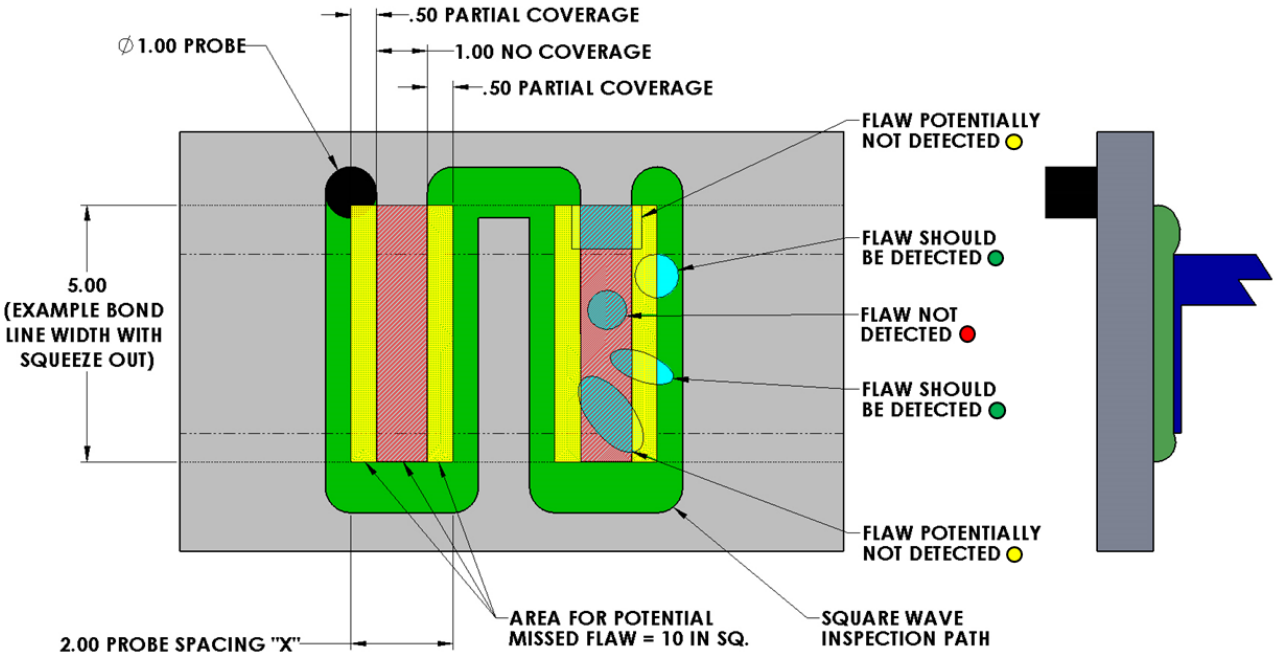

Probe Spacing "X" (in)	Area for Potential Missed Flaw (in^2)	(Red) Area of No Coverage (in^2)	(Yellow) Area of Partial Coverage (in^2)
1.00	5.00	0.00	5.00
2.00	10.00	5.00	5.00
3.00	15.00	10.00	5.00

Figure 6-19: Square Wave Inspection Coverage Pattern and Possibilities for Creating the Largest Flaw Missed Based on the Tightness of the Transducer Pattern

Human Factor: Vigilance - There are multiple human factors concerns associated with inspecting a large, complex structure. For time consuming inspections like wind blades, a primary human factors concern pertains to the ability of inspectors to maintain the proper level of concentration required for the entire multi-hour inspection task. When a large inspection task looms ahead and blade throughput is a priority this can be an impediment to achieving optimum inspection results as it can create a lack of attention to detail and diminished time spent reviewing data. During single-element UT deployment where subsequent C-scan images are not available to make flaw detection calls, the loss of concentration during inspection caused large, evident flaws to be missed. This is especially important when encountering challenging flaws with lower signal-to-noise ratios. Inspector X missed one of the larger flaws (2.5" dia.). Table 6-18 shows the improvement in Inspector X's POD level if the missed 2.5" flaw was actually detected (10 - 40% improvements). Note that almost all inspectors found this large flaw.

Similarly, if an inspector rushes his/her inspection, this can have a large effect on the overall inspection performance. One of the inspectors using a single-element UT inspection rushed through his final panel of the day in order to avoid continuing this inspection the next day. This

hastened coverage pace during inspection caused large, evident flaws to be missed. This inspector experienced more misses (4) in the final panel than in the previous 10 panels combined. Close to quitting time, this inspector's inspection time on Panel 11 was only half the time spent on the similar Panel 10. The end result is that while the inspector missed only 3 flaws in his first 10 panels, he missed 4 flaws in the final panel alone. Table 6-19 shows the improvement in POD level if the two, large, missed 2" flaws were actually detected. It can be seen that the POD would improve (decrease) by 20 - 35%. The lesson learned is that inspectors need to keep a uniform and optimum pace in their inspection coverage.

$POD_{90/95}$ Comparison: Actual Results vs. Results with One Large Flaw Miss Changed to a Hit		
Specimen Type	**Flaw Size at $POD_{90/95}$ (Dia. In.) Actual Results**	**Flaw Size at $POD_{90/95}$ (Dia. In.) - One Miss Changed to a Hit**
Laminate (Spar Cap & Spar Cap with Shear Web)	2.49	1.51
Bond Line (Spar Cap with Shear Web)	1.28	1.28
All Flaws (Spar Cap & Spar Cap with Shear Web)	1.83	1.77
All Flaws (Box Spar)	1.25	1.25
Constant Thickness	2.44	1.72
Complex Geometry	1.21	1.21
All Flaws (Box Spar, Spar Cap & Spar Cap with Shear Web)	1.51	1.35

Table 6-18: Anticipated Improvements in Overall Performance with Better Vigilance During Entire Inspection Process

What affect does a single miss have on the POD? Large flaw misses have an especially, large effect on POD levels and are important in blade inspections. Figure 6-20 shows the large effect that a single miss of a large flaw can have on the overall POD levels. POD experiments are designed to include large flaws, in this case the 2" diameter flaw, which almost all inspectors should detect. The 2" diameter flaw that inspector BB did not detect was changed to a "Hit." Figure 6-20 shows that this resulting POD improved by almost 10% from 1.143" to 1.073". The lesson learned is that additional data gates should be used to detect deeper flaws. Use of a single gate to analyze the UT A-scan data is not sufficient to detect all flaws.

$POD_{90/95}$ Comparison: Actual Results vs. Results with Two Large Flaw Misses Changed to Hits		
Specimen Type	Flaw Size at $POD_{90/95}$ (Dia. In.) Actual Results	Flaw Size at $POD_{90/95}$ (Dia. In.) - Two Large Misses Changed to Hits
Laminate (Spar Cap & Spar Cap with Shear Web)	<0.75	<0.75
Bond Line (Spar Cap with Shear Web)	1.32	1.32
All Flaws (Spar Cap & Spar Cap with Shear Web)	1.09	1.09
All Flaws (Box Spar)	2.64	1.41
Constant Thickness	<0.75	<0.75
Complex Geometry	2.06	1.29
All Flaws (Box Spar, Spar Cap & Spar Cap with Shear Web)	1.36	1.08

Note: In certain cases it was not possible to converge to a POD value because the performance was too good (i.e. not enough flaws missed); POD level was thus set at < 0.75" dia. which are the smallest flaws used in the WBFDE.

Table 6-19: Anticipated Improvements in Overall Performance if Inspector Training Produces a Few Less Flaw Misses

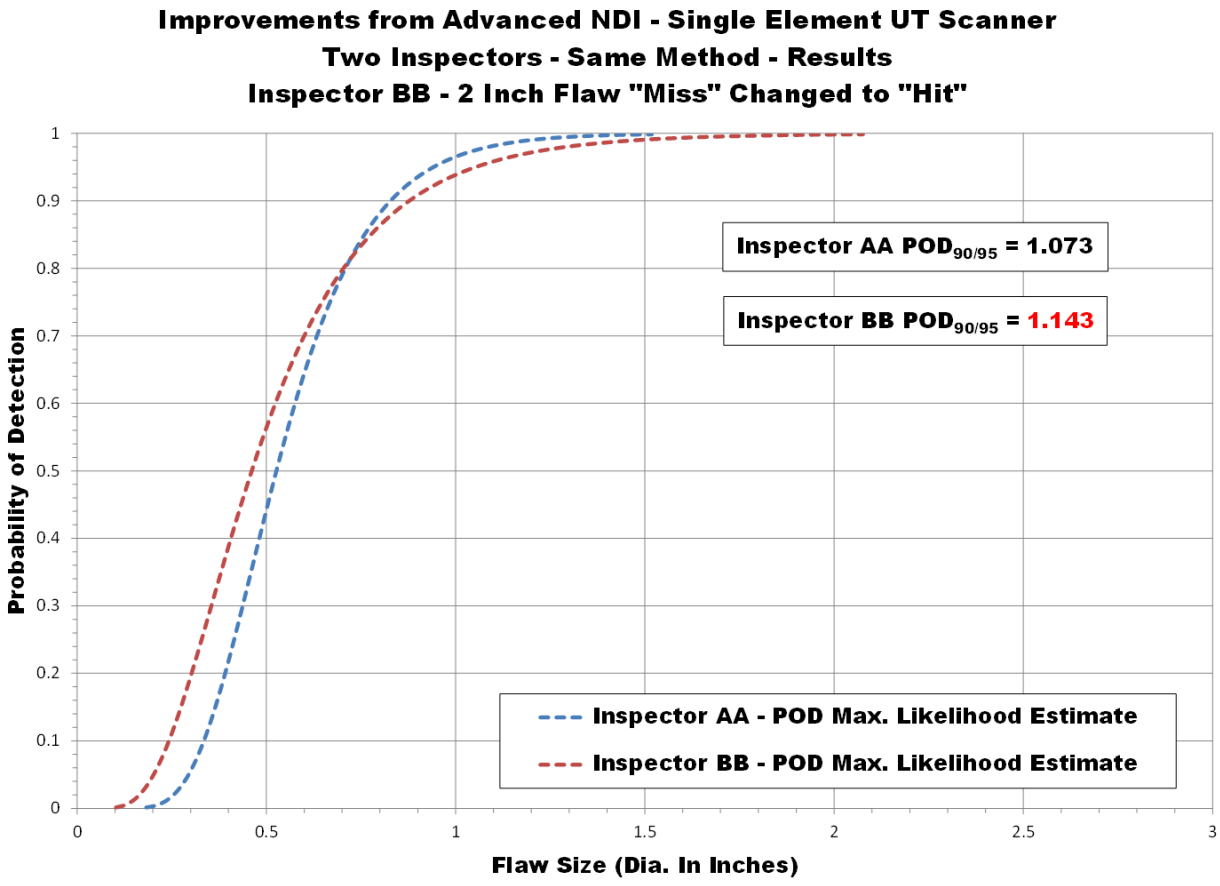

Figure 6-20: Comparison of POD Values for a Single Inspector when Proper Data Analysis is Used

6.1.5. Improving POD - Value of NDI Training and Exposure to Wind Blade Inspections

This section of the report addresses a topic that has been introduced a number of times while reviewing the POD inspection results. The topic concerns the value of focused training for wind blade inspectors along with certain type of increased exposure to wind blade inspections. Currently, the training regime for inspectors is quite limited and very ad hoc. Overall, the wind blade industry does not follow the American Society of Nondestructive Testing protocols for standardized training to produce ASNT Level I, II and III designations. Even if they did, such training is generalized to cover a wide range of industries. As a result, there is still a need for training that is focused on the very specific inspection demands of the wind blade structure and the sometimes subtle signal changes that are important to conducting an accurate, high-fidelity inspection. Furthermore, inspector proficiency will improve greatly if they are allowed to inspect specimens such as the NDI Feedback Specimens used in the WBFDE. They can conduct their inspections in a blind fashion on such specimens but immediately be provided with feedback on their performance to foster improvements in their inspection method.

With the above ideas in mind, a series of data adjustments were completed in order to quantitatively assess overall improvements in the wind industry inspection performance (baseline) if inspectors were provided with enhanced training and greater exposure/feedback on representative wind blade test specimens. Overall, when the worst performing inspectors were removed from the calculations, the POD levels improved by 5 to 20% and the spread in inspector performance (range of PODs) was reduced by 20 to 100%. Such improvements were noted in the cases for all specimens and the four regions within the specimens (all flaws, only Constant Thickness flaws, only Complex Geometry flaws, only Bond Line flaws).

Figure 6-21 shows the effects on the overall results including all test specimens when the two worst performers (highest POD levels) were removed from the inspection set. The inspectors removed from the calculation are highlighted in blue in the summary. In this case, the POD improved from 1.33” to 1.22” and the spray in results was reduced from 172% to only 82%. Figure 6-22 follows the same process where the two worst performers (highest POD levels) were removed from the inspection set of only the Constant Thickness regions in all specimens. Here, it was observed that the POD improved from 1.24” to 1.19” and the spray was reduced from 225% to only 136%. Figure 6-23 follows the same process where the two worst performers (highest POD levels) were removed from the inspection set of only the Complex Geometry regions in all specimens. The POD improved from 1.49” to 1.27” and the spray was reduced from 278% to only 178%. Finally, Figure 6-24 shows the results when the two worst performers (highest POD levels) were removed from the inspection set of only the Bond Line regions in all specimens. For this case, the POD improved from 1.23” to 1.16” and the spray was reduced from 156% to only 132%.

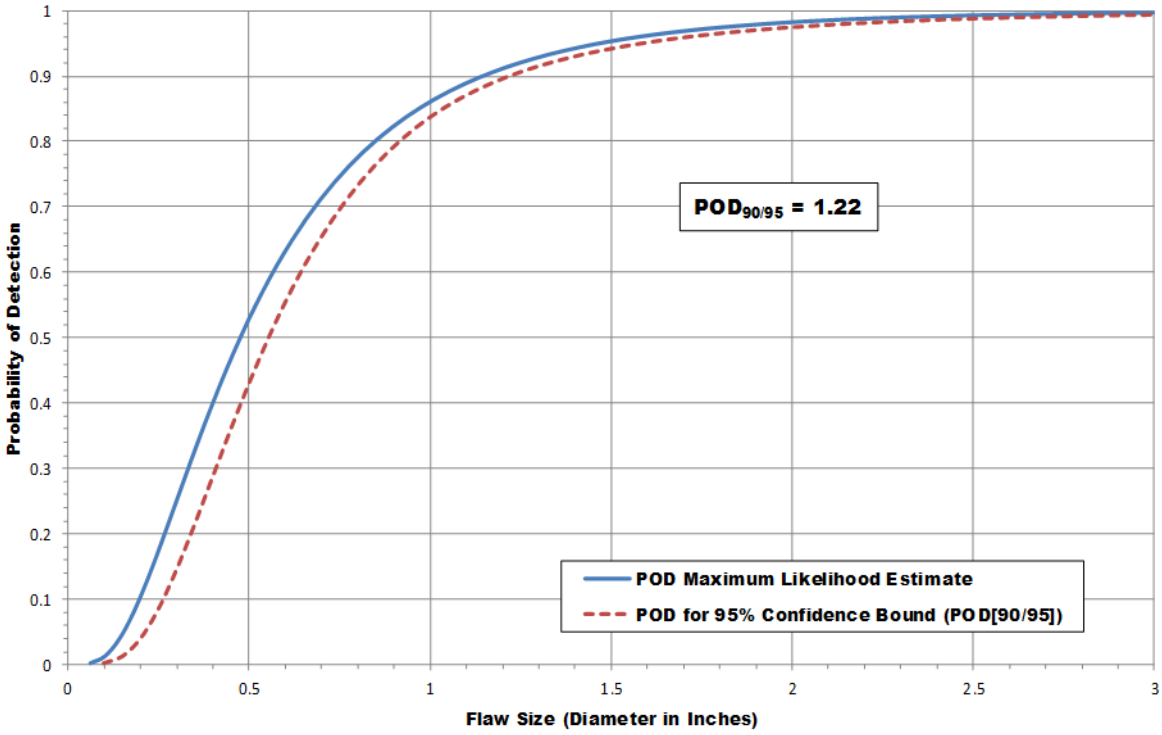

Individual Inspector POD Results Table All Spar Cap & Shear Web and Box Type Construction Conventional PE-UT - All Flaws - All Panels (1-11) Two High Removed	
Inspector	**$POD_{90/95}$ (Dia. In Inches)**
Inspector A	1.51
Inspector B - Removed	2.67
Inspector C	1.58
Inspector D	1.65
Inspector E	1.19
Inspector F	1.36
Inspector G	1.78
Inspector H	1.04
Inspector I	1.52
Inspector J	0.98
Inspector K	1.17
Inspector L - Removed	1.96
Overall Cumulative $POD_{90/95}$	**1.22**
Range Spread	**81.63%**

Figure 6-21: Cumulative POD Curve Representing Conventional PE-UT from 10 Inspectors (Two Worst POD Performers Removed) Inspecting All WBFDE Test Specimens (Spar Cap & Shear Web and Box Spar Construction)

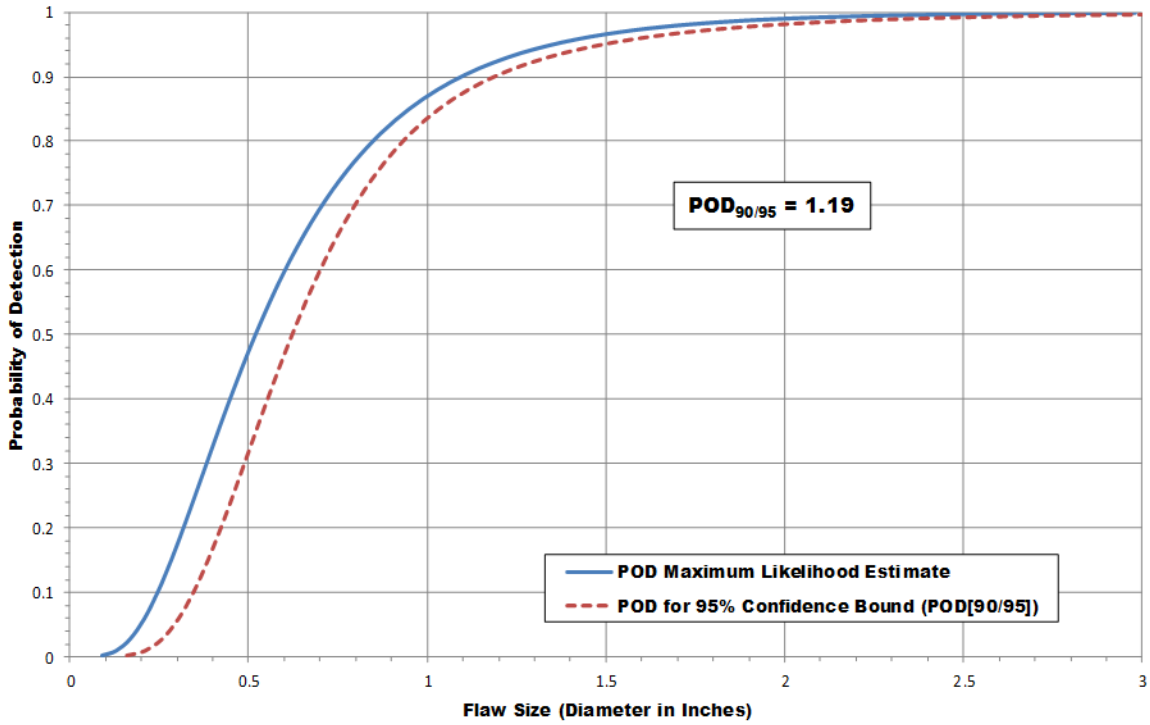

Individual Inspector POD Results Table All Spar Cap & Shear Web and Box Type Construction Conventional PE-UT - All Constant Thickness Flaws Only All Panels (1-11) - Two High Removed	
Inspector	**$POD_{90/95}$ (Dia. In Inches)**
Inspector A - Removed	2.44
Inspector B	1.58
Inspector C	1.77
Inspector D - Removed	2.44
Inspector E	1.25
Inspector F	<0.75
Inspector G	1.77
Inspector H	1.14
Inspector I	1.46
Inspector J	1.14
Inspector K	<0.75
Inspector L	1.64
Overall Cumulative $POD_{90/95}$	**1.19**
Range Spread	**136.00%**

Figure 6-22: Cumulative POD Curve Representing Conventional PE-UT from 10 Inspectors (Two Worst POD Performers Removed) Inspecting Only the Constant Thickness Regions of the WBFDE Test Specimens (Laminate and Skin Flaws)

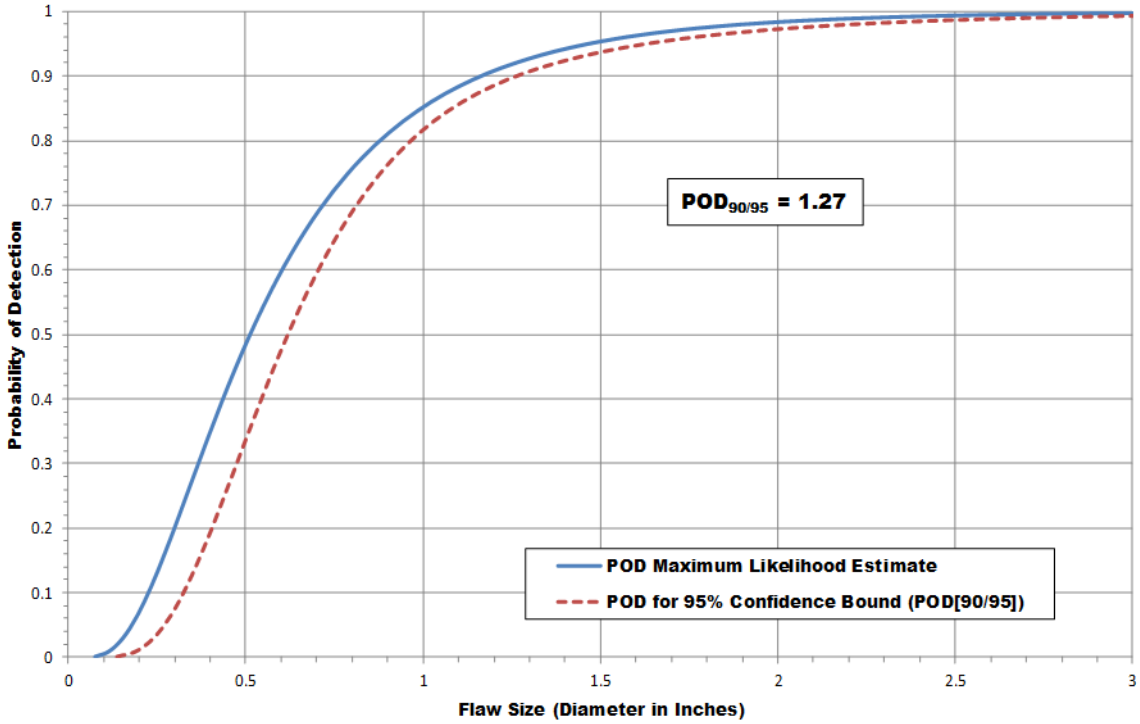

Individual Inspector POD Results Table All Spar Cap & Shear Web and Box Type Construction Conventional PE-UT - All Complex Geometry Flaws Only Panels (2, 4, 6, 8, 10 &11) Only - Two High Removed	
Inspector	**$POD_{90/95}$ (Dia. In Inches)**
Inspector A	1.21
Inspector B - Removed	2.84
Inspector C	1.63
Inspector D	1.30
Inspector E	1.36
Inspector F	2.06
Inspector G	2.09
Inspector H	1.12
Inspector I	1.86
Inspector J	<0.75
Inspector K	1.39
Inspector L - Removed	2.10
Overall Cumulative $POD_{90/95}$	**1.27**
Range Spread	**178.67%**

Figure 6-23: Cumulative POD Curve Representing Conventional PE-UT from 10 Inspectors (Two Worst POD Performers Removed) Inspecting Only the Complex Geometry Regions of the WBFDE Test Specimens (Bond Line & Laminate Under Bond)

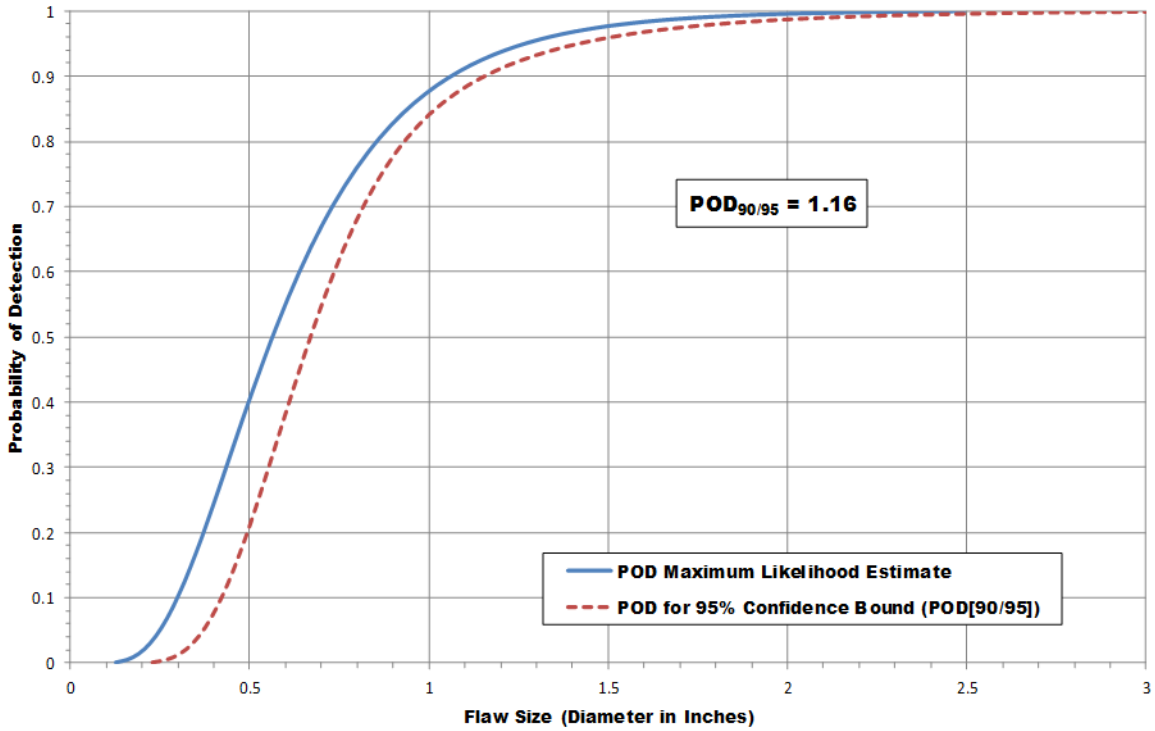

Individual Inspector POD Results Table All Spar Cap & Shear Web and Box Type Construction Conventional PE-UT - All Bond Line Flaws Only Panels (2, 4, 6, 8, 10 &11) Only - Two High Removed	
Inspector	**$POD_{90/95}$ (Dia. In Inches)**
Inspector A	1.33
Inspector B	1.74
Inspector C	1.16
Inspector D	1.31
Inspector E	1.17
Inspector F	1.19
Inspector G - Removed	1.92
Inspector H	1.19
Inspector I	1.71
Inspector J	<0.75
Inspector K	1.54
Inspector L - Removed	2.10
Overall Cumulative $POD_{90/95}$	**1.16**
Range Spread	**132.00%**

Figure 6-24: Cumulative POD Curve Representing Conventional PE-UT from 10 Inspectors (Two Worst POD Performers Removed) Inspecting Only the Bond Line Regions of the WBFDE Test Specimens (Bond Line Flaws Only)

Table 6-20 summarizes the projected overall improvements in the flaw detection capability of the wind industry if additional training, more frequent exposure to blade inspections, better inspection procedures and frequent use of Composite NDI Reference Standards are able to improve the inspectors in the "Good" category to the "Outstanding" level and inspectors in the "Average" category to the "Good" category. One scenario, affecting only the lower/average inspectors, produces a 12% overall improvement in POD from 1.33" down to 1.19". The second scenario, affecting both the lower/average and middle/good inspectors, produces a 22% overall improvement in POD from 1.33" down to 1.09". Figure 6-25 and Figure 6-26 displays these inspection improvements graphically.

Table 6-21 and Table 6-22 show the improvements possible if the largest one or two flaws missed by each inspector are changed to a hit (detection). Individually, the inspector's POD values improved by 5 to 26%. This data analysis shows the potential value of improved training where every inspector performs a little better and more repeatably. It also shows how a single, large flaw miss can drastically change an inspector's POD.

Table 6-23 and Figure 6-27 focus on possible improvements in the Spar Cap and Shear Web types of blade designs if all inspectors performed as Outstanding or Good. POD improvements as much as 28% can be brought about by additional training, more frequent exposure to blade inspections, better inspection procedures and frequent use of NDI Reference Standards. Table 6-24 and Figure 6-28 focus on possible improvements in the Box Spar types of blade designs if all inspectors performed as Outstanding or Good. In this case, POD improvements as much as 67% are possible.

Cumulative POD Results Table - Wind Blade Flaw Detection Experiment Conventional Pulse-Echo UT - All Spar Cap & Shear Web and Box Type Construction Projected Inspector Movement from Lower to Higher Performance Levels (Projected Improvements with Additional Inspector Training)	
Condition	**$POD_{90/95}$ (Dia. In Inches)**
All Flaws - 12 Inspectors - Panels (1-11) - Top 4 Inspectors (untouched), Middle 4 Inspectors (untouched), Bottom 4 Inspectors Improved to the Middle 4 Inspector Level	1.19
All Flaws - 12 Inspectors - Panels (1-11) - Top 4 Inspectors (untouched), Middle 4 Inspectors Improved to the Top 4 Inspector Level, Bottom 4 Inspectors Improved to the Middle 4 Inspector Level	1.09

Table 6-20: POD Improvements Produced when Performance of Bottom (Average) and Middle (Good) Inspectors are Shifted to High (Outstanding) and Middle (Good) Inspector Performance, Respectively

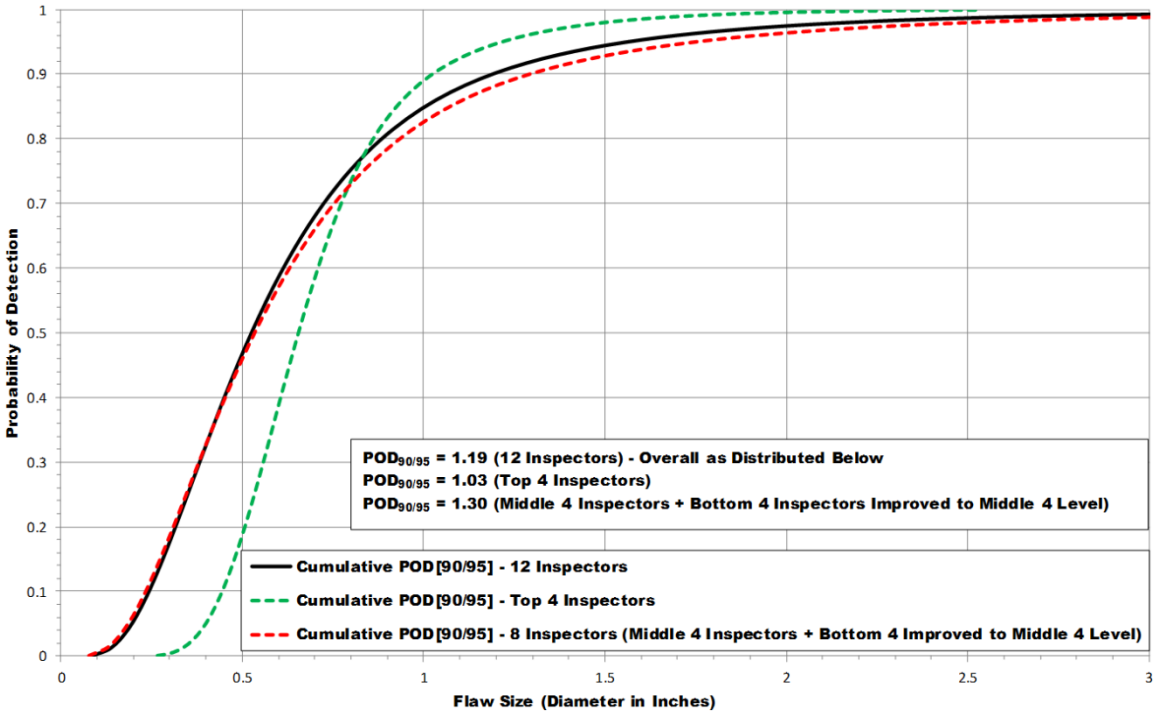

Figure 6-25: POD Curves for All WBFDE Test Specimens (Spar Cap & Shear Web and Box Spar Construction when Performance of Bottom (Average) Inspectors are Shifted to the Middle (Good) Level

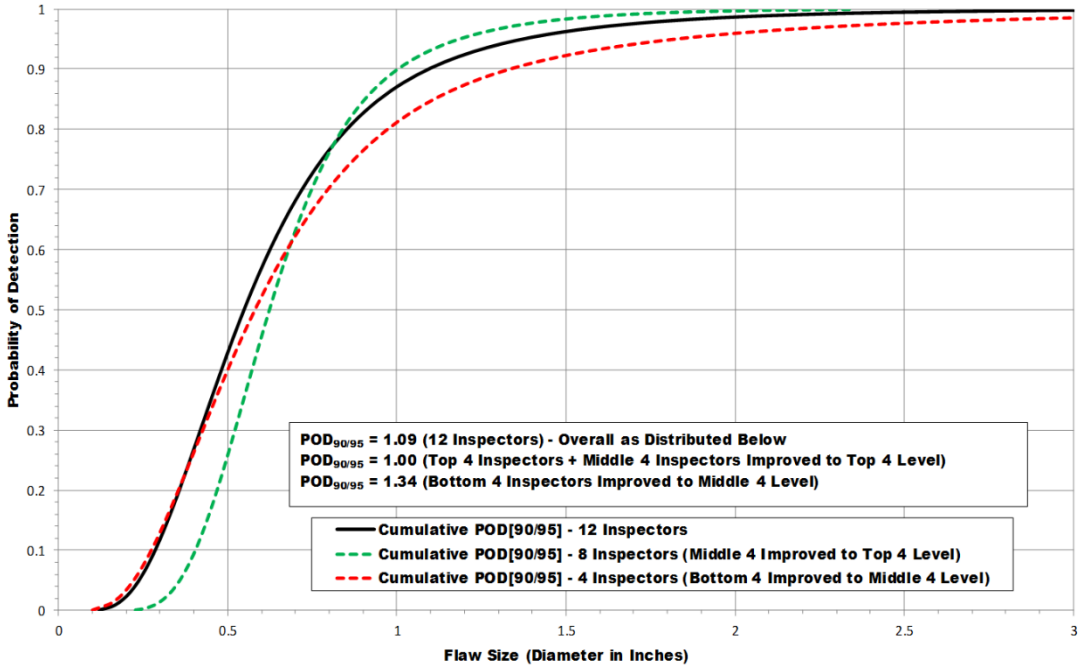

Figure 6-26: POD Curves for All WBFDE Test Specimens (Spar Cap & Shear Web and Box Spar Construction when Performance of Bottom (Average) and Middle (Good) Inspectors are Shifted to their Next Higher Level

Individual Inspector POD Results Table - All Spar Cap & Shear Web and Box Type Construction Conventional PE-UT - All Flaws - All Panels (1-11) - (Largest Miss Changed to a Detection - Each Inspector)				
Inspector	$POD_{90/95}$ (Dia. In Inches)	$POD_{90/95}$ (Dia. In Inches) Largest Miss Changed to Detection	Size of Missed Flaw Changed to Detection (Inches)	Perent Change in $POD_{90/95}$
Inspector A	1.51	1.35	2.50	10.60%
Inspector B	2.67	2.33	3.00	12.73%
Inspector C	1.58	1.45	2.00	8.23%
Inspector D	1.65	1.50	2.50	9.09%
Inspector E	1.19	1.08	1.50	9.24%
Inspector F	1.36	1.23	2.00	9.56%
Inspector G	1.78	1.70	1.50	4.49%
Inspector H	1.04	0.97	1.00	6.73%
Inspector I	1.52	1.44	1.50	5.26%
Inspector J	0.98	0.87	1.00	11.22%
Inspector K	1.17	1.00	1.50	14.53%
Inspector L	1.96	1.83	2.00	6.63%
Overall Cumulative $POD_{90/95}$	**1.33**	**1.26**		5.26%
Range Spread	**172.45%**	**167.82%**		

Table 6-21: POD Improvements Produced when the Largest Flaw Missed by Each Inspector is Changed to a Detection

Individual Inspector POD Results Table - All Spar Cap & Shear Web and Box Type Construction Conventional PE-UT- All Flaws - All Panels (1-11) - (Two Largest Misses Changed to a Detection - Each Inspector)				
Inspector	$POD_{90/95}$ (Dia. In Inches)	$POD_{90/95}$ (Dia. In Inches) Two Largest Misses Changed to Detection	Size of Missed Flaws Changed to Detection (Inches)	Perent Change in $POD_{90/95}$
Inspector A	1.51	1.27	2.50, 1.50	15.89%
Inspector B	2.67	2.12	3.00, 2.50	20.60%
Inspector C	1.58	1.37	2.00, 1.50	13.29%
Inspector D	1.65	1.37	2.50, 2.00	16.97%
Inspector E	1.19	1.03	1.50, 1.00	13.45%
Inspector F	1.36	1.08	2.00, 2.00	20.59%
Inspector G	1.78	1.62	1.50, 1.50	8.99%
Inspector H	1.04	0.86	1.00, 1.00	17.31%
Inspector I	1.52	1.36	1.50, 1.50	10.53%
Inspector J	0.98	0.86	1.00, 0.75	12.24%
Inspector K	1.17	0.87	1.50, 1.00	25.64%
Inspector L	1.96	1.70	2.00, 2.00	13.27%
Overall Cumulative $POD_{90/95}$	**1.33**	**1.19**		10.53%
Range Spread	**172.45%**	**146.51%**		

Table 6-22: POD Improvements Produced when the Two Largest Flaws Missed by Each Inspector are Changed to Detections

Cumulative POD Results Table - Wind Blade Flaw Detection Experiment Conventional Pulse-Echo UT - All Spar Cap & Shear Web Type Construction Only Inspector Performance Levels	
Condition	**$POD_{90/95}$ (Dia. In Inches)**
All Flaws - 12 Inspectors - Panels (1-9)	1.25
All Flaws - Top 4 Inspectors - Panels (1-9)	0.98
All Flaws - Middle 4 Inspectors - Panels (1-9)	1.31
All Flaws - Bottom 4 Inspectors - Panels (1-9)	1.63

Table 6-23: POD Improvements Produced when Performance of Average, Good and Outstanding Inspectors are Assessed Separately (Spar Cap and Shear Web Construction Only)

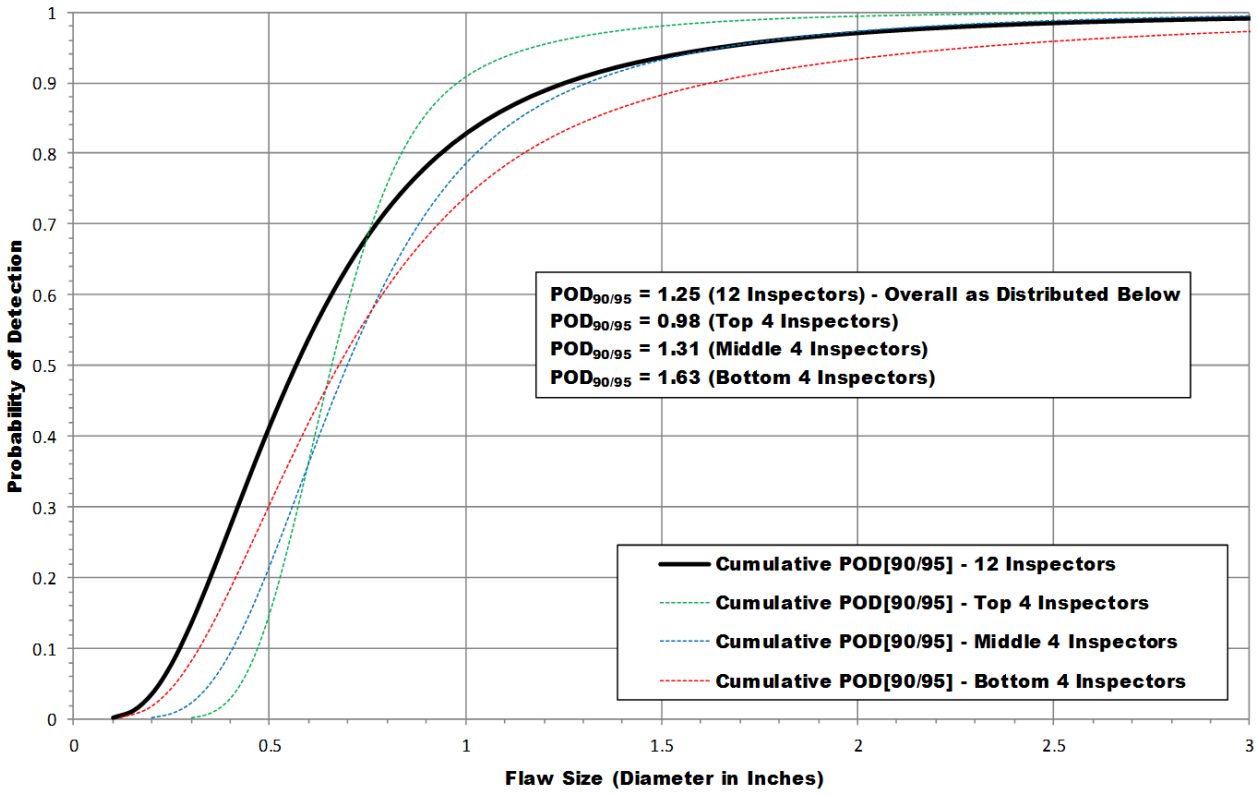

Figure 6-27: POD Curves for Spar Cap & Shear Web Specimens when Performance is Separately Assessed for Average, Good and Oustanding Inspectors

Cumulative POD Results Table - Wind Blade Flaw Detection Experiment Conventional Pulse-Echo UT - All Box Spar Type Construction Only Inspector Performance Levels	
Condition	**$POD_{90/95}$ (Dia. In Inches)**
All Flaws - 12 Inspectors - Panels (10-11)	1.62
All Flaws - Top 4 Inspectors - Panels (10-11)	0.97
All Flaws - Middle 4 Inspectors - Panels (10-1)	1.43
All Flaws - Bottom 4 Inspectors - Panels (10-11)	3.01

Table 6-24: POD Improvements Produced when Performance of Average, Good and Outstanding Inspectors are Assessed Separately (Box Spar Construction Only)

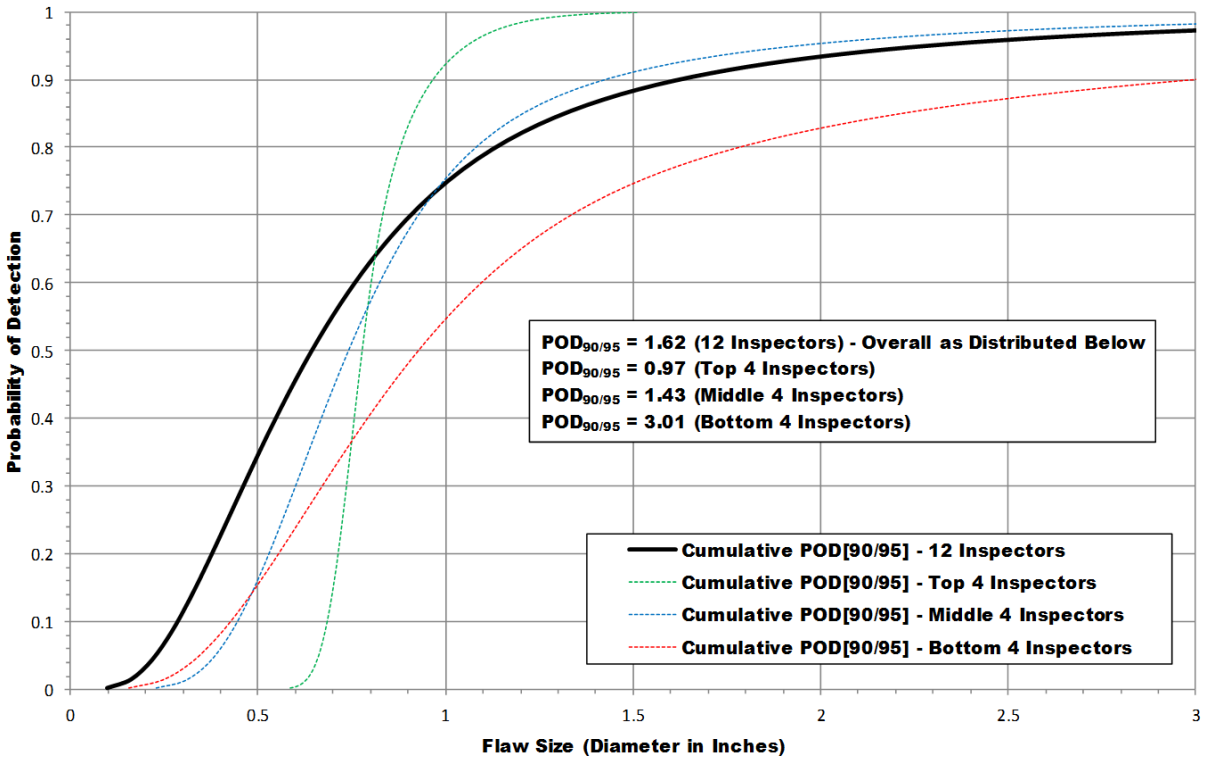

Figure 6-28: POD Curves for Box Spar Specimens when Performance is Separately Assessed for Average, Good and Oustanding Inspectors

Table 6-25 and Figure 6-29 reveal a relationship between the inspector's performance level and his experience inspecting blades. For the most part, more experienced inspectors performed better in the WBFDE. Thus, if inspectors are given additional exposure to simulated blade

inspections, through additional training and use of representative, flawed wind blade test specimens, it is expected that their performance will rise to the levels of their more experienced colleagues.

All of the examples provided in this section support the notion that wind blade inspectors should be receiving training that focuses on the specific challenges associated with wind blades and provides uniform and periodic reminders about NDI signals. Overall, the results provided in this section quantify the potential improvements in inspector's performance on wind blades as a result of increased training, apprenticeships, exposure to representative inspections, enhanced procedures, inspector teaming and awareness training on inspection obstacles.

Wind Blade Flaw Detection Experiemnt - Inspector NDT Experience Conventional Pulse-Echo UT - Sorted by Performance				
Inspector	NDT Certification Level*	Years of NDT Experience	Years of NDT Experience with Composites	Overall $POD_{90/95}$ (Dia. In Inches)
J	II	14	14	0.98
H	III	30	27	1.04
K	III	25	22	1.17
E	II	5	5	1.19
F	II	3.5	3.5	1.36
A	III	4.5	4.5	1.51
I	N/A**	7 months	7 months	1.52
C	II	5.5	5.5	1.58
D	II	7 months	7 months	1.65
G	N/A**	1.5	1.5	1.78
L	N/A**	1 week	1 week	1.96
B	N/A**	3.5	3.5	2.67
* - Certified through ASNT (SNT-TC-1A), EN 473, ISO 9712 or in-house company level certification program.				
** - N/A, no company or other certifications.				

Table 6-25: Rank of POD Performance Levels with Inspector Experience

The composite composition of wind blades coupled with difficulties associated with damage tolerance analysis of composites, has placed greater emphasis on the application of accurate NDI methods. The wind industry faces a challenge in how to develop and deliver appropriate training to personnel performing NDI on modern, complex wind blades which are almost 100% composite construction. The NDI performance assessment POD experiments described above produced a number of recommendations for improving inspection of composite wind blades. These issues included topics such as the use of guides to ensure proper surface area coverage to proper equipment calibration to recognition of critical aspects of the UT signals to the proper

deployment of transducers. Many of these issues can be mitigated by additional personnel training. Some of the training can be in the form of composite awareness training to instruct inspectors on composite materials, composite structure fabrication and typical wind blade composite construction designs. Other forms of training can stress procedural aspects of the inspections such as the use of NDI Reference Standards, proper transducer deployment aids (e.g. delay lines) and the proper use of drawings to assist in signal interpretation. A more thorough description of suggested training for wind blade inspectors is provided in Chapter 7.

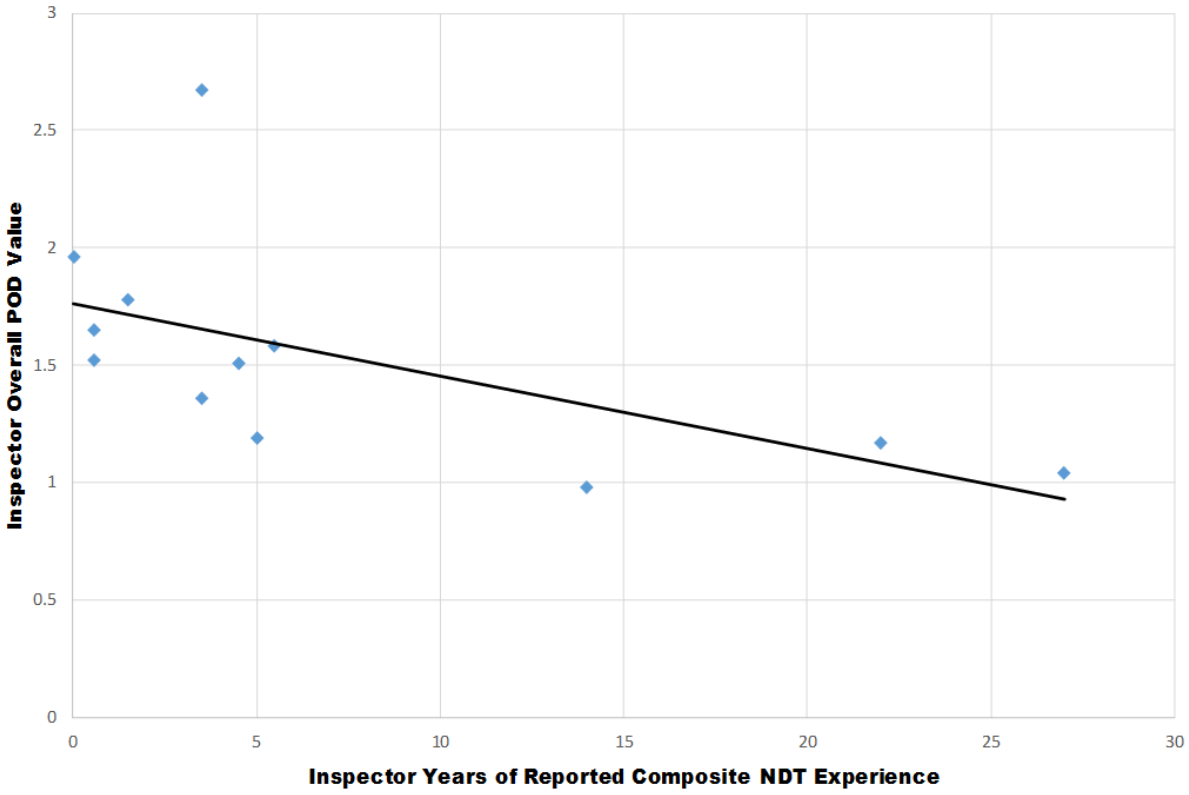

Figure 6-29: Comparison Showing a Relationship between the Inspector Performance and the Experience Level of that Inspector

6.2 Phased/Linear Array and Pulse Echo Scanning Ultrasonics

Once the industry NDI performance baseline is established for conventional inspection methods, it is then possible to assess the improvements stemming from the use of more sophisticated inspection methods. Table 6-26 provides a complete list of the advanced inspections methods deployed and the specific equipment used. Most of the advanced NDI fell into the phased array and single-element scanning UT category with the addition of some limited testing using thermography and Microwave inspection methods. These latter two NDI techniques will be address in other sections of this chapter.

6.2.1 WBFDE –POD Results Omniscan, P-Scan and Focused Single Element C-Scan Systems

The phased array UT and pulse-echo, single element scanning UT methods used in this POD experiment along with their associated equipment are shown in Figure 6-30 through Figure 6-33. The three photos along the top of Figure 6-30 show different phased array UT devices with linear encoding (position recording) mechanisms while the lower photo is a single-element UT scanning device. All of these inspection devices utilize UT waveform capture and produce a two-dimensional C-scan image. In the basic C-scan system, the scanning unit containing the transducer is moved over the surface of the test piece using a search pattern of closely spaced parallel lines. A mechanical linkage connects the scanning unit to X-axis and Y-axis position indicators which feed position data to the computer. The echo signal is recorded, versus its X-Y position on the test piece, and a color coded image is produced from the relative characteristics of the sum total of signals received. The unit is tethered to a remotely located computer for control and data acquisition. The value of using two-dimensional color coding, stemming from the sum total of the A-scan signals, to identify and size composite flaws is evident in the C-scan image. The combined use of A-scan (raw UT signal), B-scan (section view showing the depth of flaws), C-scan (2-D planform view) data enhances flaw detection and characterization. Figure 6-34 compares these various data presentation modes where conventional pulse-echo UT methods will only have the A-scan data and the X-Y scanner methods – whether they are phased array or single-element UT - will also have the B-scan and two-dimensional, color-coded C-scan information to use in making flaw calls.

Wind Blade Flaw Detection Experiment - Inspector Equipment Used - Advanced Methods				
Inspector	Probe Frequency Used	Probe Type	Advanced Method	Equipment Used
AA	0.5 MHz	Single Element, Sandia Focused Probe	Automated Scanning, Pulse-Echo UT	Boeing MAUS V
BB	1.0 MHz	64 Elements, Custom Shoe, Varied Delay	Olmypus X-Y Glider, Phased Array UT	Olympus OmniScan
CC	1.0 MHz	80 Elements, Custom Shoe, 50 mm Delay	Manual Linear Encoder, Phased Array UT	Olympus OmniScan
DD	1.0 MHz	80 Elements, Custom Shoe, 50 mm Delay	Manual Linear Encoder, Phased Array UT	Olympus OmniScan
EE	1.0 MHz	64 Elements, Custom Shoe, 35 mm Delay	Manual Linear Encoder, Phased Array UT	Olympus OmniScan
FF	0.5 MHz	Single Element, Custom Teflon Delay	Automated Scanning AMS-46, Pulse-Echo UT	Force Technology P-Scan
GG	0.5 MHz	Single Element, Custom Teflon Delay	Automated Scanning AMS-46, Pulse-Echo UT	Force Technology P-Scan
HH	0.5 MHz	Single Element, Custom Teflon Delay	Automated Scanning AMS-46, Pulse-Echo UT	Force Technology P-Scan
II	0.5 MHz	Single Element, Custom Teflon Delay	Automated Scanning ATS-1, Pulse-Echo UT	Force Technology P-Scan
JJ	0.5 MHz	Single Element	Automated Scanning (R&D), Pulse-Echo UT	Force Technology P-Scan
KK	0.5 MHz	Single Element, Custom Teflon Delay	Automated Scanning ATS-1, Pulse-Echo UT	Force Technology P-Scan
LL	n/a	n/a	IR - Pulsed Thermography	FLIR X6540 SC Camera, 750 W Heater
MM	0.5 MHz	GE RotoArray, 60 Elements	Linear Array UT	GE Mentor UT
NN	1.0 MHz	GE RotoArray, 64 Elements	Linear Array UT	GE USM Vision +

Table 6-26: List of Inspection Methods and Equipment Deployed in WBFDE

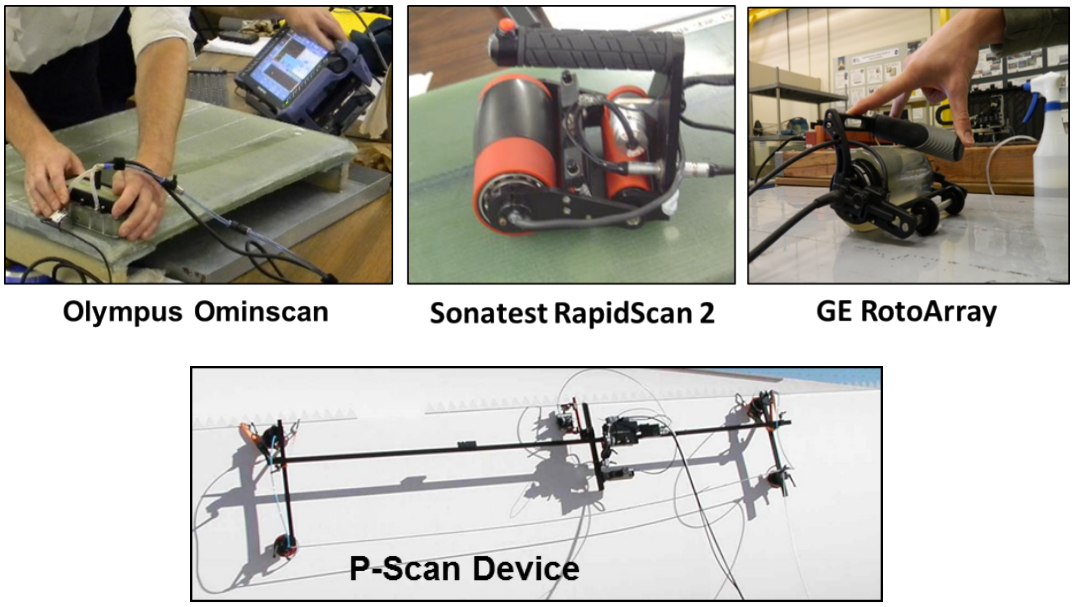

Figure 6-30: Sample Deployment of Advanced NDI Equipment - Phased Array Ultrasonics and the P-Scan Single Element UT Scanning System

Figure 6-31: Olympus OmniScan and 64 Element Phased Array Probe Deployed with an X-Y Glider for Manual Scanning

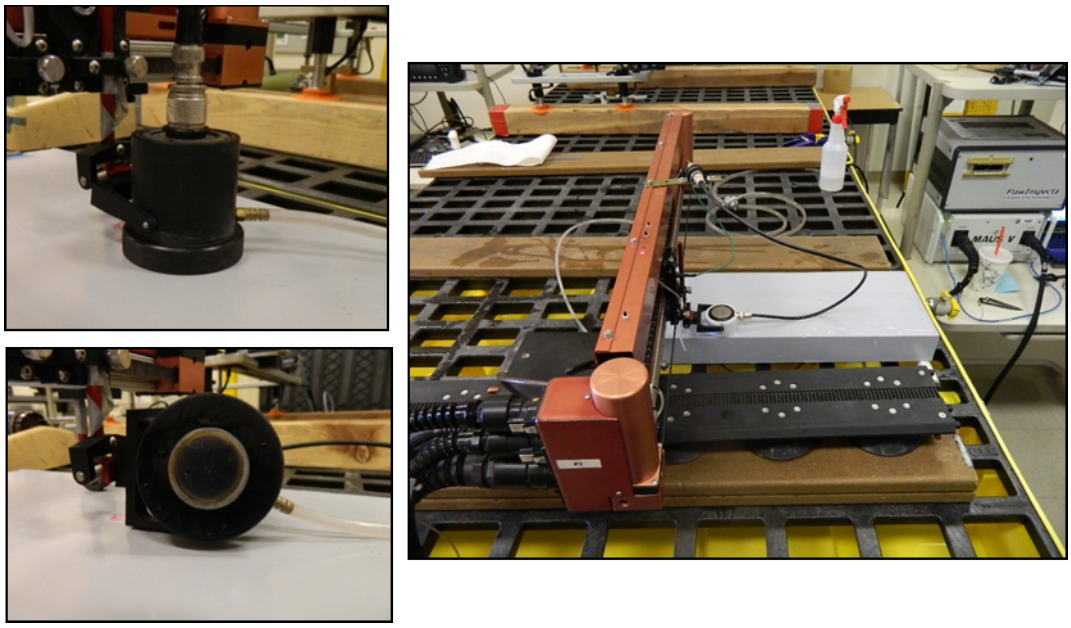

Figure 6-32: Focused Single-Element Probe Deployed in Pulse-Echo Mode Using the MAUS Automated Scanner System

Figure 6-33: Force Technology P-Scan UT System with ATS-1 Automated Track Scanner and AMS-46 Tractor Scanner

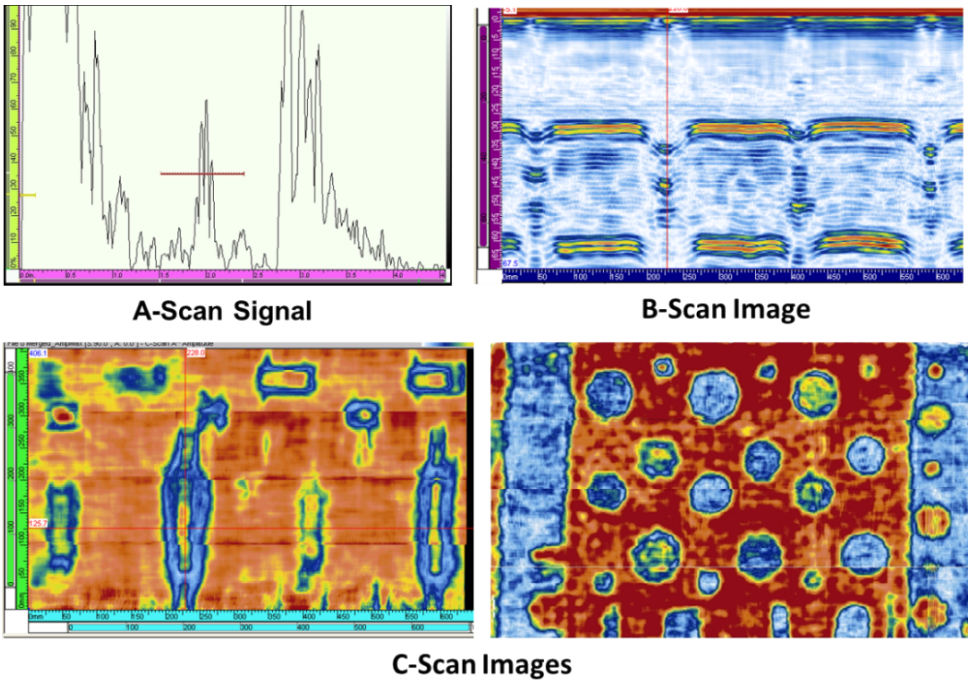

Figure 6-34: Comparison of NDI Data Presentations Used to Detect Damage in Blades

Not all phased array UT systems are expected to produce the exact same performance. Differences from one PA-UT system to the next can arise from many different design features such as: 1) hardware including the phased array transducer design (quality, placement and spacing of the elements, number of elements), transducer excitation levels (voltage), data acquisition and signal processing electronics (signal quality and noise reduction), 3) software including the ability to set multiple gates and gains/amplitude corrections, use of filters, use of PA-UT element steering and other advanced features to improve flaw detection, 4) transducer shoe used to provide proper delay line (distance from inspection surface) and signal coupling (water pool), 5) data display (human factors in presentation and use of color palettes), and 6) the availability of post-processing software to enhance signal-to-noise, focus on specific depths and other features to improve damage visualization and detection.

Following are some sample C-scan results from the application of the Omniscan PA-UT system to several of the WBFDE NDI Feedback Specimens. Wind Specimen REF-STD-4-135-SNL-1 contained two types of flaws: dry areas and out-of-plane waves. The out-of-plane waves were created by embedding pre-cured resin rods with a specific aspect ratio (width to height) between plies of the laminate prior to resin infusion. Figure 6-35 and Figure 6-36 show the PA-UT inspection results. All flaws show up quite clearly with the amplitude C-scans. All resin starved flaws are detected. Interply waves are detected clearly by their effect on the back wall signal. The amplitude in the B-scans, showing depth of flaws, is clearly affected by the waves.

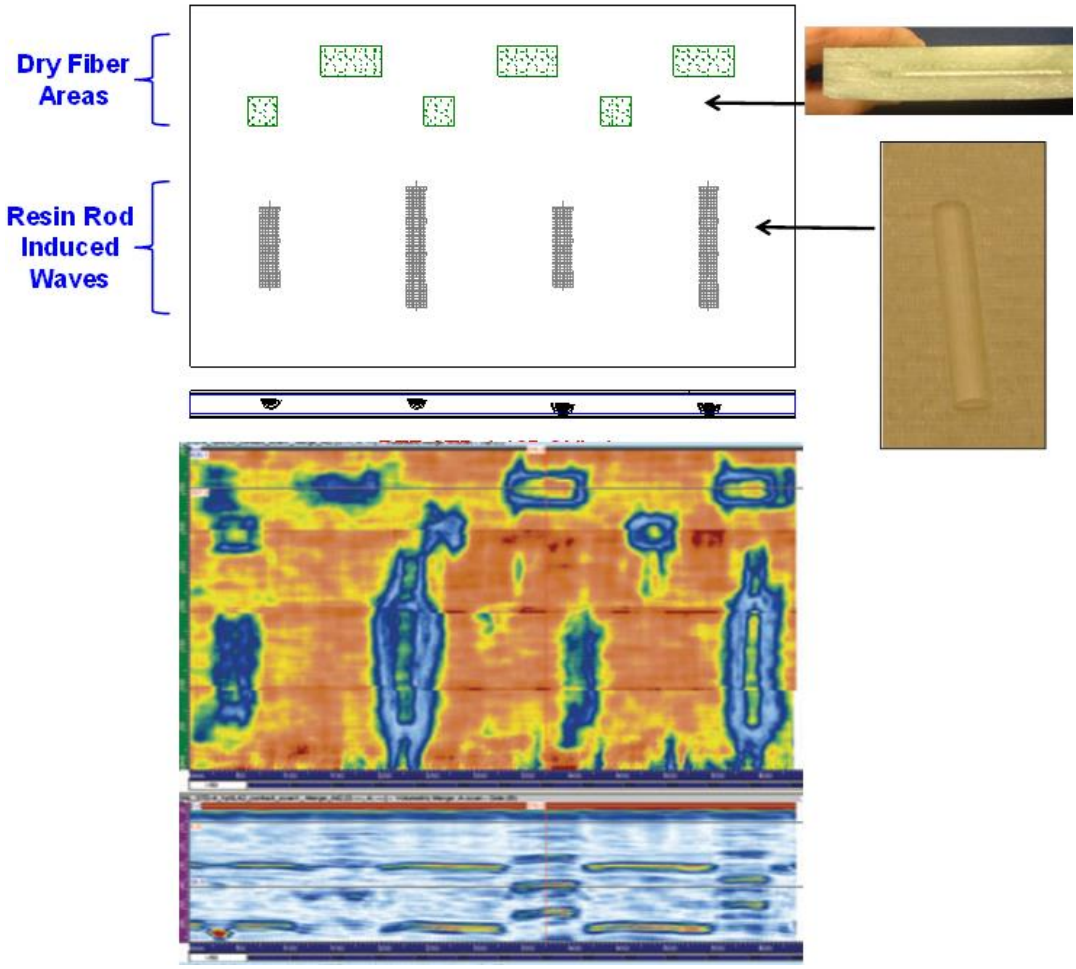

Figure 6-35: OmniScan PA-UT C-Scan of REF-STD-4-135-SNL-1 Produced by the 25 mm Water Column Shoe

Figure 6-36: OmniScan PA-UT Time-of-Flight C-Scan of REF-STD-4-135-SNL-1 Produced by the 25 mm Water Column Shoe

Wind specimen REF-STD-7-214-265-SNL-1 has a thick spar cap (2.14" vs. 1.29") and extremely thick depth to the back of the spar-to-shear web adhesive layer (2.65" vs. 1.76"). Figure 6-37 through Figure 6-39 show the PA-UT inspection results for the Omniscan deployed with the 1.5 MHz 1.5L42 probe. Note that this frequency is a bit high for such a thick specimen. The Amplitude and Time-of-Flight C-scan shows most of the flaws within the laminate with the exception of several mold release flaws at plies 23-31. Most of the flaws within the adhesive joint regions can also be detected with a Time-of-Flight C-scan with the appropriate color palette adjustment. This appears to be the only way to visualize the micro-balloon region at interface 1 (between adhesive joint and shear web). The adhesive voids in the shear web bonded joint were detected. In general, grease shows up very clearly down to a flaw size of 0.5". The microballoons can be detected regardless of where they appear within the laminate structure down to a flaw size of 1.0" and sometimes 0.5". Microballoons can be detected at the interface between the spar cap laminate and the adhesive but not on the far side of the adhesive. The pillow inserts at interface 1 do not show up in these C-scans due to the challenging noise within the laminate. Overall, the pillow inserts at interface 1 do not show up well on any C-scan. These flaws are however visible by scrolling through the A-scan data.

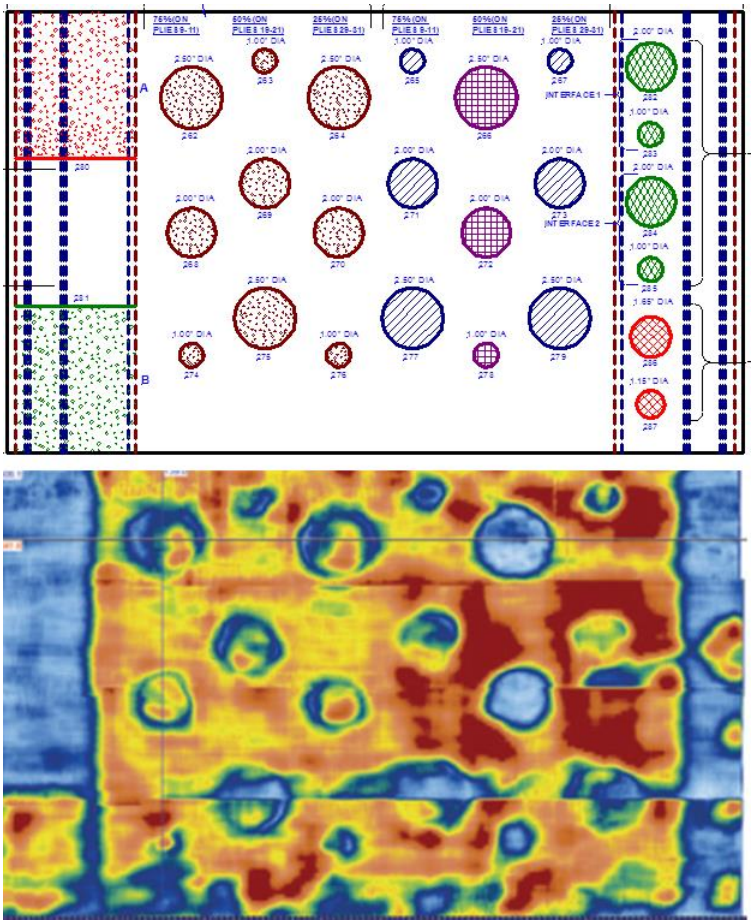

Figure 6-37: OmniScan PA-UT 1.5 MHz C-Scan of REF-STD-7-214-265-SNL-1 Produced by the Contact Wedge Shoe

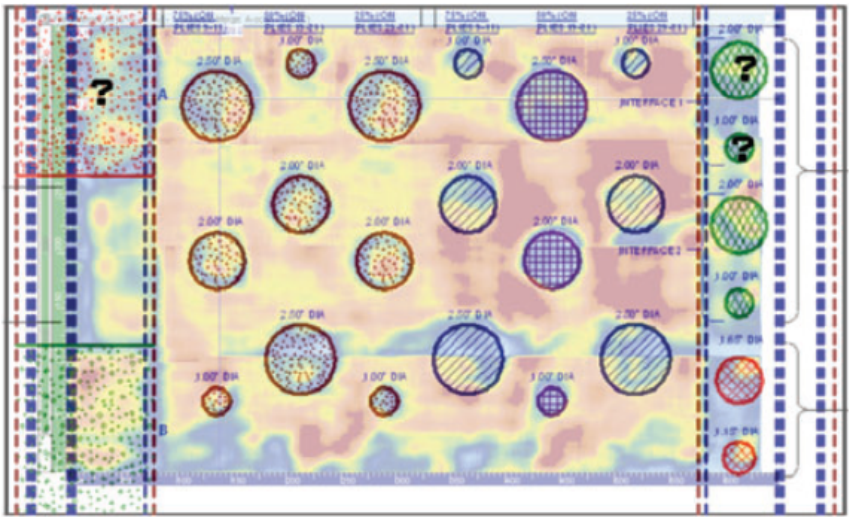

Figure 6-38: Overlay of Flaw profile with PA-UT Image Showing the Porosity and Adhesive Disbond Flaws Not Detected by the OmniScan Inspection (Contact Shoe)

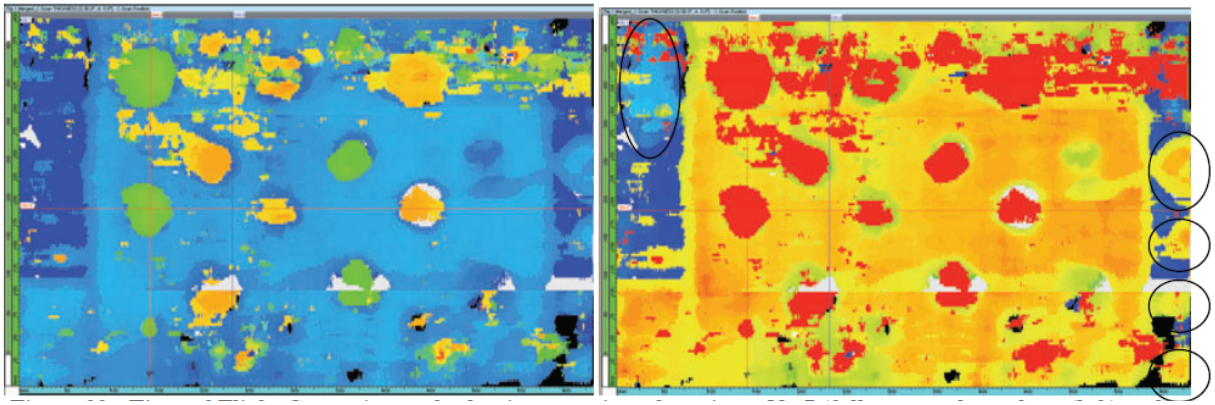

Figure 6-39: OmniScan PA-UT Time-of-Flight C-Scan of REF-STD-7-214-265-SNL-1 Produced by the Contact Shoe (full range color palette on the left and zoomed color palette on the right to show the flaws in the adhesive joint)

For the WBFDE, Olympus OmniScan was deployed with a 1 MHz 1L64 Phased Array Probe and a manually operated X-Y Glider scanner. While extensive testing to date has revealed that the optimum frequency for single-element PE-UT inspections is 500 KHz, many phased array probes are only available at a low frequency of 1 MHz. Good inspection results have also been obtained at 1 MHz as well. Figure 6-40 through Figure 6-44 show the resulting C-scans from inspection of the five NDI Feedback Specimens used by inspectors to practice and set up their equipment: 1) REF-STD-2-127-173-SNL-1, 2) REF-STD-4-135-SNL-1, 3) REF-STD-7-214-265-SNL-1, 4) REF-STD-FB10, and 5) REF-STD-FB11. Notice that the first three specimens use a naming convention where the first three-digit number pertains to the thickness of the spar

cap laminate (e.g. 2.14”) and the second three-digit number, if applicable, pertains to the total thickness of the specimen including any bond line and shear web flange (e.g. 2.65”).

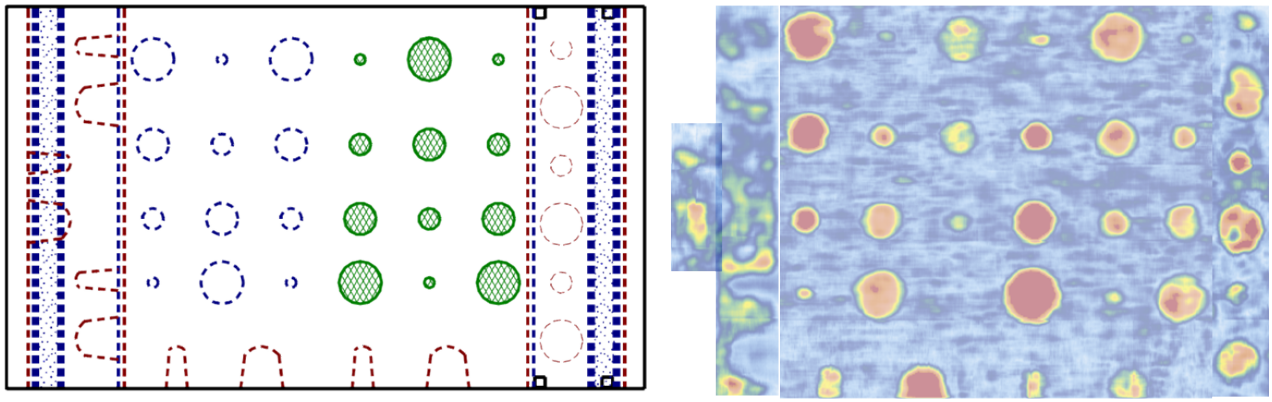

Figure 6-40: C-Scan Image of REF-STD-2-127-173-SNL-1 Specimen Produced by Omniscan PA-UT System with a 1 MHz Transducer

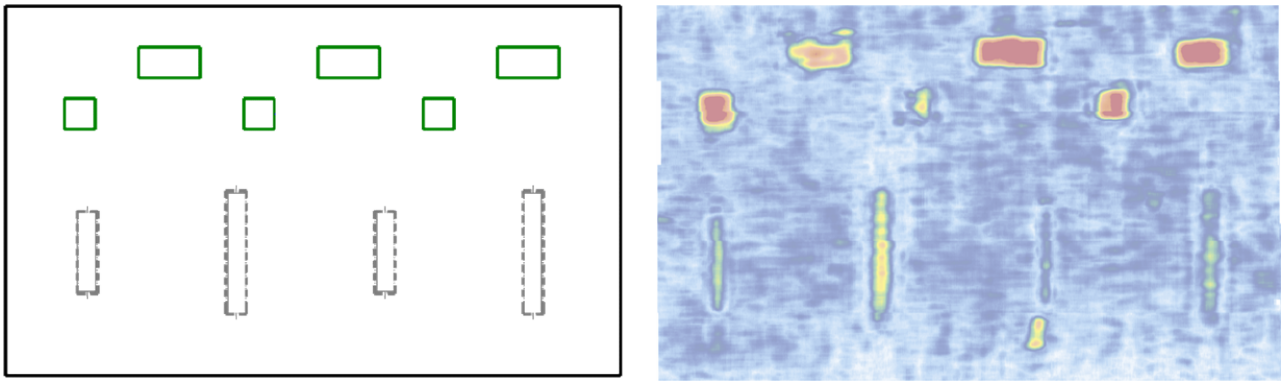

Figure 6-41: C-Scan Image of REF-STD-4-135-SNL-1 Specimen Produced by Omniscan PA-UT System with a 1 MHz Transducer

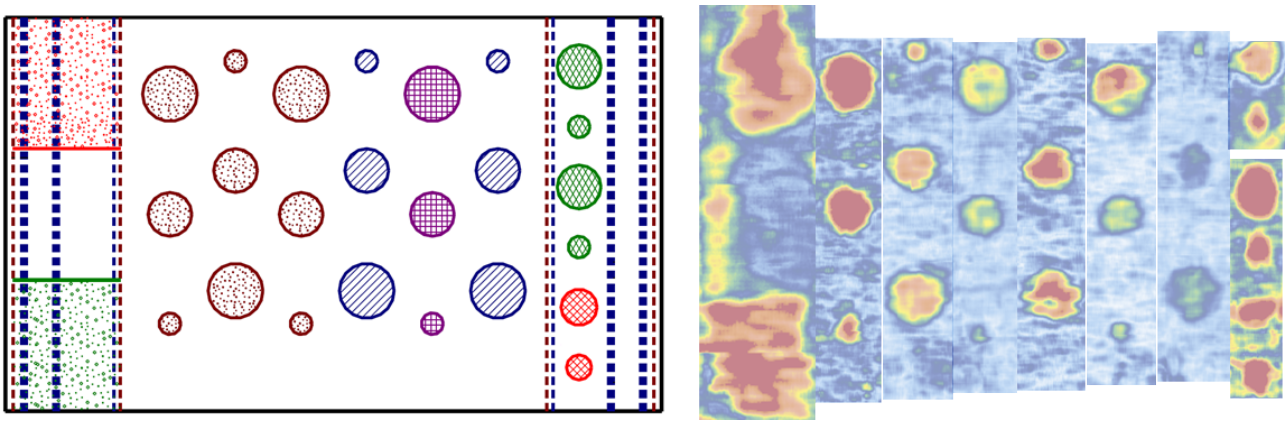

Figure 6-42: C-Scan Image of REF-STD-7-214-265-SNL-1 Specimen Produced by Omniscan PA-UT System with a 1 MHz Transducer

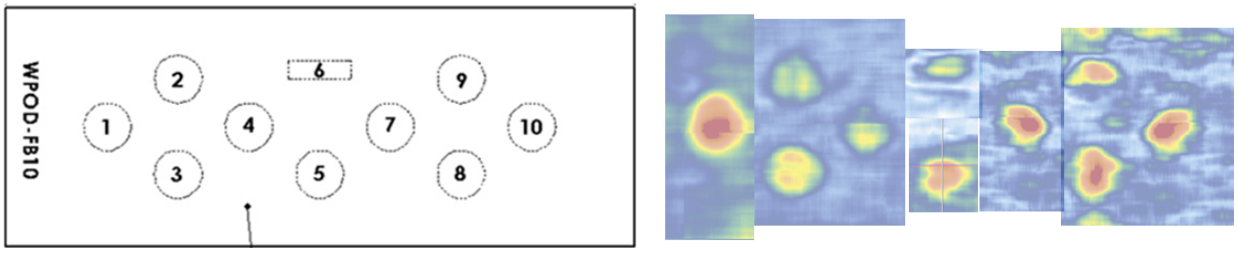

Figure 6-43: C-Scan Image of REF-STD-FB10 Specimen Produced by Omniscan PA-UT System with a 1 MHz Transducer

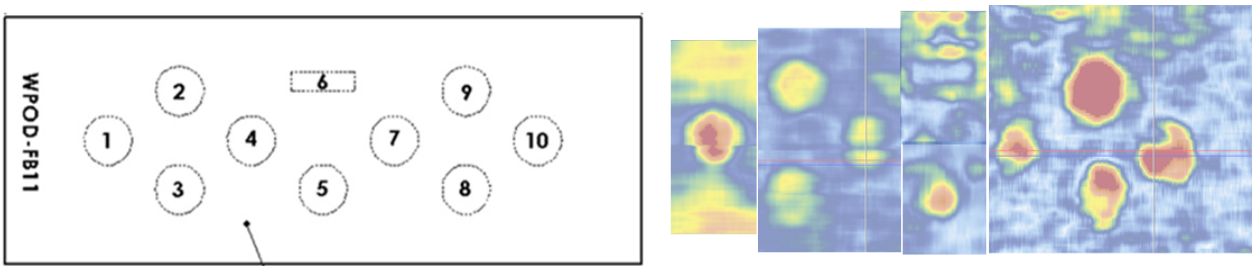

Figure 6-44: C-Scan Image of REF-STD-FB11 Specimen Produced by Omniscan PA-UT System with a 1 MHz Transducer

Figure 6-45 compares the larger footprint of the typical phased array UT probes with the inspection coverage, especially along the edges of specimens. Most of the wind blade inspections do not involve edges, however, the panels produced for this POD testing did contain flaws that were within 1" of the specimen edge. In these cases, the custom UT probe shoe sometimes experienced problems as it neared the specimen edge. The water couplant system, built into the bottom of the shoe, would lose its seal if it extended beyond the edge of the specimen, as shown in Figure 6-45. The loss of water couplant would cause signal dropout so no data was available in these locations. While this created some additional misses of flaws near the edge of the POD specimens, the phased array shoe design is not expected to have any problems during actual wind blade inspections where no edges are involved. The POD specimens were designed with approximately 8% of their flaws within 1" of edge of the panel. Thus, the performance of the phased array UT method was artificially impacted by the specimen designs and the actual POD levels for these methods are expected to be better than the results presented here.

Figure 6-46 through Figure 6-56 show the breakdown of $POD_{(90/95)}$ values for inspectors AA through KK deploying various phased array UT transducers and pulse-echo UT transducers using different C-scan devices. Each POD plot has an accompanying list of $POD_{(90/95)}$ values for the following data sets:

1. All Specimens (Spar Cap and Shear Web + Box Spar Construction) – with breakdown of POD values for Constant Thickness regions, Complex Geometry regions and Bond Line regions.

2. Spar Cap and Shear Web Specimens Only - with breakdown of POD values for Laminate regions and Bond Line regions.
3. Box Spar Specimens Only

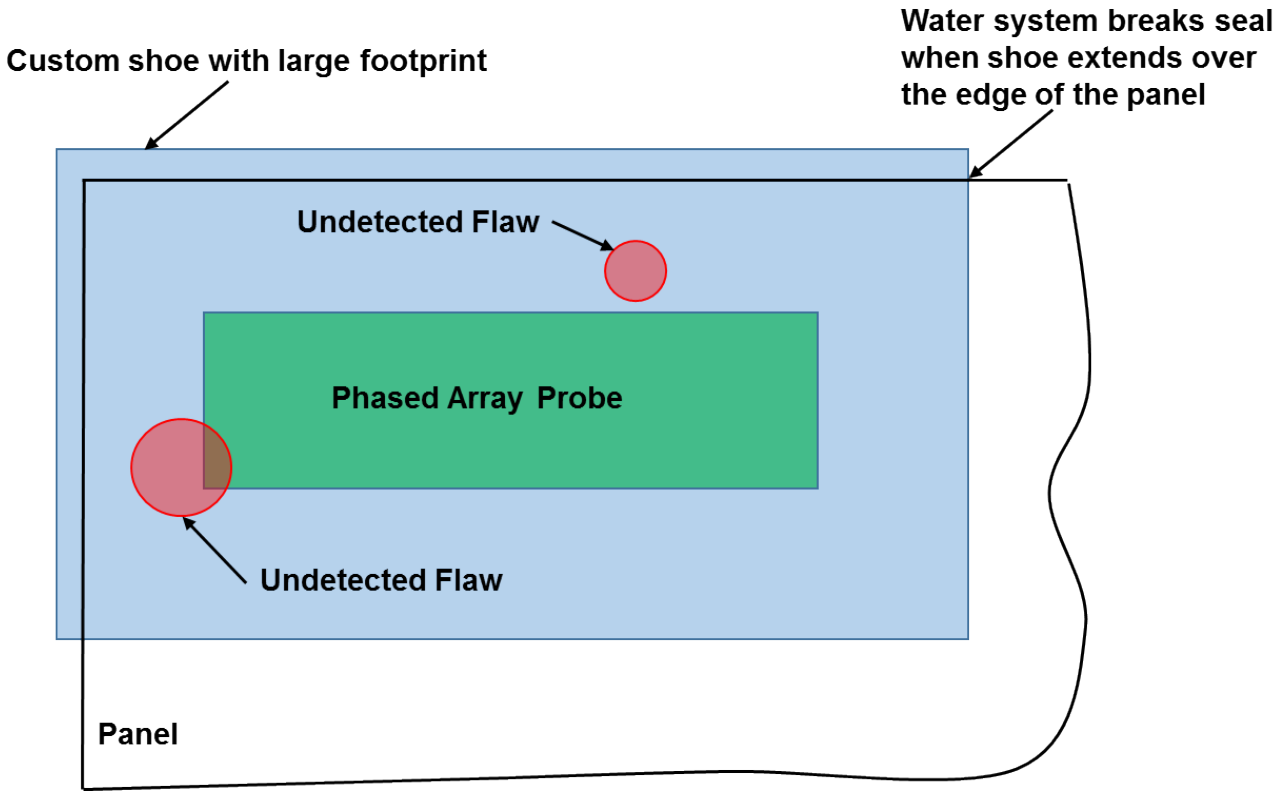

Figure 6-45: Schematic Showing Large Footprint of Phased Array UT Probe that May Affect Ability to Inspect Around Edges

Figure 6-57 and Figure 6-58 compare results for similar phased array UT devices deployed by inspectors at two different companies. The large, 85% difference between these two companies highlight several important issues: 1) the expertise required to properly deploy UT inspection methods, 2) the importance of training necessary to allow a team of inspectors to produce similar results, 3) the loss in performance if an inspection is not conducted in an optimized manner. Figure 6-59 shows the results when the low (Company X) and high (Company Y) inspection values are combined. This represents an expected outcome for the current array of inspectors with a wide variety of practices and performance levels. It has been proven that enhanced training of inspectors will reduce this performance deviation and shift the overall results toward the low POD level of 1.15" dia flaw. This will be address more in the next section.

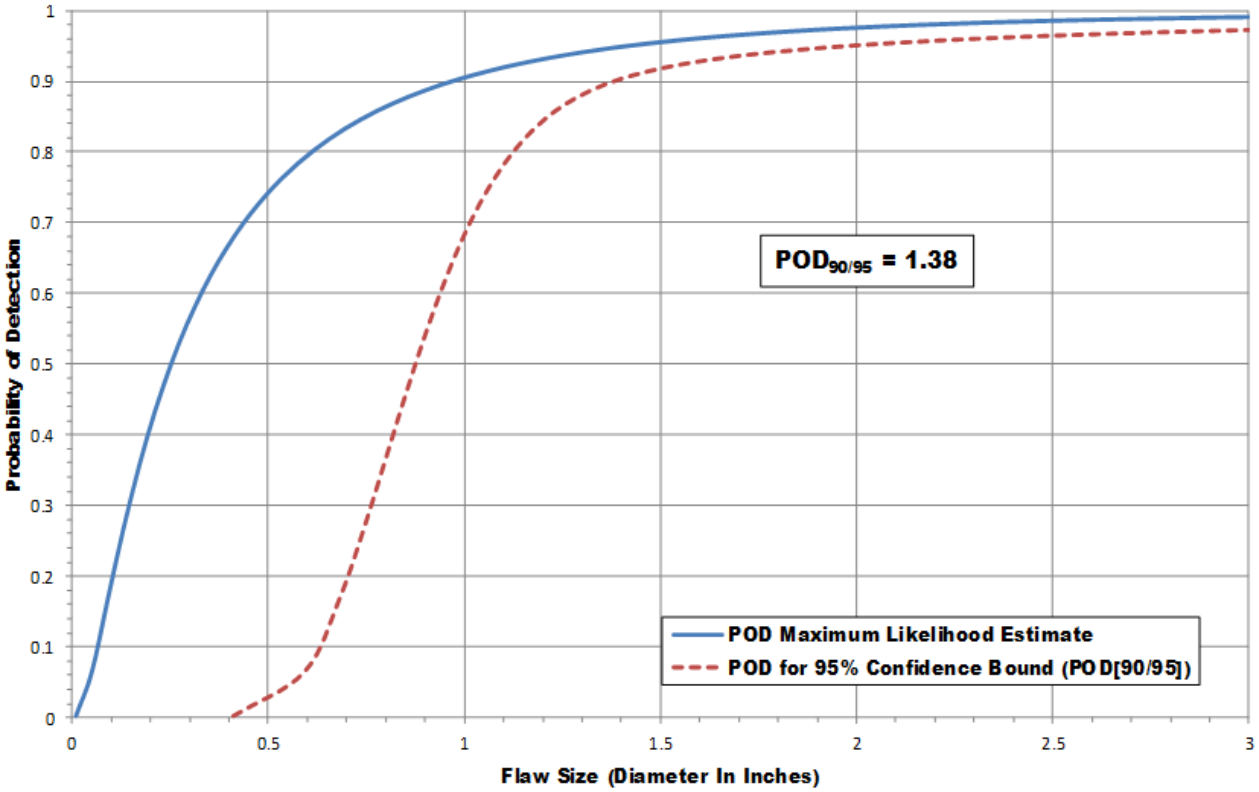

Individual Inspector POD Results Table - Wind Blade Flaw Detection Experiment Advanced NDI Methods - Inspector AA - Scanning PE-UT (500 KHz, MAUS V)	
Condition	$POD_{90/95}$ (Dia. In Inches)
All Spar Cap & Shear Web and Box Type Construction	
All Flaws - Panels (1-11)	1.38
All Constant Thickness Flaws Only - Panels (1-11)	1.37
All Complex Geometry Flaws Only - Panels (2, 4, 6, 8, 10 &11)	1.70
All Bond Line Flaws Only - Panels (2, 4, 6, 8, 10 &11)	1.17
All Spar Cap & Shear Web Type Construction Only	
All Flaws - Panels (1-9)	1.29
All Laminate Flaws Only - Panels (1-9)	1.43
All Bond Line Flaws Only - Panels (2, 4, 6, & 8)	1.28
Box Type Construction Only	
All Flaws - Panels (10-11)	2.00

Figure 6-46: $POD_{(90/95)}$ Values for Inspector AA Deploying Focused Pulse-Echo UT Using the MAUS Scanner – Results for All Specimens, Spar Cap and Shear Web Only, and Box Spar Only; Broken Down by Specific Features in Each Specimen Type

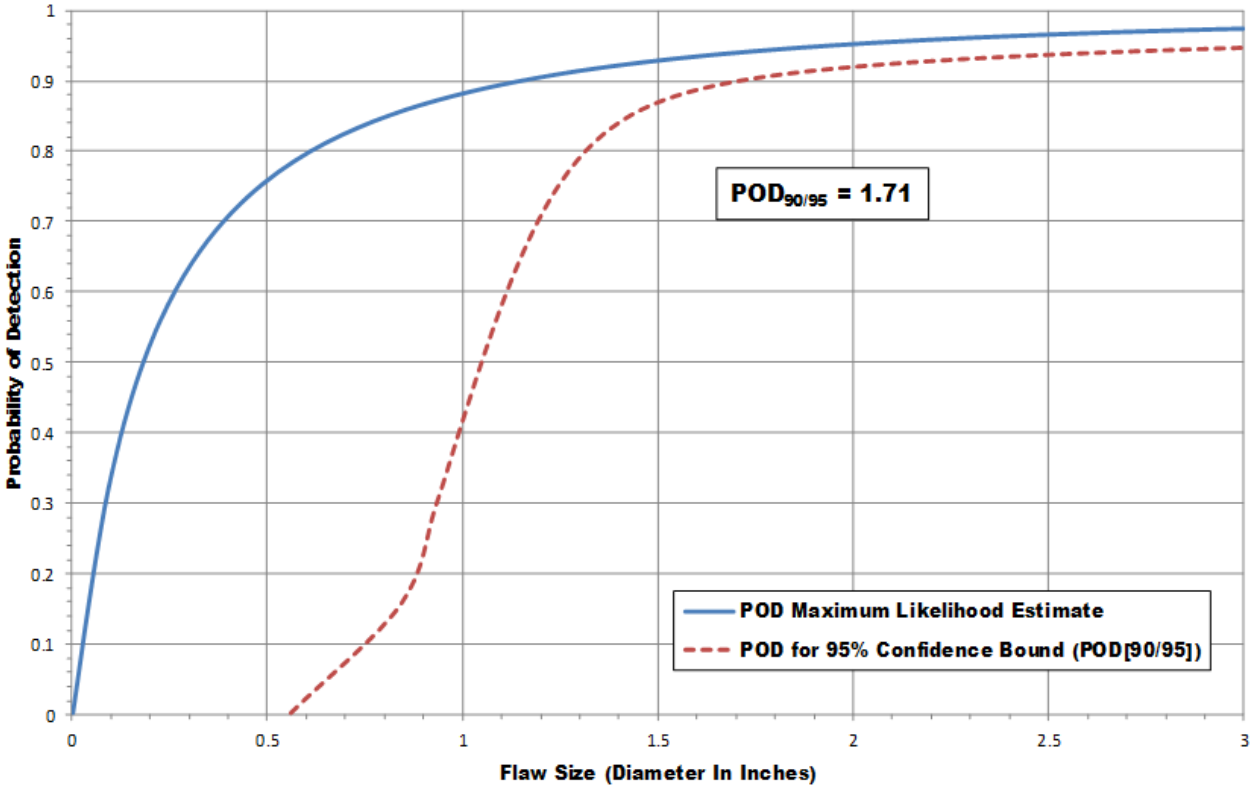

Individual Inspector POD Results Table - Wind Blade Flaw Detection Experiment Advanced NDI Methods - Inspector BB - Scanning PA-UT (1 MHz, OmniScan)	
Condition	**$POD_{90/95}$ (Dia. In Inches)**
All Spar Cap & Shear Web and Box Type Construction	
All Flaws - Panels (1-11)	1.71
All Constant Thickness Flaws Only - Panels (1-11)	<0.75
All Complex Geometry Flaws Only - Panels (2, 4, 6, 8, 10 &11)	>3.00
All Bond Line Flaws Only - Panels (2, 4, 6, 8, 10 &11)	1.17
All Spar Cap & Shear Web Type Construction Only	
All Flaws - Panels (1-9)	1.03
All Laminate Flaws Only - Panels (1-9)	<0.75
All Bond Line Flaws Only - Panels (2, 4, 6, & 8)	1.28
Box Type Construction Only	
All Flaws - Panels (10-11)	>3.00

Figure 6-47: $POD_{(90/95)}$ Values for Inspector BB Deploying Phased Array UT Using the Omniscan and Glider Scanner – Results for All Specimens, Spar Cap and Shear Web Only, and Box Spar Only; Broken Down by Specific Features in Each Specimen Type

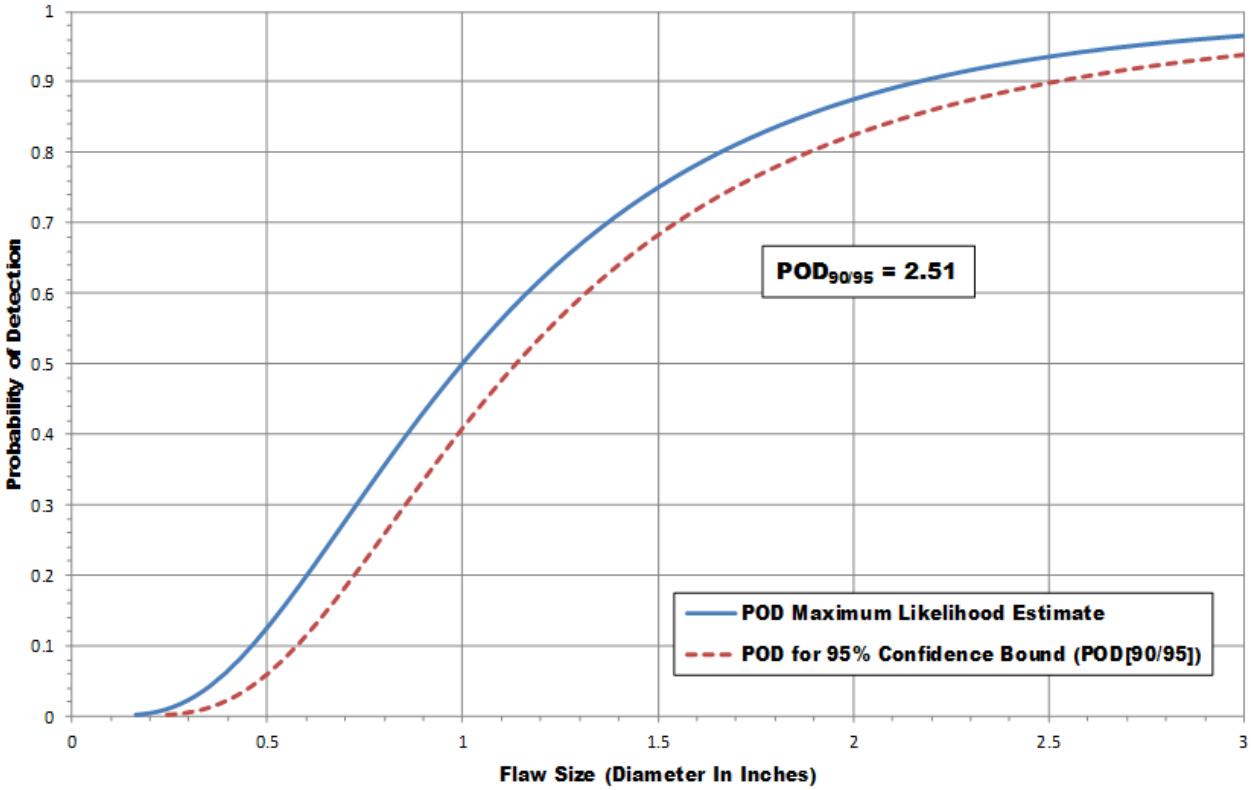

Individual Inspector POD Results Table - Wind Blade Flaw Detection Experiment Advanced NDI Methods - Inspector CC - Free Hand PA-UT (1 MHz, OmniScan)	
Condition	**$POD_{90/95}$ (Dia. In Inches)**
All Spar Cap & Shear Web and Box Type Construction	
All Flaws - Panels (1-11)	2.51
All Constant Thickness Flaws Only - Panels (1-11)	>3.00
All Complex Geometry Flaws Only - Panels (2, 4, 6, 8, 10 &11)	>3.00
All Bond Line Flaws Only - Panels (2, 4, 6, 8, 10 &11)	1.95
All Spar Cap & Shear Web Type Construction Only	
All Flaws - Panels (1-9)	>3.00
All Laminate Flaws Only - Panels (1-9)	>3.00
All Bond Line Flaws Only - Panels (2, 4, 6, & 8)	2.7
Box Type Construction Only	
All Flaws - Panels (10-11)	>3.00

Figure 6-48: $POD_{(90/95)}$ Values for Inspector CC Deploying Phased Array UT Using the Omniscan and a Manual Linear Encoder – Results for All Specimens, Spar Cap and Shear Web Only, and Box Spar Only; Broken Down by Specific Features in Each Specimen Type

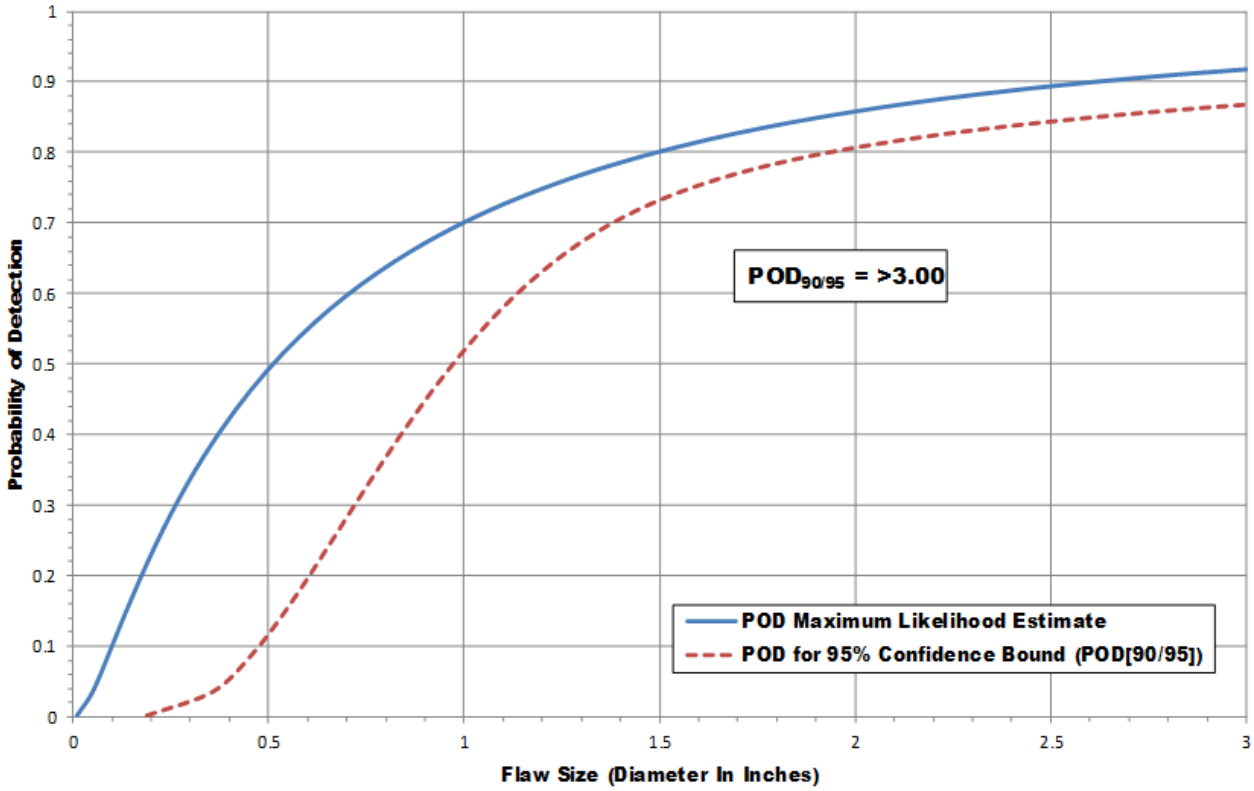

Individual Inspector POD Results Table - Wind Blade Flaw Detection Experiment Advanced NDI Methods - Inspector DD - Free Hand PA-UT (1 MHz, OmniScan)	
Condition	$POD_{90/95}$ (Dia. In Inches)
All Spar Cap & Shear Web and Box Type Construction	
All Flaws - Panels (1-11)	>3.00
All Constant Thickness Flaws Only - Panels (1-11)	2.67
All Complex Geometry Flaws Only - Panels (2, 4, 6, 8, 10 &11)	2.23
All Bond Line Flaws Only - Panels (2, 4, 6, 8, 10 &11)	2.59
All Spar Cap & Shear Web Type Construction Only	
All Flaws - Panels (1-9)	2.63
All Laminate Flaws Only - Panels (1-9)	2.97
All Bond Line Flaws Only - Panels (2, 4, 6, & 8)	2.24
Box Type Construction Only	
All Flaws - Panels (10-11)	>3.00

Figure 6-49: $POD_{(90/95)}$ Values for Inspector DD Deploying Phased Array UT Using the Omniscan and a Manual Linear Encoder – Results for All Specimens, Spar Cap and Shear Web Only, and Box Spar Only; Broken Down by Specific Features in Each Specimen Type

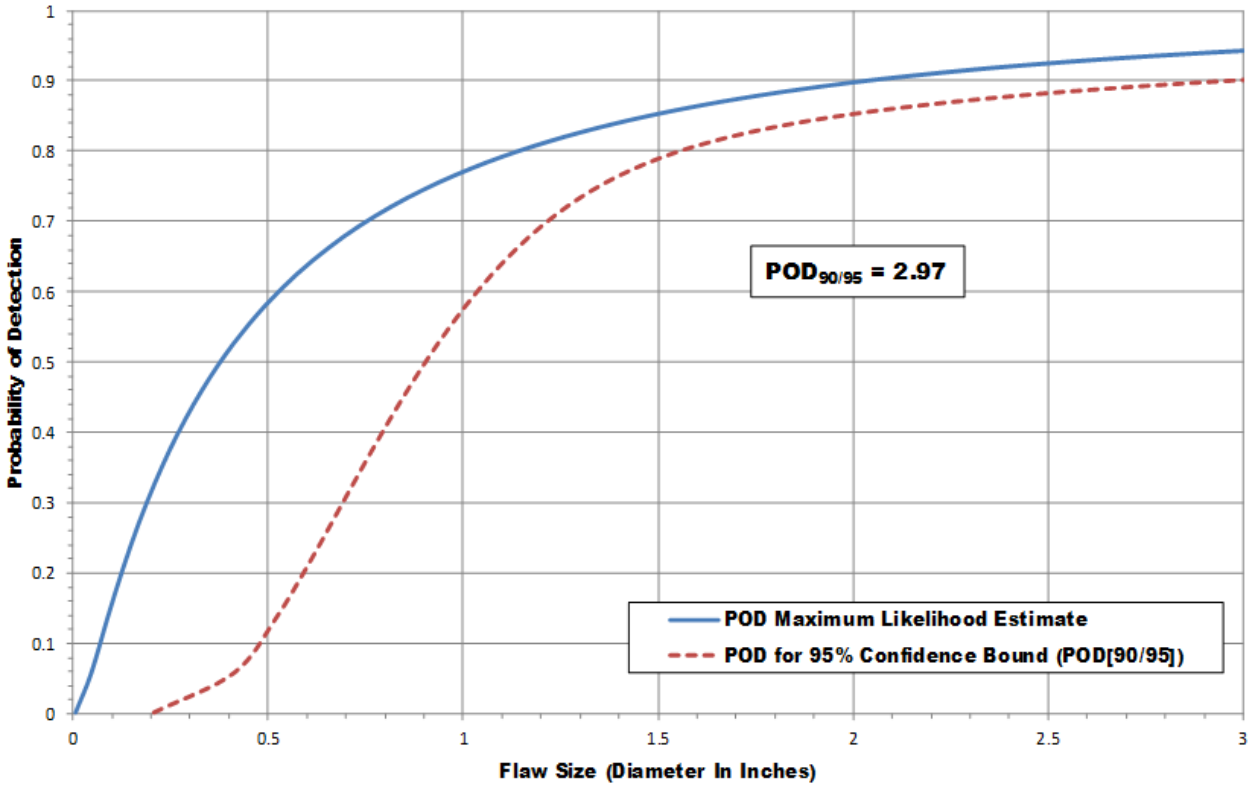

Individual Inspector POD Results Table - Wind Blade Flaw Detection Experiment Advanced NDI Methods - Inspector EE - Free Hand PA-UT (1 MHz, OmniScan)	
Condition	**$POD_{90/95}$ (Dia. In Inches)**
All Spar Cap & Shear Web and Box Type Construction	
All Flaws - Panels (1-11)	2.97
All Constant Thickness Flaws Only - Panels (1-11)	1.75
All Complex Geometry Flaws Only - Panels (2, 4, 6, 8, 10 &11)	2.49
All Bond Line Flaws Only - Panels (2, 4, 6, 8, 10 &11)	2.19
All Spar Cap & Shear Web Type Construction Only	
All Flaws - Panels (1-9)	1.86
All Laminate Flaws Only - Panels (1-9)	1.62
All Bond Line Flaws Only - Panels (2, 4, 6, & 8)	>3.00
Box Type Construction Only	
All Flaws - Panels (10-11)	>3.00

Figure 6-50: $POD_{(90/95)}$ Values for Inspector EE Deploying Phased Array UT Using the Omniscan and a Manual Linear Encoder – Results for All Specimens, Spar Cap and Shear Web Only, and Box Spar Only; Broken Down by Specific Features in Each Specimen Type

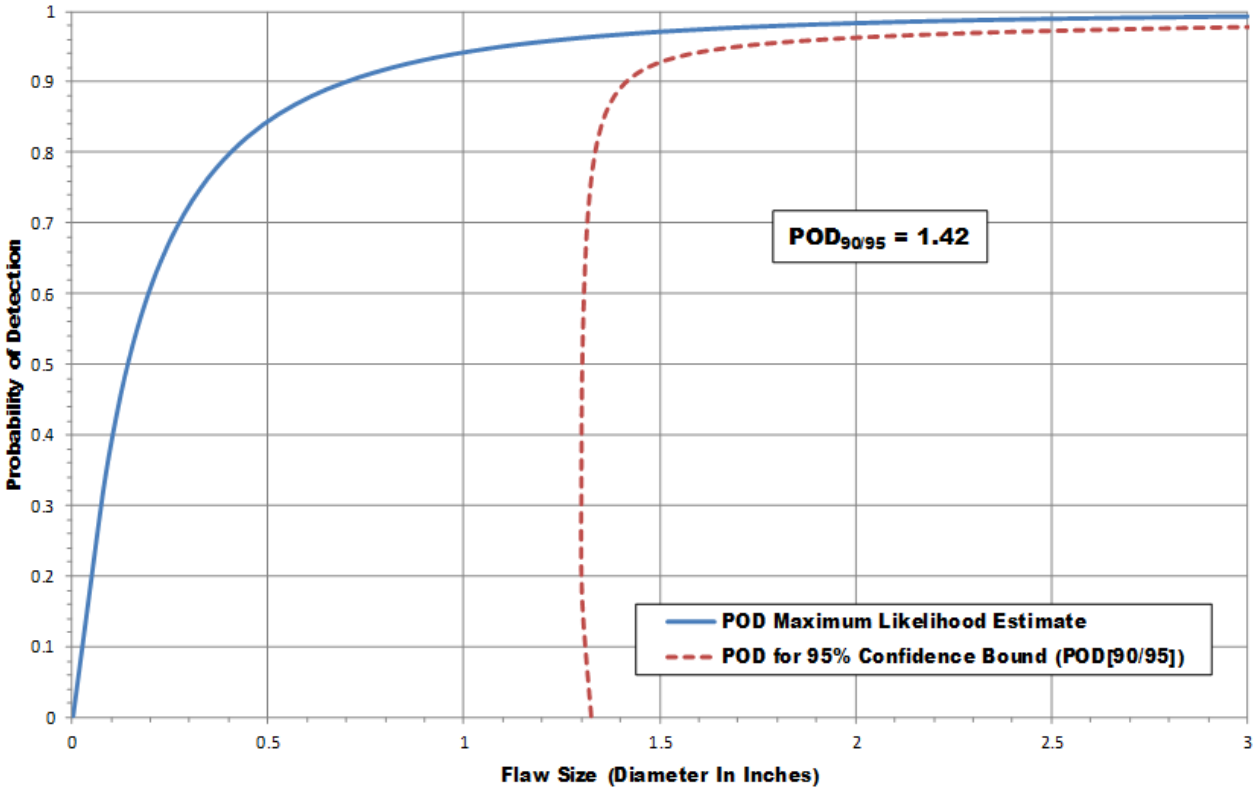

Individual Inspector POD Results Table - Wind Blade Flaw Detection Experiment Advanced NDI Methods - Inspector FF - Scanning PE-UT (500 KHz, P-Scan)	
Condition	$POD_{90/95}$ (Dia. In Inches)
All Spar Cap & Shear Web and Box Type Construction	
All Flaws - Panels (1-11)	1.42
All Constant Thickness Flaws Only - Panels (1-11)	<0.75
All Complex Geometry Flaws Only - Panels (2, 4, 6, 8, 10 &11)	1.71
All Bond Line Flaws Only - Panels (2, 4, 6, 8, 10 &11)	1.66
All Spar Cap & Shear Web Type Construction Only	
All Flaws - Panels (1-9)	1.29
All Laminate Flaws Only - Panels (1-9)	<0.75
All Bond Line Flaws Only - Panels (2, 4, 6, & 8)	2.17
Box Type Construction Only	
All Flaws - Panels (10-11)	1.67

Figure 6-51: $POD_{(90/95)}$ Values for Inspector FF Deploying Pulse Echo UT Using the Force Technology and Tractor Encoder System – Results for All Specimens, Spar Cap and Shear Web Only, and Box Spar Only; Broken Down by Specific Features in Each Specimen Type

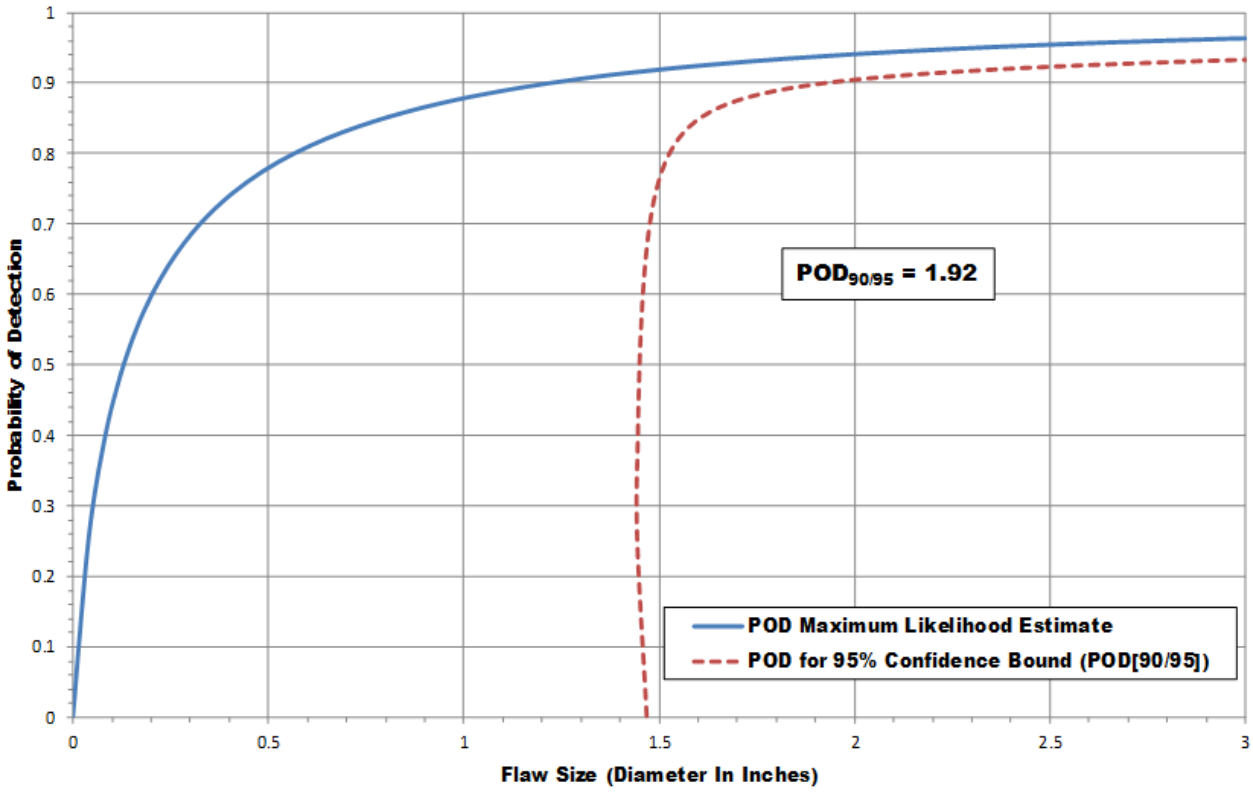

Individual Inspector POD Results Table - Wind Blade Flaw Detection Experiment Advanced NDI Methods - Inspector GG - Scanning PE-UT (500 KHz, P-Scan)	
Condition	$POD_{90/95}$ (Dia. In Inches)
All Spar Cap & Shear Web and Box Type Construction	
All Flaws - Panels (1-11)	1.92
All Constant Thickness Flaws Only - Panels (1-11)	1.84
All Complex Geometry Flaws Only - Panels (2, 4, 6, 8, 10 &11)	2.43
All Bond Line Flaws Only - Panels (2, 4, 6, 8, 10 &11)	1.47
All Spar Cap & Shear Web Type Construction Only	
All Flaws - Panels (1-9)	1.69
All Laminate Flaws Only - Panels (1-9)	1.89
All Bond Line Flaws Only - Panels (2, 4, 6, & 8)	1.72
Box Type Construction Only	
All Flaws - Panels (10-11)	>3.00

Figure 6-52: $POD_{(90/95)}$ Values for Inspector GG Deploying Pulse Echo UT Using the Force Technology and Tractor Encoder System – Results for All Specimens, Spar Cap and Shear Web Only, and Box Spar Only; Broken Down by Specific Features in Each Specimen Type

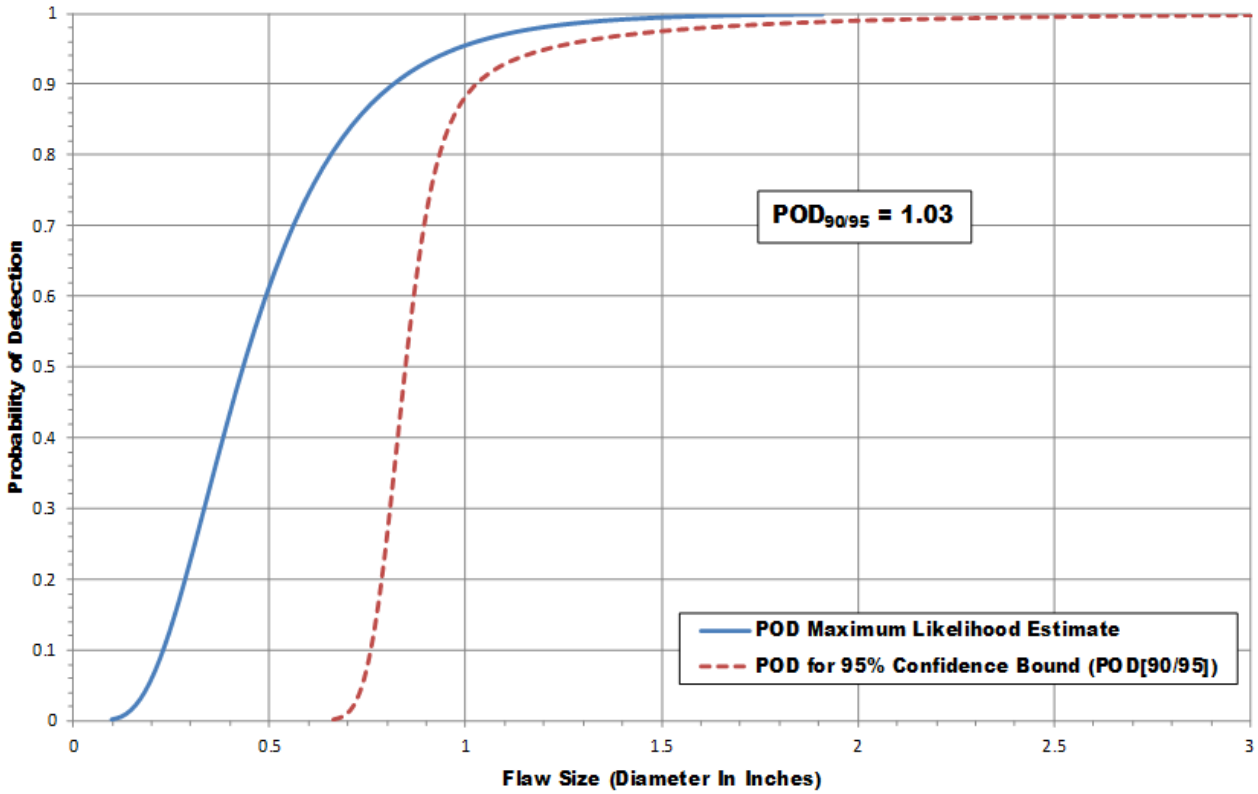

Individual Inspector POD Results Table - Wind Blade Flaw Detection Experiment Advanced NDI Methods - Inspector HH - Scanning PE-UT (500 KHz, P-Scan)	
Condition	**$POD_{90/95}$ (Dia. In Inches)**
All Spar Cap & Shear Web and Box Type Construction	
All Flaws - Panels (1-11)	1.03
All Constant Thickness Flaws Only - Panels (1-11)	<0.75
All Complex Geometry Flaws Only - Panels (2, 4, 6, 8, 10 &11)	1.21
All Bond Line Flaws Only - Panels (2, 4, 6, 8, 10 &11)	1.17
All Spar Cap & Shear Web Type Construction Only	
All Flaws - Panels (1-9)	1.09
All Laminate Flaws Only - Panels (1-9)	<0.75
All Bond Line Flaws Only - Panels (2, 4, 6, & 8)	1.32
Box Type Construction Only	
All Flaws - Panels (10-11)	1.24

Figure 6-53: $POD_{(90/95)}$ Values for Inspector HH Deploying Pulse Echo UT Using the Force Technology and Tractor Encoder System – Results for All Specimens, Spar Cap and Shear Web Only, and Box Spar Only; Broken Down by Specific Features in Each Specimen Type

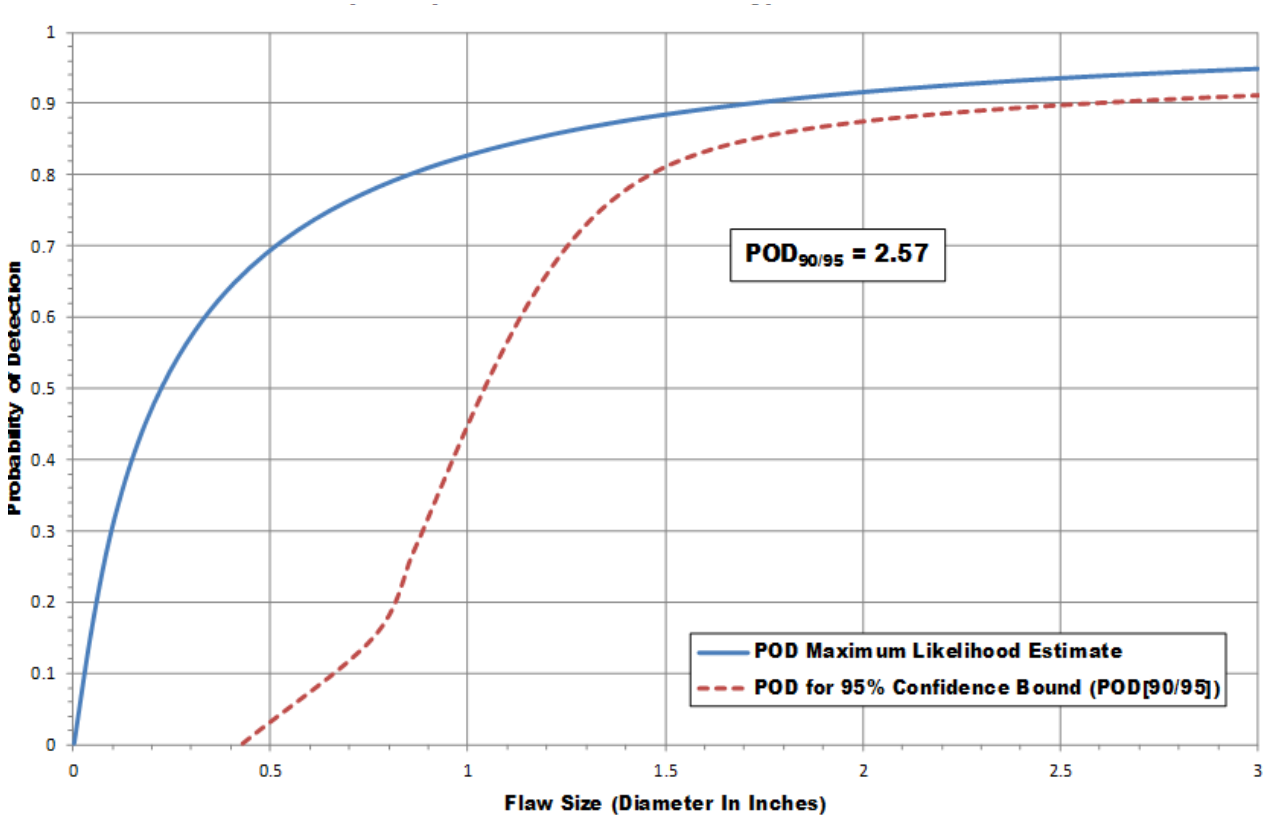

Individual Inspector POD Results Table - Wind Blade Flaw Detection Experiment Advanced NDI Methods - Inspector II - Scanning PE-UT (500 KHz, P-Scan)	
Condition	$POD_{90/95}$ (Dia. In Inches)
All Spar Cap & Shear Web and Box Type Construction	
All Flaws - Panels (1-11)	2.57
All Constant Thickness Flaws Only - Panels (1-11)	1.86
All Complex Geometry Flaws Only - Panels (2, 4, 6, 8, 10 &11)	>3.00
All Bond Line Flaws Only - Panels (2, 4, 6, 8, 10 &11)	2.36
All Spar Cap & Shear Web Type Construction Only	
All Flaws - Panels (1-9)	2.10
All Laminate Flaws Only - Panels (1-9)	1.97
All Bond Line Flaws Only - Panels (2, 4, 6, & 8)	>3.00
Box Type Construction Only	
All Flaws - Panels (10-11)	>3.00

Figure 6-54: $POD_{(90/95)}$ Values for Inspector II Deploying Pulse Echo UT Using the Force Tech and ATS-1 Auto Scanner System – Results for All Specimens, Spar Cap and Shear Web Only, and Box Spar Only; Broken Down by Specific Features in Each Specimen Type

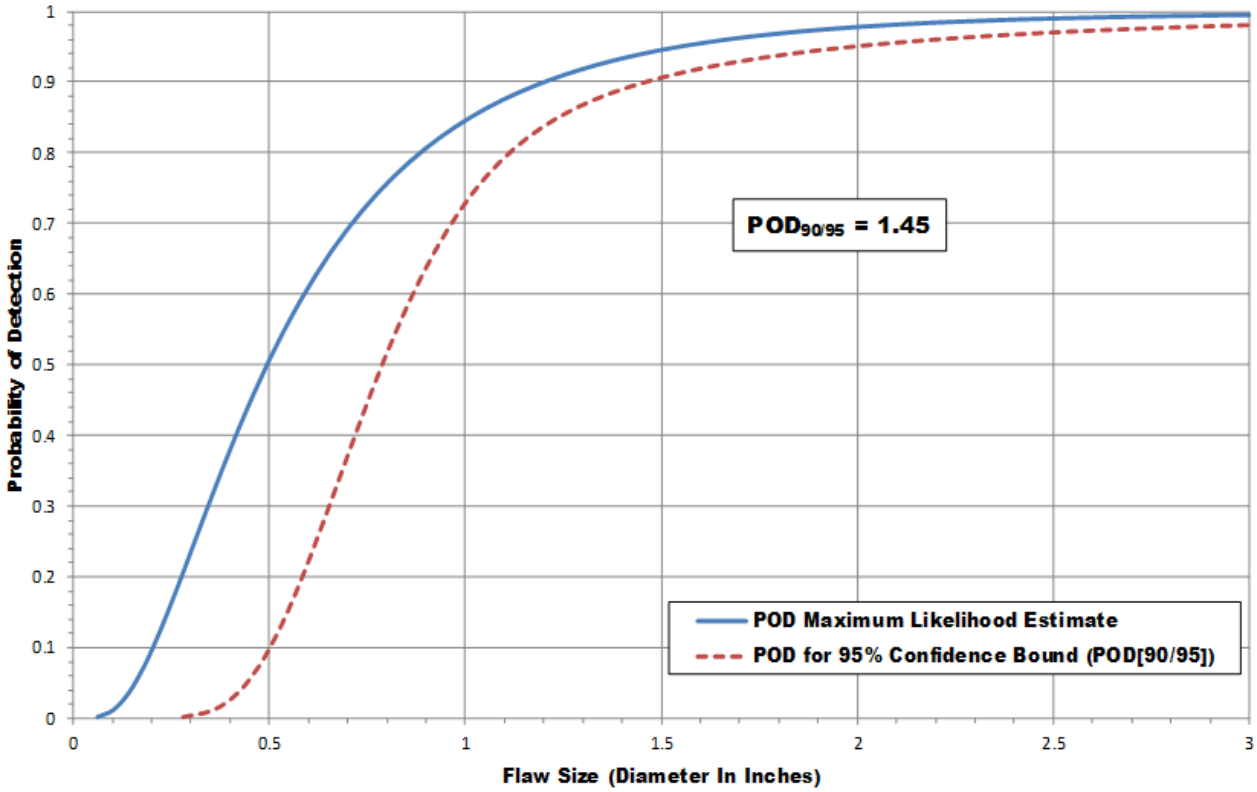

Individual Inspector POD Results Table - Wind Blade Flaw Detection Experiment Advanced NDI Methods - Inspector JJ - Scanning PE-UT (500 KHz, P-Scan)	
Condition	$POD_{90/95}$ (Dia. In Inches)
All Spar Cap & Shear Web and Box Type Construction	
All Flaws - Panels (1-11)	1.45
All Constant Thickness Flaws Only - Panels (1-11)	1.46
All Complex Geometry Flaws Only - Panels (2, 4, 6, 8, 10 &11)	1.78
All Bond Line Flaws Only - Panels (2, 4, 6, 8, 10 &11)	1.98
All Spar Cap & Shear Web Type Construction Only	
All Flaws - Panels (1-9)	1.62
All Laminate Flaws Only - Panels (1-9)	1.48
All Bond Line Flaws Only - Panels (2, 4, 6, & 8)	2.70
Box Type Construction Only	
All Flaws - Panels (10-11)	1.40

Figure 6-55: $POD_{(90/95)}$ Values for Inspector JJ Deploying Pulse Echo UT Using the Force Tech and ATS-1 Auto Scanner System – Results for All Specimens, Spar Cap and Shear Web Only, and Box Spar Only; Broken Down by Specific Features in Each Specimen Type

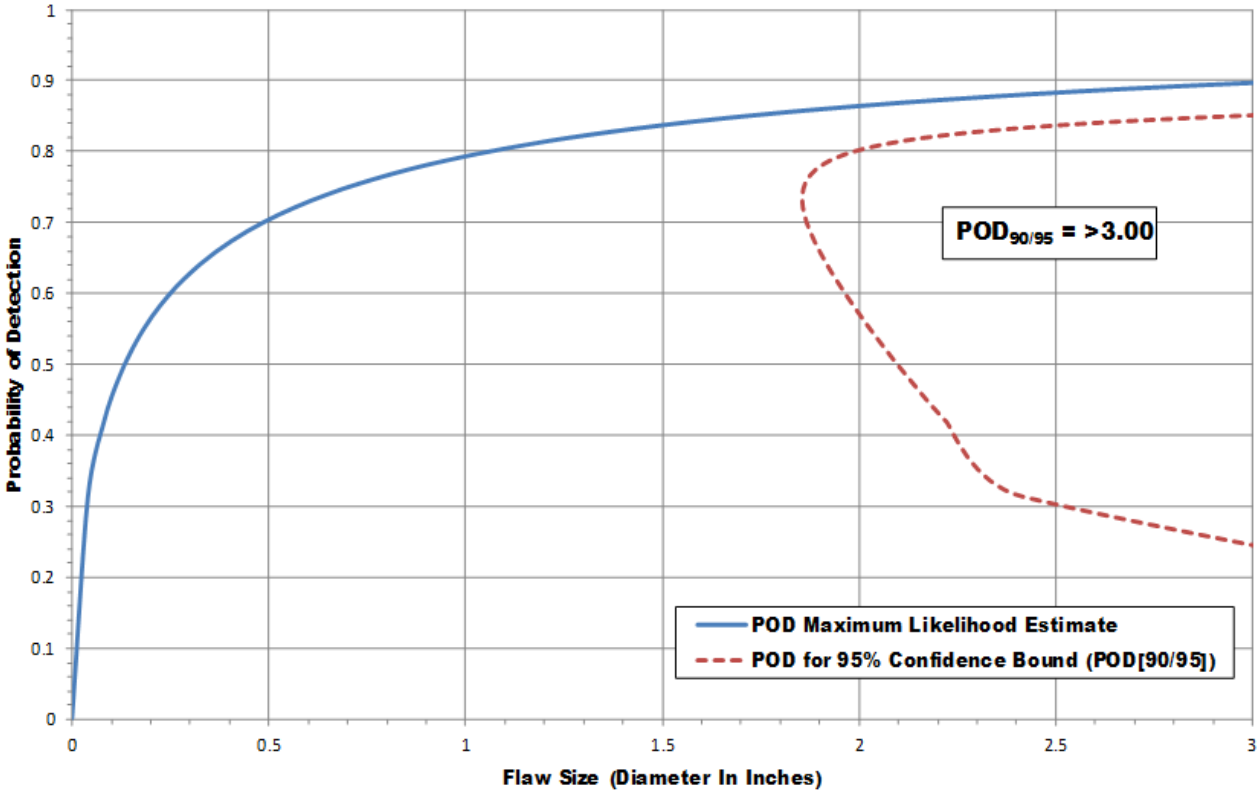

Individual Inspector POD Results Table - Wind Blade Flaw Detection Experiment Advanced NDI Methods - Inspector KK - Scanning PE-UT (500 KHz, P-Scan)	
Condition	**$POD_{90/95}$ (Dia. In Inches)**
All Spar Cap & Shear Web and Box Type Construction	
All Flaws - Panels (1-11)	>3.00
All Constant Thickness Flaws Only - Panels (1-11)	>3.00
All Complex Geometry Flaws Only - Panels (2, 4, 6, 8, 10 &11)	2.39
All Bond Line Flaws Only - Panels (2, 4, 6, 8, 10 &11)	2.25
All Spar Cap & Shear Web Type Construction Only	
All Flaws - Panels (1-9)	>3.00
All Laminate Flaws Only - Panels (1-9)	>3.00
All Bond Line Flaws Only - Panels (2, 4, 6, & 8)	2.28
Box Type Construction Only	
All Flaws - Panels (10-11)	2.64

Figure 6-56: $POD_{(90/95)}$ Values for Inspector KK Deploying Pulse Echo UT Using the Force Tech and ATS-1 Auto Scanner System – Results for All Specimens, Spar Cap and Shear Web Only, and Box Spar Only; Broken Down by Specific Features in Each Specimen Type

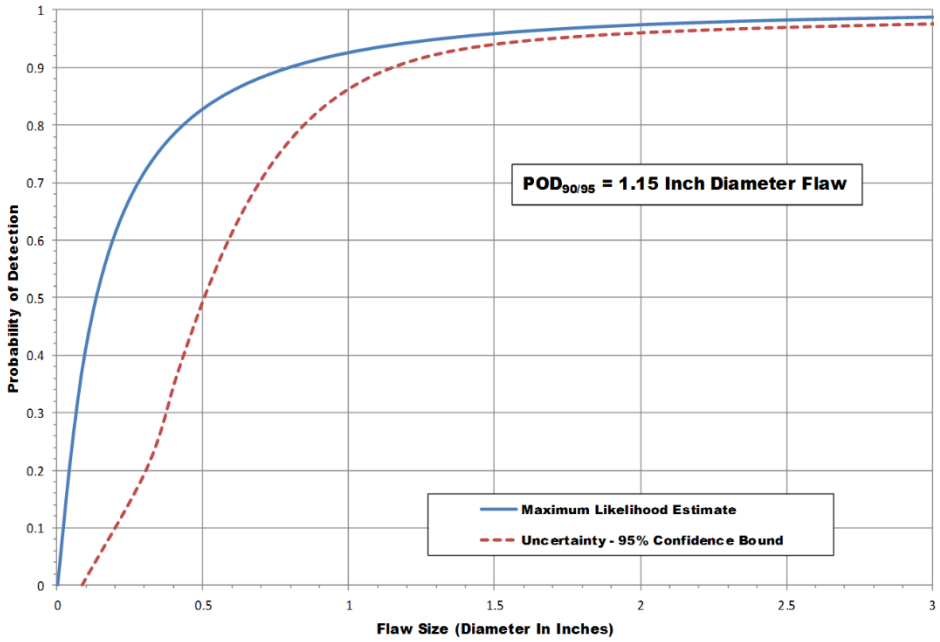

Figure 6-57: Low POD Combined Results from Company X (3 Inspectors) Deploying Pulse Echo UT (500 KHz) Using the Force Technology and Tractor Encoder System – Results for All Specimens

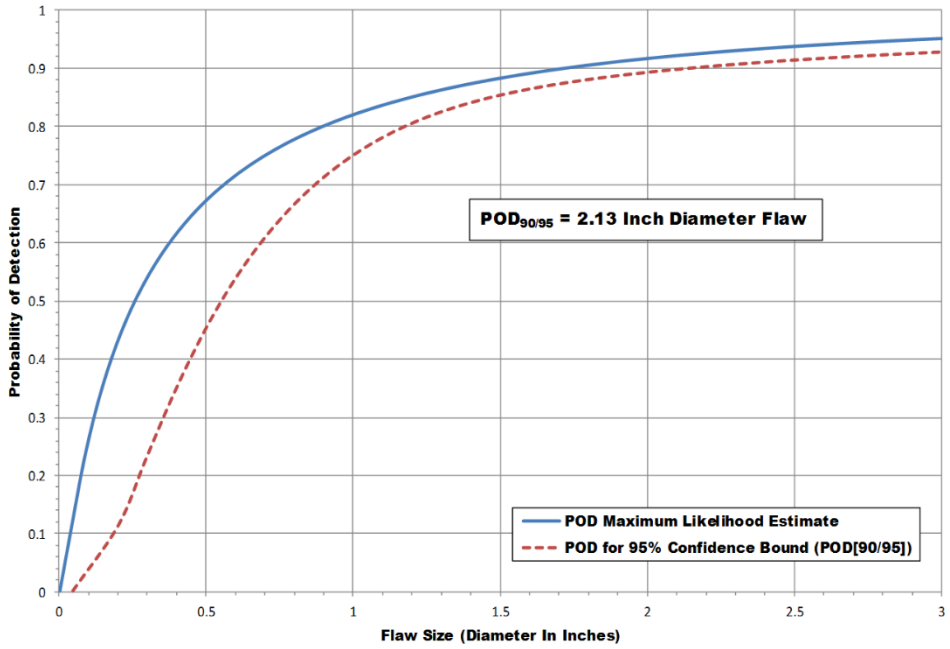

Figure 6-58: High POD Combined Results from Company Y (3 Inspectors) Deploying Pulse Echo UT (500 KHz) Using the Force Technology and ATS-1 Auto Encoder System – Results for All Specimens

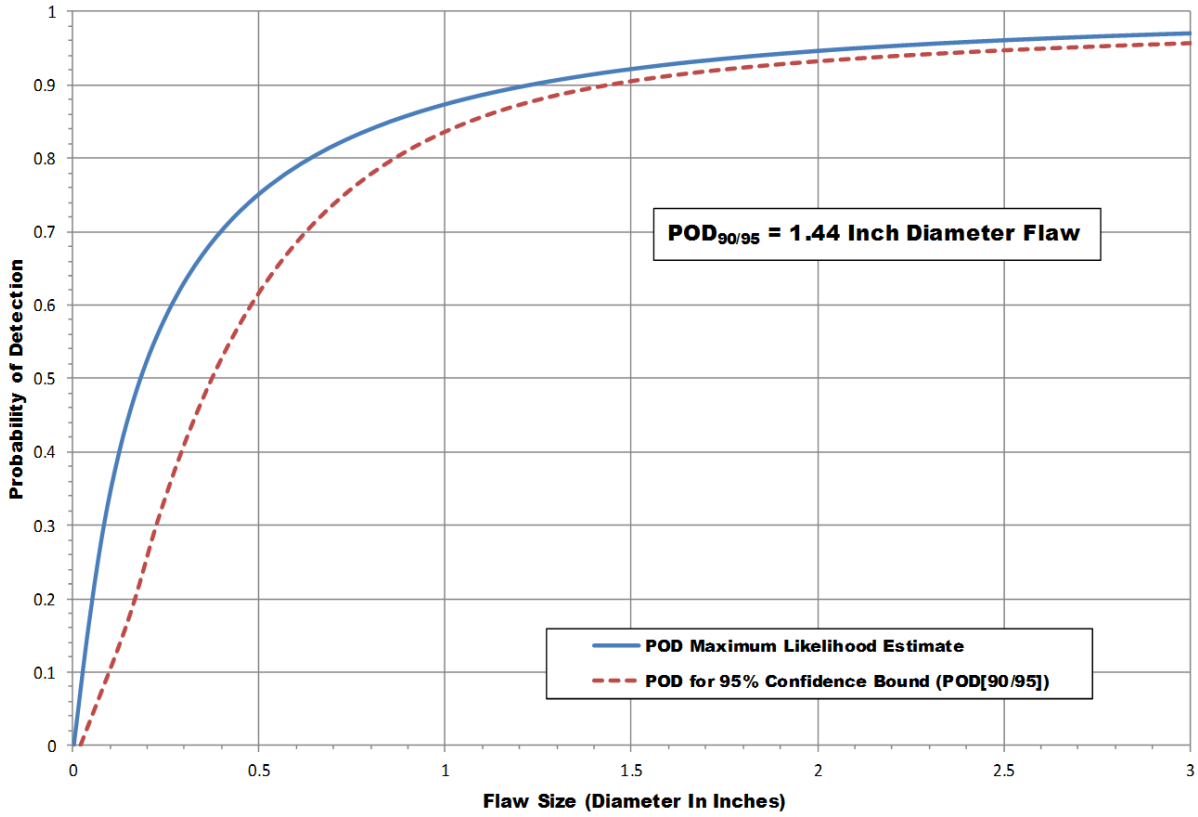

Figure 6-59: POD Results from Combining Companies X & Y (6 Inspectors) Deploying Pulse Echo UT (500 KHz) Using Force Technology Scanner Systems – Results for All Specimens

Table 6-27 through Table 6-29 summarize the inspection results for all inspectors deploying phased array and pulse echo UT methods with C-scan systems, including linear/manual position encoders. The results are divided into an overall summary of the cumulative POD results (all inspectors combined) for the full set of specimens and then broken down for the different blade designs (Spar Cap & Shear Web construction or Box Spar construction) and the different regions within those designs. The wide variety of performance levels is summarized in this table indicating that additional training would be useful for deploying advanced NDI as well. In addition, the relatively higher results for inspectors CC, DD and EE are indicated where these inspectors deployed a manual linear encoding device in a non-uniform coverage manner. Thus, the benefits of the C-scan image were not realized by these inspectors and their POD results suffered as a result.

Table 6-30 relates the POD performance of all inspectors with their level of experience in NDI and their experience with their specific equipment. In this case, unlike the similar table prepared for the conventional NDI methods, there was not a strict correlation between an inspector's experience level on wind blades and the resulting performance of the advanced NDI method.

This indicates that the C-scan methods can be more user friendly, repeatable and readily adopted by a wide range of inspectors. However, the analysis here does indicate that additional, focused wind blade inspection training can improve the performance of all inspectors.

Table 6-31 provides an overall comparison of the results from the conventional, hand-held, single-element PE-UT method with those obtained from the advanced NDI methods deploying phased-array and focused-element PE-UT using a C-scan approach. This summary compares the cumulative POD results (all inspectors combined) for the full set of specimens and then broken down for the different blade designs (Spar Cap & Shear Web construction or Box Spar construction) and the different regions within those designs. For the most part the results from both conventional and advanced NDI are very similar. Damage in the 1.0 to 1.5" diameter should be detected by inspectors deploying C-scan pulse-echo ultrasonic inspections regardless of the blade construction type. It was noted that the advanced NDI methods seemed to struggle with the Box Spar construction type and the POD levels were higher for flaw detection in this blade design. It is believed that this is due to the lack of experience in dealing with this design where the spar cap laminate is beneath the bond line. Thus, inspectors were not correctly setting their UT gates properly for a full interrogation through the blade thickness. It is further anticipated that additional training that addresses NDI of the Box Spar design will produce significant improvements in these POD results. So, as was the case with the conventional NDI evaluations, additional training, formalized procedures and the use of industry-wide NDI standards can produce improvements in these results such that: 1) it offsets other inspection difficulties to produce similar end results, or 2) compounds with current successful practices to improve the repeatability and sensitivity of inspection. This latter results will be especially useful when considering repair needs and producing the ability to install more invasive and effective repairs.

Table 6-32 compares the results from the top three inspectors (outstanding category) for both the conventional and advanced NDI methods with the POD results broken down into different blade design types (specimen types) and specific regions within those designs. It can be seen that this data breakdown – similar to improvements that might be expected from additional NDI training – shows significant lowering in POD levels where most are in the area of 1.0". The largest improvement was seen in the Box Spar construction showing that the advanced NDI methods can perform well with this blade design if the equipment is properly deployed and data properly analyzed. Finally, Table 6-33 makes a similar comparison between the conventional and advanced NDI methods for only the top inspector from each NDI method/family. Once again, very similar results are obtained. Thus, from a pure performance standpoint, both the hand-deployed and scanning-deployed PE-UT can work very well for all wind blade inspections. Then, the deciding features between these two NDI methods may come down to the level of automation required, coverage required, speed of inspections and the post-processing data analysis desired. All of these features are part of the advanced C-scan approach and could be especially useful for in-service blade inspections that could be applied remotely using robot-based deployment.

Individual Inspector POD Results Table All Spar Cap & Shear Web and Box Type Construction All Flaws - All Panels (1-11) - Advanced Methods	
Inspector	**$POD_{90/95}$ (Dia. In Inches)**
Inspector AA	1.38
Inspector BB	1.71
Inspector CC	2.51
Inspector DD	>3.00
Inspector EE	2.97
Inspector FF	1.42
Inspector GG	1.92
Inspector HH	1.03
Inspector II	2.57
Inspector JJ	1.45
Inspector KK	>3.00

Individual Inspector POD Results Table All Spar Cap & Shear Web and Box Type Construction All Constant Thickness Flaws Only - All Panels (1-11) Advanced Methods	
Inspector	**$POD_{90/95}$ (Dia. In Inches)**
Inspector AA	1.37
Inspector BB	<0.75
Inspector CC	>3.00
Inspector DD	2.67
Inspector EE	1.75
Inspector FF	<0.75
Inspector GG	1.84
Inspector HH	<0.75
Inspector II	1.86
Inspector JJ	1.46
Inspector KK	>3.00

Individual Inspector POD Results Table All Spar Cap & Shear Web and Box Type Construction All Complex Geometry Flaws Only Panels (2, 4, 6, 8, 10 &11) Only - Advanced Methods	
Inspector	**$POD_{90/95}$ (Dia. In Inches)**
Inspector AA	1.70
Inspector BB	>3.00
Inspector CC	>3.00
Inspector DD	2.23
Inspector EE	2.49
Inspector FF	1.71
Inspector GG	2.43
Inspector HH	1.21
Inspector II	>3.00
Inspector JJ	1.78
Inspector KK	2.39

Individual Inspector POD Results Table All Spar Cap & Shear Web and Box Type Construction All Bond Line Flaws Only Panels (2, 4, 6, 8, 10 &11) Only - Advanced Methods	
Inspector	**$POD_{90/95}$ (Dia. In Inches)**
Inspector AA	1.17
Inspector BB	1.17
Inspector CC	1.95
Inspector DD	2.59
Inspector EE	2.19
Inspector FF	1.66
Inspector GG	1.47
Inspector HH	1.17
Inspector II	2.36
Inspector JJ	1.98
Inspector KK	2.25

Table 6-27: Summary of POD Results for All Inspectors Deploying Phased Array and Pulse Echo UT with Various C-Scan Systems - All Specimens Broken Down by Constant Thickness, Complex Geometry and Bond Line Regions

Individual Inspector POD Results Table All Spar Cap & Shear Web Type Construction All Flaws - Panels (1-9) Only - Advanced Methods	
Inspector	**$POD_{90/95}$ (Dia. In Inches)**
Inspector AA	1.29
Inspector BB	1.03
Inspector CC	>3.00
Inspector DD	2.63
Inspector EE	1.86
Inspector FF	1.29
Inspector GG	1.69
Inspector HH	1.09
Inspector II	2.10
Inspector JJ	1.62
Inspector KK	>3.00

Individual Inspector POD Results Table All Spar Cap & Shear Web Type Construction All Laminate Flaws Only - Panels (1-9) Only Advanced Methods	
Inspector	**$POD_{90/95}$ (Dia. In Inches)**
Inspector AA	1.43
Inspector BB	<0.75
Inspector CC	>3.00
Inspector DD	2.97
Inspector EE	1.62
Inspector FF	<0.75
Inspector GG	1.89
Inspector HH	<0.75
Inspector II	1.97
Inspector JJ	1.48
Inspector KK	>3.00

Individual Inspector POD Results Table All Spar Cap & Shear Web Type Construction All Bond Line Flaws Only - Panels (2, 4, 6 & 8) Only Advanced Methods	
Inspector	**$POD_{90/95}$ (Dia. In Inches)**
Inspector AA	1.28
Inspector BB	1.28
Inspector CC	2.70
Inspector DD	2.24
Inspector EE	>3.00
Inspector FF	2.17
Inspector GG	1.72
Inspector HH	1.32
Inspector II	>3.00
Inspector JJ	2.70
Inspector KK	2.28

Table 6-28: Summary of POD Results for All Inspectors Deploying Phased Array and Pulse Echo UT with Various C-Scan Systems – Spar Cap and Shear Web Specimens Broken Down by Laminate and Bond Line Regions

Individual Inspector POD Results Table All Box Spar Type Construction All Flaws - Panels (10-11) Only - Advanced Methods	
Inspector	**$POD_{90/95}$ (Dia. In Inches)**
Inspector AA	2.00
Inspector BB	>3.00
Inspector CC	>3.00
Inspector DD	>3.00
Inspector EE	>3.00
Inspector FF	1.67
Inspector GG	>3.00
Inspector HH	1.24
Inspector II	>3.00
Inspector JJ	1.40
Inspector KK	2.64

Table 6-29: Summary of POD Results for All Inspectors Deploying Phased Array and Pulse Echo UT with Various C-Scan Systems – Box Spar Specimens Broken Down by Laminate and Bond Line Regions

Wind Blade Flaw Detection Experiment - Inspector NDT Experience - Advanced Methods							
Inspector	**NDT Certification Level***	**Years of NDT Experience**	**Years of NDT Experience with Composites**	**Years Experience Using Inspection Device**	**Method**	**Overall $POD_{90/95}$ (Dia. In Inches)**	**See Notes**
AA	II	12	10	10	Automated Scanning PE-UT	1.38	
BB	III	10	7	7	Manual Scanning PA-UT	1.71	
CC	II	20	20	8	Manual Linear Encoder PA-UT	2.51	1
DD	II	8	8	8	Manual Linear Encoder PA-UT	>3.00	1
EE	II	7.5	7.5	5	Manual Linear Encoder PA-UT	2.97	1
FF	III	30	27	3.5	Automated Scanning PE-UT	1.42	
GG	II	4.5	4.5	3.5	Automated Scanning PE-UT	1.92	
HH	II	14	14	3.5	Automated Scanning PE-UT	1.03	
I I	III	25	22	5	Automated Scanning PE-UT	2.57	
JJ	II	20	15	10	Automated Scanning PE-UT	1.45	
KK	II	7	7	2	Automated Scanning PE-UT	>3.00	
LL	n/a**	5	1	1	IR	n/a	2
MM	n/a**	15	6	6 Months	Linear Array UT, Wheel	n/a	3
NN	III	9	3	1 Week	Linear Array UT, Wheel	n/a	3
* - Certified through ASNT (SNT-TC-1A), EN 473, ISO 9712 or in-house company level certification program.							
** - N/A, no company or other certifications.							
1 - Used custom shoe & bladder with a water system (very large footprint), could not detect edge flaws due to loss of couplant near panel edges							
2 - Pulsed Thermography performed well on all near surface flaws, lack of thermal penetration, deeper subsurface flaws were impossible to find							
3 - Unfortunate equipment problems, could not complete entire experiment during visit							

Table 6-30: Summary of POD Results Arranged by Inspector Experience Level

Cumulative POD Results Table - Wind Blade Flaw Detection Experiment Conventional Pulse-Echo UT	
All Spar Cap & Shear Web and Box Type Construction	**$POD_{90/95}$ (Dia. In Inches)**
All Flaws - 12 Inspectors - Panels (1-11)	1.33
All Flaws - 10 Inspectors (High and Low Removed) - Panels (1-11)	1.30
Only Constant Thickness Flaws - 12 Inspectors - Panels (1-11)	1.24
Only Complex Geometry Flaws - 12 Inspectors - Panels (2, 4, 6, 8, 10 &11)	1.49
Only Bond Line Flaws - 12 Inspectors - Panels (2, 4, 6, 8, 10 &11)	1.23
Spar Cap & Shear Web Type Construction Only	**$POD_{90/95}$ (Dia. In Inches)**
All Flaws - 12 Inspectors - Panels (1-9)	1.25
All Flaws - 10 Inspectors (High and Low Removed) - Panels (1-9)	1.25
Only Laminate Flaws - 12 Inspectors - Panels (1-9)	1.23
Only Bond Line Flaws - 12 Inspectors - Panels (2, 4, 6, & 8)	1.34
Box Spar Type Construction Only	**$POD_{90/95}$ (Dia. In Inches)**
All Flaws - 12 Inspectors - Panels (10-11)	1.62
Only Skin Flaws - 12 Inspectors - Panels (10-11)	1.40
Only Spar Cap Laminate Flaws Under Bond Line - 12 Inspectors - Panels (10-11)*	2.22
Only Bond Line Flaws - 12 Inspectors - Panels (10-11)	1.06

Cumulative POD Results Table - Wind Blade Flaw Detection Experiment Advanced Scanning Methods Pulse-Echo UT	
All Spar Cap & Shear Web and Box Type Construction	**$POD_{90/95}$ (Dia. In Inches)**
All Flaws - 8 Inspectors - Panels (1-11)	1.33
All Flaws - 6 Inspectors (Two High Removed) - Panels (1-11)	1.12
Only Constant Thickness Flaws - 8 Inspectors - Panels (1-11)	1.09
Only Complex Geometry Flaws - 8 Inspectors - Panels (2, 4, 6, 8, 10 &11)	1.95
Only Bond Line Flaws - 8 Inspectors - Panels (2, 4, 6, 8, 10 &11)	1.31
Spar Cap & Shear Web Type Construction Only	**$POD_{90/95}$ (Dia. In Inches)**
All Flaws - 8 Inspectors - Panels (1-9)	1.22
All Flaws - 6 Inspectors (Two High Removed) - Panels (1-9)	1.06
Only Laminate Flaws - 8 Inspectors - Panels (1-9)	1.19
Only Bond Line Flaws - 8 Inspectors - Panels (2, 4, 6, & 8)	1.62
Box Spar Type Construction Only	**$POD_{90/95}$ (Dia. In Inches)**
All Flaws - 8 Inspectors - Panels (10-11)	2.46
Only Skin Flaws - 8 Inspectors - Panels (10-11)	1.21
Only Spar Cap Laminate Flaws Under Bond Line - 8 Inspectors - Panels (10-11)*	2.06
Only Bond Line Flaws - 8 Inspectors - Panels (10-11)	0.75

Table 6-31: Comparison of Conventional and Advanced Scanning PE-UT Performance for Different Blade Designs and Specific Regions Within those Designs

Cumulative POD Results - Wind Blade Flaw Detection Experiment 3 Best Inspectors - Automated Scanning PE-UT (P-Scan)	
Condition	$POD_{90/95}$ (Dia. In Inches)
All Spar Cap & Shear Web and Box Type Construction	
All Flaws - Panels (1-11)	1.10
All Constant Thickness Flaws Only - Panels (1-11)	1.01
All Complex Geometry Flaws Only - Panels (2, 4, 6, 8, 10 &11)	1.39
All Bond Line Flaws Only - Panels (2, 4, 6, 8, 10 &11)	1.40
All Spar Cap & Shear Web Type Construction Only	
All Flaws - Panels (1-9)	1.15
All Laminate Flaws Only - Panels (1-9)	1.04
All Bond Line Flaws Only - Panels (2, 4, 6, & 8)	1.74
Box Type Construction Only	
All Flaws - Panels (10-11)	1.24

Cumulative POD Results - Wind Blade Flaw Detection Experiment 3 Best Inspectors - Conventional PE-UT	
Condition	$POD_{90/95}$ (Dia. In Inches)
All Spar Cap & Shear Web and Box Type Construction	
All Flaws - Panels (1-11)	1.01
All Constant Thickness Flaws Only - Panels (1-11)	1.01
All Complex Geometry Flaws Only - Panels (2, 4, 6, 8, 10 &11)	1.08
All Bond Line Flaws Only - Panels (2, 4, 6, 8, 10 &11)	1.16
All Spar Cap & Shear Web Type Construction Only	
All Flaws - Panels (1-9)	1.06
All Laminate Flaws Only - Panels (1-9)	0.99
All Bond Line Flaws Only - Panels (2, 4, 6, & 8)	1.29
Box Type Construction Only	
All Flaws - Panels (10-11)	1.00

Table 6-32: Comparison of Upper Echelon Inspectors from Conventional (Hand-Held Single Element PE-UT) and Advanced (Phased Array UT with C-Scan) Inspection Methods

POD Comparison - Wind Blade Flaw Detection Experiment Best Inspector from Conventional and Advanced Methods		
Condition	Conv. PE-UT - $POD_{90/95}$ (Dia. In Inches)	Adv. P-Scan - $POD_{90/95}$ (Dia. In Inches)
All Spar Cap & Shear Web and Box Type Construction		
All Flaws - Panels (1-11)	0.98	1.03
All Constant Thickness Flaws Only - Panels (1-11)	1.14	<0.75
All Complex Geometry Flaws Only - Panels (2, 4, 6, 8, 10 &11)	<0.75	1.21
All Bond Line Flaws Only - Panels (2, 4, 6, 8, 10 &11)	<0.75	1.17
All Spar Cap & Shear Web Type Construction Only		
All Flaws - Panels (1-9)	1.04	1.09
All Laminate Flaws Only - Panels (1-9)	1.17	<0.75
All Bond Line Flaws Only - Panels (2, 4, 6, & 8)	<0.75	1.32
Box Type Construction Only		
All Flaws - Panels (10-11)	<0.75	1.24

Table 6-33: Comparison of Upper Echelon Inspectors from Conventional and Advanced Inspection Methods Broken Down by Blade Design Types and Specific Regions

A comparison between Figure 6-60 and Figure 6-61 reveals an overall inspection performance for the top three inspectors in the advanced (C-Scan Pulse-Echo UT) and conventional (Hand—Deployed Pulse-Echo UT). It can be seen that the top performing inspectors will produce similar results of $POD_{(90/95)} \approx 1$" and similar improvements from the full set of inspectors combined where $POD_{(90/95)} \approx 1.3$". Thus, with additional training and and more frequent practice on realistic specimens containing realistic flaws, it is expected that all inspectors will start to converge to this optimum POD level where wind blade manufacturers and wind farm operators can expect to reliably find 1" diameter flaws and larger. With this information in hand, companies in need of wind blade inspections can use additional metrics to make a decision on which NDI method to deploy. The hand-deployed PE-UT method requires less bulky equipment and is quick to apply in small sections while the automated C-scan PE-UT method can be operated quickly – once it is set-up – and will provide better, 100% area coverage of the inspection region.

A few more examples demonstrating the advantages of using advanced, C-scan PE-UT are highlighted in Figure 6-62 and Figure 6-63. The images in Figure 6-62 show a Pillow Insert flaw that is located at mid-thickness of an 8 ply laminate, however, it is challenging because it is located over the bond line. This flaw has a relatively low back wall signal-to-noise ratio of 3:1 using a 1 MHz probe and 8:1 using a 500 KHz probe. In this case, only 5 out of 12 (42% detection) inspectors detected this flaw using conventional, single-element, hand-deployed PE-UT, however, 11 out of 11 (100% detection) inspectors detected this flaw using advanced, automated C-Scan PE-UT. The images in Figure 6-63 show a Bond Line Void flaw that challenging because it is located at the backside/farside (most difficult side) of the adhesive layer. This flaw has a relatively low back wall signal-to-noise ratio of 6:1 using a 1 MHz probe and 11:1 using a 500 KHz probe. In this case, only 2 out of 12 (17% detection) inspectors detected this flaw using conventional, single-element, hand-deployed PE-UT, however, 8 out of 11 (73% detection) inspectors detected this flaw using advanced, automated C-Scan PE-UT.

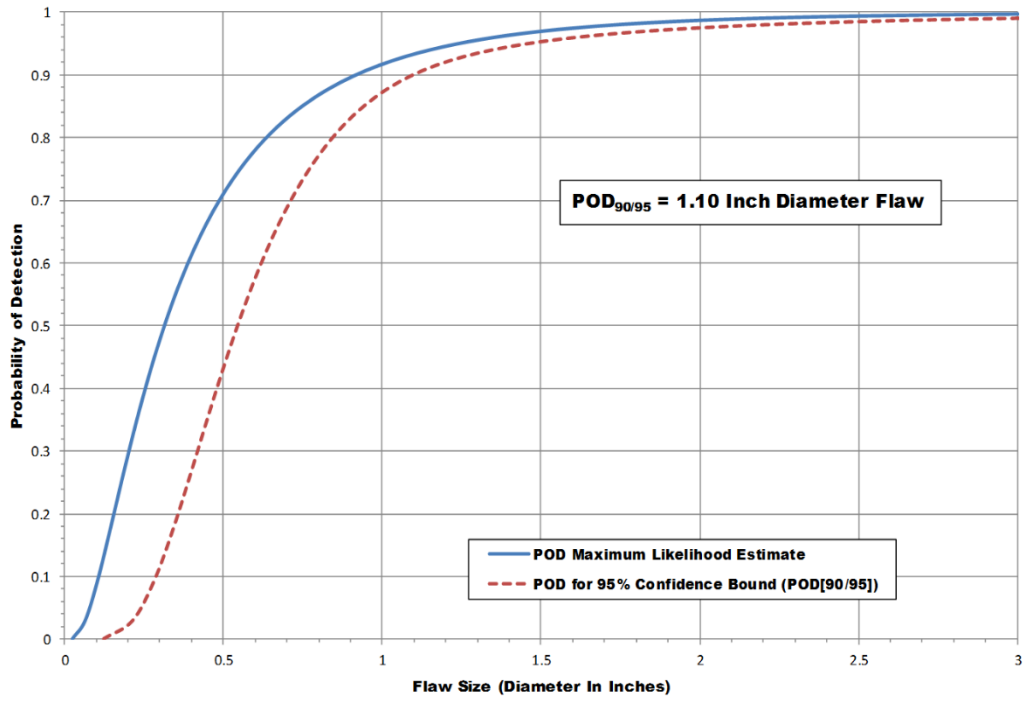

Figure 6-60: Overall POD Value for All WBFDE Specimens Produced by the Top Three Pulse-Echo Ultrasonic C-Scan Inspectors (Advanced NDI – All Inspections Completed at 500 KHz)

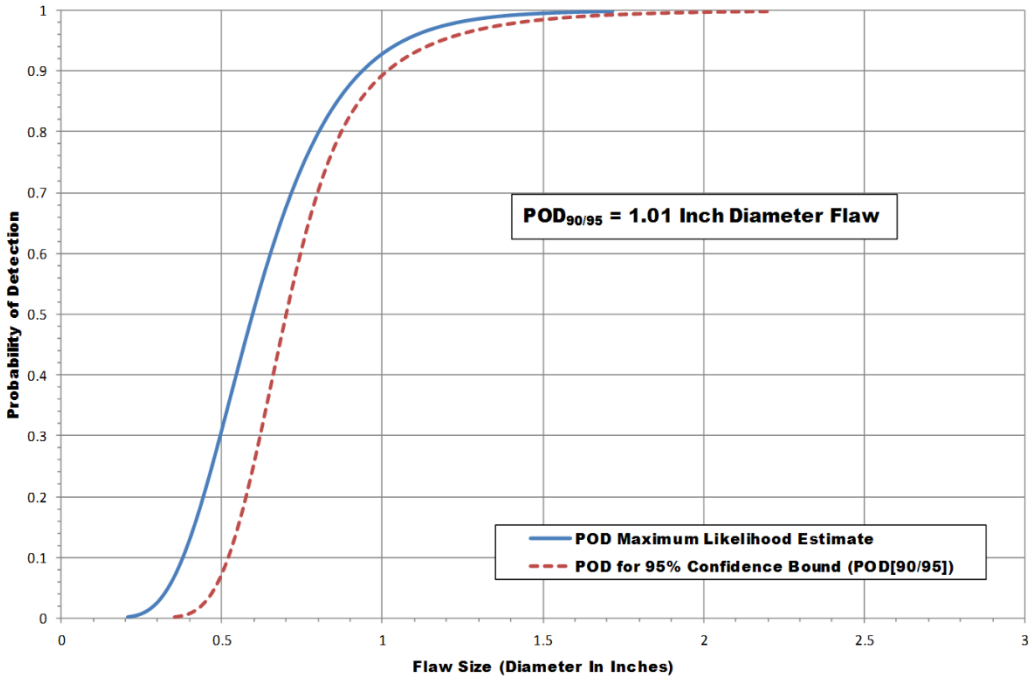

Figure 6-61: Overall POD Value for All WBFDE Specimens Produced by the Top Three Hand-Deployed Pulse-Echo Ultrasonic Inspectors

(Conventional NDI – All Inspections Completed at 500 KHz)

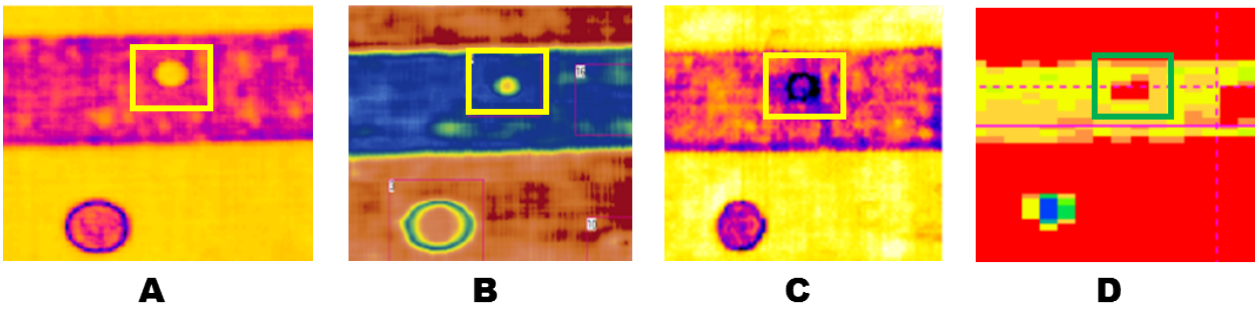

Figure 6-62: Example of Laminate Flaw Located Over the Bond Line which was Found by All Advanced NDI Methods but Very Few Conventional NDI Methods - C-scan Results from: A) Boeing MAUS V (500 KHz Focused Probe), B) OmniScan (1 MHz Phased Array), C) Boeing MAUS V (500 KHz Contact Probe), D) P-Scan (500 KHz Contact Probe)

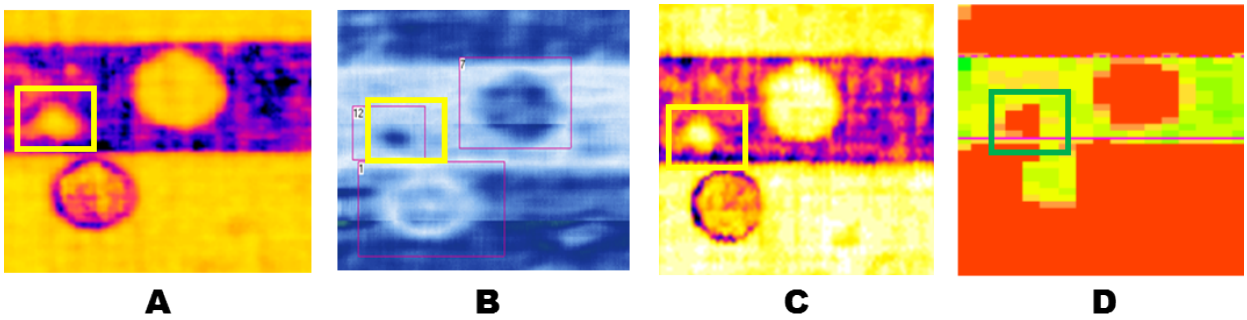

Figure 6-63: Example of Bond Line Flaw Located at the Challenging Back-Side of the Bond Line which was Found by Most Advanced NDI Methods but Very Few Conventional NDI Methods - C-scan Results from: A) Boeing MAUS V (500 KHz Focused Probe), B) OmniScan (1 MHz Phased Array), C) Boeing MAUS V (500 KHz Contact Probe), D) P-Scan (500 KHz Contact Probe)

For the advanced NDI data acquired thus far, Figure 6-64 shows that the POD level was improved by almost 20% from 1.334" to 1.105" diameter flaws through the use of advanced NDI methods.

Figure 6-64: Comparison of POD Results from Deployment of Conventional and Advanced NDI Methods

6.2.2 WBFDE Improvements Stemming from Additional Analysis and Proper Equipment Deployment - Value of NDI Training and Exposure to Wind Blade Inspections

Another observation, stemming from conducting the WBFDE experiment at wind blade factories using scanning UT methods, is that all operators do not fully utilize all capabilities of their equipment, nor do all of them use the optimum gates settings and data analysis during some of the inspections. Specifically, the UT scanning systems will allow operators to set several gates in order to detect and assess anomalies in different depths of the assembly. It was noted that sometimes the inspectors only set a single gate which emphasizes flaw detection at one particular depth. As a result, some of the flaws in the POD test specimens go undetected even though the signal acquired is able to identify the flaws. Figure 6-68 provides one such example where a C-scan image (left side of Figure 6-68) does not initially detect a certain flaw. This is due to a lack of data analysis through entire thickness of blade (full spectrum of gate settings). When the inspector is asked to revisit this same data and asked to look at a deeper region (i.e. additional gate setting), he is able to clearly image the flaw to produce a detection. In some instances, flaws as large as 2" were missed by inspectors who did not properly analyze their signals.

Observations such as the one described above, along with additional, focused analysis of the WBFDE results from the advanced NDI methods, allowed us to quantify the potential for inspection improvements stemming from additional and more focused training for inspectors as well as the benefit to be derived from additional exposure to wind blade inspections and additional practice on realistic specimens containing realistic flaws. The value of adding an improved training regimen and including additional inspector exposure to NDI Feedback Specimens can be determined by conducting specific analysis on the POD results presented above. For example, Figure 6-65 shows a set of POD results for the overall WBFDE (all Spar Cap and Shear Web and box Spar specimens) for one group of inspectors that produced a high POD level (Company Y). Then, improvements on overall performance are show as additional, high performing inspectors are added to the mix (Company X and Y combined) and when two of the poorer performing inspectors are removed. In the latter case, it is assumed that the additional training and inspection exposure produce improvements to shift these inspector's results to better

(lower) POD levels. Overall, these results show an 84% improvement in performance with a lower POD level of 1.16" diameter flaw. Similarly, Table 6-34 and Table 6-35 show the improvements possible if the largest one or two flaws missed by each inspector are changed to a hit (detection). Individually, the inspector's POD values improved by 8 to 15%. This data analysis shows the potential value of improved training where every inspector performs a little better and more repeatably. It also shows how a single, large flaw miss can drastically change an inspector's POD.

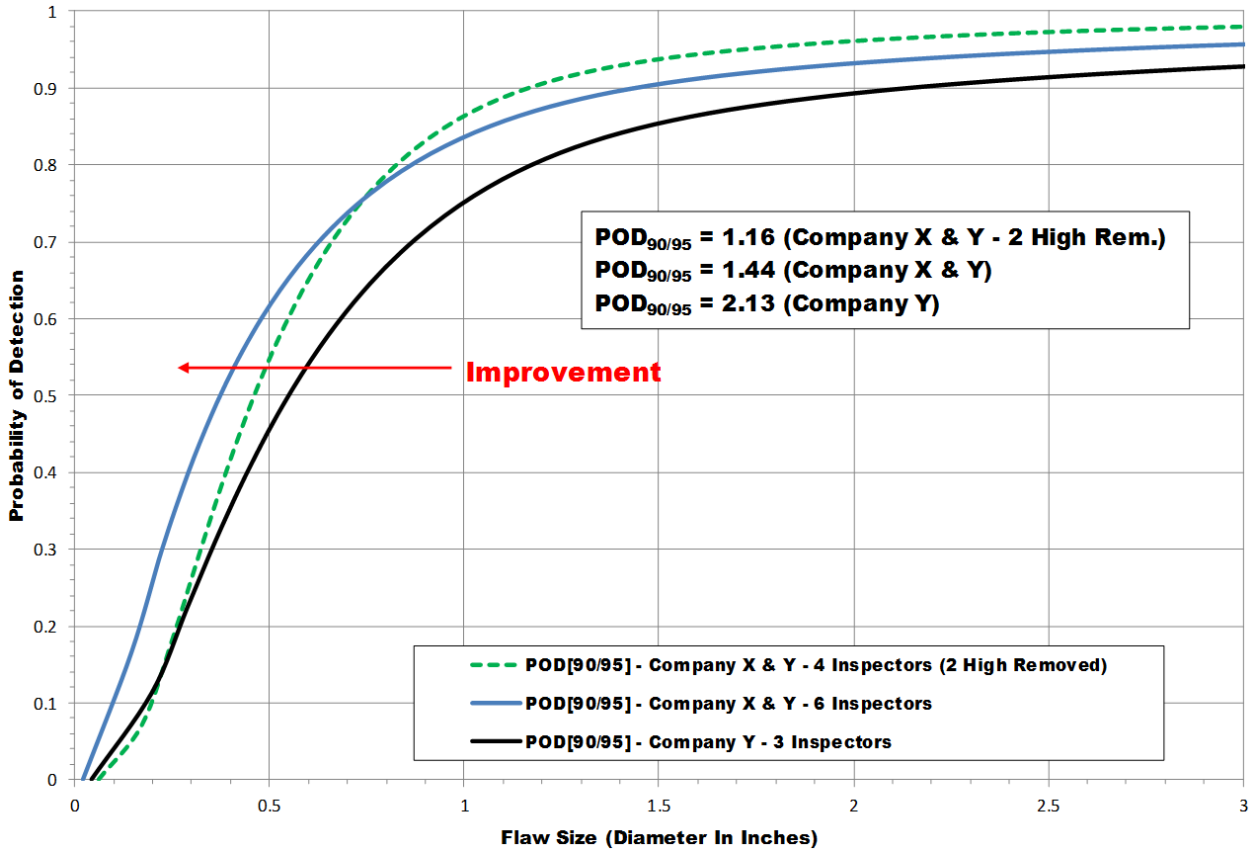

Figure 6-65: Comparison of Performance Improvements Resulting from Simulation of Inspectors Optimizing Data Acquisition and Analysis

The next set of figures describe inspection improvements that are possible if operators are better trained to fully utilize all capabilities of their equipment. This includes the use of optimum gate settings and data analysis during their inspections. First, Figure 6-66 shows attempts by the C-scan system to image two delaminations (F1 and F2) in the spar cap laminate beneath the bond line in the Box Type Construction. This is a case only 5 out of 11 (45% detection) of the advanced methods detected the F1 flaw and only 1 out of 11 (9% detection) of the advanced methods detected the F2 flaw. These flaws have a minimum back wall signal to noise ratio of 3:1. It was observed that the inspectors – who had minimal exposure to the Box Spar construction - did not properly set their gates for the laminate-beneath-the bond line construction.

As a result, the C-scan images failed to properly image these flaws and, in general, the advanced NDI performed poorly on the Box Spar specimens (reference Table 6-29). Second, Figure 6-67 reveals improvements that are possible when inspectors are asked to revisit their same data with a focus on a specific region (i.e. additional gate setting). In each of the examples provided, the inspector is able to clearly image the flaw to produce a detection. In some instances, flaws as large as 2" were missed by inspectors who did not properly analyze their signals. In all instances the inspector referred to these misses as operator mistake. A mistake that could have been eliminated with an improved training regimen. In the case of the top example in Figure 6-67, the missed bond line flaw was in a Spar Cap with Shear Web specimen. This particular inspector detected 95 of 97 flaws (98% detection, 100% detection in laminates). With a slight improvement in analysis, as shown here, this inspector could have detected 100% of the flaws.

Individual Inspector POD Results Table - All Spar Cap & Shear Web and Box Type Construction Automated Scanning PE-UT (P-Scan) - 6 Inspectors - All Flaws - All Panels (1-11) (Largest Miss Changed to a Detection - Each Inspector)				
Inspector	**$POD_{90/95}$ (Dia. In Inches)**	**$POD_{90/95}$ (Dia. In Inches) Largest Miss Changed to Detection**	**Size of Missed Flaw Changed to Detection (Inches)**	**Perent Change in $POD_{90/95}$**
Inspector FF	1.42	1.14	2.00	19.72%
Inspector GG	1.92	1.66	2.50	13.54%
Inspector HH	1.03	0.97	1.00	5.83%
Inspector II	2.57	2.09	3.00	18.68%
Inspector JJ	1.45	1.37	1.50	5.52%
Inspector KK	>3.00	>3.00	3.00	0.00%
Overall Cumulative $POD_{90/95}$	**1.44**	**1.34**		6.94%
Range Spread	**191.26%**	**209.28%**		

Table 6-34: POD Improvements Produced when the Largest Flaw Missed by One Set of Inspectors is Changed to a Detection

Individual Inspector POD Results Table - All Spar Cap & Shear Web and Box Type Construction Automated Scanning PE-UT (P-Scan) - 6 Inspectors - All Flaws - All Panels (1-11) (Two Large Misses Changed to a Detection - Each Inspector)				
Inspector	**$POD_{90/95}$ (Dia. In Inches)**	**$POD_{90/95}$ (Dia. In Inches) Two Largest Misses Changed to Detection**	**Size of Missed Flaws Changed to Detection (Inches)**	**Perent Change in $POD_{90/95}$**
Inspector FF	1.42	0.97	1.50	31.69%
Inspector GG	1.92	1.51	2.00	21.35%
Inspector HH	1.03	0.84	1.00	18.45%
Inspector II	2.57	1.84	2.50	28.40%
Inspector JJ	1.45	1.29	1.50	11.03%
Inspector KK	>3.00	>3.00	3.00	0.00%
Overall Cumulative $POD_{90/95}$	**1.44**	**1.25**		13.19%
Range Spread	**191.26%**	**257.14%**		

Table 6-35: POD Improvements Produced when the Two Largest Flaws Missed by One Set of Inspectors are Changed to a Detection

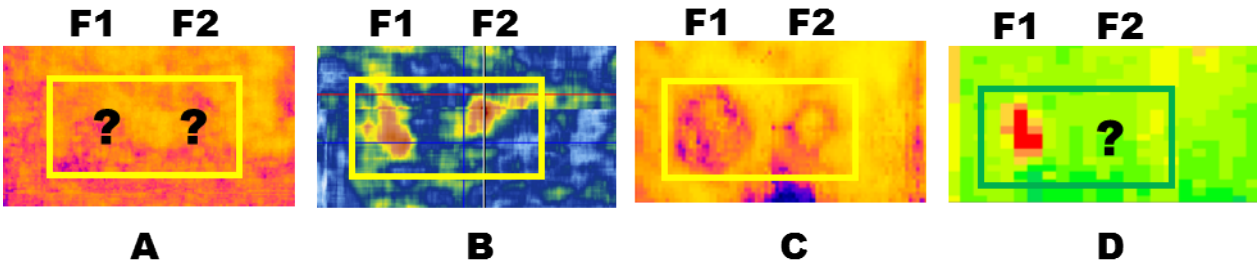

Figure 6-66: Poor Imaging of Laminate Flaw Located Beneath the Bond Line in the Box Spar Construction - C-scan Results from: A) Boeing MAUS V (500 KHz Focused Probe), B) OmniScan (1 MHz Phased Array), C) Boeing MAUS V (500 KHz Contact Probe), D) P-Scan (500 KHz Contact Probe)

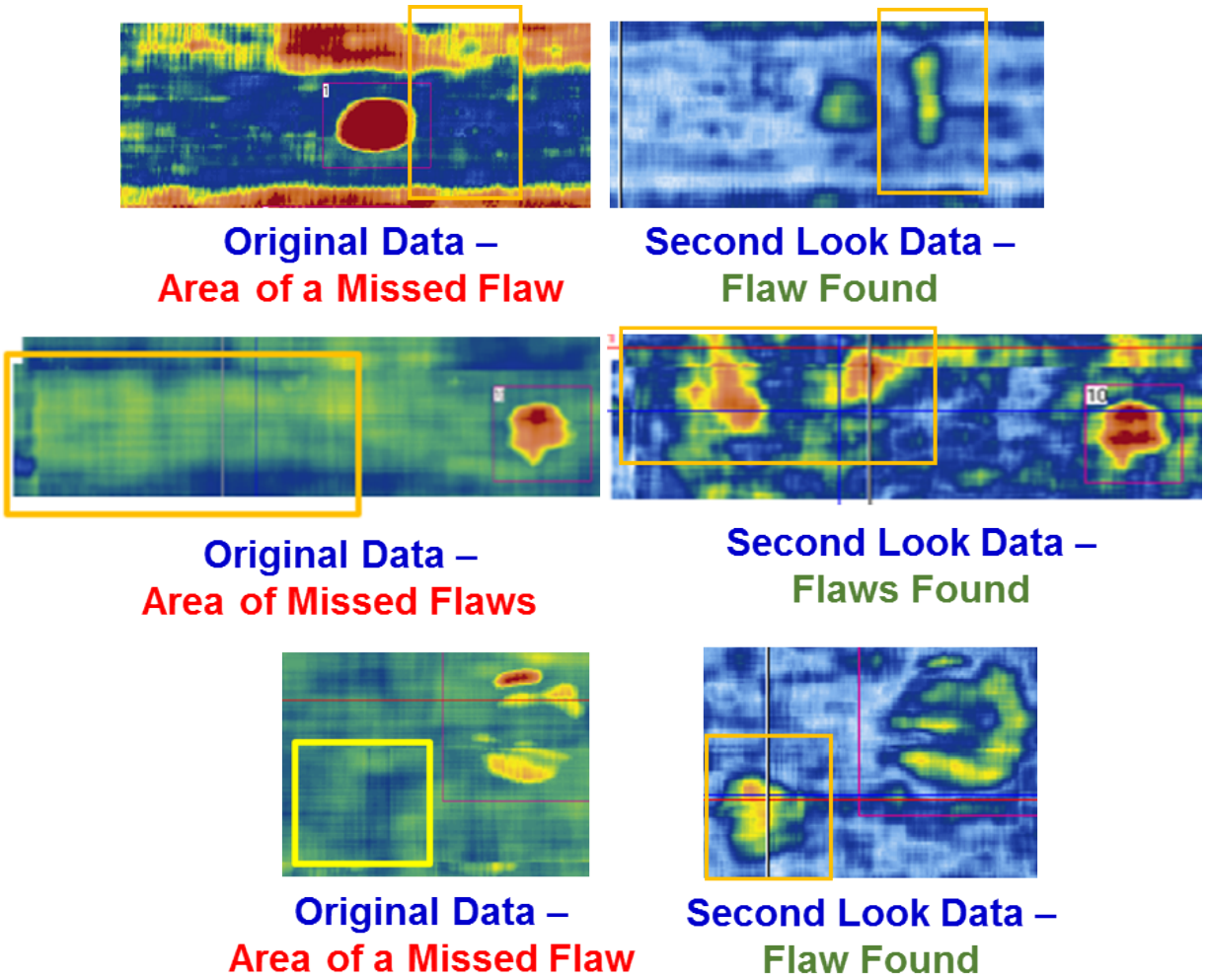

Figure 6-67: Examples of Flaws that were Initially Undetected but were Detected During a Second Analysis of the Same Inspection Data – Bond Line Void (top), Spar Cap Delamination (middle) and Bond Line Porosity (lower)

Additional examples of this phenomenon are provided in Figure 6-69 and Figure 6-70. Figure 6-69 shows before-and-after C-scan images with the eventual detection of a set of subsurface waves/wrinkles that were initially undetected. Results from a similar ultrasonic scanner system can be used to highlight the significant improvements that can be achieved through the use of additional training, both formal classroom setting and through various on-the-job training including apprenticeships. Figure 6-70 shows how non-optimal use of gate settings can allow damage to go undetected. These observations, which ranged from proper data analysis to equipment set-up and deployment, highlight the need for specific, additional training as the wind blade production facilities move into more sophisticated equipment. This is a suggested focus area for the wind NDI program. Overall, the WBFDE pointed out the advantageous use of apprentice programs within the blade production facilities. In such programs, NDI theory, proper equipment set-up and tribal knowledge of the subtle idiosyncrasies of a particular blade can be stressed and passed on by experienced personnel. Similarly, the use of blade service companies, that can provide a centralized repository of NDI expertise, advanced equipment and the benefit of repetitive deployment (experience), is a recommended source for NDI of in-service blades.

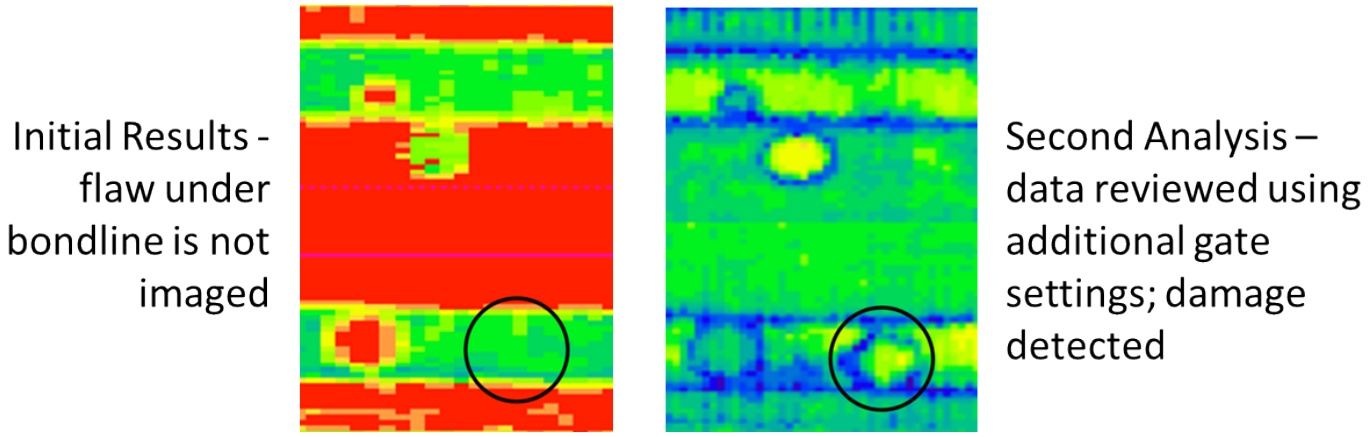

Figure 6-68: Comparisons of C-scans Highlighting the Optimization of Inspection Results and Resulting POD with Proper and More Detailed Analysis

The improvement achievable through the better deployment of scanning UT NDI equipment is highlighted in Figure 6-71. In this example POD analysis, there is a 25% improvement (lowering) of the POD value from 1.42" to 1.07" when comparing two inspectors using the same piece of equipment. One inspector used a better data analysis scheme and was able to detect more damage without increasing his false calls. Table 6-36 and Figure 6-72 highlight POD improvements for inspector BB after he subjected some of his data to a second analysis. Note that this was not a complete revisit of the entire inspection data set, rather a revisit of specific regions. Even with a second look at the data there were still two 2" flaws that were missed, causing the POD values for the Box Spar and for Complex Geometry to improve but still remain relatively high. The overall improvement (all flaws – all construction types) was 24% even with the two large, missed flaws. Similarly, Table 6-37 and Figure 6-73 highlight POD improvements for inspector II after he subjected some of his data to a second analysis. Note that this was not a

complete revisit of the entire inspection data set, rather a revisit of specific regions. Even with a second look at the data, inspector II still missed two 2" flaws causing causing the POD values for four of the categories to improve but still remain relatively high. The overall improvement (all flaws – all construction types) was 92% even with the two large, missed flaws. All three of these examples indicate that significant improvements are possible (eliminate flaw misses) with additional training and use of the associated better data analysis.

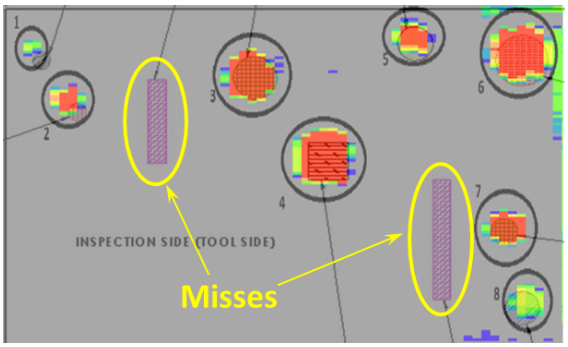

BEFORE - Original P-Scan image with superimposed flaw map showing flaw misses (Wrinkles were missed by inspector)

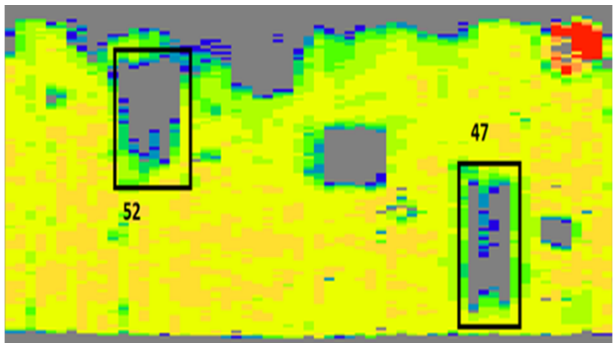

AFTER - Flaws Detected; P-Scan image after inspector revisited the same area with gates set for deeper flaws (Prompted by Sandia)

Figure 6-69: Sample of Data Re-Analysis to Reveal that Flaw Detection Could Have Been Achieved with the Original Inspection Data if the Proper Data Analysis Had Been Used

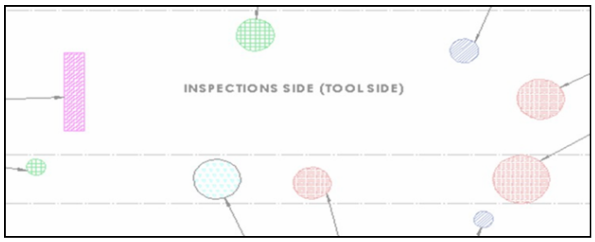

Sector of Specimen Flaw Profile (Answer)

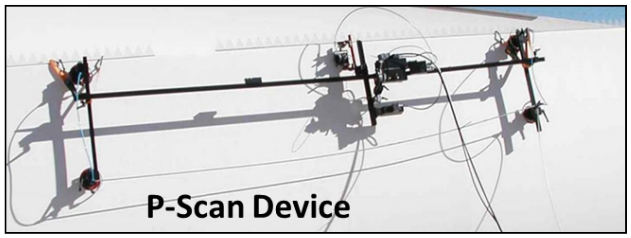

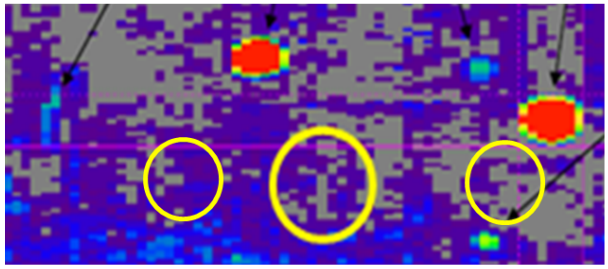

BEFORE - Original P-Scan image (Deeper flaws in spar cap bond line were missed by inspector)

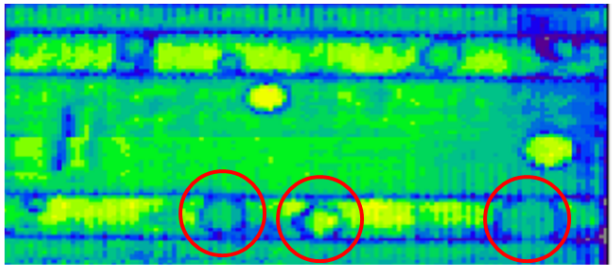

AFTER - Flaws Detected; P-Scan image after inspector revisited the same area (Prompted by Sandia)

Figure 6-70: Sample of Data Re-Analysis to Reveal that Flaw Detection Could Have Been Achieved with the Original Inspection Data if the Proper Data Analysis Had Been Used

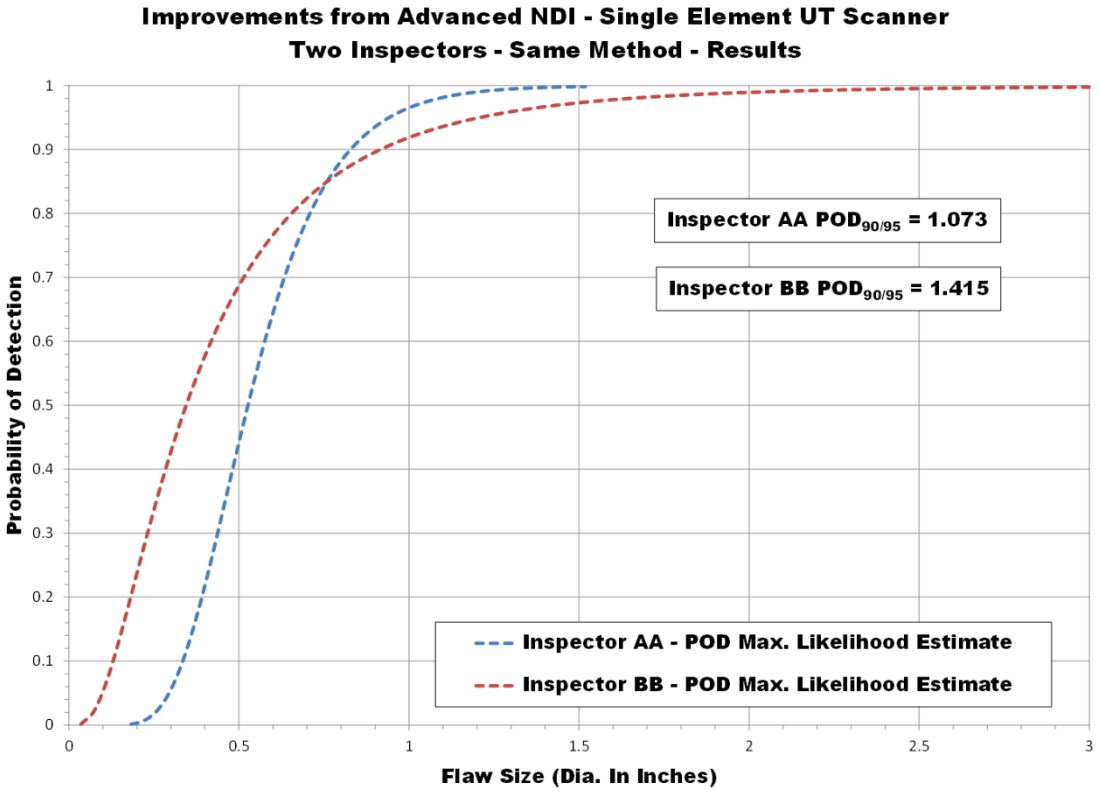

Figure 6-71: Comparison of Inspectors Deploying Similar Advanced NDI Equipment – Single Element UT Scanner System – with One Inspector Using a Better Data Analysis Method

General Inspection Data - Inspector BB			General Inspection Data - Second Look - Inspector BB		
Specimen Type	Overall Flaw Detection Percentage	Flaw Size at $POD_{90/95}$ (Dia. In.)	Specimen Type	Overall Flaw Detection Percentage	Flaw Size at $POD_{90/95}$ (Dia. In.)
Laminate (Spar Cap & Spar Cap with Shear Web)	100%	<0.75***	Laminate (Spar Cap & Spar Cap with Shear Web)	100%	<0.75***
Bond Line (Spar Cap with Shear Web)	93%	1.28	Bond Line (Spar Cap with Shear Web)	100%	<0.75***
All Flaws (Spar Cap & Spar Cap with Shear Web)	98%	1.03	All Flaws (Spar Cap & Spar Cap with Shear Web)	100%	<0.75***
All Flaws (Box Spar)	87%	>3.00	All Flaws (Box Spar)	93%	2.59
Constant Thickness*	100%	<0.75***	Constant Thickness*	100%	<0.75***
Complex Geometry**	89%	>3.00	Complex Geometry**	96%	2.00
All Flaws (Box Spar, Spar Cap & Spar Cap with Shear Web)	94%	1.71	All Flaws (Box Spar, Spar Cap & Spar Cap with Shear Web)	98%	1.38

* Refers to all flaws in spar cap & spar cap with shear web laminates (spars) and all flaws in box spar skins.

** Refers to all flaws in spar cap with shear web construction bond lines and all flaws in box spar construction bond lines and laminates (spars) below the bond line.

*** At 100% detection a POD cannot be calculated. 0.75 is the smallest flaw in the experiment.

Table 6-36: Comparison of POD Performance for Inspector BB Before and After a Second Analysis of Specific Regions of the Data

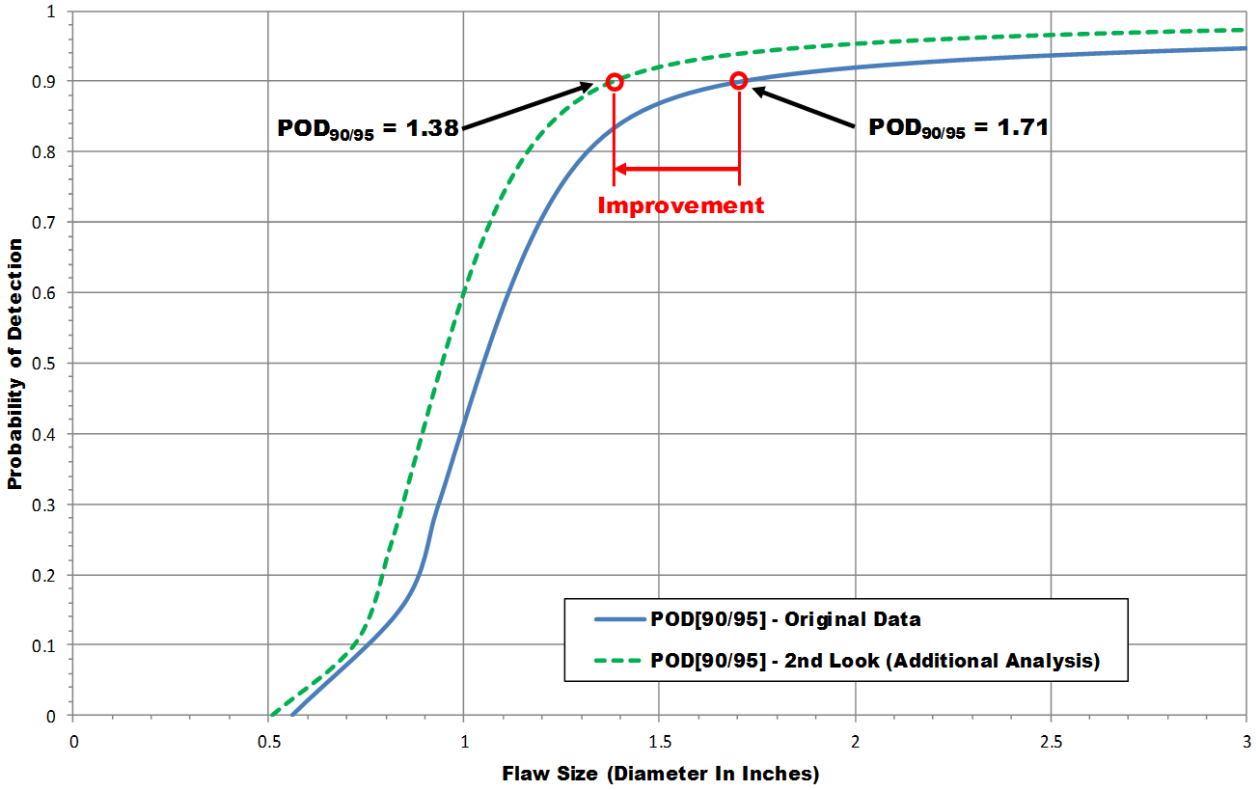

Figure 6-72: POD Improvements Observed in Inspector BB After Only Portions of the Data was Reanalysed and Additional Flaws Detected

General Inspection Data - Inspector II		
Specimen Type	Overall Flaw Detection Percentage	Flaw Size at $POD_{90/95}$ (Dia. In.)
Laminate (Spar Cap & Spar Cap with Shear Web)	91%	1.97
Bond Line (Spar Cap with Shear Web)	77%	>3.00
All Flaws (Spar Cap & Spar Cap with Shear Web)	87%	2.10
All Flaws (Box Spar)	89%	>3.00
Constant Thickness*	90%	1.86
Complex Geometry**	84%	>3.00
All Flaws (Box Spar, Spar Cap & Spar Cap with Shear Web)	87%	2.57

General Inspection Data - Second Look - Inspector II		
Specimen Type	Overall Flaw Detection Percentage	Flaw Size at $POD_{90/95}$ (Dia. In.)
Laminate (Spar Cap & Spar Cap with Shear Web)	94%	1.55
Bond Line (Spar Cap with Shear Web)	93%	0.86
All Flaws (Spar Cap & Spar Cap with Shear Web)	94%	1.32
All Flaws (Box Spar)	96%	1.84
Constant Thickness*	94%	1.49
Complex Geometry**	94%	1.49
All Flaws (Box Spar, Spar Cap & Spar Cap with Shear Web)	94%	1.34

* Refers to all flaws in spar cap & spar cap with shear web laminates (spars) and all flaws in box spar skins.

** Refers to all flaws in spar cap with shear web construction bond lines and all flaws in box spar construction bond lines and laminates (spars) below the bond line.

Table 6-37: Comparison of POD Performance for Inspector II Before and After a Second Analysis of Specific Regions of the Data

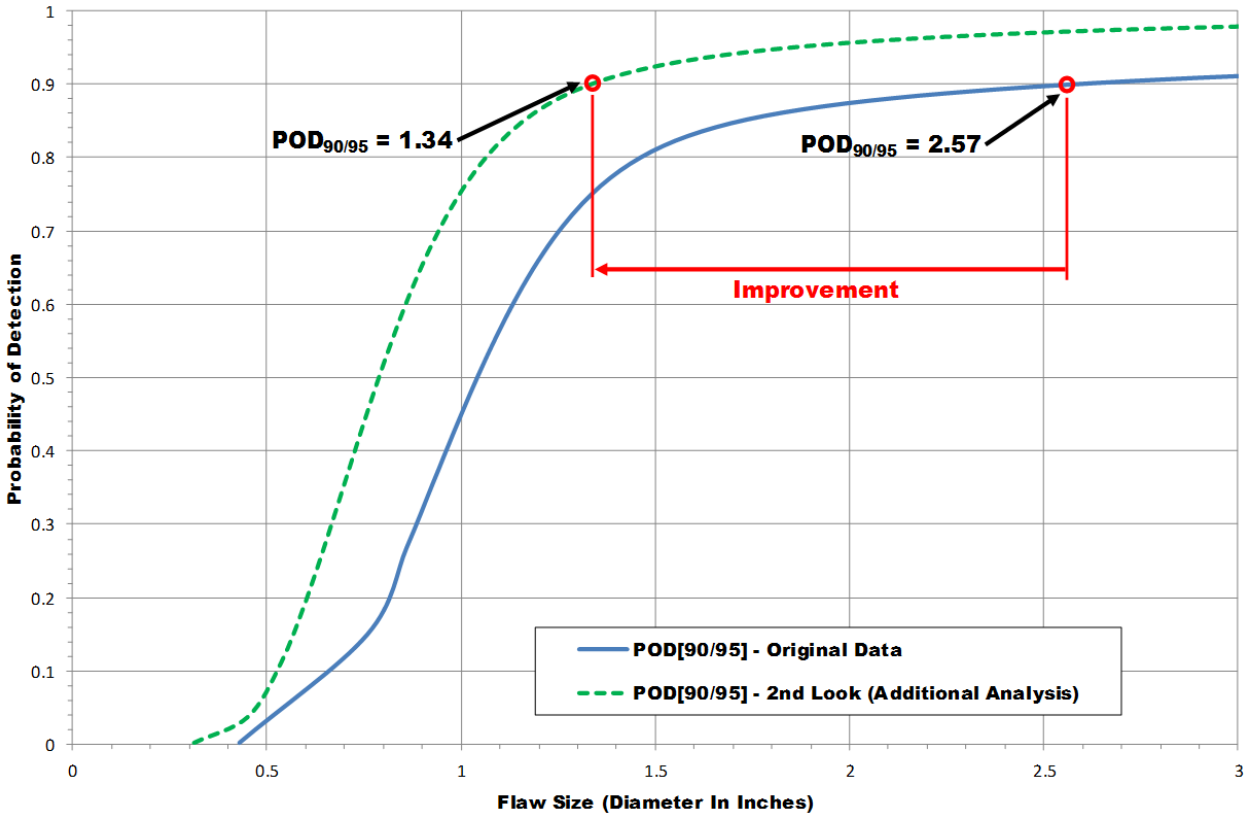

Figure 6-73: POD Improvements Observed in Inspector II After Only Portions of the Data was Reanalysed and Additional Flaws Detected

6.2.3 WBFDE – Preliminary Assessment of GE RotoArray PA-UT Device

The GE RotoArray system was applied to several of the Sandia Labs Wind Test Specimen Library includeing the WBFDE POD panels. Figure 6-74

It should be noted that, at the time of this experiment, the Mentor UT System could only fire 32 elements. This is going to 128 elements GE indicates that around the publication date of this report, the Mentor UT control device will be able to control and properly take data from a 128 element UT array. Also, it was not possible for the GE equipment to complete the POD experiment at this time so only a preliminary evaluation could be completed on the GE PA-UT method deployed with a rolling wheel transducer.

Figure 6-75 and Figure 6-76 show the GE RotoArray device, described in detail in Chapter 6, deployed on a wind NDI test specimen. Results contained here were obtained from the 1 MHz and 500 KHz RotoArray rolling wheel transducers connected to either the GE equipment shown in Figure 6-74 or the OmniScan pulser and data display device described earlier.

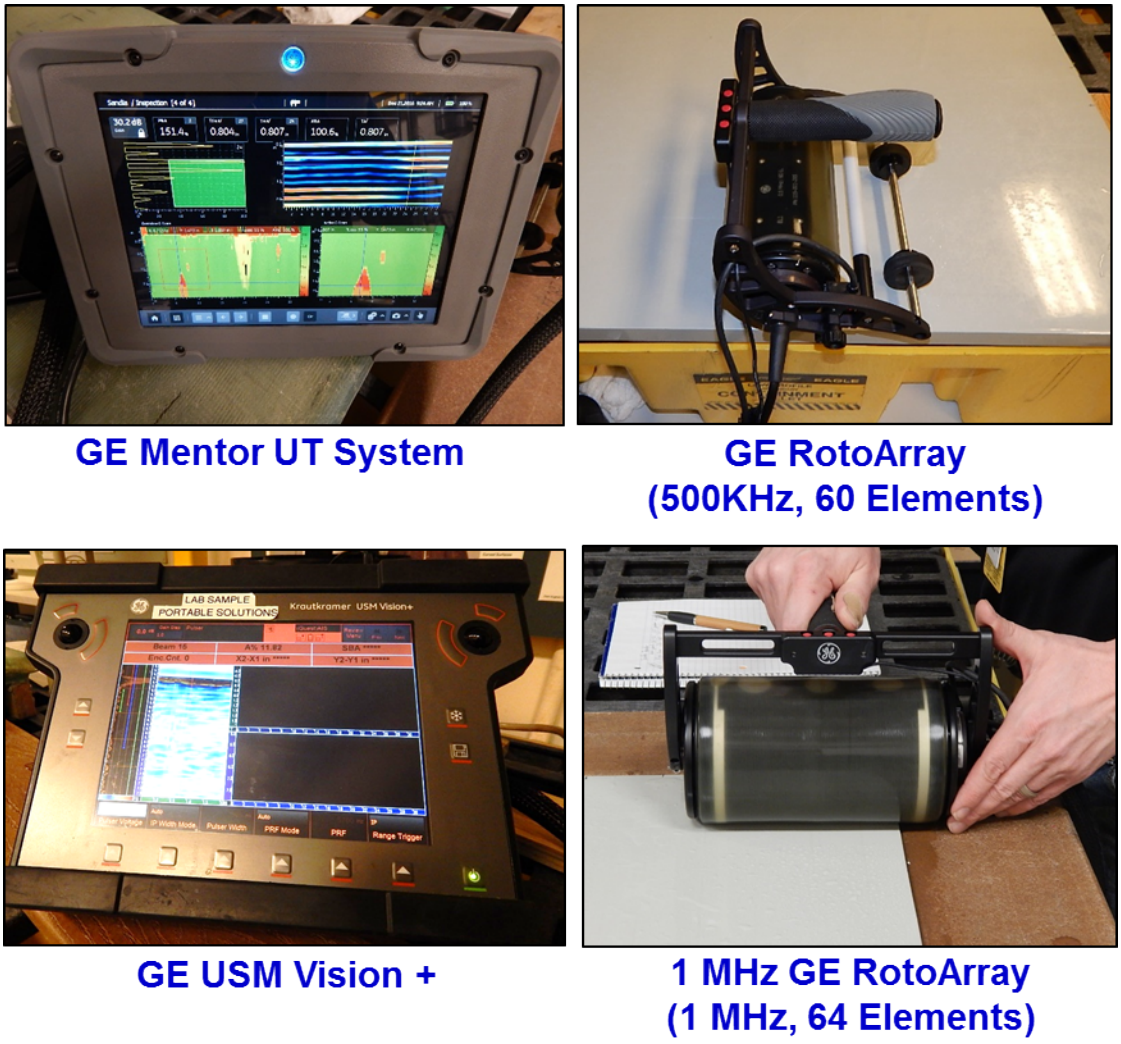

Figure 6-74: GE RotoArray Rolling Wheel Phased Array Transducers and Associated UT Equipment Deployed in Trail Mode for Preliminary Evaluations

Figure 6-77 describes the signal acquisition problem that was presented in detail in Chapter 4. This relates to the presence of signal harmonics in the UT signal time line that overlap and interfere with the observation of the reflected signal of interest. This signal masking can be eliminated through the use of the stand-off distance between the phased array UT probe and the inspection surface. This stand-off distance, which was engineered into the RotoArray wheel, pushes the harmonic signal downstream from the signals of interest as shown in Figure 6-77.

The GE RotoArray was applied to REF-STD-6-202-250-SNL-1 which has a 2.02" thick spar cap and a depth to the back of the spar-to-shear web adhesive layer of 2.5". The C-scan results are shown in Figure 6-78. Flat bottom holes in spar cap laminate were detected at the various depths and the flat bottom holes in the bonded shear web joint were also detected. It appears that all sizes of the flat bottom holes were detected (difficult to see 75% FBH – 1.0" diameter in bonded shear web joint). Pull tab flaws in laminate at 25% depth and at 75% depth were detected. The

pull tabs in the shear web bonded joint at the upper adhesive interface, were detected. Two pull tabs at interface 1 (between adhesive joint and shear web) did not show up clearly on any C-scan. Figure 6-79 shows an additional set of images – both C-scan planform and B-scan sectional/thickness images – of one of the WBFDE test specimens. Both spar cap laminate and bond line flaws are detected in these images.

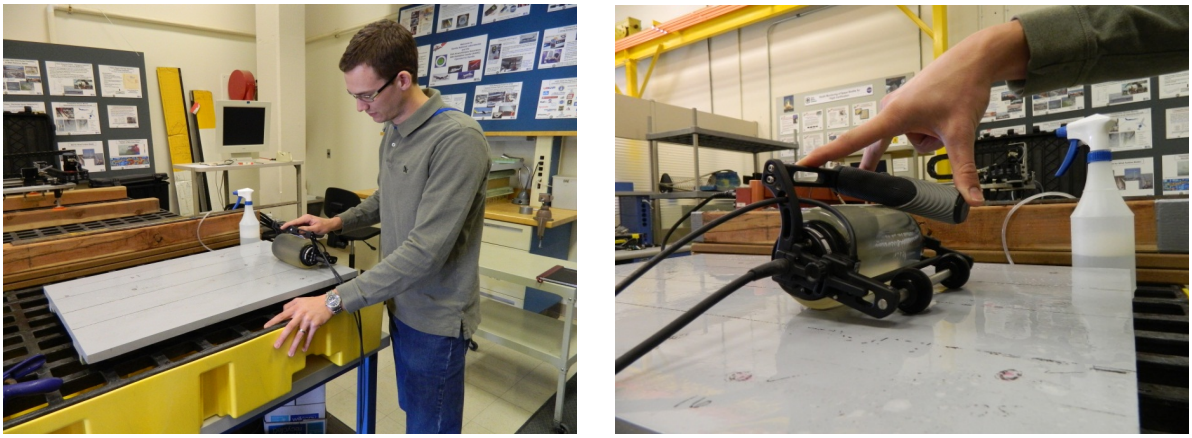

Figure 6-75: GE Phased Array UT RotoArray (1 MHz/64element) Deployed on Wind NDI Specimen with OmniScan Display Unit

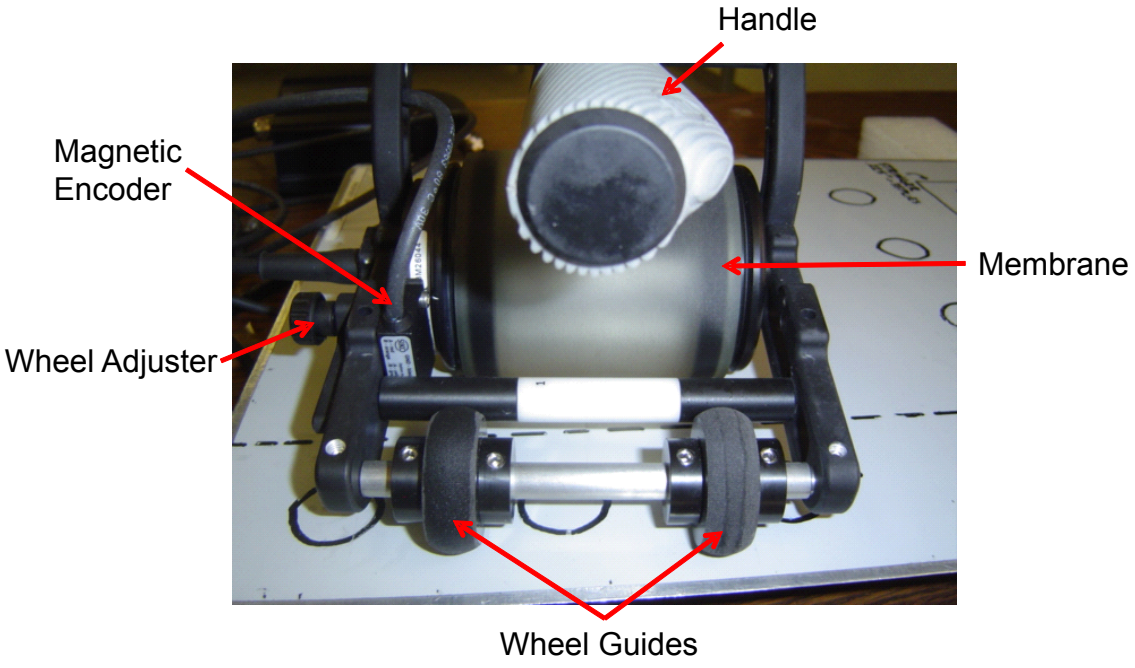

Figure 6-76: GE RotoArray – Phased Array UT Wheel Design (1 MHz, 64 Elements)

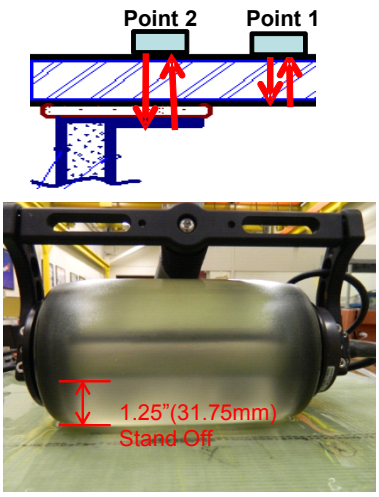

Note: In order to inspect thicker specimens, it is best to use at least 1.57" (40mm) stand off. Othewise the front surface signal multiple interferes with the appearance of the adhesive backwall.

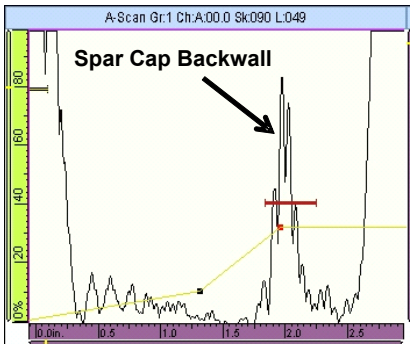

Typical A-Scan
Point 1: Spar Cap

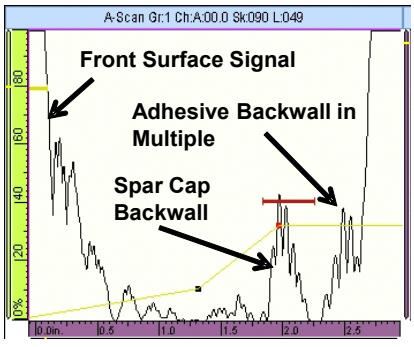

Typical A-Scan
Point 2: Spar Cap & Adhesive

Figure 6-77: A-Scan Signals from 1 MHz/64element GE RotoArray on Spar Cap and Adhesive Joint (Thickness 2.50")

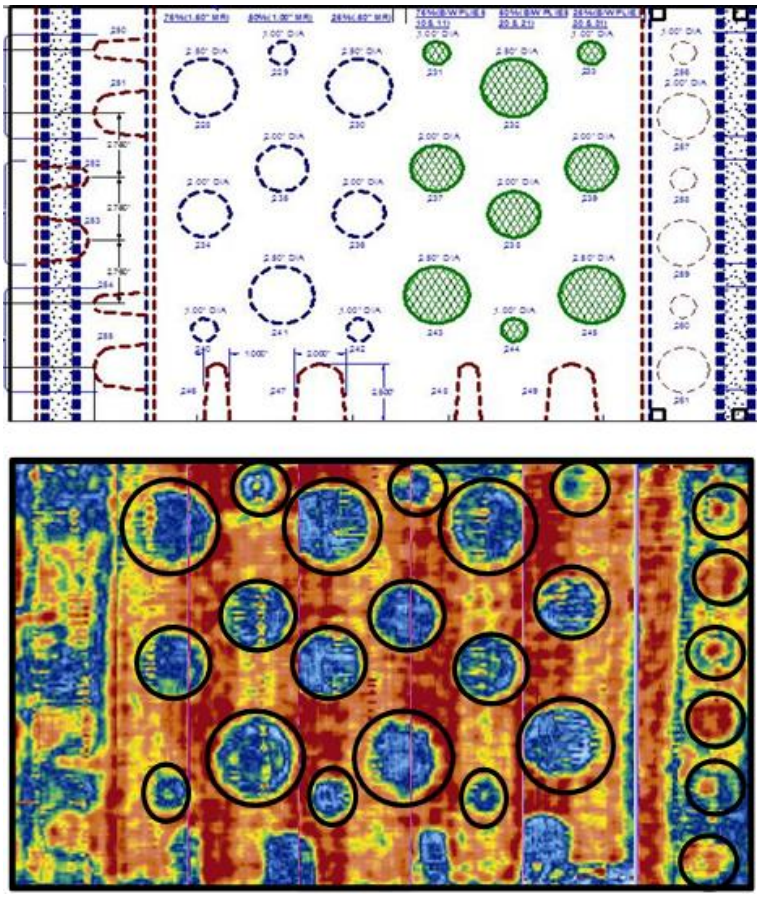

Figure 6-78: PA-UT C-Scan of REF-STD-6-202-250-SNL-1 Produced by the RotoArray 1 MHz Probe Connected to OmniScan

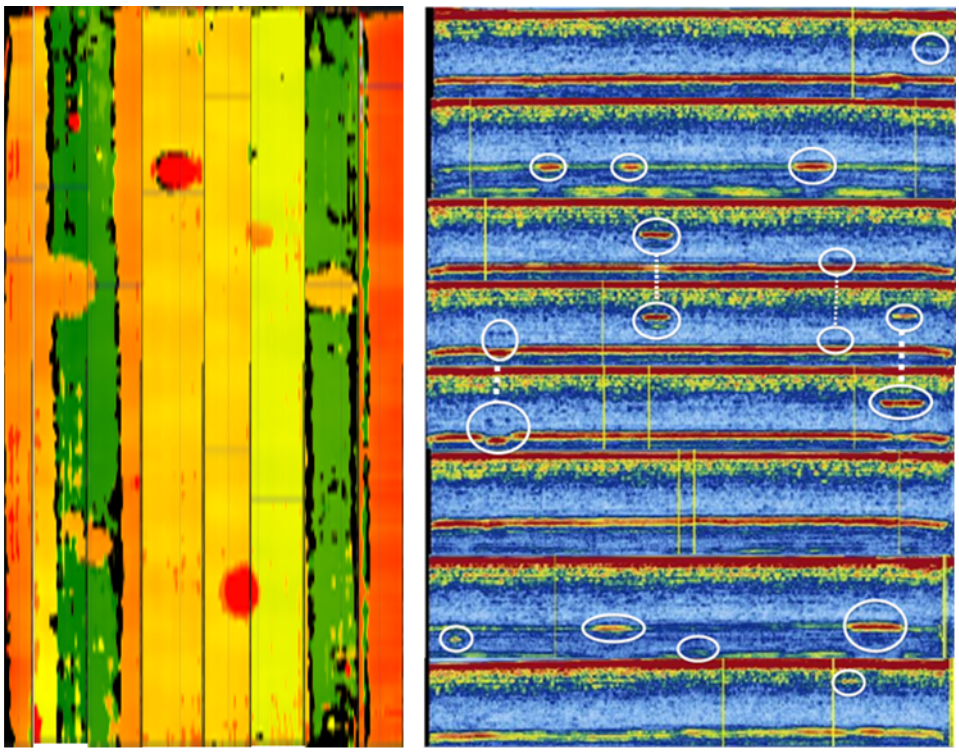

Figure 6-79: Inspection Impages Produced by the RotoArray Rolling Wheel Transducer and GE UT Control Devices

6.3 Pulsed Thermography

Vista Engineering Technologies – IR Inspection System (IRIS) - Vista Engineering Technologies has developed an automated thermography method (IRIS) for detecting defects in aluminum honeycomb aircraft composites such as disbonds and delaminations using a lower-cost, uncooled infrared (IR) camera. The method works for any type of composite (e.g. boron, fiberglass, carbon) and also works for aircraft structures with an aluminum skin bonded to aluminum honeycomb. The IRIS technology was used to evaluate a test article constructed with several flaws representative of flaws found in wind turbine blades. IRIS uses infrared images that are automatically collected, saved, and processed using a simple signal processing algorithm. Visual inspection of the IR images is not required to perform the inspection; however, the IR images can be archived if visual inspection of a particular image is needed for confirmation or further analysis. The automatic processing algorithm does a substantially better job of detecting defects and rejecting false alarms than visual inspection and interpretation of the IR images.

Vista Engineering inspected NDI test specimen REF-STD-4-TPI-1 which contains wrinkles and dry fabric. Figure 3-17 shows the drawing of REF-STD-4-TPI-1 including the various flaw types (dry regions and interply waves/wrinkles) and their locations. This specimen was inspected using the Vista IRIS device to determine if IRIS would detect the subsurface flaws engineered within the multi-ply specimen. The dry, resin-starved flaws existed in 1-layer (low), 3-layer (medium) and 5-layer (high) porosity variations. The resin-starved flaws were located at different depths within the test article. The second type of flaws were wave defects with different wave aspect ratios. The two wave defects included in this test specimen are type "A" wave where the diameter and depth of the wave are 1/6" X 2/3" respectively and of type "B" wave with a diameter and depth of 1/3" X 1".

During testing with IRIS, the top of the test article was heated and the underside of the test article was cooled. A range of parameters were tested. Throughout the testing it was determined that the best detection occurred when the change of temperature (Δt) was greatest from the top to the bottom. The final testing setup is shown in Figure 6-80. A flexible mat heater was used to heat the top and cool air was blown underneath the test article as shown in Figure 6-80. The heating mat has a surface area of approximately 2 ft^2 and the testing process for previous Air Force Work yielded testing rates of 80-100 ft^2 per hour. The cooling was accomplished by blowing cool air into the wind blade section. After heating, thermal image videos were recorded and the heat signatures were analyzed. The duration of hot and cold temperature exposure can be adjusted where longer duration exposures may be needed to detect deeply embedded flaws.

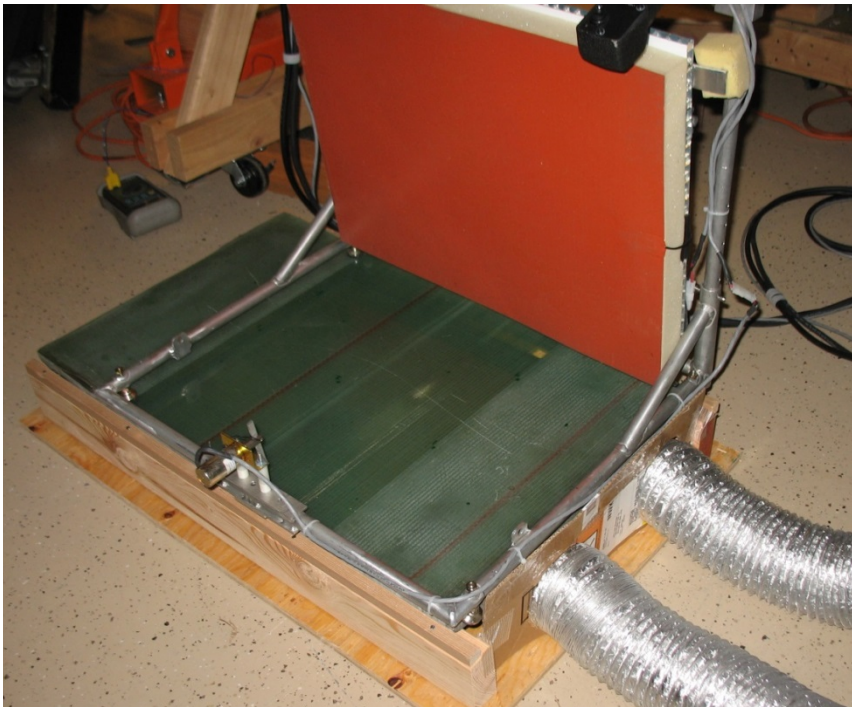

Figure 6-80: IRIS Test Setup Showing Orange Flexible Heater, the Test Specimen and Delivery of Cold Air Underneath the Test Specimen

Figure 6-81 shows the resulting thermal image that was produced from this inspection. Wave A and wave B type flaws were clearly seen in the thermal images regardless of their depth within the test piece. The type B wave flaws were seen as areas releasing greater amounts of heat. The type A wave flaw (center) in Figure 7-Tb is smaller and located further from the top surface than either of the type B wave flaws. While this size difference and location depth reduces the intensity of the heat signature, the type A wave flaw was still clearly detected by the automated processing of the data. Dry, resin-starved layer flaws showed less distinctive heat signatures. The depth of the dry resin layer flaws resulted in images that are not as distinctly defined upon visual examination of the thermal image. This is a clear demonstration of the advantage of the processing algorithm as after analysis the larger of the 3-layer and 5-layer dry resin flaws were identified**.** Vista believes that optimization of the algorithm and testing procedure is expected to result in detection of all flaws present in the test article. The bright circle in the middle of Figure 7-105 is a reflection from the IR camera.

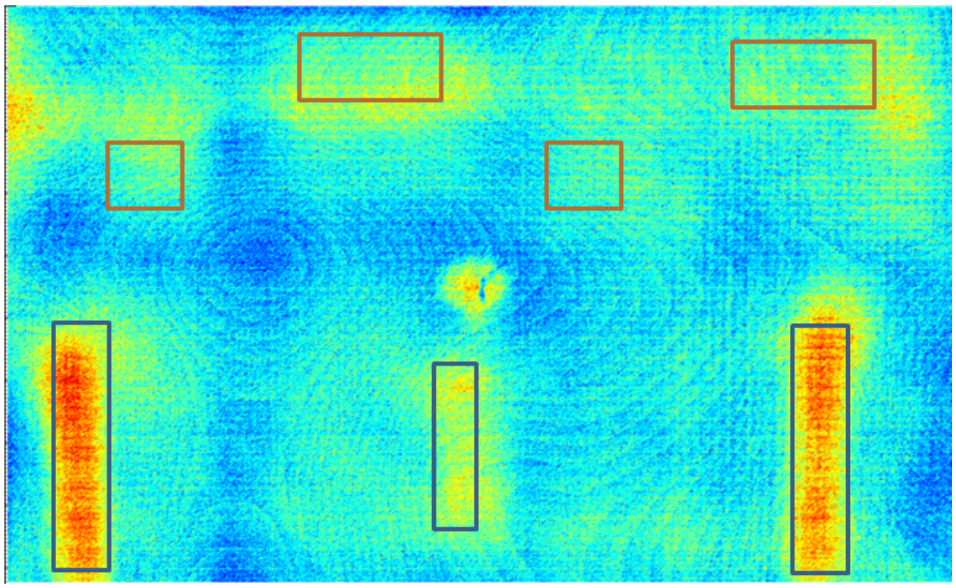

Figure 6-81: IRIS Thermal Image Showing Heat Signatures of Wave and Dry Region Flaws in NDI Test Specimen REF-STD-4-TPI-1

Initial testing revealed that IRIS could detect both types of wave and dry, resin-starved region flaws known to exist in wind blades. Initial results showed that wave A, wave B, and the larger of the 3-layer and 5-layer dry resin flaws were detected upon processing. Detection of the wave type flaws was independent of distance of the flaw from the surface of the test article. Type A wave flaws were not as distinct when viewed visually, but very clearly defined upon algorithm processing. Dry resin starved flaws were more difficult to detect, although initial results indicated that detection of the resin starved layers could be achieved with further software development. Overall, some fine tuning of IRIS would be needed to actively use the IRIS flaw detection technique on wind turbine blades.

Thermal Wave Imaging – EchoTherm Pulsed Thermography - Initial investigations to evaluate the viability of thermography for wind blade inspections were conducted several years ago. Figure 6-82 shows the deployment of a portable pulsed IR system on a thin wind blade test article. The test article was cut from an actual blade and a flat bottom hole was machined into the spar cap. Figure 6-83 shows the damage and the resulting thermographic image of the damage which is indicated as a relative hot spot in the IR image. Figure 6-84 shows the deployment of the EchoTherm system to the set of WINDIE test specimens. Normal pulsed thermography operation uses very brief flashes of quartz lamps to produce the temperature differential (heat flow) through the part. However, in thick composite sections, such as those used in wind blades, more heat energy needs to be applied in order to observe damage corresponding to heat flow variations through the part thickness. Thus, a heat gun was used on the thick WINDIE specimens in order to induce a sufficient heat differential for detecting deeply embedded flaws.

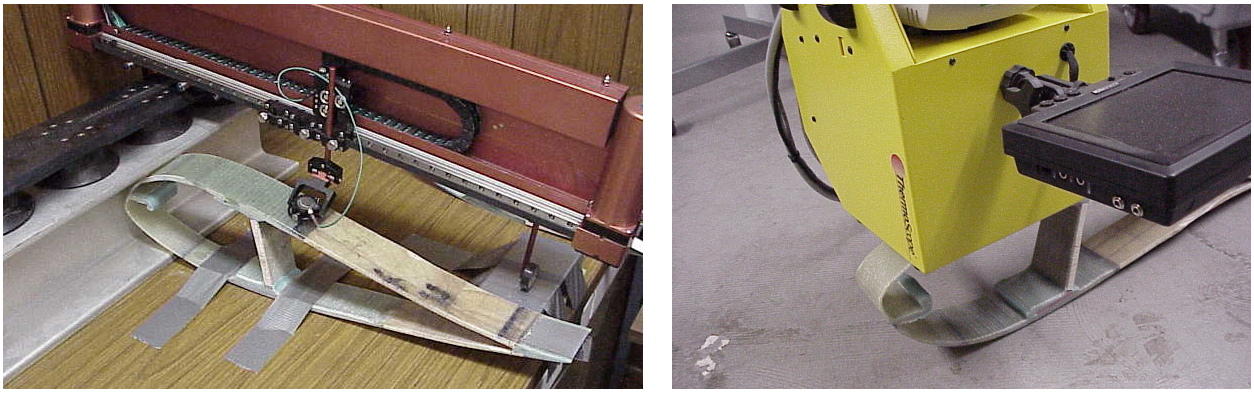

Figure 6-82: Wind Blade Section Containing Engineered Damage and Pulsed Thermography System (right) Deployed on Blade for Inspection

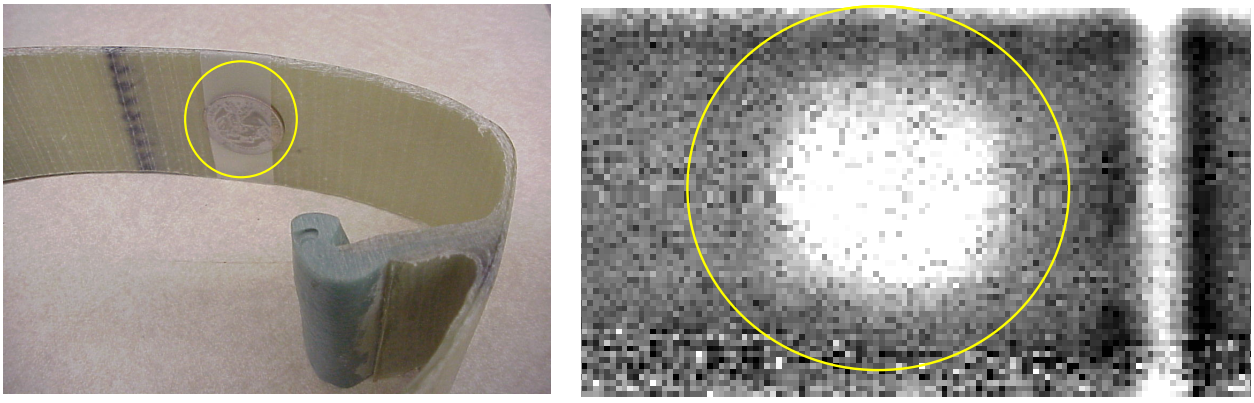

Figure 6-83: Damaged Region in Spar Cap and Thermography Image of Damage

Figure 6-85 shows one of the first tests for the TWI thermography system. The primary purpose was to assess the depth of penetration of the heat and the corresponding sensitivity of the IR system to detect deeply embedded flaws. It can be seen that simulated disbond/delamination flaws, represented by the flat bottom holes at the depths shown in Figure 6-85, were imaged

down to a depth of 0.75” when heated from the front surface. Figure 6-86 show thermography images for specimen Wind-2-044-SPAR-085 which represents thin spar caps (0.44” th.) and includes the adhesive joint at the spar cap-to-shear web flange interface (0.85” th.). It can be seen that most of the flat bottom holes are detected in the thermography images with the exception of the most challenging flaws that are located on the back side of the adhesive bond line. These flaws are further away from the inspection surface and are very close to the back wall surface making it difficult to image the very small difference in heat transfer at this depth.

Figure 6-84: TWI Thermography System Inspecting a Wind Blade NDI Specimen

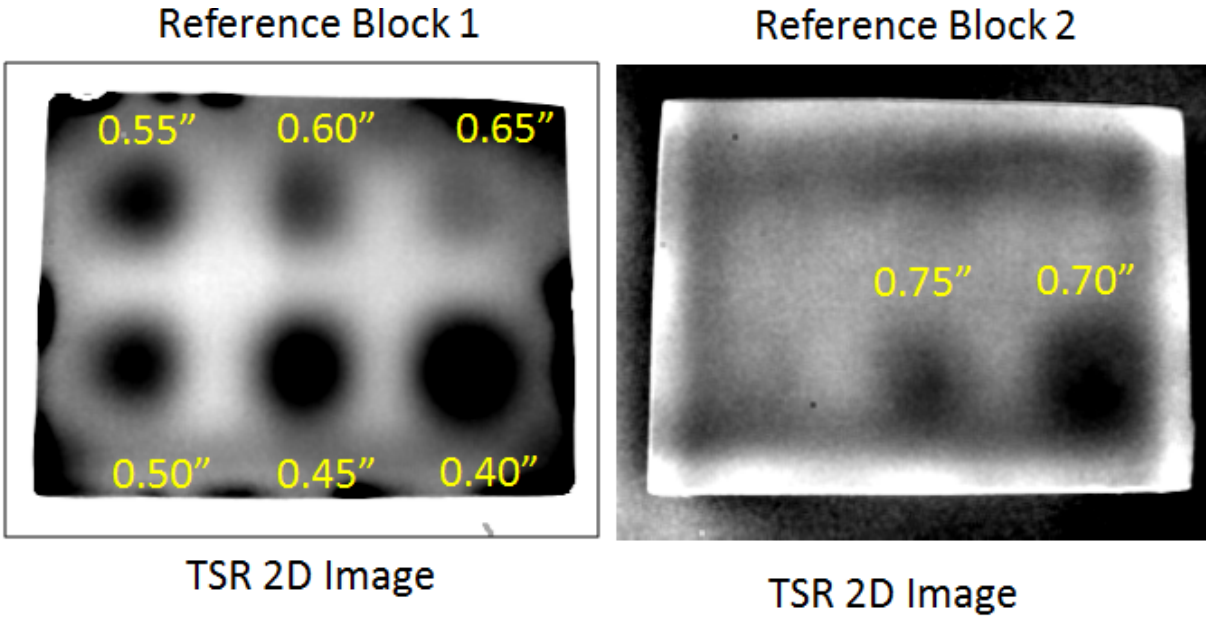

Figure 6-85: Thermography Images Produced by TWI IR System Applied to

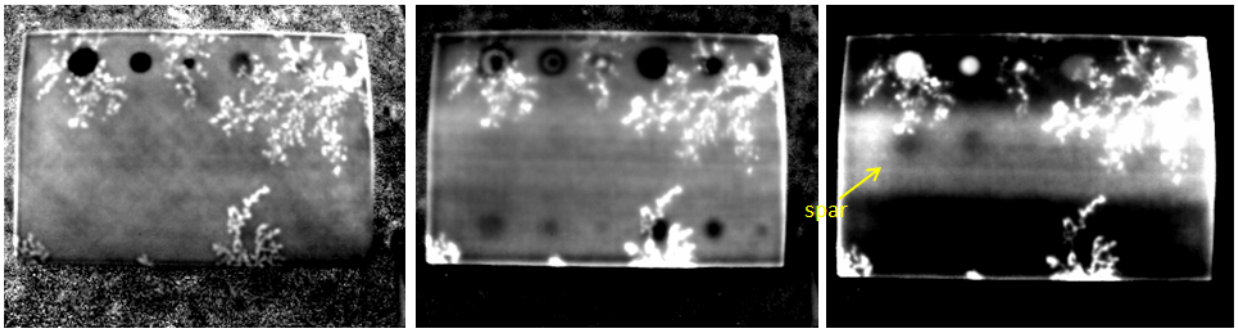

Figure 6-86: Thermography Images Produced by TWI IR System Applied to NDI Specimen WIND-2-044-SPAR-085

In addition to the laminate specimens, a sandwich core section was also inspected. REF-STD-1-050-TPI-1 contains a wide array of flaw types found in composite sandwich construction. This specimen consisted of two thin skins bonded to a two inch thick foam core. Thermography inspection results for the sandwich core WINDIE specimen are shown in Figure 6-87. Some of the interply flaws, including some of the grease contamination flaws were detected. The skin-to-core flaws produced by the pull tabs were all clearly imaged. The top row of mold release contamination was not detected.

Specimen REF-STD-2-127-173-SNL-1 includes a thicker spar cap (1.27" th.) and thicker adhesive joint at the spar cap-to-shear web flange interface (1.73" th.) than specimen Wind-2-044-SPAR-085. In Figure 6-88, flat bottom holes in spar cap laminate were detected at the various depths but the flat bottom holes in the bonded shear web joint were not detected. It appears that all sizes of the flat bottom holes were detected. Some pull tab flaws in the laminate at 25% depth were detected while the deeper pull tab flaws at 75% were not. None of the pull tabs in the shear web bonded joint, both at the upper and lower adhesive interface, were detected. It can be seen that almost all of the flaws, in both the spar cap laminate and shear web bond line, were detected. The only flaws that were not detected in this specimen were the pull tab disbond flaws in the adhesive bond line at Interface 1 (back side of the adhesive in the spar cap-to-shear web bond joint). Flat bottom holes in the spar cap laminate were detected at each of the depths and the flat bottom holes in the bonded shear web joint were also detected. Pull tab flaws in the laminate at all depths were detected.

Figure 6-89 shows thermography results for specimen REF-STD-3-129-176-SNL-1. The microballoon porosity flaws at 25% depth in the laminate spar cap were detected. The microballoons at 50% laminate depth were not detected. None of the other flaws, in both the spar cap laminate (1.29" thick) and shear web bond line (1.76" total thickness), were detected. Thus, the grease (contamination) weak bond flaws, the mold release (contamination) weak bond flaws, and disbonds and voids in the shear web bonded joint were not indicated in the

thermography images. Microballoons at the interface between the spar cap laminate and the adhesive and on the far side of the adhesive were also not detected by the IR method.

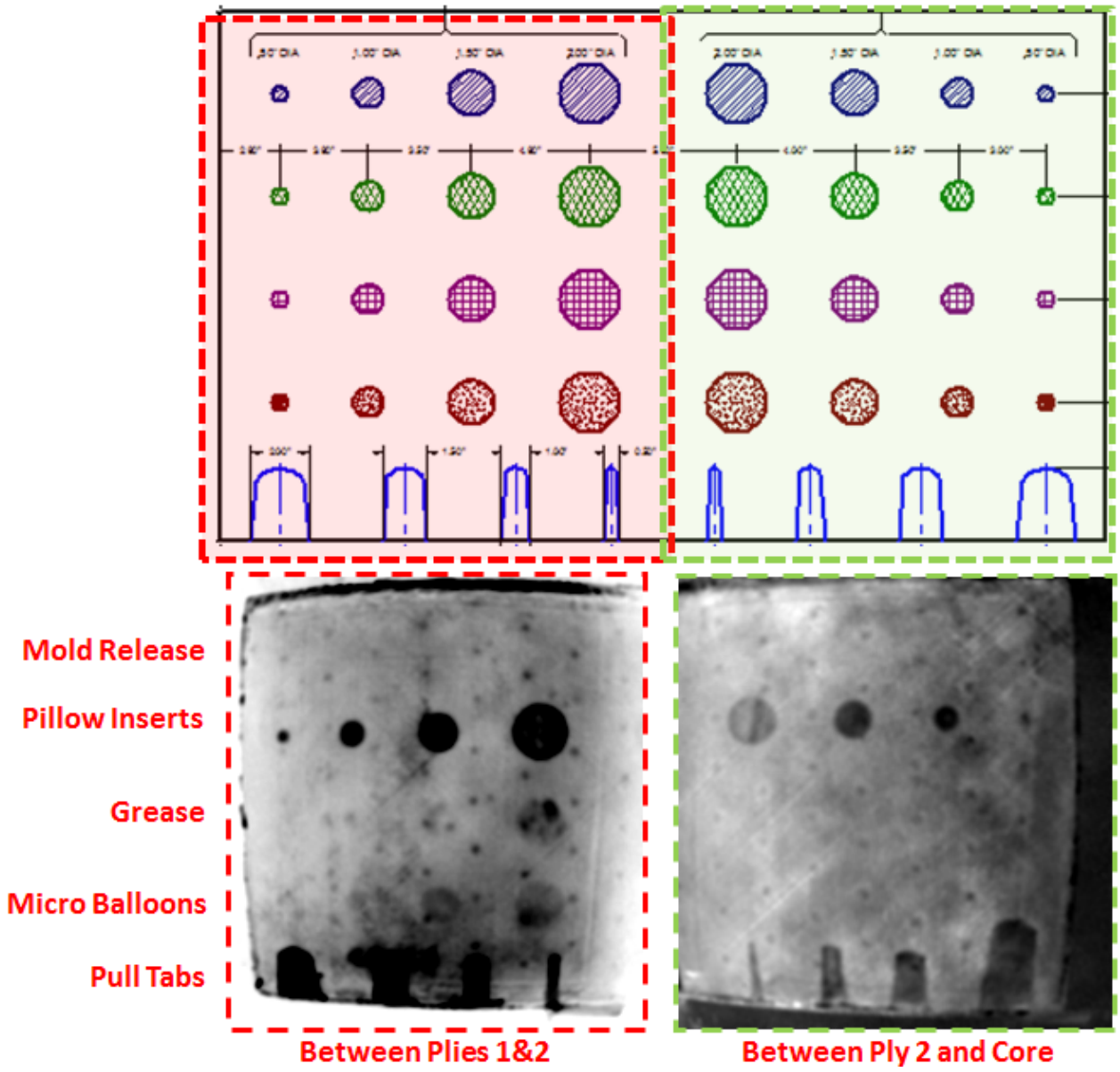

Figure 6-87: Thermography Images Produced by TWI IR System Applied to NDI Specimen REF-STD-1-050-TPI-1 Foam Core Test Specimen

Figure 6-90 shows thermography results for specimen REF-STD-4-135-SNL-1. This particular sample contained two types of flaws. They were dry areas and out-of-plane waves. The out-of-plane waves were created by embedding pre-cured resin rods with a specific aspect ratio (width to height) between plies of the laminate prior to resin infusion. Some of the wrinkles were clearly imaged and some of the deeper wrinkles were not as obvious. The same can be said for dry

fabric areas on this specimen where the flaws closer to the surface were more definitively detected by the thermography inspections.

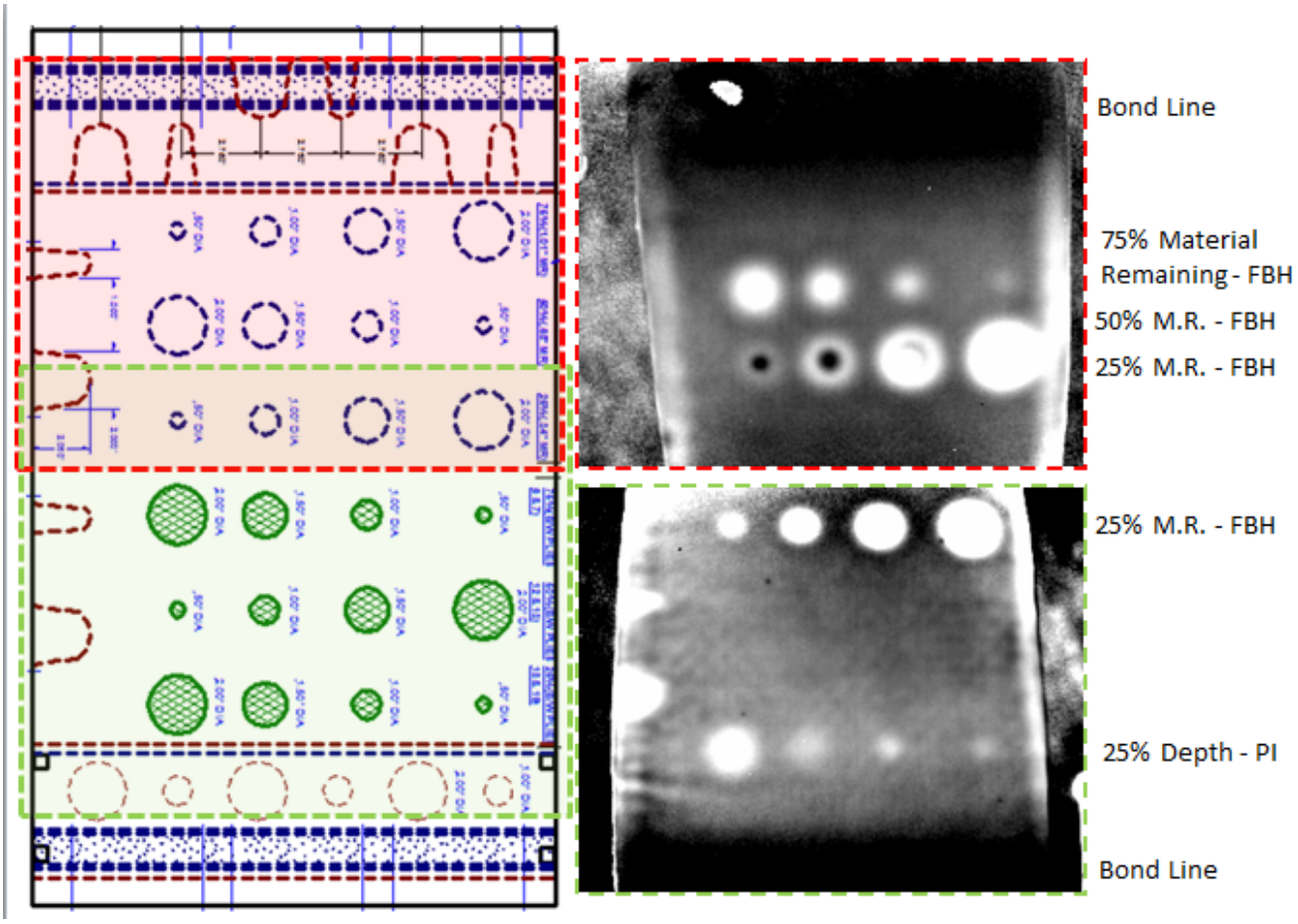

Figure 6-88: Thermography Images Produced by TWI IR System Applied to NDI Specimen REF-STD-2-127-173-SNL-1 Containing Spar Cap and Shear Web Bond Line Flaws

Results from the application of thermography to the trailing edge specimen REF-STD-5-154-SNL-1 are shown in Figure 6-91. Specimen REF-STD-5-154-SNL-1 is a sample dedicated to inspecting the adhesive joint between two laminates. All of the flaws are located at this junction and the total specimen thickness is 1.54" (0.5" depth to flaws from inspection surface). The pull tab flaws were more clearly detected in this specimen while the microballoons and pillow insert flaws were lightly imaged by the thermography system.

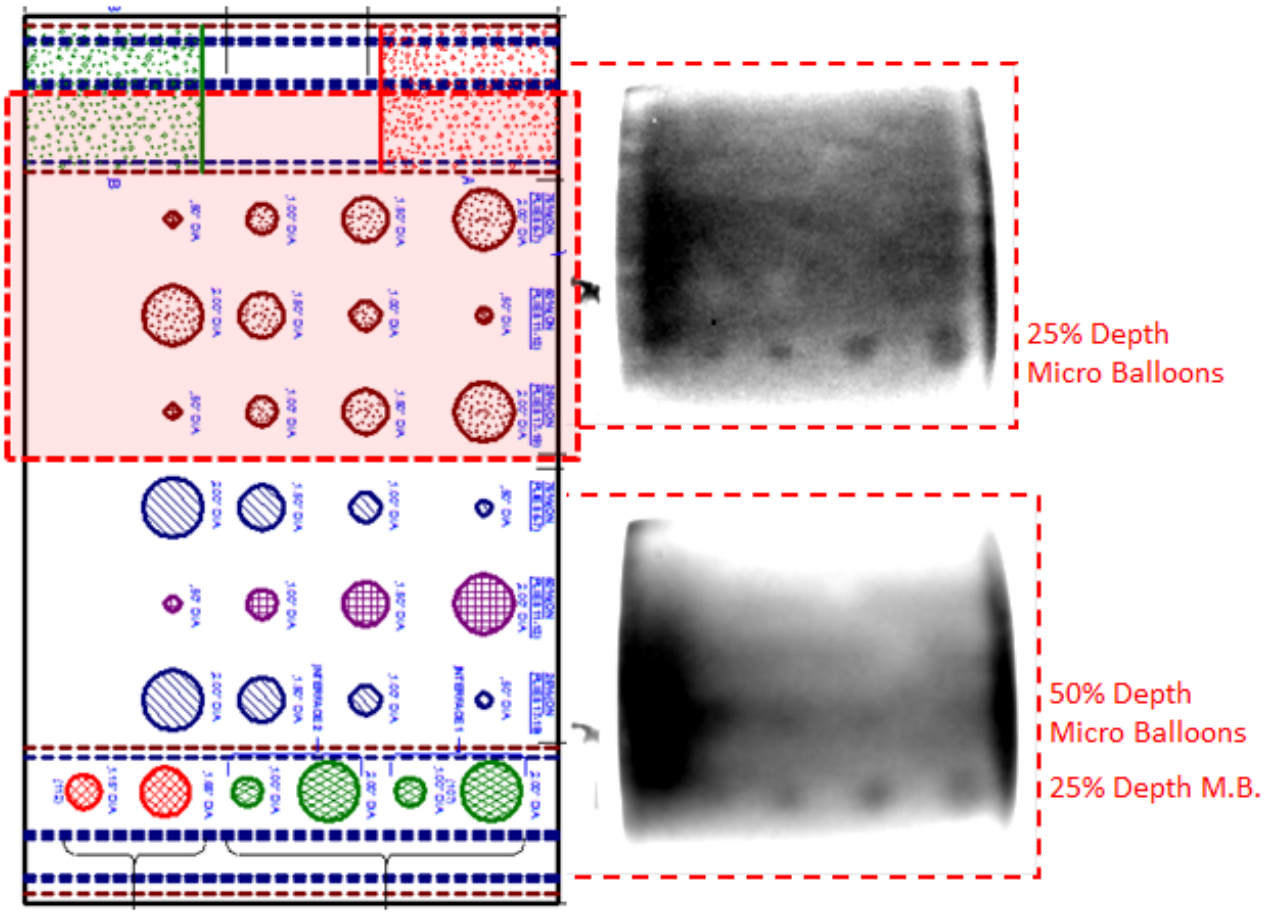

Figure 6-89: Thermography Images Produced by TWI IR System Applied to NDI Specimen REF-STD-3-129-176-SNL-1 Containing Spar Cap and Shear Web Bond Line Flaws

Overall, these results indicate that depth of penetration is a concern for thermography inspections of wind blade specimens. Other studies [7.1], along with this one, have determined that IR – and in particular this TWI EchoTherm system - performs well for wide area imaging to detect near surface flaws and performs well on sandwich core areas. Substructure flaws must manifest themselves as changes (anomalies) in the surface temperature of the part in order to be detected by thermography. Small flaws, especially those embedded deep within a structure, are difficult to image as their presence has less of an effect on surface temperature heat transfer. Thermography also works very well for NDI of sandwich construction so this method should be considered for any needs with respect to wide-area inspection of foam or balsa core regions, including post-repair inspections in the field.

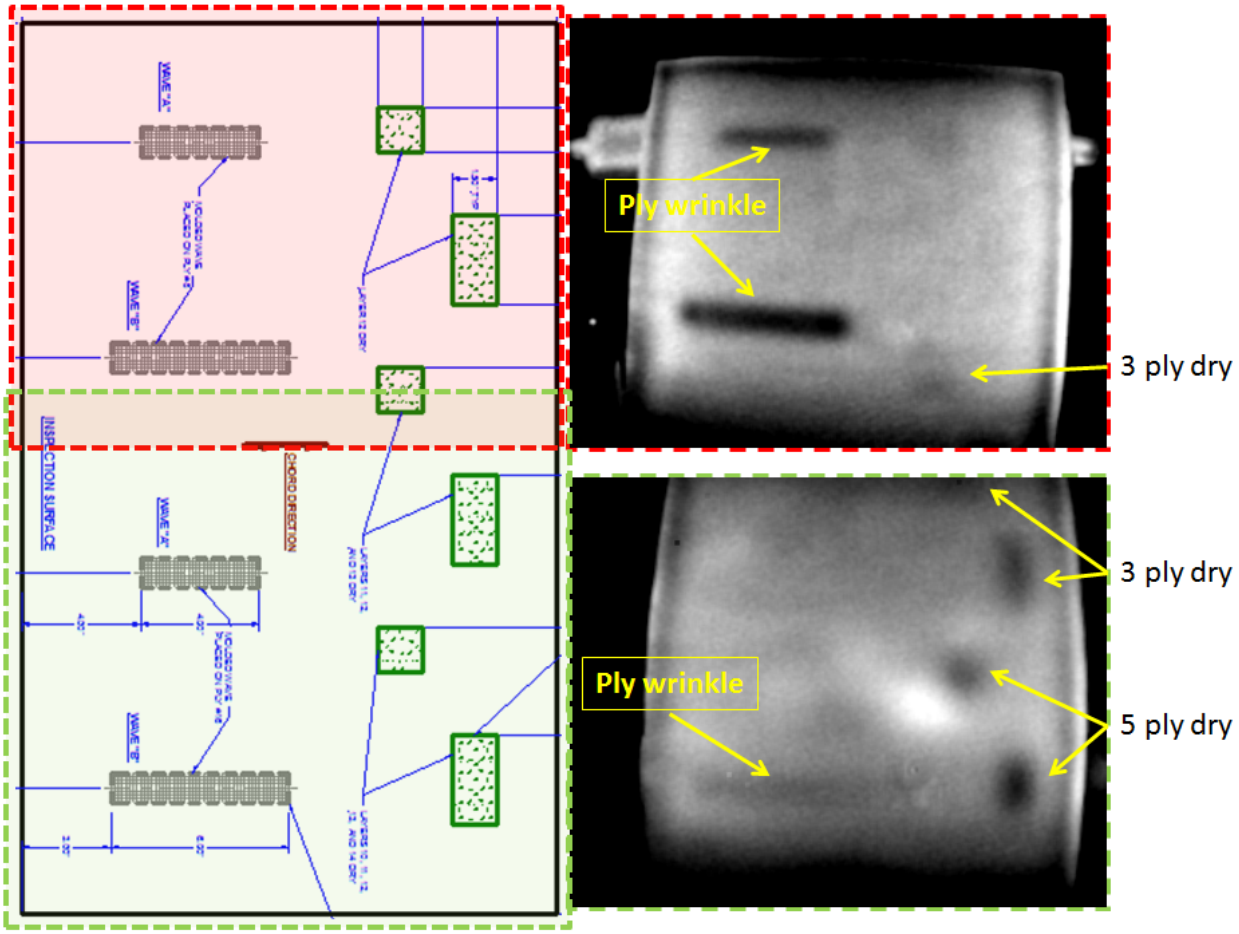

Figure 6-90: Thermography Images Produced by TWI IR System Applied to NDI Specimen REF-STD-4-135-SNL-1 Containing Wave and Dry Region Flaws

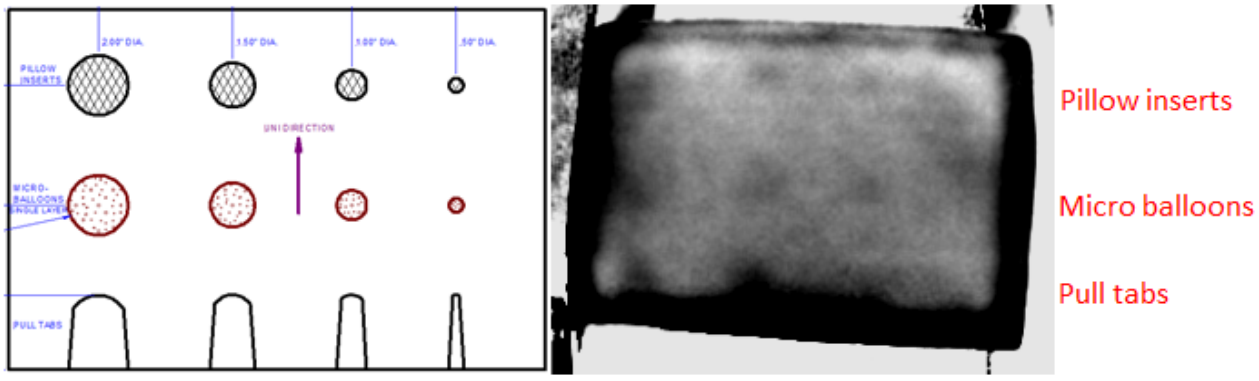

Figure 6-91: Thermography Images Produced by TWI IR System Applied to NDI Specimen REF-STD-5-154-SNL-1 Containing Spar Cap Flaws

Thermal Wave Imaging – EchoTherm Thermography - Figure 6-92 shows thermography results for specimen REF-STD-4-135-SNL-1. Some of the wrinkles were clearly imaged and some of the deeper wrinkles were not as obvious. The same can be said for dry fabric areas on this specimen where the flaws closer to the surface were more definitively detected by the thermography inspections. Thus, this technique worked well detecting the out-of-plane waves and dry areas that were closer to the surface, but didn't perform well on the flaws located deeper in the specimen.

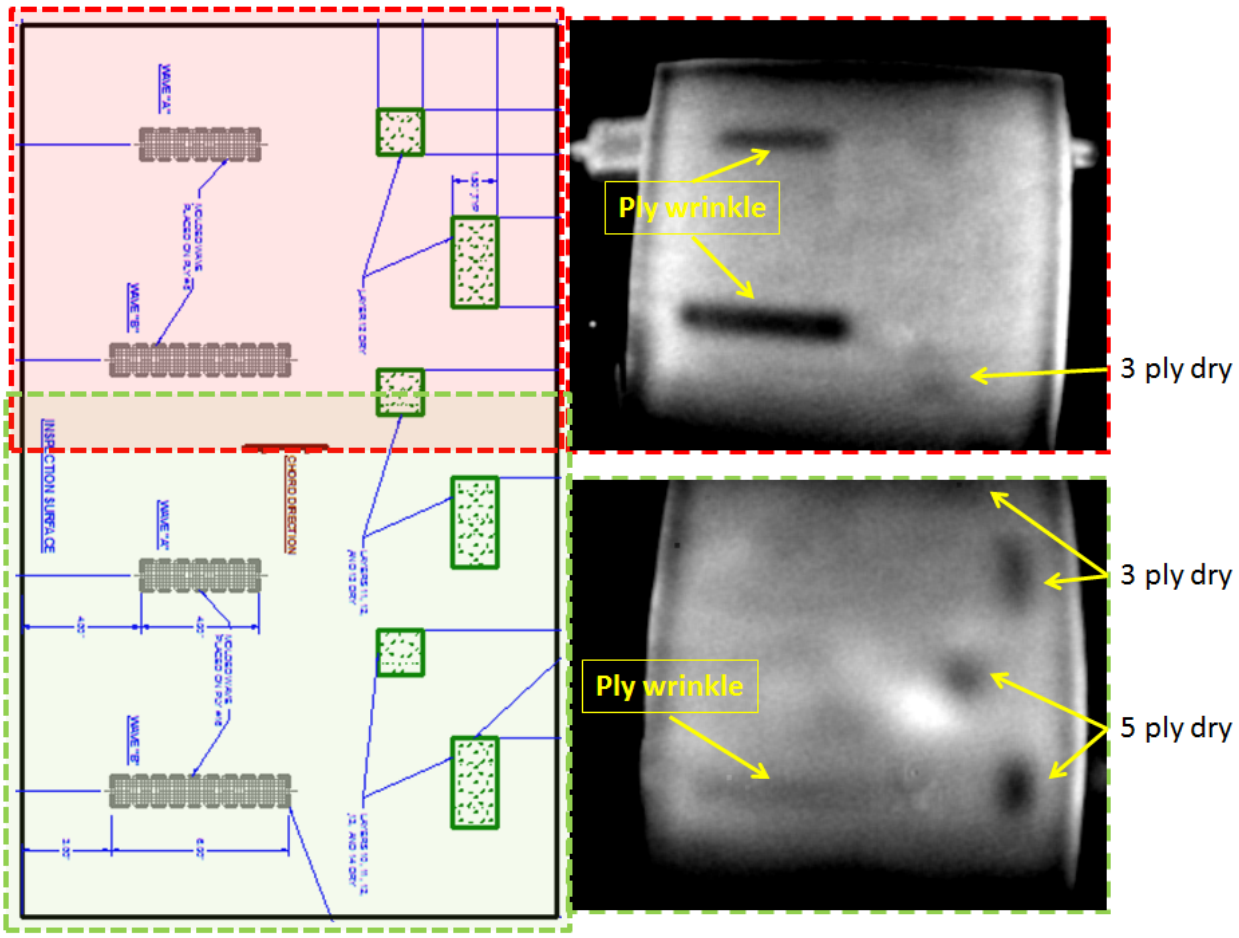

Figure 6-92: **TWI Thermography Inspection of Fiberglass Specimen REF-STD-4-135-SNL-1 and IR Images Showing Detection Capabilities**

6.4 Microwave

GE Global Research NDI Method: Microwave - The sensitivity level of microwave radar depends on several factors including power of the transmitter, frequency range and directional selectivity of the antenna. The microwave inspection technique conducted by GE provided some preliminary results. In limited testing on one wind specimen, the system, in its current

implementation, was able to detect 8 out of 10 flaws. The major benefit to microwave inspection technology is that it is a non-contact method of inspection. There is no coupling media required to inspect the part, eliminating the need for surface contouring, custom contact deployment hardware, but a gantry system or scanning method would need to be developed for field and factory use (see Figure 6-93). The GE microwave system inspects with a frequency sweep across the range of 1 -20 GHz. This is followed by the application of a Fast Fourier Transform to the data to produce A, B, and C scans. The scan head is placed approximately 0.2 m from the front of the part to be inspected.

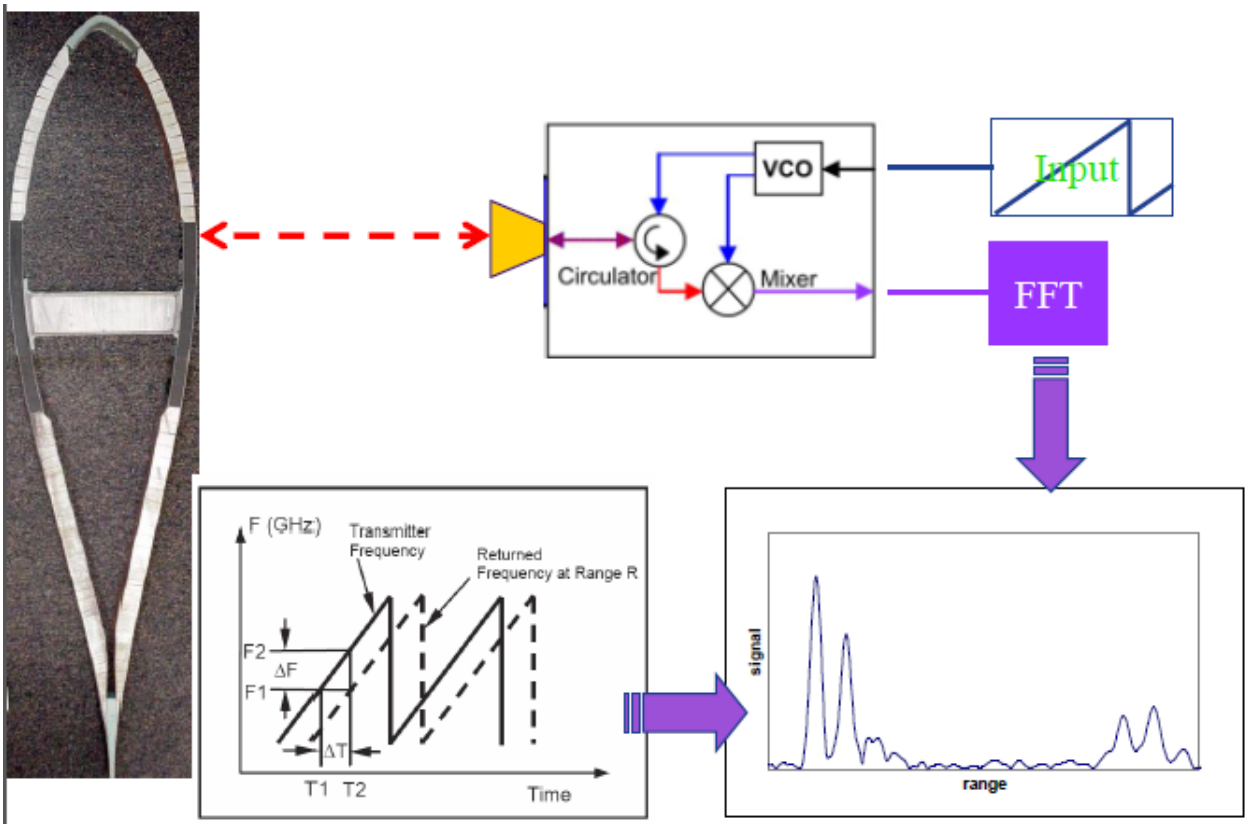

Figure 6-93: Schematic of GE Microwave Inspection Device and Set-up on Wind Turbine Blade Section Containing Flat Bottom Hole Flaws

Inspection results using the POC Microwave technique obtained from a 0.5" thick fiberglass laminate with varying size flat bottom holes can be seen in Figure 6-94. Results can be presented to the inspector in various forms including A-scans, B-scans and C-scans. If an area of concern is identified in the C-scan the inspector can focus on that area and confirm detection using the other two data presentation methods. The hardware used to inspect a WINDIE specimen with out-of-plane waves and dry regions is shown in Figure 6-95. It can be seen that there is no contact needed with the specimen to perform the microwave inspection.

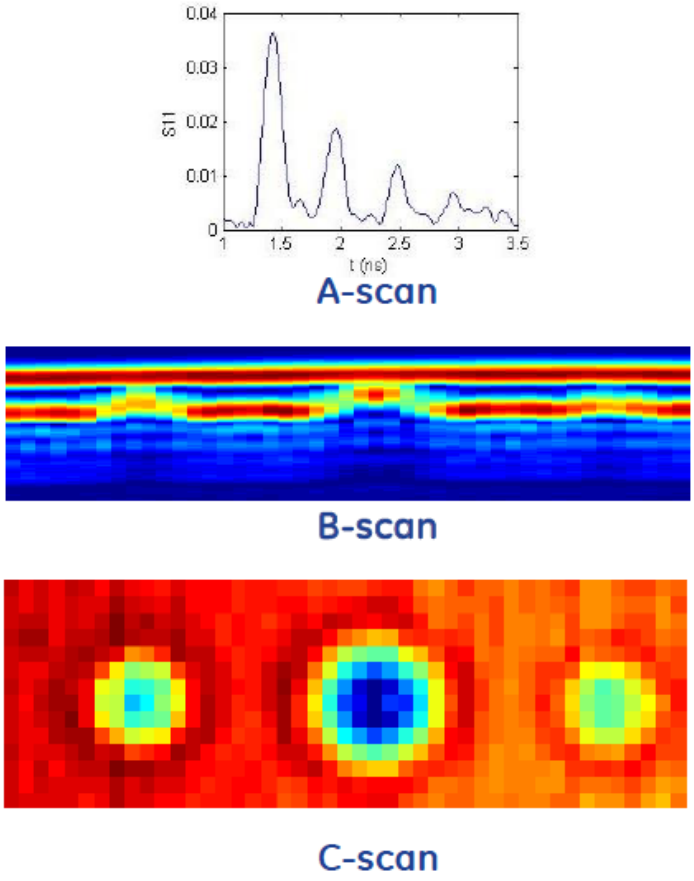

Figure 6-94: A-, B-, and C-scan Images Produced by GE Microwave System Inspecting Flat Bottom Holes in a 0.5" Thick Spar Cap

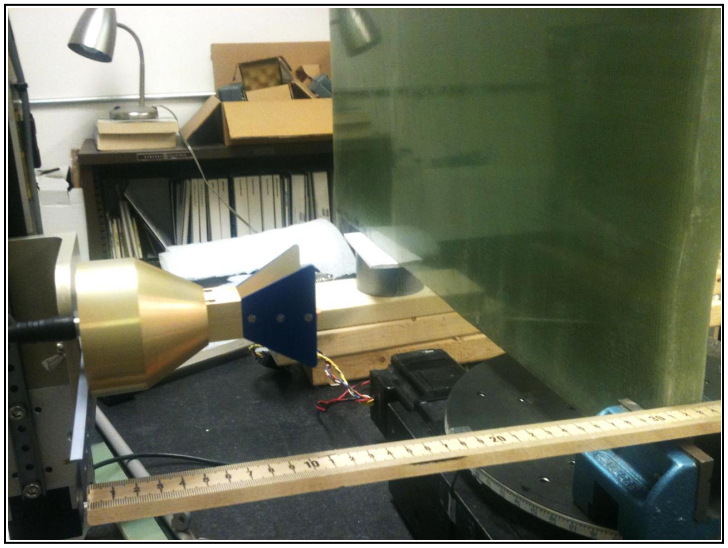

Figure 6-95: Inspection of Fiberglass Specimen (REF-STD-4-135-SNL-1) with Out-of-Plane Waves and Dry Regions Using GE Microwave System

The GE microwave system was only applied to one of the WINDIE test specimens. Figure 6-96 shows that this inspection device was able to detect 8 flaws out of 10 in the Sandia specimen containing out-of-plane waves and dry regions**.** Based on the results obtained at the Nondestructive Technologies Lab the described microwave inspection system is capable of detecting the types of defects included in specimen REF-STD-4-135-SNL-1; however, the system was not applied to other test specimens to evaluate its performance for other types of flaws found in wind turbine blades.

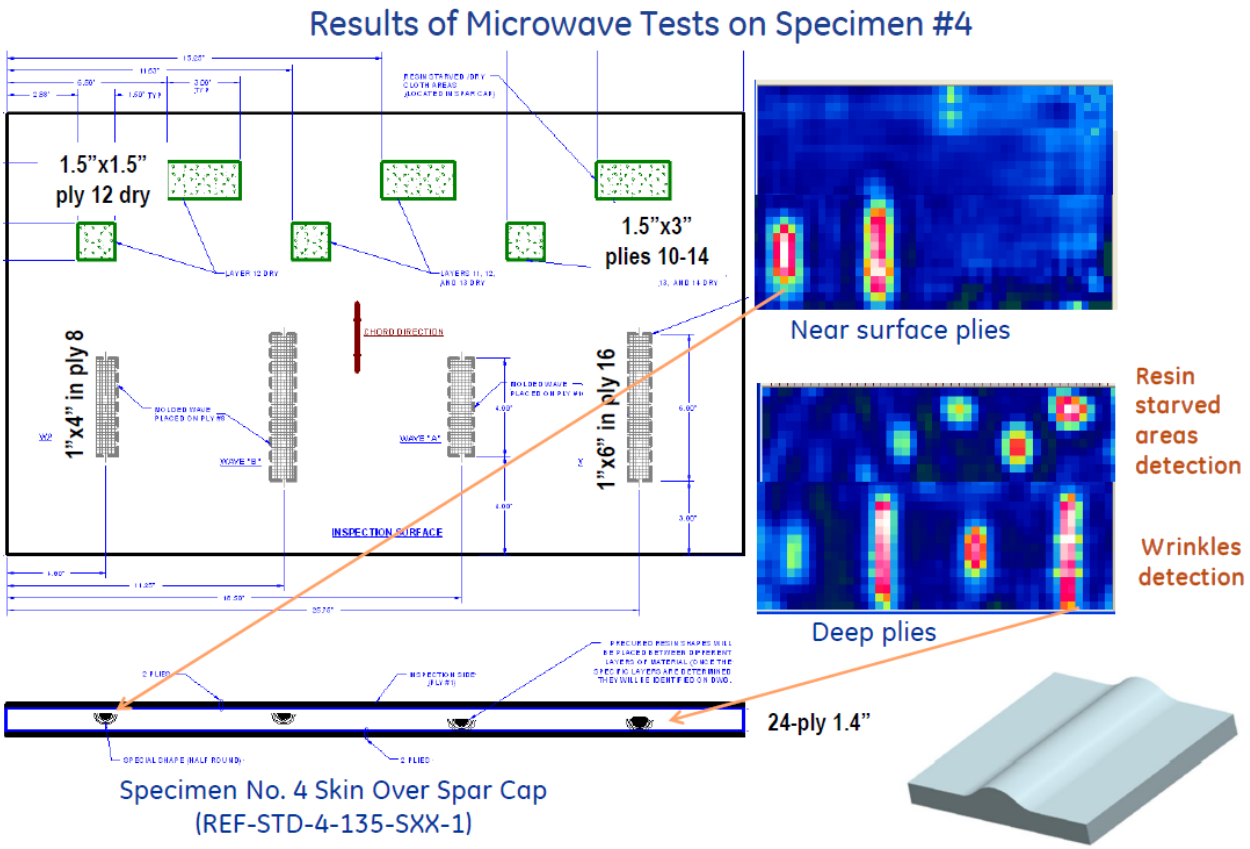

Figure 6-96: Results from GE Microwave System Inspection of REF-STD-4-135-SNL-1 with Out-of-Plane Waves and Dry Regions

Physical Optics Corporation Microwave Inspection Tool – POC inspected three wind blade test specimens to conduct probe calibration and testing. The results of the tests are summarized in this section. The tests were performed at POC's laboratories in a controlled environment and data collection ranged from approximately 10 to 20 minutes total scan time per sample. The expectation of the tests was that the 12 GHz microwaves would penetrate through the samples and reveal dielectric discontinuities with a thickness of 0.1 mm or greater and a diameter of 5 mm or larger, which was based on prior testing of the MIT on engineered samples of ¼"

thickness. An open question prior to these tests was the depth to which the MIT probes would be able to penetrate and how penetration and resolution would be affected in the case of the fiberglass-epoxy composites used in these wind blade samples.

The first wind blade sample tested was WIND-5-180 (Specimen V) shown in Figure 6-97. This sample consists of a 1.80" thick, curved fiberglass-epoxy sample with 12 flat bottom holes ranging from 1" to 2" diameter drilled to different depths across the length of the sample. The holes depths range from 0.36" to 1.44" in 0.36" increments corresponding to 1.44" to 0.36" of remaining material. We performed tests from the back of the part (i.e., hole side down). One limitation identified was due to the nature of the samples as cut-outs from large, continuous wind blade samples, so the microwave probe could not reach all the way to the edges of the parts without the Teflon feet running off the edge. This limited the ability to search for defects near the edges of the samples and therefore only half of the last row of holes was accessible. Nonetheless, the MIT scan results show in Figure 6-98 demonstrate the capability of MIT to reveal all holes at all depths with penetration through ≥ 1.44" of material.

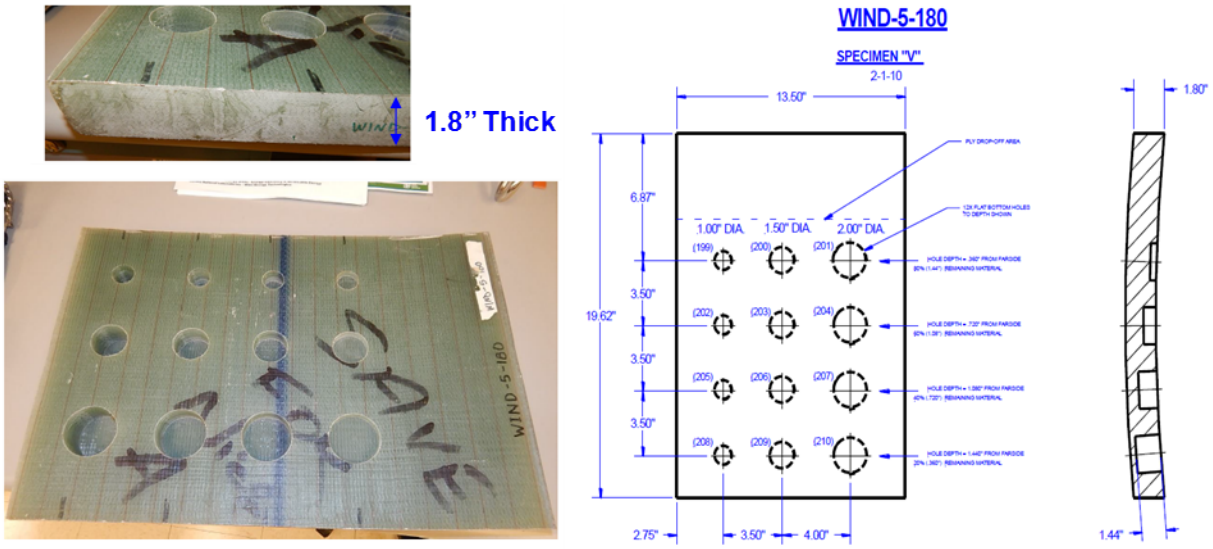

Figure 6-97: Photo and Design of Specimen Wind-5-180

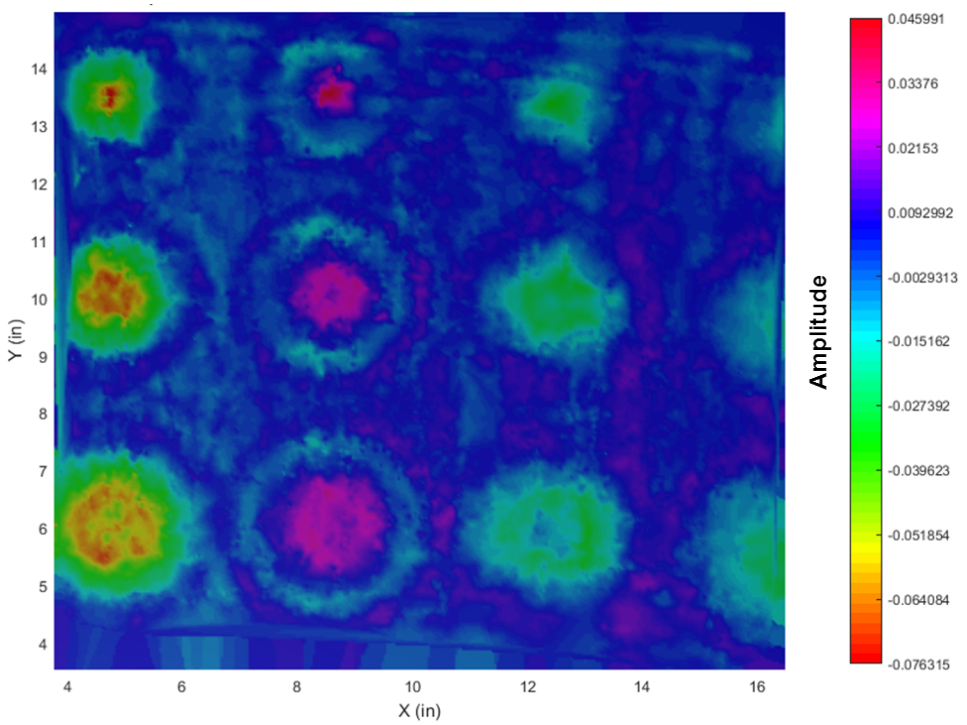

Figure 6-98: C-Scan Image from POC MIT System Inspecting WIND-5-180 Specimen

The second sample tested was WIND-2-044-SPAR-085 shown in Figure 6-99. This sample consists of a spar cap bond with a series of flat bottom holes along different portions near the bond line as well as the shell. This inspection was focused on the central bond line region as highlighted in Figure 6-99. The testing revealed all of the defects in this region including the 0.5", 1", and 1.5" diameter holes with depths of 0.310" (corresponding to 0.100" remaining bond material and 0.540" total thickness) and 1" and 1.5" holes with depths of 0.100" (corresponding to 0.310" remaining bond material and 0.750" total thickness). The 0.5" hole at 0.100" depth was too close to the edge of the part to produce an image of this flaw. The slight curvature of the part can be seen in the perspective view of the conformal C-scan shown in Figure 6-100. The conformal C-scan scaled to the actual dimensions of the sample under test enables an intuitive and fast association of the defect locations to the true locations on the actual part.

The third specimen (REF-STD-1-050-SNL-1) included a grid of pull tabs, microballoons, grease, pillow inserts, and mold release simulating a variety of defects between plies (delamination type) and between the fiberglass laminate and a foam core (disbond type). The specimen design is shown in Figure 6-101. The central region of the part was inspected using the MIT system and the resulting C-scan is shown in Figure 6-102. The tests showed the ability to detect the pillow inserts of 1" and 1.5" diameter, however the grease could not be seen. The pillow insert locations correspond to the orange regions in Figure 6-102. Similar results were obtained for both the disbond and delamination type regions. The foam core contains a periodic, triangular pattern of holes. The holes show up in the MIT C-scan images as blue and purple spots, which caused a significant amount of clutter when interpreting the results.

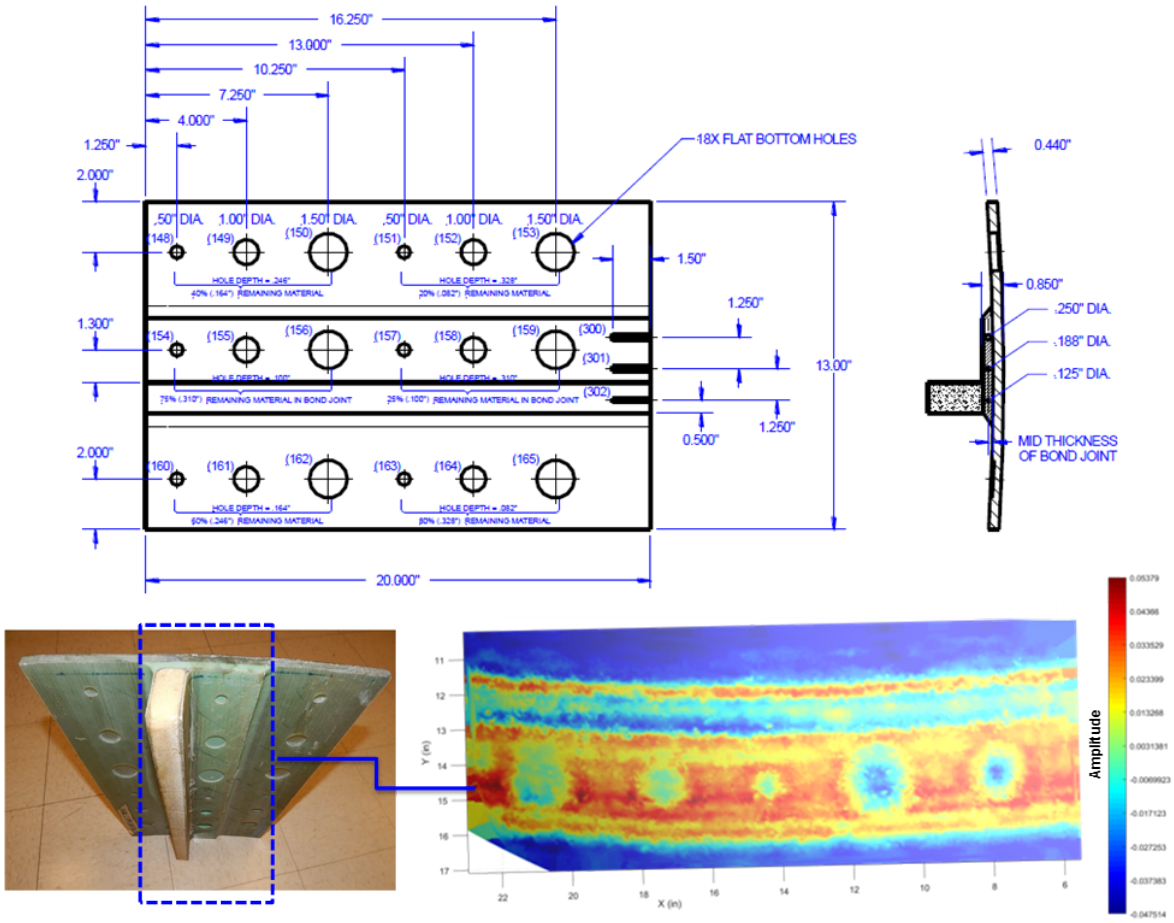

Figure 6-99: Design of Specimen WIND-2-044-SPAR-085 and C-Scan Image Resulting from Inspection with POC MIT System

The MIT testing on the wind blade test specimens indicated positive results as the MIT was able to penetrate through 1.44" using the near-field probe technique. It is believed that there was margin for the probe to penetrate a greater thickness sample, if it were tested. The ability to image all of the defects through the bond line very clearly is another strength of this technology. The MIT resolved defects down to ½" (the smallest available in these samples), which is consistent with prior testing. Additional improvements are planned for the MIT probe including optimization of the signal processing and data visualization techniques to improve contrast and enable automated highlighting of defects. Plans also exist to incorporate multi-frequency techniques to add depth resolution and defect classification capabilities.

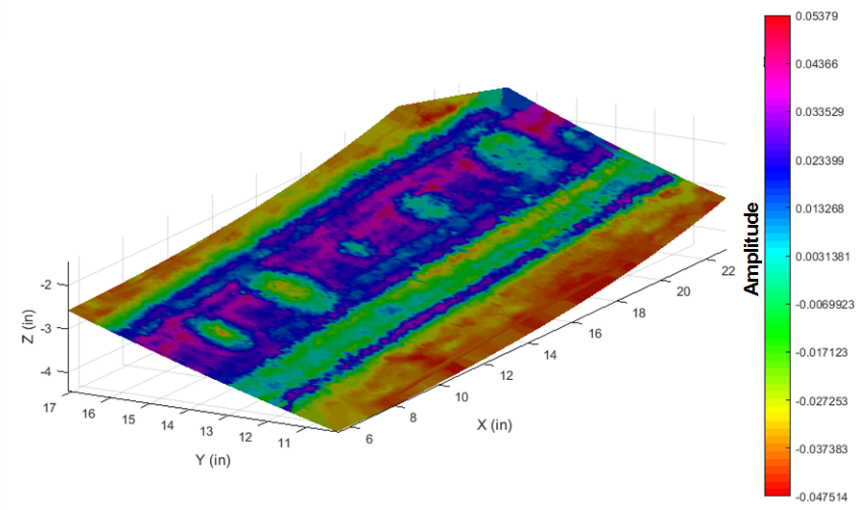

Figure 6-100: Conformal View MIT C-Scan Data Depicts the Curvature of the Surface

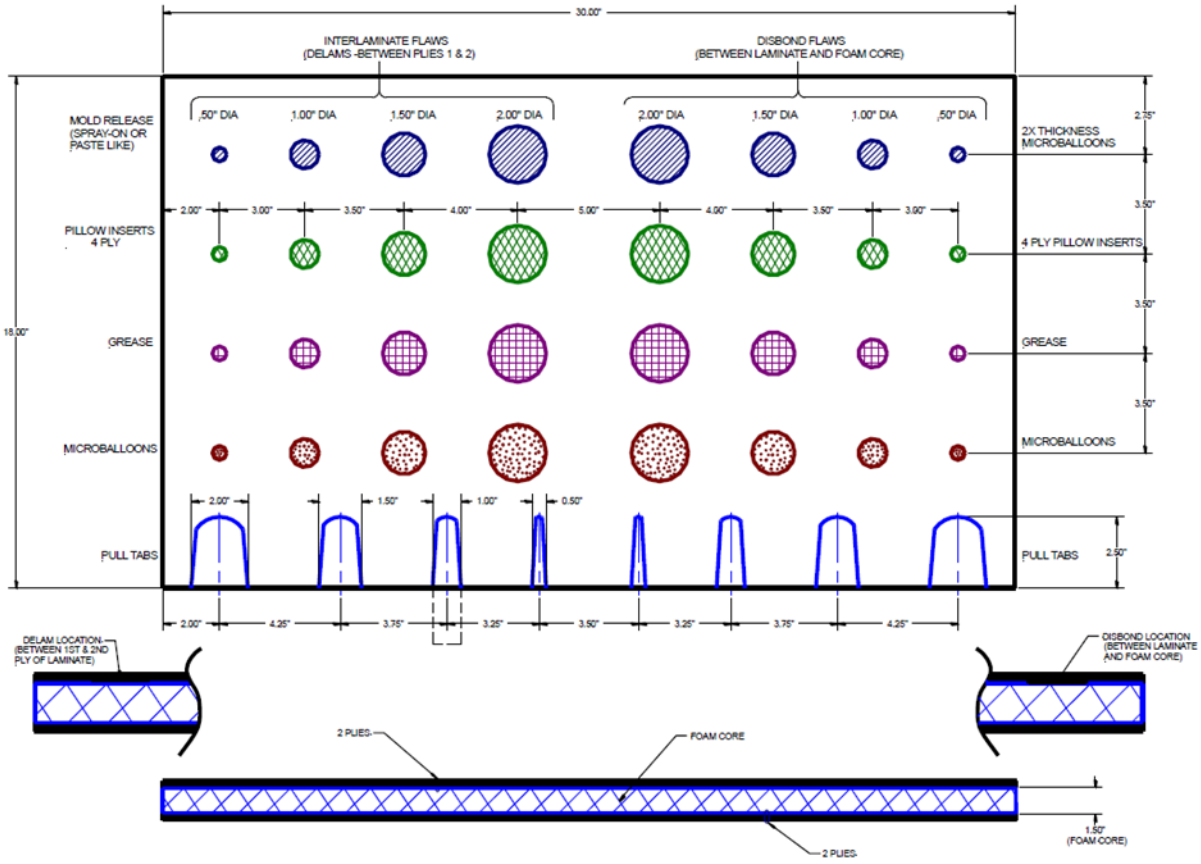

Figure 6-101: Design of WIND- REF-STD-1-050-SNL-1 Foam Core Specimen

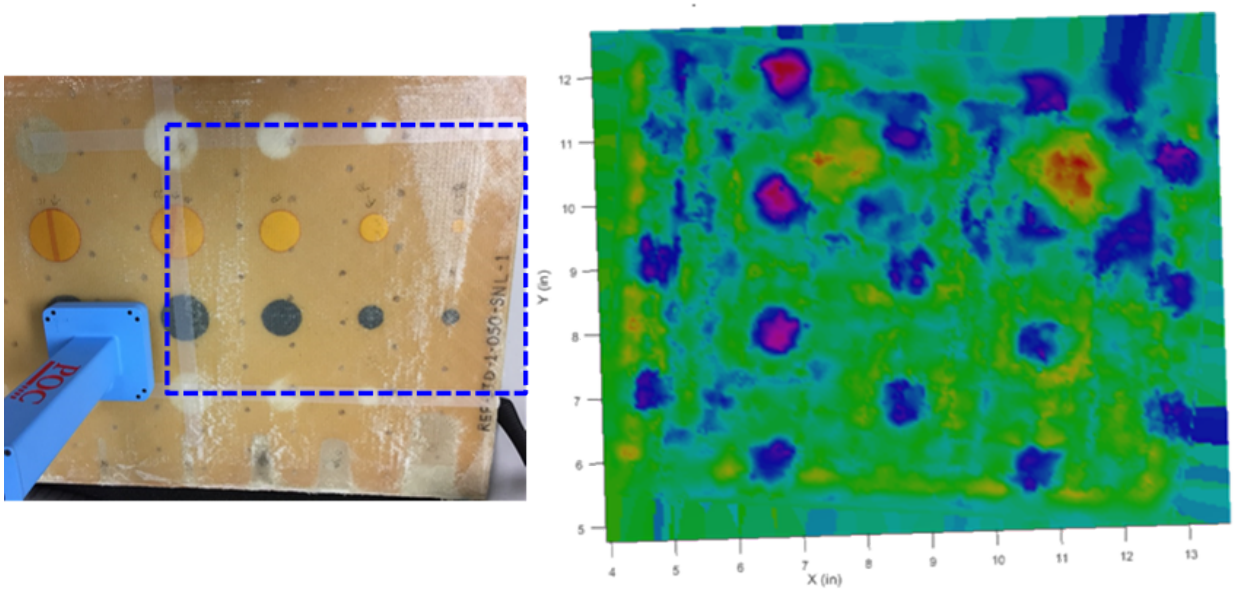

Figure 6-102: C-Scan Image Resulting from Inspection of WIND- REF-STD-1-050-SNL-1 Foam Core Specimen with POC MIT System

Evisive NDI Method: Microwave - While the Evisive Scan microwave inspection method had not been optimized for the WINDIE parts, the scan results do give the viewer an idea of the capabilities of the system on wind turbine blade sections. The images presented were created by the two separate hardware channels of the Evisive Scan transducer, each with two possible frequencies. A single scan was performed for each frequency. The two different frequencies differ in phase and hence in the depth at which the image is optimized.

Each wind part was scanned using the Evisive microwave imaging equipment. It can be seen in some of the results that the Evisive Scan system can detect and image unintentional defects in addition to the intentionally placed engineered flaws. In order to mark a flaw as detected, the scan image was reviewed and locations of areas where the return signal (voltage) differed from the general return signal for the part were identified. Where there was no direct correlation to a known surface feature that was intended by design (i.e. – label, bolt hole, etc.) it was reported as an indication in the part. Where possible, the indications were correlated to a possible cause based on previous experience with GFRP. Set up on calibration curves permits the depth of the flat bottom holes to be measured.

Two probes were used and overall the 10 GHz probe had a better signal to noise ratio than the 24 GHz probe. Flat bottom holes, pillow inserts, microballoons, out-of-plane waves, and pull tabs were imaged with the Evisive microwave technique in the spar cap laminate. However, the deeper flaws and the flaws in the adhesive bond line beneath the spar cap were more difficult to image and many of these flaws were not detected. The grease and mold release defects were not detected in either the spar cap or the adhesive joint and will need further testing to develop a reliable microwave method for detection.

- Using the Evisive NDI method, flaws are inferred by changes in the dielectric constant.
- Some probe lift-off issues were identified during the testing due to rough contours on the edges of some specimens. This made flaw calls difficult on some of the specimen edges.
- Probes could be deployed using two different scanning heads/gimbals for different deployment needs.
- Custom probes can be designed for specific applications if standard probes aren't appropriate.
- The 10GHz probe was selected for deeper penetration on thick specimens. The 24 GHz probe used did not have as much depth of penetration to detect flaws in thicker laminates.
- On specimen number 1 the inspector tested both the 24 GHz and 10 GHz probes in order to try and detect the grease contamination flaws.
- The 10GHz probe gimbal was not available during testing which would have allowed for inspecting curved/contoured specimens better
- Evisive has a hand held microwave inspection unit with encoding capability that may be appropriate for shear web bondjoints.
- The scanning system has a vacuum system that produces active suction cups for attachment to the surface being inspected.
- The scanning system also had varying indexing distances and scan speeds. It could also collect data in both directions (most common scan speed during the inspections was 2 in/sec).
- It was determined that the 10GHz probe provided better inspection results on wind specimens than the 24 GHz probe.

The Evisive scanning system with the 24 GHz transducer is shown on the left side of Figure 7-5. The 24 GHz transducer in the multi-axis gimbal is shown in the right side of this figure. This gimbal allowed it to be used on contoured surfaces.

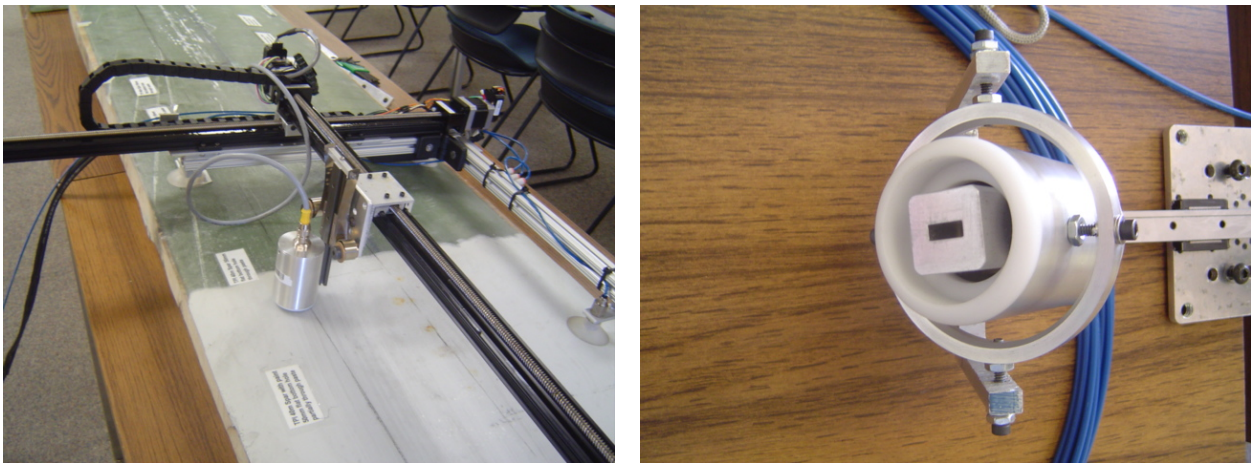

Figure 6-103: Evisive Microwave Inspection System with 24 GHz Probe

The Evisive scanning system with the 10 GHz transducer is shown in Figure 7-6. At the time the testing took place, the 10 GHz multi-axes gimbal was not available. A linear spring was used to keep the transduced in contact with the WINDIE specimen, but no couplant medium was needed.

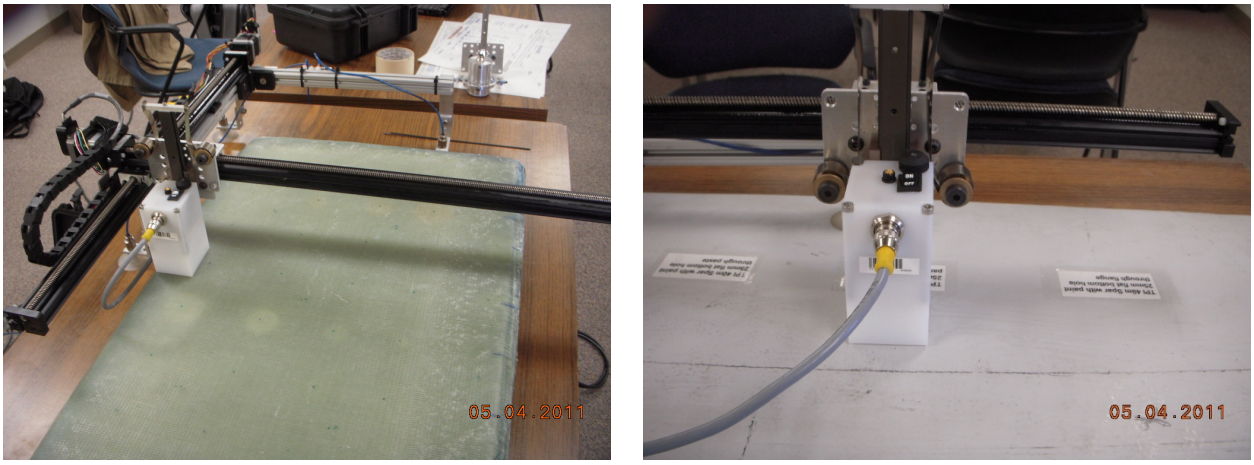

Figure 6-104: Evisive Microwave Inspection System with 10 GHz Probe

Voltage signals taken on an unflawed and flawed region of a WINDIE specimen can be seen in Figure 7-7. These signals can be compared to an A-scan signal generated in an ultrasonic inspection and are used to generate the microwave C-scan images. Figure 7-8 shows a microwave image of a specimen containing a series of flat bottom holes. The image indicates that the microwave method does have decent depth of penetration capabilities and can detect anomalies that are 0.9” deep.

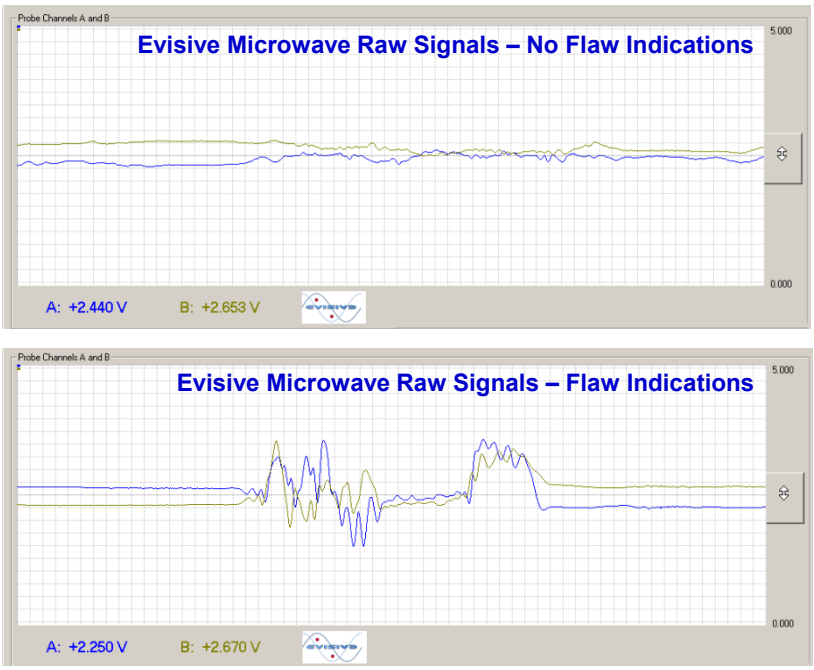

Figure 6-105: Signals Generated by Evisive Microwave Inspection System Showing the Difference Between Flawed and Unflawed Regions

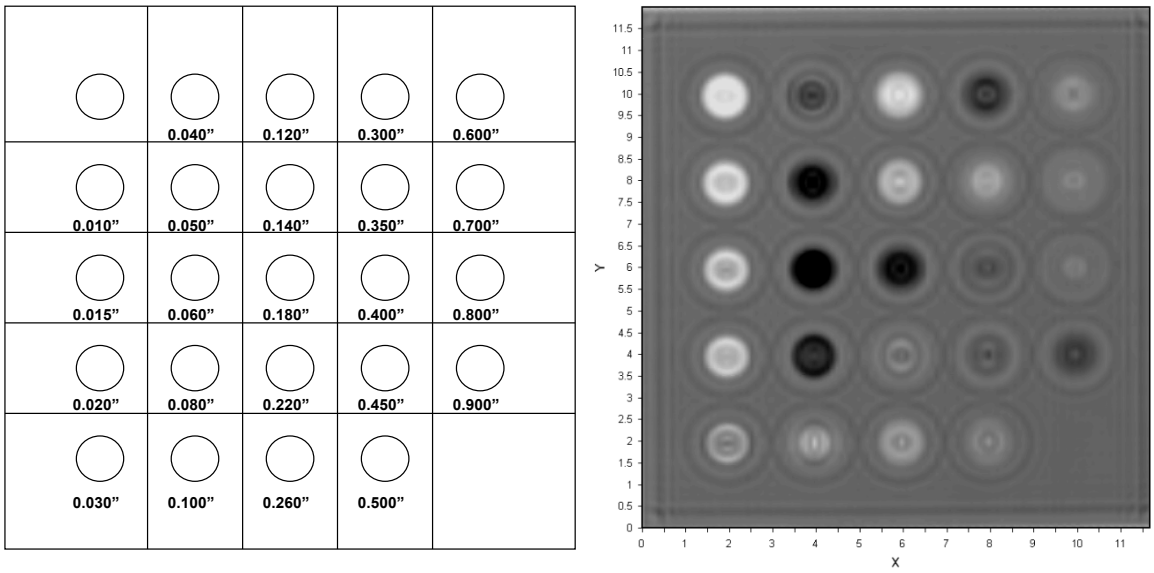

Figure 6-106: Evisive Microwave Scan of Fiberglass Wind Panel with Flat Bottom Holes Showing Depth of Penetration

Figures 7-9 and 7-10 show the inspection images produce by the Evisive microwave system when inspecting specimens REF-STD-1-050-SNL-1 and REF-STD-2-127-173-SNL-1, respectively. In Figure 7-9 pillow inserts and pull tab flaws are visible in the microwave scans.

The other flaw types (mold release, grease, microballoons) were not detected with this method in either the disbond or the delamination type of flaw designs. In Figure 7-10, flat bottom holes in spar cap laminate were detected at the various depths and the flat bottom holes in the bonded shear web joint were also detected. It appears that all sizes of the flat bottom holes were detected (difficult to see 75% FBH – 1.0" diameter in bonded shear web joint). Pull tab flaws in laminate at 25% depth were detected while the deeper pull tab flaws at 75% were not. None of the pull tabs in the shear web bonded joint, both at the upper and lower adhesive interface, were detected. Figure 7-11 shows microwave results for specimen REF-STD-3-129-176-SNL-1. The adhesive voids in the shear web bonded joint were detected (lower right portion of microwave image. The other flaw type that can be detected is the microballoons in the laminate spar cap. These are less clearly defined on the left hand side of the scanned image. None of the other flaw types, including all flaws in the adhesive joint, were detected.

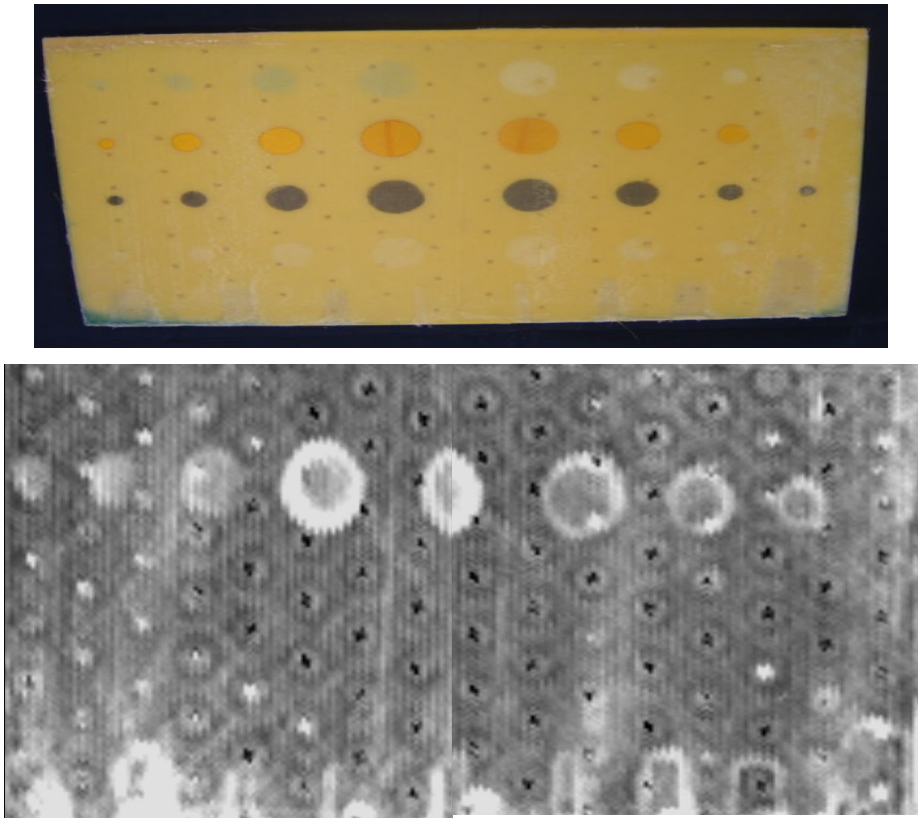

Figure 6-107: Evisive 24 GHz Microwave Scan of REF-STD-1-050-SNL-1 Foam Core Specimen

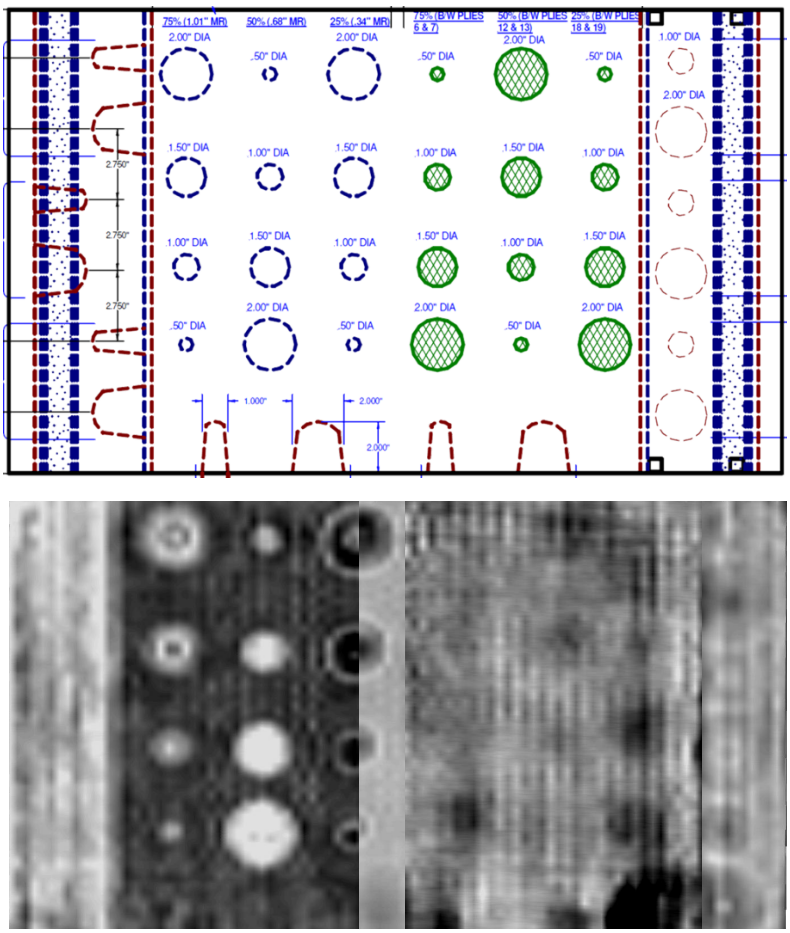

Figure 6-108: Evisive 24 GHz Microwave Scan of REF-STD-2-127-173-SNL-1 With Spar Cap and Shear Web Bond Line Flaws

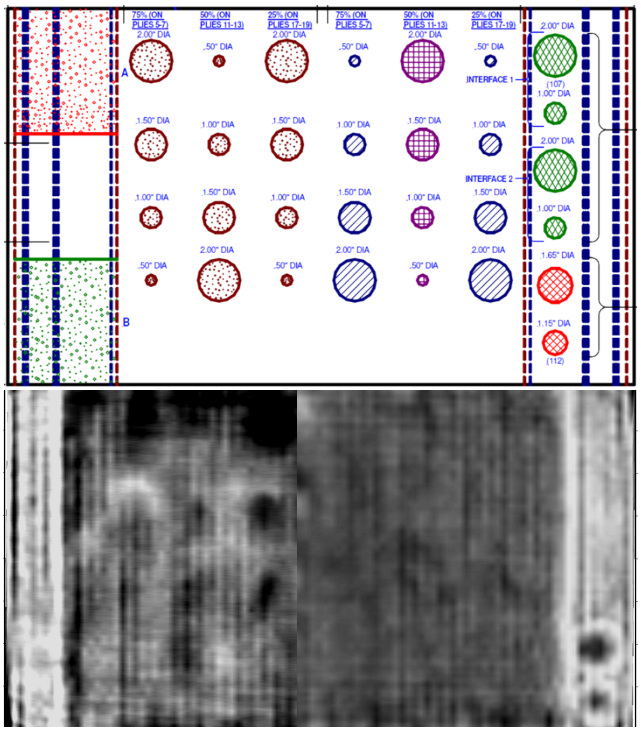

Figure 6-109: Evisive 24 GHz Microwave Scan of REF-STD-3-129-176-SNL-1 With Spar Cap and Shear Web Bond Line Flaws

Figure 6-110 shows microwave results for specimen REF-STD-4-135-SNL-1 (reference Figure 3-17). The out-of-plane waves were detected although the smallest wave was not as obvious in the microwave image. The same can be said for dry region flaws in this specimen where it appears that the larger regions can be detected and the single ply dry area is more obvious (shows up more clearly on image) than other dry regions composed of more layers of dry fiberglass plies.

Figure 6-111 shows microwave results for specimen REF-STD-5-154-SNL-1. No flaws were detected in this specimen although only the 24 GHz probe was used on this specimen and experimenters did not have chance to try 10 GHz probe which seemed to work better in the thicker laminates than the 24 GHz. Figure 6-112 shows microwave results for specimen REF-STD-7-214-265-SNL-1. The microballoon flaws are seen in the scanned image but the clarity is not very good. This microwave method was able to detect the adhesive voids in the bonded joint. In the area of the grease and mold release flaws there are some lighter areas that show in the scan and they would consider these areas of interest, but is doubtful that an inspector would delineate these as flawed areas.

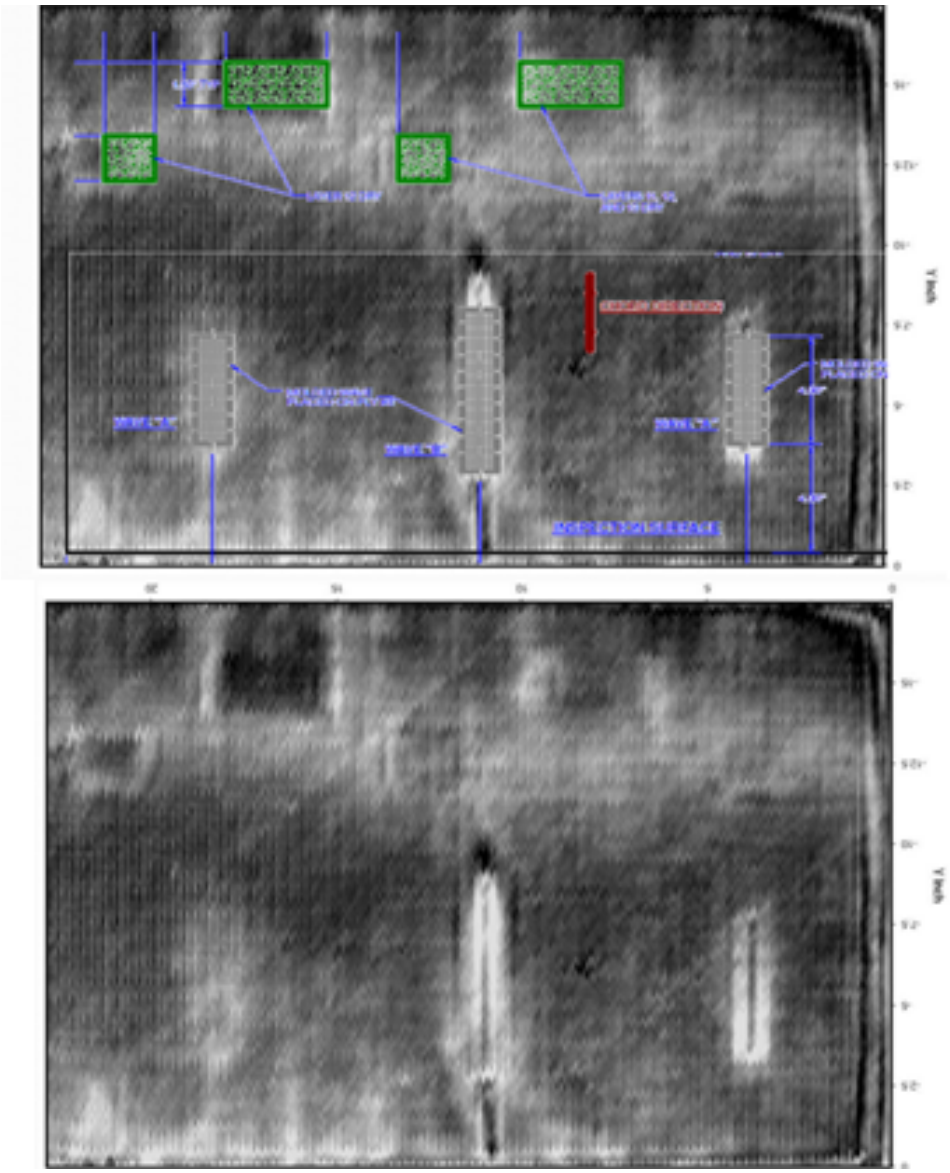

Figure 6-110: Evisive 24 GHz Microwave Scan of REF-STD-4-135-SNL-1 With Out-of-Plane Waves and Dry Regions in the Laminate

Figure 6-113 and Figure 6-114 show microwave results for specimens Wind-2-044-SPAR-085 and Wind-3-110-SPAR-150, respectively. These specimens represent thin and thick spar caps and include the adhesive joint at the spar cap-to-shear web flange interface. It can be seen that most of the flat bottom holes are detected in the microwave images with the exception of the most challenging flaws that are located on the back side of the adhesive bond line. These flaws are further away from the inspection surface and are very close to the back wall surface making it difficult to image the very small difference in wave travel.

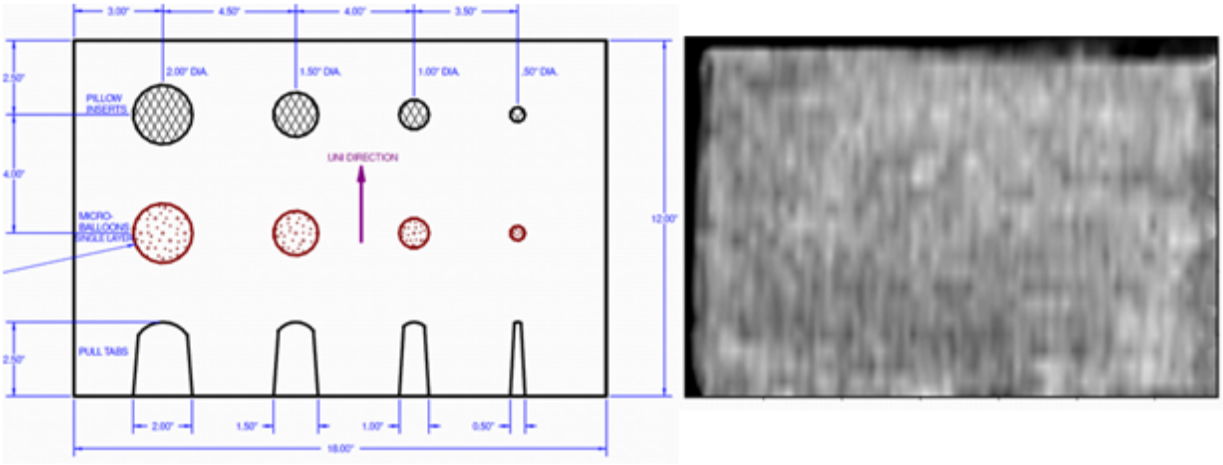

Figure 6-111: Evisive 24 GHz Microwave Scan of REF-STD-5-154-SNL-1 With Trailing Edge Flaws

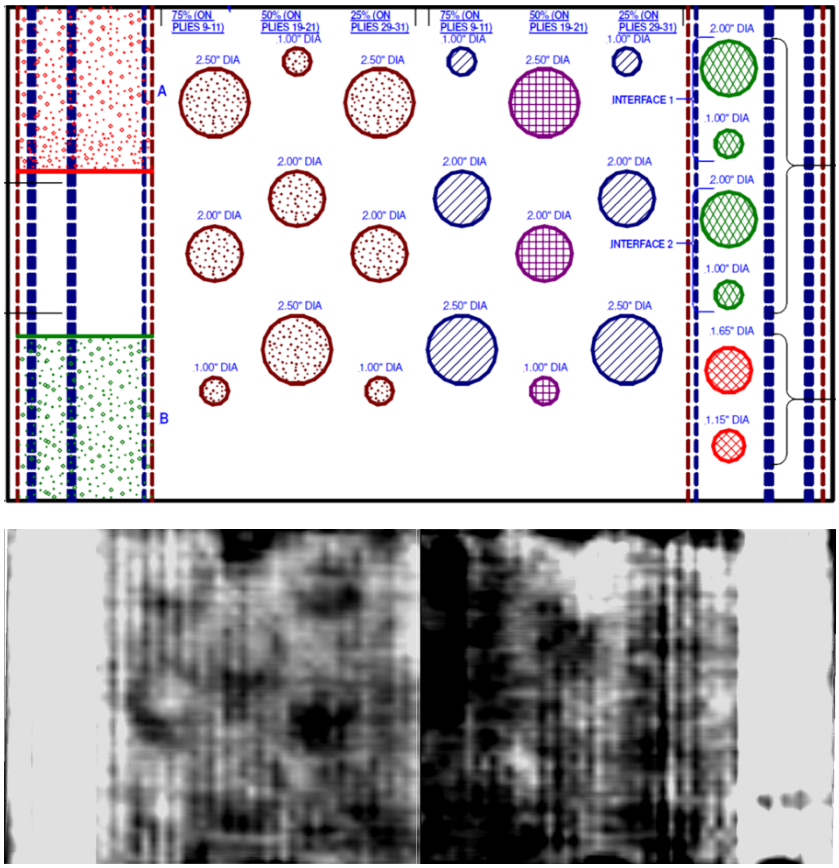

Figure 6-112: Evisive 24 GHz Microwave Scan of REF-STD-7-214-265-SNL-1 With Thick Spar Cap and Shear Web Bond Line Flaws

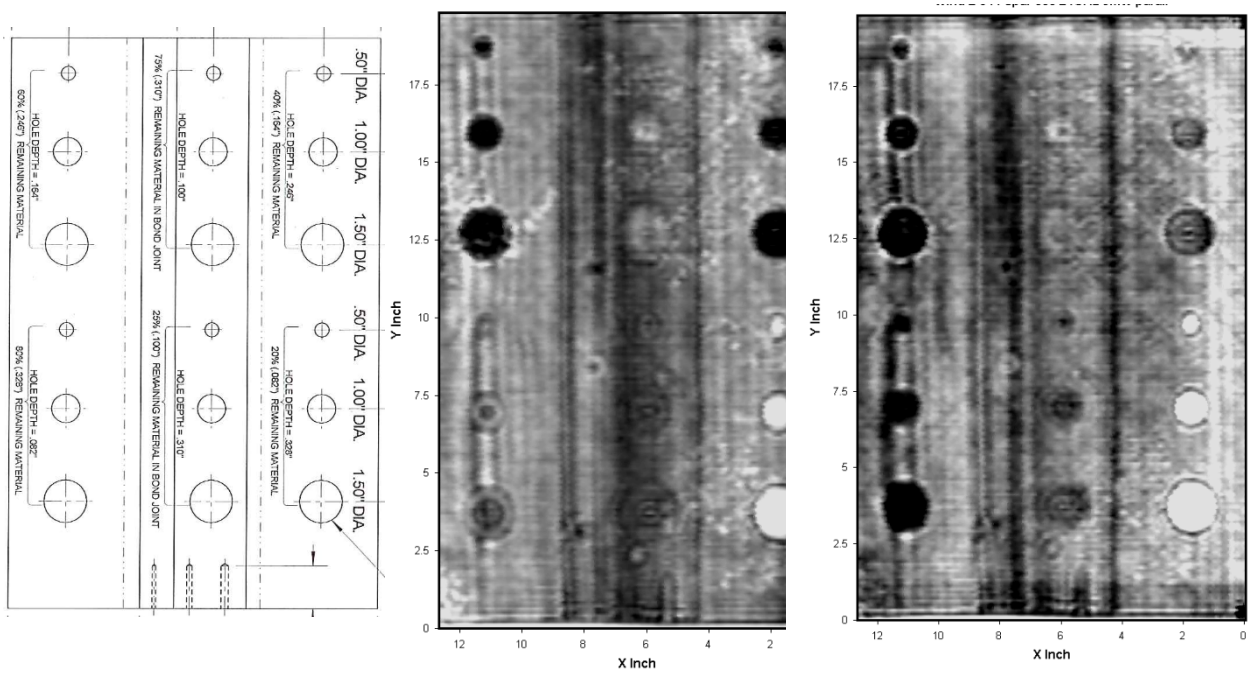

Figure 6-113: Images of Specimen Wind-2-044-SPAR-085 Showing Evisive Microwave Results for Flat Bottom Hole Flaws in Thin Spar Cap (0.44" th) and Adhesive Shear Web Bond Line (0.85" th.)

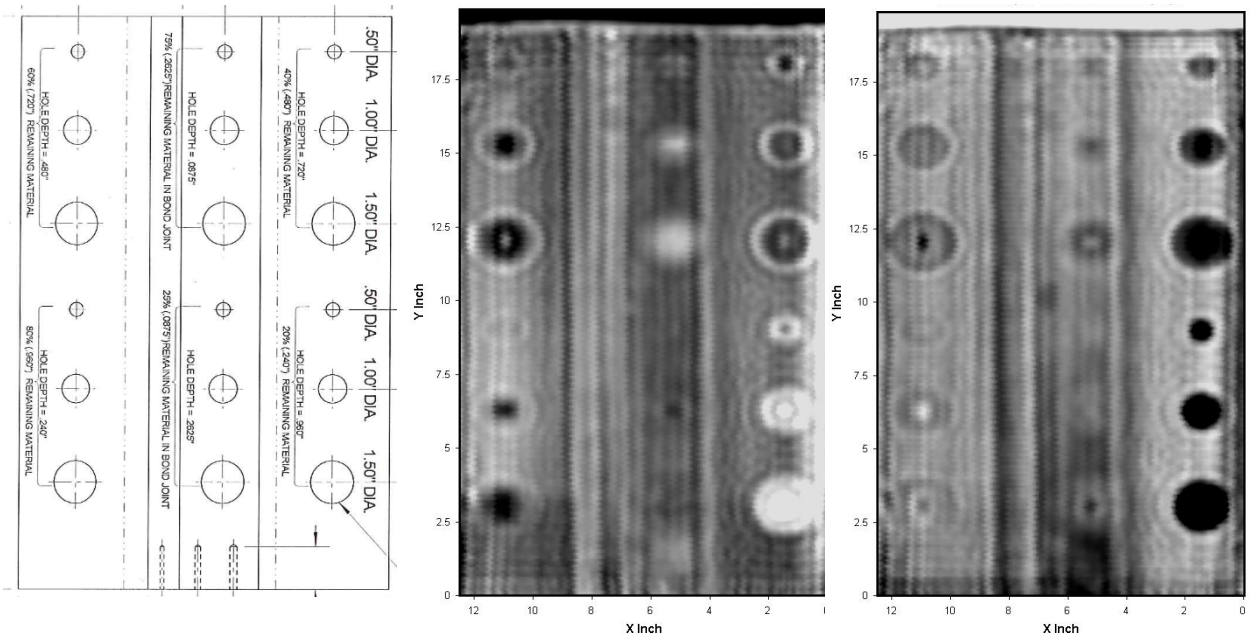

Figure 6-114: Images of Specimen Wind-3-110-SPAR-150 Showing Evisive Microwave Results for Flat Bottom Hole Flaws in 1.1" Thick Spar Cap and

Figure 6-115 shows microwave results for specimen WIND-6-180-SPAR-220 which is made from a spar cap that was cut from a blade. Once again, it is observed that all of the flat bottom holes were detected; however, to the "untrained eye," they may not be obvious due to the subtle contrast in the microwave images.

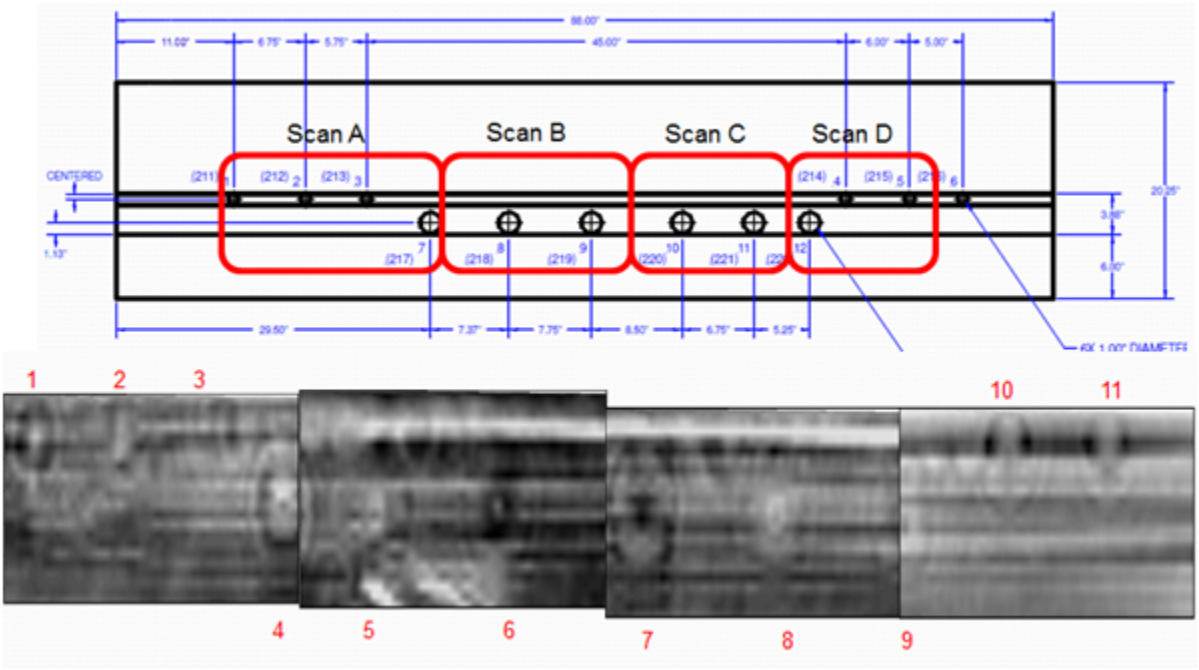

Figure 6-115: Images of Specimen Wind-6-180-SPAR-220 Showing Evisive 10 GHz Microwave Results for Flat Bottom Hole Flaws in 1.8" Thick Spar Cap and 2.2" Thick Adhesive Shear Web Bond Line

Conclusions on Evisive Microwave:

- The Evisive Scan method can be used on glass reinforced composite components to detect some defects and internal structure.
- Defects are detected by detecting changes in electromagnetic properties or the location of changes in such properties (as in a part surface).
- The 10 GHz probe had a favorable signal to noise ratio over the 24 GHz probe.
- Some of the flat bottom holes, pillow inserts, microballoons, wrinkles, and pull tabs were imaged with the Evisive technique.
- Grease and mold release defects will need further testing to develop a reliable method for detection.
- Defects of a size comparable to those intentionally introduced in the supplied parts are detectable, even in the presence of complex structure and significant thicknesses.
- For parts with a solid laminate thickness of up to 1.5 inches, the preferred interrogation frequency is 24 GHz. For thicker laminates, the preferred frequency is 10 GHz. Part number Wind-3-11-SPAR-150 was inspected using a 10 GHz Evisive Scan transducer. All other parts were inspected at 24 GHz. The resolution of the 10 GHz transducer is slightly

diminished, compared to the 24 GHz, but is adequate to detect and size the defects presented here.

- A standard 24 GHz, 5 Mw transducer was used when inspecting these parts. Transducers with higher power outputs are available, should field inspections require them. Additionally, probes with finer resolution due to smaller beam spots can be deployed.

6.5 Preliminary Efforts to Explore Wind Blade Inspection Training

Technology transfer and training initiatives were initially explored as part of the first phase of the Sandia Labs wind NDI work. Specifically, several site visits were conducted at the TPI Composites wind blade manufacturing plant in Newton, IA. The primary purpose of the site visits was to study the application of advanced NDI methods developed by Sandia Labs. However, the visits also allowed Sandia to familiarize factory inspectors with an array of inspection methods and allow them to try these techniques out on actual blades on the production floor. This included both single-element and phased array ultrasonics deployed in a scanning mode to create two-dimensional C-scan images. Figure 6-116 shows the use of two different ultrasonic methods of inspection that were deployed during these preliminary training efforts.

Figure 6-116: Blade Inspections on Factory Floor - MAUS V Scanner Deploying UT Single Element Focused Probe (left) and Inspector Practicing a Shear Web Bond Line and Spar Cap Inspection Using Phased Array Transducer with Linear Position Encoder (right)

Inspections were performed at the same time in the fabrication process as when the blades are typically inspected. The majority of inspection time was focused on inspecting the critical shear web to spar cap bonded joints on fully assembled blades. The scanner was set up and multiple gate settings were tested to obtain optimum scans. The width of the bond was determined using the adhesive "squeeze out" on each side of the bond line and was differentiated from the web bond interface itself as shown in Figure 6-117. The adhesive paste squeeze-out on either side of

the bond line is shown in dark blue and the bond line itself is shown in bright yellow between the squeeze out. Similarly, flaws in the spar cap and bond line interfaces can be detected.

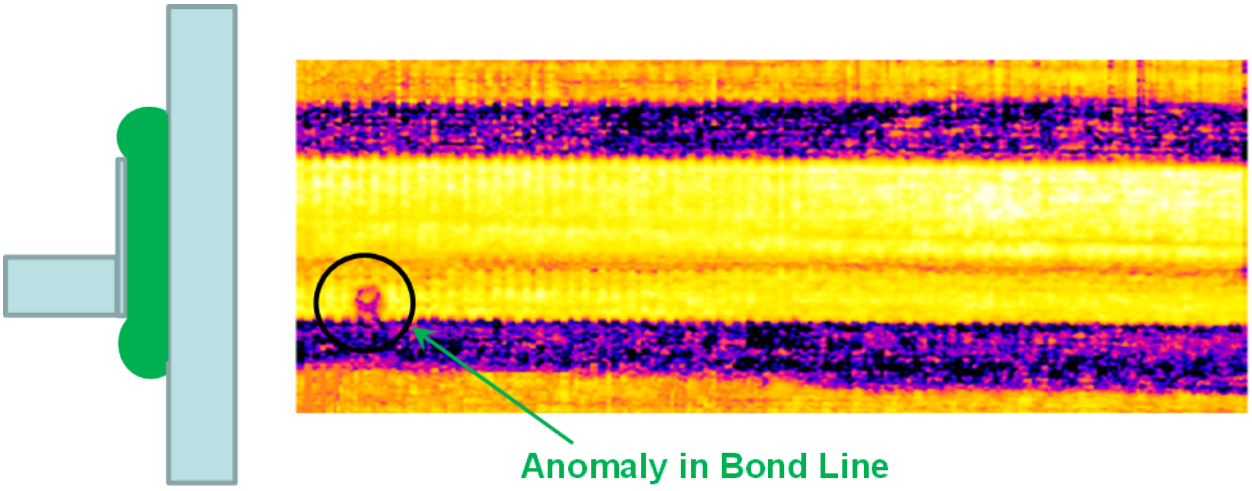

Figure 6-117: Results from Bond Line Inspections Using UT Focused Immersion Probe – Adhesive Squeeze-Out is Imaged as is the Anomaly in the Bond Line

The phased array ultrasonic (PA-UT) inspections used a linear position encoder to provide a real time C-scan image on the screen of the OmniScan device. This showed the inspector's how such a method works well for large area scanning. It also showed that PA-UT produces high resolution, deep penetrating scans that can be saved for further analysis. A wide area probe can be used to take large swaths of data, thus minimizing scan time. The inspector can not only monitor amplitude data, but also use C-scan and sectorial images when hand scanning with phased array. This allows the inspector to take multiple passes over the same inspection zone and further investigate areas of interest. One important instruction item that provides a good example of the value of the training pertained to the thickness of the transducer delay line. Inspectors were shown how harmonic surface reflection signals can interfere with the back wall signal of interest. Figure 6-118 shows some of the results from two different thickness delay lines and how the front surface reflection signal can be shifted when the thickness of the delay line is changed. It was determined that a 40-millimeter-thick, water-filled and sealed delay would provide good signal quality and allow for factory deployment of a phased array probe. Trial results were used to show inspectors how to optimize their results for the best flaw detection.

There were two parts to the training. The first was a classroom portion which included a general introduction to phased array including what a phased array probe is composed of, parameters involved when setting up a phased array inspection, and considerations involved when selecting a phased array probe. While the set of lecture notes, described here, was not used, ad-hoc lectures revealed the value of basic NDI physics discussions coupled with specific hardware optimization discussions. The hardware was then introduced and the hands-on portion of the training was conducted. Figure 6-119 shows the "classroom" portion of the training package

being presented to a wind blade manufacturing company inspector. Due to inspectors varying schedules, the training was split up and conducted when time allowed with each inspector.

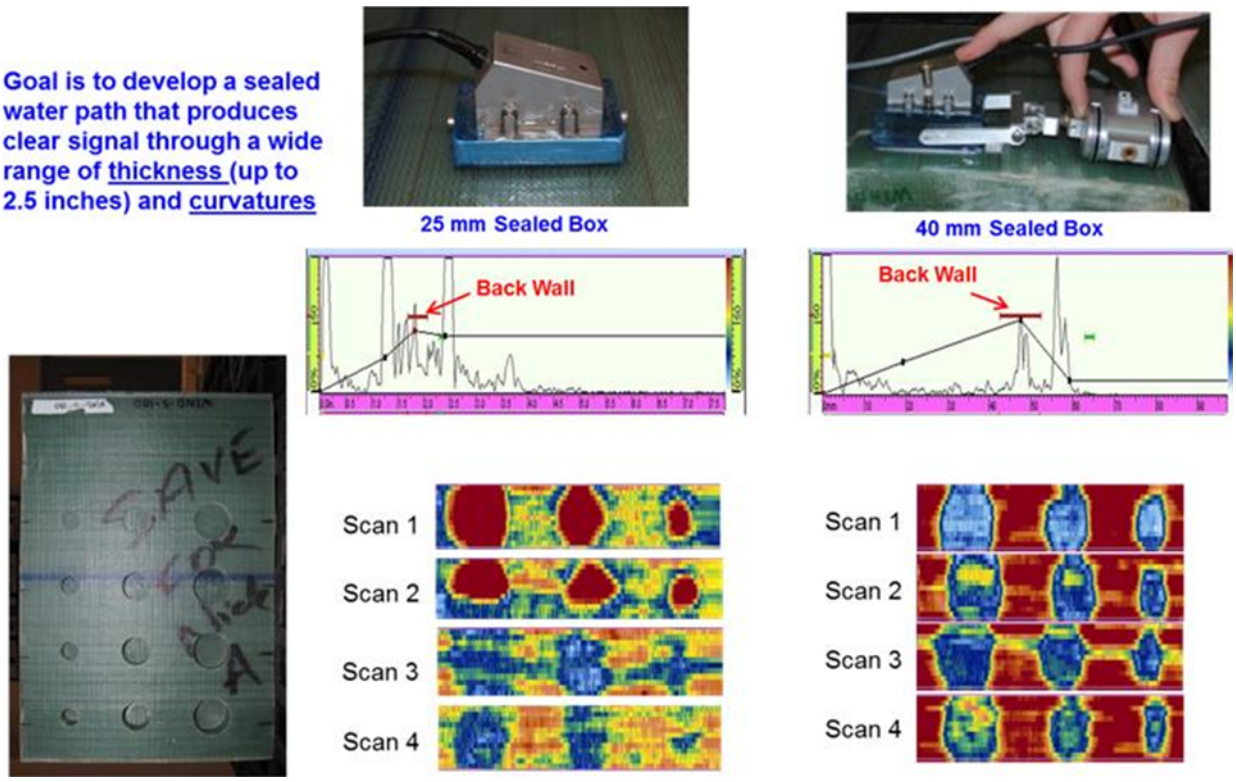

Figure 6-118: A-Scan and C-Scan Images Showing How Delay Line Thickness Effects Signal Clarity

The second part of the inspector training was the hands-on portion where the inspectors were able to use the phased array hardware. This part of the training involved using the OmniScan with the phased array probe, linear encoder and custom designed sealed water box on various fiberglass and carbon samples. In this part of the training the inspectors were able to perform scans on actual wind blade parts and on blades during the manufacturing process. Figure 6-120 shows the hands on portion of the training being conducted with three inspectors and an inspector practicing using the phased array equipment on a fiberglass spar cap.

Figure 6-119: "Classroom" Portion of Trial Phased Array Training Being Presented to a Wind Blade QA Inspector

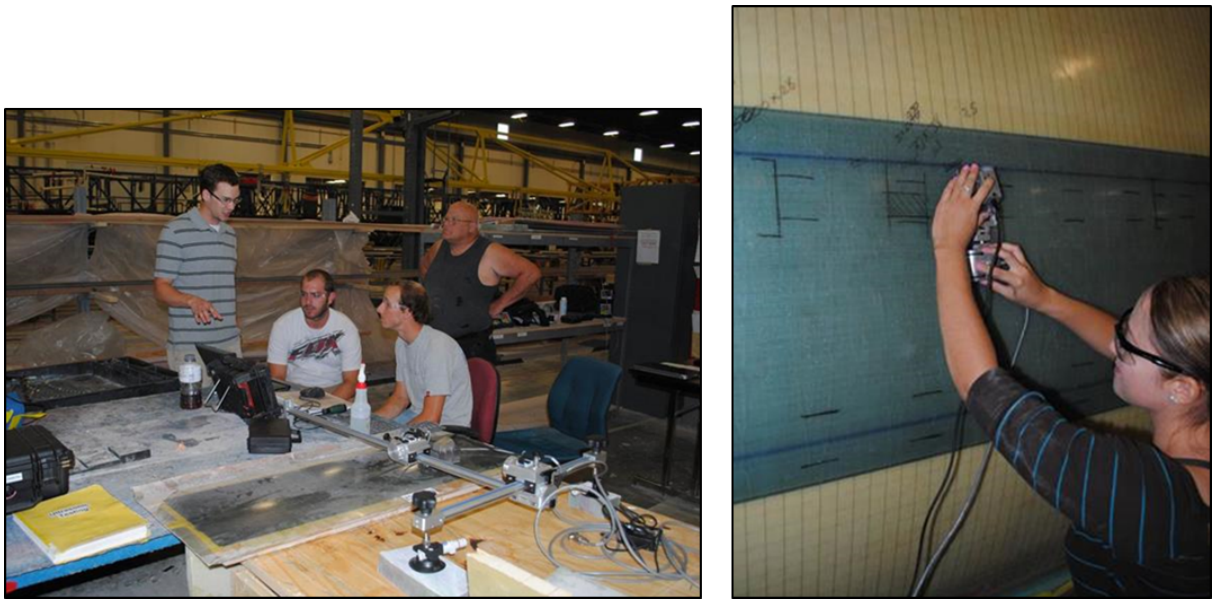

Figure 6-120: Hands on Equipment Introduction Being Presented to Blade Inspectors and an Inspector Completing a Trial of Phased Array Inspection Process

The spar cap bond line inspection on the 47 meter blades being produced at the time of the technology transfer and preliminary training visit were performed in the same manner as the inspection on the 40 meter blade. Initial inspections utilized a low frequency, single-element

ultrasonic transducer in an A-scan inspection mode. The entire length of the shear web to spar cap bond line was inspected on the blind bond side to ensure full width adhesive paste and to detect voids. While performing the width inspection the inspector drew dashed lines on the blade at the edges of the shear web. Lines drawn on the blade showing where the two shear webs are located can be seen in Figure 6-121. The first part of the inspection was to verify sufficient width of the bond line by crossing the transducer vertically over the bond while watching the ultrasonic reflection in an A-scan. Specifically, the inspector monitors for signal shift created by the adhesive squeeze out on either side of the shear web flange. Squeeze out can be seen in the A-scan data produced on either side of the shear web flange (Figure 6-121). Next, this inspection technique was used to detect adhesive voids and defects within the bond line. Figure 6-121 shows typical A-scan signals within a bond line containing voids at two different interfaces of the bond. It can be seen that there is a shift in the adhesive back wall signal and drop in amplitude when the transducer is placed over a void.

The bond line inspection was also performed using phased array with a position encoder. The phased array hardware used for this inspection can be seen in the lower left hand side of Figure 6-122 and included the 16 element phased array probe, sealed water box and linear encoder. The inspection result shown in the figure was conducted on a section of the blade that had an adhesive void. This area provided an ideal section of blade to demonstrate the PA-UT inspection hardware. C-scan inspection results can be seen in the middle of Figure 6-122. The scans on this particular section show that there is a decrease in amplitude in the upper bond line. This is shown in the scan and indicates a void in the adhesive (same back wall signal as the spar cap, blue color). This is based on how the gates were set up in the OmniScan. On-blade testing gave insights into factory deployment issues and provided real-life lessons in the following areas:

- Challenges associated with vertical and horizontal inspection surfaces
- Hand scanning – time based scanning verse linear position encoding and robotic scanners
- Flowing water and UT coupling methods
- Water box housings for phased array deployment
- Range of thickness and curvatures.

To further investigate the PA-UT inspection method, time based scanning was utilized on defects identified in a bond line. Figure 6-123 shows scans performed at 18 and 20 meter stations of a blade with voids in the bond line. The red gate in the lower right side of the figure was used to track the amplitude of the spar cap back wall signal. When the gate is set in this way, a void in the bond line results in an increase in the back wall amplitude and is shown in red in Figure 6-123. This gate setting is only preferred when inspecting for disbonds between the adhesive and the spar cap, not at the adhesive-to-shear web flange interface. The scans indicate that the disbond is at the spar cap to adhesive interface.

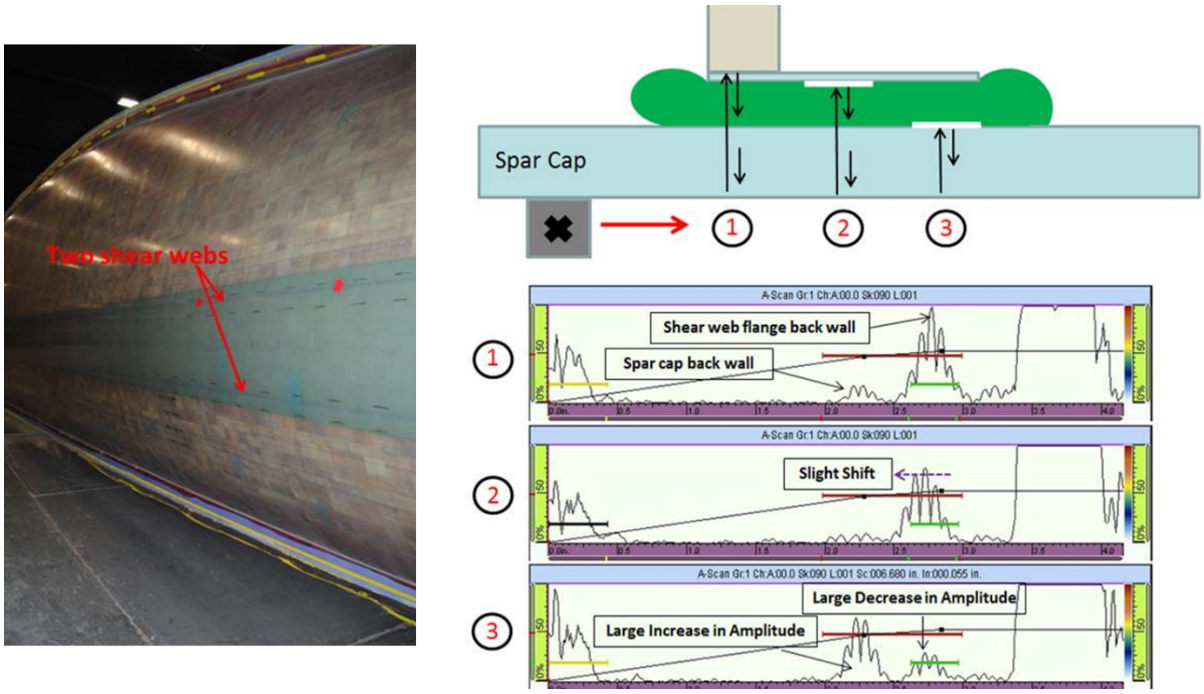

Figure 6-121: Forty-Seven Meter Fiberglass Spar Cap Blade Showing Locations of Shear Web Bond Lines and Flaw Interpretation of Signals from Hand Deployed PE-UT

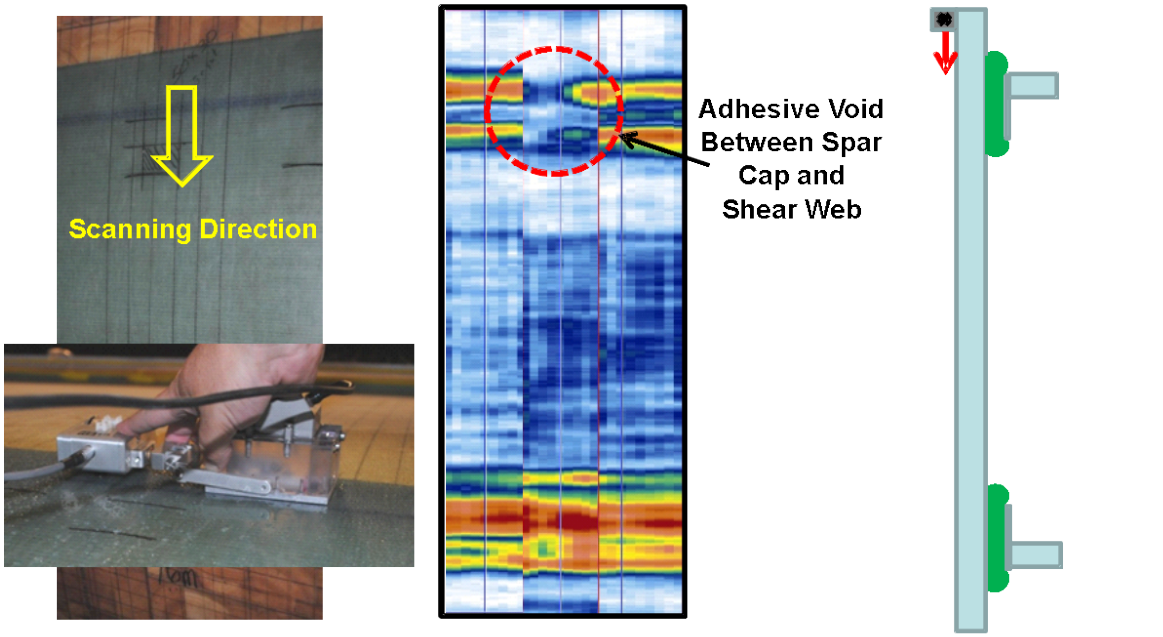

Figure 6-122: Detection of Disbond/Adhesive Void in Bond Line Using 1.5L16 Phased Array Transducer, Sealed Water Box Shoe and Linear Encoder

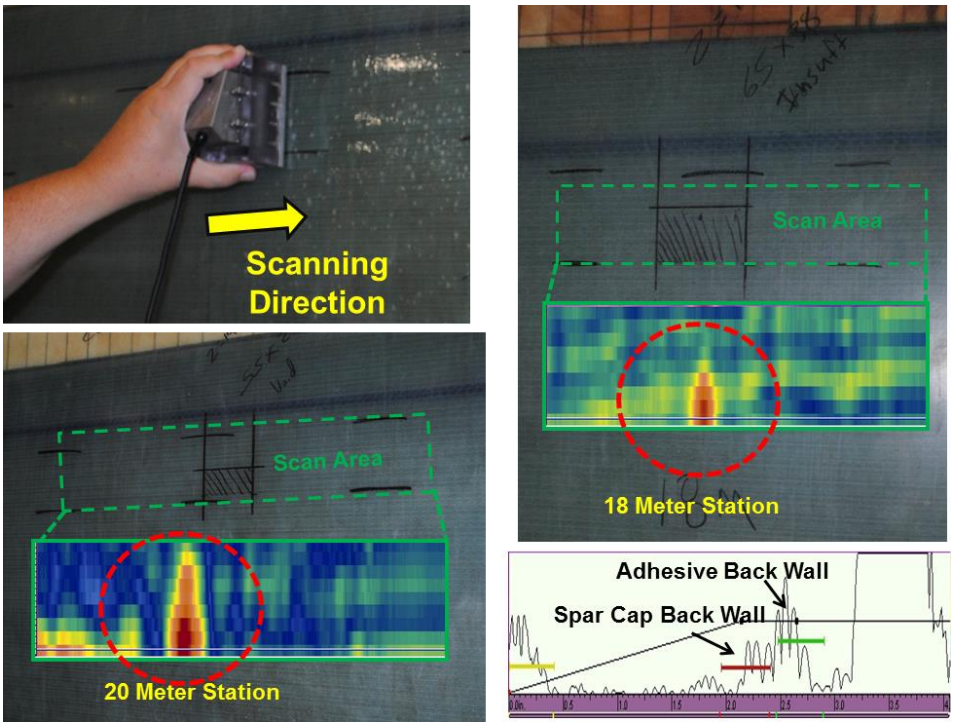

Figure 6-123: Bond Line Inspection and Results Performed with Time Based Phased Array

Single-Element and Phased Array Ultrasonic Inspection Procedures - Formal procedures are an essential element of any inspection. Currently, inspectors are provided with basic guidelines, however, the training package described here will produce very detailed procedures regarding equipment set-up and deployment with sample signals to ensure that proper data is being obtained. Sample topics to be covered in the inspection procedures include:

- Optimum hardware selection
- Set-up of the major components such as phased array ultrasonic probes, single-element ultrasonic probes, delay lines, use of coupling medium, use of position encoders or X-Y scanners, inspection control devices (e.g. OmniScan, Sonatest, Phasor)
- Adjusting water box delay line to achieve best UT signal clarity
- Use of NDI Reference Standards for initial calibration
- Typical A-scan signals and C-scan images for pristine structure to establish a proper baseline
- UT gate settings
- Use of time corrected gain to optimize signals of interest
- Sample A-scan signals and C-scan images for various types of flaws
- Use of horizontal and vertical interrogation (scanning) across area of interest
- Signal interpretation and defect detection

One example benefit of using the formal NDI procedure is when using PA-UT to inspect the bond line. Specific procedures with sample results will be provided to show how it is possible to differentiate between insufficient adhesive paste and an adhesive void. When there is insufficient adhesive in the adhesive joint, a radius of adhesive forms scattering the sound and causing a decrease in signal amplitude. The scan in Figure 6-124 shows how insufficient adhesive paste scatters the ultrasonic waves due to the geometric features associated with the lack of adhesive (the two defects that are blue in the C-scan). Also shown in the figure is an adhesive void which resulted in an increase in the spar cap back wall amplitude (the defect that is red in the C-scan on the right). A-scans explaining these anomalies and how they affect the amplitude of the ultrasonic reflections will be provided in the inspection procedures.

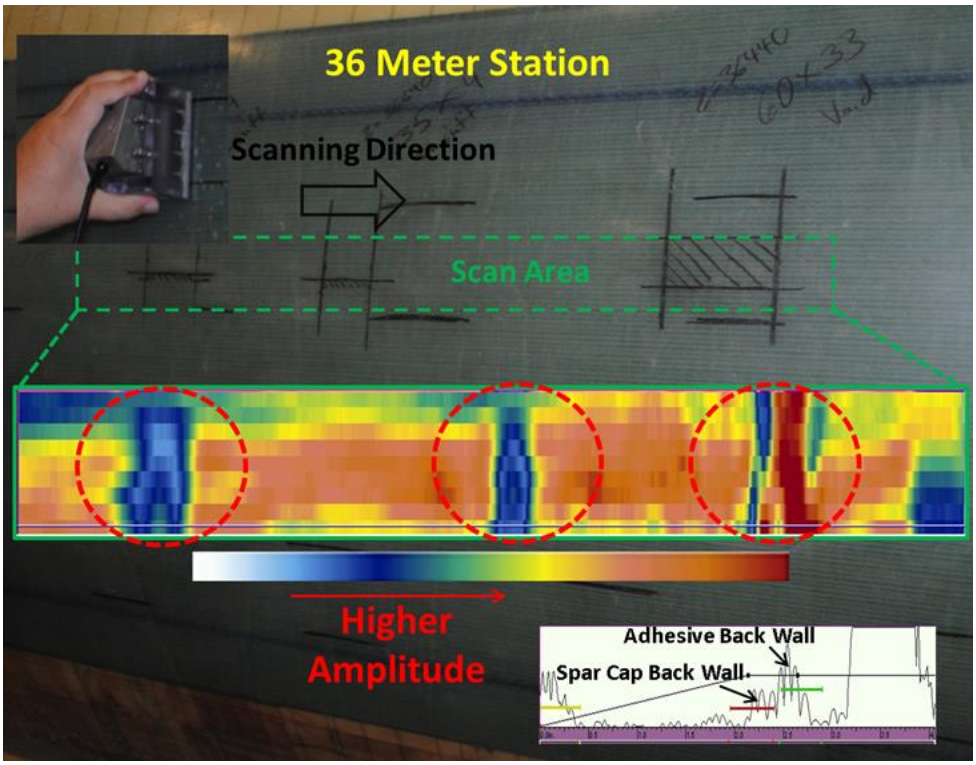

Figure 6-124: Shear Web Bond Line Inspection Indicating Insufficient Adhesive and an Adhesive Void

NDI is also necessary to firmly establish if repairs are needed and to determine the necessary size and extent of blade repairs. As the wind blades have become larger and more expensive, there is a corresponding desire to install more extensive and invasive repairs that reach many layers in depth and are placed on and around primary structure such as spar caps and root sections. The criticality of these repairs will then require the use of through-thickness depth inspection methods to ensure the quality of the repair (post-repair inspections). Such inspections will detect undesirable repair flaws that may be hidden by non-uniform resin flow and ply edge effects that are present in repairs.

Value of Wind Blade NDI Training – It has been discussed in detail and POD data analysis has been presented to describe how NDI training lead to direct improvements in the capabilities of wind blade inspectors to detect flaws and damage in the blades. In addition to the concrete examples discussed in the preceding section above, other benefits derived from the training can be quantified through additional experiences from Sandia with the Wind Blade Flaw Detection Experiment. Specifically, direct improvements in Probability of Damage Detection were quantified through several focused tests within the WBFDE.

The first instance involved the work of a very new inspector. This inspector was in his first week of regular QA inspections. The level of training received by the inspector prior to his participation in the WBFDE is unknown, however, he was rated by the wind blade manufacturing company to conduct independent QA inspections on their blades. Thus, the inspector, recorded as Inspector Z1, was rather new to his equipment. The Sandia inspector traveling with the experiment was an ASNT and NAS certified Level III inspector so he provided some cursory training for this new inspector on how to use the equipment on the feedback panels. However, after the first panel we noticed that Inspector Z1 was still struggling as highlighted by Table 6-38. The Sandia Level III inspector then conducted some more detailed training with specialized instruction on what to look for during inspections, amplitude drops, signals shifts, etc. After this focused training, Inspector Z1 returned to the blind WBFDE inspections. His results improved dramatically. In fact, Inspector Z1 actually performed better than the other inspectors on the next 8 panels. See table below. One of the observations is that the new inspector seemed to take his time, while paying careful attention to all aspects of the UT signals. Table 6-39 quantifies the degree of improvement experienced by Inspector Z1 after more extensive training.

Inspector	Inspection Experience	Insp. Time (H:M)	Total Flaws 1 Panel	Misses	Hits	% Flaws Found
Z1	1 Week	0:31	13	7	6	46.15%
Z2	1.5 Years	0:36	13	3	10	76.92%
Z3	7 Months	1:14	13	2	11	84.62%

Table 6-38: Results Comparing the Performance of a New Inspector with Little Training to the Performance of More Experienced Inspectors

Inspector	Inspection Experience	Insp. Time (H:M)	Total Flaws 8 Panels	Misses	Hits	% Flaws Found
Z1	1 Week	8:06	84	4	80	95.24%
Z2	1.5 Years	7:59	84	11	73	86.90%
Z3	7 Months	7:31	84	7	77	91.67%

Table 6-39: Results Comparing the Performance of a New Inspector with More Extensive Training to the Performance of More Experienced Inspectors

The second instance relates to the value of providing hands-on exposure to realistic inspections/structures and the associated feedback to help inspectors improve. In the cases of two different blade manufacturers, after they sent one inspector participate in the WBFDE, these companies later asked if we could visit their facility and have all their inspectors participate. They realized the value of the experiment and the training aspect for their inspectors. In both cases we were able to provide individual and company-wide results.

The third instance sited here pertains to improvements stemming from the feedback inspectors received on the inspections of the wind blade test specimens. For the advanced experiment, there were many opportunities to help inspectors with a "second look". After grading the results, we were able to send feedback to the inspectors and ask that they take a second look for flaws that they missed, solely for training purposes. Since most advanced methods capture full wave data the inspectors could reanalyze areas to look for any flaws that they may have missed. In most cases, the flaws were easily found upon reanalysis of the data. This highlights the extensive array of human factors issues that influence the performance of an inspector.

In one example, an inspector was knowledgeable in setting his ultrasonic gates for data acquisition, however, the gates were not optimized. This resulted in the missed detection of a rather large flaw as shown in Figure 6-125. Upon re-examination of the data, the inspector was influenced to adjust his gate settings. This resulted in the C-scan image shown in Figure 6-126 which clearly shows the damage. Figure 6-125 and Figure 6-126 also compare the resulting POD values with and without this damage detection. It can be seen that this improved data analysis resulted in a 28% improvement in the inspector's performance. Similar analysis on the rest of his data could have an even more significant effect on the inspector's overall performance and future capabilities. Other examples quantifying the value of an enhanced wind NDI training regimen are provided in Section 6.2.2 above.

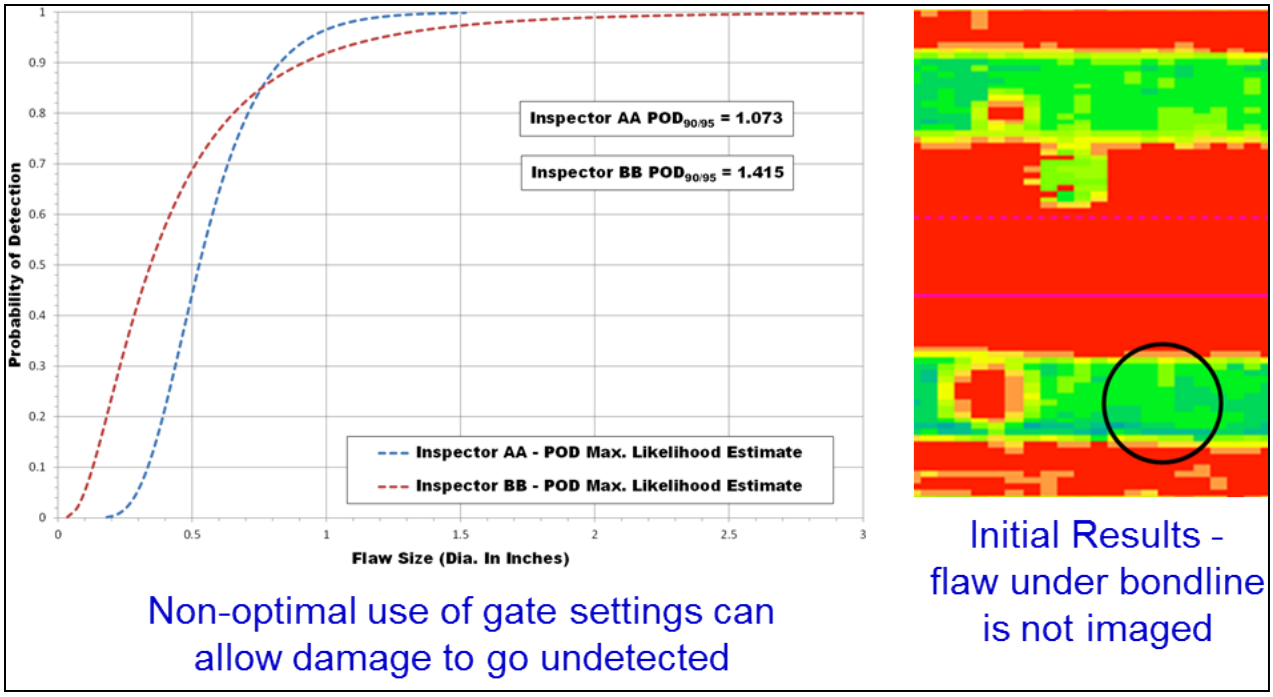

Figure 6-125: WBFDE Results for Inspector BB with Non-Optimal Gate Settings

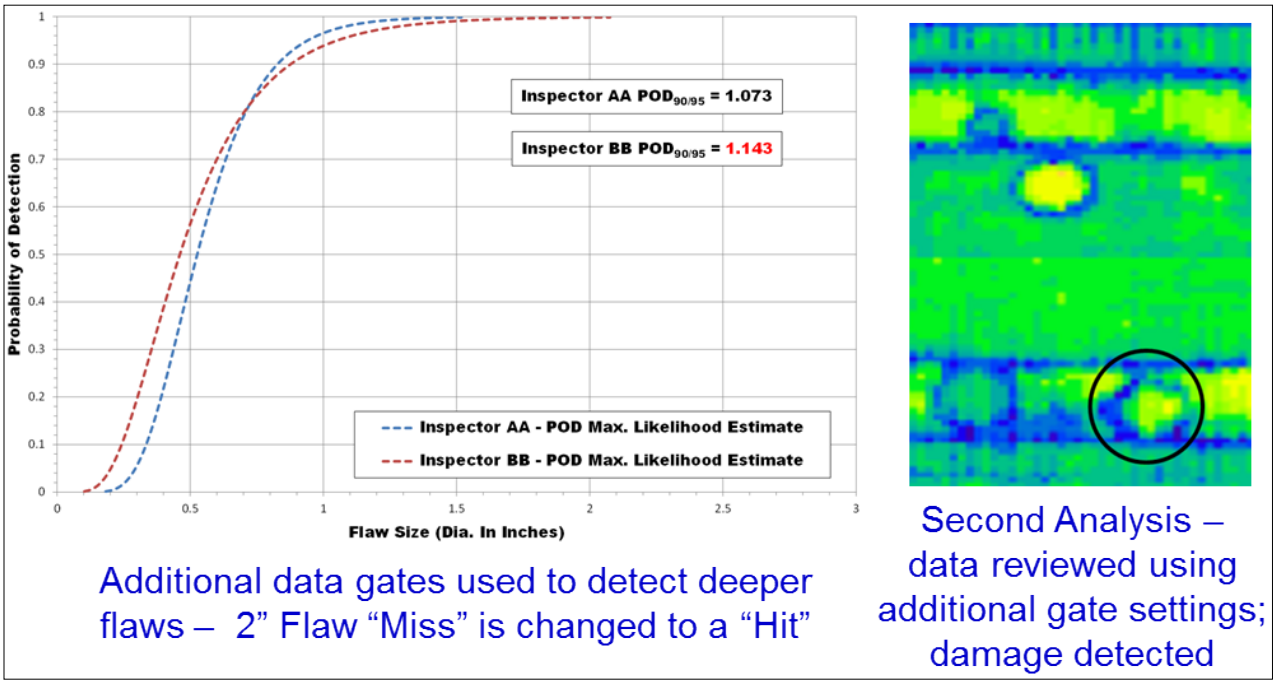

Figure 6-126: Improvements in WBFDE Results for Inspector BB with Better Data Analysis Settings

References

6.1 Roach, D., "An Inspector Calls - The Search for Hidden Flaws in Composite Honeycomb Structures," *Journal of Aerospace Testing International*, February 2004.

CHAPTER 7

7.0 Conclusions and Recommendations

7.1 Overview Thoughts on NDI for Wind Blade Structures

There is large uncertainty in the lifetime cost of maintaining and operating wind turbine rotor blades. Blades are designed for a 20-year life while blade replacements affect approximately 2-3% of the fleet per year, and typically cost $200,000 to $300,000 per replacement. The cost of these replacements is spread out over OEMs, owner-operators, and insurance companies, affecting all major components of LCOE. Furthermore, the causes are varied and range from design and manufacturing defects, to transportation and installation damage, to operational damage. The cost of these failures can be only be alleviated by appropriate flaw/damage detection and repair. However, current industry practices in diagnosing and repairing defects and damage are non-standardized and in many cases inadequate. This activity seeks to address this problem by producing improvements in inspection practices to ensure higher reliability from the factory and early detection of damage occurring in the field. The best non-destructive inspection (NDI) methods need to be implemented in factories to prevent blades leaving with flaws. The blade service industry needs reliable NDI methods that are fieldable and which can address all areas of blades.

The reliability of wind farm structures has a decisive impact on the profitability of a wind farm. To minimize the risks of costly downtime and repair periods and ensure successful functioning of a wind farm, it is necessary to conduct in-service inspections. At a minimum, in-service inspections and end-of-warranty inspections can detect imminent failures of critical components at the earliest stages, thereby, minimizing the risk of costly repair periods. As the length of blades increase and operational environments produce high stress levels in the blades, it has become increasingly important to detect the onset of damage or the propagation of fabrication defects during blade operation. The need for in-service NDI of blades at wind farms is growing. In-service NDI is critical to assess and detect defects, even those that were not seeded by manufacturing problems. Small defects can propagate to levels of concern during blade use while fatigue loading, bird/hail impact, lightning strike, erosion and other in-service conditions can lead to new damage in the blades. Additional NDI fidelity beyond what can be provided by visual methods is required to identify and repair defects before they reach a critical size.

Wind turbine blades pose a unique set of inspection challenges that span from very thick and attenuative spar cap structures to porous bond lines, varying core material and a multitude of manufacturing defects of interest. Also, due to the sheer size of blades, wide area techniques are needed to minimize inspection time and make nondestructive inspections economically viable in manufacturing environments. An increased length of blades is currently the focus of the wind industry as it pursues further reductions in the cost of wind energy. This has placed added emphasis on the use of advanced materials, sophisticated manufacturing processes and the deployment of routine inspection and health monitoring efforts. Overall, this NDI effort seeks to help wind blades reach their design life and efficiently provide the necessary life management

tasks that maximizes wind farm operations. In addition, wind blade inspections conducted in the field today are almost entirely confined to visual assessments. Such damage, and its extent, cannot always be seen by visual inspections as many of the more aggressive and destructive types of damage that can severely reduce blade life do not manifest themselves as surface demarcations. The use of in-situ NDI methods, such as high-penetration ultrasonics, on wind blades in the field is necessary to detect subsurface damage and thus, reduce failure rates. The training described here will allow advanced NDI methods to be gracefully integrated into wind farm operations. These include both up-tower NDI deployment and equipment for inspecting blades that have been removed from the wind turbine.

Detailed NDI is also necessary to firmly establish if repairs are needed and to determine the necessary size and extent of the repairs. As the wind blades have become larger and more expensive, there is a corresponding desire to install more extensive and invasive repairs that reach many layers in depth and are placed on and around primary structure such as spar caps and root sections. The criticality of these repairs will then require the use of through-thickness depth inspection methods to ensure the quality of the repair (post-repair inspections). Such inspections will detect undesirable repair flaws that may be hidden by non-uniform resin flow and ply edge effects that are present in repairs. The same techniques used to detect damage may also be used to determine the integrity of a structural repair to a blade. Enhanced NDI techniques could open up new opportunities for spar cap and root repairs. The integrity of the structural repair could be verified through inspection, giving repair designers and engineers added confidence that the blade can be recertified for use, which would lead to significant cost savings.

This report provided a comprehensive and quantitative assessment of inspection methods for use in blade inspections. Custom wind turbine blade test specimens, containing engineered defects, were used to determine critical aspects of NDI performance including sensitivity, accuracy, repeatability, speed of inspection coverage, and ease of equipment deployment. These tests provided the information needed to identify the applicability and limitations of advanced inspection methods for wind turbine blades while determining that pulse-echo ultrasonics provides the most complete inspection method to meet all of the inspection requirements. The end result is a proposed optimum advanced inspection method that considers all NDI needs such as factory deployment, field deployment, depth of penetration, sensitivity, repeatability and cost effectiveness. Customized hardware and procedures were produced for this phased array ultrasonic inspection method, technique validation was conducted and initial tech transfer activities were completed. Sandia produced and implemented the Wind Blade Flaw Detection Experiment (WBFDE) to establish the Probability of Detection (POD) and other critical performance attributes for inspection methods. This experiment provided a report card on the state of current inspection capabilities of the wind industry including an assessment of inspectors, flaw detection sensitivity, the possibility for false calls and limitations/deficiencies in NDI equipment utilization. It also quantified the level of improvements that can be achieved through the deployment of more sophisticated inspection methods.

Sandia Labs has developed and adapted customized single element and phased array pulse-echo ultrasonic inspection (PE-UT and PA-UT) methods to optimize sensitivity and depth of signal penetration in large wind turbine blades. Specific hardware, system deployment and data analyses approaches were conceived to overcome the unique challenges associated with blade

inspections. Some of the key items include optimized inspection frequency, use of focused transducers and focusing apparatus, use of compatible pulser excitations, use of data filters, transducer housing to improve signal coupling, and multiple gate settings to uncouple and identify signals of interest. These innovations optimize signal strength and clarity while allowing the user to focus on key signatures within the blade. This allows for interrogation of both the composite laminate structures and the bond lines below the spar cap and at the trailing edge. Automated and encoded phased array UT inspections were integrated to enable the production of two-dimensional, color coded C-scan images of wide area inspections. This feature improves probability of damage detection, minimizes false calls and improves overall health assessment efforts. Inspection procedures, necessary for the comprehensive and repeatable deployment of the PA-UT technique, were also produced.

In order to realize the benefits stemming from improved inspection methods, procedures and deployment practices, it is necessary to conduct a detailed NDI technology transfer effort. This can be achieved using the focused wind blade inspection training initiative that has been discussed throughout this report. Concrete examples were provided to quantify the estimated improvements in inspection performance that can be produced by such a focused training effort. Section 7.3 of this report delves into the details of such a technology transfer and training activity.

As the application of wind turbines continues to expand, there is an increased emphasis on ensuring the quality, and thus the reliability, of wind turbine blades. Blade reliability is rapidly becoming one of the highest cost elements of plant operations because blade failure can cause extensive down time and lead to expensive repairs. In addition, blades are being delivered to the site in a condition that occasionally requires additional treatment of quality issues before they can be installed. Blade repair contractors for US wind plant developers and operators report that a significant percentage of the blades they repair have never been operated. Blade reliability issues need early attention because of the lost production and cost of significant failures. The NDI performance study presented here addresses these important reliability issues as they impact development and operations costs. This effort recognizes and is addressing the need to improve the quality of blades as they are delivered to the field through enhanced inspection capabilities and associated quality metrics. The need for viable, accurate NDI technology becomes more important as the cost per blade, and lost revenue from downtime, grows. NDI methods described in this paper are able to contend with the challenges associated with inspecting extremely thick composite laminates and subsurface bond lines but also address new inspection requirements stemming from the growing understanding of blade structural aging phenomena.

7.2 Wind Blade Flaw Detection Experiment – Steps to Improve Probability of Flaw Detection and Overall Wind Blade Inspections

The intention of this study was to determine which Nondestructive Inspection (NDI) technologies are most promising for wind turbine blade inspections, assess those technologies, and transfer the technology to industry through inspection procedure development and inspector training. The Sandia Wind Blade Flaw Detection Experiment was completed to evaluate different NDI methods that have demonstrated promise for interrogating wind blades for

manufacturing flaws or in-service damage. The purpose of the WBFDE was to determine the capability of conventional and advanced NDI methods to identify flaws in wind turbine blades. The WBFDE effort was used to study the capabilities and limitations of applicable NDI methods in identifying the different flaw types in wind blade construction. The general goal was to determine which NDI method(s) have high sensitivity, accuracy and reliability in order to facilitate improvements in both quality assurance measures during blade production and critical damage detection during service. This effort also identified the factors influencing composite wind blade inspections on this type of structure so that improved methods and procedures can be developed.

These tests provided the Probability of Detection information needed to generate industry-wide performance curves that quantify: 1) how well current inspection techniques are able to reliably find flaws in wind turbine blades (industry baseline) and 2) the degree of improvements possible through integrating more advanced NDI techniques and procedures. Based on the WBFDE results, a number of recommendations can be made to help improve existing blade inspection practices using conventional NDI methods. In addition, phased array ultrasonics (PA-UT) has been identified as the optimum advanced NDI method for introduction at blade manufacturing facilities and to assess blades operating in the field.

In order to facilitate the optimum, uniform and reliable deployment of the PA-UT inspection method to address blade inspections, Sandia also developed custom hardware. Inspection procedures were produced and beta tested at blade production facilities. Both laboratory and field tests were conducted to study this NDI technology and to ensure that all deployment issues were properly addressed. In addition to flaw and damage detection, customized pulse-echo UT can provide diagnostic information regarding bond line thickness and porosity levels in the assembly. This study has identified one best overall NDI method while determining complimentary NDI methods that can be applied to produce a comprehensive blade inspection system. The detection of fabrication defects helps enhance plant reliability and increase blade life. Improved inspection of operating blades can result in efficient blade maintenance, facilitate repairs before critical damage levels are reached and minimize turbine downtime while increasing blade operation lifetimes.

A summary of findings and recommendations stemming from the WBFDE are:

- Value of WBFDE and Guidance Produced - Overall, the results from this study provide input and recommendations to the wind industry regarding new NDI techniques and guidance that can enhance the wind blade inspection process. Wind blade factories and wind farm operators can use these results to guide NDI deployment and training, to define what flaws/damage can be reliably found by inspectors and to reduce the human factors issues in order to produce improved NDI performance. Key adjustments in inspection procedures were identified to optimize performance.

  The WBFDE provided many insights into how to optimize blade inspections and revealed specific issues that can be addressed through training and the deployment of advanced NDI methods. For example, the degree of flaw detection improvement – ranging from 20 to over 50% - stemming from the use of optimized NDI practices was quantified. In addition, testing of current inspectors showed that: 1) there is a large spread (up to 70% difference)

in the ability of inspectors to detect flaws in blades, and 2) basic instruction in NDI can produce tremendous improvements in performance to reduce this extreme spread in inspection results.

- Challenges with Complex Joints - There is a need for additional inspector training in order to generate the performance improvements possible via optimized NDI deployment, sufficient knowledge of the inspection idiosyncrasies and increased exposure to realistic, composite inspection demands. When inspecting thick composites with substructure bond lines or other elements, for example, additional signal penetration requirements coupled with a more extensive set of complex reflections, results in a clear reduction in NDI performance in the region of substructure elements. Additional NDI training and use of more representative NDI Reference Standards is recommended to improve flaw detection in complex structures.

- Conventional vs Advanced NDI Inspection Methods - For an inspector deploying conventional, hand-held, pulse-echo ultrasonic inspection methods, the overall $POD_{[90/95]}$ level for blade structures occurs when the flaw, or damage, is approximately 1.33" in diameter. Through the use of more sophisticated NDI methods this $POD_{[90/95]}$ level can be reduced to damage that is 1.11" in diameter. It has been demonstrated that the use of color-coded or gray-scale images, coupled with wide-area coverage that accommodates comparisons with adjacent areas, is extremely helpful in both identifying flaws and reducing false calls. It may be useful to conduct composite laminate inspections using the scanning methods evaluated here and then complete flaw confirmation inspections on questionable regions only using conventional PE-UT where focused A-scan signals can nicely compliment the C-scans. Another advantage of the advanced NDI systems is that they have the ability to store the images for future use. This allows for additional image interpretation from other inspectors, as well as an ability to track questionable regions to determine if subtle shadings remain unchanged over time or if they evolve into something that is clearly damage in the part. Phased array and linear array wheel probes have the same advantages as traditional array scanning systems, but offer the ability to scan surface structures without scanner set-up time. Another advantage is that wheel probes maintain better contact with the inspection surface and virtually eliminate probe wobble. One drawback of rolling wheel probes is that their size can create deployment challenges and make it difficult to inspect in tight spaces.

  When considering overall inspection performance for the top three inspectors in the advanced (C-Scan Pulse-Echo UT) and conventional (Hand—Deployed Pulse-Echo UT) categories, it can be seen that the top performing inspectors will produce similar results of $POD_{(90/95)} \approx 1$" and similar improvements from the combined results from all inspectors where $POD_{(90/95)} \approx 1.3$". Thus, with additional training and and more frequent practice on realistic specimens containing realistic flaws, it is expected that all inspectors will start to converge to this optimum POD level where wind blade manufacturers and wind farm operators can expect to reliably find 1" diameter flaws and larger. With this information in hand, companies in need of wind blade inspections can use additional metrics to make a decision on which NDI method to deploy. The hand-deployed PE-UT method requires less bulky equipment and is quick to apply in small sections while the automated C-scan PE-UT

method can be operated quickly – once it is set-up – and will provide better, 100% area coverage of the inspection region.

- The overall assessment of the pulse-echo ultrasonic inspection method using a single-element, focused probe with signal optimization is:
  - Overall noise levels, transducer ringdown and signal harmonics are a concern as they mask signals of interest
  - Use of an immersion probe with a custom probe holder (water column coupling) improves UT signals, and the resultant images, beyond those produced by normal contact transducers
  - 1 MHz, 2" focus probe (1.25" dia.) produced the strongest signals at an offset of 1.15" from the inspection surface
  - A new probe holder was designed with larger membrane diameter to allow for transducer positioning close to the inspection surface (optimize focus for specimen thickness)
  - An adjustable water path probe holder was designed and evaluated to prove that it is able to eliminate the presence of the confounding signals in the time-base region of interest
  - Adhesive studies and UT signal modeling may reveal additional methods to optimize penetration into the adhesive layer and improve flaw recognition in laminate-to-shear web joints.

- Sandia has focused on the development of sealed water column shoes with customized heights to optimize UT inspections. Overall, the advantages of using water shoes to optimally deploy single-element or phased array UT include:
  - Better/cleaner scanning signal response (less noise) which results in a better signal-to-noise ratio for flaw detection
  - Better coupling - no signal dropout and easier clean-up than gel couplant
  - Easier to deploy over a scanned surface
  - The enclosed water column, which uses a bladder system, allows the inspector to maintain a seal when deploying vertically.

- Two significant observations related to equipment set up for wind turbine blade inspections were made during the assessment of UT inspection techniques. They include:
  - The importance of optimum gate settings for detecting flaws and clearly imaging them. It was determined that optimum inspection results are obtained from the use of two gates, one that is narrow and focuses on the back wall of the spar cap laminate and one that focuses on the back wall of the shear web beneath the adhesive layer.
  - When driving an ultrasonic transducer with a pulser, the shape of that excitation input to the transducer crystal is critical to the energy levels of the inspection.

- Phased and linear array ultrasonics performed exceptionally well in the spar cap and spar cap to shear web bond line inspection areas, including detection of deep subsurface flaws. The ultrasonic family of NDI produced the best all-around results when considering sensitivity, versatility, repeatability and deployment issues. These methods were also able

to detect near surface flaws in spar structure, but are less well-suited for inspecting flaws in thin-skinned sandwich core structure.

- Single-element pulse-echo ultrasonics, deployed using a scanner, produced similar performance levels as those obtained from phased and linear array ultrasonics. The C-scan capability provides far better visualization compared to hand deployed pulse echo ultrasonic A-scans. In prior work it was determined that C-scan imaging vs. A-scans is a major factor influencing an inspector's ability to detect and interpret flaws. The primary drawback with single-element pulse-echo ultrasonics is that it has a slower scan rate than the phased/linear array UT systems. Thus, inspection throughput can be a concern.

- Microwave methods showed promise for inspecting spar cap regions, sandwich structure, deep surface flaws and near surface flaws. Different frequency ranges work well depending on the thickness of the material. One of the limitations for using microwave is its inability to inspect carbon, due to the material's conductive properties.

- Thermography performed well on the thinner wind blade specimens, but depth of penetration is a concern for thermography inspections of thick wind blade specimens. Substructure flaws must manifest themselves as changes (anomalies) in the surface temperature of the part in order to be detected by this technique. Small flaws, especially those embedded deep within a structure, are difficult to image as their presence has less of an effect on surface temperature heat transfer. Other studies, along with this one, have determined that thermography performs well for wide area imaging of detect near-surface flaws. They also works very well for NDI of sandwich construction so these methods should be considered for any needs with respect to wide-area inspection of foam or balsa core regions, including post-repair inspections in the field.

- Advantage of Inspection Images - The advantage of scanning pulse echo ultrasonics (the phased and linear array UT methods studied in this experiment) is the addition of C-scan imaging to compliment the A-scan signals used in conventional, single element PE-UT. The advantages of the scanning ultrasonic methods are: 1) C-scan area views provide the inspector with easier-to-use and more reliable data with which to recognize flaw patterns, while eliminating the human factors concerns related to continuously observing and detecting subtle changes in A-scan signals, 2) scanning approach ensures full coverage of the inspection region and allows for more rapid inspections of large surface areas, 3) multiple gate settings can be used simultaneously to optimize flaw detection at different depths within complex structures.

- Confounding Effects of Signal Harmonics - Signal harmonics can appear in the range of interest when harmonics from front wall ("initial bang") fold into the same time frame as the actual signals of interest generated from the back wall of a laminate or bond line. In these cases, the recommendation is to use custom transducer shoes to improve signal coupling into the part and to shift the signal of interest beyond the noise generated by the front wall.

- Probe Size Versus Flaw Size – An important experiment design feature to keep in mind is that the inspectors were asked to detect flaws as small as 0.5" in diameter. The ultrasonic transducers that were used to conduct the inspections, and transducers that are typically used in the 0.5-1 MHz range, were typically 1" in diameter. This means that even if the transducer was centered directly over 0.5" flaws (i.e. flaws less than the diameter of the transducer), the transducer signal would be composed partly of information from a flaw region and partly of information from the unflawed region around the small flaws. Thus, the overall effect of the flaw on the transducer response would be lessened. So, if it is desired to detect flaws of 0.5" diameter, smaller diameter or focused single-element transducers [1] - which might only be realistically applied in localized inspections – should be used.

- Amount of Overall Time Spent Inspecting – The time required to compete a full blade inspection can be a concern. The WBFDE, like actual blade inspections requires concentration for multiple hours in a row and covers large inspection regions. Sandia demonstrated in the smaller, more focused POD experiment, that inspectors performed much better when directed to specific regions (i.e. shorter, more focused inspections) [4-5]. When subjected to exceptionally long inspections, it is not unusual for the inspector's attention to wane at times which increases the possibility of missing a flaw. From a human factors perspective, the inspection of large areas can reduce NDI performance. The recommendation is that wide area inspections associated with large composite structures be divided into a series of smaller inspection regions to allow for the necessary inspection focus. In addition, some of the more demanding inspections that involve larger regions or complex structure should be inspected using a two-man team. Discussions on signal quality and interpretation between the two inspectors should improve the overall flaw detection performance.

- Use of Aids to Ensure Proper Coverage – The inspection procedures discuss proper coverage of the inspection area and even suggest the use of grids or other methods to ensure that the UT transducer is moved over the entire surface area. Some inspectors completed their work using simple freehand (unguided) motion over the entire surface area of each specimen. Some inspectors divided the test specimens into quadrants, while still moving the transducer in a freehand motion, so that they could better monitor their coverage and transducer movement. Some inspectors used straight edges to guide their transducer movement. Inspection results showed improvements in POD for inspectors used some aids to ensure complete coverage of the inspection surface. When inspectors are inspecting large areas as may be the case in composite wind blades, they should use some form of guides or grids to ensure proper coverage of the inspection area.

- Full Inspection of Wind Blades – Currently, many blade manufacture facilities conduct QA checks by applying their NDI in a sampling approach. That is, the inspection does not cover 100% of the critical spar and bond line region. Instead a zig-zag NDI sampling pattern is used to assess portions of the blade. Such a search pattern can reduce POD levels substantially. Full area coverage was used for the WBFDE, however, the experiment could be redeployed several times to quantify the performance reduction when only a subset of the critical region is inspected as a statistical sampling QA approach.

- Lack of Exposure to Composite Laminate Inspections – While all of the inspectors that participated in this experiment received some training to inspect wind blade composite structures, some did not have extensive exposure to such inspections or their equipment. Use of appropriate NDI Reference Standards, or even more challenging NDI Proficiency Specimens, that allow for unlimited inspector use, can help overcome this issue. This finding indicates that additional training and exposure to wind blade laminate inspections – and the unique challenges associated with inspecting complex, multi-layered composite structures – could help improve these POD results even further. Inspectors would benefit from periodic refresher classes that will renew, or even improve, their level of expertise with respect to UT inspection methods in general, as well as with the unique aspects of composite laminate inspections.

- In-Service Wind Blade Inspections - The reliability of wind farm structures has a decisive impact on the profitability of a wind farm. To minimize the risks of costly downtime and repair periods and ensure successful functioning of a wind farm, it is necessary to conduct in-service inspections. At a minimum, in-service inspections and end-of-warranty inspections can detect imminent failures of critical components at the earliest stages, thereby, minimizing the risk of costly repair periods. Many wind farm owners and operators have observed that some components, although designed to last the predicted lifetime of a turbine, fail earlier than anticipated, causing unexpected downtime and adversely affecting the overall success of a wind farm. In-service inspections involve a series of activities, wherein various components of a wind turbine are regularly inspected and monitored throughout their entire operational lifetime [6]. Using a system of diverse inspection and analysis methods ensures that any unexpected degradation from normal conditions is detected as early as possible to prevent unnecessary damage.

- Training – The issues described above can also be addressed via additional personnel training. Some of the training can be in the form of composite awareness training to instruct inspectors on composite materials, composite structure fabrication and typical wind blade composite construction designs. Other forms of training can stress procedural aspects of the inspections such as the use of NDI deployment aids, optimization of equipment set-ups and data analysis schemes, and the proper use of drawings to assist in signal interpretation. This experiment revealed that human factors issues exist for both conventional and advanced NDI deployment. For scanning inspections methods, it was observed that a second, improved POD curve was generated by results obtained when the inspector revisited the same UT C-scan data but spent additional time to study potential flaws in the images. When the data was analyzed a second time, it was observed that the POD value improved by as much as 25%. This indicates that flaw detection, and potentially reductions in false calls, can be improved through the use of additional training

- Overall Wind Blade NDI Training Recommendations - Successful efforts to transition inspectors from “average” to “good” or “outstanding” performance levels will have a significant effect on $POD_{[90/95]}$ levels. Possible measures to achieve this include: increased training, apprenticeships, exposure to representative inspections, enhanced procedures, inspector teaming and awareness training on inspection obstacles.

- More specialized training needs to be developed to specifically address wind blade inspections. It would help to have a class that focuses on the unique challenges and signal differences associated with blade inspections. Signal characteristics related to ply tapers, bond lines and composite repairs, for example, could be discussed so that it is easier for inspectors to distinguish flaw signals from those generated by pristine structure.
- Some of the specific composite NDI training needs can be addressed by more On-the-Job Training and apprentice programs. An apprentice program could rotate inspectors into composite shops so that they can learn about composite construction while exploring the effects of different construction scenarios on NDI.
- Experiment participants requested additional guidance related to composite NDI training from industry groups, such as Sandia Labs and the DOE Blade Reliability Collaborative, in the areas of specific instrument training, specific methods training, repair inspections, composite construction training and reference standard fabrication and use. Programs supporting the evolution of such training should be initiated and pursued in an industry-wide approach.
- NDI Proficiency Specimens - Exposure to more realistic flaw specimens is one way to keep the inspectors attentive to the challenges associated with wind blade inspections. So, in addition to formal composite NDI training classes, blade inspectors should conduct routine practice inspections on representative wind blade structures (NDI Proficiency Specimens) that contain realistic damage. Such test specimens should be more complex and varied than NDI Reference Standards, used for equipment set-up, and contain known, but non-uniformly-spaced flaw profiles. Added exposure to available flaw specimens is viewed as a way to keep the inspectors ready, well-trained and current on composite inspections. Industry teams that allow for participation from blade manufacturers, wind farm operators and third party service organizations should carry out an initiative to develop such test specimens along with specifications for specimen acquisition and use.

- NDI Inspection Standards and Associated Specimens for Equipment Set-Up and Training – The wind industry has grown to the point where, like the heavily regulated aviation industry, it should promote the development and use of industry standards. Specifically, Wind Blade Inspection Standards should be produced, endorsed and disseminated by the wind industry. Two such industry-wide committee efforts are underway. The IEA 35 Rotor Blade Test Committee, operating under the auspices of the International Energy Agency, seeks to establish standards and guidelines for the performance testing and nondestructive inspection of wind blades. Similarly, the IEC 61400-5 Rotor Blade Design and Manufacturing Committee is promoting related industry standards. The Sandia Labs wind NDI team is participating on these committees and producing NDI guidance that will help ensure uniform and reliable NDI processes for wind blades. These guidelines can also promote industry-accepted NDI test specimens. These can include both the simple, NDI Reference Standards – used for NDI equipment set-up – and the more challenging NDI Proficiency Specimens described above.

7.3 Inspection Improvements Via Technology Transfer and Focused Wind Inspector Training

Nondestructive inspection (NDI) and Quality Assurance (QA) requirements, methods and practices vary widely within the wind industry and different blade manufacturers utilize different levels of rigor and different inspection techniques on their product before it leaves the factory. However, small defects can propagate to levels of concern during blade use while fatigue loading, impact, lightning strike and other in-service conditions can lead to new damage in the blades. As the length of blades increase and operational environments produce high stress levels in the blades, it has become increasingly important to detect fabrication defects that arise during blade manufacture and to follow that QA with periodic monitoring of blade health during operation. Through interactions and on-site work with multiple blade manufacturers, it was observed that there is less consistency in inspection quality than what exists in other industries. In many cases, this was due to gaps in training or lack of knowledge of better equipment and how to implement it. Similarly, current wind farm operations can be hindered by a lack of a complete range of expertise in wind blade inspection, maintenance and repair. The inspection training initiative presented here will help produce the level of expertise needed to accurately detect and track damage in wind blades before it reaches critical size.

A critical element in deploying any NDI method is ensuring that the inspectors have sufficient training to optimally use their equipment. Currently, much of the training that wind blade inspectors at blade manufacturing plants receive is developed in-house and can vary widely across the industry. There are no inspection standards. Interactions and plant visits by Sandia Labs have revealed that some of the training would be considered marginal and that inspectors, while qualified to perform their work, are not adequately trained, especially in the intricacies of inspecting thick composite structure. Inspectors provided by wind service companies may be trained according to overall multi-industry recommendations, such as ASNT or NAS, however, this standard UT training must address inspection demands from a very diverse range of structures such as pipelines, automobiles, bridges, welded structures and metallic components. As a result, there is little-to-no consideration for the inspection of composite materials with instructions on how to properly interpret A-scan signals, signatures produced by common flaws in composite materials, how to achieve needed depth-of-penetration in thick, high attenuation parts, optimum use of signal gates to produce clear C-scans and a host of other items pertinent to their unique inspection challenges. A focused “Wind Blade Inspection Training Class” can address these important topics while providing hands-on exercises that can produce significant improvements in an inspector’s performance.

The best way to achieve the most comprehensive technology transfer is through a focused NDI training class. In addition, such a class would provide critical instruction to inspectors on the proper set-up and use of their equipment. During the deployment of Sandia’s Wind Blade Flaw Detection Experiment to quantify the performance of current wind blade inspectors, it was discovered that some inspectors were not using their equipment properly or following the best data analysis schemes. This was a similar finding from Sandia’s aviation-based Composite Laminate Probability of Flaw Detection Experiment. Mostly, this stems from the fact that NDI technicians receive general UT training which does not delve into the subtleties and challenges associated with composite inspections. Even within the wind industry, Sandia’s visits to blade

manufacturing plants revealed that much of the inspector's training is general ad-hoc, in-house training that does not reflect the Level I, II, or III designations associated with formal ASNT or NAS training. Instead the Level X designations are made by the company itself. The relatively-low NDI experience levels and limited training for most inspectors in the wind industry is exacerbated by high turnover rates within these jobs. An industry-wide training initiative will facilitate a comprehensive technology transfer while producing more uniform, sensitive and reliable inspections across the wind blade manufacturing industry. The benefit will be optimum deployment of automated or semi-automated NDI to detect undesirable flaws and damage in blades while minimizing the time and cost required to complete the inspections. Better detection of production flaws will help avoid subsequent in-service failures.

The proposed training would center around the NDI methods that have consistently demonstrated the highest level of performance and high deployment viability over the full range of inspection demands for assessing wind blades. These are ultrasonic-based methods. It is important to note that this involves better ways to deploy conventional, single-element UT, as well as the use of phased array UT which produces both engineering and economic benefits. Some of the basic physics behind ultrasonics will be taught along with the specific challenges facing wind blade inspectors and the solution to those challenges.

This training will allow blade inspectors to: 1) see the proper approaches to their tasks, 2) realize the value of their actions in realistic inspection, maintenance and repair scenarios, and 3) understand the relationship between their activities (e.g. inspection performance, repair process, coatings, damage assessment) and the structural integrity of the composite part. Results of Sandia's Wind Blade Inspector Training course and associated NDI hands-on NDI Proficiency Specimens will be used to facilitate routine training for inspectors in the factory and in the field so that technique optimization, deployment issues and human factors concerns - identified and overcome in Sandia studies - can be addressed with inspectors at blade OEMs, wind farms and wind blade service companies. The course work developed in this project will present NDI challenges and means to address them – geometry (e.g. taper, substructure, curvature), signal interpretation (many samples highlighting complex signal reflections, confounding presence of signal harmonics, rapid variations produced by changing/complex geometry), and highly attenuative materials.

There are many, far-reaching benefits that will arise through the deployment of wind blade inspection training. On the front end of the blade's design life, it will produce better inspection performance at plants using conventional single-element UT inspections and further improvements in flaw detection sensitivity, inspection coverage and throughput for those companies that choose to adopt multi-element phased array UT methods. In addition, extremely limited, visually-based inspections in the field can be supplemented by sensitive through-thickness inspections to detect damage, allow for repairs and avoid blade replacement.

Wind Blade Inspection Training Class - Course Content - The focused inspector training accomplished with the "Wind Blade Inspection Training Class" can allow blade manufacturers to produce the best and most efficient flaw detection before the blade leaves the factory floor and allow wind farm operators to properly monitor the integrity of their blades before critical damage levels hinder operation. This activity represents the logical conclusion of the array of blade

inspection efforts that Sandia completed over the past few years. The goal is to conduct technology transfer activities to introduce blade inspectors to optimized ultrasonic inspection practices and advanced phased array ultrasonic options.

The training will cover the basics of blade construction as it effects NDI, the primary types of damage to be detected, optimized inspection procedures – including equipment set-up and transducer selection – and the proper use of both single-element and phased array ultrasonic (UT) techniques. As opposed to general UT training received by all inspectors, this class will emphasize the subtleties associated with inspecting composites, the challenges involved in obtaining full waveform penetration in thick laminate parts and the lessons learned from working with a myriad of wind blade inspectors around the world. The class will introduce the advantages and use of automated inspections via robotic scanning systems. The class will be customized to address the unique needs of the wind industry and will prepare blade manufacturers to adopt more sensitive and rapid NDI methods. The advantageous use of NDI Reference Standards, rarely given much attention in the wind industry thus far, will be demonstrated in order to make this a routine part of wind blade inspections. As motivation and to provide a better learning tool, results from Sandia's wind NDI development work will be presented along with results and recommendations from Sandia's Wind Blade Flaw Detection Experiment. The introduction to other promising methods such as thermography and terahertz inspections can be included in this class as well. Finally, hands-on exercises will be incorporated into the training so that specific guidance and class topics can be reinforced and optimized NDI practices can be ingrained with the inspectors. NDI Proficiency Specimens from Sandia's Wind Test Specimen Library, along with custom NDI specimens produced to support specific class exercises, will be used to provide realistic inspection challenges and real-time feedback on inspector performance

The inspections must address all deployment issues including: a) vertical and horizontal inspection surfaces, b) hand scan vs. attachable scanner, c) signal coupling via water flow or other signal couplant, d) wide range of thicknesses which may require equipment adjustments such as transducer selection and gate adjustments in ultrasonic inspections, e) need for quantitative information, f) ease of equipment use to minimize human factors concerns and performance variations, and g) rate of inspection to produce necessary coverage. Some inspection considerations and impediments that must be overcome in order to produce the desired NDI performance include: a) some methods may need access to both sides of blade, b) wide area inspection methods may be needed (scanners), c) porosity/attenuation levels of blades are high, d) depth of penetration and sensitivity at depth is needed, and e) inspections must accommodate surface curvature and complex geometries. The class will address both conventional pulse-echo UT and phased-array UT. As such it will discuss the limitations/challenges of current inspection practices and the use of more sophisticated NDI methods and devices to improve inspection coverage of blades while also improving damage detection sensitivity and reliability.

"Wind Blade Inspection Training Class" – Course Syllabus

Class Description

This is a 2 to 3-day class designed for Level I to Level III certified conventional UT Inspectors and engineers. The course provides training in the principles of conventional and phased array inspection, probe designs, scanning techniques, beam focusing, beam steering, phased array instruments, instrument set up, element checks and calibration, data collection, and ultrasonic software. The class will focus on the unique aspects of inspecting wind blades and the unique challenges associated with inspecting thick, high-attenuation composite structures. The course will be an even mix of classroom learning and hands-on exercises that will reinforce optimized inspection procedures. Use of the NDI Proficiency Specimens – which contain realistic flaws and geometry - will provide inspectors with critical exposure to inspections with real-time feedback on their performance. This class can be used by wind blade manufacturing plants, wind farm operators and wind service companies to enhance an inspector's preparation and training by focusing on the unique challenges associated with blade inspections. The end results will be optimized wind blade utilization and extended lifetimes.

General Training Content

- Present NDI challenges and means to address them – geometry (e.g. taper, substructure, curvature), signal interpretation (many samples highlighting complex signal reflections, confounding presence of signal harmonics, rapid variations produced by changing/complex geometry), attenuative materials
- NDI - theory & physics, methods & usage by application (alternatives; where & how to apply); deployment; reiterate proper use of procedures (use of laminate NDI procedure); training on navigation of guidance documents
- Field issues – repair and/or NDI common errors; human factors concerns
- Use of NDI Proficiency Specimens - usage processes/modes for feedback & learning
- Hands-on portion of class – designed exercises, equipment, selection of transducer, proper use of NDI Reference Standards; highlight lessons learned with lab exercises

Learning Objectives

- This course is intended to educate and refresh NDT inspectors in all aspects of composite laminate inspections while providing a foundational understanding of the fabrication flaws and in-service damage that must be detected
- To produce a general understanding of composite materials, how composite parts are manufactured and the need for damage detection.
- To produce an in-depth understanding of the nondestructive testing methods used to inspect wind blades.
- To provide an understanding of the fundamental ultrasonic principles and the specific use of UT for composite NDI.
- To allow students to recognize critical aspects of A-Scan, B-Scan and C-Scan signals and to understand the analysis of ultrasonic pulse echo signals to include bond lines and substructures.
- To produce a high inspection proficiency on wind blades made up of a variety of structural configurations to include: laminates, laminates with substructure, co-cured

bond lines, secondary bond lines, tapered laminates, effects of adhesive squeeze-out in the inspection zone, and various types of damage to include disbonds, delaminations, wrinkles, porosity and impact damage.

Module 1: Introduction, Motivation, Objectives & Expected Outcome from Class
Module Learning Objectives

- General motivation and need for well-executed and sensitive inspection of wind blades
- Training content including overview of hands-on exercises
- Use of guidance documents, formal NDI procedures and NDI Reference Standards to form a sound basis of comparison and ensure proper equipment set-up.
- Use of material property and calibration curves to guide NDI deployment and signal interpretation and to set proper accept-reject thresholds.
- General deployment of NDI and human factors issues.
- Introduction to Probability of Detection and POD goals.
- Employment of a hybrid inspection approach that can rapidly include A-scan conventional and C-scan analysis during phased array inspection.

Module 2: Composite Awareness and NDI Deployment – Blade Fabrication, Manufacturing Flaws, In-Service Sustained Damage, Inspection Deployment, and Various Inspection Considerations

Manufacturing Flaws

- Describe various manufacturing flaws to include: disbonds, interply delaminations, dry resin starved regions, porosity, adhesive voids, wrinkles, ply waviness, and snow flaking.
- Show Examples of flawed Wind Blade parts
- Describe the problems with Wind Turbine Blades
- Robustness of Wind Turbine Blades – detecting required damage levels

In-Service Sustained Damage

- Stress
- Erosion
- Impact
- Lightning strikes
- Fluid ingress
- Stress risers occurring during wind blade installation.

Inspection Deployment

- Vertical vs. Horizontal Inspections
- Hand Scan vs. Attachable Scanner
- Signal Coupling via Water Flow or Couplant
- Various thickness orientations and the effects on ultrasonic sound
- Human Factors of Deployable Equipment
- Inspection impediments and Accessibility to include scan rates.

Various Inspection Considerations

- Part Accessibility
- Wide Area Inspections- scanners
- Porosity/Attenuation Levels
- Ultrasonic Depth of Penetration

- Surface Curvature and Complex Geometries
- Leading Edge Bond
- Spar Caps
- Spar Cap to Shear Web Flange Bond Line
- Trailing Edges

Module 3: Wind Turbine NDI –Theory and Practice

- Inspection requirements – flaw size allowable (area dependent), coverage, classification; flowchart for damage characterization process
- Visual inspection processes – camera vs. drone inspections
- Pulse echo UT – theory and practice of conventional and phased array options
- UT equipment types
- Suitable frequencies and sensor types; delay lines; types of wedge material

NDI Deployment

- Review of procedures and best practices.
- Process for set-up with NDI Reference Standards
- Coupling types, transducer shoes
- Signal interpretation
- Mapping damage

Description of Inspection Methods

- Single-element UT, phased array UT, linear array UT, light tests, and tap testers
- UT imaging
- Advantages of C-scan over A-scan; use of B-scan
- Use of NDI Wind Reference Standards
- Use of proper gate settings
- Use of amplitude information
- Scan indexing distance
- Attenuation & use of transfer functions

Probability of Flaw Detection

- Performance assessments
- Critical issues affecting POD – inspector-controlled elements
- Smallest flaw found vs largest defect missed (detectable vs rejectable)
- Overcome fear of unknown with NDI of wind turbine blades.

Additional Considerations

- Lessons learned to optimize - human factors considerations, use of apprenticeships.
- Adhesive bond line assessment
- Interpretation of signals from normal structure
- Shear web considerations
- Bonded substructures
- Inspecting repairs
- Assessing porosity
- Avoiding False Calls

Module 4: Wind Turbine Repair Awareness- Challenges & Lessons Learned

- Common manufacturing flaws to include: lack of adhesive, adhesive voids, presence of foreign material, contamination in the laminate or bond line, and disbonds between laminate and adhesive.
- Common in-service flaws: scarf repairs, blisters, repairs to leading and trailing edges, lightning strikes, tip repairs, and repairs over balsa wood.
- Use of NDI to assess damage limits (area, depth)
- Introduction to repair procedures.
- Repairs to primary structure and need for post-repair inspection.

Lessons Learned from Wind Farm Operators and Wind Blade Repair Companies

- Case studies - Examples with photos, damage detection, outcome

Module 5: Wind NDI Proficiency Specimens

- Introduction to Wind NDI Proficiency Specimens – what they are and how they can be used
- Description of configurations and design considerations – critical features and inspection challenges.
- Design and manufacture of specimens.
- Flaw profiles with sample inspection results (characterization).
- Learning objectives – use in hands-on exercises.

Module 6: Composite NDI – Hands-On Exercises

The set of proficiency specimens containing engineered defects and representative damage will be used to reinforce teaching points of the course and can be used to "test" inspector's proficiency. Specific exercises are still being defined but current thoughts include the following structured hands-on exercises:

- Exercise 1 – Calibration: set material velocity and Time Corrected Gain curves
- Exercise 2 – Calibration: phased array ultrasonic equipment
- Exercise 3 – Identifying substructure to aid signal interpretation
- Exercise 4 – Setting gates
- Exercise 5 – Analyzing A-scan signals and C-scan results
- Exercise 6 – Defect detection in uniform thickness skin and in complex geometries
- Exercise 7 – Inspection of bonded substructure

As the length of blades increase and operational environments produce high stress levels in the blades, it has become increasingly important to detect fabrication defects that arise during blade manufacture and to follow that QA with periodic monitoring of blade health during operation. Detailed NDI is also necessary to firmly establish if repairs are needed and to determine the necessary size and extent of the repairs. With the advent of improved ultrasonic inspection hardware and the development of new phased-array UT methods, there are numerous improvements that can be achieved if such NDI advances are accompanied by specific, focused training. Improvements can be realized in both quality assurance measures during blade production and damage detection during operation in the field to improve sensitivity, accuracy, repeatability & speed of inspection coverage. Detection of fabrication defects helps enhance plant reliability while improved inspection of operating blades can result in efficient blade

maintenance to increase blade life; facilitate repairs before critical damage levels are reached and minimize turbine downtime

The primary goal of a wind blade NDI training package is to address the issues listed above. Ultrasonic-based inspection methods currently provide the best option for inspecting wind blades due to the technologies' exceptional depth of penetration, signal resolution and wide variation in deployment options. Recent NDI development activities have successfully addressed capabilities for large area, rapid scanning, focused inspections (i.e. bond lines), improved data presentation, enhanced sensitivity, versatility to meet multiple inspection demands, defect characterization, automated analysis, and advanced sensors/probes.

Joint efforts with blade OEMs and experienced, blade in-service inspectors will be used to design training modules that are focused on improving blade inspections. The benefit will be optimum deployment of NDI methods to detect undesirable flaws and damage in blades before they leave the factory floor, as well as new damage that originates during blade operation in the field. This will help the blades reach their design lifetime or beyond.

7.4 Summary of Key Points and Best NDI Practices

Ultimately, the proper combination of several inspection methods may be required to produce the best inspection sensitivity and reliability for both near-surface and deep, subsurface damage. This study has identified one best overall NDI method while determining complimentary NDI methods that can be applied to produce a comprehensive blade inspection system. The detection of fabrication defects helps enhance plant reliability and increase blade life while improved inspection of operating blades can result in efficient blade maintenance, facilitate repairs before critical damage levels are reached and minimize turbine downtime.

The reliability of wind farm structures has a decisive impact on the profitability of a wind farm. To minimize the risks of costly downtime and repair periods and ensure successful functioning of a wind farm, it is necessary to conduct in-service inspections. At a minimum, in-service inspections and end-of-warranty inspections can detect imminent failures of critical components at the earliest stages, thereby, minimizing the risk of costly repair periods. Many wind farm owners and operators have observed that some components, although designed to last the predicted lifetime of a turbine, fail earlier than anticipated, causing unexpected downtime and adversely affecting the overall success of a wind farm. In-service Inspections involve a series of activities, wherein various components of a wind turbine are regularly inspected and monitored throughout their entire operational lifetime. Using a system of diverse inspection and analysis methods ensures that any unexpected degradation from normal conditions is detected as early as possible to prevent unnecessary damage.

The need for in-service inspection often conflicts with tight operation budgets and resistance to taking the turbine out of service for long periods of time. This inspection need will become greater as larger, more expensive blades move into routine use. Current wind farm operations can be hindered by a lack of a complete range of expertise in wind blade inspection, maintenance and repair. Cost considerations may make on-site expertise in all disciplines hard to retain,

however, third-party wind service companies can fill these capability voids. The conceptual ideas described in this report could help wind farm operators address their inspection needs while minimizing costs and disruption of service.

When a blade is placed into service, intended and unintended load situations, coupled with environmental factors and the presence of small, undetectable flaws arising during blade production, can cause damage that can propagate in a blade. Wind blade inspections conducted in the field today are almost entirely confined to visual assessments. Such damage, and its extent, cannot always be seen by visual inspections as many of the more aggressive and destructive types of damage that can severely reduce blade life do not manifest themselves as surface demarcations. The use of in-situ NDI methods, such as high-penetration ultrasonics, on wind blades in the field is necessary to detect subsurface damage and thus, reduce failure rates, lower repair costs and lower operation costs by allowing blades to reach their design life with less interruption of service. Detailed NDI is also necessary to firmly establish if repairs are needed. The inspections results will determine the size and extent of repairs needed. In-service NDI can also provide post-repair inspections to ensure the viability of the installed repair.

THIS PAGE INTENTIONALLY LEFT BLANK

Appendix A

Experimenter Briefing and Information Packet for Wind Blade Flaw Detection Experiment

Wind Energy
Blade Reliability Collaborative (BRC)

Detection of Hidden Flaws in Composite Wind Turbine Blade Structure

EXPERIMENTER BRIEFING AND INFORMATION PACKET

Experiment Coordinators: Tom Rice (505) 844-7738
Dennis Roach (505) 844-6078

Infrastructure Assurance and NDI Department
Sandia National Labs

Experimenter Briefing and Information

Introduction

The Sandia National Labs' Infrastructure Assurance and Non-Destructive Inspection Department, under direction from the Department of Energy (DOE) Sandia Wind Energy Group, is conducting an experiment to assess flaw detection in wind turbine blade structures. The Wind Turbine Blade Flaw Detection Experiment (BFDE), including a set of 11 wind test specimens containing engineered flaws, will travel to wind blade manufacturing companies, wind blade service companies, and NDI developer labs to acquire flaw detection (NDI performance) data. One phase of this effort will utilize wind turbine blade personnel to study pulse echo UT inspections with a Probability of Detection (POD) experiment to formulate improvements in this critical inspection procedure. The experiment will require approximately 2-2½ days of each inspector's time. In general, inspectors will be asked to locate and size hidden flaws in the test specimens. After a sufficient number of inspectors have completed the experiment, industry-wide performance curves will be established that determine: 1) how well current inspection techniques are able to reliably find flaws in wind structures, and 2) the degree of improvements possible through the integration of more advanced NDI techniques and procedures. The inspections will emphasize flaw detection methods applicable to wind turbine blade structures ranging from 8 plies (0.45" thick laminate, 0.85" thick with adhesive bond line) to 32 plies (1.80" thick, 2.20" thick with adhesive bond line), for both shear web and box type bond line construction. The results will be published as industry-wide performance measures and all links to individuals and specific wind turbine blade companies will be permanently removed.

Inspectors will gain experience and feedback on the implementation of your inspections on representative wind turbine blade structure. No individual inspector's names will be linked to any experiment results. Similarly, no organization's name will be linked to any group of experiment results. However, results of all participants will be combined and potential users will be able to compare the results of competing inspection techniques and systems.

The inspectors will receive feedback on how they performed in the experiment. This will come in the form of tabulated results indicating the number of flaws correctly detected, the number of flaws missed, the number of false calls made, and the ability of the inspector to accurately size the flaws they detected. We can also provide feedback on the type of flaws that were detected and missed so that the inspector will learn what types of flaws they have trouble detecting. It is important to note that the feedback to the inspectors is kept confidential. In the final aggregate results, we ensure that the participants are always kept anonymous so that there is no way to correlate any results to a specific person or manufacturer.

Background

The inspection category for evaluation in this experiment is the inspection for representative disbonds, interply delamination's, dry areas, out-of-plane waves and bond line flaws. The test articles are modeled after the general range of construction scenarios found on wind turbine blades. The test program is intended to evaluate the technical capability of the inspection procedures and

the equipment (i.e. NDI technique). Evaluation of inspector specific or environment specific factors associated with performing this inspection are not the primary objective of this experiment. However, notice will be taken by the experiment monitor if such factors seem to influence results or if unplanned events occur which could impact the results of the inspection. Specific notice will be taken if issues such as deployment or maneuverability adversely affect the outcome of the inspection.

For this experiment a set of test specimens containing engineered flaws have been manufactured. The inspections will be conducted on a series of test specimens ranging in different thicknesses, some with adhesive substructure (bond lines). These specimens will be placed on small wood rails to support the specimen and isolate if form the table or working surface. You will be asked to inspect each test specimen and provide any information you can about the presence of applicable flaws. If you determine that flaws are present, you should then provide size and shape information about each detected flaw. The results should be marked directly on the test specimen using only markers provided by the experiment monitors. *Inspectors should use any positive indications to find flaws as small as 3/4" in diameter.* Experimenters should work at a pace that is comfortable for them. Although monitors will note start and stop times for your inspection, time to inspect is a secondary variable of the experiment. Inspectors should take whatever time is necessary to assure that any and all flaws in the test specimens are found.

1. Test Specimens and the Flaw Detection Experiment

Engineered Specimens - Engineered specimens have been manufactured that mimic the inspection applications of interest and include realistic flaws found in those structures. Specific information on the construction of the test panels follows. Experimenters will be told the configuration of each panel they inspect and be provided with drawings for reference.

- **Laminate Type** – Fiberglass.
- **Laminate (spar) Thickness** – Panels have 8 (~0.45”), 16 (~0.90”), 24 (~1.35”), and 32 (~1.80”) plies.
- **Paint** – All panels are painted to hide flaws in the experiment.
- **Adhesive Bond Line Thickness** – Panels with shear webs have bond lines of 10 mm (0.40”) thick. The box spar panels have bond lines of 10 mm (0.40”) and 5 mm (0.20”) thick.
- **Specimen Deployment** – During testing, panels will be placed on two wood rails on a flat surface to isolate the specimen from the work surface. Spar cap with shear web specimens are self-supported and don’t need the wood rails.
- **Flaw Detection** – Inspectors should use any positive indications to find flaws as small as ¾” in diameter.
- **Inspection Device** – For the most part, the inspector will utilize their own NDI equipment. We will provide acceptable inspection devices to be used for this testing and the inspectors will make the final choice based on availability and familiarity with that equipment. Some testing with non-standard devices may also be conducted in order to form a basis of comparison with results obtained using the recommended pulse echo UT devices.
- **There are two separate experiments.** One set of specimens are to represent a Spar Cap & Spar Cap with Shear Webs and the other represents a Box Spar type construction.

Equipment Calibration and Familiarization - Each blind inspection process will be preceded by inspections on appropriate training/feedback specimens supplied by the experiment monitors. The inspector will be given information on the manufactured flaws present in the training/feedback specimens and will be allowed to use them for check-out of their inspection equipment. The training/feedback specimens will have similar construction as the blind test specimens and include similar flaws. Thus, they also can be used to allow inspectors to become familiar with an inspection device and learn about a specific equipment's response for the various wind turbine blade structures and flaws within those structures. The training/feedback specimens will be used as a training tool prior to starting the experiment and will also be used by inspectors during the course of the experiment to set-up their equipment. Figures A-1 through A-6 show the flaw profiles of all the training/feedback specimens.

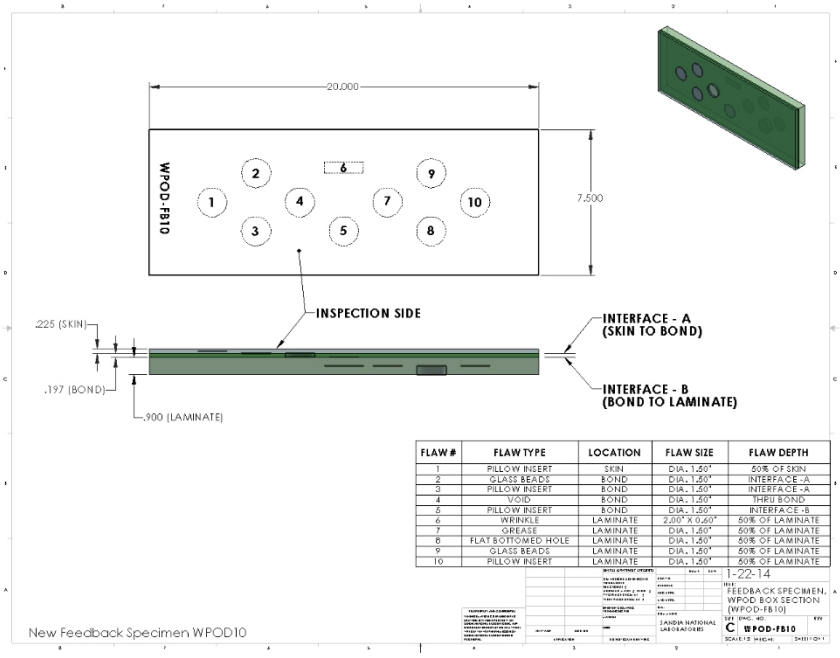

FLAW #	FLAW TYPE	LOCATION	FLAW SIZE	FLAW DEPTH
1	PILLOW INSERT	SKIN	DIA. 1.50"	50% OF SKIN
2	GLASS BEADS	BOND	DIA. 1.50"	INTERFACE - A
3	PILLOW INSERT	BOND	DIA. 1.50"	INTERFACE - A
4	VOID	BOND	DIA. 1.50"	THRU BOND
5	PILLOW INSERT	BOND	DIA. 1.50"	INTERFACE - B
6	WRINKLE	LAMINATE	2.00" X 0.60"	50% OF LAMINATE
7	GREASE	LAMINATE	DIA. 1.50"	50% OF LAMINATE
8	FLAT BOTTOMED HOLE	LAMINATE	DIA. 1.50"	50% OF LAMINATE
9	GLASS BEADS	LAMINATE	DIA. 1.50"	50% OF LAMINATE
10	PILLOW INSERT	LAMINATE	DIA. 1.50"	50% OF LAMINATE

Figure A-1: Wind POD Box Section Feedback Specimen (WPOD-FB10)

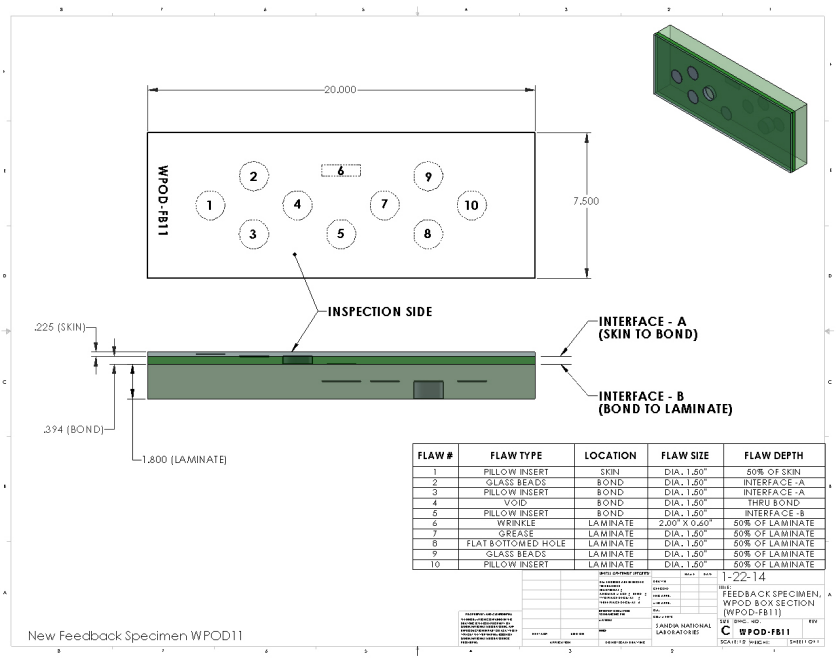

FLAW #	FLAW TYPE	LOCATION	FLAW SIZE	FLAW DEPTH
1	PILLOW INSERT	SKIN	DIA. 1.50"	50% OF SKIN
2	GLASS BEADS	BOND	DIA. 1.50"	INTERFACE - A
3	PILLOW INSERT	BOND	DIA. 1.50"	INTERFACE - A
4	VOID	BOND	DIA. 1.50"	THRU BOND
5	PILLOW INSERT	BOND	DIA. 1.50"	INTERFACE - B
6	WRINKLE	LAMINATE	2.00" X 0.60"	50% OF LAMINATE
7	GREASE	LAMINATE	DIA. 1.50"	50% OF LAMINATE
8	FLAT BOTTOMED HOLE	LAMINATE	DIA. 1.50"	50% OF LAMINATE
9	GLASS BEADS	LAMINATE	DIA. 1.50"	50% OF LAMINATE
10	PILLOW INSERT	LAMINATE	DIA. 1.50"	50% OF LAMINATE

1-22-14
FEEDBACK SPECIMEN, WPOD BOX SECTION (WPOD-FB11)
SANDIA NATIONAL LABORATORIES
C WPOD-FB11

Figure A-2: Wind POD Box Section Feedback Specimen (WPOD-FB11)

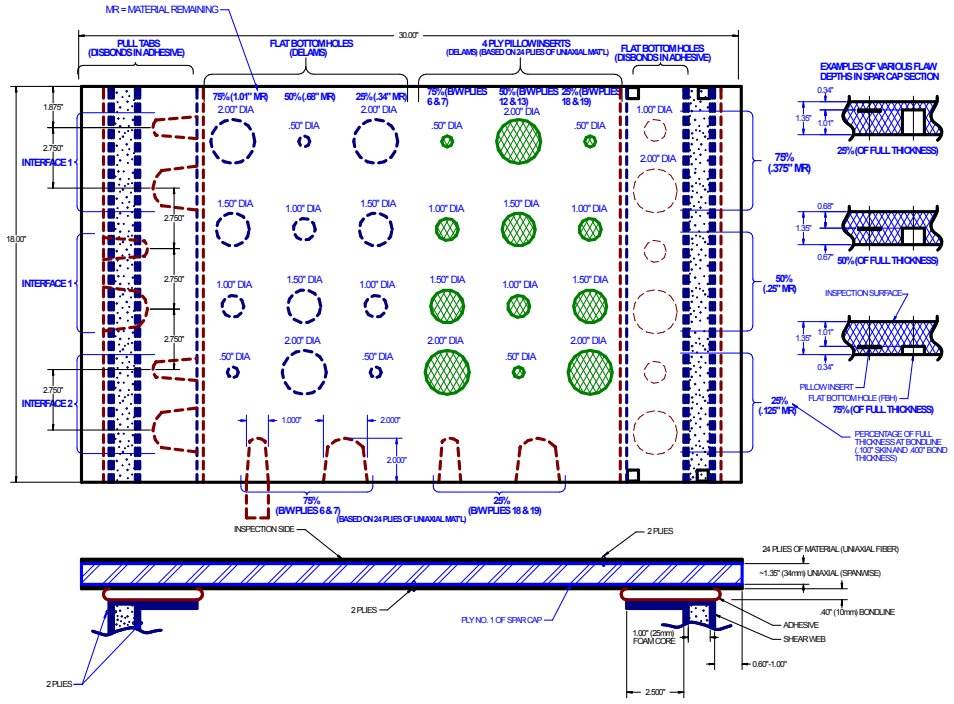

Figure A-3: Wind POD Spar Cap with Shear Web Feedback Specimen (REF-STD-2-127-173-SNL-1)

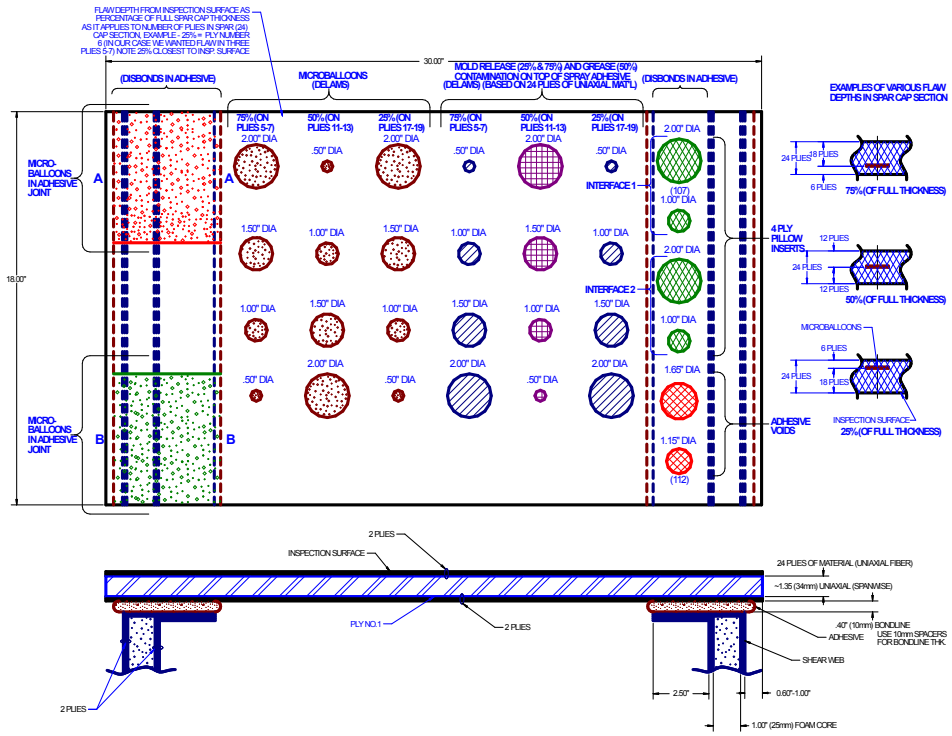

Figure A-4: Wind POD Spar Cap with Shear Web Feedback Specimen (REF-STD-3-129-176-SNL-1)

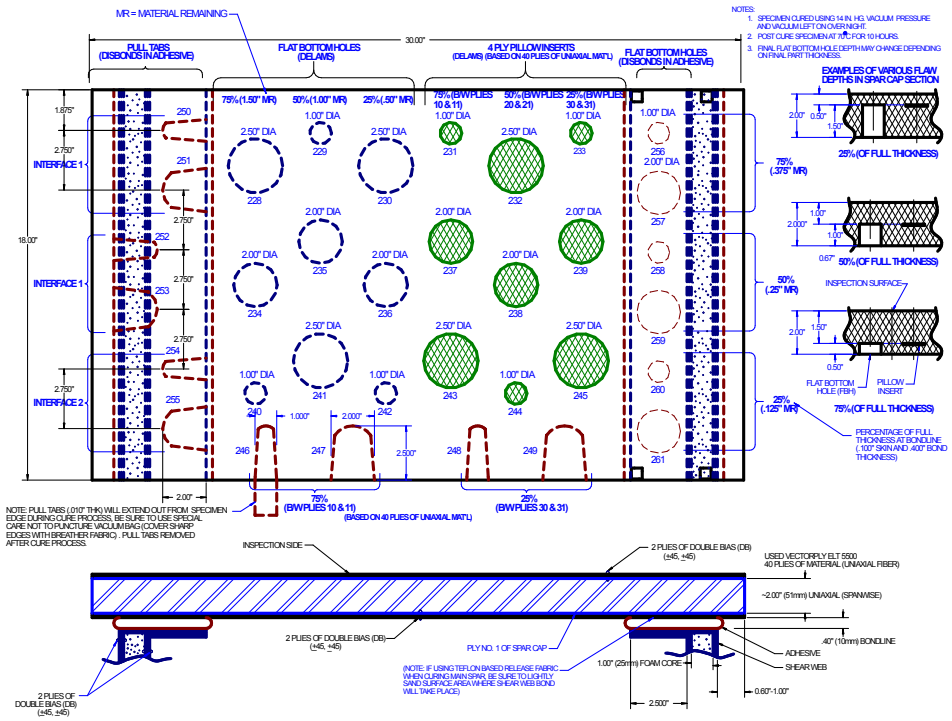

Figure A-5: Wind POD Spar Cap with Shear Web Feedback Specimen

(REF-STD-6-202-250-SNL-1

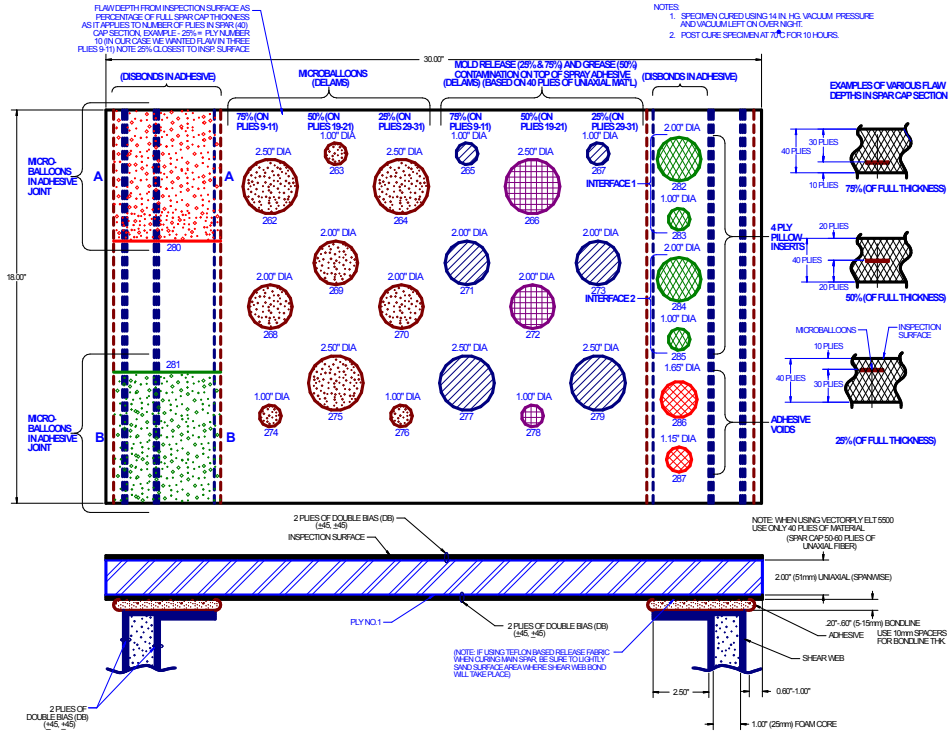

Figure A-6: Wind POD Spar Cap with Shear Web Feedback Specimen (REF-STD-7-214-265-SNL-1

2. Performance Metrics

Multiple performance attributes will be discussed in the final report for this experiment. These are given in the table below and are briefly discussed following the table. Quantitative metrics (standards applied to events that can be numerically counted or quantified) will be applied when appropriate but many of the performance attributes will be discussed using qualitative metrics (standards that rely on human judgments of performance). Where practical, qualitative assessments will be based on predetermined criteria to ensure grading consistency. The intent is to provide useful summaries of the major factors that would influence the user communities' perception of the viability of the technique or specific equipment. Because different users may have different priorities, we will not rank or prioritize the various measures.

Quantitative Metrics - objective standards applied to events that can be numerically counted or quantified.

Qualitative Metrics - subjective standards that rely on human judgments of performance; where practical, qualitative assessments will be based on predetermined criteria to ensure grading consistency.

STRUCTURED EXPERIMENT EVALUATION CRITERIA
1. ..1.1 Accuracy and Sensitivity
2. Data Analysis Capabilities
3. Versatility
4. Portability
5. Complexity
6. Human Factors
7. Inspection Time

1. Accuracy and Sensitivity
   Accuracy is the ability to **detect** flaws reliably and correctly in composite structures and repairs without overcalling (false calls). Sensitivity is the extent to which the inspection system responds to flaws as a function of size, type, and location (e.g., proximity to edges, underlying or adjacent structural elements) in the structure.

   Test results will be graded to evaluate the accuracy of quantitative measurements and to assess qualitative measurement parameters. The test results will identify hits (calls with any amount of overlap between the call and the solution), misses (no call for an area of a known flaw), false calls (call with no overlap of a flaw), degree of overlap between experimenter calls and actual flaw areas, and accuracy of quantitative call.

2 Data Analysis Capabilities
   Data analysis capabilities define how well the inspection system and process can correctly characterize flaws. Analysis capabilities include, but are not limited to, the ability to identify the flaw size (e.g., lateral extent), flaw location, and flaw type (i.e., distinguish between disbonds and delaminations). Quantitative aspects of the data analysis capabilities are provided by evaluating the accuracy and sensitivity as discussed above. Also, the repeatability, reliability, degree of automation, data storage and retrieval capabilities and constraints, and subjective interpretation requirements are considered when assessing the data analysis capabilities.

3. Versatility
   Versatility is the capability of the inspection system to be easily adapted for application to varying inspection tasks and conditions (e.g., varying surface conditions, specimen orientations and accessibility). Versatility is primarily assessed using qualitative metrics, such as calibration and equipment reconfiguration requirements to address differing inspection applications. Furthermore, variations in system performance due to changes in the surface condition (e.g., paint variations, front and/or back surface contaminants, surface scratches or dents), and specimen configuration (e.g., accessibility and orientation).

4. Portability
   Portability is the capability of the inspection system to be easily moved and used in standard aircraft inspection applications. Portability is assessed using qualitative metrics such as the inspection system's size, weight, apparent ease of use in each evaluated inspection application, and inspection restrictions (i.e., limitations created by power requirements, tethering or remote control issues, safety, or other factors that may restrict equipment usage). Equipment storage and shipment requirements will also be considered when evaluating the system portability.

5. Complexity
   Complexity is the intricacy of the tasks required to perform the inspections and data analysis. The inspection system should be suitable for use by qualified wind NDI personnel. Also, the inspection process should be efficient, repeatable, and reliable. Complexity is assessed using qualitative metrics, such as: the number of people required to perform the inspection; the number and difficulty of the range of tasks required for the inspection (including setup, calibration, system reconfiguration for changing inspection requirements, data acquisition, and data analysis); the number of simultaneous tasks required; tasks requiring unusual manipulative skills (as compared to traditional inspection needs) or which place the inspector in awkward positions that may be uncomfortable; and tasks that require advanced interpretative skills (including calibration, data acquisition, and data analysis - both qualitative and quantitative).

6. Human Factors
   For purposes of this evaluation, human factors include procedures or equipment (hardware or software) related inspection elements that may act as a source of human error. Environmental factors such as temperature, noise, and lighting level will not be considered. The Human Factors criterion is assessed subjectively considering: man-machine interface issues (e.g., data presentation clarity and ease of interpretation, presentation speed, layout and usability of knobs and dials, opportunities for operational or interpretative errors, glare effects, safety to the inspector and others in the surrounding area, etc.); written procedure usability (e.g., clarity, correctness, correlation to tasks actually performed); inspector education, training (initial and recurring) and experience requirements; objective versus subjective calibration, inspection, and analysis processes.

7. Inspection Time
   Inspection time is assessed quantitatively. Set up, clean up, inspection, and analysis time will be measured. This includes re-calibration and equipment reconfiguration time to move to differing inspection applications.

3. Experimenter Flaw Calls and Data Logging

The purpose of this experiment is to determine the capability of various inspection methods to detect and measure flaws in wind turbine blade structures. The Wind Flaw Detection

Experiment will travel to wind turbine blade manufactures, field operators, and NDI developer labs to acquire flaw detection data.

For this experiment a set of test specimens containing engineered flaws have been manufactured. The inspections will be conducted on a series of test specimens ranging in different thicknesses and adhesive substructures. Specimens without shear webs will be placed on two wood rails to isolate the panel from the work surface. You will be asked to inspect each test specimen and provide any information you can about the presence of applicable flaws. If you determine that flaws are present, you should then provide size and shape information about each detected flaw. The results should be marked directly on the test specimen using only markers provided by the experiment monitors.

If instructed by the experiment monitors, inspection results can also be marked on a full-scale sheet of tracing paper. Registration points/lines should be used on the tracing paper to assure location accuracy of the flaws. Also, test specimen numbers should be logged onto each log sheet. Figure A-7 shows a sample set of flaw marks on one of the wind turbine blade test specimens. This study would like to assess performance for flaws as small as ¾" in diameter. Inspectors should use any positive indications to find flaws as small as ¾" in diameter. It is not necessary to track small anomalies, such as porosity, that are less than ¾" in length.

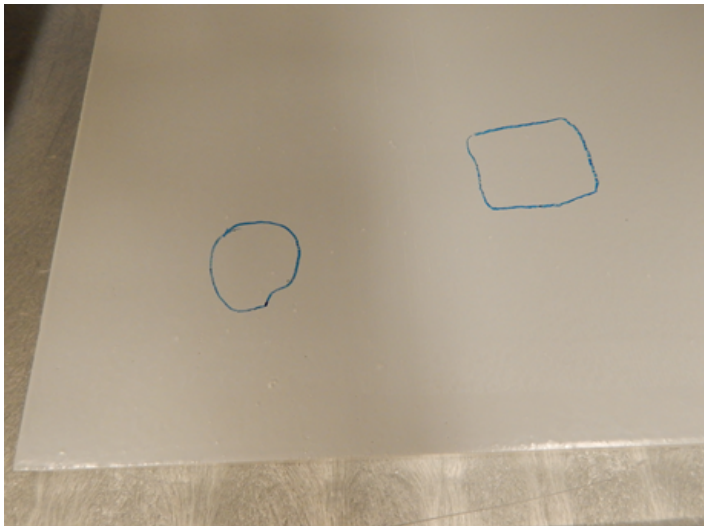

Figure A-7: Sample Set of Inspector's Flaw Marks on a Wind Turbine Blade Specimen

Specimen Deployment

During the inspections, the specimens without shear webs will be placed on wood rails to isolate the panel from the work surface. The specimens with shear webs were designed to stand on the work surface without the need for further isolation. The test specimens should not be turned over at any time. The wood rails, supplied, should be assembled as per Figure A-8 to support the panels properly. The order of inspections will be set forth by the experiment monitors. The inspection order may be varied, but once started on a specific panel the inspector will be expected to complete that panel before moving onto another. The BDFE blind test specimens and some of the training/feedback specimens are painted.

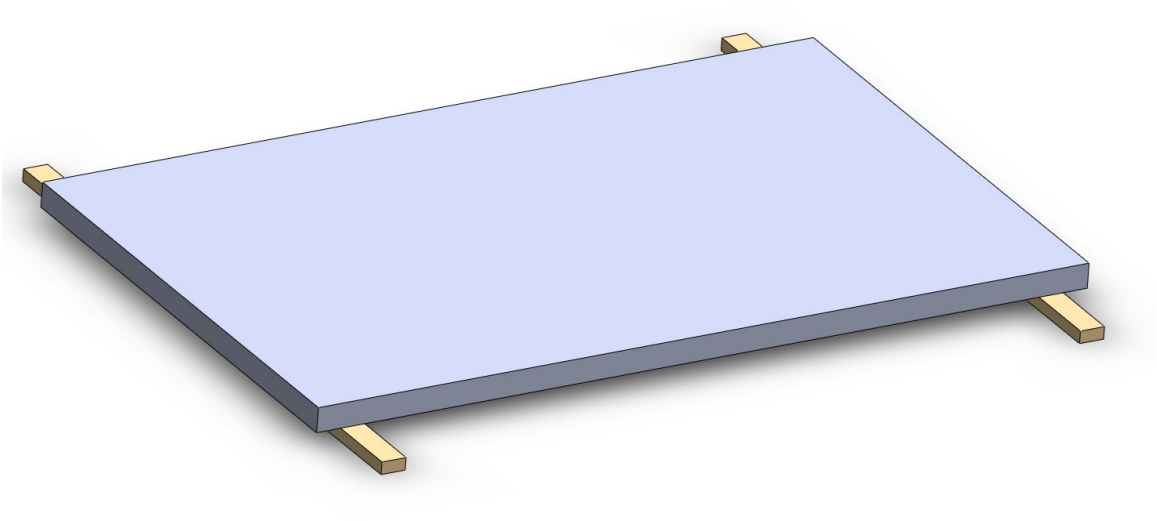

Figure A-8: During Inspections, Place the Spar Cap and Box Spar Panels on Wood Rails to Isolate the Panel from the Work Surface.

Typical Signals & Flaw Calls

Figures A-9 and A-10 show a series of representative ultrasonic signals that may be produced during a pulse-echo UT inspection of a wind turbine blade structure. When inspecting wind turbine blades, there are two distinct areas that must be looked at. One is the spar cap and the other is the bond line. Figure 9 shows typical signals that might be expected from an inspection on spar cap laminate as the transducer engages flaws at various depths in the structure. Figure 10 shows a similar set of signals that would be typical from an inspection of the bond line adhesive under the spar cap laminate.

A schematic of the signal travel through the flawed and unflawed regions beneath the transducer is shown in Figure A-11. UT waves at points (A) and (C) are unaffected by the presence of the small delamination flaw but the UT waves at point (C) interact with the delamination. These waves around point (C) cause the backwall signal to be reduced and also create an intermediate signal between the front and back wall. Inspectors should utilize the small flaws in the feedback panels in order to understand the type of signals associated with these flaws. This will be helpful in interpreting the flaw signals in this experiment.

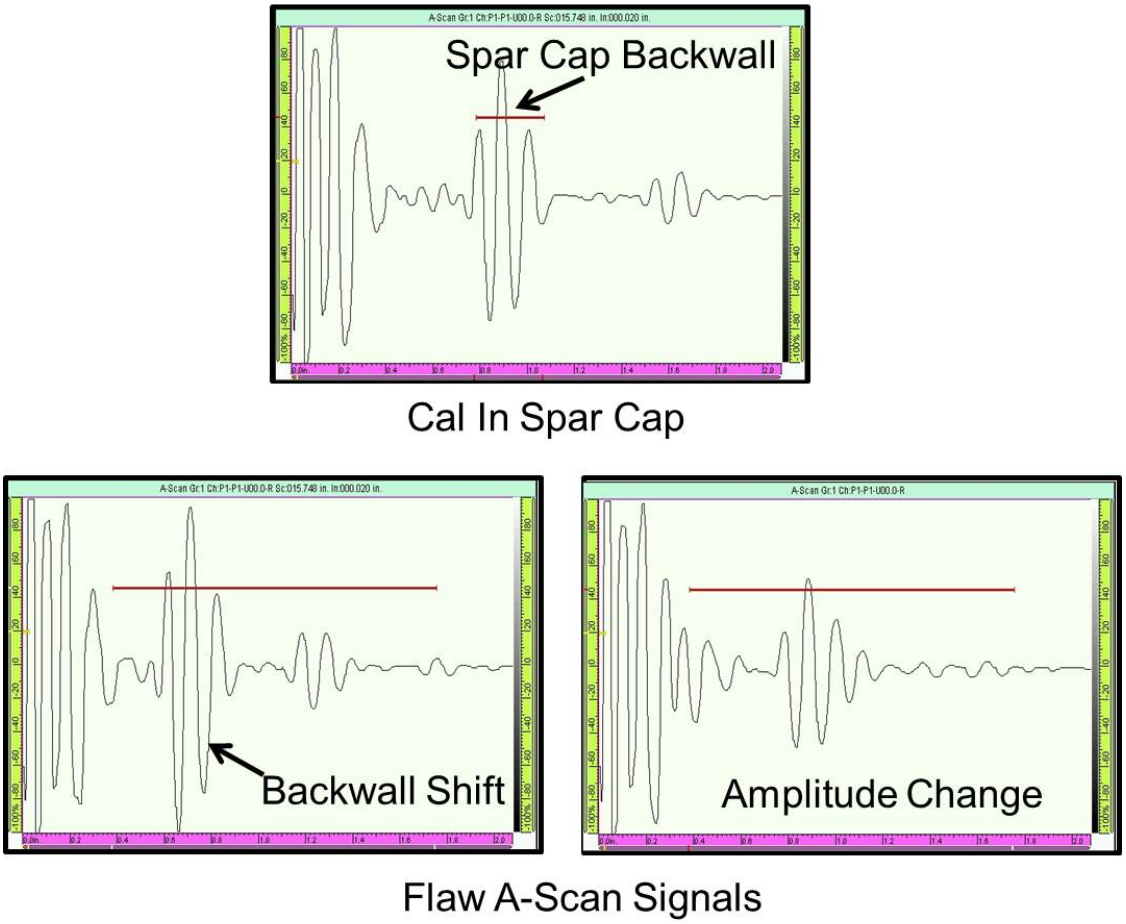

Figure A-9: Example Spar Cap Backwall and Flaw A-Scan Signals

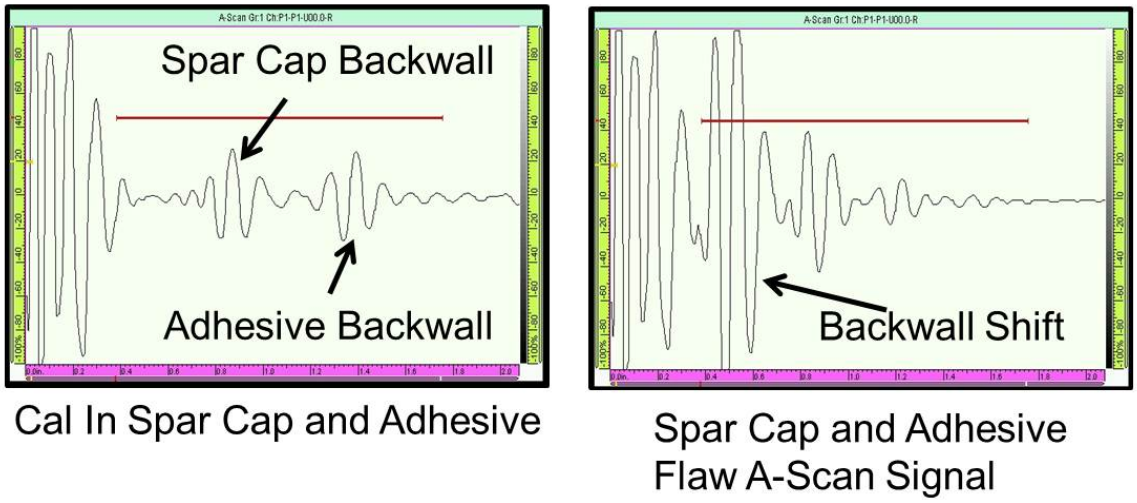

Figure A-10: Example Spar Cap with Shear Web Bond Line (Adhesive) and Flaw A-Scan Signals

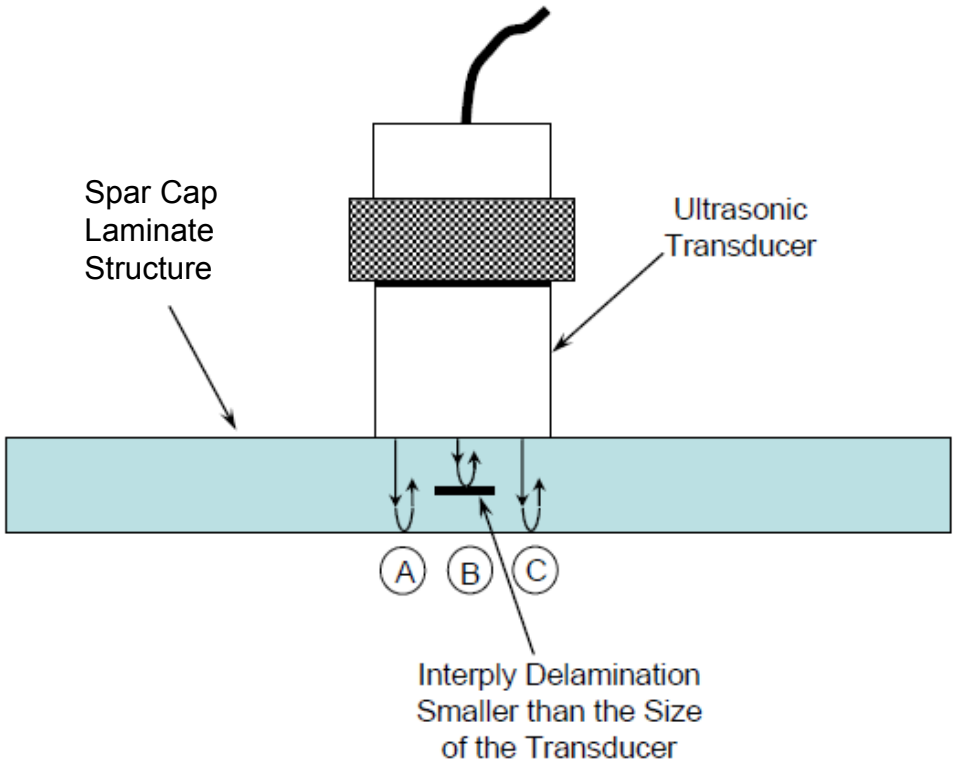

Figure A-11: Schematic Showing Reflection of Pulse-Echo UT Signals When the Transducer Footprint is Larger than the Size of the Delamination Flaw

Additional guidance for inspectors performing this experiment are as follows:

- Experimenters should work at a pace that is comfortable for them. Although monitors will note start and stop times for your inspection, time to inspect is a secondary variable of the experiment.
- Inspectors should use their own judgment as to how to perform the inspection (i.e. a strict procedure will not be enforced).
- Inspection coverage should be 100% of the panel with the exception of a small 1.00" band around the perimeter of the panels where edge effects may create problems.
- The Wind Turbine Blade Training/Feedback Specimens, or equivalent, should be used to set-up the equipment. Minor equipment adjustments stemming from in-situ calibration on the parts being inspected are allowed.
- Inspectors should draw the entire size/shape of the flaw (i.e. delineate the edges).
- Training/feedback specimens should be used as an aid to determine where to make flaw call edges. This is based on the diameter of the probe and how much of the probe needs to be over the flaw in order to react/detect.
- Inspectors do not need to determine the type of flaw just the location, size, and shape of the suspected anomaly.
- Inspectors should ignore any visual clues (surface anomalies in the paint or small surface marks) and to avoid using these as flaw detection aids. Such anomalies may be

intentionally planted to add complexity to the inspection. Inspectors should only make a call on those flaws that are highlighted by their inspection device.

Test results will be graded to evaluate the accuracy of quantitative measurements and to assess qualitative measurement parameters. The test results will identify hits (calls with any amount of overlap between the call and the solution), misses (no call for an area of a known flaw), false calls (call with no overlap of a flaw), and the degree of overlap between experimenter calls and actual flaw areas. Figure A-12 is a grading parameter drawing that shows an example of how the hits-misses-false calls results will be graded. Percentage of flaw covered will be another variable of primary interest. Error in lateral extent of flaw and maximum linear extent of overcall are variables of secondary concern and are not currently being considered as part of the grading plan.

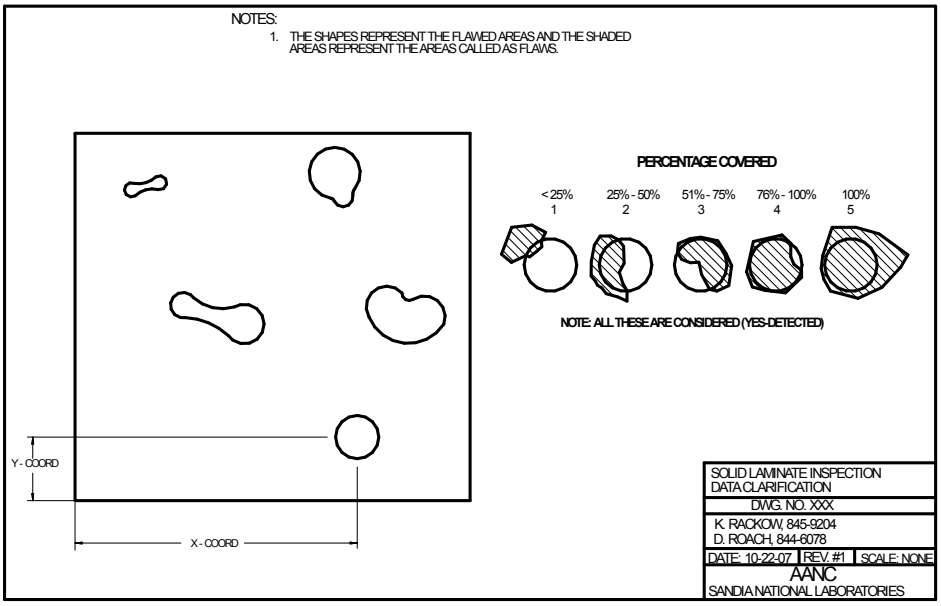

Figure A-12: Schematic Showing the Sizing Categories Comparing Experimenter Flaw Calls with Actual Flaw Information

4. Sample NDI Procedures for Pulse Echo Ultrasonic Inspection of Wind Turbine Blade Structures

Attached is a generic procedure for the inspection of composite wind turbine blades. The procedures are for general deployment of NDI equipment that is relevant to this flaw detection experiment. The NDI procedures are included here as general information to aid inspectors in preparing for the flaw detection experiment. It is not expected that these procedures are sufficient to train an inexperienced inspector. Rather, they provide additional background and guidance to inspectors who are already familiar with the equipment and have experience in performing this type of wind turbine blade inspection. The Wind Turbine Blade Training/Feedback Specimens provided with this experiment can be used in lieu of the standards described in the following procedure.

Wind Energy
Blade Reliability Collaborative (BRC)

Generic Procedure for the Inspection (NDI) of Composite Wind Turbine Blades

Ultrasonic Inspection of Composite Wind Turbine Blades

Prepared by: T. Rice, D. Roach, S. Neidigk and R. Duvall
Infrastructure Assurance and NDI Department
Sandia National Labs

Note: This procedure is for Reference Only

Ultrasonic Inspection of Composite Wind Turbine Blades

1. Assessment:

1.1 This procedure provides the generic requirements for the inspection of composite wind turbine blades.

2. Definitions and Terms:

2.1 *Adhesive Bond Line* - The adhesive material volume acting as a bonding agent between two or more structural members.

2.2 *Amplitude* – The vertical height of a received signal on an A-scan. It is measured from peak to peak for an RF presentation

2.3 *Flaw Indication* – The ultrasonic response from or the evidence of a discontinuity in material condition or structure.

2.4 *Full Screen Height (FSH)* - The full vertical deflection of the ultrasonic screen display to the maximum graticule marking or 100% FSH.

2.5 *Gain* - Signal amplification regulating the strength of the echo's being received

2.6 *Inspection Plan* – A summary providing detailed inspection information for the geometry being inspected.

2.7 *Loss of Backwall Signal* – Absence or significant reduction of amplitude from the back surface of the structure.

2.8 *Noise* – Any undesired signal that obscures the signal of interest, typically form the structures dimensional or property variations.

2.9 *Noise Level* – The amplitude of the peak noise associated with the structure's material.

2.10 *Shell* – The outside skin of the blade, consisting of laminated fabric and resin with a core in some areas and a spar cap in other areas. Two shells put together create the shape of the wind turbine blade.

2.11 *Shear Web* – Structural members connecting the two shells in the mid chord area of a wind turbine blade. The shear webs are often made of foam or balsa incased in laminated fabric and resin and are adhesively bonded to the spar cap areas.

2.12 *Shear Web Flange* – Part of the shear web, a flange typically perpendicular to the structural support, used for bonding to the spar cap.

2.13 *Spar Cap* – Primary load carrying structural elements often consisting of unidirectional composite ply material.

3. Engineering Requirements:

3.1 **Inspector Certification** – The inspections shall be performed by personnel qualified and certified through an established program that incorporates all the guidelines provided in ASNT Document SNT-TC-1A, prEN 4179 or CAN/CGSB-48.9712-95 for qualification. It is required of all inspectors to have Level II ultrasonic testing certification with one exception, UT Level I inspectors may perform inspections under the direct supervision of a certified Level II or Level III inspector. Data analysis and evaluation results may only be reported by Level II or Level III inspectors. Note: This is a generic procedure provided as an example, ASNT Certification not required to participate in the BFDE experiment, just inspection experience in the wind industry.

3.2 **Inspection Plan** – An inspection scan plan for each type of wind turbine blade shall be prepared. The inspection plan should contain the following; 1) Inspection Plan issue date, 2) Wind turbine blade part/drawing number, 3) Material, 4) Company specification and revision numbers, 5) Drawing of scan zones, 6) Transducer required for each zone, 7) Transducer frequency, 8) Equipment required, 9) Acceptance criteria, 10) Calculated values for each part geometry, 11) Signature of Level II or III inspector, and 12) Signature line for final approval.

3.3 **Shear Web Bond Line Testing Coverage** – The entire volume of the adhesive bond line between all shear webs and the spar caps shall be inspected using ultrasonic longitudinal wave testing (shown as adhesive bond line in Figure 1).

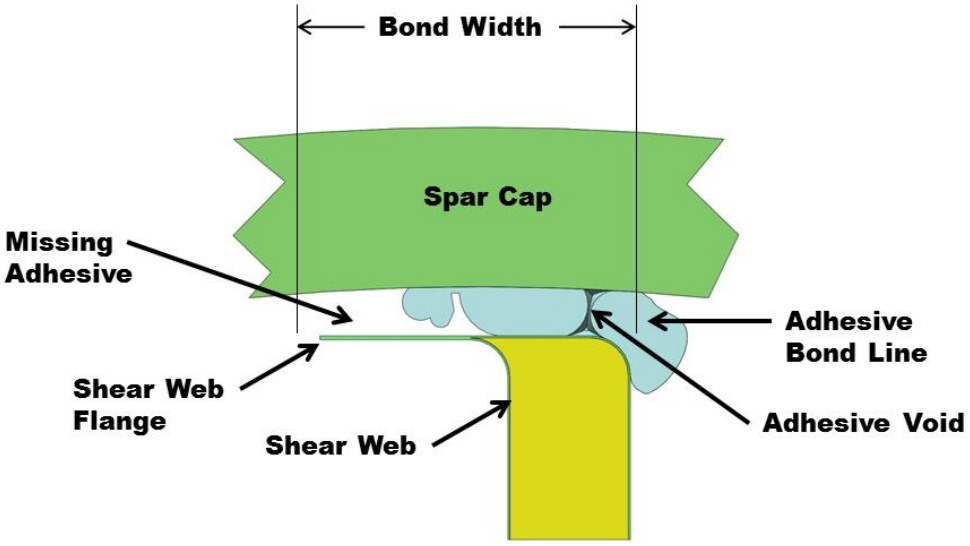

Figure 1: Example of Shear Web to Spar Cap Bond with Insufficient Adhesive Paste

3.3.1 **Inspection Area** – The inspection area shall include the thickness of the blade spar, spar cap, adhesive bond line thickness and the shear web flange.

3.3.2 **Width of the Shear Web Bond Line** – The width of the shear web bond line must be inspected for the full length of the shear web.

3.4 **Leading and Trailing Edge Bond Line Inspection** – The entire volume of the adhesive bond joints at the trailing and leading edge shall be inspected using pulse echo ultrasonics (longitudinal wave) and/or the through transmission method. If adhesive contact can be ensured by visual inspection ultrasonic testing may be removed. (See Figures 1 & 2)

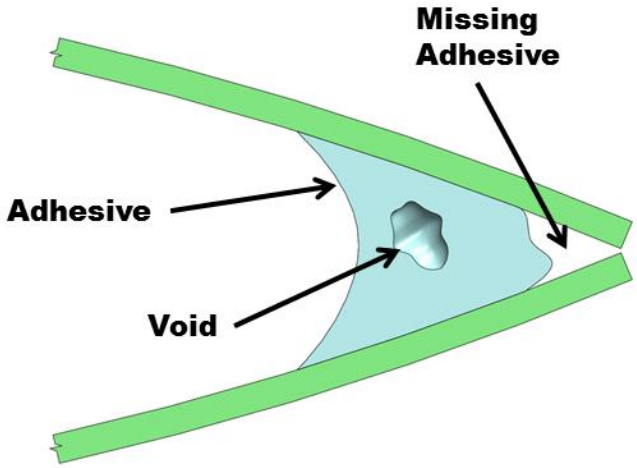

Figure 2: Example of Trailing Edge Adhesive Bond

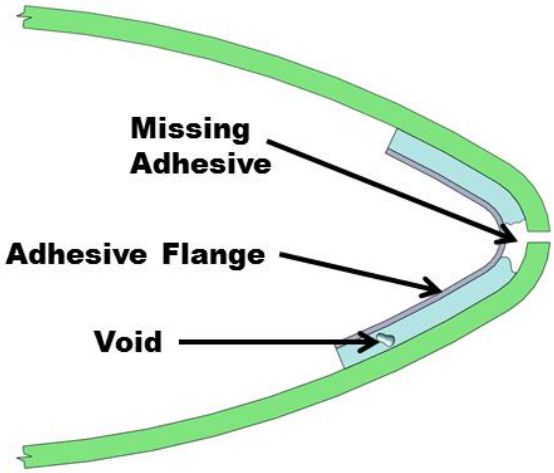

Figure 3: Example of Leading Edge Adhesive Bond

3.4.1 **Through Transmission Requirement** – Through transmission will be required when the surfaces of the leading or trailing edge are no longer parallel enough for pulse echo ultrasonics (back wall signal no longer visible due to angle).

4. Inspection Requirements:

4.1 General Requirements:

4.1.1 Equipment Type:

4.1.1.1 **Ultrasonic Instrument** – An ultrasonic instrument that is capable of inspection from 500 KHz to 5.0 MHz shall be used. Required calibration dates displayed on the instrument; date of the last calibration and date of the next required calibration. Calibration interval is 12 months.

4.1.1.2 **Probes** –Inspections shall be performed using a single element Panametrics 500 KHz, 1.0 inch longitudinal wave probe for the shear web bond line inspection. For leading and trailing edge inspection use a Panametrics 1 MHz, 1.0 inch longitudinal wave probe. An approved delay line may be used for any of these inspections. Approval is required for use of other probe sizes or frequencies.

4.1.1.3 **Scanning Systems** – Automated scanning systems using pulse echo, phased array or through transmission may be used with prior approval. There must be a method established to store the data for analysis.

4.1.1.4 **Couplant –** Water or water soluble couplant shall be used and shall not leave a visible residue on the blade surface. Other couplants may be used but approval is required.

4.1.2 Reference or Feedback Panels

4.1.2.1 The reference/feedback panels will be used to set inspection sensitivity. The panels will be manufactured using the same materials that are specified for the wind turbine blade being inspected, including the adhesive, laminate materials and any gelcoat or paint applied to the finished blade. See Figure 4 and 5 for examples.

4.1.2.2 The reference/feedback panels should represent the thickest section through the spar cap shear web area. Flaws may be inserted, during manufacture, to aide an inspector with equipment set-up and flaw characterization. Pillow inserts and flat bottom holes are the desired flaws, but other flaw types may be added. The panels should be a minimum of 7.5 inches by 20 inches (to accommodate scanning systems).

4.1.2.3 **Identification** - The reference/feedback panels will be identified with a unique part number accompanied with a drawing, showing thicknesses, flaw sizes and depths.

4.1.2.4 **Thickness and Sensitivity Calibration** - Using the reference/feedback panels, a thickness calibration should be performed prior to each blade inspection to show that the instrument display is within 5% of the actual panel thickness. To test the sensitivity, a shift in the back wall signal from the total thickness, with the back wall set at 80% FSH, to the thickness at a flat bottom hole is visible and within 5% of the actual thickness to the flat bottom hole. See Figures 6 and 7.

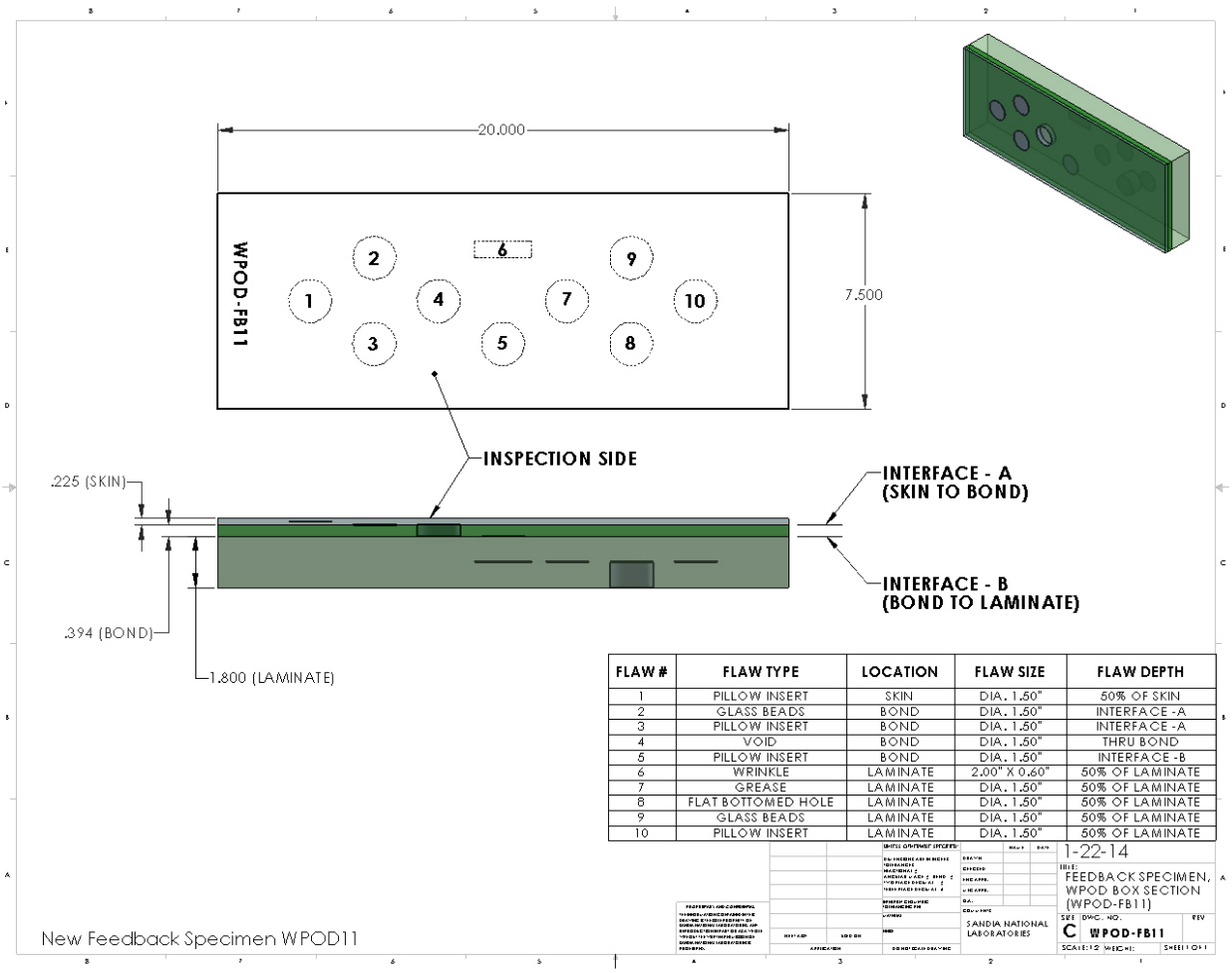

FLAW #	FLAW TYPE	LOCATION	FLAW SIZE	FLAW DEPTH
1	PILLOW INSERT	SKIN	DIA. 1.50"	50% OF SKIN
2	GLASS BEADS	BOND	DIA. 1.50"	INTERFACE -A
3	PILLOW INSERT	BOND	DIA. 1.50"	INTERFACE -A
4	VOID	BOND	DIA. 1.50"	THRU BOND
5	PILLOW INSERT	BOND	DIA. 1.50"	INTERFACE -B
6	WRINKLE	LAMINATE	2.00" X 0.60"	50% OF LAMINATE
7	GREASE	LAMINATE	DIA. 1.50"	50% OF LAMINATE
8	FLAT BOTTOMED HOLE	LAMINATE	DIA. 1.50"	50% OF LAMINATE
9	GLASS BEADS	LAMINATE	DIA. 1.50"	50% OF LAMINATE
10	PILLOW INSERT	LAMINATE	DIA. 1.50"	50% OF LAMINATE

Figure 4. Example Feedback Specimen – Box Section

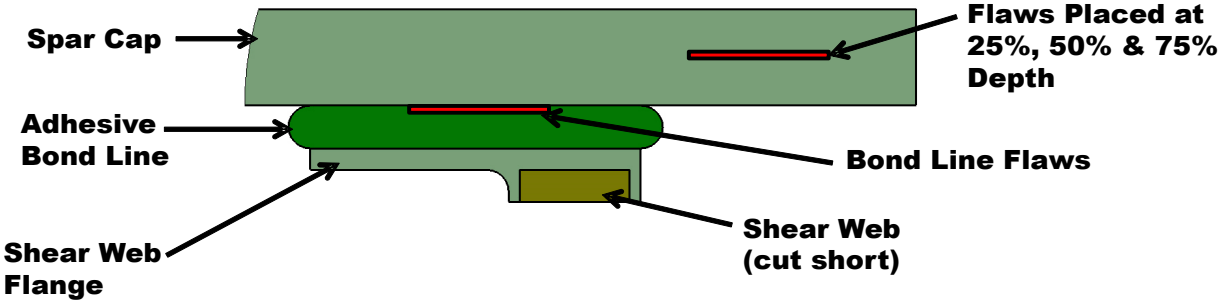

Figure 5. Example Feedback Specimen – Shear Web Section

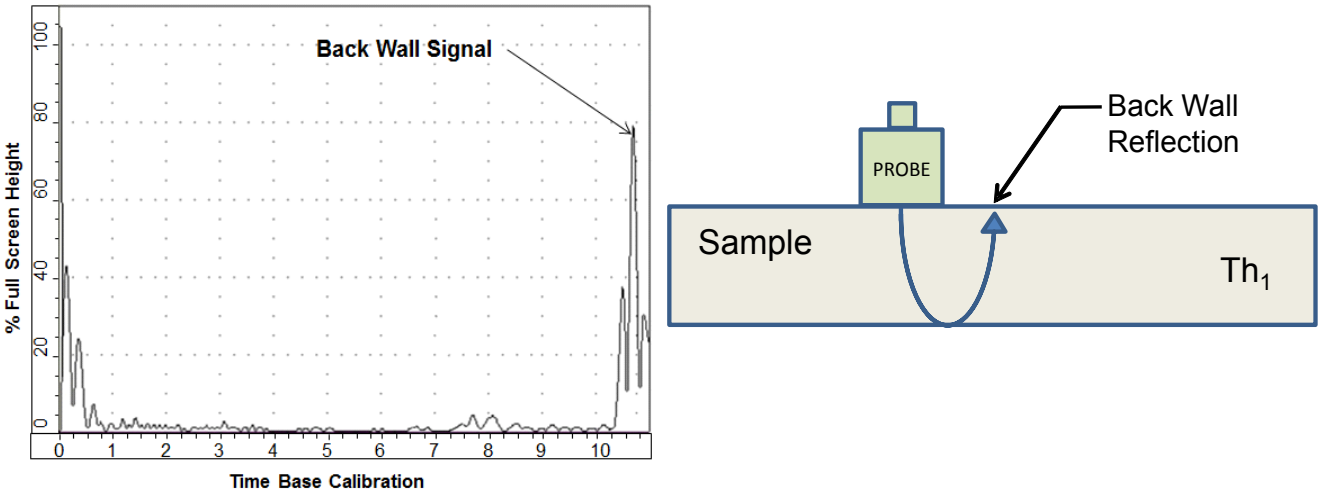

Figure 6. Example Thickness Calibration

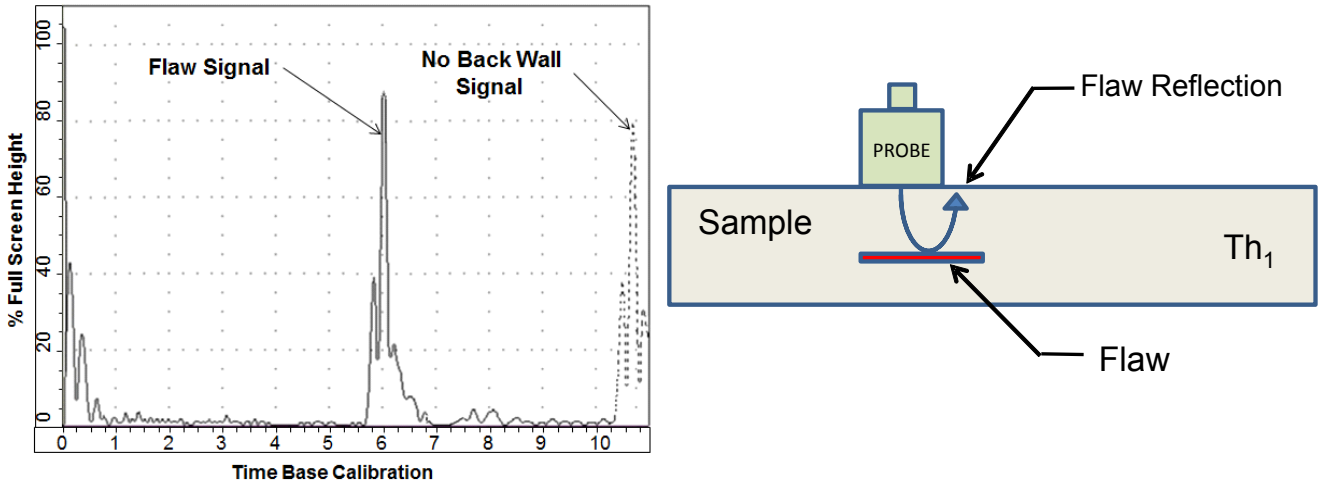

Figure 7. Example Sensitivity Test – Shift in Backwall Signal Due to the Presence of a Flaw

4.1.3 **Scanning Speed –** Inspectors should use a scanning speed that is comfortable to them, usually between 4-6 inches/second. Automated scanning systems may use faster scanning speeds based on equipment manufacturers recommendations.

4.1.4 **Scanning Index –** The recommended scanning index should be around 50% of the transducer diameter, but can't exceed 75% of the transducer diameter.

4.1.5 **Blade Surface Finish –** Ultrasonic inspection requires the blade surface to be clean and free of any foreign material or markings that may interfere with the inspection signal.

4.2 **Inspection Sensitivity:**

4.2.1 **Shear Web Bond Line Inspections –** The instrument gain should be established by placing the transducer on the skin, in the spar cap region, over the shear web bond line area and setting the back wall signal to 80% FSH. The inspection method should be able to detect non-bonded or missing adhesive in the bond line area. This would be for both missing adhesive between the spar cap and the adhesive, and missing adhesive between the adhesive and the shear web flange.

4.2.2 **Leading Edge and Trailing Edge Inspections –** For parallel surfaces, the instrument gain should be established by placing the transducer on the skin over the bonded edge area and setting the back wall signal to 80% FSH. For surfaces that are not parallel, the area should be inspected with through transmission. Using two ½" probes held opposite each other, over the bonded edge area, then increase the gain to achieve 80% FSH.

4.3 **Reporting:**

4.3.1 **Recording Indications** – For hand held or manual scanning, all indications or loss of back wall signal that are not acceptable must be documented in the final report. For automated scanning systems, all indications or loss of back wall signal that are not acceptable must be recorded. All electronically stored data must be maintained.

4.3.2 **Evaluating Indications:**

4.3.2.1 The 6 db drop method shall be used to determine the edge of the adhesive bond line. This can be achieved by identifying the location where the back wall signal height is reduced by 6 db or a the point where the back wall signal shifts to within 0.16 inches (4 mm) of the spar cap thickness. This location shall be marked on the spar cap section of the blade (over the bond line area) if the location is out of compliance with the adhesive bond line area specified in the inspection plan.

4.3.2.2 For through transmission inspection of the leading or trailing edges, any location where the signal height is reduced by 12 db shall be marked on the blade if the location is out of compliance with the adhesive bond areas specified in the inspection plan.

4.3.3 **Acceptance Limits:**

4.3.3.1 **Shear Web** – Refer to the inspection plan for the expected/designed adhesive bond line width. The inspected shear web adhesive bond line width must be at least 80% of the designed

adhesive bond line width. Any missing adhesive in the shear web bond line area with a dimension greater than 0.80 inch (20 mm) in any direction shall be rejected.

4.3.3.2 **Leading and Trailing Edges** – All missing adhesive inspection indications at the exterior points of the leading or trailing edges are not acceptable. Any missing adhesive in the leading or trailing edge bond area (area shown in the inspection plan) with a dimension greater than 0.80 inch (20 mm) in any direction shall be rejected.

5. Inspection Record

5.1 Inspection Report – An inspection report shall be submitted and include the following:

5.1.1 Inspection company name

5.1.2 Inspector name and certification level

5.1.3 Date of inspection

5.1.4 Blade manufacturer, power rating and overall length

5.1.5 Sketch of the wind turbine blade referencing the scan zones

5.1.6 Location and size for each questionable adhesive bond area. Location distances to be measured from the blade root and from the leading or trailing edge

6. Reference Documents:

6.1 American Society for Nondestructive Testing, Inc. (ASNT). Recommended Practice SNT-TC-1A, Personnel Qualifications and Certifications in Nondestructive Testing.

6.2 European Standard EN 4179, Qualification and Approval of Personnel for Nondestructive Testing.

6.3 Canadian National Regulations contained in CAN/CGSB-48.9712-95, Qualification and Certification of Nondestructive Personnel.

Distribution List

Vineesh Agrawal
Clipper Windpower, LLC
Carpinteria, CA

Jim Ahlgrimm
U.S. Dept of Energy
Washington, D.C.

Tasdiq Ahmed
TWI
Ferndale, MI

Kevin Alewine
Shermco Industries Inc.
Irving, CA

Daryoush Allaei
SheerWind
Chaska, MN

Matt Allen
University of Wisconsin - Madison
Madison, WI

Nick Althoff
Pointis Engineering
LaCrosse, WI

Shreyas Ananthan
U.S. Dept of Energy
Washington, DC

Clemens Asmussen
Repower Systems SE
Osterrönfeld, SH Germany

Greg Atchley
General Dynamics Satcom Technologies
Richardson, TX

Mohammad Attia
GE Global Research
Niskayuna, NY

Jared Baker
University of Wyoming
Laramie, WY

Jonathan Baker
Frontier Wind
Rocklin, CA

Pramod Bangalore
Chalmers University of Technology
SE 412 96 Gothenburg, Sweden

Dan Barnard
Iowa State University
Ames, IA

Dev Barpanda
The Dow Chemical Company
Midland, MI

Natalie Barrett
Purdue Center for Systems Integrity
Lafayette, IN

Rashi Bates
Shell WindEnergy Inc.
Houston, TX

Christina Beller
Technical University of Denmark
Roskilde, Denmark

Matt Benoist
ITW Polymer Technologies
Montgomeryville, PA

Chad Benton
Mesalands Community College
Tucumcari, NM

William Berger
Duke Energy
Charlotte, NC

Rob Bergman
GE Energy
Schenectady, NY

Phil Berling
MTS Systems Corporation
Eden Prairie, MN

Derek Berry
NREL/NWTC
Golden, CO

Jay Bhatia
BASF Corporation
Florham Park, NJ

Gunjit Bir
Clipper Windpower
Carpinteria, CA

Keith Blackwell
Milliken & Company
Spartanburg, SC

Chris Bley
Rope Partner
Santa Cruz, CA

Chris Bley
InspecTools
Santa Cruz, CA

Eric Book
Shell WindEnergy Inc.
Houston, TX

John Borgmann
Ocean Power Technologies
Pennington, NJ

Knowledge Centre Wind Turbine
Maaik Borst
Wieringerwerf, The Netherlands

Carlo Bottasso
Politecnico di Milano
Milano, Italy

Francis Boudreault-Leclerc
Olympus NDT
Montreal, Canada

Techical Univ Delft
Cyril Boussion
Delft, The Netherlands

Tony Brandon
Milliken and Company
Spartanburg, SC

Lisa Brasche
Iowa State University
Ames, IA

Wesley Bratton
Vista Engineering Technologies
Richland, WA

Ralph Brillhart
ATA Engineering
San Diego, CA

Ethan Brown
TPI Composites
Warren, MI

Joshua Bryant
Sandia - SWiFT Facility
Houston, TX

Bruce Burton
Huntsman Corporation
The Woodlands, TX

Gregor Cadman
Google Inc.
San Carlos, CA

Doug Cairns
Montana State University
Bozeman, MT

Scott Campbell
Milliken and Company
Dayton, OH

Nannan Cao
Frontier Wind
Rocklin, CA

Mark Capellaro
University Stuttgart
Stuttgart, Germany

Pepe Carnevale
Blade Dynamics
HampshireUK

Mike Carr
Office of the Assistant Secretary - EERE
Washington, DC

Christopher Caruso
GE Energy
Greenville, SC

Luciano Castillo
Texas Tech University
Lubbock, TX

Luis Cerezo
Electrical Power Research Institute
Charlotte, NC

Luis Cerezo
EPRI
Charlotte, NC

Karun Chakravarthy
Dassault Systemes
Waltham, MA

Santhosh Chandrabalan
3M Company
Maplewood, MN

David Chang
Raycon
San Jose, CA

Xiao Chen
University of Houston NWEC
Houston, TX

Phillip Chiu
UCLA
Los Angeles, CA

John Christiansen
MTS Systems Corporation
Eden Prairie, MN

Thomas Christiansen
Strategic Power Systems, Inc.
Charlotte, NC

David Clark
Bachmann Electronic Corp.
Grayslake, IL

Jonathan Colby
Verdant Power
New York, NY

Bill Cole
University of Houston NWEC
Houston, TX

Taylor Coleman
Poseidon Systems, LLC
Rochester, NY

Craig Collier
Collier Research Corporation
Newport News, VA

Matthew Conwell
Invenergy
Chicago, IL

Dean Corren
Verdant Power
New York, NY

Joshua Crayton
Rope Partner
Santa Cruz, CA

Matt Crompton
Dantec Dynamics
Del Rey Oaks, CA

Marty Crotty
Up Wind Solutions
San Diego, CA

Daggumati Subbareddy
GE Global Research,
Bangalore, Karnataka -India

Rick Damiani
RRD Engineering
Arvada, CO

Rory Davis
ATA Engineering
San Diego, CA

Salvatore Della Villa
Strategic Power Systems, Inc.
Charlotte, NC

Tom DeMint
Owens Corning
Seattle, WA

Mike Derby
U.S. Dept of Energy
Washington, DC

Mike Desmond
National Renewable Energy Laboratory
Golden, CO

Sharon Donohoe
Clipper Windpower
Carpinteria, CA

PJ Dougherty
SMI Inc.
Washington, DC

Timothy Downey
Department of Transportation
Washington, DC

Vuk Dragovic
Wing d.o.o.
Belgrade, Serbia

Rodrigo Duarte
SSE Renewables Portugal
Lisbon, Portugal

Marc Dubios
iPhoton Solutions LLC
Ft. Worth, TX

Paul Dvorak
WTWH Media LLC
Cleveland, OH

Katherine Dykes
National Renewable Energy Laboratory
Golden, CO

Chris Edwards
Fulcrum Composites Inc.
Midland, MI

Kate Edwards
Ocean Power Technologies
Pennington, NJ

Dave Eisenberg
Siemens Energy Inc.
Boulder, CO

Andrew Elliott
MSC Software
Mesa, AZ

Kevin Elsken
Bayer Material Science
Pittsburgh, PA

Senvion SE
Enno Eyb
Osterronfeld, Germany

Tim Fallon
TPI Composites
Warren, RI

Bob Farris
Momentive Specialty Chemicals
Stafford, TX

Stefan Faulstich
Fraunhofer IWES
Bremerhaven, Germany

Brian Feeny
Michigan State University
East Lansing, MI

Albert Fisas-Camanes
ALSTOM Power Inc.
Richmond, VA

Cash Fitzpatrick
U.S. Dept of Energy
Washington, DC

Alex Fleming
Ecomerit
Santa Barbara, CA

Vince Foody
Milliken and Company
Spartanburg, SC

Matthew Frank
Iowa State University
Ames, IA

Xu Fu
GE Global Research
Shanghai, China

Bernie Fu
BASF
Florham Park, NJ

Bill Fuller
Exxon Mobil Corp.
Irving, TX

Enrique Garcia
Gamesa Wind Power
Sarriguren, Spain

Benjamin Gaskill
Shell WindEnergy Inc.
Houston, TX

Anis Gawandi
Siemens Wind Power
Boulder, CO

Steve Gibbs
Clipper Windpower
Cedar Rapids, IA

Adrian Gill
Vestas
Boulder, CO

Ben Givens
AEP
Trent, TX

Chad Glinsky
Romax Technology Inc.
Nottingham, United Kingdom

Clint Goolsbay
Hexcel Composites
Arlington, TX

Carol Graham
Creative Foam Corporation
Fenton, MI

Francesco Grasso
ECN
Petten, Netherlands

Anne Marie Graves
GL Garrad Hassan
Houston, TX

Karl Gregory
Vestas
Boulder, CO

Ronald Grife
EDPR
Houston, TX

Ernesto Grossmann
CU Boulder
Boulder, CO

Joel Gruhn
NEPTCO Inc.
Pawtucket, RI

Qiang Guo
Iowa State University
Ames, IA

Todd Haber
Micron Optics Inc.
Atlanta, GA

Jason Habermehl
Olympus NDT
Montreal, Canada

Berthold Han
Fraunhofer IWES
Kassel, Germany

Mohsan Haider
Clipper Windpower LLC
Carpinteria, CA

Kurt Hallamasek
Google, Inc.
San Carlos, CA

Jeffrey Hammit
NextEra Energy Resources
Boca Raton, FL

Scott Hearon
ITW WindGroup
Neptune, NJ

Jeremey Heinks
LM Wind Power
Grand Forks, ND

Troy Hetherington
Stran Technologies
Naugatuck, CT

Mark Higgins
U.S. Department of Energy
Washington, DC

Satyanarayana Himakuntla
Enercon India Ltd.,
Daman – India

Juan Hodelin
Physical Optics Corp.
Torrance, CA

D.M. Hoyt
NSE Composites
Seattle, WA

Irfan Huda
BASF
Tarrytown, NY

Gary Huff
ER Systems
Rockford, MN

Scott Hughes
National Renewable Energy Laboratory
Golden, CO

Byungsun Hwang
Korea Inst. Of Materials Science
Changwon, Korea

Eric Jacobsen
GE Global Research
Greenville, SC

Salim Jaffer
General Electric - Bently Nevada
Phoenix, AZ

Anant Jain
Texas Tech University
Lubbock, TX

Chuck Jenkins
General Electric - Bently Nevada
Hamilton, OH

John Jeno
LM Windpower
Grand Forks, ND

Find Mølholt Jensen
Bladena Aps
Ringsted, Denmark

Jae-ho Jeong
Samsung Heavy Indus/Wind Turbine Div.
Geoje-si, Korea

Joyce Jin
Worldwide Aeros Corp.
Montebello, CA

Kevin Joesel
Fusion UV Systems, Inc.
Gaithersburg, MD

Wade Johanns
Iowa State University
Ames, IA

Justin Johnson
EDP Renewables North America LLC
Houston, TX

Perry Johnson
UCLA, Wirz Research Group
Los Angeles, CA

Desiree Johnson
Iberdrola Renewables
Portland, OR

Nick Johnson
U.S. Department of Energy
Golden, CO

James Jones
Composites Consulting Group
DeSoto, TX

Yellavenkatasunil Jonnalagadda
Siemens energy, Inc. - Wind Power
Boulder, CO

Wandan Joo
Doosan
Daejeon, Republic of Korea

Peter Joosse
CTC Engineering
Hengelo, Netherlands

Rob Kamisky
WINDprove, Inc.
Davis, CA

Gary Kanaby
Molded Fiber Glass Companies
Sherman, CA

Aaron Kaplan
Luna Technologies
Blacksburg, VA

Hirokazu Karasawa
Toshiba Power System Inspection Services
Tokyo, Japan

Stefan Kern
GE Global Research
Garcging n. Munich

Ole Kils
Clipper Windpower
Carpinteria, CA

Seong-Hun Kim
Samsung Heavy Industries/Wind Turbine
Geoje-si, Gyeongsangnam-do, South Korea

Mac Klingler
M.G. Klingler, Ltd.
Galena, IL

Dave Klozik
Comau Inc.
Southfield, MI

Justin Klure
Northwest Energy Innovations
Portland, OR

Sandie Klute
Luna Innovations
Blacksburg, VA

Keith Konieczka
Owens Corning
Wauseon, OH

Steven Kopf
Northwest Energy Innovations
Portland, OR

Sriram Krishnamurthy
GE Global Research,
Bangalore, Karnataka – India

David Kroeker
Texas Tech University
Lubbock, TX

Annie Kyriakides
GE Energy
Schenectady, NY

Richard LaFountain
Molded Fiber Glass Companies
Gainesville, TX

Carl LaFrance
Molded Fiber Glass Companies
Ashtabula, OH

Kevin Lambrych
Ashland Performance Materials
Dublin, OH

Brenda Langley
NW Nat'l Marine Renewable Energy Center
Corvallis, OR

Francesco Lanza di Scalea
UC San Diego
LaJolla, CA

Scott Larwood
University of the Pacific
Stockton, CA

Bernard Laskowski
Analatom Inc
Sunnyvale, CA

Bob Lasser
Imperium Inc.
Beltsville, MD

John Leahey
Vestas
Boulder, CO

Jihyun Lee
Samwon Millennia
Seongnam, South Korea

Ken Lee
Wetzel Engineering, Inc.
Lawrence, KS

Sanghonn Lee
Doosan
Daejeon, Republic of Korea

Yeon-Seung Lee
Korea Adv Inst. of Science & Technology
Yuseong-gu, Daejeon, Republic of Korea

Hak Gu Lee
Wind Turbine Tech Research Center
Daejeon, Republic of Korea

Paul Legac
J. P. Morgan
Chicago, IL

Thierry Lemaigre
Dow Corning Corporation
Seneffe, Belgium

Obdulia Ley
Mistras
Princeton Junction, NJ

Jianfu Li
Chinese Wind Energy Association
Beijing, China

Bob Liekar
Fluitec Wind
Jersey City, NJ

Wendy Lin
GE Global Research
Niskayuna, NY

Lindberg Lindberg
Electric Power Research Institute

Jack Little
Evisive Inc
Baton Rouge, LA

Marcus Lihua Liu
Owens Corning
Shanghai, China

K.H. Lo
University of Houston NWEC
Houston, TX

Kevin Long
JRL Ventures
Cape Coral , FL

Peter Lucon
Resodyn Corporation
Butte, MT

Matthew Lueker
University of Minnesota
Minneapolis, MN

Doug Lutz
GE Sensing &Inspection Technologies
Lewistown, PA

Liangkai Ma
The Dow Chemical Company
Midland, MI

Helge Madsen
Risøe National Laboratory
Roskilde, Denmark

Andrew Magstadt
University of Wyoming
Laramie, WY

Mark Main
BASF Corporation
Canton, MI

Ninochska Maldonado
eDF-RE
Palm Beach Gardens, FL

Matt Malkin
DNV
Seattle , WA

John Mandell
Montana State University
Bozeman, MT

Christophe Mattei
Exova
Jonkoping, Sweden

Timothy McCarthy
Materia Inc.
Pasadena, CA

Megan McCluer
Dept of Energy
Washington, DC

Bill McCroskey
Intl Health Monitoring Systems
Dayton, OH

Jarlath McEntee
Ocean Power Renewable Company
Portland, ME

Ken McGraw
Wind Energy Services
Gainesville, TX

Thomas McKay
BASF Corporation
South Lyon, MI

Rock McNeil
BASF Corporation
Southfield, MI

Suchit Meshram
Enercon India Ltd.,
Daman – India

Hendrik Mester
Repower Systems SE
Osterrönfeld, SH Germany

Angie Miller
Huntsman
The Woodlands, TX

William Miller
Huntsman Advanced Materials
The Woodlands, TX

Akira Miyase
University of Houston NWEC
Houston, TX

David Model
Triton
Chelmsford, MA

Dave Modos
IMCORP
Manchester, CT

Jiwon Mok
GE Global Research
Niskayuna, NY

Robert Monroe
Fulcrum Composites Inc.
Midland, MI

Iain Montghomery
AGY
Aiken, SC

Jin Bum
Wind Turbine Tech Research Center
Daejeon, Republic of Korea

Pat Moriarty
NREL/NWTC
Golden, CO

Willard Morris
Imperium Inc.
Beltsville, MD

Justin Morse
ALSTOM Power Inc.
Richmond, VA

Patrick Muglia
AmTech Composites
Wapato , WA

Eduardo Munoz
Applus RTD
Houston, TX

Noah Myrent
Purdue Center for Systems Integrity
Lafayette, IN

Jacques Nader
Siemens
Boulder, CO

Mala Nagarajan
Owens Corning
Granville, OH

Kamesh Narasimhan
NEPTCO Inc.
Granite Falls, NC

Jonathan Naughton
University of Wyoming
Laramie, WY

Ryan Neahr
General Dynamics Satcom Technologies
Richardson, TX

Jared Nelson
Montana State University
Bozeman, MT

Jeff Nelson
Transalta
Calgary, Canada

John Newman
Laser Technology Inc.
Norristown, PA

Khanh Nguyen
National Wind Technology Center/NREL
Louisville, CO

Chris Niezrecki
UMass Lowell
Lowell, MA

Rogier Jijssen
Knowledge Centre Wind Turbine
Wieringerwerf, The Netherlands

Pourya Nikoueeyan
University of Wyoming
Laramie, WY

Simeon Andrew Ning
NREL/NWTC
Golden, CO

Maya Nissim
EDP Renewables
Houston, TX

Steve Nolet
TPI Composites
Warren, RI

Global Blade Technology
Mark Noordanus
Wieringerwerf, The Netherlands

Germán Moreno Notario
Applus+ LGAI
Barcelona, Spain

John Obrecht
Siemens
Boulder, CO

Frank O'Connor
ServusNet Informatics
Cork, Ireland

Ryan O'Connor
EDF-RE
Denver, CO

Ganzalo Palacio
Gamesa Wind Power
Vizcaya, Spain

Sharon Papke
Bayer MaterialScience
Pittsburgh, PA

James Parle
Muir Data Systems
Pasadena, CA

James Payant
Janicki Industries
Sedro-Woolley, WA

Jim Payant
Janicki Industries
Sedro , WA

Raymond Pearson
Lehigh University
Bethlehem, PA

Eduardo Perez
Power Equipment Maintenance, Inc.
Piedmont, SC

Will Perry
GEIT
Lewistown, PA

Frank Peters
Iowa State University
Ames, IA

Soren Horn Petersen
Bladena Aps
Ringsted, Denmark

Stanton Peterson
BP Wind Energy
Houston, TX

Lars Pettersson
Vattenfall AB
Stockholm, Sweden

Tyler Phillips
Energetx
Holland , MI

Yuri Plotnikov
GE Global Research
Niskayuna, NY

Alejandro Ponce
Tecsis dba WindCom Services
Houston, TX

David Potter
National Instruments
Austin, TX

Eric Powell
Ashland, Inc.
Dublin, OH

Amar Pradhan
Fluitec Wind
Jersey City, NJ

Larry Preston
Heartland Energy Solutions
Mt Ayr, IA

Charles Previte
DIAB Sales, Inc.
DeSoto, TX

Padmakumar Puthillath
Milliken and Company
Spartanburg, SC

Jaime Rabell
Dow Corning
Mexico City, Mexico

Venkat Ramakrishnan
Michigan State University
East Lansing, MI

John Register
R-Conn NDT Inc
Menomonie, WI

Pat Rezza
Resolute Marine Energy
Boston, MA

Ken Rhinefrank
Columbia Power Technologies
Corvallis, OR

Amir Riahi
GE Wind
Greenville, SC

William Riddle
Montana State University
Livingston, MT

Garth Ripton
Iberdrola Renewables
Portland, OR

Richard Roberts
Hexcel
Dublin, CA

James Rodgers
Airgia LCC
Mesa, AZ

Daniel Rodriguez
AOC LLC
Collierville, TN

Bjoern Roscher
EWEM
Delft

Stan Rosinski
Electrical Power Research Institute (EPRI)
Charlotte, NC

Ralph Rotolante
MovieTherm
Boxborough, MA

James Sadlo
3M-Industrial & Transporation Business
Round Rock, TX

Jon Salmon
enXco Corporation
Forest City, IA

Angelica Sanchez
Cabot Corporation
Billerica, MA

Daniel Sanchez
U.S. Department of Energy
Albuquerque, NM

Chris Sauer
Ocean Power Renewable Company
Portland, ME

Hely Ricardo Savio
Jade Systems S.I.
Zizur Mayor Navarra, Spain

Philip Schell
Zoltek Corporation
St. Louis, MO

Thomas Schmack
InspecTools
Santa Cruz, CA

John Schroeder
Texas Tech University
Lubbock, TX

Juan Serrano
PPG Industries
Shelby, NC

Roland Sesselmann
Siemens Energy
Boulder, CO

Shawn Sheng
NREL/NWTC
Golden, CO

Chris Shennan
HEXCEL
Duxford, United Kingdom

Steve Shepard
Thermal Wave Imaging
Ferndale, MI

Mark Shepler
Creative Foam Corporation
Fenton, MI

Robert Sherwin
EAPC Wind Energy
Norwich, VT

Rick Shumaker
Heron Wind
Traverse City, MI

Ryan Sievers
Siemens Wind Power
Boulder, CO

Elizabeth Sims
Cabot Corporation
Billerica, MA

Susan Skemp
SE Nat'l Marine Renewable Energy Center
Boca Raton, FL

Jesse Skramstad
NDT Solutions
New Richmond, WI

Jeff Smith
Gamesa
Trevose, PA

Ron Smith
Verdant Power
New York, NY

James Snelson
Infigen Energy
Sweetwater , TX

Dave Snowberg
NREL/NWTC
Golden, CO

Seyed Soltani
Wichita State University
Wichita, KS

Felipe Soriano
DIAB Sales, Inc.
DeSoto, TX

Sritharan Sri
Iowa State University
Ames, IA

Bill Staby
Resolute Marine Energy
Boston, MA

Bob Stakenborghs
Evisive
Baton Rouge, LA

Kevin Standish
Siemens Energy Inc.
Boulder, CO

Markus Stieglbauer
BASF Coatings
Oldenburg, Germany

Fred Stoll
Milliken and Company
West Chester, OH

Jan Sumfleth
Repower Systems SE
Schleswig-Holstein, Germany

Ryan Suncheefore
U.S. Dept of Energy
Washington, D.C.

Henry Swales
Clipper Windpower
Santa Barbara, CA

Paul Sweat
National Instruments
Thornton, CO

Todd Tagatz
MTS Systems Corporation
Eden Prairie, MN

Jason Testa
General Electric
Greenville, SC

Jim Thomas
Strategic Power Systems, Inc.
Charlotte, NC

Henrik Stensgaard Toft
Aalborg University/EMD International A/S
Aalborg, Denmark

Ville Turkia
VTT Tehnical Research Centre of Finland
P.O. Box 1000, Fl-02044 VTT, Finland

Alan Turner
Micron Optics Inc.
Atlanta, GA

Paul Ubrich
Momentive Specialty Chemicals
Stafford, TX

Mary Uchida
University of Colorado
Boulder, CO

Hans Urich Thornberg
Bach Composites
Ft. Lupton, CO

C.P. (Case) Van Dam
University of California - Davis
Davis, CA

Ehren Van Schmus
Clipper Windpower
Santa Barbara, CA

Paul Veers
National Renewable Energy Laboratory
Boulder, CO

Luis Vega
Hawai'i Nat'l Marine Renewable Energy Center
Honolulu, HI

Dayal Vinay
Iowa State University
Ames, IA

Alexander Vossler
General Electric
Greenville, SC

Tomas Vronsky
Vestas
Boulder, CO

Chris Walford
Wind Energy
Seattle, WA

Su Su Wang
University of Houston NWEC
Houston, TX

Siyong Wang
Chinese Wind Energy Association
Beijing, China

Carsten Westergaard
NextraTEC, Inc.
Houston, TX

Kyle Wetzel
Wetzel Engineering
Austin, TX

John Wirt
VEC Technology, LLC
Greenville, PA

Hoon ill Won
Texas Tech University
Lubbock, TX

Geoff Wood
Profile Composites
Sidney BC, Canada

David Woodcock
Huntsman Corporation
The Woodlands, TX

Sean Xun
U.S. Dept of Energy
Washington, DC

Ke Yang
Institute of Engineering Thermohphysics
Beijing, China

Aaron Yarbrough
General Electric
Greenville, SC

Chandra Yerramalli
GE Electric-GRC
Schenectady, NY

Dong-Jin Yoon
Korea Research Inst of Stds & Science
Daejeon, Korea

Mostafa Yossef
Arab Academy for Science and Technology
Cairo Egypt

Usama Younes
Bayer Material Science LLC
Pittsburgh, PA

Robert Youssi
G.E.
Fallbrook, CA

Tung Pei Yu
University of Houston NWEC
Houston, TX

Wenbin Yu
Utah State University/AnalySwift LLC
Logan, UT

Paul Zakian
Bruel and Kjaer
San Diego, CA

Jose Zayas
U.S. Department of Energy
Washington, DCChina

Mingming Zhand
Institute of Engineering Thermohphysics
Beijing, China

Huiyi Zhand
Iowa State University
Ames, IA

Qi (Joyee) Zhu
GE Energy
Greenville, SC

Siqi Zhu
Iowa State University
Ames, IA

Sandia National Labs:

160 Valerie Salim-Meza
162 Erik Ridley
1515 Matthew Barone
1523 Brian Owens
1534 Rich Jepsen
1815 Bernadette Hernandez-Sanchez
2667 Luke Watson
2722 Lorenzo Gutierrez
3555 Alyssa Archibeque
3651 Stephanie Holinka
6000 Jill Hruby
6100 Carol Adkins
6111 Stanley Atcitty
6112 Roger Hill
6120 Janet Snow
6120 Juan Torres
6121 Jonathan Berg
6121 Joshua Bryant
6121 David Maniaci
6121 Phillip Richards
6121 Dale Berg
6121 Lenore Boulton
6121 Wesley Johnson
6121 Benjamin Karlson
6121 Bruce LeBlanc
6121 David Minster
6121 Brian Naughton
6121 Joshua Paquette
6121 Brian Resor
6121 Jonathan White
6122 Diana Bull
6122 Todd Griffith
6122 Daniel Laird
6122 Carlos Michelen
6122 Vincent Neary
6122 Jesse Roberts

6124 Sandra Begay-Campbell
6133 Bruce Thompson
6600 Billy Marshall
6610 Jeff Danneels
6620 Roberto Mata
6620 Willy Morse
6620 Dennis Roach
6621 Michel Bode
6621 Randy Duvall
6621 Steve Heffelfinger
6621 Stephen Neidigk
6621 Tom Rice
6622 Robert Baca
6623 Mark Soo Hoo
6625 Barry Boughton
6630 Brad Parks
7931 Krista Houmpheng
7931 Natalie Pitcher
9513 Alistair Ogilvie
9532 Recorded Information Management
10661 Mario Pino
35543 Jade Cook
85155 Eric Johnson


Sandia National Laboratories